ČESKÉ VYSOKÉ UČENÍ TECHNICKÉ V PRAZE

FAKULTA STAVEBNÍ

Katedra hydrauliky a hydrologie

Hmotnostní toky v půdním prostředí

Habilitační práce

2017 Ing. Jaromír Dušek, Ph.D.

Poděkování

Na tomto místě bych rád poděkoval prof. Ing. Tomáši Vogelovi, CSc. za vždy podnětné a povzbuzující diskuze a připomínky. Stejné poděkování patří i dalším kolegům a spolupracovníkům z Fakulty stavební, ČVUT v Praze. V předkládané habilitační práci jsou prezentovány výsledky, které byly získány v rámci těchto grantových projektů: Identifikace hydrofyzikálních vlastností způsobujících gravitačně podmíněné proudění v porézních materiálech (Grantová agentura ČR), Antropogenní tlaky na stav půd, vodní zdroje a vodní ekosystémy v české části mezinárodního povodí Labe (Ministerstvo životního prostředí ČR), Revitalizace vodního systému krajiny a měst zatíženého významnými antropogenními změnami (Ministerstvo školství, mládeže a tělovýchovy ČR), Hydrologické toky v systému půda-rostlina-atmosféra (Grantová agentura ČR), Izotermické a neizotermické proudění vody a transport látek v pórovitém prostředí v blízkosti nasycení (Grantová agentura ČR) a Podpovrchový transport vody, uhlíku a tepla - kombinovaný hydrologický, geochemický a izotopový přístup (Grantová agentura ČR).

Obsah

Komentář k souboru publikovaných prací 1
Úvod 1
Studie zahrnuté do souboru publikovaných prací 3
Shrnutí 10
Literatura 11
Soubor publikovaných prací 13
Numerical analysis of ponded infiltration experiment under different experimental conditions, Soil and Water Research, 2009. 13
Short-term transport of cadmium during a heavy rain event simulated by a dual-continuum approach, Journal of Plant Nutrition and Soil Science, 2010. 20
Effect of plastic mulch on water flow and herbicide transport in soil cultivated with pineapple crop: A modeling study, Agricultural Water Management, 2010. 33
Field leaching of pesticides at five test sites in Hawaii: study description and results, Pest Management Science, 2010. 43
Field leaching of pesticides at five test sites in Hawaii: modeling flow and transport, Pest Management Science, 2011. 60
Combining dual-continuum approach with diffusion wave model to include a preferential flow component in hillslope scale modeling of shallow subsurface runoff, Advances in Water Resources, 2012. 73
Hillslope hydrograph analysis using synthetic and natural oxygen-18 signatures, Journal of Hydrology, 2012. 87
Transport of iodide in structured soil under spring barley during irrigation experiment analyzed using dual-continuum model, Biologia, 2013. 101
Modeling subsurface hillslope runoff dominated by preferential flow: One- vs. two-dimensional approximation, Vadose Zone Journal, 2014. 107
Transport of bromide and pesticides through an undisturbed soil column: A modeling study with global optimization analysis, Journal of Contaminant Hydrology, 2015. 121
Hillslope-storage and rainfall-amount thresholds as controls of preferential stormflow, Journal of Hydrology, 2016. 138
Dynamics of dissolved organic carbon in hillslope discharge: Modeling and challenges, Journal of Hydrology, 2017. 155

Komentář k souboru publikovaných prací

Úvod

Důležitost časoprostorové informace o objemovém toku vody a hmotnostním toku chemických látek v pórovitém prostředí je zřejmá v mnoha oborech lidské činnosti. Objemové a hmotnostní toky mají přímý vliv na kvantitu i kvalitu vody v recipientech, potravinovou produkci a biomasu, klima, zdroje podzemní vody, transport živin, stabilitu svahů, erozi, apod. Proudění vody ve vadózní zóně je ze své podstaty značně komplikované nelinearitou a hysterezí hydraulických vlastností půdního prostředí (včetně heterogenity fyzikálně-chemických vlastností) a výraznou citlivostí vůči změnám atmosférických a hydraulických podmínek.

Experimentální data sloužící k vyhodnocení režimu odtoku vody a transportu ve vodě rozpuštěných látek v půdách jsou obvykle nedostatečně reprezentativní v čase a prostoru. Hmotnostní toky jsou navíc obtížně měřitelné a jejich prostorová variabilita způsobená prostorovou heterogenitou pórovitého prostředí a variabilitou hydraulických charakteristik je často významná, a to jak v přirozených půdách (horských půdních profilech) tak v zemědělských půdách s antropogenními zásahy. Terénní data jsou rovněž zatížena nejistotou danou například nepřesnou kalibrací a teplotní závislostí. Nezastupitelnou úlohu proto v analýzách spojených s pohybem vody a transportu látek v pórovitém prostředí hraje matematické modelování. Fyzikálně založené modely slouží k lepšímu pochopení relevantních procesů a vyhodnocení jednotlivých dílčích vlivů na režim odtoku a transportu. Fyzikálně založené modely navíc poskytují představu o procesech, které ovlivňují pohyb vody a transport látek. Modelování se například používá v rozhodovacím řízení zaměřeném na vyhodnocení rizik kontaminace organickými látkami. Základní výzva spojená s aplikací fyzikálně založených modelů je jejich parametrizace, což je jeden z důvodů používání zjednodušených empirických přístupů.

Preferenční proudění je fenomén, který významně ovlivňuje hmotnostní toky v půdách a jejich časoprostorovou variabilitu. Tento typ proudění může být vyvolán různými příčinami a může se také různým způsobem projevovat. Preferenční proudění se uplatňuje na různých úrovních prostorového (mikroskopická úroveň až měřítko svahu/povodí) a časového měřítka (sekundy až roky). K preferenčnímu proudění a transportu dochází v případě toku infiltrující vody a rozpuštěných látek relativně malou objemovou částí pórového prostoru (preferenčními cestami). Preferenční tok významně ovlivňuje hydrologickou reakci na srážku a má proto výrazný vliv na kvantitu i kvalitu podzemních a povrchových vod. Charakteristickým znakem preferenčního proudění je nerovnováha stavových veličin (tlaková výška půdní vody a koncentrace chemické látky) mezi půdní matricí a rychlými cestami proudění (makropóry, biopóry, trhliny, strukturní části půdy, půdní agregáty apod.). Preferenční proudění může rovněž vznikat díky prostorové variabilitě rychlostí způsobené heterogenitou pórovitého prostředí na úrovni pórů („pore scale“) a makroskopickém měřítku („Darcy scale“). Aplikace matematických modelů pro takovéto případy stále představuje nesnadný úkol (Jarvis et al., 2016).

Významnost a/nebo intenzitu projevů preferenčního proudění lze kvantifikovat různými matematickými indexy a ukazateli s využitím experimentálních dat o tocích, efektivním nasycení nebo koncentraci rozpuštěné látky. Mezi nejrozšířenější experimentální přístupy patří zhodnocení prostorové (experiment se stopovačem) nebo časové (koncept průnikové křivky) variability koncentrace chemické látky. Experimenty se stopovačem-barvivem mohou naznačit morfologii a prostorovou strukturu preferenčních cest, objemový podíl makropórů a jejich interakci (přenos) s okolní půdní matricí. Z tvaru průnikové křivky lze usuzovat o vlivu preferenčního transportu; pomocí modelových přístupů je možné vliv preferenčního proudění a transportu kvantifikovat, například použitím „two-region" modelu s mobilní a nemobilní zónou proudění.

Matematické modely preferenčního proudění vody a transportu látek je možné z hlediska zahrnutí geometrie preferenčních cest do konceptuálního modelu rozdělit na modely implicitní a explicitní. V implicitních modelech je systém preferenčních cest reprezentován samostatnou doménou proudění, druhou doménu tvoří půdní matrice (Obrázek 1). Tento přístup je nazýván modelem duálního kontinua (duální permeability). Obě pórové domény mají odlišné hydraulické charakteristiky a mezi doménami dochází k výměně vody a rozpuštěných látek. Jako model pohybu vody je v preferenční doméně používána Richardsova rovnice (Gerke a van Genuchten, 1993) nebo rovnice kinematické vlny (Larsbo et al., 2005). Transport chemických látek je obvykle popsán řešením advekčně disperzních rovnic v obou pórových systémech.

Explicitní modely jsou založeny na konkrétním prostorovém vyjádření zón rychlého proudění (preferenčních cest). Jednou z možností je použití algoritmu pohybu *Lumbricus terrestris* (Vogel et al., 2006) nebo stochastické generování distribuce makropórů na základě terénního pozorování (Klaus a Zehe, 2011).

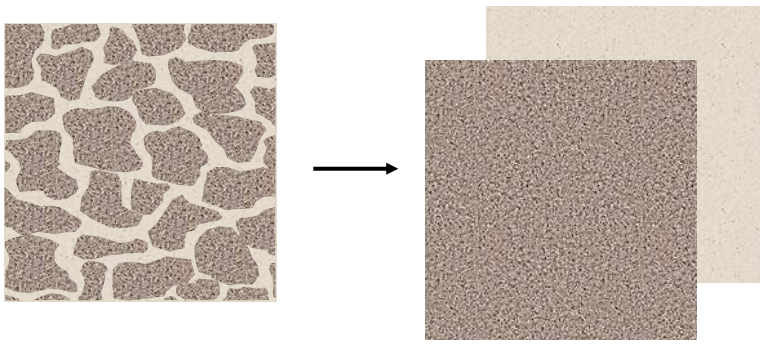

Obrázek 1. Model duálního kontinua. Strukturní pórovité prostředí je nahrazeno dvěma doménami proudění: půdní matricí a preferenční doménou (Vogel et al., 2010).

V matematických modelech je často opomíjena časová variabilita hydraulických charakteristik. Během vegetačního období je vznik makropórů a biopórů formovaných půdní faunou (například *Lumbricus terrestris*) intenzivní, rovněž tak zvýšení počtu a objemového podílu trhlin vzniklých během letních teplých období v půdách s obsahem jílových minerálů.

Sezónní dynamika pohybu vody se však obvykle uvažuje s časově neměnnými hydraulickými charakteristikami. Tento předpoklad může být velmi nereálný především u zemědělských půd, kde se v průběhu roku technickými zásahy i přirozenými procesy mění struktura svrchní vrstvy. Dynamika odezvy na srážku tak může být v průběhu roku velmi rozdílná.

U fyzikálně založených matematických modelů je nezbytné definovat počáteční a okrajové podmínky. Okrajové podmínky jsou v terénních úlohách definované s větší nejistotou v porovnání s kontrolovanými podmínkami v laboratoři. Nejednoznačnost v definování okrajových podmínek se obvykle propaguje do simulovaných výsledků. Pro půdní povrch s přítomnými preferenčními cestami se jedná o komplexní separaci a přerozdělování objemových a hmotnostních toků. Okrajové podmínky pro půdní matrici a preferenční cesty jsou pro specifické případy rozdílné. Doposud však nebyly navrženy takové experimentální techniky, které by byly schopny měřit hmotnostní toky samostatně pro každou pórovou doménu proudění. Vedle okrajových podmínek může být definování počáteční podmínky stejně problematické, ovšem počáteční podmínky ovlivňují především epizodní simulace.

Ve studiích zaměřených na analýzu pohybu vody a transportu látek nenasycenou zónou je velmi často nutné uvážit odběr vody kořenovým systémem. Kvantifikace makroskopické intenzity odběru a její hodnověrnost ovlivňuje bilanci půdní vody a rozpuštěných látek. Evapotranspirační tok během vegetační sezóny může pro horská povodí v mírném klimatickém pásmu dosahovat až dvou třetin srážkového úhrnu; evapotranspirace tak tvoří důležitou složku celkové bilance půdní vody. V posledních letech bylo uveřejněno několik studií, které ukázaly zdokonalenou konceptualizaci procesu odběru vody kořeny a tím realističtější intenzity odběru, včetně hydraulické redistribuce půdní vody a kompenzačního mechanismu (například Vogel et al., 2013). Vedle hydraulických charakteristik pórovitého prostředí je v případě aplikace těchto modelů nutné definovat vlastnosti kořenového systému a rostliny (prostorovou hustotu kořenů, průměr aktivního kořene a radiální odpor, kapacitu xylemu). Díky pokroku v experimentálních metodách mohou být výsledky modelování porovnávány s daty toku vody rostlinou („sap flow“). Rovněž nové neinvazivními techniky umožňují vizualizaci kořenové architektury a odhad parametrů kořenového systému.

Hlubší a detailnější poznání fyzikálně-chemických procesů a mechanismů ovlivňujících pohyb vody a transport chemických látek v půdách je základem pro realistické předpovědi pomocí deterministických simulačních modelů. Transportní procesy odehrávající se v půdním prostředí jsou komplexní a jsou ovlivněny četnými přímými i nepřímými faktory (Vereecken et al., 2016), jejichž nezávislá parametrizace je často obtížná. Z tohoto důvodu se v konceptuálním modelu zahrnují pouze relevantní fyzikální, chemické a biologické vlivy a procesy, což mnohdy vyžaduje interdisciplinární přístup.

Studie zahrnuté do souboru publikovaných prací

Tato práce obsahuje soubor 12 studií publikovaných během období 2009 až 2017 v časopisech indexovaných v databázích Web of Science a Scopus. Předkladatel habilitační práce byl u všech studií uveden jako hlavní a s redakcí časopisu korespondující autor.

Dušek, J., Dohnal, M., Vogel, T., 2009, Numerical analysis of ponded infiltration experiment under different experimental conditions, Soil and Water Research, 4, S22–S27.

Výtopová infiltrace se v hydropedologii používá jako standardní *in situ* experiment k zjišťování hodnoty nasycené hydraulické vodivosti svrchní půdní vrstvy. Nasycená hydraulická vodivost (K_s) je z hlediska matematického modelování jeden z nejdůležitějších parametrů pórovitého prostředí; parametr K_s patří mezi nejcitlivější parametry hydrologických modelů. Její hodnota se avšak poměrně nesnadno zjišťuje pro strukturní a heterogenní půdy. Hodnota K_s je zcela určující pro rozdělování hmotnostních toků mezi infiltraci a povrchový odtok. Experimentální infiltrační data jsou často ovlivněna různými vlivy, které znesnadňují jejich interpretaci a vyhodnocení. V článku byly pomocí třírozměrného matematického modelování postupně analyzovány následující vlivy: 1) průměr infiltračního válce, 2) výška vodní hladiny v infiltračním válci během experimentu, 3) hloubka zaražení válce do půdního profilu, 4) tvar a velikost výpočetních elementů sítě v blízkosti stěny válce a 5) dvouválcové uspořádání experimentu. Numerickou analýzou bylo zjištěno, že hloubka zaražení válce významně ovlivňuje infiltrační rychlost. Infiltrační rychlost je rovněž ovlivněna tvarem výpočetní sítě, tj. anizotropií elementů v blízkosti stěny válce. Ustálená infiltrační rychlost je u dvouválcové metody výrazně vyšší než hodnota K_s svrchní vrstvy.

Dušek, J., Vogel, T., Lichner, L., Čipáková, A., 2010, Short-term transport of cadmium during a heavy rain event simulated by a dual-continuum approach, Journal of Plant Nutrition and Soil Science, 173, 536–547.

Intenzifikace transportu rozpuštěných látek v půdách hraje díky preferenční složce odtoku klíčovou roli při úlohách zabývajících se znečištěním podzemních vod. Cílem této studie bylo pomocí numerického modelování analyzovat transport kadmia (Cd) v reakci na extrémní srážkovou událost. Tato studie vznikla ve spolupráci s Ústavem hydrologie Slovenské akademie věd (L. Lichner) a slovenským Státním zdravotním ústavem (A. Čipáková). Hlavním zdrojem kadmia jsou hnojiva, která mohou obsahovat až 170 mg Cd kg^{-1}. Jednorozměrným modelem založeným na konceptu duálního kontinua byl odhadnut průnik kadmia třemi texturně odlišnými půdními profily (písčito-hlinitá půda, hlinitá půda a jílovitá půda) v Podunajské nížině. Tato oblast je charakteristická extenzivním zemědělstvím a relativně malou mocností nenasycené zóny. Na základě laboratorních adsorpčních experimentů, které provedli slovenští partneři, bylo předpokládáno kadmium relativně mobilní v preferenčních cestách (nižší hodnota distribučního koeficientu K_d než v půdní matrici). Pro dva typy půd (hlinitá a jílovitá) bylo modelováním prokázán pohyb Cd pod kořenovou zónu během krátkého časového období. Nejhlubší průnik Cd byl zjištěn pro těžkou jílovitou půdu, kde byl preferenční transport významný vzhledem ke kontrastním vlastnostem domén půdní matrice a preferenčních cest. Z environmentálního hlediska představují výsledky simulací nejnepříznivější situaci tím, že kadmium zůstává přítomné v kořenové zóně a tím přístupné odběru rostlinami a zároveň poměrně hluboký pohyb kadmia, což může představovat zvýšené riziko kontaminace podzemních vod.

Dušek, J., Ray, C., Alavi, G., Vogel, T., Šanda, M., 2010, Effect of plastic mulch on water flow and herbicide transport in soil cultivated with pineapple crop: A modeling study, Agricultural Water Management, 97, 1637–1645.

Studie věnovaná vyhodnocení transportu herbicidu bromacil vznikla ve spolupráci s americkou univerzitou (University of Hawaii). Bromacil je ve vodě rozpuštěná chemická organická látka, která se používá na zemědělských plochách k likvidaci plevele. K vyhodnocení režimu transportu bromacilu na ploše s ananasy byl použit jednorozměrný vertikální a dvourozměrný model. Oba modely jsou založeny na řešení Richardsovy rovnice pro pohyb vody a advekčně disperzní rovnice pro transport chemické látky. Byly provedeny tranzientní simulace proudění vody a transportu reaktivní chemické látky během 18 měsíců růstového cyklu ananasu. Půdních povrch ananasových plantáží je obvykle až z 50% pokryt nepropustnou plastovou fólií, která snižuje výpar závlahové vody a vytěkávání aplikovaných chemických látek z půdy. Předchozí studie naznačila, že závlaha včetně aplikovaného herbicidu a srážka se z nepropustných ploch povrchovým tokem přerozděluje na nepokryté části zemědělské plochy (Alavi et al., 2008). Simulace byly proto navrženy s čtyřmi různými scénáři, které zohledňovaly vliv nepropustné plastové fólie na půdním povrchu na pohyb vody a transport herbicidu v nezakrytých částech plochy. Ve studii bylo provedeno porovnání měřených a modelovaných tlaků půdní vody a reziduálních koncentrací herbicidu v půdním profilu. Z analýzy vyplynula nezbytnost zahrnutí příspěvku vody a hmotnostního toku herbicidu z nepropustné plochy – jestliže se nezohlednil tento příspěvek, předpověď modelu byla neuspokojivá. Jednorozměrný přístup k odhadu transportu chemické látky se ukázal jako dostatečný pouze v případě zahrnutí toků vody a rozpuštěné látky z nepropustné fólie.

Dušek, J., Šanda, M., Loo, B., Ray, C., 2010, Field leaching of pesticides at five test sites in Hawaii: study description and results, Pest Management Science, 66, 596–611.

Studie pojednává o terénních experimentech, které byly uskutečněny během pracovního pobytu na University of Hawaii. V rámci výzkumného projektu Ministerstva zemědělství státu Hawaii (HDOA) „Posouzení transportu vybraných pesticidů v různých hydrologických podmínkách“ byly v letech 2002–04 provedeny extenzivní laboratorní a terénní experimenty, které vyhodnocovaly mobilitu a perzistentnost organických látek (pesticidů). HDOA musí posoudit všechny nové chemické produkty, které jsou plánovány ke komerčnímu používání pro zemědělské účely ve státu Hawaii. Důvodem pro zvýšenou ochranu podzemní vody před ohrožením nežádoucími polutanty je naprostá nezastupitelnost tohoto zdroje pitné vody pro všechny ostrovy tohoto amerického státu. Terénní experimenty byly provedeny na pěti různých zemědělských plochách třech ostrovů státu Hawaii. Během 16 týdnů experimentu byl sledován průnik šesti pesticidů a konzervativního stopovače bromidu půdním profilem. V laboratoři byly pro jednotlivé chemické sloučeniny a půdy provedeny adsorpční zkoušky a inkubační testy. Data z terénního experimentu ukázala, že koncentrační profily většiny pesticidů byly omezeny hloubkou 80 cm. Byly zjištěny významné rozdíly v laboratorně určeném poločasu rozpadu mezi jednotlivými pesticidy. Během experimentální části byla získána rozsáhlá databáze pedologických, hydrologických a chemických údajů, která byla využita v následující studii zaměřené na numerické modelování transportních procesů v tropické půdě.

Dušek, J., Dohnal, M., Vogel, T., Ray, C., 2011, Field leaching of pesticides at five test sites in Hawaii: modeling flow and transport, Pest Management Science, 67, 1571–1582.

Ministerstvo zemědělství státu Hawaii využívá k posouzení chemického produktu (pesticidu) tzv. tier-I modely. Tyto modely jsou založeny na kritériích určující potenciální transport látek v půdách. Potenciální index šíření (leachability index) nového pesticidu je porovnáván s dvěma referenčními chemickými látkami – jedna je v podmínkách tropického prostředí známa jako vysoce mobilní látka a druhá jako nemobilní látka. Modely, které ministerstvo rutinně používá, však neposkytují předpověď koncentrace chemické látky v půdním profilu ani v půdním roztoku. HDOA má pravomoc chemické látky, které se projeví jako relativně mobilní zcela zakázat nebo povolit pouze s určitými omezeními. Tato studie byla zaměřena na vyhodnocení mobility šesti pesticidů a konzervativního stopovače bromidu během terénního experimentu pomocí tier-II modelu. Použitý tier-II model byl jednorozměrný numerický model s Richardsovou rovnicí pro pohyb vody a advekčně disperzní rovnicí pro transport rozpuštěných látek. Modelovaný pohyb pesticidů a bromidu s reaktivními transportními parametry (distribuční koeficient K_d a poločas rozpadu $t_{1/2}$) odhadnutými z laboratorních experimentů neposkytl uspokojivou shodu s měřenými koncentračními profily. Proto bylo použito inverzní modelování k odhadu efektivních reaktivních transportních parametrů. V cílové funkci byly zahrnuty jak koncentrační profily tak rovněž poloha (hloubka) těžiště koncentračního profilu. Výsledky modelování s optimalizovanými parametry ukázaly vyšší míru shody s měřenými koncentračními profily i polohou těžiště koncentračního profilu. Odhadnuté transportní parametry pesticidů byly také využity pro tier-I model; relativní mobilita jednotlivých pesticidů zjištěná tier-I modelem byla poté v souladu s pozorovanou polohou těžiště koncentračního profilu. Publikovaná studie přispěla k posouzení stávajícího přístupu HDOA, který výrazně přehlíží dynamiku proudění vody a transportu látek v půdách.

Dušek, J., Vogel, T., Dohnal, M., Gerke, H.H., 2012, Combining dual-continuum approach with diffusion wave model to include a preferential flow component in hillslope scale modeling of shallow subsurface runoff, Advances in Water Resources, 44, 113–125.

Studie zaměřená na popis dynamiky hypodermického odtoku vznikla ve spolupráci s německým partnerem (Leibniz-Center of Agricultural Landscape Research). Mělký podpovrchový hypodermický odtok je v případě absence povrchového odtoku jedním z nejdůležitějších mechanismů hydrologické odezvy pramenných povodí. Hypodermický odtok vzniká na méně propustné vrstvě, obvykle na rozhraní nebo v přechodové vrstvě mezi půdním profilem a skalním podložím. Jakákoliv snaha zahrnout vliv preferenčního odtoku v hydrologických studiích je omezena tím, že tloušťka propustné půdy je většinou výrazně menší ve srovnání s délkou svahu. Dynamika odtoku je na sledovaném svahu Tomšovka (povodí Uhlířská, Jizerské hory) relativně rychlá a intenzivní z důvodu mělkého půdního profilu a přítomnosti vertikálních a laterálních preferenčních cest. Cílem této studie bylo popsat preferenční hypodermický odtok ze svahu pomocí kombinace jednorozměrného vertikálního modelu a jednorozměrného laterálního modelu. Vertikální model proudění vody ve vadózní zóně je založen na přístupu duálního kontinua, řešeny jsou dvě Richardsovy rovnice. Laterální model pro nasycené laterální proudění je založen na řešení difuzní vlny

(Vogel, 2005). Tento přístup byl použit k modelování dynamiky odtoku ze svahu během vybraných srážko-odtokových epizod. Bylo provedeno kvantitativní srovnání modelových intenzit odtoku s měřenými odtoky podpovrchovým příkopem umístěným na rozhraní mezi půdou a skalním podložím. Významná transformace vertikálního signálu laterálním modelem byla zjištěna pro delší svah, menší efektivní vodivost a vyšší efektivní pórovitost. Použitý přístup založený na kombinaci dvou jednorozměrných modelů umožňuje zjednodušený popis jak preferenčního proudění ve vertikálním směru tak také v laterálním směru.

Dušek, J., Vogel, T., Šanda, M., 2012, Hillslope hydrograph analysis using synthetic and natural oxygen-18 signatures, Journal of Hydrology, 475, 415–427.

Hypodermický odtok je považován za nejdůležitější mechanismus odtoku pro pramenná povodí nacházející se v mírném klimatickém pásmu. Odezva mělkého podpovrchového odtoku na významnou srážku je urychlena přítomností makropórů a biopórů v půdním profilu, které mohou vytvářet síť vzájemně propojených preferenční cest. Tyto cesty mají podstatný vliv na formování odtoku v měřítku svahu. Transportní procesy v strukturních a heterogenních půdách však stále nejsou spolehlivě poznány a modelovány. Experimentální data konzervativního stopovače izotopu kyslíku (^{18}O) získaná na svahu Tomšovka nevykazovala intuitivní transformaci ale spíše komplexní chování izotopu v půdě. Motivací této studie bylo lepší pochopení transportních procesů pomocí popisu transformace vstupního signálu (tj. koncentrace izotopu ve srážce) na výstupní signál (tj. koncentrace izotopu v odtoku ze svahu). Stabilní izotopy vody nabízejí potenciál studovat relevantní mechanismy transportu v různých prostorových měřítcích, často se používají k rozlišení příspěvku „staré“ vody (voda přítomna v půdě před srážkovou událostí) a „nové“ vody (srážková voda) hydrogramu odtoku. V této studii byl použit model vertikálního proudění vody a transportu izotopu kyslíku ^{18}O v nenasycené zóně a laterálního proudění a transportu na svahu. Byly vybrány a studovány srážko-odtokové epizody zaznamenané během tří vegetačních sezón. Ačkoli hrálo preferenční proudění důležitou roli při tvorbě odtoku ze svahu, příspěvek „staré“ vody byl významný – tvořil 47–74% z celkového objemu odtoku. Výsledky simulací potvrdily hypotézu o výrazném mixování srážkové vody a vody přítomné v půdním profilu nad méně propustným podložím před příčinnou srážkou.

Dušek, J., Lichner, L., Vogel, T., Štekauerová, V., 2013, Transport of iodide in structured soil under spring barley during irrigation experiment analyzed using dual-continuum model, Biologia, 68, 1094–1098.

Experimenty s chemickou látkou poskytují časoprostorové údaje o režimu transportu v pórovitém prostředí. Na rozdíl od experimentu s barvivem-stopovačem, který je omezen pouze na jednu časovou úroveň v důsledku svého destruktivního charakteru, má metoda radioaktivního izotopového měření potenciál poskytovat vícenásobné informace během experimentu při současně zanedbatelném porušení půdní struktury. Ve studii byl vyhodnocen radioaktivní izotopový experiment s jodidem sodným pomocí jednorozměrného modelu duálního kontinua. Experiment byl proveden v jílovito-hlinité půdě slovenským partnerem (Slovenská akademie věd, Ústav hydrologie) během teplého letního období, které způsobilo viditelné rozpukání půdního povrchu. Trhliny, konceptualizované preferenční

doménou, zaujímaly relativně vyšší objemový podíl z celkového objemu půdy (15%). Profily relativní koncentrace jodidu byly určeny pro několik časových úrovní během experimentu, také byl určen časový vývoj koncentrace v hloubce 30 cm. Naměřené koncentrace reaktivního traceru jodidu byly porovnány s modelovanými hodnotami. Experimentální data shodně s výsledky modelování naznačovala, navzdory procesu sorpce, relativně hluboký průnik jodidu (cca 60 cm) během krátké doby trvání terénního experimentu. Radioizotopový experiment a numerické modelování umožnily vyhodnotit režim transportu nekonzervativního stopovače ve strukturní půdě.

Dušek, J., Vogel, T., 2014, Modeling subsurface hillslope runoff dominated by preferential flow: One- vs. two-dimensional approximation, Vadose Zone Journal, 13. doi:10.2136/vzj2013.05.0082.

V minulých letech bylo navrženo několik rozdílných přístupů popisujících odtok z mělkého svahového segmentu. V této studii bylo provedeno detailní porovnání dvou konceptuálně odlišných aproximací k modelování dynamiky odtoku ze svahu. Jedná se o přístupy jednorozměrné a dvourozměrné, které se od sebe odlišovaly uváženou dimenzionalitou a tím také složitostí geometrických, materiálových a okrajových podmínek. Jednorozměrný přístup zjednodušuje proudové pole pouze na vertikální a laterální směr; tento přístup výrazně snižuje výpočetní nároky. Dvourozměrný přístup rigorózně popisuje směr proudění ve svahovém segmentu a separaci toku na rozhraní mezi půdou a podložím, jeho výpočetní nároky jsou však značné a možné propojení s hydrologickými modely povodí limitované. Oba použité přístupy byly založeny na konceptu duálního kontinua. Odtok ze svahu nastával pouze ve formě nasyceného hypodermického (podpovrchového) proudění preferenčními cestami. Validace obou modelových přístupů sestávala z kvantitativního porovnání simulovaného hypodermického odtoku a tlaku půdní vody s experimentálními daty ze svahu Tomšovka. Oba odlišné přístupy naznačily obdobnou dynamiku hypodermického odtoku ze svahu, vyznačující se krátkodobými odtokovými událostmi jako odezvy na významné srážky. Tlak půdní vody na svahu (a tím také zásoba půdní vody) byl v blízkosti experimentálního příkopu modelován realističtěji dvourozměrným přístupem, neboť jednorozměrný přístup nabízí pouze efektivní vertikální oblast proudění bez uvážení prostorové variability nasycené zóny. Analýza citlivosti hydraulických charakteristik půdy a přechodové horninové vrstvy potvrdila významný vliv nasycené hydraulické vodivosti podloží na simulovaný odtok ze svahu. Jednodušší jednorozměrný přístup založený na kombinaci vertikálního proudění a laterálního odtoku poskytuje dostatečnou aproximaci složitějšího dvourozměrného systému a zároveň je z hlediska výpočetní náročnosti velmi efektivní.

Dušek, J., Dohnal, M., Sněhota, M., Sobotková, M., Ray, C., Vogel, T., 2015, Transport of bromide and pesticides through an undisturbed soil column: A modeling study with global optimization analysis, Journal of Contaminant Hydrology, 175–176, 1–16.

Používání pesticidů v zemědělství celosvětově stoupá. Roční aplikace pesticidů v České republice a Spojených státech amerických je téměř shodná, FAO (2017) uvádí hodnotu 2 kg aktivní složky pesticidu na 1 ha. Transportní procesy v tropických půdách jsou v porovnání s chováním organických látek v půdách mírného pásmu méně analyzovány a poznány.

Tropické půdy jsou charakteristické celkovým kladným nábojem a vysokým podílem mikropórů. Rovněž reaktivní parametry pesticidů a modelové přístupy nejsou pro tropické půdy prozkoumány takovým způsobem jako v případě půd mírného pásmu. Studie se zabývá vyhodnocením laboratorního transportního experimentu pomocí numerického modelování. Experiment sestával z několika cyklů zkrápění a přerušování, během nichž byl aplikován roztok pěti pesticidů a konzervativního stopovače bromidu. Pro účely vyhodnocení byly použity tlakové výšky půdní vody ve vzorku, intenzita výtoku a průnikové čáry jednotlivých chemických látek. Ve studii byly uváženy dva základní scénáře – okamžitá (rovnovážná) nelineární sorpce a kinetická (nerovnovážná) lineární sorpce. Byly navrženy a provedeny statisíce přímých simulací s různými kombinacemi reaktivních transportních parametrů jednotlivých pesticidů. Z výsledků byly vybrány simulace s vyšší shodou a byla zhodnocena nejistota určení transportních parametrů pomocí predikčních limitů průnikových křivek. Odhadnuté transportní parametry poskytovaly také konfidenční intervaly. Numerické experimenty potvrdily nekonzervativní chování bromidu, což bylo pravděpodobně způsobeno přítomností oxidů železa a tím celkových kladným nábojem půdy (bromid se adsorboval na pevnou fázi intenzivněji než většina pesticidů). Byla zjištěna relativně výrazná mobilita pesticidů (nízká hodnota K_d) a intenzivní degradace (nízké hodnoty $t_{1/2}$). Kinetická sorpce se ukázala být vhodnější k popsání průnikových křivek tří herbicidů. Odhadnuté transportní parametry pomohly vyhodnotit chování jednotlivých organických látek v tropické půdě.

Dušek, J., Vogel, T., 2016, Hillslope-storage and rainfall-amount thresholds as controls of preferential stormflow, Journal of Hydrology, 534, 590–605.

Transformace srážky půdním svahovým segmentem na odtok má komplexní charakter, neboť je ovlivněna statickými (prostorové uspořádání svahu, půdní charakteristiky, topografie rozhraní mezi půdním profilem a skalním podložím) a dynamickými (charakteristiky srážky, počáteční vlhkostí a jejím rozložením na svahu, vegetací) faktory. Jednotlivé faktory působí současně a tím je obtížné jejich dílčí vlivy kvantifikovat. Tato studie byla věnována bilanci svahu Tomšovka v povodí Uhlířská v Jizerských horách během tří vegetačních sezón, kde byl k dispozici hypodermický odtok ze svahu měřený podpovrchovými příkopy. Pomocí dvourozměrného modelu založeného na přístupu duálního kontinua byla provedena detailní analýza složek hydrologické bilance svahu během vybraných srážko-odtokových epizod. Jednotlivé složky bilance svahu – vertikální odtok přes rozhraní půda/podloží, hypodermický odtok a změna zásoby vody ve svahu – byly rovněž vyhodnoceny pro syntetické srážkové epizody. Celkem byly provedeny stovky simulací, při nichž bylo studováno prahové hydrologické chování svahu na příčinnou srážku systematickou změnou počátečního nasycení svahu, velikosti a časového rozložení srážek. Byl zjištěn hysterezní vztah mezi zásobou vody ve svahovém segmentu a hypodermickým odtokem i bez uvážení hystereze hydraulických charakteristik. Vztah mezi srážkou a hypodermickým odtokem, stejně jako mezi srážkou a vertikální odtokem, vykazoval značnou nelinearitu pro nižší hodnoty počátečního nasycení svahu. Studie ukázala vzájemný účinek jednotlivých složek bilance půdní vody na nelineární charakter odtoku ze svahu.

Dušek, J., Vogel, T., Dohnal, M., Barth, J.A.C., Šanda, M., Marx, A., Jankovec, J., 2017, Dynamics of dissolved organic carbon in hillslope discharge: Modeling and challenges, Journal of Hydrology, 546, 309–325.

Hodnověrná předpověď hmotnostních toků ve vodě rozpuštěných látek ve strukturní půdě je z důvodu okrajových podmínek a heterogenity prostředí nesnadná. U kvantifikace toků rozpuštěného organického uhlíku (dissolved organic carbon – DOC) je navíc obtížná parametrizace transformačních procesů této látky. Poslední z předkládaných studií byla zaměřena na modelování dynamiky transport DOC ve svahovém segmentu; studie vznikla ve spolupráci s německým partnerem (Friedrich-Alexander-Universität Erlangen-Nürnberg). Souběžně s DOC byl studován transport přirozeného a stabilního izotopu kyslíku ^{18}O. DOC byla uvážena jako reaktivní látka podléhající transformacím v půdním prostředí (zdroj nultého řádu, rovnovážná lineární sorpce a degradace prvního řádu). Transformace jsou navíc závislé na vlhkosti půdní vody a teplotě, což vyžadovalo propojení řídících rovnic pohybu vody a transportu tepla a DOC. Jelikož se parametry ovlivňující transformace DOC velmi obtížně nezávisle stanovují, byl jednorozměrný vertikální model s přístupem duálního kontinua spuštěn 100,000 s různými kombinacemi transportních parametrů DOC. Simulované koncentrace ^{18}O a DOC byly porovnány s měřenými koncentracemi v hypodermickém odtoku ze svahu Tomšovka. Značný počet přímých simulací umožnil kvantifikovat nejistotu spojenou s parametrizací transportu DOC. Variabilita izotopu kyslíku v odtoku i v půdní vodě byla modelem poměrně dobře reprodukována. Navzdory komplexním mikrobiálním transformacím DOC, které způsobily nejistotu v určení parametrů modelu a následnou předpověď transportu DOC, ukázaly simulované koncentrace v odtoku podobné chování jako měřené. Byla zjištěna podstatně větší variabilita simulovaného DOC v odtoku v porovnání s nejistotou reprezentovanou predikčními limity. Celkový hmotnostní tok DOC z jednotkové plochy svahu byl díky zahrnutí preferenčního příspěvku vyšší než hmotnosti uváděné v dostupné literatuře.

Shrnutí

V habilitační práci je předložen soubor výzkumných studií s jedním integrujícím tématem – transportem chemických látek v přírodních pórovitých formacích a související kvantifikací objemových a hmotnostních toků. Jednotlivé studie se liší dimenzionalitou řešené úlohy – byly provedeny jednorozměrné, dvourozměrné a třírozměrné analýzy. Rozdílné bylo rovněž prostorové měřítko – dynamika půdní vody byla pomocí matematického modelování popsána v měřítku laboratorního vzorku, půdního profilu a svahového segmentu. Důležitým rysem bylo u několika studií zahrnutí preferenčního proudění a transportu do konceptuálního modelu.

Matematické modely poskytují efektivní nástroj k vyhodnocení režimu odtoku vody a transportních procesů v pórovitém prostředí. Dostupná literatura naznačuje budoucí dynamický růst v oblasti jejich vývoje i použití. Univerzální model pro rozdílné typy proudění však v současné době není k dispozici, používají se tak specifické modely pro konkrétní mechanismy a režimy odtoku. Současná generace modelů rovněž neposkytuje popis dynamiky odtoku pro různé příčiny projevů preferenčního proudění. Rozvoj

experimentálních technik a metod (například nové přístupy v určování okrajových podmínek a ve vizualizaci a detekování proudění a transportu) nicméně umožní dokonalejší pochopení procesů a mechanismů ovlivňující pohyb vody a chemických látek. Tento rozvoj se velmi pravděpodobně projeví také ve zvýšené hodnověrnosti matematických modelů. K zahrnutí relevantních procesů na větším prostorovém měřítku a během delších časových období bude zapotřebí zdokonalit numerické techniky řešení řídících rovnic a výrazně zvýšit výpočetní výkon. Detailní parametrizace fyzikálně založených modelů bude i nadále představovat nesnadnou úlohu. Budoucí matematické přístupy budou pravděpodobně hlouběji integrovat hydrologické procesy s procesy biologickými a chemickými, včetně vzájemných interakcí.

Otevřenou výzvou zůstává rutinní a věrohodná parametrizace efektivních hydraulických a transportních parametrů heterogenních pórovitých systémů. Pro modely založené na konceptu duálního kontinua je nutné zdokonalit odhad přenosových koeficientů pro vodu a rozpuštěné chemické látky, včetně objemových podílů jednotlivých domén proudění. Experimentální výzkum by proto měl směřovat k spolehlivým a snadno reprodukovatelným metodám pro získávání vstupních parametrů modelů duálního kontinua. Současně je třeba vývoj zaměřit na interakci mezi transportními a hydraulickými parametry, například zahrnutí vlivu chemických reakcí na hydraulické vlastnosti půdního prostředí může zdokonalit modelové předpovědi transportu látek v půdách. Rovněž zahrnutí vlivu časové dynamiky hydraulických charakteristik, zejména propojení a spojitosti preferenčních cest, by mělo přispět k realističtější kvantifikaci hmotnostních toků.

Literatura

Alavi, G., Sanda, M., Loo, B., Green, R.E., Ray, C., 2008, Movement of bromacil in a Hawaii soil under pineapple cultivation – a field study, Chemosphere, 72, 45–52.

Food and Agriculture Organization of the United Nations (FAO), 2017, http://www.fao.org/.

Gerke, H.H., van Genuchten, M.T., 1993, A dual-porosity model for simulating the preferential movement of water and solutes in structured porous media, Water Resour. Res., 29, 305–319.

Jarvis, N., Koestel, J., Larsbo, M., 2016, Understanding preferential flow in the vadose zone: recent advances and future prospects, Vadose Zone J., 15. doi:10.2136/vzj2016.09.0075.

Klaus, J., Zehe, E., 2011, A novel explicit approach to model bromide and pesticide transport in connected soil structures, Hydrol. Earth Syst. Sci., 15, 2127–2144.

Larsbo, M., Roulier, S., Stenemo, F., Kasteel, R., Jarvis, N., 2005, An improved dual-permeability model of water flow and solute transport in the vadose zone, Vadose Zone J., 4, 398–406.

Vereecken, H., Schnepf, A., Hopmans, J.W., Javaux, M., Or, D., Roose, T., Vanderborght, J., et al., 2016, Modeling soil processes: review, key challenges, and new perspectives, Vadose Zone J., 15. doi:10.2136/vzj2015.09.0131.

Vogel, H.-J., Cousin, I., Ippisch, O., Bastian, P., 2006, The dominant role of structure for solute transport in soil: Experimental evidence and modelling of structure and transport in a field experiment, Hydrol. Earth Syst. Sci., 10, 495–506.

Vogel, T., 2005, Simplified dual continuum approach to modeling subsurface runoff from a hillslope segment. In: General assembly, European Geophysical Union, Vienna, Austria.

Vogel, T., Brezina, J., Dohnal, M., Dusek, J., 2010, Physical and numerical coupling in dual-continuum modeling of preferential flow, Vadose Zone J., 9, 260–267.

Vogel, T., Dohnal, M., Dusek, J., Votrubova, J., Tesar, M., 2013, Macroscopic modeling of plant water uptake in a forest stand involving root-mediated soil water redistribution, Vadose Zone J., 12. doi:10.2136/vzj2012.0154.

Soubor publikovaných prací

Numerical analysis of ponded infiltration experiment under different experimental conditions, Soil and Water Research, 2009.

Numerical Analysis of Ponded Infiltration Experiment under Different Experimental Conditions

Jaromír DUŠEK, Michal DOHNAL and Tomáš VOGEL

Department of Hydraulics and Hydrology, Faculty of Civil Engineering, Czech Technical University in Prague, Prague, Czech Republic

Abstract: One of the most important properties, affecting the flow regime in the soil profile, is the topsoil saturated hydraulic conductivity (K_s). The laboratory-determined K_s often fails to characterise properly the respective field value; the K_s lab estimation requires labour intensive sampling and fixing procedures, difficult to follow in highly structured and stony soils. Thus, simple single- or double-ring ponded infiltration experiments are frequently performed in situ to obtain the field scale information required. In the present study, several important factors, affecting the infiltration rate during the infiltration experiments, are analysed using three-dimensional axisymmetric finite-element model S2D. The examined factors include: (1) the diameter of the infiltration ring, (2) the depth of water in the ring, (3) the depth of the ring insertion under the soil surface, (4) the size and the shape of the finite-element mesh near the ring wall, and (5) the double- vs. single-ring setup. The analysis suggests that the depth of the ring insertion significantly influences the infiltration rate. The simulated infiltration rates also exhibit high sensitivity to the shape of the finite-element mesh near the ring wall. The steady-state infiltration rate, even when considering a double-ring experiment, is significantly higher than the topsoil saturated hydraulic conductivity. The change of the water depth in the outer ring has only a small impact on the infiltration rate in the inner ring.

Keywords: infiltration; single-ring infiltrometer; saturated hydraulic conductivity; depth of insertion; ponding depth; soil hydraulic properties; three-dimensional axisymmetric flow

The topsoil saturated hydraulic conductivity (K_s) is one of the most important properties affecting the flow regime in the soil profile. The laboratory-determined K_s often fails to characterise properly the respective field value; the K_s lab estimation requires labour intensive sampling and fixing procedures, difficult to follow in highly structured and stony soils. Thus simple double- or single-ring ponded infiltration experiments are frequently performed in situ to obtain the field scale information required.

The infiltration experiment may be performed using mini-disk infiltrometers, with adjustable capillary pressure, or ring infiltrometers, to establish the ponded conditions. The localised water supply from both types of infiltrometer inevitably causes a three-dimensional character of flow under the circular source. At the beginning of the infiltration experiment, capillary forces dominate. As the infiltration rate approaches a quasi steady-state condition, the gravity forces become also important.

Supported by the Czech Science Foundation, Project No. 526/08/1016 and by the Ministry of Environment of the Czech Republic, Project No. SP/2e7/229/07.

From the disk steady-state infiltration rate it is possible to determine the hydraulic conductivity using analytical solution (Ankeny *et al.* 1991). Transient infiltration data can be used as well to accomplish this goal; however the inverse procedures must be invoked (e.g. Ramos *et al.* 2006). The inverse analysis was used to obtain K_s from a field ponded infiltration experiment e.g. by Vogel and Císlerová (1993).

Recently, several studies on the geometrical setup of single- or double-ring infiltration experiments (e.g. the depth of water in the ring, the ring diameter and the ring insertion) were published. Chowdary *et al.* (2006) analysed in situ the geometrical setup of the infiltration aiming at a proper design and management of field irrigation systems. Three-dimensional numerical studies of the field infiltration experiments were carried out by e.g. Reynolds and Elrick (1990) and Wu and Pan (1997). Wu and Pan (1997) attempted to develop a generalised infiltration solution and evaluated the respective geometrical effect on the infiltration curve. Reynolds and Elrick (1990) defined an effective shape factor which assesses the geometrical setup of the infiltration experiment; in their study, the shape factor was used to calculate the field K_s. Numerical studies of the infiltration experiment were also conducted by e.g. Šimůnek (1988) and Touma *et al.* (2007).

The objective of this paper is to evaluate numerically different factors that determine the infiltration rates during the field infiltration experiments and the resulting values of the saturated hydraulic conductivity. The analysed factors include: (1) the diameter of the infiltration ring, (2) the depth of water in the ring, (3) the depth of the ring insertion under the soil surface, (4) the size and shape of the finite-element mesh near the ring wall, and (5) the double- vs. single-ring setup. The individual and combined effects were analysed in detail by means of three-dimensional axisymmetric simulations carried out by two-dimensional numerical model S2D (Vogel *et al.* 2000).

MATERIALS AND METHODS

The mathematical modelling involved three-dimensional axisymmetric simulations carried out by the two-dimensional code S2D. To parameterise the unsaturated hydraulic conductivity function, modified Mualem-van Genuchten approach was used (Vogel *et al.* 2001).

The governing partial differential equation (Richards' equation) was assumed in the following form

$$C\frac{\partial h}{\partial t} = \nabla \cdot (K\nabla h) + \nabla \cdot (K\nabla z) \quad (1)$$

where:

h – soil water pressure head (L)

K – hydraulic conductivity tensor (L/T)

C – specific capacity (1/L)

z – vertical coordination oriented upward (L)

t – time (T)

The conductivity tensor was assumed to be isotropic, i.e. the conductivity is defined at any particular location and time by a single scalar value.

Table 1 shows the soil hydraulic parameters of coarse sandy loam used for the numerical experiments. In this study, we assumed a homogeneous soil profile. The soil characteristics are based on the soil samples taken from the soil profile of Dystric Cambisol in the Volynka river watershed, Sumava Mountains, Southern Bohemia (Císlerová *et al.* 1988).

As the initial condition, soil water pressure head was set equal to –1000 cm in the entire flow domain. The two-dimensional finite-element mesh (see Figure 6) rotates along the central axis of the infiltration ring, thus creating three-dimensional axisymmetric domain with dimensions of 200 × 150 cm. The vertical dimension of the flow domain was chosen to be large enough to meet the requirement that the lower boundary does not affect the infiltration rate on the soil surface. A Dirichlet boundary condition with the prescribed value of the pressure head was used for the flooded area of the infiltration ring. The lower boundary was treated as a unit hydraulic gradient boundary.

Table 1. Parameters of soil hydraulic properties (modified Mualem-van Genuchten parameterisation)

Depth (cm)	θ_r (–)	θ_s (–)	h_s (cm)	α (1/cm)	n (–)	K_s (cm/h)
0÷150	0.01	0.461	–3.42	0.083	1.111	5.0

All other parts of the flow domain boundary were assumed to be impermeable.

The geometry of a single-ring infiltration experiment is depicted in Figure 1. In a series of three subsequent simulation runs, the diameter of the infiltration ring varied from 35.7 cm to infinity (D = 35.7, 61.8, ∞). For the simulation run corresponding to the ring diameter of infinite length, one-dimensional code HYDRUS 5.0 (Vogel *et al.* 1996) was used instead of S2D code. The depth of water H in the ring was alternatively assumed to be 0, 5, and 10 cm, respectively. The depth of the ring insertion I under the soil surface was set at 0, 5, 10, and 20 cm, respectively. For the numerical experiments with the double-ring setup, the diameter of the outer ring was 61.8 cm. Finally, the impact of the size and shape of the finite-element mesh near the ring wall was tested by using two different finite-element meshes.

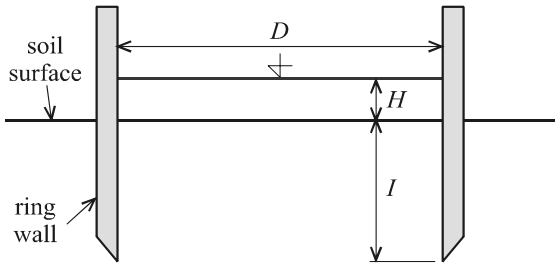

Figure 1. Schematic of the single-ring infiltration experiment; symbol D stands for the diameter of the ring, H for the depth of water in the ring, and I denotes the depth of the ring insertion under the soil surface

RESULTS AND DISCUSSION

Figure 2 illustrates the effect of changing the diameter of the infiltration ring by showing the infiltration rate vs. time throughout the infiltration experiment. Note that the one-dimensional simulation rates (marked as D = ∞ in Figure 2) approach asymptotically the value of the saturated hydraulic conductivity. For the three-dimensional scenarios, the steady-state infiltration rate is higher than K_s. This is caused by the three-dimensional character of the wetting front. The smaller the diameter of the ring, the higher the steady-state infiltration rate. By increasing further the ring diameter, the 3D simulation results will converge to the D = ∞ infiltration curve. A similar trend in the infiltration rates in response to varying D has been also predicted for other combinations of the water depth H and ring insertion I (not shown in this paper).

In Figure 3, the effect of varying the depth of water H in the ring is shown. From the figure it seems obvious that a higher water level maintained in the ring produces higher infiltration rates due to a greater pressure gradient. Again, a similar trend in the infiltration rates in response to varying H is simulated for other combinations of D and I (not shown here).

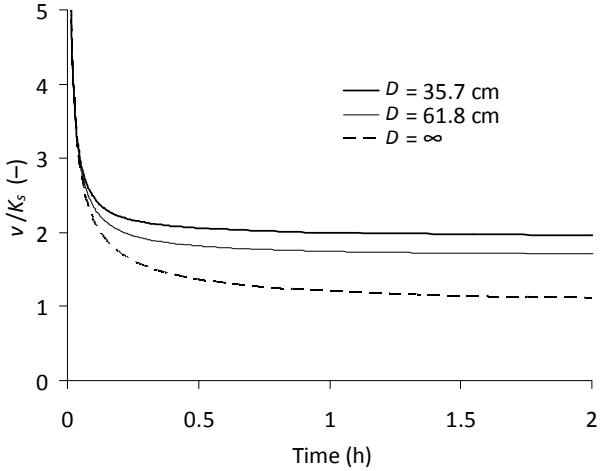

Figure 2. The effect of changing the ring diameter D; the depth of water in the ring H = 5 cm, the depth of the ring insertion I = 5 cm; the ring diameter of infinite length corresponds to one-dimensional water flow simulation (D = ∞)

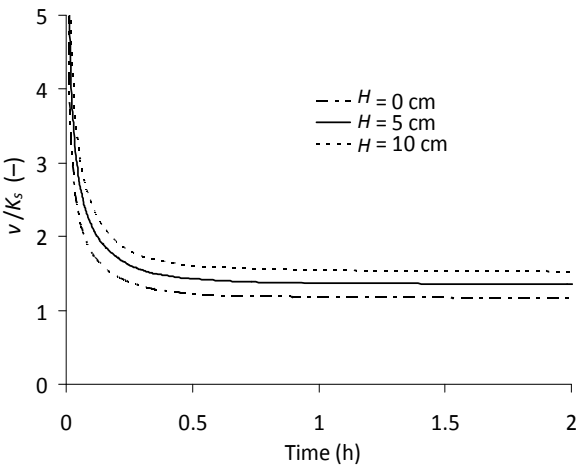

Figure 3. The effect of changing the depth of water H in the ring; the ring diameter D = 61.8 cm, the depth of the ring insertion I = 20 cm

The effect of changing the depth of the ring insertion on the infiltration rate is shown in Figure 4. Substantial deviations among the simulations with different I are predicted. It is evident that, if the ring insertion is not considered in the mathematical modelling of the ponded infiltration, a significant overestimation of the infiltration rate is obtained. For our particular case study, the simulation with zero depth of insertion delivered the steady-state infiltration rate higher than 3 K_s. The effect of the depth of the ring insertion is enhanced for greater depths of water in the ring H. As one can expect, the effect of the insertion depth becomes less important for larger sizes of the infiltration ring (i.e., the infiltration rate at the steady-state was about 2.5 K_s for the simulation with zero depth of insertion, using H = 10 cm and D = 61.8 cm).

The effects of changing the size and shape of the finite-element mesh near the ring wall are shown in Figure 5 and Figure 6. Figure 5 depicts the simulated infiltration rate (for D = 35.7 cm, H = 5 cm, and I = 10 cm) as a function of time for the scenario with two different finite-element meshes. The two simulation scenarios are referred to as wrong mesh and correct mesh, respectively. The correct mesh was constructed from triangular elements of continuously changing sizes, in contrast to the wrong mesh. In addition, the minimum allowed element angle for the correct mesh was specified so that the mesh anisotropy was kept small. As follows from Figure 5, the simulated infiltration rates exhibit a high sensitivity to the shape of the finite-element mesh near the ring wall.

The 2D cross-section of the pressure head field below the ring at t = 20 min is shown in Figure 6.

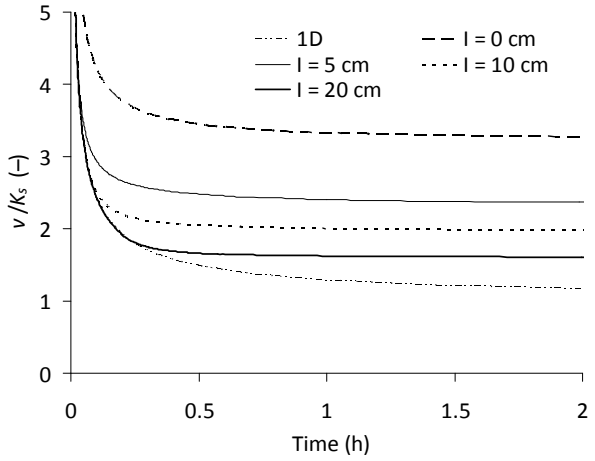

Figure 4. The effect of changing the depth of the ring insertion I; the depth of water in the ring H = 10 cm, the ring diameter D = 35.7 cm

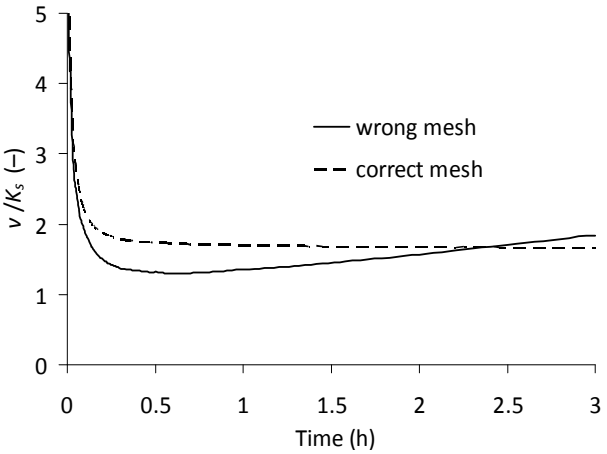

Figure 5. The effect of changing the size and shape of the finite-element mesh near the ring wall; the results for the simulations using wrong and correct computational meshes are shown; scenario with D = 35.7 cm, H = 5 cm, and I = 10 cm

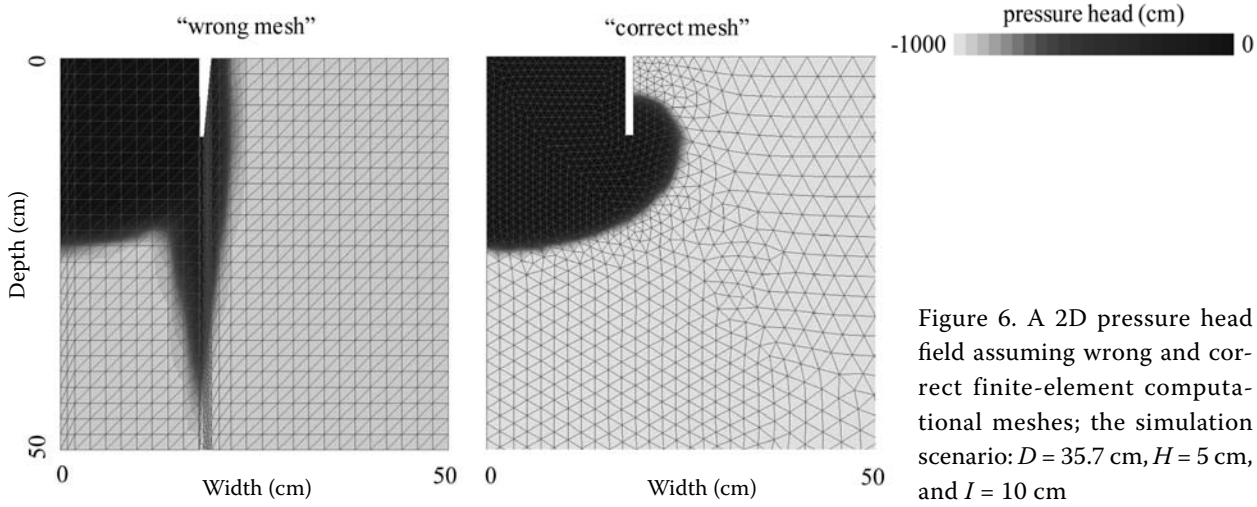

Figure 6. A 2D pressure head field assuming wrong and correct finite-element computational meshes; the simulation scenario: D = 35.7 cm, H = 5 cm, and I = 10 cm

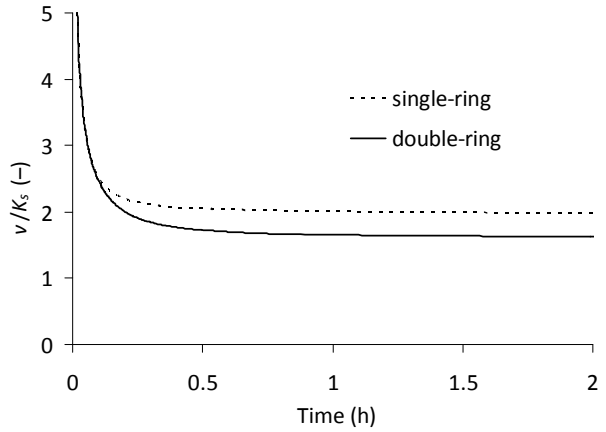

Figure 7. The effect of using double-ring vs. single-ring. The single-ring infiltration rate is compared with the inner ring rate of the double-ring setup; the simulation scenario: D = 35.7 cm, H = 10 cm, and I = 10 cm

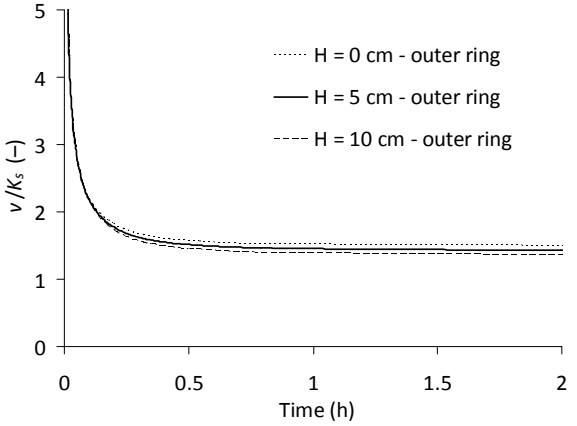

Figure 8. The effect of changing the water depth in the outer ring of the double-ring infiltration experiment. Infiltration rates in the inner ring are shown; the simulation scenario: D = 35.7 cm, H = 5 cm (inner ring), and I = 10 cm

The detail is based on the wrong and correct finite-element meshes, which are shown as well. Note that the computational elements near the ring wall exceed the recommended height-to-width ratio due to the mesh deformation technique used to generate the mesh. The mesh anisotropy induced the development of a finger-like water flow along the ring wall.

The comparison between the infiltration rates in a single-ring infiltrometer (D = 35.7 cm) and in the inner ring of a double-ring infiltrometer, assuming H = 10 cm and I = 10 cm, is depicted in Figure 7 (the outer ring diameter was 61.8 cm). The water flow in the outer ring caused a slight reduction of the infiltration rate in the inner ring. However, it can be seen that even if the double-ring setup is considered, the steady-state infiltration rate is significantly higher than K_s. This implies the well known, but not always fully respected, fact that the double-ring experiment does not deliver directly the value of the saturated hydraulic conductivity, and thus the steady-state infiltration rate cannot be interpreted as K_s. Again, the increase of the water depth in the infiltration ring leads to more pronounced differences between the steady-state infiltration rates for single- and double-ring setups and, as mentioned above, a deeper ring insertion makes the infiltration rate smaller.

In Figure 8, the effect of the water depth in the outer ring of the double-ring setup is examined. The depth of water in the inner ring was kept constant (H = 5 cm) while the water depth in the outer ring was lowered/raised by 5 cm. Such differences seem to be realistic due to the difficulties often encountered during the field double-ring infiltration experiments. The results suggest only a negligible effect of the water depth in the outer ring on the infiltration rate in the inner ring. Note that smaller infiltration rates in the inner ring are predicted for the case of a higher water depth in the outer ring. This is caused by the reduction of the lateral flow component. In this context, it is worth mentioning that the water transfer between the outer and inner rings may be more pronounced in soils with preferential pathways, but such effects are beyond the scope of this study.

CONCLUSIONS

In this study, five important factors were analysed determining the infiltration rate and the water flow regime during the ponded infiltration experiments as well as the subsequent evaluation of the surface hydraulic properties. The factors include: (1) the diameter of the infiltration ring, (2) the depth of water in the ring, (3) the depth of the ring insertion under the soil surface, (4) the size and shape of the finite-element mesh near the ring wall, and (5) the double-ring vs. single ring setup of the experiment.

The results of the numerical study confirm that the effects related to the geometry of the experimental setup significantly influence the water flow in the soil profile. The depth of the ring insertion under the soil surface was found to be the most important geometrical factor. Neglecting the ring insertion in the numerical model may lead to false or biased conclusions, e.g. when the model is used

to verify various methods for the determination of sorptivity and/or hydraulic conductivity. Steady-state infiltration rates, even considering the double-ring experiment, are significantly higher than the saturated hydraulic conductivity. The change of the water depth in the outer ring has only a small impact on the resulting infiltration rates in the inner ring (provided that the preferential flow effects are negligible).

As far as the mathematical modelling of the ponded infiltration experiment is concerned, special attention should be paid to the design of the finite-element mesh and to the proper parameterisation of the soil hydraulic properties near saturation.

References

Ankeny M.D., Mushtaque A., Kaspar T., Horton R. (1991): Simple field method for determining unsaturated hydraulic conductivity. Soil Science Society of American Journal, **55**: 467–470.

Chowdary W.M., Rao M.D., Jaiswal C.S. (2006): Study of infiltration process under different experimental conditions. Agricultural Water Management, **83**: 69–78.

Císlerová M., Šimůnek J., Vogel T. (1988): Changes of steady-state infiltration rates in recurrent ponding infiltration experiments. Journal of Hydrology, **104**: 1–16.

Ramos T.B., Goncalves M.C., Martins J.C., van Genuchten M.Th., Pires F.P. (2006): Estimation of soil hydraulic properties from numerical inversion of tension disk infiltrometer data. Vadose Zone Journal, **5**: 684–696.

Reynolds W.D., Elrick D.E. (1990): Ponded infiltration from a single ring: I. Analysis of steady flow. Soil Science Society of American Journal, **54**: 1233–1241.

Šimůnek J. (1988): Infiltration – numerical simulation. Vodohospodářský časopis, **36**: 407–420. (in Czech)

Touma J., Voltz M., Albergel J. (2007): Determining soil saturated hydraulic conductivity and sorptivity from single ring infiltration tests. European Journal of Soil Science, **58**: 229–238.

Vogel T., Císlerová M. (1993): A scaling-based interpretation of a field infiltration experiment. Journal of Hydrology, **142**: 337–347.

Vogel T., Huang K., Zhang R., van Genuchten M.Th. (1996): The HYDRUS code for simulating One-Dimensional Water Flow, Solute Transport, and Heat Movement in Variably-Saturated Media. Version 5.0 [Research Report No. 140.] U.S. Salinity Lab., ARS, USDA, Riverside.

Vogel T., Gerke H.H., Zhang R., van Genuchten M.Th. (2000): Modelling flow and transport in a two-dimensional dual-permeability system with spatially variable hydraulic properties. Journal of Hydrology, **238**: 78–89.

Vogel T., van Genuchten M.Th., Císlerová M. (2001): Effect of the shape of soil hydraulic functions near saturation on variably-saturated flow predictions. Advances in Water Resources, **24**: 133–144.

Wu L., Pan L. (1997): A generalized solution to infiltration from single-ring infiltrometers by scaling. Soil Science Society of American Journal, **61**: 1318–1322.

Corresponding author:

Ing. Jaromír Dušek, Ph.D., České vysoké učení technické v Praze, Fakulta stavební, katedra hydrauliky a hydrologie, Thákurova 7, 166 29 Praha 6-Dejvice, Česká republika
tel.: + 420 224 354 355, e-mail: jaromir.dusek@fsv.cvut.cz

Short-term transport of cadmium during a heavy rain event simulated by a dual-continuum approach, Journal of Plant Nutrition and Soil Science, 2010.

Short-term transport of cadmium during a heavy-rain event simulated by a dual-continuum approach

Jaromir Dusek[1]*, Tomas Vogel[1], Lubomir Lichner[2], and **Andrea Cipakova[3]**

[1] Faculty of Civil Engineering, Czech Technical University in Prague, Thakurova 7, 166 29 Prague, Czech Republic
[2] Institute of Hydrology, Slovak Academy of Sciences, Racianska 75, 831 02 Bratislava, Slovakia
[3] Regional Public Health Authority, Ipelska 1, 042 20 Kosice, Slovakia

Abstract

The transport of solutes in soils, and its intensification due to preferential flow, plays crucial role when problems related to the groundwater pollution are dealt with. The objective of this study was to examine transport of cadmium (Cd) in response to an extreme rainfall event for three different soils using numerical modeling. The $^{115m}Cd^{2+}$ concentration profile had been measured in the Bodiky reference site (Danubian Lowland, Slovakia) by the radioactive-tracer technique and used for the calibration of the dual-continuum model S1D. The Cd transport during a single rain event was predicted with the S1D model for light, medium-heavy, and heavy soil in the same region. The Cd transport through the soil profile was simulated by the one-dimensional dual-permeability model, which assumes the existence of two pore domains: the soil-matrix domain and the preferential-flow domain. The model is based on Richards' equation for water flow and advection-dispersion equation for solute transport. A modified batch technique enables to distinguish process of adsorption in the matrix domain and the preferential pathways. Modeling with classical single-permeability approach and dual-continuum approach without considering the particle-facilitated transport led to negligible Cd penetration. The rainfall event with extremely high rainfall intensity induced deep penetration of Cd in the medium-heavy and heavy soil, which may indicate increased vulnerability to shallow groundwater pollution for the respective sites in Danubian Lowland region. The highest Cd leaching was predicted for heavy clay soil, where the preferential particle-facilitated transport of Cd through the soil profile was significant due to the contrasting properties of the soil-matrix domain and the preferential-flow domain. The results of the sensitivity analysis suggested only slight effect of the transfer rate coefficients on simulated Cd leaching.

Key words: cadmium / transport / preferential flow / macropores / dual-continuum / sorption / particle-facilitated transport / vadose zone

Accepted July 14, 2009

1 Introduction

The increased vulnerability of freshwater resources, with regard to a widespread use of agricultural fertilizers containing traces of cadmium (Cd), requires a careful assessment of the potential paths of contamination from the soil surface to groundwater. Especially in lowland regions of Central and E Europe, such as the Danubian Lowland, the use of fertilizers has a long history (*Lichner* et al., 2006) and thus poses significant threat for both terrestrial organisms and humans (*ATSDR*, 1999). The main sources of Cd are P-based fertilizers, which may contain up to 170 mg kg^{-1} of Cd (*Singh*, 1994). Release of Cd into the environment may be induced by other significant sources. For instance, sludge slurries may contain considerable amount of sorbed Cd; the US Environmental Protection Agency (*EPA*, 1985) estimated Cd concentrations in sewage sludge from <1 mg kg^{-1} to >1000 mg kg^{-1}. Additionally, Cd in highway runoff has been detected at levels of up to 60 μg L^{-1} (*ATSDR*, 1999).

In regions exposed to pollution, Cd concentrations in soil of up to 30 mg kg^{-1} have been reported (*Seuntjens* et al., 2001). Topsoil concentrations are often more than twice as high as subsoil levels as the result of atmospheric fallout and contamination (*Pierce* et al., 1982). Long-term effects of sewage-sludge applications on soil properties, Cd availability and distribution in arable soil were presented, *e.g.*, by *Bergkvist* et al. (2003). Contamination of soil by Cd is of concern because Cd is efficiently taken up by plants, and therefore enters the food chain for humans and animals (*Vos* et al., 1990; *Almås* and *Singh*, 2001). A low soil pH, due to acid rain or soil liming activity, increases the uptake of Cd by plants (*Elinder*, 1992). Cadmium, relatively persistent in all media, is known to be highly toxic for aquatic organisms. Harmful impact on zooplankton and fish was observed even for concentrations in magnitude of micrograms per liter (*ATSDR*, 1999).

* Correspondence: Dr. J. Dusek; e-mail: dusek@mat.fsv.cvut.cz

In soils, pH, oxidation–reduction reactions, and formation of complexes are important processes influencing the mobility of Cd (*Herrero* and *Martin*, 1993). One of the processes that significantly affect the transport of Cd in soils is preferential flow. Whenever preferential flow develops, chemicals dissolved in water can travel at considerably high velocities through preferential pathways concurrently bypassing the porous matrix. As a result, chemicals are not homogeneously distributed in soils. This may represent a serious contamination risk for groundwater (*e.g., Steenhuis* et al., 1996; *Bundt* et al., 2000). Preferential flow has been proven to be triggered by various causes, *e.g.*, by textural stratification, soil water repellency, air entrapment, and surface desaturation (*Baker* and *Hillel*, 1990; *Wang* et al., 1998; *Dekker* and *Ritsema*, 1994; *Ritsema* and *Dekker*, 2000; among others). Preferential flow through interaggregate pore space, highly aggregated and spatially heterogeneous soils has been also reported (*Booltink* and *Bouma*, 1991; *Lennartz* et al., 1999; *Vervoort* et al., 1999). All above mentioned types of preferential flow may considerably shorten travel and residence times of contaminants in the vadose zone.

It is well recognized that the sorbing chemicals such as heavy metals and pesticides may be transported as mobile colloidal particles through macropores (*de Jonge* et al., 1998; *Levin* et al., 2006; *Burkhardt* et al., 2008). Beside preferential-flow effects, transport of colloid particles makes the model prediction of contaminant transport even more difficult (*e.g., Massoudieh* and *Ginn*, 2007; *Chatzikosma* and *Voudrias*, 2007). Mathematical modeling of particle-facilitated transport still poses a complex research challenge (*e.g., Laegsmand* et al., 2007; *Ilina* et al., 2008). To overcome the estimation of parameters controlling the colloid attachment/detachment and other processes, *Vogel* et al. (2007) presented a simplified approach to describe particle-facilitated transport of Cd using a dual-continuum model. In particular, *Vogel* et al. (2007) reanalyzed a field infiltration experiment performed by *Lichner* (1998) in a macroporous soil in Danubian Lowland (Bodiky site). In his study, Cd penetration at the depth of 0.65 m into sandy-loam soil was observed by radiotracer technique; it was further hypothesized that Cd sorbed on soil particles < 0.01 mm caused such deep breakthrough.

In regard to Cd field transport in soils, numerous model applications were reported (*e.g., Streck* and *Richter*, 1997; *Seuntjens* et al., 2002; *Ingwersen* and *Streck*, 2006) but only few studies explicitly considered preferential-flow effects using dual-continuum approach (*e.g., Moradi* et al., 2005; *Dusek* et al., 2006). In this study, we use the dual-permeability approach of *Gerke* and *van Genuchten* (1993a) modified by *Vogel* et al. (2000) and further extended by *Ray* et al. (2004). The dual-permeability model invokes local nonequilibrium in pressure head and solute concentration between the two pore domains. This is achieved through dividing the liquid-phase continuum into that of the preferential-flow domain (further on abbreviated with PF domain) and the soil-matrix domain (SM domain). A difficult parameterization of the dual-continuum models (increased number of soil-hydraulic parameters, need to determine the volumetric fractions of the flow domains and to define the interdomain mass-transfer coefficients) is the main drawback, which prevents wider use (*Gerke*, 2006). However, detailed suggestions on estimation of the hydraulic parameters of structured and/or macroporous soils have been proposed by *Zurmühl* and *Durner* (1998) and *Köhne* et al. (2002a, b). Furthermore, various techniques for the quantification of mass-transfer rate coefficients between the pore systems in dual-permeability approach have been investigated by *Gerke* and *van Genuchten* (1993b, 1996), *Gerke* and *Köhne* (2002), *Köhne* et al. (2004), and *Dolezal* et al. (2007).

Radioactive-tracer techniques and relevant computational methods are recognized as promising tools for solute-transport parameterization and modeling/prediction in the unsaturated zone of soils. The $^{115m}Cd^{2+}$-concentration profile, measured at the Bodiky site with the radioactive-tracer technique, was used for the calibration of the dual-continuum model S1D in the previous study of *Vogel* et al. (2007). The aim of the present modeling study is to predict Cd penetration into light, medium-heavy, and heavy soils, in response to an extreme rainfall event. In particular, distinct sorption coefficients for each of the two flow domains of the dual-permeability system, adopted from the previous study, are used to estimate the effect of particle-facilitated transport of Cd through macropores.

2 Materials and methods

2.1 Governing equations

The dual-continuum approach (*Gerke* and *van Genuchten*, 1993a; *Vogel* et al., 2000) assumes that the porous medium consists of two separate domains (SM domain and PF domain) with specific hydraulic properties. One-dimensional variably saturated water flow in the dual-continuum model is described by a pair of Richards' equations. Similarly, a coupled pair of advection-dispersion equations is solved to model solute transport. The exchange of water and solute between the matrix and the macropore domains is assumed to be proportional to the local pressure difference and the concentration gradient between the two pore systems. Details of model description and numerical implementation can be found in *Vogel* et al. (2004).

Richards' equations, governing one-dimensional variably saturated water movement in the two domains of dual-continuum porous medium, can be written as follows (considering the vertical coordinate, *z*, to be positive upward)

$$\frac{\partial w_m \theta_m}{\partial t} = \frac{\partial}{\partial z}\left(w_m K_m(h_m)\left(\frac{\partial h_m}{\partial z} + 1\right)\right) + \Gamma_w, \quad (1)$$

$$\frac{\partial w_f \theta_f}{\partial t} = \frac{\partial}{\partial z}\left(w_f K_f(h_f)\left(\frac{\partial h_f}{\partial z} + 1\right)\right) - \Gamma_w, \quad (2)$$

where the subscripts *m* and *f* denote the SM domain and the PF domain, respectively, *K* is the unsaturated hydraulic conductivity function (L T^{-1}), which is dependent upon *h*, the pressure head (L). Above, θ_m and θ_f are the volumes of water in each domain per unit volume of that domain. The hydraulic functions $\theta(h)$ and $K(h)$ differ between the two domains. The symbol Γ_w stands for the water-transfer term, which is defin-

ed as the volume of fluid moving from the PF to the SM domain per unit bulk volume of the medium per unit time (T^{-1}). The terms w_m and w_f are volume fractions of the SM and PF domain per unit volume of the bulk soil, respectively, with $w_m + w_f = 1$. The respective water contents of the two domains are related by

$$\theta = w_f\theta_f + w_m\theta_m, \quad (3)$$

where θ is the volumetric water content of the soil.

The following first-order formula is used for the evaluation of the water transfer term between the two pore domains

$$\Gamma_w = \alpha_w\ (h_f - h_m), \quad (4)$$

in which

$$\alpha_w = \alpha_{ws}K_{ar}, \quad (5)$$

where α_{ws} denotes the water-transfer rate coefficient at saturation ($L^{-1}\ T^{-1}$), and K_{ar} is the relative-hydraulic-conductivity function of the interface between the SM and the PF domain. Values of K_{ar} range from 0 to 1 taken as the minimum of the PF and SM domain conductivities evaluated for upstream pressure, *i.e.*: $K_{ar} = \min\{K_{fr}(h_f), K_{mr}(h_f)\}$ for $h_f \geq h_m$ and $K_{ar} = \min\{K_{fr}(h_m), K_{mr}(h_m)\}$ for $h_f < h_m$ (*Ray* et al., 2004; *Gerke* et al., 2007). The parameter α_{ws} can account for mass transfer reduction due to, for instance, aggregate coating effects (*e.g., Gerke* and *Köhne*, 2002).

The pair of advection-dispersion equations is solved in order to predict concentration in a dual-continuum system as follows:

$$\frac{\partial w_m R_m\theta_m c_m}{\partial t} + \frac{\partial w_m q_m c_m}{\partial z} - \frac{\partial}{\partial z}\left(w_m\theta_m D_m\frac{\partial c_m}{\partial z}\right) = +\Gamma_s, \quad (6)$$

$$\frac{\partial w_f R_f\theta_f c_f}{\partial t} + \frac{\partial w_f q_f c_f}{\partial z} - \frac{\partial}{\partial z}\left(w_f\theta_f D_f\frac{\partial c_f}{\partial z}\right) = -\Gamma_s, \quad (7)$$

where c is the solute concentration ($M\ L^{-3}$), D is the hydrodynamic dispersion coefficient ($L^2\ T^{-1}$), and q is the Darcy flux ($L\ T^{-1}$). The equilibrium sorption is controlled by the retardation factor $R = 1 + \rho K_d/\theta$ where K_d is the equilibrium sorption distribution coefficient ($L^3\ M^{-1}$) and ρ is the soil bulk density ($M\ L^{-3}$). In the above, Γ_s is the solute-exchange term ($M\ L^{-3}\ T^{-1}$), which controls the transfer of chemical between the two domains.

In Eq. 6 and 7, the solute-coupling term Γ_s is defined as the mass flux of solute being transported from one domain to another per unit bulk volume. Solute exchange between pore domains is modeled as a first-order process and is expressed as

$$\Gamma_s = \Gamma_w c_i + \alpha_s(c_f - c_m). \quad (8)$$

The first term on the right side of Eq. 8 defines the advective exchange of solute due to a movement of water, Γ_w, from one domain to the other because of the water pressure difference between the two domains. The second term of the right side of Eq. 8 accounts for the diffusive exchange of solute due to a concentration gradient between the two domains. In case water flows from the SM domain to the PF domain $c_i = c_m$, for flow in the opposite direction $c_i = c_f$.

The solute-exchange coefficient α_s (T^{-1}) was shown by *Gerke* and *van Genuchten* (1993a) to be dependent upon the effective diffusion coefficient, moisture content, and aggregate radius of the matrix domain, similar to its flow counterpart. The following formulation for α_s is used in the present study

$$\alpha_s = \alpha_{ss}\theta_{ar}, \quad (9)$$

where α_{ss} is the solute transfer rate coefficient at saturation (T^{-1}). The interface relative saturation $\theta_{ar} = \theta_a/\theta_{as}$ of the SM/PF domain interface is assumed to be equal to the relative saturation of the PF domain (*Ray* et al., 2004).

The respective solute concentrations in the two domains are related by

$$c = (w_f\theta_f c_f + w_m\theta_m c_m)/\theta, \quad (10)$$

where c is the composite concentration.

The dual-continuum model S1D assumes validity of laminar flow in both domains and no dissolution-precipitation due to chemical interaction, among other simplifications (*van Genuchten* et al., 1999). The dual sets of governing equations for flow of water and transport of Cd are solved numerically by the computer code S1D (*Vogel* et al., 2007), which is an extended version of the HYDRUS 5 code (*Vogel* et al., 1996). The soil-hydraulic functions were described using the modified version of the van Genuchten-Mualem formulation (*Vogel* et al., 2001).

2.2 Soils and soil hydraulic properties

All the studied sites were situated in the SW part of the Danubian Lowland, which is a large (1260 km^2) agriculturally managed area situated in the SW of Slovakia, with a shallow (0.5–3.8 m deep) underlying aquifer containing ≈10 km^3 of freshwater.

The reference study site was located at the Kralovska luka meadow in the territory of Bodiky village. The sandy-loam soil under study was classified as Calcaric Fluvisoil (*WRB*, 1998). It was covered by permanent grass. Penetration of $^{115m}Cd^{2+}$ into the soil during field ponded infiltration was observed in a controlled experiment. The dual-continuum model S1D was then used to model $^{115m}Cd^{2+}$ transport (*Vogel* et al., 2007). In the present study, the same model was used to predict the Cd fate at three different sites of the region (Kalinkovo, Macov, and Jurova).

The first site was located in the territory of Kalinkovo village. The studied light sandy-loam soil was classified as Calcaric Fluvisoil (*WRB*, 1998). It was sown with oilseed rape. The second site was located at Macov village. The medium-heavy loamy soil was classified as Calcari-Haplic Chernozem (*WRB*, 1998). It was sown with winter wheat. The third site

was situated at Jurova village. The studied heavy clay soil was classified as Calcari-Mollic Fluvisol (*WRB*, 1998). It was sown with winter wheat. All three soils were plowed conventionally in a late autumn to a depth of 0.2 m. Cadmium transport at the Macov site was already examined by *Dusek* et al. (2006).

The soil stratification for all three sites was determined by a standard soil-survey procedure (involving soil color, texture, structure, and composition). The laboratory retention measurements were performed on small-undisturbed soil samples (100 cm^3) using the pressure-plate apparatus with three replicates for each layer. The hydraulic parameters of the soil matrix (including nonzero capillary height h_s) were obtained by fitting van Genuchten's modified prediction model (*Vogel* et al., 2001) to data points.

The volumetric portion of the fast domain, w_f, was set to 10% of the bulk soil for the Macov and Jurova sites. For Macov, the field-ponded-infiltration experiment using the Briliant Blue dye tracer proved the existence of biopore system (*Dohnal* et al., 2009). The biopore network in the soil profile originated from the activity of *Lumbricus terrestris* L. The coefficient w_f was estimated from the digital image analysis of stained area below the infiltration ring. The heavy–clay soil profile in the Jurova site contained fissures and cracks which originated from prolonged rainless period. The estimation of w_f was based on the visual inspection of the soil profile.

The measurements of the topsoil hydraulic conductivity were carried out *in situ* using a tension infiltrometer (*Lichner* and *Houskova*, 2001; *Lichner* et al., 2006). The measurement of the infiltration rate was performed in 10 replicates. The observed infiltration rates were used to determine the saturated hydraulic conductivity K_s and the unsaturated conductivity K(–3 cm) (Tab. 8–10 in *Lichner* et al., 2006). First, the saturated hydraulic conductivity of the SM domain K_{sm} was estimated from the measured hydraulic conductivity at $h = -3$ cm using the modified prediction model of $K(h)$ (*Vogel* et al., 2001). Then, having the composite saturated hydraulic conductivity K_s and the volumetric fraction of the PF domain ($w_f = 0.1$), it was possible to compute the saturated hydraulic conductivity of the PF domain K_{sf} from the following formula

$$K_s = w_m K_{sm} + w_f K_{sf}. \quad (11)$$

The saturated hydraulic conductivities K_{sm} for the SM domain of the remaining soil layers were derived by a pedotransfer-function model (*Schaap* et al., 2001) based on textural classes. The parameters used in the simulations for the three sites are listed in Tab. 1–3. Since measured K_s and K(–3 cm) for the Kalinkovo site did not differ significantly, the preferential-flow component was not considered. Therefore, the simulation of Cd transport for Kalinkovo was predicted using a single-continuum approach.

The retention properties of the preferential pathways are less important compared to their conductivity and thus were approximated by properties of a coarsely textured porous media (*Gerke* and *van Genuchten*, 1993a; *Gerke* et al., 2007). No stratification in the PF domain was assumed. The water-transfer rate coefficient at saturation $\alpha_{ws} = 0.015\ cm^{-1}\ d^{-1}$ for a sandy-loam soil was estimated by the inverse dual-continuum simulation (*Vogel* et al., 2007). In this study, we used $\alpha_{ws} = 0.01\ cm^{-1}\ d^{-1}$ for the Macov and Jurova sites in a more lumped manner as in a originally suggested formulation (*Gerke* and *van Genuchten*, 1993b). Similarly, the solute-transfer rate coefficient at saturation α_{ss} was set equal to

Table 1: Soil hydraulic parameters for the Kalinkovo site (light sandy-loam soil).

Depth / m	**0–0.25**	**0.25–0.5**	**0.5–0.9**	**0.9–1.0**
θ_s*	0.484	0.499	0.466	0.465
θ_r	0.031	0.029	0.020	0.200
α / cm^{-1}	0.002	0.011	0.020	0.013
n	1.567	1.369	1.303	1.387
h_s / cm	–0.76	–0.51	–0.24	–0.66
K_s / cm d^{-1}	87.0	56.0	72.0	104.0

* θ_s and θ_r, saturated and residual volumetric water content; α and n, fitting parameters; h_s, air-entry value; K_s, saturated hydraulic conductivity. The modified van Genuchten model was used in the simulations (*Vogel* et al., 2001).

Table 2: Soil hydraulic parameters for the Macov site (medium-heavy loamy soil).

	SM domain					**PF domain**
Depth / m	**0–0.2**	**0.2–0.3**	**0.3–0.5**	**0.5–0.8**	**0.8–1.0**	**0–1.0**
θ_s	0.498	0.486	0.502	0.452	0.479	0.600
θ_r	0.000	0.000	0.000	0.000	0.073	0.050
α / cm^{-1}	0.018	0.042	0.057	0.026	0.016	0.145
n	1.212	1.176	1.184	1.215	1.647	2.680
h_s / cm	–1.62	–2.06	–0.80	–2.61	–2.88	0.00
K_s / cm d^{-1}	119.0	23.9	18.9	17.6	31.7	2029.0
w_f						0.1
α_{ws} / $cm^{-1}\ d^{-1}$						0.01
α_{ss} / d^{-1}						0.01

Table 3: Soil hydraulic parameters for the Jurova site (heavy clay soil).

	SM domain			**PF domain**
Depth / m	**0–0.4**	**0.4–0.8**	**0.8–1.0**	**0–1.0**
θ_s	0.610	0.531	0.553	0.600
θ_r	0.079	0.070	0.093	0.050
α / cm^{-1}	0.190	0.128	0.049	0.145
n	1.170	1.133	1.215	2.680
h_s / cm	–1.98	–0.23	–0.55	0.00
K_s / cm d^{-1}	76.0	27.0	6.0	14516.0
w_f				0.1
α_{ws} / $cm^{-1}\ d^{-1}$				0.01
α_{ss} / d^{-1}				0.01

0.01 d^{-1} for both simulated sites. A simple sensitivity analysis is presented to demonstrate the significance of transfer coefficients on Cd leaching.

2.3 Batch tests

The sorption distribution coefficient for the SM domain, K_{dm}, which describes the partitioning between the solid and liquid phase, was experimentally determined by standard lab batch experiments as described, *e.g.*, in *Selim* et al. (1992) and *Cipakova* and *Mitro* (1997). In contrast, the sorption distribution coefficient for the PF domain, K_{df}, was determined by modified batch technique (*Lichner* and *Cipakova*, 2002). In case of the latter domain, the liquid phase contained not only Cd in aqueous phase, but also Cd adsorbed to soil particles < ≈0.01 mm. These soil particles may be highly mobile in the macropore network (*Laegsmand* et al., 1999), thus may travel to considerable depths as suspension.

For all measurements, ^{109}Cd, as an easily detectable radioactive isotope of Cd, was used. In each sorption experiment, 10 g of dry soil (sieved through a 2 mm sieve) were dispersed in 40 mL water with the radioactive tracer ^{109}Cd plus carrier solution (with the ^{109}Cd half-life of 330 d, chemical form $CdCl_2$, initial Cd concentration 50.9 mg L^{-1}, and initial specific activity a_0). In case of the standard batch test, soil, water, and Cd mixture were shaken for 5 s in a 100 mL plastic bottle. After 1 min of Cd–soil contact, 5 mL sample of the dispersion were taken from the bottle and centrifuged for 2 min at 2000 rpm. The specific activity of the ^{109}Cd in the liquid phase was then measured by multi-channel gamma-spectrometer Canberra (Series 35 Plus, Canberra Industries Inc., Meriden, Conn., USA) with Ge/Li detector.

The amount of Cd absorbed on the solid phase and the respective distribution coefficient were computed from the measured activities. The resulting distribution coefficient, denoted as K_{dm}, characterizes the process of adsorption in the SM domain:

$$K_{dm} = \frac{V}{m}\frac{(a_0 - a)}{a}, \qquad (12)$$

where a_0 and a are the initial and final specific activities of Cd in the liquid phase, respectively, m is the amount of dry soil in the batch test (M), V is the volume of distilled water in the batch test (L^3).

To obtain the distribution coefficient for the PF domain, the modified batch test was used. In this case, the 5 mL sample of the dispersion was taken from the bottle after 5 s of shaking and 1 min of sedimentation. This time, no centrifugation was applied. According to the Stokes' sedimentation law, the particles < 0.01 mm, carrying a significant part of the adsorbed Cd, had not enough time to sediment and thus remained dispersed in the sample. The specific activity of the combined amount of Cd in both liquid and solid phases (including Cd adsorbed on particles < 0.01 mm) was then measured by the gamma-spectrometer. The distribution coefficient K_{df} was calculated by applying a formula analogous to Eq. 12.

For all batch tests, the same procedure was applied also for longer Cd–soil contact times (up to 60 min). All batch tests were carried out in duplicate.

2.4 Domain-specific sorption and transport parameters

When considering domain specific sorption, each pore domain (the SM and PF domain) has its own sorption properties. In our study, both pore domains are assumed to contain only equilibrium sorption sites characterized by the distribution coefficients K_{dm} for the SM domain and K_{df} for the PF domain (*Lichner* and *Cipakova*, 2002; *Vogel* et al., 2007). The distribution coefficient for the PF domain is always smaller than that for the matrix due to the fact that the soil particles < 0.01 mm (loaded with the adsorbed Cd) are assumed to move with the soil water. The colloids are assumed to be completely immobile in the SM domain of the dual-continuum system but fully mobile in the PF domain. It is further assumed that the colloids move by the same mechanism as the dissolved Cd (*i.e.*, by advection and dispersion) and therefore the advection-dispersion equations can be used to approximate the combined transport of dissolved and colloid-sorbed Cd. Obviously our highly simplified approach is not capable of predicting all complexities and processes involved in the colloid-facilitated transport. In this conceptual model, the mobile colloid density is predetermined by the results of the batch tests and by the mobility/immobility assumptions (*Vogel* et al., 2007).

To illustrate the preferential Cd movement without a provision for colloid-bound transport the distribution coefficient for the flow domains (*i.e.*, the SM and PF domain) was set equal to K_{dm} evaluated by standard lab batch experiment.

Based on the review of the field-scale dispersivities (*Vanderborght* and *Vereecken*, 2007) where an upper limit of 0.1 m for dispersivity was reported, a reasonable estimate of 0.05 m was used in this study. The molecular diffusion coefficient was set equal to 6.2×10^{-5} m^2 d^{-1} (*Marcus*, 1997). The distribution coefficients for both pore domains, determined from the conventional and modified batch tests, of the three studied soils are presented in Tab. 4. The large differences in K_{dm} between the sites can be explained by different composition of soils; mainly by differences in C_{ox} content (*Lichner* et al., 2006).

Table 4: Distribution coefficients for the SM and PF domain of the three soils. Bulk densities are reported for the topsoil.

Studied soil	Kalinkovo	Macov	Jurova
K_{dm} / cm^3 g^{-1}	1596	138.9	483.8
K_{df} / cm^3 g^{-1}	–	7.01	3.95
ρ / g cm^{-3}	1.41	1.35	1.35

2.5 Initial and boundary conditions

At the beginning of the simulated period, 14 h prior to the rainstorm event of interest, Cd was applied in a definite pulse of water with the concentration load 2 mg L^{-1}. The pulse

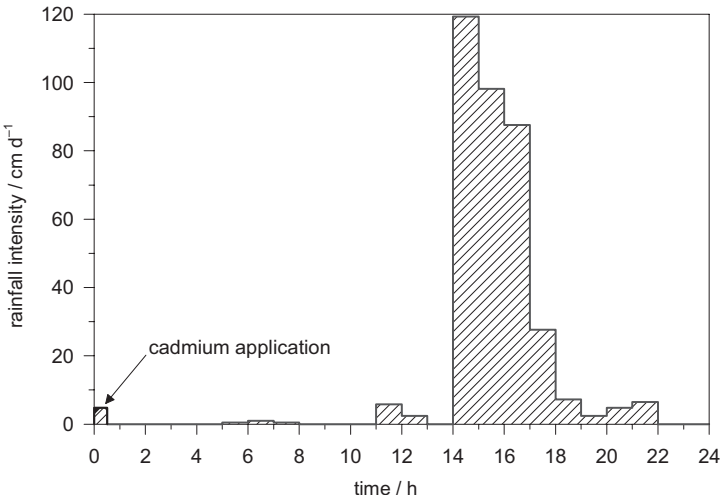

Figure 1: Rainfall measured at Pezinok-Myslenice on July 17, 1999.

lasted for 0.5 h and comprised of 1 mm of water column. The Cd mass was distributed according to volumetric proportions of the SM and PF domains. Applied concentration was considered to be a reasonable estimate based on the assumption that the fertilizer-application rate is ≈900 kg ha^{-1} and 1 kg of fertilizer may contain up to 24 mg of Cd. The amount of 24 mg of Cd in 1 kg of fertilizer seems to be quite high, but not so long ago this amount was still meeting the limits for use in agriculture (*Lichner*, 1998). As a result of the simulated application, 1 cm^2 of the soil surface received 0.2 μg of Cd in total. The initial soil profile was assumed to be Cd-free. The bottom boundary condition was set to zero concentration gradient to allow the contaminant to pass freely the lower boundary at the depth of 1 m.

The soil surface was treated as "atmospheric boundary condition". This type of boundary condition allows for switching between the Neumann and Dirichlet type conditions, *i.e.*, when the top soil is not capable to transmit water during heavy rain, the flux condition is changed to pressure condition. In this case, a surplus water may either generate surface runoff or stay retained at the soil surface. The unit-hydraulic-gradient condition was used at the lower boundary, allowing water to leave the soil profile at the rate equal to unsaturated hydraulic conductivity. The initial condition for water flow was defined as so called "field-capacity condition" (*i.e.*, fully saturated soil profile left to drain freely for 72 h). No evaporation was taken into account for the simulated period of 24 h.

The rainfall event used in our analysis was recorded at Pezinok-Myslenice weather station in the Danubian region. The recorded storm occurred on July 17, 1999, and total cumulative rate amounted to 150 mm rain during 17 h. Considerable amount of precipitated water, 130 mm, was observed during three consecutive hours (2 p.m. till 5 p.m.), which represents an extreme rainfall event with a 100 y return period in the SW of Slovakia. The temporal pattern of the rainfall is depicted in Fig. 1.

3 Results and discussion

The simulation results indicate that at the peak rainfall intensity of the tested rainstorm the soil matrix becomes at all three sites fully saturated near the soil surface. The surplus water from the matrix is diverted to the PF domain at the Macov and Jurova sites. At Kalinkovo, the saturation excess water contributes to the formation of temporary surface storage or surface runoff, due to the absence of the preferential pathways. The algorithm for the redistribution between the

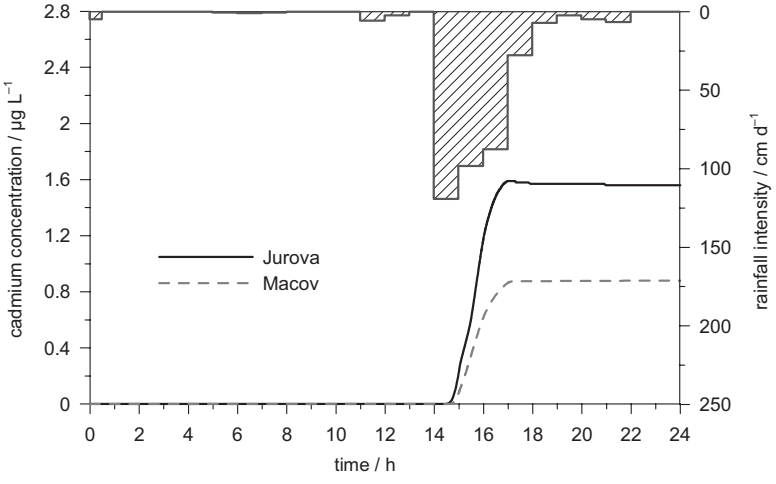

Figure 2: Simulated Cd breakthrough curves in the PF domain at the depth of 0.15 m (liquid concentrations). At the Kalinkovo site no Cd breakthrough occurred.

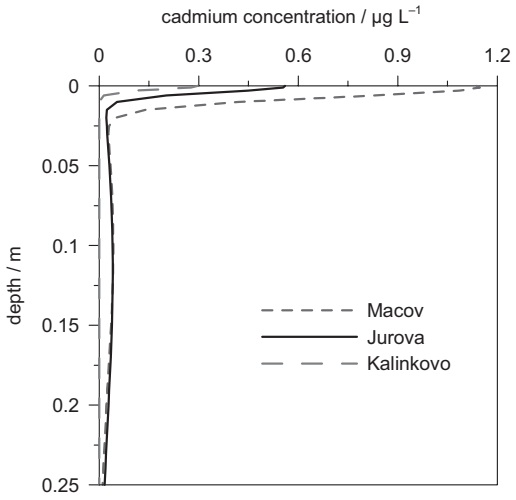

Figure 3: Simulated Cd concentration profile for all studied soils after the rainfall.

pore domains is described in more detail in *Ray* et al. (2004) and *Dusek* et al. (2008).

The breakthrough curves for the PF domain, simulated by the dual-permeability model, are shown in Fig. 2, where Cd resident concentrations in the liquid phase at the depth of 0.15 m are depicted. In the model, both the higher hydraulic conductivity and the lower distribution coefficient of the PF domain controlled the deeper and more intense Cd penetration in the PF domain leading to increased concentrations deeper in the soil profile. The increase of concentration is clearly associated with the commencement of the intense rainfall. Higher concentration in the PF domain is predicted for heavy clay soil in Jurova than for medium-heavy soil in Macov. It is important to note that the maximum predicted Cd concentration for the Jurova site (≈1.6 µg L^{-1}) is below the maximum level of Cd in drinking water suggested by the US EPA (5 µg L^{-1}). However, Cd concentration above the detection limit (≈0.2 µg L^{-1}) was predicted in the PF domain at the 0.45 m depth in Jurova. Similarly, the depth of Cd penetration above the detection limit for the Macov site was 0.35 m. The distribution coefficients seem to control the contaminant leaching, which was already proven by previous studies (*e.g., Dubus* et al., 2003; *Roulier* et al., 2006; *Stenemo* et al., 2007); *i.e.*, lower K_{df} at Jurova as compared to the Macov site. The single-domain simulation for the Kalinkovo site revealed no concentration increase at the depth of interest.

The simulated composite concentration profiles for the three sites of interest are shown in Fig. 3. In this figure, Cd distribution in the liquid phase is depicted for t = 24 h. Different concentration maxima for the three soils at the soil surface result from different K_d values and actual water content. It is evident that the single-continuum model for the Kalinkovo site predicts all applied Cd in the uppermost part of the topsoil layer (0–0.01 m). The two dual-continuum simulations (Macov and Jurova) show elevated Cd concentrations to 0.25 m but only in minor absolute values. The secondary concentration peaks below 0.025 m depth for these two cases are related to the transport of Cd through the preferential-flow domain.

The Cd mass in soil sublayers down to 0.25 m beneath the soil surface is shown in Fig. 4. The figure shows total mass including both the mobile and immobile (adsorbed) contribution. The Cd amount in the first sublayer (0–0.05 m) mainly reflects the presence of Cd in the SM domain. The deeper-layer Cd contents are exclusively associated with leaching in the PF domain. The leached Cd mass below the plowing depth (0.20 m) is in the following order: Jurova (0.0045 µg cm^{-2}, *i.e.*, 2.3% of applied Cd) > Macov (0.003 µg cm^{-2}, *i.e.*, 1.5% of applied Cd) > Kalinkovo (0 µg cm^{-2}). The highest Cd leachate is predicted for Jurova soil, which can be explained by the lowest K_{df} among the sites. However, the difference in Cd leaching between Macov and Jurova is not significant. The deeper leaching in the PF domain for the Jurova site is in case of Macov compensated by the matrix transport. The SM-domain sorption distribution coefficient for Macov is ≈3.5 times smaller than K_{dm} for Jurova (see Tab. 4).

In Fig. 5, simulated depth–time development of Cd concentration in the PF domain for the Jurova site is presented. Note, the scale of Cd concentrations is logarithmic. The 2D plot shows the simulated changes of Cd concentration in soil water flowing through the preferential pathways. It can be

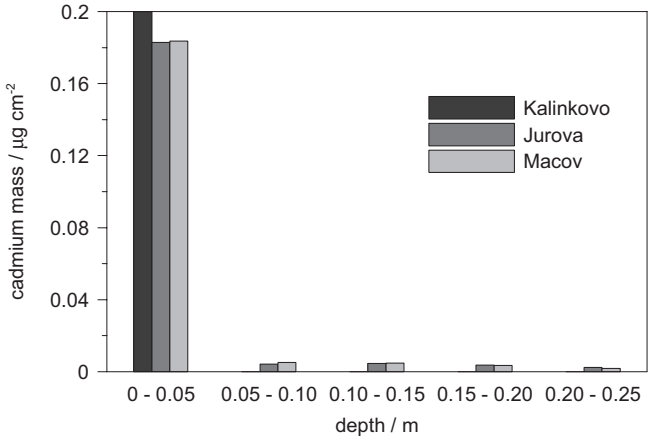

Figure 4: Total simulated Cd mass for the three soils in 0.05 m increments after the rainfall event (t = 24 h).

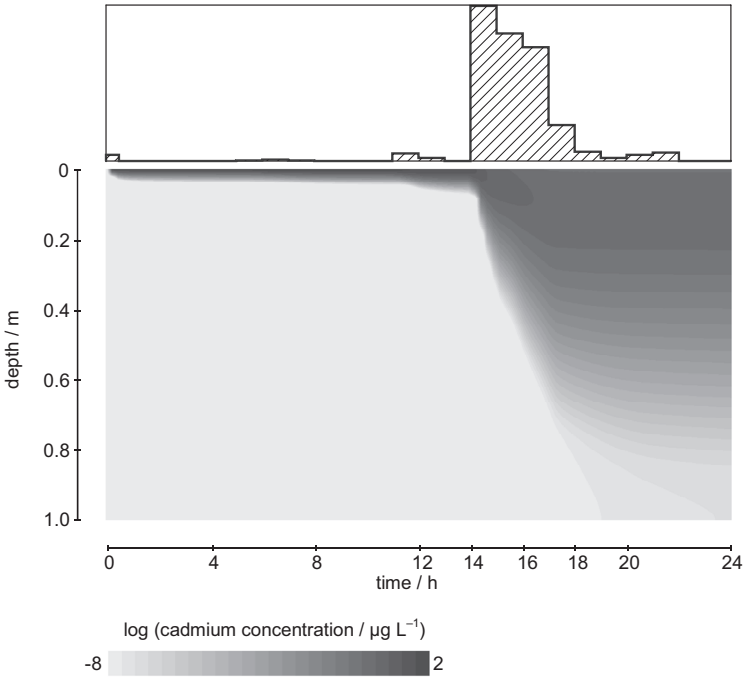

Figure 5: Depth–time development of mobile Cd concentration in the PF domain for the Jurova site. The rainfall pattern is superimposed atop.

seen that the dynamics of Cd transport closely corresponds to the infiltration process. At the end of the recorded rainfall event, Cd traces are predicted even at the bottom of the 1 m deep soil profile.

The results of the dual-continuum scenario excluding the colloid transport for Macov and Jurova are shown in Fig. 6. The depth of Cd penetration can be directly compared with Fig. 4 where the particle-facilitated transport in the dual-permeability soil is additionally considered. Such a comparison reveals very weak downward Cd migration for scenarios excluding the colloid transport, which is caused by high K_d values used for the flow domains. If particle-facilitated transport is not considered in modeling, Cd stayed near the soil surface. The comparison of results based on particle-facilitated and preferential Cd transport highlights the importance of appropriate consideration of relevant transport processes in the conceptual model.

A sensitivity analysis of water (α_{ws}) and solute (α_{ss})-transfer rate coefficients is shown in Fig. 7 and 8. The simulations refer to the Macov site. Small values of the transfer coefficients lead to more intense preferential-flow effects, whereas a large value leads to near-equilibrium case. The smaller the water rate coefficient, the deeper the predicted Cd penetration (Fig. 7). In one simulation scenario, the mass-transfer term Γ_s was set equal to zero, so that no exchange of the dissolved Cd between the matrix and the PF domain could take place. The scenario, in which no transfer of cadmium between the flow domains is considered, shows identical Cd penetration as other scenarios (Fig. 8). Similar results were obtained for the Jurova site (not shown). The results of the sensitivity analysis suggest only slight effect of the transfer rate coefficients on simulated Cd leaching. This conclusion is in a direct contradiction with our previous study (*Vogel* et al., 2007) where Cd transport was predicted during the field tracer infiltration experiment. The difference between the two studies can be attributed to different flow regime, which governs the Cd distribution among the flow domains.

The results from the conventional batch technique suggest that nearly all of Cd dissolved in water would be adsorbed on soil particles of the studied soils during the first minutes of a rain or irrigation event following application (*Lichner* and *Cipakova*, 2002; *Lichner* et al., 2006). In accordance with the findings of *Jacobsen* et al. (1997), a part of Cd adsorbed on particles < 0.01 mm and mobilized by erosive impact of rain or irrigation could be transported *via* soil macropores. Burrows formed by the *Lumbricus terrestris* L. earthworm, for

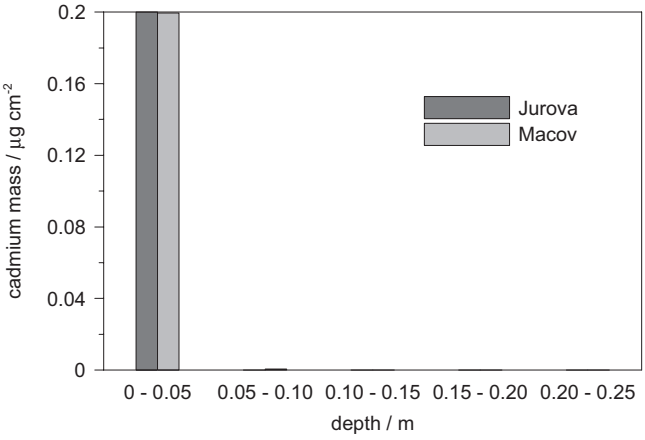

Figure 6: Total simulated Cd mass for the two soils in 0.05 m increments after the rainfall event (t = 24 h). The simulation scenario accounts for the preferential Cd movement but excludes particle-facilitated transport.

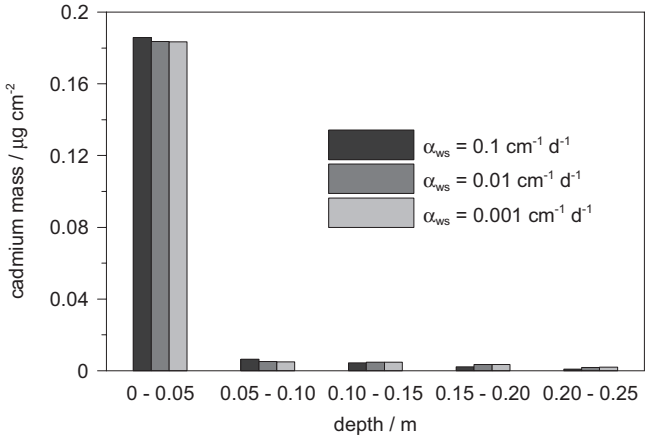

Figure 7: Total simulated Cd mass for Macov in 0.05 m increments after the rainfall event (t = 24 h) for three different water-transfer rate coefficients α_{ws}. The solute-transfer rate coefficient is fixed at α_{ss} = 0.01 d^{-1}.

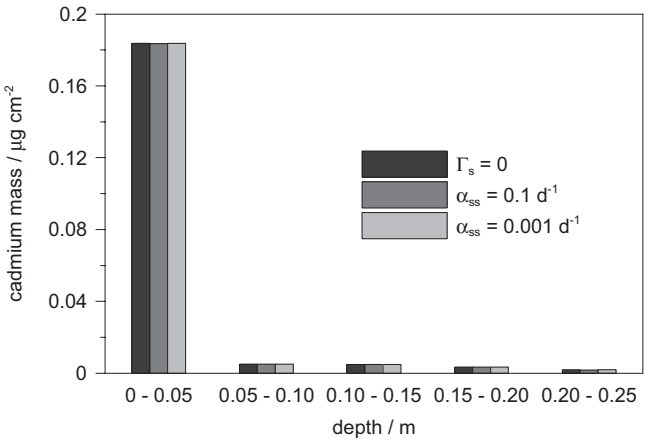

Figure 8: Total simulated Cd mass for Macov in 0.05 m increments after the rainfall event (t = 24 h) for three different Cd between-domain communications. The water-transfer rate coefficient is fixed at α_{ws} = 0.01 cm^{-1} d^{-1}.

example, can have a diameter up to 12 mm and depth of penetration up to 2.4 m (*Shipitalo* and *Gibbs*, 2000). These and other soil macropores may accentuate the above mentioned particle- (*Jacobsen* et al., 1997) or colloid-facilitated (*Laegsmand* et al., 1999) transport of Cd, causing the deep penetration of Cd into the soil profile and shallow-groundwater pollution. During its transport in the macropore system, the mobility of Cd adsorbed on soil particles < 0.01 mm is not influenced by the depth-varying properties of the soil matrix. The batch-test results also indicate that significant amount of Cd, adsorbed on the soil particles < 0.01 mm, may be available for transport through macropores.

The pH (KCl) of the three soils ranged from 7.4 to 7.7 (*Lichner* et al., 2006). *Adriano* (2001, p. 279) reported that the precipitation of Cd as $CdCO_3$ may occur at pH > 7 in calcareous soils. In that case, Cd mobile in soil macropores would consist of three components: Cd in the liquid phase, Cd adsorbed on soil particles < 0.01 mm, and Cd precipitated as $CdCO_3$. However, the lab batch experiments did not suggest any Cd precipitation for all three soils. In a different study on soils with similar pH from the Danubian Lowland, *Kovacova* (2000) also did not observe deviations from the isotherm due to Cd precipitation. Hence, the key assumption of the modeling approach (see above) was complied.

As stated earlier, the conceptual model for Cd transport is based on the assumption that the Cd attached to colloids moves with the same mechanism as the Cd dissolved in soil water, *i.e.*, by advection and dispersion (*Vogel* et al., 2007). The first condition, needed to fulfill this assumption, is the presence of mobile colloids in the preferential pathways. Particle analysis shows that the Macov and Jurova sites contain ≈ 34% and 60% soil particles < 0.01 mm, respectively (*Lichner* et al., 2006). It is further assumed that the heavy-rainfall event may initiate the transport of these particles in the macropores. Nevertheless, soil plowing destroys the topsoil part of macropore systems, thereby greatly reducing preferential-flow effects shortly after this activity. This may be counteracted by soil fauna (*e.g.*, earthworms), which can form new macropore (biopore) systems in the soil shortly after destroying the old ones (*Farenhorst* et al., 2000). In addition, natural weathering may produce desiccation cracks in the plow layer, although this usually takes a longer time (*e.g., Cornelis* et al., 2006).

Chemical adsorption with different sorption bonds in separate flow domains may imply wider applications in modeling solute transport through natural porous systems. For instance, reduced distribution coefficient of the preferential domain may be due to low sorption capacity or coatings on macropore walls (*Rasmussen* et al., 2001; *Vanderborght* et al., 2002). *Hansen* et al. (1999) hypothesized that the macropore walls may have different sorption properties compared to the bulk soil. This is due to the specific mineralogy characteristics and the preferential-flow regime prevailing in the macropore network. In addition, the adsorption process in the macropore domain may be, under specific conditions, better characterized as kinetic sorption rather than equilibrium sorption (*Hansen* et al., 1999; *Ray* et al., 2004). From the physical point of view, high water fluxes through the macropores may limit the sorption process which may lead to a kinetically controlled sorption reaction or even to no sorption case in the PF domain (*Ray* et al., 2004). For reactive compounds, the biodegradation may vary between the flow domains as well. Both laboratory and field experiments showed faster degradation in the macropores compared to the matrix (*Pivetz* and *Steenhuis*, 1995; *Bolduan* and *Zehe*, 2006). Such a difference could be attributed to higher bacterial activity in the more aerobic PF domain than in the less aerobic soil matrix. Therefore the chemical composition and thus the properties of the preferential pathways are important aspects to be considered when predicting nonequilibrium transport.

Recent modeling studies dealing with Cd transport in soils focused on the field-scale leaching or considered Cd fate in a long-time span (*e.g., Streck* and *Richter*, 1997; *Bergkvist* and *Jarvis*, 2004; *Seuntjens* et al., 2002; *Moradi* et al., 2005; *Ingwersen* and *Streck*, 2006). A good agreement between

observed and simulated concentration profiles was often found without accounting for the preferential-flow effects and colloid transport. In some studies (*Streck* and *Richter*, 1997; *Ingwersen* and *Streck*, 2007), the application of the stream-tube model (*Jury* and *Roth*, 1990) with spatially variable sorption characteristics delivered reasonable match with observations. In this study, different modeling concept was used with emphasis on the short-term water and Cd dynamics. From the long-term perspective, certain transport processes, which are relevant from the short-term view, may dampen out.

Several studies indicated small risk of groundwater contamination by Cd (*Streck* and *Richter*, 1997; *Moradi* et al., 2005; *Ingwersen* and *Streck*, 2006). On the contrary, our modeling approach predicted Cd displacement (≈ 2% of applied Cd) below 0.20 m depth within 1 d; Cd migration was exclusively attributed to colloid transport through the preferential pathways. If the rain events with high intensity are frequent in the studied region and the intensity of irrigation/rainfall is higher than the infiltration rate into the soil matrix (resulting in the infiltration of water/water suspension into the surface-vented soil macropores), the Cd load toward the groundwater table becomes intensified. The experimental research on the field-scale particle-facilitated preferential transport of sorbing compounds also indicated significant leaching (*e.g., Villholth* et al., 2000; *de Jonge* et al., 2004; *Schelde* et al., 2006).

4 Conclusions

The effect of extreme rainfall on Cd transport through three different soils in the Danubian Lowland was examined. The results of laboratory batch tests were used to distinguish different Cd transport regime for the soil-matrix domain and preferential-flow domain. For two soils (medium-heavy and heavy clay), it has been demonstrated by numerical model based on dual-permeability approach that Cd may percolate below the root zone within a short period of time. Deeper Cd penetration in macropores was caused by significantly smaller distribution coefficient for the PF domain obtained from the modified batch test. The highest Cd leaching was predicted for heavy clay soil, which was attributed to the lowest sorption distribution coefficients in the preferential-flow domain.

The results of the sensitivity analysis indicated only slight effect of the transfer rate coefficients on simulated Cd leaching. Modeling with classical single-permeability approach and dual-continuum approach without considering the particle-facilitated transport led to negligible Cd penetration.

The simulation results suggested for two of the three examined sites the most unfavorable situation: retention of Cd in the root zone, where it can be accessible to plants, and, at the same time, quite deep Cd penetration, which can pose contamination risk for groundwater. This conclusion is, at this point, based on numerical modeling, supported by limited laboratory and field experiments. Thus, more thorough experimental confirmation is still needed.

Acknowledgments

The study has been supported by the research fund of the *Ministry of Education of the Czech Republic (MSM 6840770002)*. Additional support was provided by the *Slovak Scientific Grant Agency project VEGA 2/0170/09* and *Czech-Slovak project SK-CZ-0066-07/MEB 0808114.* The comments of Dr. *O. Sracek* and two anonymous reviewers are gratefully acknowledged.

References

Adriano, D. C. (2001): Trace Elements in Terrestrial Environments: Biogeochemistry, Bioavailability, and Risks of Metals. 2nd edn., Springer-Verlag, New York.

ATSDR (Agency for Toxic Substances and Disease Registry) (1999): Toxicological profile for cadmium. U.S. Department of Health and Human Services, Public Health Service, Atlanta, GA, USA.

Almås, Å. R., Singh, B. R. (2001): Plant uptake of cadmium-109 and zinc-65 at different temperature and organic matter levels. *J. Environ. Qual.* 30, 869–877.

Baker, R. S., Hillel, D. (1990): Laboratory tests of a theory of fingering during infiltration into layered soils. *Soil Sci. Soc. Am. J.* 54, 20–30.

Bergkvist, P., Jarvis, N. (2004): Modeling Organic Carbon Dynamics and Cadmium Fate in Long-Term Sludge-Amended Soil. *J. Environ. Qual.* 33, 181–191.

Bergkvist, P., Jarvis, N., Berggren, D., Carlgren, K. (2003): Long-term effects of sewage sludge applications on soil properties, cadmium availability and distribution in arable soil. *Agric. Ecosyst. Environ.* 97, 167–179.

Bolduan, R., Zehe, E. (2006): Abbau von Isoproturon in Regenwurm-Makroporen und in der Unterbodenmatrix – Eine Feldstudie. *J. Plant Nutr. Soil Sci.* 169, 87–94.

Booltink, H. W. G., Bouma, J. (1991): Physical and morphological characterization of bypass flow in a well-structured clay soil. *Soil Sci. Soc. Am. J.* 55, 1249–1254.

Bundt, M., Albrecht, A., Froidevaux, P., Blaser, P., Fluehler, H. (2000): Impact of preferential flow on radionuclide distribution in soil. *Env. Sci. Tech.* 34, 3895–3899.

Burkhardt, M., Kasteel, R., Vanderborght, J., Vereecken, H. (2008): Field study on colloid transport using fluorescent microspheres. *Eur. J. Soil Sci.* 59, 82–93.

Chatzikosma, D. G., Voudrias, E. A. (2007): Simulation of polychlorinated biphenyls transport in the vadose zone. *Environ. Geol.* 53, 211–220.

Cipakova, A., Mitro, A. (1997): Influence of agrochemical characteristics on ^{85}Sr and ^{137}Cs sorption in soil samples from the localities around nuclear power plants in Slovak Republic. *J. Radioecology* 5, 3–8.

Cornelis, W. M., Corluy, J., Medina, H., Diaz, J., Hartmann, R., Van Meirvenne, M., Ruiz, M. E. (2006): Measuring and modelling the soil shrinkage characteristic curve. *Geoderma* 137, 179–191.

de Jonge, H., Jacobsen, O. H., de Jonge, L. W., Moldrup, P. (1998): Particle-facilitated transport of prochloraz in undisturbed sandy loam soil columns. *J. Environ. Qual.* 27, 1495–1503.

de Jonge, L. W., Moldrup, P., Rubæk, G. H., Schelde, K., Djurhuus, J. (2004): Particle leaching and particle-facilitated transport of phosphorus at field scale. *Vadose Zone J.* 3, 462–470.

Dekker, L. W., Ritsema, C. J. (1994): How water moves in a water repellent sandy soil. I. Potential and actual water repellency. *Water Resour. Res.* 30, 2507–2517.

Dohnal, M., Dusek, J., Vogel, T., Cislerova, M., Lichner, L., Stekauerova, V. (2009): Ponded infiltration into soil with biopores – field experiment and modeling. *Biologia* 64, 580–584.

Dolezal, F., Zumr, D., Vacek, J., Zavadil, J., Battilani, A., Plauborg, F., Hansen, S., Abrahamsen, P., Bizik, J., Takac, J., Mazurczyk, W., Coutinho, J., Stekauerova, V. (2007): Dual permeability soil water dynamics and water uptake by roots in irrigated potato fields. *Biologia* 62, 552–556.

Dubus, I. G., Brown, C. D., Beulke, S. (2003): Sensitivity analyses for four pesticide leaching models. *Pest Manag. Sci.* 59, 962–982.

Dusek, J., Vogel, T., Lichner, L., Cipakova, A., Dohnal, M. (2006): Simulated cadmium transport in macroporous soil during heavy rainstorm using dual-permeability approach. *Biologia* 61(Suppl. 19), S251–S254.

Dusek, J., Gerke, H. H., Vogel, T. (2008): Surface boundary conditions in 2D dual-permeability modeling of tile drain bromide leaching. *Vadose Zone J.* 7, 1241–1255.

Elinder, C. G. (1992): Cadmium as an environmental hazard. *IARC Sci. Pub.* 1118, 123–132.

EPA (1985): Cadmium contamination of the environment: An assessment of nationwide risk. EPA-440/4–85-023, U.S. Environmental Protection Agency, Office of Water Regulations and Standards, Washington, DC, USA.

Farenhorst, A., Topp, E., Bowman, B. T., Tomlin, A. D. (2000): Earthworm burrowing and feeding activity and the potential for atrazine transport by preferential flow. *Soil Biol. Biochem.* 32, 479–488.

Gerke, H. H. (2006): Preferential flow descriptions for structured soils. *J. Plant Nutr. Soil Sci.* 169, 382–400.

Gerke, H. H., Köhne, J. M. (2002): Estimating hydraulic properties of soil aggregate skins from sorptivity and water retention. *Soil Sci. Soc. Am. J.* 66, 26–36.

Gerke, H. H., van Genuchten, M. Th. (1993a): A dual-porosity model for simulating the preferential movement of water and solutes in structured porous media. *Water Resour. Res.* 29, 305–319.

Gerke, H. H., van Genuchten, M. Th. (1993b): Evaluation of a first-order water transfer term for variably saturated dual-porosity models. *Water Resour. Res.* 29, 1225–1238.

Gerke, H. H., van Genuchten, M. Th. (1996): Macroscopic representation of structural geometry for simulating water and solute movement in dual-porosity media. *Adv. Water Resour.* 19, 343–357.

Gerke, H. H., Dusek, J., Vogel, T., Köhne, J. M. (2007): Two-dimensional dual-permeability analyses of a bromide tracer experiment on a tile-drained field. *Vadose Zone J.* 6, 651–667.

Hansen, H. C. B., Jensen, M. B., Magid, J. (1999): Phosphate sorption to matrix and fracture wall materials in a Glossaqualf. *Geoderma* 90, 243–261.

Herrero, T. C., Martin, L. F. L. (1993): Evaluation of cadmium levels in fertilized soils. *Bull. Environ. Contam. Toxicol.* 50, 61–68.

Ilina, T., Panfilov, M., Bues, M., Panfilova, I. (2008): A pseudo two-phase model of colloid transport in porous media. *Transp. Porous Media* 71, 311–329.

Ingwersen, J., Streck, T. (2006): Modeling the environmental fate of cadmium in a large waste water irrigation area. *J. Environ. Qual.* 35, 1702–1714.

Jacobsen, O. H., Moldrup, P., Larsen, C., Konnerup, L., Petersen, L. W. (1997): Particle transport in macropores of undisturbed soil columns. *J. Hydrol.* 196, 185–203.

Jury, W. A., Roth, K. (1990): Transfer functions and solute movement through soils: Theory and applications. Birkhäuser Verlag, Basel, Switzerland.

Köhne, J. M., Gerke, H. H., Köhne, S. (2002a): Effective diffusion coefficient of soil aggregates with surface skins. *Soil Sci. Soc. Am. J.* 66, 1430–1438.

Köhne, J. M., Köhne, S., Gerke, H. H. (2002b): Estimating the hydraulic functions of dual-permeability models from bulk soil data. *Water Resour. Res.* 38, 1121, doi:10.1029/2001 WR000492.

Köhne, J. M., Mohanty, B. P., Simunek, J., Gerke, H. H. (2004): Numerical evaluation of a second-order water transfer term for variably saturated dual-permeability models. *Water Resour. Res.* 40, W07409, doi:10.1029/2004 WR003285.

Kovacova, V. (2000): Estimation of adsorption parameters of cadmium for choiced types of soils (in Slovak). *J. Hydrol. Hydromech.* 48, 367–377.

Laegsmand, M., Villholth, K. G., Ullum, M., Jensen, K. H. (1999): Processes of colloid mobilization and transport in macroporous soil monoliths. *Geoderma* 93, 33–59.

Laegdsmand, M., Moldrup, P., De Jonge, L. W. (2007): Modelling of colloid leaching from unsaturated, aggregated soil. *Eur. J. Soil Sci.* 58, 692–703.

Lennartz, B., Michaelsen, J., Wichtmann, W., Widmoser, P. (1999): Time variance analysis of preferential solute movement at a tile-drained field site. *Soil Sci. Soc. Am. J.* 63, 39–47.

Levin, J. M., Herman, J. S., Hornberger, G. M., Saiers, J. E. (2006): Colloid mobilization from a variably saturated, intact soil core. *Vadose Zone J.* 5, 564–569.

Lichner, L. (1998): Cadmium transport in a loamy soil as influenced by macropore flow (in Slovak). *J. Hydrol. Hydromech.* 46, 207–217.

Lichner, L., Cipakova, A. (2002): Cadmium distribution coefficients and Cd transport in structured soils. *Rostlinná výroba* 48, 96–100.

Lichner, L., Houskova, B. (2001): Temporal variability of hydraulic conductivity of macropore soils. *Acta Hydrologica Slovaca* 2, 1–8.

Lichner, L., Dlapa, P., Sir, M., Cipakova, A., Houskova, B., Fasko, P., Nagy, V. (2006): The fate of cadmium in field soils of the Danubian lowland. *Soil Tillage Res.* 85, 154–165.

Marcus, Y. (1997): Ion Properties. Marcel Dekker, New York.

Massoudieh, A., Ginn, T. R. (2007): Modeling colloid-facilitated transport of multi-species contaminants in unsaturated porous media. *J. Contam. Hydrol.* 92, 162–183.

Moradi, A., Abbaspour, K. C., Afyuni, M. (2005): Modelling field-scale cadmium transport below the root zone of a sewage sludge amended soil in an arid region in Central Iran. *J. Contam. Hydrol.* 79, 187–206.

Pierce, F. J., Dowdy, R. H., Grigel, D. F. (1982): Concentrations of six trace metals in some major Minnesota Soil Series. *J. Environ. Qual.* 11, 416–422.

Pivetz, B. E., Steenhuis, T. S. (1995): Soil matrix and macropore biodegradation of 2,4-D. *J. Environ. Qual.* 24, 564–570.

Rasmussen, L. H., Ernstsen, V., Hansen, H. C. B. (2001): Redoximorphic macropore environments in an Agrudalf. *Nord. Hydrol.* 32, 333–352.

Ray, C., Vogel, T., Dusek, J. (2004): Modeling depth-variant and domain-specific sorption and biodegradation in dual-permeability media. *J. Contam. Hydrol.* 70, 63–87.

Ritsema, C. J., Dekker, L. W. (2000): Preferential flow in water repellent sandy soils: principles and modeling implications. *J. Hydrol.* 231/232, 308–319.

Roulier, S., Baran, N., Mouvet, C., Stenemo, F., Morvan, X., Albrechtsen, H. J., Clausen, L., Jarvis, N. (2006): Controls on atrazine leaching through a soil-unsaturated fractured limestone sequence at Brevilles, France. *J. Contam. Hydrol.* 84, 81–105.

Schaap, M. G., Leij, F. J., van Genuchten, M. Th. (2001): ROSETTA: a computer program for estimating soil hydraulic parameters with hierarchical pedotransfer functions. *J. Hydrol.* 251, 163–176.

Schelde, K., de Jonge, L. W., Kjaergaard, C., Laegdsmand, M., Rubæk, G. H. (2006): Effects of manure application and plowing on transport of colloids and phosphorus to tile drains. *Vadose Zone J.* 5, 445–458.

Selim, H. M., Buchter, B., Hinz, C., Ma, L. (1992): Modeling the transport and retention of cadmium in soils: Multireaction and multicomponent approaches. *Soil Sci. Soc. Am. J.* 56, 1004–1015.

Seuntjens, P., Tirez, K., Simunek, J., van Genuchten, M. Th., Cornelis, C., Geuzens, P. (2001): Aging effects on cadmium transport in undisturbed contaminated sandy soil columns. *J. Environ. Qual.* 30, 1040–1050.

Seuntjens, P., Mallants, D., Simunek, J., Patyn, J., Jacques, D. (2002): Sensitivity analysis of physical and chemical properties affecting field-scale cadmium transport in a heterogeneous soil profile. *J. Hydrol.* 264, 185–200.

Shipitalo, M. J., Gibbs, F. (2000): Potential of earthworm burrows to transmit injected animal wastes to tile drains. *Soil Sci. Soc. Am. J.* 64, 2103–2109.

Singh, B. R. (1994): Trace element availability to plants in agricultural soils, with special emphasis on fertilizer imputs. *Environ. Rev.* 2, 133–146.

Steenhuis, T. S., Ritsema, C. J., Dekker, L. W. (1996): Introduction to Special Issue: Fingered flow in unsaturated soil: from nature to model. *Geoderma* 70, 83–85.

Stenemo, F., Lindahl, A. M. L., Gardenas, A., Jarvis, N. (2007): Meta-modeling of the pesticide fate model MACRO for groundwater exposure assessments using artificial neural networks. *J. Contam. Hydrol.* 93, 270–283.

Streck, T., Richter, J. (1997): Heavy metal displacement in a sandy soil at the field scale: II. Modeling. *J. Environ. Qual.* 26, 56–62.

van Genuchten, M. Th., Schaap, M. G., Mohanty, B. P., Simunek, J., Leij, F. J. (1999): Modeling flow and transport processes at the local scale, in Feyen, J., Wiyo, K. (eds.): Modelling of transport processes in soils at various scales in time and space. Leuven, Belgium.

Vanderborght, J., Vereecken, H. (2007): Review of Dispersivities for Transport Modeling in Soils. *Vadose Zone J.* 6, 29–52.

Vanderborght, J., Gähwiller, P., Flühler, H. (2002): Identification of transport processes in soil cores using fluorescent tracers. *Soil Sci. Soc. Am. J.* 66, 774–787.

Vervoort, R. W., Radcliffe, D. E., West, L. T. (1999): Soil structure development and preferential solute flow. *Water Resour. Res.* 35, 913–928.

Villholth, K. G., Jarvis, N. J., Jacobsen, O. H., de Jonge, H. (2000): Field investigations and modeling of particle-facilitated pesticide transport in macroporous soil. *J. Environ. Qual.* 29, 1298–1309.

Vogel, T., Huang, K., Zhang, R., van Genuchten, M. Th. (1996): The HYDRUS code for simulating One-Dimensional Water Flow, Solute Transport, and Heat Movement in Variably-Saturated Media, Version 5.0. Research Report No. 140, U.S. Salinity Laboratory, ARS, USDA, Riverside, CA, USA.

Vogel, T., Gerke, H. H., Zhang, R., van Genuchten, M. Th. (2000): Modeling flow and transport in a two-dimensional dual-permeability system with spatially variable hydraulic properties. *J. Hydrol.* 238, 78–89.

Vogel, T., van Genuchten, M. Th., Cislerova, M. (2001): Effect of the shape of soil hydraulic functions near saturation on variably-saturated flow predictions. *Adv. Water Resour.* 24, 133–144.

Vogel, T., Dohnal, M., Dusek, J. (2004): Description of the available bench scale modeling approaches with emphasis on the input data requirements and output data structure. Deliverable COMPUTE1.1, Integrated Project AquaTerra.

Vogel, T., Lichner, L., Dusek, J., Cipakova, A. (2007): Dual-continuum analysis of a cadmium tracer field experiment. *J. Contam. Hydrol.* 92, 50–65.

Vos, G., Lammers, H., Kan, C. A. (1990): Cadmium and lead in muscle tissue and organs of broilers, turkeys and spent hens and in mechanically deboned poultry meat. *Food Addit. Contam.* 7, 83–92.

Wang, Z., Feyen, J., Ritsema, C. J. (1998): Susceptibility and predictability of conditions for preferential flow. *Water Resour. Res.* 34, 2169–2182.

WRB (1998): World reference base for soil resources. World Soil Resources Reports, No. 84, FAO, Rome.

Zurmühl, T., Durner, W. (1998): Determination of parameters for bimodal hydraulic functions by inverse modeling. *Soil Sci. Soc. Am J.* 62, 874–880.

Effect of plastic mulch on water flow and herbicide transport in soil cultivated with pineapple crop: A modeling study, Agricultural Water Management, 2010.

Agricultural Water Management 97 (2010) 1637–1645

Contents lists available at ScienceDirect

Agricultural Water Management

journal homepage: www.elsevier.com/locate/agwat

Effect of plastic mulch on water flow and herbicide transport in soil cultivated with pineapple crop: A modeling study

J. Dusek[a,*], C. Ray[b], G. Alavi[b], T. Vogel[a], M. Sanda[a]

[a] Czech Technical University in Prague, Faculty of Civil Engineering, Thakurova 7, 166 29 Prague, Czech Republic
[b] Civil and Environmental Engineering and Water Resources Research Center, University of Hawaii at Manoa, Honolulu, HI, USA

ARTICLE INFO

Article history:
Received 15 March 2010
Accepted 19 May 2010
Available online 17 June 2010

Keywords:
Pesticide transport in soil
Bromacil
Tropical soil
Soil water flow
Field leaching
Irrigation

ABSTRACT

In Hawaii, pineapple is typically grown in raised beds covered with impervious plastic mulch. Field measurements of a commonly used herbicide (bromacil) mass beneath mulch-covered pineapple beds and inter-bed open areas revealed that open areas contained a mass of bromacil about 3.5 times greater than was originally applied, based on label instructions, to the entire field. The broadcast bromacil ended up in the inter-bed open areas through water runoff from the plastic mulch covering the pineapple beds. The objective of this study was to evaluate the impact of surficial management on water dynamics and bromacil concentration in the soil on a pineapple plantation using the one- (1D) and two-dimensional (2D) flow and transport models. Flow and transport processes were simulated in a 2D vertical cross-section perpendicular to the plant rows. The 1D simulation was limited to the open inter-bed areas. Several simulation scenarios were proposed to evaluate the effect of plastic mulch on bromacil transport in soil. In our simplified approach, the water and solute boundary fluxes for the non-covered areas were increased to simulate the water and solute contribution from the plastic mulch surface. The simulation results were compared with field observations of soil water potentials and resident bromacil concentration profiles. The field and laboratory-measured hydraulic and transport parameters were used for all simulation scenarios. Reasonably good agreement between the model-predicted and observed soil water potentials and bromacil concentration profiles was obtained. Biased 1D and 2D results were predicted when the water runoff from plastic mulch was neglected. The 1D approach to quantify bromacil transport beneath the inter-bed open areas seemed to be sufficient in case the water runoff from the mulch was taken into account.

1. Introduction

Pineapple crop is grown by several companies on the islands of Oahu and Maui, in Hawaii, USA, where it is a major part of the agricultural economy, and is sold as fresh fruits in the USA market. Bromacil is a major herbicide used for weed control over the crop cycle (pineapples remain on the field for about 36–48 months, which corresponds to two or three fruit crop cycles). It is a systemic uracil herbicide that non-selectively inhibits plant photosynthesis and may persist up to 6 months in common agricultural soils. The detection of bromacil in depths below the root zone and in groundwater has prompted an evaluation of farming practices with the goal of reducing leaching (e.g., Li et al., 2001; Zhu and Li, 2002; Alavi et al., 2008).

In Hawaii, pineapple is grown in raised beds covered with plastic mulch to prevent the volatilization of nematicides injected into the soil to control plant-parasitic nematodes. Usually, there are two pineapple rows under each mulch sheet. Open areas between the sheets effectively comprise about 50% of the total area. If an herbicide is uniformly (broadcast) applied to the fields at the label dose, an excess dose arrives on the open areas because the herbicide falling on the plastic mulch sheet moves to open areas with rain or overhead sprinkler irrigation water. A recent investigation indicated that a large part of the bromacil broadcast ended up in the open, uncovered areas (Alavi et al., 2008). In their work, the calculated mass of residual bromacil from the sampled zone in the uncovered inter-bed areas was on average 3.5 times higher than the dose applied to the field on an areal basis.

Mathematical models of water and chemical transport are effective tools to evaluate the impact of modifications in farming practices aimed at reducing herbicide leaching. Most models currently used for pineapple plantations are one-dimensional (1D). Two-dimensional (2D) models are however more suitable because of the spatial configuration of the farming methods on pineapple plantations, and the ability of 2D models to make spatial distribution predictions of water and chemicals in the soil profile.

* Corresponding author. Tel.: +420 22435 4355; fax: +420 22431 0782.
E-mail address: dusek@mat.fsv.cvut.cz (J. Dusek).

0378-3774/$ – see front matter © 2010 Elsevier B.V. All rights reserved.
doi:10.1016/j.agwat.2010.05.019

In this study, S1D and S2D numerical models, developed at the Czech Technical University in Prague, were used to model water flow and herbicide transport underneath a pineapple crop. The 1D and 2D models are based on Richards' equation and an advection–dispersion equation (Vogel et al., 2000, 2007). The models have previously been used for water flow and chemical transport in various soils (Vogel et al., 2000; Dusek et al., 2006; Gerke et al., 2007) including those with macropores (Ray et al., 2004; Dolezal et al., 2007; Dusek et al., 2008).

The aim of this study was to evaluate the impact of surficial management on water dynamics and bromacil concentration in the soil on a pineapple plantation using the S1D and S2D models. Field- and laboratory-derived soil hydraulic and transport parameters were used for simulations while field measurements of water dynamics and bromacil leaching pattern were compared to the 1D and 2D model predictions. In addition, the results of the 1D and 2D simulations were cross-compared to analyze the impact of model dimensionality on predictions of water and bromacil movement.

2. Materials and methods

2.1. Site description and experimental set-up

A detailed description of the experimental site is given by Alavi et al. (2008) and thus the description presented here will be limited to the most important characteristics of the field leaching experiment. The experiment was conducted in a pineapple field in the Kunia area of central Oahu, Hawaii. The pineapple cultivar planted at the field was *Smooth Cayenne*. The soil in the field is an Oxisol of the Wahiawa series. The soil surface is nearly level to moderately sloping. The soil is dark reddish-brown silty clay and has a subangular blocky structure. The substratum is highly weathered basalt. The organic carbon content (f_{oc}) of surficial Oxisols ranges from 1.6% to 3.9% (Peterson et al., 1985). It decreases with depth and reaches less than 1% at a depth of 1 m, and is as low as 0.03% by 10 m. The mean annual rainfall is about 1500 mm (Giambelluca et al., 1986) with most rainfall occurring between November and March. The mean annual soil temperature is 22 °C.

The leaching study was conducted in a 600 m × 200 m pineapple plot. Initially, the field was covered with plant mulch from a previous planting. Subsequently, the plot was deep plowed. During the installation of the beds and placement of the plastic mulch, a drip irrigation tubing was placed at a depth of 0.05 m in the middle part of the raised beds under the plastic mulch. Soon after planting (June 23, 2002), 20 mm of irrigation water was applied using a movable overhead sprinkler to set the pineapple crowns so that roots could develop. Following planting, the field was sprayed with 2.25 kg ai (active ingredient)/ha bromacil (June 26, 2002). The drip irrigation started within a month after overhead sprinkler irrigation. It was calibrated to apply water at the rate of 3 mm/h based on antecedent rainfall. A second bromacil application followed on June 11, 2003.

Once the plants were established, four sites were selected between the pineapple rows for monitoring soil water potentials. Conventional tensiometers (Soilmoisture Equipment Corp., Santa Barbara, California) were vertically installed at depths of 0.15 m, 0.30 m, 0.45 m, and 0.60 m. At each site, 8–11 tensiometers were installed. They were read manually once a week or fortnight from July 20, 2002 to February 9, 2003 using a digital tensimeter from Soil Measurement Systems of Tucson, Arizona. This scarcity of tensiometer readings was due to site access and limitation on manpower available for measurement. Soil samples were collected once before the bromacil application (reference concentration on March 1, 2002) and on three occasions after the first bromacil application. The final sampling was carried out after the second bromacil application (June 11, 2003). Details of the sampling and pesticide analytical procedures used can be found in Alavi et al. (2008).

2.2. Measurement of soil hydraulic properties

Prior to planting, four soil pits were dug across the study plot. Three undisturbed soil cores, each 72 mm in diameter and 42 mm long, were taken at depths of 0.02 m, 0.15 m, 0.35 m, 0.60 m, and 1 m. Soil water content was determined for each core using a box with hanging water column at pressures of −0.1 kPa, −0.7 kPa, −1 kPa, −2 kPa, and −4.2 kPa and in a pressure chamber at pressures of −10 kPa, −50 kPa, −100 kPa, and −350 kPa (Klute, 1986). The bulk density was estimated for each soil core. At the same depths, the near saturated hydraulic conductivity was determined *in situ* using a tension infiltrometer (Ankeny et al., 1988) for water potentials ranging from −0.01 kPa to −1 kPa.

2.3. Sorption and degradation experiments

The laboratory sorption and degradation experiments of bromacil were conducted at the University of Hawaii.

Core samples collected prior to planting were used for sorption measurements. A total of 64 samples (eight sites and eight depth intervals) were analyzed. Each sample was equilibrated with three to four bromacil concentration solutions. For equilibration, 5 g of dry soil was added to 20 ml of solution having bromacil concentrations of 0.5 mg/l, 5 mg/l, or 50 mg/l. After mixing the soil in the solution inside 40 ml vials, the vials were loaded into a rotary shaker. The rotation speed was 30 rpm and the mixing time was 18 h. After that, the samples were centrifuged at 5000 rpm for 20 min and the supernatant was filtered through a 0.45-μm glass fiber filter and analyzed by high performance liquid chromatography (HPLC). The distribution coefficients (K_D) were estimated by plotting residual concentration in the liquid phase versus the adsorbed concentration.

Bromacil degradation was studied for soil samples from depth intervals of 0–0.3 m, 0.3–0.6 m, and 0.6–0.9 m. Aerobic degradation tests were conducted in a dark room at a temperature of 22 °C ± 3 °C. In total, 36 soil samples were collected over a period of 23 weeks. The samples were watered weekly to keep the water content close to −10 kPa potential for optimal microbial activity. Approximately 10 g of each subsample was taken at 7–51 day intervals. A total of 96 subsamples were analyzed for residual bromacil concentration.

2.4. Climate data

Rainfall data were collected from the nearest meteorological station (operated by the National Oceanic and Atmospheric Administration (NOAA) at the Wheeler Air Force Base, Oahu, Hawaii) located less than 2 km from the experimental site. One-hour rainfall intensities were used for the modeling. During the summer of 2003 when rain data from this station was missing, rainfall data from the next nearest station, NOAA's Mililani station, which is about 7 km from the study site, was used. Drip irrigation amounts were derived from the actual irrigation record of water applied throughout the study period. Daily potential evapotranspiration (ET) was based on the pan evaporation recorded at the Honolulu International Airport meteorological station, which is about 20 km from the study site.

2.5. Model description

The S1D and S2D models are based on Richards' equation for water flow and the advection–dispersion equation for reactive solute transport. Both models use the Galerkin linear finite element

method for numerical solution of the flow and transport equations (Vogel et al., 2000). Water flow is given by:

$$C\frac{\partial h}{\partial t} = \nabla \cdot (K\nabla h) + \nabla \cdot (K\nabla z) \; - \; S \tag{1}$$

where h is the soil water potential (m), K is the hydraulic conductivity tensor (m/s), C is the specific water capacity (1/m), S is the sink term accounting for the root water uptake (1/s) (Feddes et al., 1978), z is the vertical coordinate taken to be positive upward (m), and t is the time (s). The modified van Genuchten–Mualem model (Vogel and Cislerova, 1988; Vogel et al., 2001), which is used to describe the soil hydraulic functions, introduces a non-zero air entry value, h_s (m). It was shown that the modified approach provides more adequate prediction of the unsaturated hydraulic function especially near saturation (Vogel et al., 2001).

Transport of reactive solutes is described by the advection–dispersion equation as follows:

$$\frac{\partial\left(\theta R c\right)}{\partial t} = \nabla \cdot \left(\theta D \nabla c\right) - \nabla \cdot (qc) - \lambda_w \theta c - \lambda_s \rho s - S c_s \tag{2}$$

where c is the solute concentration (kg/m^3), θ is the soil water content (−), D is the dispersion coefficient tensor (m^2/s) comprising the molecular diffusion and dispersion, q is the soil water flux (m/s), λ_w and λ_s are the first-order decay coefficients (1/s) for the liquid and solid phases, respectively, c_s is the solute taken up by plant roots (kg/m^3), s is the adsorbed concentration (kg/kg), and ρ is the soil bulk density (kg/m^3). The linear equilibrium sorption is incorporated through the dimensionless retardation factor R (−), which is directly related to the distribution coefficient K_D (m^3/kg):

$$R = 1 + \frac{\rho}{\theta} K_D \tag{3}$$

The hydraulic conductivity and dispersion tensors in 2D were both assumed to be isotropic, and hence fully determined by scalar functions. For the S1D model, these two variables are scalar functions. More details on the numerical models can be found in Vogel et al. (2000, 2004). To compare the simulated bromacil concentration with observed values, the simulated solute concentrations (i.e. in the liquid phase) were converted into total concentration expressed in ng/g of dry soil. For this conversion, soil bulk density, water content, and distribution coefficient were used (Alavi et al., 2007).

2.6. Parameterization of the models

The models were parameterized using measured data and run without calibration (Table 1). The one-dimensional model considered a profile depth of 3 m and it was assumed to be located beneath the center of the inter-bed area. The soil profile consisted of five different soil layers. The depth of soil layers ranged from 0.05 m to 2.2 m (Table 1). Altogether, 300 nodes were used to numerically discretize the 3-m domain.

For two-dimensional scenarios, the soil profile was 3 m in depth and 0.54 m wide. The pineapple row was elevated by 0.05 m above the inter-bed area. The drip tube was located 0.05 m beneath the pineapple row. Details of the flow domain are shown in Fig. 1. The finite element mesh was refined near the soil surface, at the soil horizon interfaces and in the vicinity of the dripper where high water fluxes were expected. Four observation points were selected beneath the center of the inter-bed area at 0.15 m, 0.30 m, 0.45 m, and 0.60 m depths. The profile was divided into triangular finite elements representing 0.01 m thick vertical slices through the system. It was oriented perpendicularly to the principle pineapple row direction and contained one pineapple plant and one dripper section. The axial symmetry enabled us to simulate only one-half of the original flow domain.

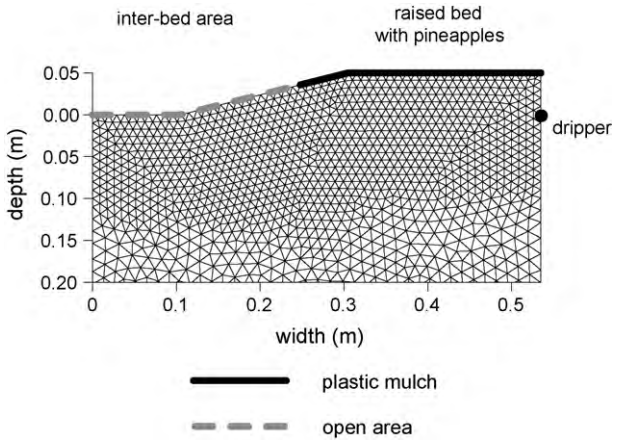

Fig. 1. Scheme of the surface configuration and detail of the two-dimensional finite element mesh.

The RETC program (van Genuchten et al., 1991) was used to simultaneously fit the expressions of van Genuchten (1980) and Mualem (1976) functions to observed median values of water retention and unsaturated hydraulic conductivity in each depth. An optimization was performed using the least sum of squares method to estimate the soil hydraulic parameters. The estimated soil hydraulic parameters are listed in Table 1.

The pineapple root zone is usually shallow thus the deepest level with roots (0.30 m) was used (Schneider et al., 1992). A linear decrease of the root density from soil surface to the root depth was adopted. Potential evapotranspiration rates were estimated from measured pan evaporation data using a coefficient of 0.2 (Gavenda et al., 1996). The estimated potential evapotranspiration rates ranged from 0.1 mm/day to 3.8 mm/day. Cultivated pineapple crop is known to be highly productive in water limited availability conditions (Ekern, 1965). For instance, Azevedo et al. (2007) estimated pineapple evapotranspiration in Brazil in the range from 2.8 mm/day to 6.0 mm/day during the full crop cycle. Relatively low values for parameters that govern the water stress function (Feddes et al., 1978) were used as the field was irrigated. This resulted in similar values of the potential evapotranspiration rates and actual evapotranspiration rates determined by the numerical models.

Table 1
Measured (bulk density, θ_s, f_{oc}) and estimated (K_s, θ_r, α, n, l) soil parameters.

Depth (m)	Bulk density (g/cm^3)	f_{oc} (%)	K_s (m/day)	h_s (m)	θ_s (−)	θ_r (−)	α (m^{-1})	n (−)	l (−)	K_D (cm^3/g)
0–0.05	1.39	1.78	1.0	−0.359	0.54	0.17	0.1	1.4	6	4.97
0.05–0.25	1.19	1.49	1.4	−0.049	0.51	0.26	2.3	1.1	6	4.81
0.25–0.45	1.26	0.90	1.7	−0.030	0.51	0.32	1.8	1.3	6	4.6
0.45–0.8	1.33	0.61	1.0	0.0	0.51	0.38	1.9	2.1	6	4.21
0.8–3.0	1.40	0.56	1.4	−0.038	0.51	0.38	2.3	1.6	6	2.59

The parameters K_s, θ_r, α, n, and l were estimated using the RETC program with the van Genuchten/Mualem model. The air entry values h_s were estimated as well. The distribution coefficient K_D is based on laboratory measurement.
θ_s and θ_r, saturated and residual volumetric water content, respectively; α and n, fitting parameters; h_s, air entry value; l tortuosity factor; K_s, saturated hydraulic conductivity.

The decreasing trend of lab-measured K_D with depth which was obtained closely corresponds with the decreasing organic carbon content with depth. The distribution coefficients are presented in Table 1.

The laboratory degradation data showed considerable variations in concentrations among the samples and with time. This could be caused by analytical errors or by soil heterogeneity. Therefore, the field degradation half-life was used for all simulation scenarios knowing that these values can be somewhat shorter than lab values, as the chemical is exposed to other loss mechanisms. The half-life was determined from its total mass found in each location over the set of three sampling events. The average half-life found at various locations for these three sampling events was 250 days ± 50 days. Thus the bromacil degradation half-life used for the simulations was set to 250 days.

The longitudinal dispersivity was assumed to be 0.2 m, while the transverse dispersivity for the 2D model was fixed at 0.02 m. The molecular diffusion coefficient in water was set to 5.4×10^{-5} m^2/day (Russo et al., 1997). It was further assumed that no bromacil uptake by the pineapple crop occurred, i.e. $c_s = 0$.

2.7. Method of identifying effects of different surficial management

The following one- and two-dimensional scenarios were considered:

1. "Original" – reference scenario assuming a pineapple plantation with plastic mulch cover but the impervious sheet does not increase the water and bromacil input in the open areas.
2. "Increased 1" – a scenario with the spatial field configuration according to Fig. 1. Plastic mulch covers about 53% of the total field area which yields a value of 2.1 for the ratio of open area to plastic mulch area. Hence the precipitation and application inputs for the open areas were increased by a factor of 2.1. The open areas receive both rain that falls directly on the uncovered area and also rain that falls on the mulch-covered area. The latter ends up in the open area through surface runoff.
3. "Increased 2" – a scenario where precipitation and mass of applied bromacil were multiplied by 2.8. Such a multiplication factor translates into about 64% area coverage of the total field area by plastic mulch. This scenario serves as an intermediate scenario between "increased 1" and "increased 3".
4. "Increased 3" – a scenario where precipitation and bromacil application mass were increased by a factor of 3.5 as observed from measured bromacil mass in the field (Alavi et al., 2008). The "increased 3" scenario is proposed to evaluate the most pronounced runoff from plastic mulch on bromacil leaching through the soil profile. A value of 3.5 would imply that about 71% of the total field area is covered by plastic mulch (much wider plastic mulch than the one used in this case).

2.8. Statistical analysis

Graphical comparisons of simulated and measured soil water potential and concentration were made to observe the general agreement between the models and the field measurements. Model performance in predicting quantitatively the soil water potential and concentration was tested using the root mean square error (RMSE). RMSE is defined as:

$$\mathrm{RMSE} = \left[\frac{1}{N-1} \left(\sum_{i=1}^{N} (o_i - m_i)^2 \right) \right]^{1/2} \quad (4)$$

where N is the number of measurements, o and m are the observed and simulated responses, respectively. The unit of the RMSE criterion is identical as the compared variables (i.e. soil water potential and concentration). Smaller value of RMSE indicates better agreement between model prediction and experimental data. If the simulated and the observed values are the same, the RMSE is zero (the lower limit).

2.9. Initial and boundary conditions

The simulation period lasted from March 1, 2002 to August 28, 2003. A linear transition between initial soil water potential at the top ($h = -300$ cm) and the bottom ($h = 0$ cm) was considered at the start of simulation. The simulation started 4 months before the actual pesticide application so that the soil water profile equilibrated to field conditions at the time of pesticide application. An open area was treated as "atmospheric boundary condition" (Vogel, 1987; Dusek et al., 2008) where natural rainfall, irrigation and evapotranspiration took place. If the infiltration capacity of the uppermost soil layer is exceeded, the flux condition (Neumann type) is switched to a pressure boundary condition (Dirichlet type). The surplus water will temporarily be stored and allowed to resume infiltrating at the end of the irrigation event. This procedure eliminated potential surface runoff and routing. A no-flow boundary was considered for the whole length of the impervious plastic mulch (2D simulation scenarios). Fig. 1 depicts the schematic layout of boundary condition configuration on the soil surface. Free drainage (unit pressure gradient) was applied as the bottom boundary condition at a depth of 3 m. Flux condition (Neumann type) was assumed for the drip tube (Bear and Verruijt, 1987) for the 2D simulation scenarios.

For the solute transport simulation, bromacil was assumed to have been applied on the open areas where natural rainfall conditions were assumed. A pulse of bromacil diluted in 20 mm of water was applied for 30 min on June 26, 2002. This concentration equaled an application rate of 2.25 kg ai/ha bromacil (the current application rate for weed control at the study site) and was used for the "original" scenarios. The corresponding application rates for the three "increased" scenarios were 4.74 kg ai/ha, 6.30 kg ai/ha and 7.88 kg ai/ha, respectively. Initial concentration of bromacil in the soil profile was derived from the pre-application measurement of concentration (March 1, 2002). The bottom boundary was assumed to be a free-exit boundary (zero concentration gradient).

3. Results

Fig. 2 depicts the comparison of the simulated two-dimensional model to the observed soil water potentials at two depths in the inter-bed areas. The "increased" scenarios have smaller RMSE values, thus showing a closer agreement with measured data than the "original" scenario (Table 2). During the late summer period (August–September 2002), the "original" simulations show much drier conditions than that observed resulting in poor agreement and RMSE values higher than 150 cm. Aside from the late summer period, the water content was generally high throughout the soil profile because of high rainfall. The simulated response to rainfall was fast at all soil layers which can be explained by the high hydraulic conductivity assumed (Table 1).

Fig. 3 displays measured and simulated (1D) bromacil profiles beneath the inter-bed area. A large variation in bromacil concentration data was observed in the topsoil (0–0.25 m depth). Similarly, large variation of pesticide concentrations in tropical soils was previously reported by Dusek et al. (2010). The bromacil concentration of the topsoil is underestimated significantly on April 29, 2003 for all simulation scenarios. Observed bromacil concentration in the topsoil indicates that bromacil did not decay substantially over a

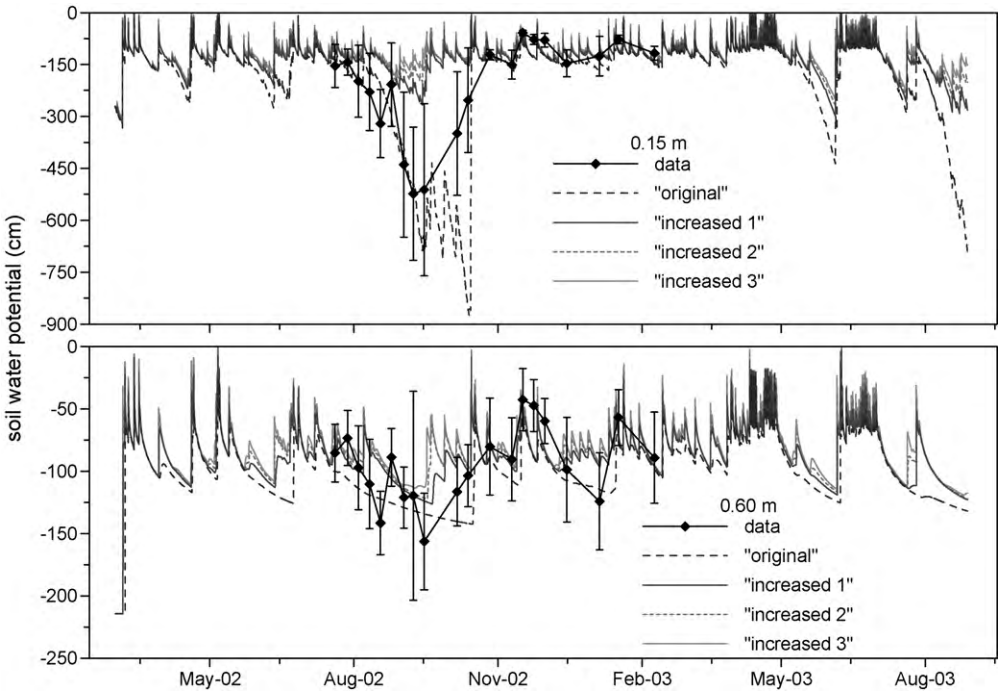

Fig. 2. Comparison of simulated two-dimensional (2D) and measured (mean values and standard deviations) values of soil water potentials at two depths below the inter-bed area. Lines connecting tensiometric data (symbols) represent only guides to field soil water potential development.

period of 10 months. The simulated bromacil concentrations in the deeper soil layers on July 23, 2002 and October 23, 2002 resulted from the reference concentrations used as the initial condition. Table 2 presents the criteria of bromacil comparison with data for all proposed simulation scenarios ("increased" and "original" in 1D and 2D). The "increased" scenarios always delivered improved agreement over the "original" simulations. The RMSE criterion is not a dimensionless measure of the fit; it is influenced by the absolute concentration values in the soil profile.

The measured and simulated (2D) bromacil profile beneath the plastic mulch is shown in Fig. 4. The results reflect the last sampling (August 27, 2003) conducted more than 2 months after the second bromacil application (June 11, 2003). Close agreement between simulated and measured bromacil concentration profiles was obtained. Simulated elevated bromacil concentrations below 1.7 m depth were due to the bromacil initially present, not by downward leaching.

Different transport regimes between the four simulation scenarios were predicted for 1D and 2D simulations (Table 3). It is obvious that with increasing bromacil input, the leachate fraction from the simulated domain also increases. The dissipated bromacil mass in the domain, evaluated in respect to total mass, exhibits a declining trend with increasing bromacil application (Table 3). However, degradation was enhanced for "increased" scenarios in absolute terms since the degradation process is based on the first-order model (the dissipated mass depends on the initial bromacil mass). Different leaching patterns of bromacil can also be clearly elucidated using the bromacil balance in the simulated domain. The "original" scenario predicted a decrease of bromacil mass in the soil profile during the simulated period while the "increased" scenarios suggested a net increase of bromacil mass in the profile. The measured bromacil profiles showed an increase of bromacil mass in the soil profile over the study period of eighteen months as well.

Table 2
One- (1D) and two-dimensional (2D) RMSE values for water (expressed in cm) and bromacil (in ng/g) for all considered simulation scenarios.

Simulation scenario	1D				2D			
	Original	Increased 1	Increased 2	Increased 3	Original	Increased 1	Increased 2	Increased 3
Water	333.1	84.4	74.9	90.9	151.0	73.2	84.2	91.4
Bromacil	425.9	288.8	262.2	279.7	446.4	368.9	323.8	298.5

Water criterion was computed from measured soil water potentials at four depths (averaged from 8 to 11 locations). Bromacil criterion was computed from herbicide concentration profiles beneath the inter-bed open area (averaged from 8 locations).

Table 3
One- (1D) and two-dimensional (2D) predicted values of leachate and dissipated mass of bromacil for all simulation scenarios.

Simulation scenario	1D				2D			
	Original	Increased 1	Increased 2	Increased 3	Original	Increased 1	Increased 2	Increased 3
Leachate (%)	0.9	1.7	2.0	2.2	0.6	1.1	1.4	1.6
Dissipation (%)	60.2	53.9	51.8	50.6	66.6	60.3	57.8	55.9

The bromacil leachate and dissipation in percentage was calculated with respect to total bromacil mass for the individual scenario.

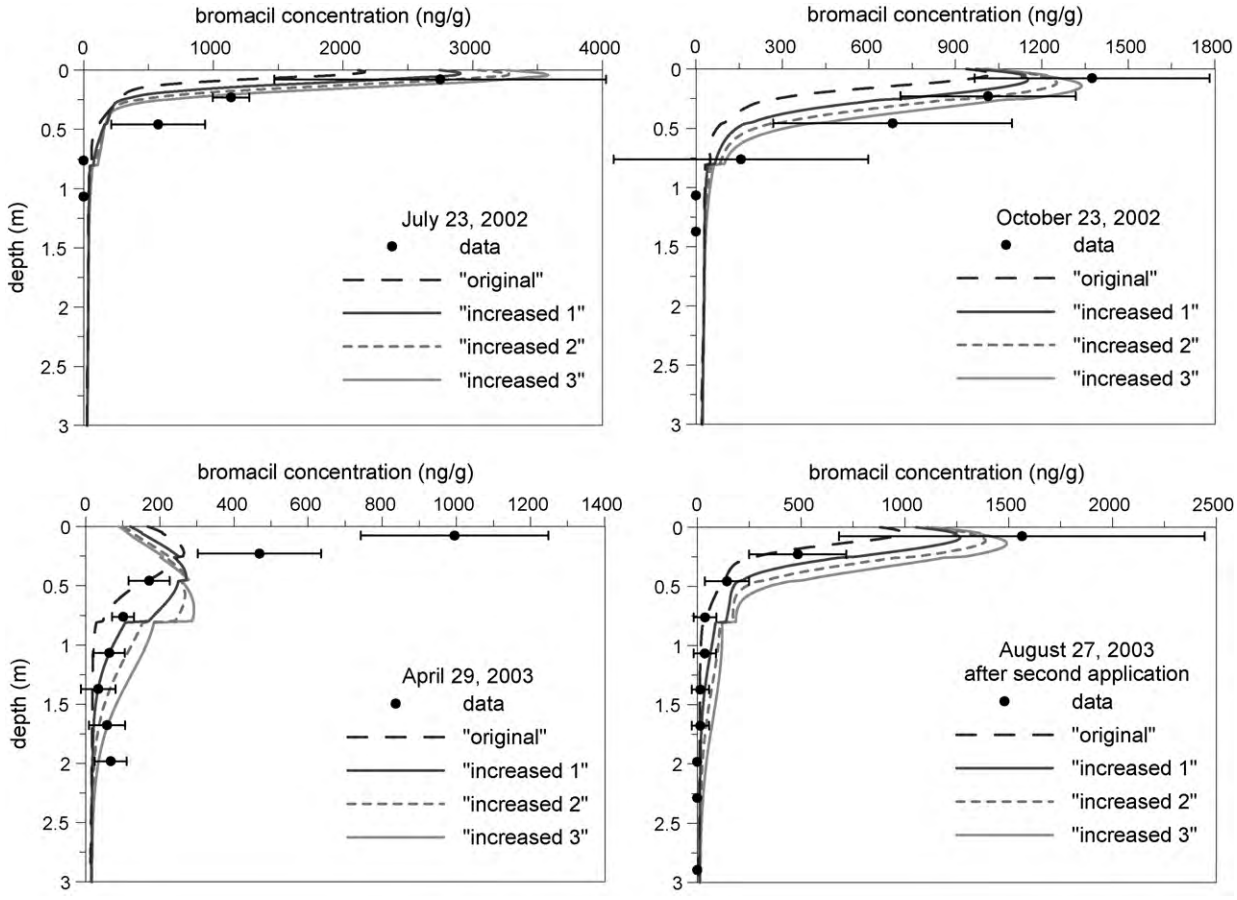

Fig. 3. Comparison of predicted one-dimensional (1D) and measured (mean values and standard deviations) bromacil concentration profiles below the center of the inter-bed area. Bromacil concentration refers to total concentration, i.e. the sum of bromacil present in the liquid and solid phases.

The simulated (2D, scenario "increased 2") bromacil distribution during the application event on June 26, 2002 is shown in Fig. 5. The scale of bromacil solute concentrations is logarithmic. The non-uniform water infiltration diluted the bromacil concentrations beneath the inter-bed area whereas high bromacil concentrations can be found below the raised beds (Fig. 5A). The bromacil application to the inter-bed open area accompanied with the water infiltration caused, besides expected vertical transport, lateral bromacil movement towards the dripper. It can be seen from Fig. 5 that increased bromacil concentrations were predicted for the near-surface soil beneath the plastic mulch, which could partly be attributed to lateral transport of bromacil from the inter-bed area and to initial conditions (Fig. 5C). Overall, the 2D figures exhibit mainly vertical transport of bromacil. The vertical profiles soon after application (Fig. 5B) and four days after application (Fig. 5C) do not differ significantly due to strong soil–chemical adsorption in the topsoil and lack of larger rain storms during this period.

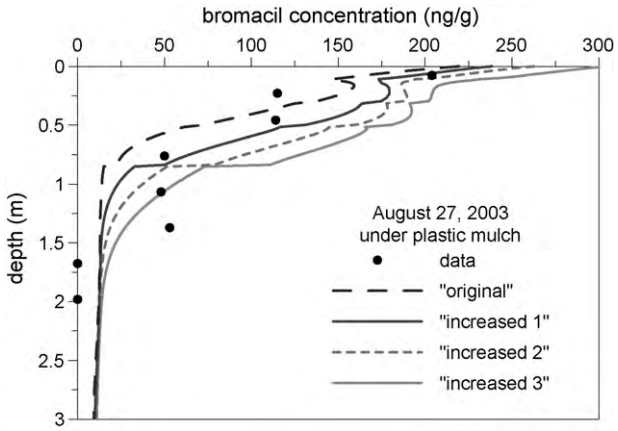

Fig. 4. Comparison of predicted two-dimensional (2D) and measured bromacil concentration profiles below the plastic mulch. Bromacil concentration refers to total concentration, i.e. the sum of bromacil present in the liquid and solid phases.

4. Discussion

In this study, the transport parameters were not calibrated nor adjusted to obtain closer agreement with experimental data. For instance, no bromacil residues below 0.6 m were detected at the first bromacil sampling after the application (July, 2002); however, the simulation results using a half-life of 250 days predicted bromacil below the depth of 0.6 m (Fig. 3). The primary focus of this study was to analyze the impact of the plastic mulch on bromacil transport. In the study of Dohnal et al. (2006), an RMSE value of about 20 cm was obtained by inverse modeling of the soil hydraulic parameters, and this was considered as an indicator of good agreement between measured and predicted soil water potentials. In our study, the soil hydraulic and transport parameters were derived from laboratory and field experiments. Hence, the fit of simulated soil water potential to measured values may be still considered as reasonable (RMSE ranging from 73.2 cm to 91.4 cm for the "increased" scenarios). For bromacil simulations, relatively low RMSE values (<369 ng/g) were obtained for different sizes of open areas (Table 2). The lower RMSE values for bromacil were obtained for the simulation scenarios where the bromacil application mass was increased. It can be further speculated that a

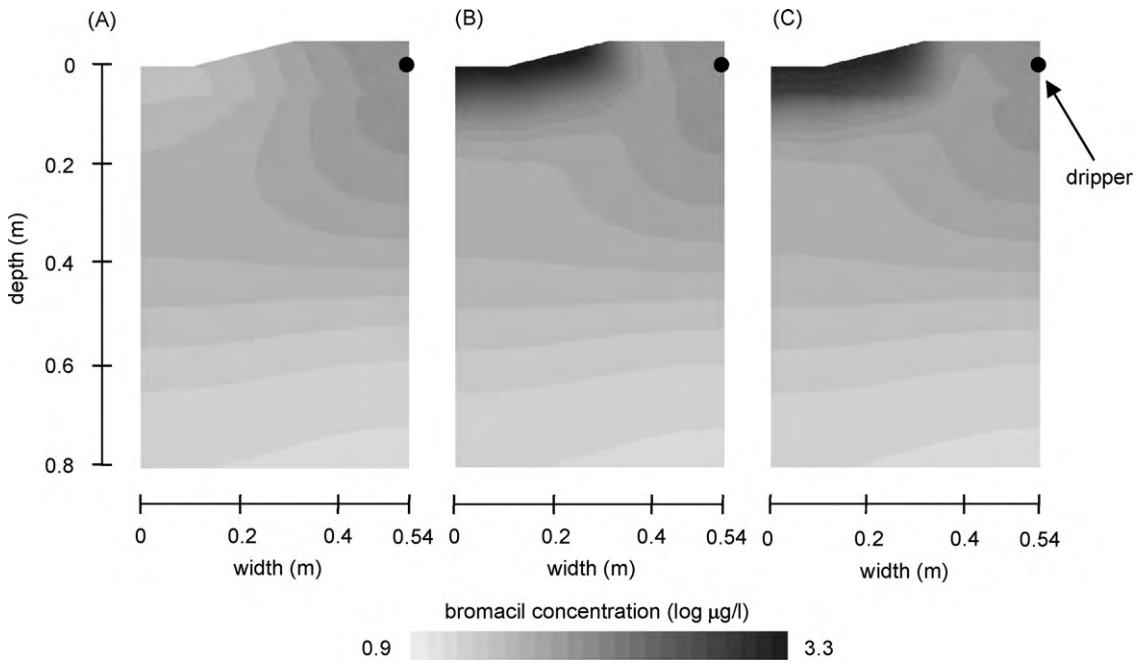

Fig. 5. Vertical cross-sectional images presenting results of the two-dimensional (2D) model (scenario "increased 2") of bromacil transport during the application period in June, 2002. Two-dimensional (2D) plots of bromacil concentrations in the liquid phase are shown for the period: (A) before application (June 25), (B) soon after application (June 26), and (C) 4 days after application (June 30).

closer match between the model predictions and observations can be achieved by optimizing the open/covered area ratio.

The foliage of a pineapple crop gradually develops in the first year and reaches a peak towards the end of the year, after about 14 months (Rebolledo-Martinez et al., 2005). The crop maintains near-peak foliar coverage for the next 2 years. At the study site, the entire inter-bed open area becomes fully covered at the full growth stage of pineapple (i.e. before the last sampling event in August 2003). Once the plants grow and the canopy covers both the mulch surface and the open areas, more rain water is captured by the plants and funneled to the plastic mulch. Some water may enter the soil in the immediate vicinity of the plant and some may move to open inter-bed areas. Thus, not only the plastic mulch but also the foliage of pineapple contributes to the effective covered area at field-scale. The "increased" scenarios assume that about 53–71% of the total field area is effectively covered and water reaching the mulch is routed to uncovered areas. Based on the RMSE criterion and graphical comparisons the "increased" simulation scenarios seem to correlate with field conditions.

A simplified approach to evaluate the effect of plastic mulch on bromacil leaching was presented in this study. In the simulations the runoff was distributed evenly and homogeneously on top of the non-covered soil and not locally near the edge of the plastic sheets as is the actual case. In fact it is clear that the slope of the uncovered areas is non-uniform resulting in local depressions. Furthermore, some fraction of rainfall and bromacil pools on plastic-covered areas which may result in photo-degradation and possible water evaporation losses. However, previous studies have shown very weak photo-degradation of bromacil (FOOTPRINT, 2007). In addition, evapotranspiration is coupled together (i.e. sum of evaporation from bare soil surface and transpiration from pineapple crop) and modeled through the sink term. All the above-mentioned factors may influence the bromacil concentration profiles; however, these factors are believed to play a minor role in the leaching pattern. More elaborate and sophisticated flow and transport models, which would couple surface and subsurface processes, are beyond the scope of this study.

Bromacil transport under plastic mulch could not be simulated by the 1D model as accurately as the 2D model because of the radial nature of water distribution around the dripper. The measured and simulated bromacil concentration profiles indicated that lateral movement was not a key transport process but rather vertical advection and dispersion governed the leaching pattern. The bromacil beneath the inter-bed area was transported by episodic storm events because the irrigation water was applied only through drip tubes located under the plastic mulch. The 1D model seemed to be sufficient to simulate movement of bromacil beneath the open area if the water runoff from the mulch was taken into account (Table 2). On the contrary, biased 1D and 2D results were found when the water runoff from plastic mulch was neglected (RMSE > 425 ng/g). The values of RMSE for prediction of water flow and bromacil transport turned out to be similar for both the 1D and 2D models (Table 2). Generally, the 1D and 2D modeling approaches showed similar profiles (Figs. 6 and 7). The 1D model simulated a drier soil than the 2D model during dry periods (Fig. 6). The 2D model

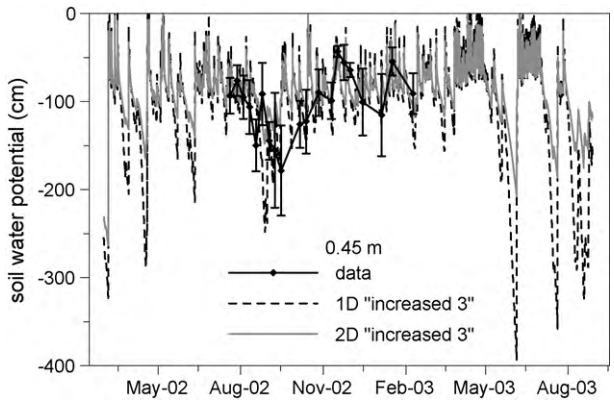

Fig. 6. Comparison of soil water potentials at the depth of 0.45 m beneath the inter-bed area using one- (1D) and two-dimensional (2D) models.

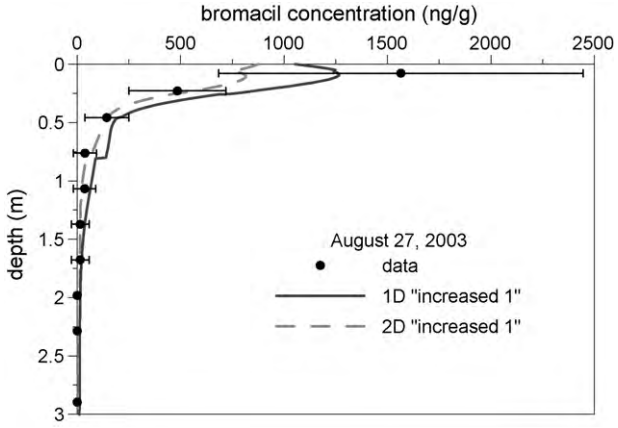

Fig. 7. Comparison of bromacil concentration profiles beneath the inter-bed area using one- (1D) and two-dimensional (2D) models.

simulated a slightly lower bromacil concentrations and leachates than the 1D model (Fig. 7 and Table 3). This may be attributed to the lateral spread in the 2D domain. Comparison of 1D and 2D results indicates that the impact of the drip irrigation on the transport of bromacil beneath the inter-bed area was negligible.

Gavenda et al. (1996) reported that reactive solutes may stay adsorbed to the intra-particle pores of aggregates in Oxisols and slowly leach with incoming rain producing non-Gaussian (long tailed) concentration profiles. This may be the cause behind the discrepancy between the measured and simulated bromacil concentration in the uppermost 0.2 m soil layer on the sampling event of April 29, 2003 (Fig. 3). The intra-particle pores were proven to change the shape of the concentration profile and to be responsible for the unusual pattern of pesticide transport (Rao et al., 1974). No provision for preferential flow was made in our conceptual model. The bromacil leaching pattern predicted by the classical advection–dispersion equation showed a moderate to slow transport regime. Despite the fact that aggregated Oxisols are known to be prone to preferential flow, the field measurements of soil samples did not suggest any indication of preferential transport (i.e. deep and rapid bromacil breakthrough, existence of a bimodal pore region, etc.). No attempts were made to collect pore water samples for bromacil because of site access and maintenance of pore water samplers.

5. Conclusions

Different surficial management yielded distinct soil water regime and chemical leaching patterns in the soil profile. When the water infiltration and bromacil application to the open areas were increased as a result of plastic mulch, a reasonably good agreement with observed soil water potentials and bromacil concentration profiles was obtained. Biased one- (1D) and two-dimensional (2D) results were predicted if the water runoff from plastic mulch was neglected. The 1D approach was sufficient to quantify bromacil transport beneath the inter-bed open area if the water runoff from the mulch was taken into account.

The simulated results from 1D and 2D modeling delivered similar water flow dynamics and bromacil concentration profiles in the open areas. The drip irrigation located below the plastic mulch had little effect on the bromacil transport beneath the inter-bed area. It is rainfall which played the major role in pesticide leaching. This means that drip irrigation represents an efficient irrigation method and also does not increase the risk of chemical leaching. The results from 2D modeling and field sampling indicate a predominantly vertical transport of bromacil.

Acknowledgments

The modeling component of the study was supported by the research fund of the Ministry of Education of the Czech Republic (MSM 6840770002). The field and laboratory experiments were funded by the Hawaii Department of Agriculture (HDOA), Pesticides Branch. This paper is published as a part of the continuing series "Contributed Papers" of the Water Resources Research Center, University of Hawaii at Manoa.

References

Alavi, G., Dusek, J., Vogel, T., Green, R.E., Ray, C., 2007. Evaluation of dual-permeability models for chemical leaching assessment to assist pesticide regulation in Hawaii. Vadose Zone Journal 6, 735–745.
Alavi, G., Sanda, M., Loo, B., Green, R.E., Ray, C., 2008. Movement of bromacil in a Hawaii soil under pineapple cultivation – a field study. Chemosphere 72, 45–52.
Ankeny, M.D., Kaspar, T.C., Horton, R., 1988. Design for an automated tension infiltrometer. Soil Science Society of America Journal 52, 893–896.
Azevedo, P.V., de Souza, C.B., da Silva, B.B., da Silva, V.P.R., 2007. Water requirements of pineapple crop grown in a tropical environment, Brazil. Agricultural Water Management 88, 201–208.
Bear, J., Verruijt, A., 1987. Modelling Groundwater Flow and Pollution. D. Riedel Comp.
Dohnal, M., Dusek, J., Vogel, T., 2006. The impact of the retention curve hysteresis on prediction of soil water dynamics. Journal of Hydrology and Hydromechanics 54, 258–268.
Dolezal, F., Zumr, D., Vacek, J., Zavadil, J., Battilani, A., Plauborg, F., Hansen, S., Abrahamsen, P., Bizik, J., Takac, J., Mazurczyk, W., Coutinho, J., Stekauerova, V., 2007. Dual permeability soil water dynamics and water uptake by roots in irrigated potato fields. Biologia 62, 552–556.
Dusek, J., Vogel, T., Lichner, L., Cipakova, A., Dohnal, M., 2006. Simulated cadmium transport in macroporous soil during heavy rainstorm using dual-permeability approach. Biologia 61 (Suppl. 19), S251–S254.
Dusek, J., Gerke, H.H., Vogel, T., 2008. Surface boundary conditions in 2D dual-permeability modeling of tile drain bromide leaching. Vadose Zone Journal 7, 1241–1255.
Dusek, J., Sanda, M., Loo, B., Ray, C., 2010. Field leaching of pesticides at five test sites in Hawaii: study description and results. Pest Management Science 66, 596–611.
Ekern, P.C., 1965. Evapotranspiration of pineapple in Hawaii. Plant Physiology 40, 736–739.
Feddes, R.A., Kowalik P.J., Zaradny H., 1978. Simulation of Field Water Use and Crop Yield. Simulation Monographs. Pudoc, Wageningen, The Netherlands.
FOOTPRINT, 2007. Creating tools for pesticide risk assessment and management in European Union FOOTPRINT program. http://www.eu-footprint.org/ppdb.html (accessed February 23, 2010).
Gavenda, R.T., Green, R.E., Schneider, R.C., 1996. Leaching of pesticides in selected Hawaii Oxisols and Andisols as influenced by soil profile characteristics. HITAHR Research Series 075. University of Hawaii, Honolulu, HI, p. 35.
Gerke, H.H., Dusek, J., Vogel, T., Köhne, J.M., 2007. Two-dimensional dual-permeability analyses of a bromide tracer experiment on a tile-drained field. Vadose Zone Journal 6, 651–667.
Giambelluca, T.W., Nullet, M.A., Schroder, T.A., 1986. Rainfall Atlas of Hawaii. Division of Water and Land Development, Department of Land and Natural Resources, State of Hawaii, Water Resources Research Center, University of Hawaii at Manoa, Honolulu, HI.
Klute, A., 1986. Water retention: laboratory methods. In: Klute, A. (Ed.), Methods of Soil Analysis, Part 1. Physical and Mineralogical Methods. Monograph, vol. 9. Am. Soc. Agron, Madison, Wisconsin, pp. 635–660.
Li, Q.X., Hwang, E.C., Guo, F., 2001. Occurrence of herbicides and their degradates in Hawaii's groundwater. Bulletin of Environmental Contaminant and Toxicology 66, 653–659.
Mualem, Y., 1976. A new model for predicting the hydraulic conductivity of unsaturated porous media. Water Resources Research 12, 513–522.
Peterson, F.L., Green, K.R., Green, R.E., Ogata, J.N., 1985. Drilling Program and Pesticide Analysis of Core Samples from Pineapple Fields in Central O'ahu. Special Report 7.5:85, Water Resources Research Center, University of Hawaii at Manoa, Honolulu, HI.
Rao, P.S.C., Green, R.E., Balasubramanian, V., Kanihero, Y., 1974. Field study of solute movement in a highly aggregated Oxisol with intermittent flooding. II. Picloram. Journal of Environmental Quality 3, 197–202.
Ray, C., Vogel, T., Dusek, J., 2004. Modeling depth-variant sorption and domain-specific biodegradation in dual-porosity media. Journal of Contaminant Hydrology 70, 63–87.
Rebolledo-Martinez, A., del Angel-Perez, A.L., Becerril-Roman, A.E., Rebolledo-Martinez, L., 2005. Growth analysis for three pineapple cultivars grown on plastic mulch and bare soil. Interciencia 30, 758–763.
Russo, D., Tauber-Yasur, I., Laufer, A., Yaron, B., 1997. Numerical analysis of field-scale transport of bromacil. Advances in Water Resources 21, 637–647.
Schneider, R.C., Zhang, J., Anders, M.M., Bartholomew, D.P., Caswellchen, E.P., 1992. Nematicide efficacy, root-growth, and fruit yield in drip-irrigated pineapple parasitized by rotylenchulus–reniformis. Journal of Nematology 24, 540–547.

van Genuchten, M.Th., 1980. A closed form equation for predicting the hydraulic conductivity of unsaturated soils. Soil Science Society of America Journal 44, 892–898.
van Genuchten, M.Th., Leij, F.J., Yates, S.R., 1991. The RETC Code for Quantifying the Hydraulic Functions of Unsaturated Soils. U.S. EPA Rep. 600/2–91/065. Environ. Protect. Agency, Washington DC, p. 85.
Vogel, T., 1987. SWMS II: Numerical model of two-dimensional flow in a variably saturated porous medium. Research Report No. 87. Dept. of Hydraulics and Catchment Hydrology, Agriculture Univ., Wageningen, The Netherlands.
Vogel, T., Cislerova, M., 1988. On the reliability of unsaturated hydraulic conductivity calculated from the moisture retention curve. Transport in Porous Media 3, 1–15.
Vogel, T., Gerke, H.H., Zhang, R., van Genuchten, M.Th., 2000. Modeling flow and transport in a two-dimensional dual-permeability system with spatially variable hydraulic properties. Journal of Hydrology 238, 78–89.
Vogel, T., van Genuchten, M.Th., Cislerova, M., 2001. Effect of the shape of soil hydraulic functions near saturation on variably-saturated flow predictions. Advances in Water Resources 24, 133–144.
Vogel, T., Dohnal, M., Dusek, J., 2004. Description of the available bench scale modeling approaches with emphasis on the input data requirements and output data structure. Deliverable COMPUTE1.1, Integrated Project AquaTerra.
Vogel, T., Lichner, L., Dusek, J., Cipakova, A., 2007. Dual-continuum analysis of a cadmium tracer field experiment. Journal of Contaminant Hydrology 92, 50–65.
Zhu, Y., Li, Q.X., 2002. Movement of bromacil and hexazinone in soils of Hawaiian pineapple fields. Chemosphere 49, 669–674.

Field leaching of pesticides at five test sites in Hawaii: study description and results, Pest Management Science, 2010.

Research Article

Received: 31 August 2009 Revised: 15 October 2009 Accepted: 18 November 2009 Published online in Wiley Interscience: 2 February 2010

(www.interscience.wiley.com) DOI 10.1002/ps.1914

Field leaching of pesticides at five test sites in Hawaii: study description and results

Jaromir Dusek,[a] Martin Sanda,[a] Binh Loo[b] and Chittaranjan Ray[c]*

Abstract

BACKGROUND: Following the discovery of pesticides in wells, the Hawaii Department of Agriculture (HDOA) supported research to evaluate the likelihood of pesticide leaching to the groundwater in Hawaii. The aim of this study was to evaluate the relative leaching pattern of five pesticides at five different sites on three islands and to compare their leaching behavior with bromide and a reference chemical (atrazine) that is known to leach in Hawaiian conditions. Laboratory measurements of sorption and degradation of the pesticides were made.

RESULTS: Most of the applied mass of pesticides was still present in the top 80 cm after the 16 week study period. The aggregated oxisol at Kunia showed the most intensive leaching among the five sites. The revised attenuation factor screening approach used by the HDOA indicated that all chemicals, with the exception of trifloxystrobin, had the potential to leach. Similarly, the groundwater ubiquity score ranked trifloxystrobin as a non-leacher. The field leaching data, however, suggested that trifloxystrobin was the most mobile compound among the pesticides tested.

CONCLUSION: Although the results were variable among the sites, the field and laboratory experiments provided useful information for regulating use of these pesticides in Hawaii.

Supporting information may be found in the online version of this article.

Keywords: pesticide; transport; water flow; degradation; sorption; field leaching

1 INTRODUCTION

Groundwater is the primary source of drinking water on all the Hawaiian Islands, and alternative sources are non-existent in many areas. Chemical use on pineapple plantations in Hawaii increased dramatically after World War II, where dibromochloropropane (DBCP) and ethylene dibromide (EDB) were used. A number of herbicides, including bromacil, atrazine and ametryn, were used or are being used on pineapple crops as well. Aside from these herbicides, hexazone was also used on sugarcane plantations for weed control. After the detection of DBCP and EDB in drinking water wells in the late 1970s,[1] these chemicals were banned. Atrazine, hexazinone and bromacil have also been detected in groundwater during surveys conducted by the State of Hawaii and the pesticide registrants.[2,3] Degradation products of many of these herbicides were also found in detectable concentrations.[4]

Following the discovery of pesticides in groundwater, the Hawaii Department of Agriculture (HDOA), the agency charged with regulating the use of pesticides in the state, supported research to evaluate the likelihood of leaching to groundwater of pesticides that are used in Hawaii. The HDOA receives applications for licensing pesticide products for use in the state (a license is valid for 3 years). For evaluation of the leaching potential of the chemicals, the HDOA currently uses a tier-I leaching model, derived from the commonly named revised attenuation factor (AFR) approach.[5,6] The HDOA evaluations are primarily based on the potential of the compound to contaminate groundwater, using a known leacher and a known non-leacher as references.

Field leaching experiments have been fully established as an effective means of evaluating the fate of pesticides in soils.[7–9] Residual concentration profiles in the soil are usually sampled and analyzed to estimate the pesticide persistence and mobility.[10,11] Several studies have made use of lysimeters[12,13] and sites with tile drains[14,15] for accurate chemical balance determination under field conditions. The fate of pesticides in tropical soils is still not as well understood as it is for soils in temperate regions,[16,17] as the majority of field studies have so far been undertaken in temperate regions. For instance, the effect of temperature on degradation and sorption characteristics for tropical soils requires further evaluation.[18]

The objective of the present study was to evaluate the leaching behavior of five pesticides under consideration for licensing in the state of Hawaii (S-metolachlor, imazaquin, sulfometuron-methyl, trifloxystrobin and imidacloprid), plus atrazine and bromide, at

* *Correspondence to: Chittaranjan Ray, Department of Civil and Environmental Engineering, University of Hawaii at Manoa, Honolulu, HI 96822, USA. E-mail: cray@hawaii.edu*

a *Czech Technical University in Prague, Faculty of Civil Engineering, Prague, Czech Republic*

b *Chemical Analysis Laboratory, Hawaii Department of Agriculture, Honolulu, Hawaii, USA*

c *Civil and Environmental Engineering and Water Resources Research Center, University of Hawaii at Manoa, Honolulu, Hawaii, USA*

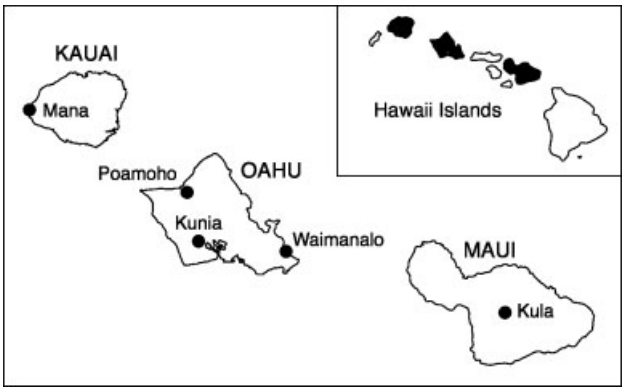

Figure 1. Experimental sites for evaluating the leaching of pesticides in the tropical soils of Hawaii.

five sites representing diverse soil and hydrological conditions found in the state. The selection of the six pesticides was based on their potential importance in Hawaiian agriculture and urban pest control. The leachability of the five new pesticides was evaluated with reference to the leachability of bromide tracer and atrazine. Atrazine was used as the reference pesticide because it has been extensively used in Hawaii and its leaching behavior is well understood in Hawaiian conditions. Field leaching experiments and laboratory studies were performed to examine the fate and transport of these chemicals in soils. An additional objective was further to evaluate modeling approaches currently being used by the HDOA in its regulatory assessment of pesticides.

2 MATERIALS AND METHODS

2.1 Field leaching experiment

Four herbicides (atrazine, S-metolachlor, imazaquin, and sulfometuron-methyl), the insecticide imidacloprid and the fungicide trifloxystrobin were tested under field conditions during the 16 week study. Atrazine and S-metolachlor are herbicides used in corn, grain and potato production, imazaquin and sulfometuron-methyl are herbicides used for grass and broadleaf weed control, trifloxystrobin is a fungicide used mostly in fruit and vegetable production and imidacloprid is an insecticide used for termite and pest control.

2.1.1 Site characteristics

Five sites, each representing different soil/hydrological conditions, were selected for the leaching study. These sites represent agriculturally important soils in Hawaii. Three were located on the island of Oahu (Kunia, Poamoho and Waimanalo), one on the island of Kauai (Mana) and one on the island of Maui (Kula) (Fig. 1). Detailed information about the sites is given in Table 1.

The soils at the five sites differ in terms of their moisture and temperature regimes, mineralogy and physical and chemical properties. Two of the five soils are oxisols, two are vertisols and one is an andisol (Table 1).[20] The Poamoho, Kunia and Waimanalo sites have deep profiles[7] owing to intense weathering of the parent material. The Kula site has a shallow soil profile above bedrock at a depth of 75 cm.[21] At Kula, the soil, primarily volcanic ash, was mixed when a terrace was constructed. At the Mana site, coralline rock fragments were encountered at depths less than 75 cm.

2.1.2 Plot layout and site preparation and irrigation system design

At each site, an 18.3 × 12.2 m area was divided into four identical plots arranged as shown in Fig. 2. Owing to spatial limitations, the plots at the Kula site were configured in a 36.6 × 6.1 m rectangle, having the same total plot area, but arranged linearly along a narrow constructed terrace. Following tillage, herbicides were applied on two of the four plots, and fungicide and insecticide were applied on the remaining two plots at each site.

A sprinkler irrigation system, consisting of a set of surface rotating sprinklers, was set up at each site. The irrigation helped to enhance the leaching within the timeframe of the study. Irrigation was automatically timed to operate during early morning hours when the effect of wind was at its lowest, to ensure the most uniform application. Irrigation application, determined by the irrigation uniformity test, ranged between 7.5 and 13.7 mm h^{-1} for all sites, except for Kula. At Kula, the system produced an intensity of 20.3 mm h^{-1}. Irrigation uniformity was evaluated using the distribution uniformity (DU) coefficient. The DU was calculated as the average of the lowest quarter of samples divided by the average of all samples. The higher the DU, the better is the performance of the irrigation system. A DU value higher than 70% is considered 'good' for sprinkler irrigation systems.[22]

2.1.3 Site instrumentation and data collection

To study hydrological processes as driving forces for the transport of pesticides, several manual and automatic devices were installed to measure climate and soil water regime variables.

At each site, soil temperature at 30 and 60 cm below the soil surface and air temperature at the surface and at 200 cm above the surface were measured using a Campbell Scientific 107-L temperature probe. Soil water pressure within the soil profile was monitored using a set of six automated tensiometers (Soilmoisture Equipment Company, Goleta, CA), installed at two locations in nests of three at depths of 30, 60 and 90 cm (Fig. 2). At Kula, the tensiometers were installed at 25, 50 and 75 cm depths owing to spatial limitations of the shallow soil profile. All automated measurements were recorded at 5–15 min intervals, depending on logger memory availability and data acquisition logistics at each site.

Four nests of three manual tensiometers were additionally installed at the same depths as the automated tensiometers (Fig. 2). A Tensimeter™ – a digital manual meter with a portable transducer – was used to acquire the soil water pressure from the manual tensiometers. Two nests of time domain reflectometry (TDR) buriable uncoated probes were installed at each site to measure soil moisture content (Fig. 2). The probes were placed horizontally at the same depths as tensiometers. Soil moisture content and soil water pressure were measured weekly or biweekly using the TDR probes and manual tensiometers. At all sites, except Mana, an evaporation pan was installed 30 cm above the soil surface to collect data daily. It was not possible to maintain an evaporation pan at Mana owing to its remote location.

2.1.4 Soil hydraulic properties

Sets of undisturbed soil core samples were collected at the study sites for the purpose of measuring soil water retention characteristics. At each site, three samples were collected at 15, 45 and 75 cm depths at two locations, for a total of eighteen samples per site. At the Kula site, soil samples were taken from depths of 5, 25 and 50 cm.

Table 1. Summary information of the five sites for the pesticide leaching study

Site	Soil type	Soil series	Soil taxonomy	Elevation (m above sea level)	Mean annual rainfall (mm)[a]
Poamoho	Silty clay oxisol	Wahiawa	Rhodic Eutrustox	213	1000
Waimanalo	Clay vertisol	Waialua	Vertic Haplustolls	30	1500
Kunia	Silty clay oxisol	Molokai	Typic Eutrotorrox	85	600
Kula	Loam andisol	Kula	Typic Eurtandepts	911	750
Mana	Silty clay loam vertisol	Malama	Typic Haplusters	3	500

[a] Data from Giambelluca *et al.*[19]

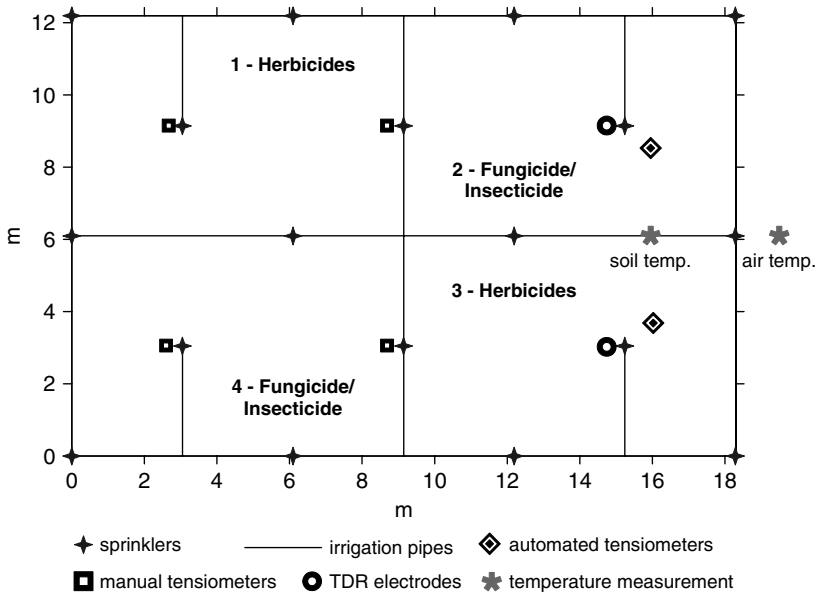

Figure 2. Experimental plot design for the field leaching experiment. The Kula site had plots in a linear set-up (in a row).

In situ infiltration rates were measured using a 20 cm diameter tension disc infiltrometer at two pits outside and adjacent to the plot boundaries, following the method of Perroux and White.[23] Infiltration measurements were performed at the same depths from which undisturbed soil samples for water retention measurement were removed. Three replicate measurements were conducted at each depth. In these experiments, infiltration rates were conducted at five or six different pressure heads.

2.1.5 *Pesticide application and sampling procedure*

Soil samples were collected from the field for laboratory analysis prior to pesticide application. These samples were used in studies of pesticide degradation and sorption, and for measurement of pH and organic carbon (OC) content. A single borehole was drilled in each plot at each site using a manually operated stainless steel wide bucket auger. Samples were taken from these boreholes at several depths. These pre-application sampling depths were similar to the final post-application sampling depths. The post-application sampling depths for all sites are summarized in Table 2. The sampling depths were based on initial estimates of bromide movement in the soil.

After the monitoring equipment had been installed, the irrigation system calibrated and the pre-application soil samples collected, the chemicals were applied to the plots, including the conservative tracer potassium bromide, which was applied on each plot at a rate of 39.09 kg ha^{-1} in aqueous solution prior to the pesticide application.

The pesticides were applied by two researchers walking over the plots carrying a 3.0 m long tube equipped with six spray nozzles between them. The rate at which they walked over the plots was measured, and the actual application concentration was calculated from this. Owing to variations in walking speed during application, the actual application rates varied slightly between the five sites. Application was performed in the early morning hours to minimize the impact of wind, which could have affected the uniformity of application.

The application rates of the active ingredient of the commercial products were as follows: atrazine 5.41 kg ha^{-1} as 900 g kg^{-1} WG (Aatrex Nine-O®; Syngenta), S-metolachlor 2.87 kg ha^{-1} as 920 g L^{-1} EC (Dual II Magnum®; Syngenta), imazaquin 0.7 kg ha^{-1} as 700 g kg^{-1} WG (Image 70 DG®; BASF), sulfometuron-methyl 0.53 kg ha^{-1} as 750 g kg^{-1} WG (Oust®; DuPont), trifloxystrobin 1.56 kg ha^{-1} as 500 g kg^{-1} WG (Compass®; Bayer CropScience) and imidacloprid 0.62 kg ha^{-1} as 240 g L^{-1} SC (Admire®; Bayer CropScience). The application rates were at or below the USEPA/HDOA maximum allowable application rates over a season. At Poamoho, Waimanalo and Kula, imidacloprid 240 g L^{-1} SC (Premise®) was applied at the termiticidal rate, 39–41 kg AI ha^{-1}. For termiticidal application, insecticides are generally applied into a narrow trench around the footprint of a house (rather than sprayed uniformly) prior to its construction, thus resulting in a

Table 2. Sampling depths for soil sampling at the three sites on Oahu and the sites on Kauai and Maui[a,b]

Oahu and Kauai soil depth (cm)	Soil sample collected for chemicals: 1 DAA[c]	7 DAA	14 DAA	28 DAA	56 DAA	84 DAA	112 DAA	336 DAA
0–15	A	A	A	A	A	A	A	P
15–30		A	A	A	A	A	A	P
30–60			A	A	A	A	A	P
60–90				A	A	A	A	P
90–120					A	A	A	P
120–150						A	A	P
150–180							A	P
180–210							A	P

Maui soil depth (cm)	Soil sample collected for chemicals: 1 DAA	7 DAA	14 DAA	21 DAA	28 DAA	45 DAA	74 DAA	113 DAA
0–15	A	A	A	A	A	A	A	A
15–30		A	A	A	A	A	A	A
30–45			A	A	A	A	A	A
45–60				A	A	A	A	A
60–75					A	A	A	A

[a] A – all chemicals (four herbicides, fungicide, insecticide, and bromide).
[b] P – imidacloprid plots at the Poamoho station only.
[c] DAA – days after application.

higher concentration in a smaller area. Imidacloprid is the active ingredient in both Admire® and Premise®, but they are formulated for different uses.

After the application of bromide and the pesticides, the irrigation system was operated for 1 h to allow the chemicals to move into the soil profile and to prevent their photodegradation. One day after application, a 5 cm thick layer of wheat straw was spread over the entire application area further to prevent photodegradation and reduce evaporation from the bare soil, as no crop was grown on the plots during the leaching experiment.

Soil samples were collected from each of the four plots for pesticide residue analysis. Samples were taken 1 day and 1, 2, 4, 8, 12 and 16 weeks after the application. Sampling depths increased with time in order to try to recover the full mass of the chemicals as they moved downward. The sampling depth intervals over time are presented in Table 2.

Three holes were drilled per plot to retrieve the soil samples through the full depth of the holes each time samples were taken over the following 16 weeks. These sampling holes were located randomly with the intention of sampling all regions of the plot. For soil sampling from deeper zones, a PVC sleeve was used to prevent surface soil from falling and contaminating the lower samples. For each sampling event, new borehole locations were selected. Samples collected from the identical depths taken from each of the three different holes on each plot were thoroughly mixed together in a plastic bag. From this mixture, a subsample was placed in a glass jar. The samples were transferred in a cooler to a refrigerator and then to the analytical laboratory. Samples were frozen in the laboratory prior to chemical analysis.

2.1.6 *Field profile and center of mass analysis*

The concentrations of the applied pesticides in the soil samples taken from the five sites were determined, and the results were used to calculate the mass of pesticides present in the soil profile. Similarly, each sample's bromide concentration was used to estimate its mass in the soil. The mass per unit area ($\mu g\ m^{-2}$) was calculated by multiplying the concentration ($\mu g\ kg^{-1}$) in a sample from a given depth interval (m) by the bulk density ($kg\ m^{-3}$) in that depth interval. The total calculated pesticide mass in the soil profile at each successive sampling interval was then used to estimate field dissipation rates using the first-order degradation process.[7]

For asymmetric concentration profiles, a meaningful way to evaluate the relative leachability of a compound through the soil is to locate its center of mass (COM) and compare it with that of other compounds.[7] The COM is a reference point at which 50% of the pesticide mass is above and the other 50% is below. In this study, COMs were determined from the measured concentration profiles. Obviously, the COM does not indicate the location of the concentration front of the chemicals. It is important to note that, for asymmetric concentration profiles, the total depth of leaching could be much more than twice the depth to the COM.

To allow a direct comparison of the leachability between the five sites, predictions of COM were made on the basis of a linear extrapolation from observed values under known water application regimes. This analysis thus made it possible to predict a chemical's COM for a given cumulative water application. When a pesticide was not detected in the soil profile at a sampling event owing to its dissipation, the COM measured from previous sampling (when the pesticide was still present in the profile) was used for the new sampling event. This procedure was used to reduce an overestimation of extrapolated COM. Nearly complete dissipation was observed for atrazine, imazaquin and S-metolachlor over the study period.

2.1.7 *Leachability indices*

The leaching potential of pesticides can be estimated by a so-called groundwater ubiquity score (GUS) index.[24] The GUS is calculated using the following equation:

$$\mathrm{GUS} = \log t_{1/2}\,(4 - \log\ K_{\mathrm{OC}}) \tag{1}$$

where $t_{1/2}$ is the pesticide half-life (days) and K_{OC} is the soil organic carbon sorption coefficient ($mL\ g^{-1}$). If GUS is higher than 2.8, the pesticide is classified as a leacher. A pesticide with a GUS value lower than 1.8 is said to be a non-leacher. Pesticides with GUS values between 1.8 and 2.8 are considered as transient compounds.

The attenuation factor (AF) proposed by Rao *et al.*[5] was originally used by the HDOA to evaluate leaching potential. Later, the revised attenuation factor (AFR)[6,25] was established as a tier-I model for registration purposes. The AFR is defined as

$$\mathrm{AFR} = \ln\left(\frac{d\mathrm{RF}\theta_{\mathrm{FC}}}{qt_{1/2}}\right) + k \tag{2}$$

where d is the compliance or groundwater depth (m), θ_{FC} is the water content at field capacity, q is the average water flow rate through the soil (or recharge rate) (m/day), k is a constant ensuring that the AFR is positive and RF is the retardation factor, evaluated

as

$$RF = 1 + \frac{\rho_b f_{OC} K_{OC}}{\theta_{FC}} \quad (3)$$

where ρ_b is the soil bulk density (g cm^{-3}) and f_{OC} is the fractional organic carbon content.

For evaluation of the relative leachability of a pesticide using AFR in the present experiments, the parameters varied among the five sites. The input parameters were derived from the laboratory measurements (ρ_b, θ_{FC}, f_{OC}) or field observations (q). The compliance depth $d = 0.5$ m was chosen for all sites. Changing the compliance depth results in different absolute values of the AFR; nevertheless, the effect is the same for all pesticides and does not change the relative classification.[25] The parameters K_{OC} and $t_{1/2}$ are discussed in Section 3.10.

2.2 Laboratory experiments

2.2.1 *Soil water retention measurements*

The drainage part of the water retention curve was measured for all the soil samples in the range from saturation to 15 bar negative pressure, using seven suction–water content equilibrium measurements following the method of Dane and Topp.[26] From the undisturbed soil core samples, porosity and bulk density were also determined. Each of the measured retention curves was fitted by the van Genuchten–Mualem model.[27] Based on the sets of fitted curves, reference retention curves were established using the scaling method of Vogel *et al*.[28] for each site.

2.2.2 *Organic carbon*

An organic carbon analyzer (model WR-112; Leco Corp., St Joseph, MI) was used to determine the organic carbon content of the soil samples using the dry combustion method. The instrument utilized an infrared detector to measure the carbon dioxide gas produced during combustion.

2.2.3 *pH*

Soil pH values were measured in a soil–water slurry (1 : 1 paste of soil: 1 M KCl) after 30 min of equilibration. A pH electrode (Corning Inc., Corning, NY) was used to determine the pH of the slurry.

2.2.4 *Bromide analysis*

For the bromide analysis, about 10 g of soil was placed in a 40 mL vial. One sample from each plot (resulting in four samples from the site) was analyzed for bromide concentration for each sampling depth. Deionized water was added, to produce a final ratio of 2 : 1 water : dry soil. The samples were thoroughly mixed in the vial for 2 h at 30 rpm and centrifuged (5000 rpm for 30 min) to produce a clear supernatant. The supernatant was again centrifuged (at 11 000 rpm for 20 min) in 5 mL centrifuge tubes to remove fine particulate matter. The final solution was analyzed using an ion chromatograph (model DX-120; Dionex Corp., Sunnyvale, CA). The minimum detectable bromide concentration was 0.2 mg L^{-1}.

2.2.5 *Pesticide adsorption experiments*

Batch sorption tests of the soils collected from the different depths prior to the field application were conducted in a constant-temperature laboratory at 22 °C. Duplicate samples from all sites from depths listed in Table 2 were used. The 180–210 cm layer was not collected at the Mana site, as hard coral was encountered at that depth.

For each soil sample, competitive batch equilibration tests of the four herbicides or the insecticide and fungicide mixture were carried out. In the herbicide batch, the initial concentrations of atrazine, S-metolachlor, imazaquin and sulfometuron-methyl in the solution were 20, 31, 10 and 20 μg mL^{-1} respectively. In the insecticide/fungicide batch, initial concentrations of imidacloprid and trifloxystrobin were 6 and 0.6 μg mL^{-1} respectively. Mixtures containing 40, 15 and 5% of the above solutions, were prepared for the equilibration experiments.

Sorption of the metabolites of selected compounds was conducted following the same procedure as for parent compounds. Desethyl atrazine, desisopropyl atrazine, S-metolachlor CGA-37735 [*N*-(2-ethyl-6-methylphenyl)-2-hydroxyacetamide] and S-metolachlor CGA-354743 [sodium 2-[(2-ethyl-6-methylphenyl)(2-methoxy-1-methylethyl)amino]-2-oxoethanesulfonate] were mixed together with initial concentrations of 5, 5, 25 and 25 μg mL^{-1} respectively. (*Z*,*Z*)-Trifloxystrobin acid and (*E*,*E*)-trifloxystrobin acid were mixed into a solution having initial concentrations of 25 μg mL^{-1} each. Two dilutions of the above compound mixtures, containing 40 and 15% of the initial solution, were used.

The procedure involved adding 10 g of moist soil into a 40 mL glass vial containing 20 mL of the pesticide solution. The soil was mixed for 24 h at 30 rpm. The slurry was then centrifuged at 5000 rpm for 30 min. The supernatant was then transferred into 5 mL centrifuge tubes, and centrifuged again at 11 000 rpm for 20 min to produce a clear supernatant for analysis by high-performance liquid chromatography.

The mass of the pesticide adsorbed to unit mass of dry soil (calculated from moisture content) was determined from the difference between the initial and equilibrated concentrations, the solution volume and the amount of soil present in the slurry. Assuming the sorption linear isotherm model, the isotherm was constructed by plotting the equilibrated concentration versus the amount adsorbed per mass of soil. The sorption distribution coefficient K_d was calculated from the slope. From the organic carbon content analyzed for various depths, the organic carbon partition coefficient K_{OC} was estimated.

2.2.6 *Pesticide degradation experiments*

Degradation experiments were conducted on the soil samples collected prior to field application in a constant-temperature room at 22 °C. In order to reduce the laboratory analyses to a manageable number, degradation experiments from three depths (0–15, 15–30 and 60–90 cm) were carried out for the three Oahu sites and the Mana site. For the Kula site, samples from 15–30, 30–45 and 60–75 cm depths were used for the experiments.

Each sample of about 1000 g was air dried and sieved through a 2 mm mesh sieve. The mixed soil was split into three replicates and placed in aluminum containers. The mass application of pesticides in the laboratory study was estimated on the basis of field application. The application concentrations for the samples from 0–15 cm depth were the following: 3200 ng g^{-1} dry soil for atrazine, 1600 ng g^{-1} for S-metolachlor, 400 ng g^{-1} for imazaquin, 320 ng g^{-1} for sulfometuron-methyl, 800 ng g^{-1} for trifloxystrobin and 320 ng g^{-1} for imidacloprid. Deeper samples received 75 and 25% of the estimated concentrations. Degradation studies for imidacloprid were conducted using the agricultural application rate.

A mixture of the four herbicides was applied to one set of soil samples. A mixture of the insecticide and the fungicide was applied to another sample set. The solutions were applied to the surface

of air-dried soils in aluminum pans. Deionized water was added to achieve the desired moisture content for microbial degradation during the experiment. The sampling regime followed the same pattern as the field sampling regime. Approximately 10 g of soil from each of the pans was collected in glass vials on the sampling day and submitted to the laboratory for chemical analysis.

2.2.7 *Pesticide extraction from soil and analytical conditions*

The method of extraction of the pesticides from the soil varied according to the compound. Details of the analytical procedures for the individual compounds used in this study are presented in Ray *et al*.[29] The following is a summary of these. The minimum detectable concentrations ranged from 0.2 ng g^{-1} (sulfometuron-methyl) to 50 ng g^{-1} (imazaquin) for the pesticides. In the present case, the limit of detection (LOD) was the same as the limit of quantitation (LOQ). The LOQ was defined as a signal-to-noise (S/N) ratio of 10. The average analytical recovery for all pesticides was 90%, with a standard deviation of 26%.

Atrazine, S-metolachlor and their metabolites were extracted from 10 g of soil with acetonitrile + water (90 + 10 by volume) using an accelerated solvent extractor (ASE 200; Dionex Corp., Sunnyvale, CA). The following extraction conditions were similar for all of these pesticides: oven temperature 100 °C, pressure 10 MPa, static time 5 min, flush volume 60% of the cell volume, nitrogen purge 60 s at 1 MPa, static cycle 1.

Imidacloprid was extracted with 100% acetonitrile using the ASE. The sample extract was then concentrated to an appropriate volume by a nitrogen evaporator before analysis by GC/MS. For imidacloprid, the sample extracts were derivatized with *N*-methyl-*N*-trifluoroacetamide.

Imazaquin was extracted with 100 mL of 0.5 M NaOH. The sample was placed in a shaker. The extract was filtered and acidified (to pH 0.75–1.0) with 6 M HCl. The acidified extract was partitioned with dichloromethane and the solvent was exchanged with acetone. The sample extract was then methylated with tetrabutylammonium and iodomethane. The methylated sample was analyzed using a Hewlett-Packard HP 5890 GC, a Hewlett-Packard HP 5972 MSD and a Hewlett-Packard HP 7673 autosampler.

Sulfometuron-methyl was extracted with methanol + 0.1 M ammonium carbonate (1 + 9 by volume) using the ASE under the conditions described for the other herbicides. The extract was cleaned using solid-phase extraction cartridges (Oasis HLB; Waters Corp., Milford, MA). The extract was transferred to a mixture of acetonitrile and ammonium formate for analysis using a liquid chromatograph with a mass spectrometer (LC/MS) detector. The mobile phase in the LC/MS was composed of 50% solvent A (acetonitrile) and 50% solvent B (10 mM ammonium formate, 10 mM formic acid pH = 3 and 2% acetonitrile).

Trifloxystrobin and its metabolites were first extracted from the soil using the ASE. The extraction solvent was methanol + water (50 + 50 by volume). The oven temperature was maintained at 40 °C. All other conditions were as described for the other herbicides. The extract was diluted with methanol to which an internal standard was added. Analysis was performed using LC/MS. The mobile phase was 75% solvent A (methanol) and 25% solvent B (10 mM ammonium formate pH = 6 and 2% acetonitrile).

3 RESULTS

3.1 Sprinkler uniformity

Irrigation uniformity tests for each site produced DU coefficients of about 85%. At the Kunia site, the sprinkler systems could not be well calibrated owing to fluctuating water pressure in the pipeline, so DU equaled 77%. Based on the values of DU, the sprinkler systems produced relatively uniform irrigation application.[22]

3.2 Rainfall, irrigation and evaporation

Rainfall along with irrigation and pan evaporation data for the Kula site is presented in Fig. 3. The cumulative water application (rainfall plus irrigation) was lower than the cumulative pan evaporation for all of the sites, with the exception of Kula. At Kunia, the pan evaporation was significantly higher than (nearly twice that) of the other sites on Oahu owing to its location in a relatively dry and warm part of the island. Although the cumulative pan evaporation for most of the sites was higher than total water application, actual evaporation from soil at each of the sites was expected to be low owing to the absence of plants. The sites were also covered with straw mulch, decreasing the evaporation rate. For instance, Gavenda *et al*.[7] estimated evaporation from straw-covered soils to be about 20% of pan evaporation.

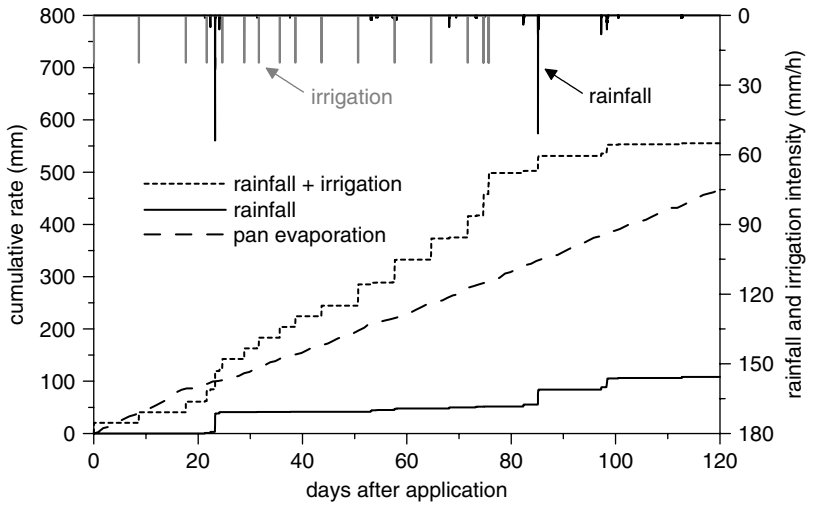

Figure 3. Rainfall, irrigation and evaporation data at the Kula site (Maui).

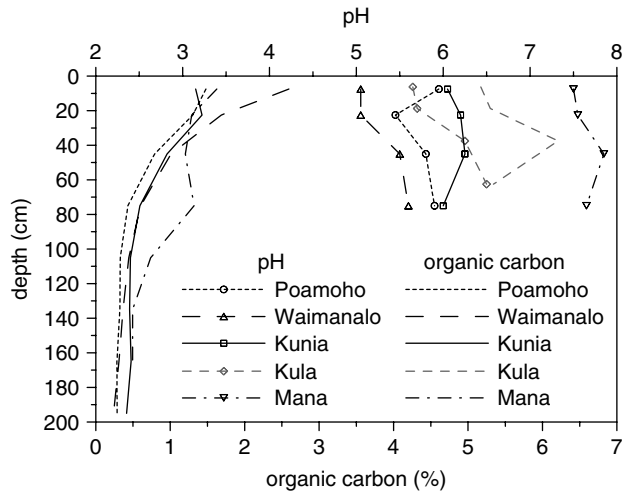

Figure 4. Profile of soil pH and organic carbon for the five sites.

The cumulative irrigation rate varied between 375 and 500 mm among the five sites over the 16 week study duration. This amounted to about 25–30 mm per week. In this study, the amount of irrigation water was less than that used by Gavenda *et al*.[7] The irrigation rate used in this study is quite typical for commercial field crops such as seed corn and vegetables.[30]

3.3 Soil physical and hydraulic properties

Figure 4 shows the soil pH values, which ranged from 5 to 8 for the five sites at 80 cm depth. There was no significant change in pH with depth. The highest pH was observed at the Mana site owing to the presence of limestone fragments.

The profiles of organic carbon in the top 200 cm for all the soils are also shown in Fig. 4. The OC of the Kula soil was high compared with that of the other soils, as the Kula soil developed from volcanic ash. The Kula soil had the highest OC at a depth of 40 cm (more than 6%). For the other soils, the OC was about 2% at the surface and decreased to less than 0.5% at a depth of 200 cm. The OC profiles were similar at the four other sites.

The bulk density values for the Kula soils were less than 1.0 g cm^{-3}, which is a typical value for volcanic ash soils. For the other soils, the topsoil bulk density ranged from 1.2 g cm^{-3} at Poamoho and Kunia to 1.5 g cm^{-3} at Mana. The Waimanalo soil also showed relatively low bulk density.

The values of saturated hydraulic conductivity (K_s) for all the soils, with the exception of Kula, centered around 0.0001 m s^{-1}. For the Kula soil, K_s was about 20% of this value. All sites (again except at Kula), revealed a gradual decrease in K_s with depth. At Kula, the K_s had a nearly constant value within the soil profile because the shallow soil profile was plowed well prior to the study.

3.4 Pesticide sorption

A linear relationship was found between the adsorbed concentration of pesticides (and their metabolites) and equilibrium liquid-phase concentrations over the range of concentrations used in the batch tests. Hence, the linear isotherm model was fitted to data. The K_d values ranged from 0.05 (imazaquin at Mana) to 23.9 mL g^{-1} (trifloxystrobin at Poamoho) for all compounds for the five sites (supporting Table S1). The highest K_d values were obtained for soils from the Kula site, which might be explained by the fact that this soil had the highest OC (Fig. 4). The K_{OC} values in supporting Table S1 were estimated by dividing the K_d values by the respective fractions of the OC at the corresponding depths. The calculated K_{OC} values were not much different from those reported in the literature.[31] The K_{OC} values used by the US Environmental Protection Agency by its registration division are also reported in the table (Rothmann G, private communication, USEPA). The K_{OC} value of imidacloprid used by USEPA was substantially smaller than the value estimated in this study, and also than the K_{OC} value reported by the FOOTPRINT database.

Theoretically, the K_{OC} values should be uniform with depth. However, the reactivity and spatial heterogeneity of OC are believed to have played a major role in the observed variations. Additionally, the contribution of the soil mineral fraction to sorption (and possible degradation) of organic sorbates may invalidate the use of K_{OC} as a predictor of sorption in soils, especially at depths below the cultivated layer. In supporting Table S1, the K_{OC} values for S-metolachlor were slightly higher than those for atrazine, a known leacher under Hawaii conditions, at four of the five sites (not the case at Kunia). Both imazaquin and sulfometuron-methyl showed low K_{OC} values at all sites. For example, these values were less than 10 mL g^{-1} at Kula and less than 20 mL g^{-1} at Mana. Trifloxystrobin and imidacloprid showed higher estimated K_{OC} values than the herbicides. However, trifloxystrobin exhibits rapid photodegradation (half-life about 2.7 days).[31] Photodegradation of trifloxystrobin could have resulted in overestimation of calculated K_d and K_{OC} values, as it decreased trifloxystrobin concentration in the solution, thus overestimating adsorbed mass in the calculation.

The K_d values for metabolites showed a general declining trend with depth, with a few exceptions (supporting Table S2). For most of the metabolites, the K_d and K_{OC} values were lower than for the parent compounds. In particular, the metabolites of S-metolachlor (CGA-37735 and CGA-354743) had K_{OC} values lower than 10 mL g^{-1} in the Kula soil. Overall, the lowest sorption was found for CGA-354743 at all sites, followed by CGA-37735.

3.5 Pesticide degradation in laboratory conditions

The resident concentration of pesticides in soils during aerobic degradation in the laboratory varied with time. Although the concentrations were expected to decrease with time, sporadic spikes in the samples of certain compounds towards the later part of the degradation study were observed. Improper mixing might have contributed to these discrepancies.

The laboratory-determined half-lives are summarized in supporting Table S3. In this table, the standard deviations, calculated from three replicate samples at each depth, are also reported. The degradation half-life of each compound varied according to soil depth. In general, the half-life was longer in the subsoil than in the topsoil. Although the experimental values showed wide variations, all or portions of data for each of the compounds, with the exception of imidacloprid, were used to estimate degradation half-life for the chemicals at three depths (supporting Table S3). In particular, it was difficult to estimate the half-life for imidacloprid, as the laboratory data showed extreme fluctuations with time. Nevertheless, for the portions of the data that showed monotonic decay, the estimated average half-life was about 313 days, with a standard deviation of about 200 days. The calculated standard deviations showed wide variations (supporting Table S3). For example, the standard deviation for sulfometuron-methyl at Waimanalo was only 1% of the half-life value, while the standard deviation for atrazine at Poamoho equaled 82% of its half-life.

Overall, the median standard deviation of all pesticides was about 20% from all soil horizons and sites.

The literature-reported laboratory degradation half-life values for each compound are also listed in supporting Table S3. The values determined from the present experiment were longer for trifloxystrobin than those reported in the literature.[31] Atrazine showed shorter half-life values than those found in the literature.[31] For S-metolachlor, imazaquin and sulfometuron-methyl, the literature values were within the range of measured values.

3.6 Field dissipation rates

Definitive values of field-dissipation half-life were difficult to estimate for the sites because of highly variable concentrations of the chemicals in both space and time. As stated earlier, there was variability in the application of irrigation water. As the post-application soil samples were collected randomly from each site, areas of plots receiving greater amounts of irrigation water would have showed deeper migration of the chemicals. In the early part of the study period, the sampling depths were shallow (see Table 2). The observed concentration profiles suggested that some of the chemicals went past the sampling depth anticipated as the maximum penetration depth for the given time between application and sampling. As a result, the measured mass for certain sampling events showed less mass than was actually present in the soil profile. The values of field-dissipation half-life were not further used in the analyses.

3.7 Recovery mass from field sampling

Mass recoveries of only selected chemicals at two sites are presented to keep the results concise and comprehensible. Field recoveries of bromide, sulfometuron-methyl, trifloxystrobin and imidacloprid at the Kula and Poamoho sites are shown in Fig. 5. The graph presents the calculated amount of a given chemical present in the soils from the sampled depth per unit area of the plot (g m^{-2}) as a function of time. The depletion of the chemicals in the soil profile could be due to degradation or leaching beyond the sampled zone.

At Poamoho there was an initial loss of bromide in the first sampling event. This could have been due to (i) run-off loss from the plots, (ii) adsorption to the soil and (iii) incomplete recovery from the soil extract. At Kula, a consistent reduction in mass per unit area with time for the sampled depth was observed. Because of its conservative nature, the primary cause of the bromide mass reduction was leaching to the underlying consolidated rocks at 75 cm depth.

As shown in Fig. 5 for Poamoho as well as Kula, sulfometuron-methyl showed a gradual reduction in field recovery, which was mainly attributed to its degradation. It is believed that the majority of this compound was present in the sampling zone. Imidacloprid at Poamoho exhibited only a small mass reduction over a period of 48 weeks. At Kula, the degradation of imidacloprid also seemed to be negligible for a period of 14 weeks. As stated for the laboratory degradation experiments, the imidacloprid concentration (and thus mass) fluctuated with time.

The fast photodegradation of trifloxystrobin probably caused rapid initial decrease in mass in the sampled zone. Later, the trifloxystrobin mass remained almost constant during the study period without significant field dissipation. A similar field recovery pattern of trifloxystrobin was observed at three other sites (not shown).

3.8 Bromide and pesticide concentration profiles

Owing to ease and concise presentation of the results, only the bromide and selected pesticide concentration profiles during the field leaching experiment for the five sites are shown in Fig. 6. It seemed that the sampling depth used 14 days after pesticide application was too shallow; this sampling probably did not capture the leading front of some chemicals (e.g. bromide, S-metolachlor, imidacloprid). Trifloxystrobin topsoil concentration profiles showed substantial dissipation over the study period at Mana. However, the compound continued to leach downward steadily, although the observed concentrations were lowered by one order of magnitude with respect to application. At Kula, atrazine resident concentrations indicated negligible mass in the soil profile after 16 weeks, which could be due to both dissipation and leaching beyond the sampling depth. For imazaquin and S-metolachlor, only topsoil contained concentrations higher than the detection level at the end of the study. Sulfometuron-methyl at Kula showed significant leaching without substantial dissipation. Imidacloprid at the Mana site indicated an unexpected leaching pattern, i.e. the 8 week sampling revealed no chemical below 30 cm, while the sampling events at 12 and 16 weeks showed elevated imidacloprid concentrations in the subsoil. This was accompanied with an increase in mass of imidacloprid at the 12 and 16 week samplings compared with the 8 week sampling event. In addition, an increase in the topsoil concentration in time for a few sampling events can be seen. Bromide at Waimanalo showed leaching to 200 cm depth at the end of the study period.

3.9 COM estimates based on water application

Table 3 shows the calculated COM for various chemicals at the five sites as functions of cumulative water application. The most leaching was calculated for trifloxystrobin. For example, the calculated COM exceeded 1 m for 600 mm of water application at Poamoho, Waimanalo, Kunia and Mana. Bromide center of mass varied between 70 and 155 cm, with the shallowest at Kula and the deepest at Kunia. The presence of all pesticides, with the exception of trifloxystrobin and sulfometuron-methyl at Mana, was limited to 1 m depth for 600 mm of water application. If the COM of a given compound remained constant with increasing water application, the pesticide dissipated or strongly adsorbed to soil (e.g. atrazine at Kula and Mana).

Table 3 also presents the ratio of the pesticide COM to that of bromide for all five sites. Only trifloxystrobin at Poamoho and Waimanalo had ratios greater than 1.0, i.e. the estimated COM of trifloxystrobin migrated below the estimated COM of bromide. The ratios mostly showed a declining trend with increasing time (increasing cumulative water application). This trend could be partly attributed to the overestimation of pesticide COMs in the early part of the experiment. As the first sampling was only 15 cm deep, the measured COM for bromide and the pesticides was identical (i.e. 7.5 cm). Therefore, the initial overestimation of pesticide penetration could have resulted in higher ratios for projected pesticide COMs based on 50 mm water application.

3.10 Evaluation of leaching potential using GUS and AFR

The GUS index for all pesticides and sites is presented in Table 4. In Table 4, the uncertainty of GUS evaluation was assessed by the range of GUS values. The range was calculated using the laboratory-measured half-life values with and without the standard deviation (supporting Table S3). Owing to the lack of laboratory half-life data for imidacloprid in this study, the GUS for this

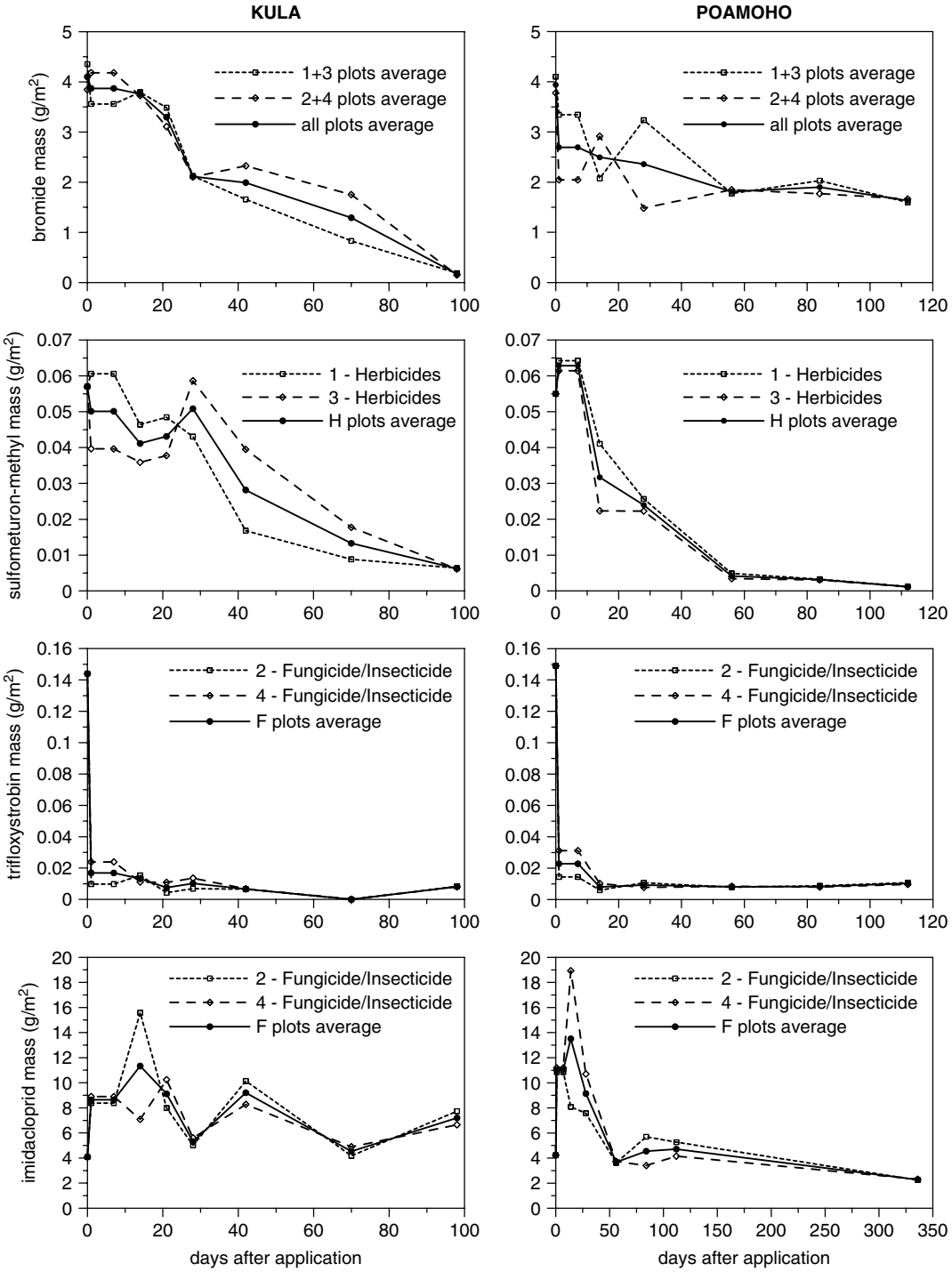

Figure 5. Recoveries of bromide, sulfometuron-methyl, trifloxystrobin and imidacloprid at the Kula and Poamoho sites.

compound was determined on the basis of $t_{1/2}$ values found in the literature.[31] The GUS values in Table 4 are exclusively based on the laboratory results, i.e. estimation of half-life and K_{OC} from K_d using measured OC. According to calculated GUS using the K_{OC} (Rothmann G, private communication, USEPA) and literature $t_{1/2}$ values,[31] imazaquin and imidacloprid were ranked as the most mobile compounds. On the other hand, trifloxystrobin was classified as the least mobile compound using both FOOTPRINT and USEPA K_{OC} values. S-metolachlor was categorized as a transient compound. Atrazine and sulfometuron-methyl were characterized as leachers (GUS $>$ 2.8) using the FOOTPRINT database.

At Kunia, in topsoil, S-metolachlor showed a short half-life (supporting Table S3) and hence was ranked as having low leaching potential. At other sites, S-metolachlor was a mobile chemical. GUS indicated that all herbicides exhibited high leaching potential under the tropical conditions of this experiment. The fungicide trifloxystrobin was ranked as a non-leacher in topsoil of all sites. Imazaquin showed the most leaching potential for all sites (GUS from 3.8 to 9.2).

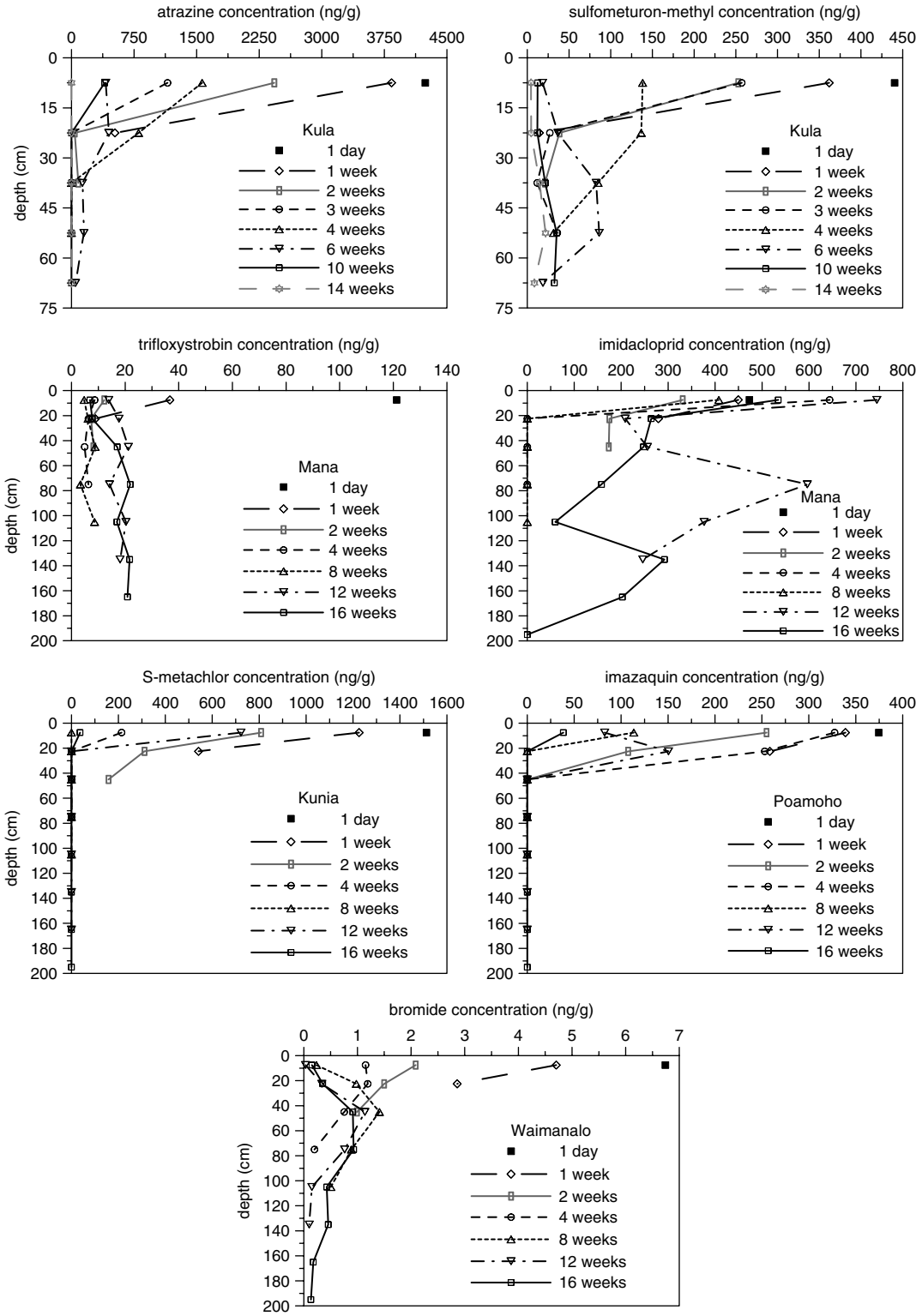

Figure 6. Field content of selected pesticides and bromide at the five sites.

The relative leachability of the new chemicals was also evaluated using the AFR approach.[25] Atrazine and endosulfan were considered as the two reference chemicals; atrazine was the likely leacher and endosulfan was a non-leacher. The mean and standard deviations of K_{OC} and $t_{1/2}$ for the pesticides used for leaching assessment are shown in Table 5. Laboratory-determined sorption as well as degradation data for the five soils were used for estimating these parameters. The calculated AFR values and their corresponding uncertainties, expressed as standard deviations, are summarized in Table 6. Compared with the atrazine–endosulfan pair, most compounds appeared to be likely leachers, with the exception of trifloxystrobin. Imazaquin,

Table 3. Estimates of the locations of the center of mass (COM) for chemicals as a function of water application at the five sites

	Poamoho		Waimanalo		Kunia		Kula		Mana	
Cumulative water application (mm)	COM (cm)	Ratio[a]	COM (cm)	Ratio[a]	COM (cm)	Ratio[a]	COM (cm)	Ratio[a]	COM (cm)	Ratio[a]
Atrazine										
50	12	0.72	17	0.88	14	0.65	10	0.59	10	0.49
200	13	0.32	21	0.47	14	0.25	10	0.33	11	0.21
400	15	0.21	27	0.35	15	0.14	11	0.21	12	0.12
600	18	0.17	34	0.29	16	0.10	11	0.15	13	0.09
Imazaquin										
50	12	0.73	19	1.00	20	0.94	13	0.75	10	0.47
200	14	0.34	25	0.55	36	0.63	21	0.65	10	0.19
400	17	0.23	32	0.40	58	0.55	31	0.60	11	0.11
600	20	0.19	39	0.34	80	0.51	40	0.58	12	0.08
S-metolachlor										
50	11	0.70	17	0.91	16	0.76	9	0.51	10	0.47
200	12	0.29	22	0.49	19	0.33	9	0.29	10	0.19
400	13	0.17	28	0.36	23	0.22	10	0.19	11	0.11
600	13	0.13	35	0.30	27	0.17	10	0.14	11	0.08
Imidacloprid										
50	10	0.63	10	0.53	11	0.52	9	0.51	9	0.43
200	23	0.56	21	0.47	33	0.58	15	0.47	29	0.55
400	40	0.55	36	0.46	63	0.59	23	0.44	57	0.59
600	57	0.54	50	0.44	93	0.60	30	0.43	85	0.62
Bromide										
50	16		19		21		18		21	
200	41		45		57		32		53	
400	73		79		106		51		96	
600	105		114		155		70		138	
Trifloxystrobin										
50	19	1.19	21	1.11	13	0.62	15	0.87	17	0.81
200	50	1.22	48	1.07	41	0.72	26	0.83	46	0.87
400	92	1.26	85	1.08	79	0.75	41	0.81	83	0.86
600	133	1.27	122	1.07	116	0.75	56	0.80	121	0.88
Sulfometuron- methyl										
50	13	0.81	14	0.74	11	0.52	14	0.77	12	0.57
200	16	0.39	29	0.64	23	0.40	24	0.76	43	0.81
400	21	0.29	49	0.62	40	0.38	39	0.76	85	0.89
600	26	0.25	69	0.61	56	0.36	53	0.76	127	0.92

[a] Ratio = (COM for pesticide)/(COM for bromide).

imidacloprid and sulfometuron-methyl showed higher leaching potential than a reference leacher (atrazine) at all five sites. Trifloxystrobin leachability was near that of endosulfan at all sites. The standard deviation of each pesticide's AFR value was similar for all sites (Table 6). The standard deviations of AFR values for all pesticides were low, except for S-metolachlor at all sites and imazaquin at Poamoho and Waimanalo. At these two sites, high recharge rates caused low AFR values, which in turn increased relative uncertainty of imazaquin AFR values. High uncertainty in S-metolachlor leaching was caused by high standard deviation of half-life (Table 5), which resulted from very different half-life values obtained among the five sites (supporting Table S3).

Both leachability indices used in this study showed similar results, as the calculation of AFR and GUS involved the use of the same laboratory-determined input data. Both AFR and GUS ranked trifloxystrobin as a non-leacher. Imazaquin was ranked as the most mobile compound among the group by both indices.

4 DISCUSSION

4.1 Influence of soil properties on leaching

To evaluate the effect of soil properties on leaching, a simple score sheet analysis was performed. Based on the depth of projected COMs for 600 mm of water application (Table 3), each site was assigned a number describing the leaching potential for each chemical (one representing the deepest COM and five for the shallowest COM). After summing the numbers for all seven chemicals, the overall site ranking was determined. The higher the total score, the less deep was the leaching. The relative intensity of leaching at the five different sites was in the following order: Kunia

Table 4. Calculated GUS index for pesticides at the five sites. For USEPA calculation of the GUS, USEPA K_{OC} values and $t_{1/2}$ values from the FOOTPRINT database were used. The numbers in parentheses indicate the range of GUS values[a]

Site	Depth interval (cm)	Atrazine	Imazaquin	Imidacloprid	S-metolachlor	Sulfometuron-methyl	Trifloxystrobin
Poamoho	0–15	2.8 (1.3–3.3)	7.0 (6.2–7.5)	–	4.4 (3.4–4.8)	4.5 (4.0–4.9)	0.6 (0.5–0.7)
	15–30	3.6 (3.5–3.6)	7.0 (6.7–7.3)	–	4.9 (3.6–5.4)	4.3 (3.7–4.6)	0.8 (0.7–0.8)
	60–90	3.2 (3.1–3.4)	5.2 (4.8–5.5)	–	2.8 (2.7–2.9)	3.0 (2.9–3.0)	0.7 (0.7–0.7)
Waimanalo	0–15	2.7 (2.6–2.7)	7.2 (5.6–7.9)	–	2.3 (2.1–2.4)	2.9(2.7–3.2)	1.6 (1.5–1.7)
	15–30	2.6 (2.4–2.7)	6.3 (4.6–7.0)	–	2.5 (2.1–2.7)	2.8 (2.8–2.9)	1.9 (1.5–2.2)
	60–90	2.2 (2.2–2.3)	3.8 (3.2–4.2)	–	2.8 (2.7–2.8)	4.0 (3.9–4.0)	2.2 (1.8–2.5)
Kunia	0–15	2.3 (1.5–2.7)	7.2 (6.4–7.6)	–	1.3 (1.3–1.4)	3.9 (3.7–4.1)	1.2 (1.2–1.3)
	15–30	2.8 (2.7–2.9)	6.8 (6.3–7.1)	–	2.2 (1.9–2.4)	3.7 (3.4–3.9)	1.9 (1.9–2.0)
	60–90	2.6 (2.1–2.9)	6.0 (4.3–6.6)	–	2.7 (2.6–2.8)	4.2 (4.1–4.3)	2.6 (2.1–2.9)
Kula	15–30	2.8 (2.6–2.9)	7.5 (7.3–7.6)	–	2.5 (2.4–2.7)	4.5 (4.2–4.8)	1.3 (1.1–1.4)
	30–45	2.2 (2.1–2.3)	9.2 (8.1–9.8)	–	5.3 (4.1–5.8)	5.3 (5.0–5.5)	2.1 (1.5–2.5)
	60–75	2.4 (2.1–2.6)	7.6 (7.3–7.9)	–	3.8 (3.7–4.0)	6.6 (6.0–7.0)	2.4 (1.9–2.7)
Mana	0–15	3.8 (3.7–3.9)	6.5 (6.4–6.7)	–	2.7 (2.1–3.1)	4.4 (4.2–4.6)	1.4 (1.1–1.5)
	15–30	2.0 (1.5–2.3)	8.7 (7.9–9.2)	–	3.7 (3.4–3.9)	4.1 (4.1–4.2)	1.2 (1.0–1.4)
	60–90	3.1 (2.9–3.2)	7.3 (7.1–7.5)	–	3.1 (3.1–3.2)	4.7 (4.5–4.9)	1.9 (1.8–2.0)
USEPA		–	4.5	7.3	2.0	4.0	0.3
FOOTPRINT (2007)		3.6	5.5	3.7	1.9	2.9	0.2

[a] Shaded area represents a non-leacher (index value GUS < 1.8).

Table 5. Sorption and degradation values of the five pesticides used in the AFR approach

Pesticide	K_{OC} (mL g^{-1})	SD (K_{OC})[a]	Half-life (days)	SD (half-life)[a]
Imazaquin	14	8	269	169
Imidacloprid	280	261	313	200
S-metolachlor	100	31	34	114
Sulfometuron-methyl	23	14	29	17
Trifloxystrobin	688	648	10	10
Atrazine (likely to leach)[b]	147	56.5	75	49.3
Endosulfan (unlikely to leach)[b]	5150	4060	64.3	27.2

[a] SD = standard deviation.
[b] Data from Stenemo *et al.*[25]

> Waimanalo > Mana > Poamoho > Kula. In this evaluation, great variation between compounds was found in ranking the sites for leaching potential. For instance, Poamoho showed the deepest COM for trifloxystrobin but the shallowest COM for sulfometuron-methyl of all sites (Table 3).

Through COM analysis, the greatest overall leaching appeared to occur at the Kunia site. Hence, this site was identified as the most vulnerable to leaching. The Kula site, on the other hand, showed minimal chemical transport. The saturated hydraulic conductivity of the soils did not appear to have a significant effect on chemical transport. The mean K_s values were within one order of magnitude among the five sites. The soil at Kunia had one of the lowest organic carbon contents among the sites (Fig. 4). On the other hand, the Kula site had the highest organic carbon content (Fig. 4). The soil pH at the Kunia site was the second highest among the sites (Fig. 4), which could favor the leaching process.

Another possible explanation for deep solute movement at the Kunia site could be preferential transport. Preferential flow for aggregated oxisols was previously reported in the literature.[32,33] However, as pointed out by Scorza *et al.*,[15] the resident concentrations in the soil profile do not allow detection of preferential transport. In their work, the flux concentrations in drain water proved to be a sensitive detector of preferential flow. The concentration profile data acquired during the field leaching experiment in this study could not prove or disprove the possibility of preferential transport.

Based on the pesticide pKa values and their structure diagrams, the effect of soil pH on non-hydrophobic sorption was evaluated. Only two pesticides, imazaquin and sulfometuron-methyl, were expected to show decreasing sorption with increasing pH. This was supported by batch tests (supporting Table S1), where the Mana site (which had the highest pH values) (Fig. 4) showed low sorption potential for these two compounds. However, the pH effect is not believed to play a major role in sorption processes for the pH values seen in this study.

The estimation of COM locations for the pesticides and bromide (Table 3) further suggested that the tracer did not behave conservatively. The clay mineralogy of the weathered tropical soils is typically dominated by kaolinite and the oxides of iron and aluminum. This mineralogy creates positive charge sites on metal oxide surfaces. Negatively charged anions such as bromide may undergo sorption in these tropical soils.[34,35]

4.2 Influence of pesticide properties on leaching

As with the soils, the effect of pesticide properties on leaching was evaluated using estimated COMs. Overall, the relative leachability of the chemicals had the following order: bromide > trifloxystrobin > sulfometuron-methyl > imidacloprid > imazaquin > atrazine > S-metolachlor. This ranking was consistent at all sites, i.e. all the chemicals exhibited similar COMs at all five sites.

Table 6. Calculated AFR values for pesticides at the five sites. The numbers in parentheses indicate the standard deviations

Pesticide	Poamoho	Waimanalo	Kunia	Kula	Mana
Imazaquin	0.62 (0.72)	0.36 (0.72)	1.53 (0.73)	1.63 (0.77)	2.65 (0.73)
Imidacloprid	2.43 (1.14)	2.19 (1.14)	3.44 (1.15)	3.87 (1.18)	4.51 (1.15)
S-metolachlor	3.78 (3.38)	3.53 (3.38)	4.76 (3.39)	5.14 (3.39)	5.85 (3.38)
Sulfometuron-methyl	3.03 (0.72)	2.78 (0.72)	3.96 (0.73)	4.15 (0.79)	5.08 (0.73)
Trifloxystrobin	6.71 (1.42)	6.47 (1.42)	7.73 (1.42)	8.19 (1.43)	8.80 (1.42)
Atrazine (likely to leach)	3.30 (0.84)	3.05 (0.84)	4.29 (0.84)	4.69 (0.86)	5.37 (0.84)
Endosulfan (unlikely to leach)	6.83 (1.00)	6.59 (1.00)	7.85 (1.00)	8.32 (1.00)	8.92 (1.00)

The herbicide S-metolachlor was identified as the least mobile compound in the group. Atrazine, although known as a leacher under Hawaii conditions, had the second lowest mobility potential among the pesticides tested. Nevertheless, both leachability indices used in this study categorized atrazine as a leacher. That atrazine leaches is also indicated by its detection in Hawaii groundwater.[4]

Trifloxystrobin turned out to be the most mobile compound after the bromide tracer. On the other hand, the obtained AFR and GUS values classified trifloxystrobin as a non-leacher. The leachability of trifloxystrobin using AFR and GUS was evaluated using laboratory data ($t_{1/2}$ and K_{OC}). Batch sorption tests indicated high K_d (in turn K_{OC}), and a relatively short half-life (compared with those of the other compounds tested) was determined from the degradation experiments. However, the observed concentration profiles suggested deep trifloxystrobin leaching. It is important to note that trifloxystrobin concentrations in the soil profile a few days after application were significantly lower than the applied concentration (Fig. 6). The difference between field leaching and laboratory sorption data could be due to overestimation of the lab-determined K_d values for trifloxystrobin owing to photodegradation during the batch tests. Waimanalo and Kula showed significantly lower trifloxystrobin K_{OC} values than Poamoho, Kunia and Mana (supporting Table S1); however, the estimated K_{OC} values for these three sites were comparable with those shown in the FOOTPRINT pesticide database. Another possible explanation might be that trifloxystrobin desorption under field conditions favored deep leaching. Additionally, trifloxystrobin did not follow the laboratory-determined half-life under field conditions, i.e. trifloxystrobin showed larger half-life dissipation values in the field than were determined in the laboratory. It may be further speculated that the field microbial activity was not sufficient for dissipation, as trifloxystrobin is a new compound to Hawaii soils. From these results, the discrepancy between the laboratory data and field experiments became evident.

Imidacloprid at Kunia and Mana (agricultural rates) had a deeper estimated COM than at Poamoho, Waimanalo and Kula (high termicidal rates) (Table 3). The measured subsoil concentrations of imidacloprid were similar regardless of the application rate at all five sites. This leaching pattern could not be explained by advection-dispersion-based theory assuming a linear equilibrium isotherm. However, the imidacloprid leaching pattern could be explained by considering Freundlich sorption isotherms for sites with termicidal rates and linear isotherms for sites where the agricultural rates were applied. The linear equilibrium isotherm for termicidal rates was most likely invalid owing to the limited number of sorption sites in the bulk soil. It is important to mention that the entire range of field concentrations of imidacloprid (agricultural and termicidal rates) was not covered in the laboratory batch sorption tests.

Laboratory sorption data showed that imazaquin and sulfometuron-methyl had a low sorption potential ($K_d < 1$ mL g^{-1}) (supporting Table S1). Regitano *et al.*[17] reported similar K_d values for imazaquin for tropical soils in Brazil. For sulfometuron-methyl, Oliveira *et al.*[36] reported K_d values of about 1 mL g^{-1} for six tropical soils. Observed resident concentrations during the 16 week study period showed that transport of sulfometuron-methyl (ranked as the second highest pesticide leacher by COM analysis) was limited to 80 cm depth (with the exception of the Mana site). Similarly, for imazaquin the concentration profiles suggested negligible downward transport below 40 cm (with the exception of Kula and Kunia). A recent study of imazaquin in tropical soils[17] indicated that batch tests alone were not sufficient to evaluate leaching owing to the assumption of chemical equilibrium in the batch tests, disregarding the physical processes such as rate-limited diffusion. Regitano *et al.*[37] concluded that imazaquin's high mobility potential (owing to low K_d) could be reduced in highly weathered soils because of their acidic nature and high Fe and Al oxide content. The results presented in this study point to a need for cross-comparison of laboratory sorption data and actual field concentration profiles for adequate evaluation of pesticide leaching under field conditions.

Sorption properties indicated that the metabolites of atrazine, S-metolachlor and trifloxystrobin had potential to leach down the soil profile (supporting Table S2). Among the atrazine metabolites, only the desethyl metabolite showed sporadic spikes in the soil profile. Metabolite CGA-51202 of S-metolachlor [(2-ethyl-6-methylphenyl)(2-methoxy-1-methylethyl)amino-oxoacetic acid] was detected early on in the field experiment at all sites. Trifloxystrobin degraded to a number of metabolites within 1 week of application. However, these metabolites showed steady leaching at all five sites.

For this work, the authors followed the study of Gavenda *et al.*[7] which follows earlier studies conducted in Hawaii.[38–40] Many US scientists have carried out sorption and degradation experiments using methods developed in their own laboratories, not closely following the OECD guidelines for the testing of chemicals.[41,42] In order to ascertain whether the present results fell within the reported values in the literature, the results from the experiments were compared with the FOOTPRINT database and other studies. The FOOTPRINT database is widely accessed for research and registration purposes because of its easy availability. It is worth noting that this pesticide database is compiled from different sources with different confidences on the quality of data used. Other pesticide databases in the USA have compiled information in which some of the studies have not followed OECD procedures.

4.3 COM analysis

The need to use COM analysis for the cross-comparison of chemical leaching between sites was apparent from the observed shape of the solute concentration profiles. Well-defined peaks were not generally observed for the pesticides, most likely owing to a complex interaction of sorption and transport processes in the aggregated soils.[7,43] Chemicals retained in intra-aggregate pore spaces of tropical weathered soils are known slowly to leach downward with time.[43,44] Therefore, the COM values could not be approximated by solute peaks in the concentration profiles.

The analysis of projected COMs could be questionable owing to an episodic flow regime, spatially variable irrigation intensities, different application rates for imidacloprid, incomplete chemical recovery on the sampling event, etc. In addition, the actual evaporation was not accounted for in the COM analysis, i.e. only rainfall and irrigation were assumed. It is intuitive that projected COMs could only be interpreted within the timeframe of the field leaching experiment (i.e. 16 weeks), which approximately corresponded to 600 mm of water application for all sites. The use of COM analysis for pesticides with short half-life values is limited owing to complete dissipation of the compound. However, for more persistent compounds and time projection beyond 16 weeks (and hence higher cumulative water application), the estimated COM can still be used, as the dissipation process only decreases the total mass of the pesticide in the soil profile without changing COM.

Furthermore, different coefficients of determination for the COM trendlines were obtained in the regression analysis. Several predicted COMs exhibited strong correlation with measured COM (high coefficient of determination), and hence the estimated COM as a function of water application was more reliable than for cases with low correlation. For compounds showing rapid field dissipation (i.e. atrazine, imazaquin, S-metolachlor), a low correlation of determination was acquired.

Processes such as sorption, field dissipation, rainfall, irrigation and evaporation affected the chemical transport. Thus, the COM was expected to vary among the sites and chemicals. The COM is a relative indicator of the center of mass of the chemical profile in soil. It should be emphasized that the COM did not account for the actual mass of chemical present in soil. So, for certain sites, the COM of imidacloprid was shallow, although its mass was greater than any of the other chemicals. This excess mass could be available to future leaching during periods of heavy precipitation. For specific conditions in Hawaii, episodic storms with daily total rainfall exceeding 200 mm could occur. This could cause severe leaching of chemicals, so the COMs found in this study would not be valid. Although the COM approach is a generalization of the leachability in a given area, it did capture the transport process of chemicals at the five sites.

4.4 Field and laboratory data validity

As discussed by Flury,[45] mass recovery during field experiments varies considerably, especially for pesticides. A complete mass balance of reactive solutes is extremely difficult to obtain. In the present study, analytical difficulties and soil heterogeneity contributed to observed unexpected behavior of the pesticides. Leaching of chemicals beyond the sampling depth could be partially responsible for incomplete recoveries during the field experiment (Fig. 5). Based on expected values, the acquired pesticide dataset might be subjectively ranked as 'excellent' (e.g. S-metolachlor at Kunia) (Fig. 6), 'moderately good' (e.g. bromide at Waimanalo) (Fig. 6) or 'poor' (e.g. imidacloprid at Mana) (Fig. 6). The 'moderately good' and 'excellent' data with more confidence will be subject to future modeling efforts.

In general, the measured spatial distribution of irrigation rates at each study site could be useful in evaluating apparent inconsistencies in field profile concentrations of the pesticides from one sampling date to another. However, the use of a composite sample from three boreholes for each depth increment precluded any analysis of variation between sample holes; the compositing practice was necessary to avoid overloading the analytical laboratory with samples. The compositing of three samples for each depth of each hole sampled provided a kind of 'physical averaging' of concentrations in the three sampled holes, a logical practice where there were limitations in analytical services. In this study, a total of 1582 samples were analyzed for pesticide residues.

5 CONCLUSIONS

The field and laboratory studies provided useful information to compare the relative leachability of the four herbicides, the insecticide and the fungicide. Further, the study addressed the leaching behavior of the pesticides under specific Hawaiian conditions. Leaching profiles among the five sites varied owing to differences in (i) soil properties, (ii) pesticide properties and (iii) water recharge. Within a given site, the variations in chemical profiles were attributed to differences in pesticide properties and partly due to variability in water application. In the early part of the study period, the concentration front of certain chemicals was not captured. Deeper sampling from the beginning would have helped to capture the complete profile. Nevertheless, the measured resident concentration profiles of most pesticides were limited to the top 80 cm after the study period. The variations in laboratory degradation half-life among chemicals appeared to be significant.

Based on COM analysis, the most mobile compound was the fungicide trifloxystrobin, although the lab sorption and degradation experiments suggested low mobility and short persistence of this compound. Although the projected rate of movement of the COM of trifloxystrobin was the greatest among the pesticides, the actual concentrations in the subsoil were low owing to rapid photodegradation. The herbicide S-metolachlor was identified as the least mobile compound.

The most leaching of all the compounds occurred in aggregated oxisol at Kunia. On the other hand, the andisol profile at Kula showed the least chemical transport among the tested sites.

The two leachability indices used in this study delivered similar outcomes, as the calculation of the indices was based on the same lab-determined input data. The revised attenuation factor (AFR) screening approach suggested that all chemicals, with the exception of trifloxystrobin, had the potential to leach. Similarly, the groundwater ubiquity score (GUS) ranked trifloxystrobin as a non-leacher. The discrepancy between laboratory and field leaching data for trifloxystrobin could be attributed to overestimation of sorption properties because of potential photodegradation during laboratory experiments. Similarly, the interaction of imazaquin with mineral oxide surfaces could have contributed to its dissipation. The results suggested that the laboratory data alone were not sufficient for proper assessment of the field leaching of pesticides. Although AFR and GUS indices were not able to predict the fate of trifloxystrobin and imazaquin adequately for the five sites, use of more appropriate model parameters (e.g. a lower organic carbon sorption coefficient for

trifloxystrobin or a shorter half-life for imazaquin, accounting for additional degradation at the mineral surfaces) would have resulted in index values consistent with field observations.

Aside from the field and laboratory data, the final recommendation, which would either support or reject the use of each of the five tested chemicals in Hawaii, is based on a set of complex factors. In spite of the uncertainty in obtained results, the HDOA may use the information to restrict the use of new pesticide compounds at certain locations and remonitor them. Furthermore, not only the field leaching data but also the mode of pesticide use and the application rate are additional aspects to be considered in the registration procedure. For example, in spite of its high leaching potential, the HDOA registered trifloxystrobin as an unrestricted-use pesticide, as the compound is rarely applied to soil in current practice. Sulfometuron-methyl and imazaquin are considered as potential leachers. The pesticide advisory committee of the state of Hawaii recommended monitoring of groundwater in areas where these compounds are being applied. The state may keep records of their use in databases and may restrict their application to certified applicators. For imidacloprid, a final decision is pending. The HDOA considers it as a potential leacher if the compound is used on agricultural crops or in uncovered sites.

ACKNOWLEDGEMENTS

This project was funded by the Hawaii Department of Agriculture, under project #49506. Additional support was provided by the research fund of the Ministry of Education of the Czech Republic (MSM 6840770002). The authors sincerely thank Dr Richard E Green for his guidance during this study. They thank Joseph Lichwa and Martina Sobotkova for helping them with the laboratory measurements. They also thank the managers of the University of Hawaii Agricultural Experiment Station, Roger Corrales, David Oka and Susan Migita, for accommodating them during the field experiment. In addition, they appreciate the help provided by the Hawaii Agricultural Research Center and Pioneer-HiBred for the use of their land for the study. They thank Dr Michael Kawate, Julie Coughlin and James Kam of the University of Hawaii for performing the pesticide applications. They also thank Keith Yabusaki for helping them to design the irrigation system. The project manager for this research was Mr Steven Matsuda from the HDOA. The authors thank him and Mr Robert Boesch for their support. This paper is published as part of the continuing UHM Water Resources Research Center 'Contributed Papers' series.

SUPPORTING INFORMATION

Supporting information may be found in the online version of this article.

REFERENCES

1 Oki DS and Giambelluca TW, DBCP, EDB, and TCP contamination of ground water in Hawaii. *Ground Water* **25**:693–702 (1987).
2 Proposed groundwater quality protection strategy. Draft III. State of Hawaii Department of Health, May (1988).
3 Zhu Y and Li QX, Movement of bromacil and hexazinone in soils of Hawaiian pineapple fields. *Chemosphere* **49**:669–674 (2002).
4 Li QX, Hwang EC and Guo F, Occurrence of herbicides and their degradates in Hawaii's groundwater. *B Environ Contamin Tox* **66**:653–659 (2001).
5 Rao PSC, Hornsby AG and Jessup RE, Indices for ranking the potential for pesticide contamination of groundwater. *Soil Crop Sci Soc Fla* **44**:1–8 (1985).
6 Li ZC, Yost RS and Green RE, Incorporating uncertainty in a chemical leaching assessment. *J Contam Hydrol* **29**:285–299 (1998).
7 Gavenda RT, Green RE and Schneider RC, Leaching of pesticides in selected Hawaii oxisols and andisols as influenced by soil profile characteristics. CTAHR Research Series 075, University of Hawaii, Honolulu, HI (1996).
8 Close ME, Lee R, Sarmah AK, Pang LP, Dann R, Magesan GN, *et al*, Pesticide sorption and degradation characteristics in New Zealand soils – a synthesis from seven field trials. *N Z J Crop Hort* **36**:9–30 (2008).
9 Kazemi HV, Anderson SH, Goyne KW and Gantzer CJ, Atrazine and alachlor transport in claypan soils as influenced by differential antecedent soil water content. *J Environ Qual* **37**:1599–1607 (2008).
10 Close ME, Sarmah AK, Flintoft MJ, Thomas J and Hughes B, Field and laboratory study of pesticide leaching in a Motupiko silt loam (Nelson) and in a Waikiwi silt loam (Southland). *Aust J Soil Res* **44**:569–580 (2006).
11 Capel PD, McCarthy KA and Barbash JE, National, holistic, watershed-scale approach to understand the sources, transport, and fate of agricultural chemicals. *J Environ Qual* **37**:983–993 (2008).
12 Laabs V, Amelung W, Pinto A and Zech W, Fate of pesticides in tropical soils of Brazil under field conditions. *J Environ Qual* **31**:256–268 (2002).
13 Sakaliene O, Papiernik SK, Koskinen WC, Kavoliunaite I and Brazenaitei J, Using lysimeters to evaluate the relative mobility and plant uptake of four herbicides in a rye production system. *J Agric Food Chem* **57**:1975–1981 (2009).
14 Zehe E and Fluhler H, Preferential transport of isoproturon at a plot scale and a field scale tile-drained site. *J Hydrol* **247**:100–115 (2001).
15 Scorza RP, Smelt JH, Boesten JJTI, Hendriks RFA and van der Zee SEATM, Preferential flow of bromide, bentazon, and imidacloprid in a dutch clay soil. *J Environ Qual* **33**:1473–1486 (2004).
16 Racke KD, Skidmore MW, Hamilton DJ, Unsworth JB, Miyamoto J and Cohen SZ, Pesticides report 38. Pesticide fate in tropical soils. *Pure Appl Chem* **69**:1349–1371 (1997).
17 Regitano JB, Prata F, Rocha WSD, Tornisielo VL and Lavorenti A, Imazaquin mobility in tropical soils in relation to soil moisture and rainfall timing. *Weed Res* **42**:271–279 (2002).
18 Bernard H, Chabalier PF, Chopart JL, Legube B and Vauclin M, Assessment of herbicide leaching risk in two tropical soils of Reunion Island (France). *J Environ Qual* **34**:534–543 (2005).
19 Giambelluca TW, Nullet MA and Schroder TA, *Rainfall Atlas of Hawaii*. Division of Water and Land Development, Department of Land and Natural Resources, State of Hawaii, Water Resources Research Center, University of Hawaii, Honolulu, HI (1986).
20 Foote DE, Hill EL, Nakamura S and Stephens F, *Soil Survey of Islands of Kauai, Oahu, Maui, Molokai and Lanai, State of Hawaii*. Soil Conservation Service, USDA, Washington, DC (1972).
21 Green RE and Guernsey CW, Soil–water relations and physical properties of irrigated soils in the Kula area, Island of Maui, Hawaii. Research Bulletin 173, Hawaii Agricultural Experiment Station, CTAHR, University of Hawaii, Honolulu, HI (1981).
22 Landscape irrigation scheduling and water management. Irrigation Association Water Management Committee, Falls Church, VA (2005).
23 Perroux KM and White I, Designs for disc permeameters. *Soil Sci Soc Am J* **52**:1205–1215 (1988).
24 Gustafson DI, Groundwater ubiquity score: a simple method for assessing pesticide leachability. *Environ Toxicol Chem* **8**:339–357 (1989).
25 Stenemo F, Ray C, Yost R and Matsuda S, A screening tool for vulnerability assessment of pesticide leaching to groundwater for the islands of Hawaii, USA. *Pest Manag Sci* **63**:404–411 (2007).
26 Dane JH and Topp GC, *Methods of Soil Analysis, Part 4: Physical Methods*. Soil Science Society of America, Inc., Madison, WI (2002).
27 van Genuchten MTh, A closed-form equation for predicting the hydraulic conductivity of unsaturated soils. *Soil Sci Soc Am J* **44**:892–898 (1980).
28 Vogel T, Cislerova M and Hopmans JW, Porous media with linearly variable hydraulic properties. *Water Resour Res* **27**:2735–2741 (1991).
29 Ray C, Sanda M, Dusek J, Loo B, Pavelkova H, Sobotkova M, *et al*, Leaching behavior of selected pesticides in Hawaii soils as influenced by soil properties and hydrologic conditions: field and laboratory evaluations. WRRC-2007-03, University of Hawaii, Honolulu, HI, 186 pp. (2008).

30 Kemble JK and Sanders DC, Basics of vegetable crop irrigation. ANR-1169, Alabama A&M and Auburn Universities (2000).
31 *Creating Tools for Pesticide Risk Assessment and Management in European Union FOOTPRINT Program*. [Online]. FOOTPRINT (2007). Available: http://www.eu-footprint.org/ppdb.html [14 August 2009].
32 Loague K, Miyahira RN, Green RE, Oki DS, Giambelluca TW and Schneider RC, Chemical leaching near the Waiawa Shaft, Oahu, Hawaii: 2. Modeling results. *Ground Water* **33**:124–138 (1995).
33 Loague K, Bernknopf RL, Green RE and Giambelluca TW, Uncertainty of groundwater vulnerability assessments for agricultural regions in Hawaii: Review. *J Environ Qual* **25**:475–490 (1996).
34 Clay DE, Zheng Z, Liu Z, Clay SA and Trooien TP, Bromide and nitrate movement through undisturbed soil columns. *J Environ Qual* **33**:338–342 (2004).
35 Wong MTF and Wittwer K, Positive charge discovered across Western Australian wheatbelt soils challenges key soil and nitrogen management assumptions. *Aust J Soil Res* **47**:127–135 (2009).
36 Oliveira RS, Koskinen WC and Ferreira FA, Sorption and leaching potential of herbicides on Brazilian soils. *Weed Res* **41**:97–110 (2001).
37 Regitano JB, Alleoni LRF, Vidal-Torrado P, Casagrande JC and Tornisielo VL, Imazaquin sorption in highly weathered tropical soils. *J Environ Qual* **29**:894–900 (2000).
38 Lee CC, Green RE and Apt WJ, Transformation and adsorption of fenamiphos, f. sulfoxide and f. sulfone in Molokai soil, and simulated movement with irrigation. *J Contam Hydrol* **1**:211–225 (1986).
39 Schneider RC, Green RE, Apt WJ, Bartholomew DP and Caswell EP, Field movement and persistence of fenamiphos in drip irrigated pineapple soils. *Pestic Sci* **30**:243–257 (1990).
40 Buxton DS and Green RE, Desorption and leachability of sorbed DBCP residues in Hawaii soils. WRRC Technical Report No. 180, University of Hawaii, Honolulu, HI, 60 pp. (1992).
41 OECD guideline for the testing of chemicals 106: Adsorption–desorption using a batch equilibrium method. OECD, adopted 21 January (2000).
42 OECD guideline for the testing of chemicals 307: Aerobic and anaerobic transformation in soil. OECD, adopted 24 April (2002).
43 Rao PSC, Green RE, Balasubramanian V and Kanihero Y, Field study of solute movement in a highly aggregated oxisol with intermittent flooding: II. Picloram. *J Environ Qual* **3**:197–202 (1974).
44 Rao PSC, Green RE, Balasubramanian V and Kanihero Y, Field study of solute movement in a highly aggregated oxisol with intermittent flooding: I. Nitrate. *J Environ Qual* **2**:359–362 (1973).
45 Flury M, Experimental evidence of transport of pesticides through field soils: a review. *J Environ Qual* **25**:25–45 (1996).

Field leaching of pesticides at five test sites in Hawaii: modeling flow and transport, Pest Management Science, 2011.

Research Article

Received: 11 October 2010 Accepted: 27 April 2011 Published online in Wiley Online Library: 16 June 2011

(wileyonlinelibrary.com) DOI 10.1002/ps.2217

Field leaching of pesticides at five test sites in Hawaii: modeling flow and transport

Jaromir Dusek,[a]* Michal Dohnal,[a] Tomas Vogel[a] and Chittaranjan Ray[b]

Abstract

BACKGROUND: Physically based tier-II models may serve as possible alternatives to expensive field and laboratory leaching experiments required for pesticide approval and registration. The objective of this study was to predict pesticide fate and transport at five different sites in Hawaii using data from an earlier field leaching experiment and a one-dimensional tier-II model. As the predicted concentration profiles of pesticides did not provide close agreement with data, inverse modeling was used to obtain adequate reactive transport parameters. The estimated transport parameters of pesticides were also utilized in a tier-I model, which is currently used by the state authorities to evaluate the relative leaching potential.

RESULTS: Water flow in soil profiles was simulated by the tier-II model with acceptable accuracy at all experimental sites. The observed concentration profiles and center of mass depths predicted by the tier-II simulations based on optimized transport parameters provided better agreements than did the non-optimized parameters. With optimized parameters, the tier-I model also delivered results consistent with observed pesticide center of mass depths.

CONCLUSION: Tier-II numerical modeling helped to identify relevant transport processes in field leaching of pesticides. The process-based modeling of water flow and pesticide transport, coupled with the inverse procedure, can contribute significantly to the evaluation of chemical leaching in Hawaii soils.

Supporting information may be found in the online version of this article.

Keywords: pesticide transport in soil; soil water flow; tropical soil; tier-I model; tier-II model; pesticide registration

1 INTRODUCTION

Physically based deterministic (tier-II) models may serve as possible alternatives to expensive field and laboratory leaching experiments. After adequate calibration to an existing database, tier-II models help to predict the fate and transport of pesticides under varying scenarios (e.g. change of agricultural practices, different weather patterns, etc.). Tier-II modeling may also provide information about pesticide concentration profiles in soil, the flux of leachate towards groundwater and quantitative chemical balance.

In Hawaii, the Hawaii Department of Agriculture (HDOA) currently uses a tier-I screening model to evaluate leaching of pesticides that are candidates for registration in the State. The HDOA originally used a tier-I model based on the attenuation factor (AF)[1] approach, and it currently uses an updated model based on the revised attenuation factor approach (AFR).[2,3] These two approaches only evaluate the relative leaching potential using independently measured pesticide properties and lack the capacity to make detailed predictions of pesticide fate and transport in soils; i.e. the results from tier-I modeling cannot be compared directly with data from field leaching experiments. In Hawaii, the AFR tier-I model primarily serves as a tool in the decision process of pesticide registration where the subject pesticide is judged as a 'leacher' or 'non-leacher' compared with two pesticides – a known leacher and a known non-leacher under Hawaii conditions. This approach is taken by the HDOA because it cannot afford to conduct field leaching experiments for every product entering the state market. The United States Environmental Protection Agency (US EPA) makes use of a regression-based tier-I screening concentration in ground water model (SCI-GROW), along with the tier-II pesticide root zone model (PRZM),[4] to assess the risk posed to groundwater by a pesticide.

To evaluate the reliability of pesticide leaching predictions based on tier-I modeling, Kleveno *et al.*[5] compared the leaching behavior of twenty chemicals at a site where pesticides were known to have leached. They compared the tier-I AF model and PRZM and concluded that AF predictions compared well with PRZM predictions. In separate studies, PRZM was used to simulate pesticide transport in soils found in Hawaii, and the results were compared with field data.[6,7] Loague *et al.*[6,7] stated that the general shape of the concentration profile simulated by PRZM matched field data reasonably well; however, the actual concentrations did not match.

* *Correspondence to: Jaromir Dusek, Department of Hydraulics and Hydrology, Faculty of Civil Engineering, Czech Technical University in Prague, Thakurova 7, 166 29 Prague, Czech Republic. E-mail: dusek@mat.fsv.cvut.cz*

a *Faculty of Civil Engineering, Czech Technical University in Prague, Prague, Czech Republic*

b *Civil and Environmental Engineering and Water Resources Research Center, University of Hawaii at Manoa, Honolulu, Hawaii, USA*

The root zone water quality model (RZWQM)[8] and leaching estimation and chemistry model (LEACHM)[9] are other tier-II models frequently applied to predict fate and transport of pesticides in the unsaturated zone. The pesticide leaching model (PELMO),[10] PRZM and pesticide emission assessment at regional and local scales (PEARL)[11] are tier-II models that are being employed for pesticide registration purposes in the European Union (EU) (FOCUS leaching scenarios[12]). For structured soils, the use of the MACRO tier-II model[13] is recommended within the European Union pesticide registration guidelines. The S1D (tier-II) model,[14] the successor to the original HYDRUS code,[15] was recently compared with the MACRO model to assist in the evaluation of pesticide leaching in Hawaii.[16] Unfortunately, the data used, from an earlier field leaching experiment performed on a Hawaii oxisol, were not sufficient in terms of temporal observations for detailed cross-comparison of the S1D and MACRO models.[16]

The various models noted above differ in the complexity of their approach to solving either water flow or solute transport. Some of these models are based on simple descriptions of water flow dynamics (e.g. PELMO and PRZM), while others are capable of simulating preferential flow and transport (e.g. MACRO and S1D). The advection-dispersion equation is used to describe chemical movement within the soil matrix. Traditionally, a first-order decay process is implemented in the models for predicting pesticide degradation. A comprehensive review of pesticide models was most recently provided by Köhne *et al.*[17]

The primary objective of the present study was to predict pesticide fate and transport using a one-dimensional numerical tier-II S1D model during a field leaching experiment. The data from an earlier field leaching experiment performed by Dusek *et al.*[18] at five different test sites in Hawaii were used for comparison with the model predictions. The purpose of the field study was to collect data to validate the tier-II model. As it was not possible to reproduce some of the observed concentration profiles with the tier-II model on the basis of laboratory-measured reactive parameters, inverse modeling was used to obtain more accurate parameters. The pesticide concentration profiles and centers of mass were then predicted using the tier-II model with optimized transport parameters. The estimated transport parameters of pesticides were also used in the AFR tier-I modeling, to comply with the HDOA pesticide registration assessment. The results obtained from tier-II modeling were compared with the tier-I model predictions to evaluate the validity of the tier-I model and its continued use in pesticide registration protocols.

2 MATERIALS AND METHODS

2.1 Field and laboratory experiments

Detailed description of the field and laboratory experiments used in the present evaluation of the models may be found in Dusek *et al.*[18] Only a brief summary of the experiments, pertaining to the modeling efforts, is presented here.

Three herbicides (S-metolachlor, imazaquin and sulfometuron-methyl), the insecticide imidacloprid, the fungicide trifloxystrobin and a bromide tracer were tested under field conditions during the 16 week study. The five pesticides were under consideration either for new licensing or for license renewal by the HDOA for use in Hawaii. In addition, the herbicide atrazine, a known leacher under Hawaii conditions (based on the fact that it has been found in groundwater in Hawaii), was used as a reference pesticide.

Five sites, representing different soil and hydrological conditions, were selected for the leaching study. Three were located on the island of Oahu (Kunia, Poamoho and Waimanalo), one was on the island of Kauai (Mana) and one was on the island of Maui (Kula). Two of the five soils are oxisols (Kunia and Poamoho), two are vertisols (Waimanalo and Mana) and one is an andisol (Kula).

At each site, four plots of 56 m^2 (noted as 1H, 2F, 3H and 4F) were established. A sprinkler irrigation system, consisting of rotating sprinklers, was set up at each site. Irrigation varied between the sites at rates from 25 to 30 mm of water per week. Each site was equipped with automatic tensiometers installed at three depths below the soil surface.

Bromide tracer (as KBr) was applied on all four plots, the three herbicides were applied on two of the four plots (1H and 3H) and imidacloprid and trifloxystrobin were applied on the remaining two plots at each site (2F and 4F) at label rates. At Poamoho, Waimanalo and Kula, imidacloprid was applied at the termicidal rate. It was applied at the agricultural rate (about 65 times lower than the termicidal rate) at Kunia and Mana.

One day after application, a layer of wheat straw was spread over the entire application area to prevent photodegradation and reduce evaporation from the bare soil. Soil samples were taken at each plot from several depths 1 day and 1, 2, 4, 8, 12 and 16 weeks after the application. For each sampling depth, samples were taken from three different holes and combined into a composite sample for analysis. The samples from the greatest depth (210 cm for all sites except for Kula) were only taken during later sampling events to reduce the samples to a manageable number for analysis. At Kula, the soil profile was situated on a 75 cm deep man-made terrace with underlying rock fragments, so sample depth was limited to 64 cm below the surface.

Analysis of pesticide residue was performed on a liquid chromatograph using a mass spectrometer or gas chromatograph with a mass spectrometer detector. The bromide tracer was analysed using an ion chromatograph.

The saturated hydraulic conductivities were evaluated at each site *in situ*, taking six repeated measurements at three depths using a disk tension infiltrometer. In the laboratory, the drainage branch of the water retention curve was measured in six replicate soil samples from 3–5 depths depending on the site. Experimental data were fitted by the van Genuchten–Mualem model.[19,20] The reference retention curves were established using the scaling method of Vogel *et al.*[21] Soil bulk density was also determined using undisturbed soil core samples. Pesticide batch sorption tests and degradation experiments were performed in the laboratory on samples collected from both topsoil and subsoil horizons.

For asymmetric concentration profiles, a meaningful way to evaluate the relative leachability of a compound through the soil is to locate its center of mass (COM).[22,23] The COM is defined as the depth at which 50% of the chemical mass is above and the other 50% is below. Note that the measured COM does not necessarily specify the depth of the peak concentration of a chemical. For asymmetric concentration profiles, the total depth of leaching could be much more than twice the depth of the COM.[24]

2.2 Revised attenuation factor approach

The revised attenuation factor (AFR)[2,3] model is accepted by the HDOA as a tier-I model for registration purposes to evaluate the leaching potential of pesticides. The AFR index is defined as

$$\mathrm{AFR} = \ln\left(\frac{d\,\mathrm{RF}\,\theta_{\mathrm{FC}}}{I\,t_{1/2}}\right) + k \qquad (1)$$

where d is the compliance or groundwater depth (m), θ_{FC} is the water content at field capacity ($m^3\ m^{-3}$), I is the average water

flow rate through the soil (m day^{-1}), $t_{1/2}$ denotes the pesticide half-life (day), k is a constant ensuring positive AFR index values and RF is the retardation factor which is evaluated as

$$RF = 1 + \frac{\rho f_{OC} K_{OC}}{\theta_{FC}} \quad (2)$$

where ρ is the soil bulk density (kg m^{-3}), K_{OC} is the soil organic carbon sorption coefficient (L kg^{-1}) and f_{OC} is the organic carbon content (–).

2.3 Flow and transport model

The one-dimensional numerical S1D model,[14] based on Richards' equation for water flow and the advection-dispersion equation for conservative and reactive solute transport, was employed in this study. The S1D model has previously been used to predict water flow and chemical transport in various soils,[25–27] including those with well-developed structure.[28–30] These earlier studies considered the transport of many compounds, from conservative tracers[30] to pesticides[26,28] and heavy metals.[25,27] The S1D model utilizes the Galerkin linear finite element method for numerical solution of the flow and transport equations. More details on the numerical model can be found elsewhere.[14,31] Water flow is described in the S1D model as

$$\frac{\partial \theta}{\partial t} = \frac{\partial}{\partial z}\left(K(h)\left(\frac{\partial h}{\partial z} + 1\right)\right) \quad (3)$$

where θ is the soil water content (m^3 m^{-3}), h is the pressure head (m), K is the hydraulic conductivity function (m day^{-1}), z is the vertical coordinate (assigned positive values for the upward direction in meters) and t denotes time (day). The van Genuchten–Mualem model[19,20] is used to describe the soil hydraulic functions in the S1D model.

The transport of solutes is given by the advection-dispersion equation:

$$\frac{\partial \theta c}{\partial t} + \frac{\partial \rho s}{\partial t} = \frac{\partial}{\partial z}\left(\theta D \frac{\partial c}{\partial z}\right) - \frac{\partial q c}{\partial z} - \lambda_w \theta c - \lambda_s \rho s \quad (4)$$

where c is the solute concentration (kg m^{-3}), D is the hydrodynamic dispersion coefficient (m^2 day^{-1}) comprising the molecular diffusion and dispersion, q is the soil water flux (m day^{-1}), s is the adsorbed concentration (kg kg^{-1}) and λ_w and λ_s are the first-order degradation coefficients (day^{-1}) for the liquid and solid phases respectively. The coefficients λ_w and λ_s are calculated using the half-life value $t_{1/2}$ as $\lambda = \ln(2)/t_{1/2}$. For this study, the first-order degradation coefficients in the liquid and solid phases were assumed to be identical. The sorption distribution coefficient K_d (L kg^{-1}) is used to calculate the adsorbed concentration s from the solute concentration c as

$$s = K_d c^{\kappa} \quad (5)$$

where κ is the empirical fitting coefficient (–). If the exponent $\kappa = 1$, the non-linear form of the sorption isotherm simplifies to a linear equilibration isotherm.

To compare the simulated pesticide concentrations with observed values, the simulated solute concentrations c (i.e. in the liquid phase) were converted into total concentrations expressed in mg kg^{-1} of dry soil. For this conversion, soil bulk density, water content and distribution coefficients were used.[16] As bromide is assumed to be a conservative tracer, only the values for soil bulk density and water content were necessary in this case. The predicted total concentrations in numerical nodes were averaged over the sampled zone to produce a single value, which could then be compared with the measured concentration at that sample increment.

The S1D model takes into account the effect of soil water content dynamics on pesticide degradation. This effect was, however, not considered in the simulations in the present study, as the experimental plots were regularly irrigated during the study and the clay content of the soils prevented substantial variations in water content. Furthermore, the effect of temperature on pesticide degradation was neglected because soil temperature does not fluctuate dramatically in Hawaii.

2.4 Parameterization of the models

Input parameters were varied among the five sites when using AFR to evaluate the relative leachability of a pesticide. Parameters were derived from both laboratory measurements (ρ, θ_{FC}, f_{OC}) and field observations (I). The compliance depth was chosen as $d = 0.5$ m for all sites. The soil organic carbon sorption coefficient and half-life values used for the AFR approach were derived from the inverse modeling of the reactive transport (see Section 3.4).

Both field and laboratory experiments (see Section 2.1) were performed for parameterization of the S1D model. The measured soil hydraulic parameters for the five sites are shown in supporting information Table S1. For sites where the hydraulic parameters were not measured at depths below 90 cm, deeper soil properties were assumed to be the same as those in the overlying soil layer.

The values of K_d and $t_{1/2}$ for the five sites were derived from batch sorption tests and laboratory degradation experiments.[18] The linear isotherm was found to be valid for the range of concentrations tested. The molecular diffusion coefficient for the pesticides was fixed at a general value of 0.43 cm^2 day^{-1}.[32] The molecular diffusion coefficient for the bromide tracer (1.2 cm^2 day^{-1}) was taken from the literature.[33] Based on a review of field-scale dispersivities,[34] the dispersivity value was, for simplicity, fixed at 10 cm for all sites.

2.5 Initial and boundary conditions for the tier-II model

The numerical simulation of soil water flow and solute transport was considered for the period of the field leaching experiment (i.e. 16 weeks). The initial condition corresponded to the soil water pressure profile measured by tensiometers before the pesticide application. The upper boundary condition involved natural rainfall, artificial irrigation and potential evaporation. Rainfall and irrigation intensities were organized in 1 h series. Daily potential evaporation was estimated from pan evaporation measurements. The lower boundary of the simulated domain was treated as the unit hydraulic gradient boundary, allowing water to leave the soil profile at a rate equal to the unsaturated hydraulic conductivity. Except for the Kula site, the simulated domain was defined to be 220 cm deep for all sites. For the Kula site, a domain depth of 75 cm was defined for the simulations. The simulated domain was numerically discretized into computational nodes with a spacing of 1 cm.

For the solute transport simulations, the chemical-free soil profile was used as the initial condition for simulation at each of the field sites. For the herbicides plots (1H and 3H), the herbicides and bromide tracer were applied separately over a period of 30 min in 5 L of water. Mimicking spray concentrations

typical for commercially applied insecticides and fungicides, imidacloprid and trifloxystrobin as well as bromide tracer were applied separately over a period of 30 min in 10 L of water to the insecticide/fungicide plots (2F and 4F). Thus, a third-type boundary condition with prescribed solute mass flux was employed to match the field applied mass. The bottom boundary was a zero concentration gradient condition, which would allow the bromide tracer and pesticides to pass through it.

2.6 Inverse modeling and RMSE

Inverse modeling involved the calibration of the soil hydraulic characteristics to improve the agreement with observed pressure heads. The measured soil hydraulic parameters listed in supporting information Table S1 were used as the initial estimates for the inverse modeling. The S1D model was coupled with the model independent parameter estimator (PEST) package,[35] which is based on the Levenberg–Marquart algorithm, to minimize the differences between simulated and observed responses. The fitting parameter α in the van Genuchten retention model and the saturated hydraulic conductivity (K_s) values were optimized in the least-squares sense. The objective function contained observed pressure head values.

Once the water flow model was calibrated, the transport model was run using the laboratory-determined values of the reactive transport parameters (i.e. K_d and $t_{1/2}$) to predict chemical concentrations in the soil profile and COMs. In the next step, the transport parameters were estimated through inverse modeling to obtain a better match between the data and model predictions. The S1D coupled with PEST was used to estimate K_d and $t_{1/2}$ values. In field leaching experiments, the $t_{1/2}$ parameter refers to dissipation rather than degradation half-life. The estimated field dissipation half-life values can be somewhat shorter than the laboratory-measured degradation half-life values, as the chemical is exposed to other loss mechanisms (e.g. volatilization, photodegradation). The objective function contained chemical concentration profiles measured during the leaching experiment and information about the observed position of the COM. Because of different absolute values and numbers of data in the objective function (i.e. the concentration soil profiles and the depths of the COM), each measurement set and each measured value were weighted to counterbalance their relative weight.[36] The weight factor for depths of the COM was normalized by the number of measurements. The weight factor for the concentration soil profiles was calculated as the logarithm of the measured values and subsequently normalized by the number of measurements. For concentrations below the detection limit for the respective pesticide, a weight factor calculated for the smallest detected concentration was used. As a result, the weight factors for the pesticide concentration profiles slightly increased the relative importance of the later sampling events as the measured concentrations decreased with time.

It is well known that reactive transport parameters may gradually change with depth.[12] However, to reduce overparameterization of the inverse problem, only topsoil (0–30 cm for all sites except Kula, where it was 0–25 cm) and subsoil (below 30 cm for all sites except Kula, where it was below 25 cm) values of K_d and $t_{1/2}$ were optimized. Bromide simulations were run only with the optimized sets of soil hydraulic characteristics (see above), i.e. no other parameters were adjusted.

A quantitative measure of agreement between the model predictions and experimental data was evaluated using the root mean square error (RMSE), which is defined as

$$\mathrm{RMSE} = \left[\frac{1}{N-1} \left(\sum_{i=1}^{N} (w_i o_i - w_i m_i)^2 \right) \right]^{1/2} \tag{6}$$

where N is the number of measurements, w is the weight factor and o and m are the observed and simulated responses respectively. The RMSE for pressure heads is in cm, while RMSE for pesticide concentration profiles is in mg kg^{-1}. The smaller the RMSE value, the better the agreement between model predictions and experimental data. Should the model prediction and experimental data be identical, the RMSE will be zero. The pressure head and bromide concentration values used for the calculation of RMSE were not weighted (i.e. $w = 1$).

3 RESULTS

3.1 Water flow regime

A graphical comparison of simulated and observed pressure heads at the Kunia site is provided in Fig. 1. The figure shows generally close agreement between the field data and simulated pressure heads using optimized soil hydraulic parameters (RMSE = 16 cm). This is undoubtedly due to the calibration of the water flow model to fit the observed pressure heads. Figure 1 additionally depicts the simulated pressure heads using measured hydraulic parameters (labeled as 'before optimization', RMSE = 138 cm). Agreement between predicted and observed pressure heads at the other experimental sites was similar to that obtained for Kunia. The optimized soil hydraulic parameters for all sites are summarized in supporting information Table S2. RMSE values of pressure heads after the optimization were substantially lower compared with scenarios based on measured hydraulic parameters (average RMSE values for scenarios before and after optimization were respectively 217 and 19 cm for all five sites).

3.2 Chemical concentration profiles in soil

Figure 2 presents a comparison of predicted and observed concentration profiles for selected sites and compounds. The figure displays predicted concentration profiles after using optimized K_d and $t_{1/2}$ values. Abrupt transitions in simulated bromide concentration profiles at soil horizon interfaces are caused by changes in bulk density and actual water content. Field concentration profiles of imidacloprid at the Waimanalo site were characterized by significant variations in the insecticide's mass in the sampled zone, generating some very low levels of correlation between the observed profiles and those predicted by the numerical model (Fig. 2).

RMSE values based on measured and optimized transport parameters are shown in Table 1. RMSE values for bromide for all five sites are also shown in Table 1. Average RMSE values based on laboratory-measured K_d and $t_{1/2}$ parameters and optimized reactive parameters were respectively 0.289 and 0.160 mg kg^{-1} for all five sites.

The optimized values for K_d and $t_{1/2}$ are listed in supporting information Tables S3 and S4. Optimized K_d values ranged from 0.00 mL g^{-1} (trifloxystrobin at Waimanalo) to 4.41 mL g^{-1} (S-metolachlor at Kula) for all pesticides at the five sites (supporting information Table S3). In supporting information Table S3, the soil organic carbon sorption coefficients K_{OC}, calculated as $K_{OC} = K_d/f_{OC}$, are shown for all pesticides. The values of K_{OC} ranged

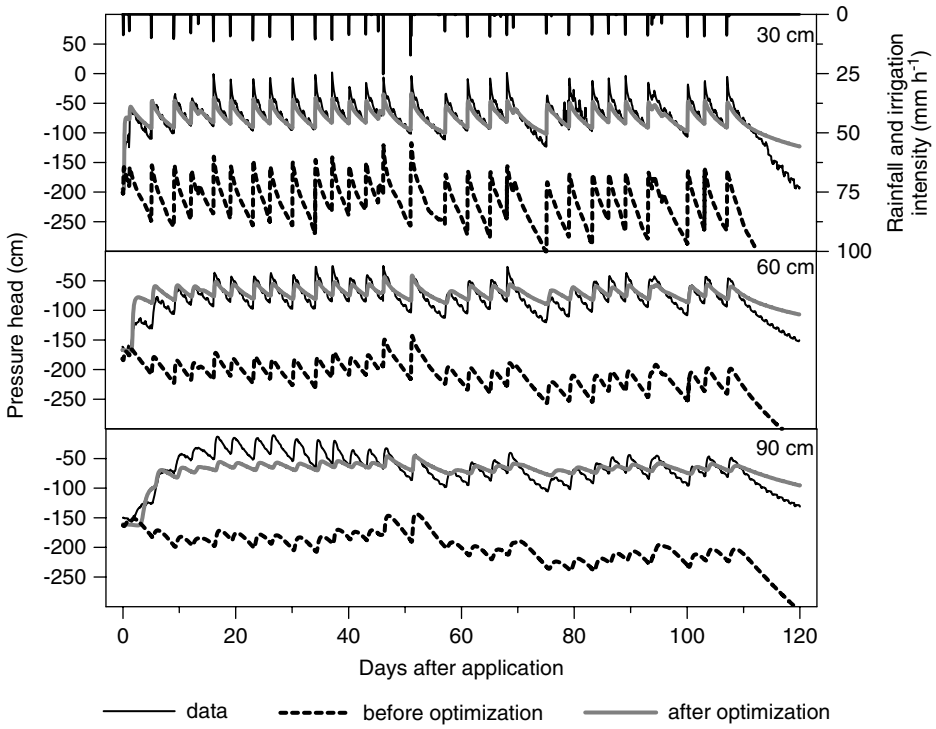

Figure 1. Simulated and observed pressure head development at three depths at the Kunia site.

Table 1. RMSE values (mg kg^{-1}) computed for scenarios based on optimized reactive transport parameters. The RMSE values (mg kg^{-1}) for scenarios based on laboratory-measured transport parameters are shown within parentheses. For bromide simulations, the RMSE was not weighted and transport parameters were not optimized

Site	Bromide	Atrazine	Imazaquin	Imidacloprid	S-metolachlor	Sulfometuron-methyl	Trifloxystrobin
Poamoho	0.979	0.013 (0.171)	0.035 (0.057)	0.428 (0.487)	0.128 (0.273)	0.0004 (0.004)	0.166 (0.261)
Waimanalo	0.525	0.012 (0.091)	0.045 (0.052)	0.187 (0.339)	0.015 (0.035)	0.001 (0.002)	0.384 (0.394)
Kunia	1.367	0.023 (0.081)	0.049 (0.053)	0.028 (0.040)	0.017 (0.018)	0.001 (0.005)	0.013 (0.039)
Kula	4.241	0.061 (0.131)	0.086 (0.089)	2.435 (4.855)	0.037 (0.056)	0.019 (0.020)	0.458 (0.471)
Mana	1.881	0.017 (0.164)	0.012 (0.045)	0.115 (0.168)	0. 011 (0.177)	0.001 (0.010)	0.013 (0.090)

from 0 mL g^{-1} (trifloxystrobin at Waimanalo) to 607 mL g^{-1} (S-metolachlor at Poamoho). The optimized half-lives ranged from 1.2 days (atrazine at Mana) to 616.6 days (imidacloprid at Mana) for all sites and pesticides (supporting information Table S4).

In addition to the optimization of K_d and $t_{1/2}$ values, the exponent κ in equation (5) was estimated by inverse modeling for the imidacloprid applied at the high termicidal rate (Poamoho, Waimanalo and Kula). It was hypothesized previously that the linear equilibrium isotherm for termicidal application rates was most likely invalid owing to the limited number of sorption sites in the bulk soil.[18] However, RMSEs and COMs did not differ significantly for predictions based either on the linear or non-linear isotherms at these three sites. Thus, in the present case it can be concluded that the assumption of the linear isotherm was also adequate in the modeling of imidacloprid transport at high termicidal application rates.

3.3 Center of mass comparison

Comparisons of the measured COM and the simulated pesticide COM for optimized scenarios are presented in Table 2. The COMs of bromide predictions, run in non-optimized mode, are also shown in Table 2. Ratios higher than 1 between the observed and the predicted COMs indicate that the COM was underpredicted. The average ratio of observed COMs to predicted COMs for bromide was 1.11, which implies a negligible overall underprediction of COMs. For the pesticides, the averages of observed-to-predicted COMs for scenarios based on measured K_d and $t_{1/2}$ values and optimized reactive parameters were 3.48 and 1.19 respectively. The scenarios using optimized reactive parameters showed only slight underestimation of predicted COMs. The best and worst fits based on the comparison of measured and predicted COMs were obtained for imazaquin at Kula and S-metolachlor at Mana respectively (Table 2).

3.4 AFR comparison

Optimized K_d and $t_{1/2}$ values (shown in supporting information Tables S3 and S4) were used to run the AFR model for the five sites and the five new pesticides. This was a different procedure to that used in the present authors' previous study[18] where laboratory-measured K_d and $t_{1/2}$ values were considered. In the present study,

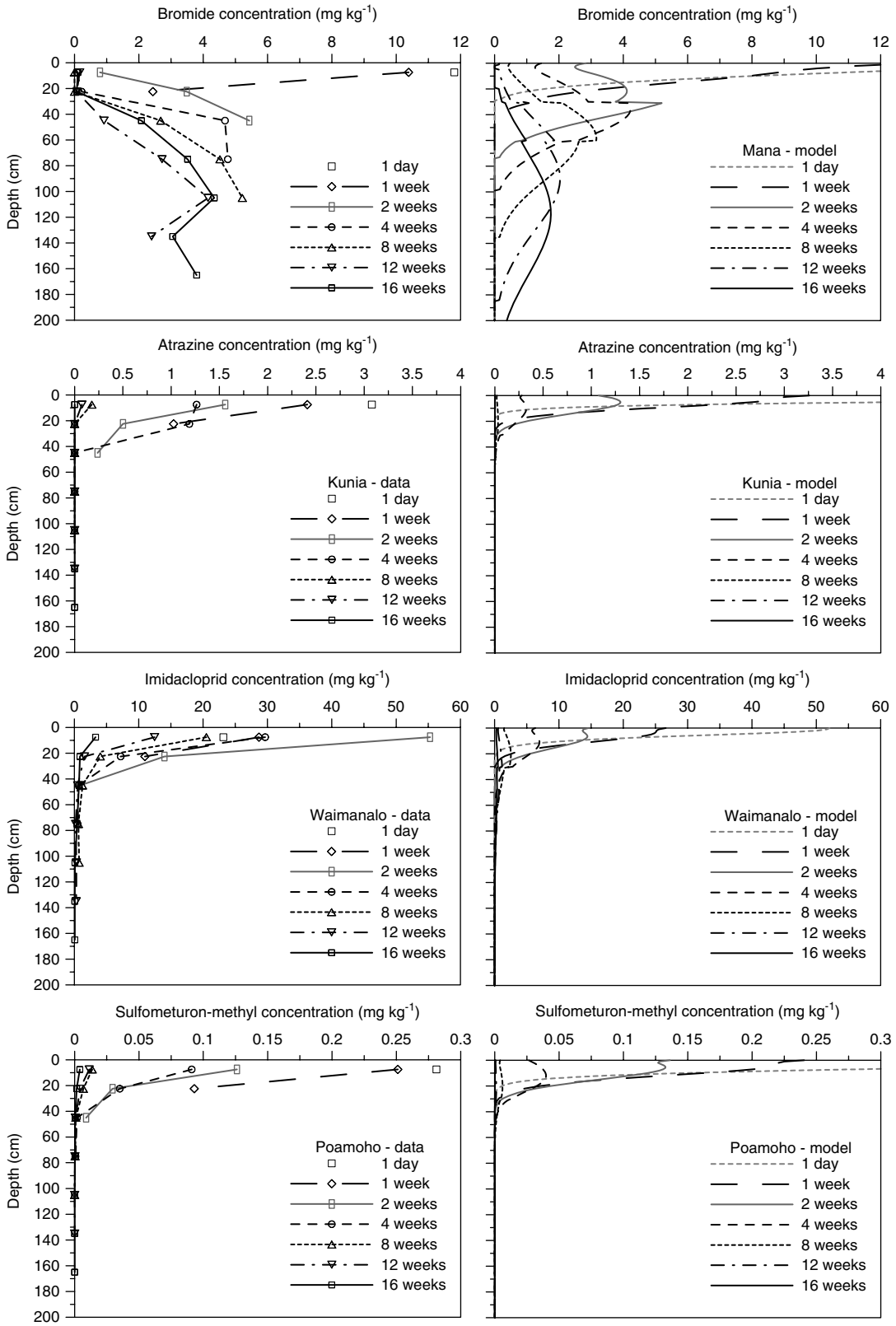

Figure 2. Simulated and measured concentration profiles of selected pesticides and bromide. Left panel, observed profiles; right panel, simulated profiles based on optimized values of K_d and $t_{1/2}$. Bromide simulation was not optimized.

Table 2. Measured COM/simulated COM for all chemicals at five sites. Simulated pesticide COM values are based on the optimized scenarios. Bromide simulations were not optimized

Site	Weeks after application	Bromide	Atrazine	Imazaquin	Imidacloprid	S-metolachlor	Sulfometuron-methyl	Trifloxystrobin
Poamoho	1	0.91	1.60	2.98	1.55	2.85	1.61	1.17
	2	1.05	1.20	2.06	1.16	2.15	1.88	1.34
	4	1.20	0.93	1.53	1.03	0.82	1.04	1.61
	8	1.04	ND/NS	0.54	1.05	ND	0.92	1.07
	12	0.92	NS	1.08	0.74	0.40	0.89	0.98
	16	0.96	ND/NS	0.37	1.12	0.32	1.00	1.05
Waimanalo	1	1.17	1.07	1.52	1.78	1.26	1.54	0.90
	2	1.69	1.61	2.25	1.25	1.71	1.23	1.69
	4	1.34	0.39	0.38	1.02	0.32	1.17	1.77
	8	1.41	ND/NS	ND	1.10	ND/NS	1.12	1.63
	12	1.09	ND/NS	0.16	0.87	NS	0.43	0.39
	16	1.31	ND/NS	0.14	1.05	ND/NS	0.82	1.55
Kunia	1	0.84	2.13	1.40	1.18	1.11	1.66	1.04
	2	1.36	2.56	1.90	0.82	1.34	1.47	1.39
	4	1.16	1.12	2.01	1.19	0.2	1.17	1.43
	8	0.98	0.37	0.56	1.09	ND/NS	0.90	1.08
	12	1.08	0.33	1.10	1.21	NS	1.05	0.97
	16	1.09	ND/NS	0.53	0.86	NS	0.99	1.15
Kula	1	0.85	2.34	1.33	2.08	3.36	1.18	1.66
	2	0.73	1.47	1.10	1.48	2.11	1.04	1.39
	3	0.70	1.01	1.01	1.19	1.48	0.99	1.66
	4	1.08	0.97	0.83	1.08	0.89	0.87	1.89
	6	1.05	1.44	ND	1.00	1.53	1.03	1.34
	10	0.92	0.40	0.81	0.88	0.49	0.84	0.98
	14	0.91	ND/NS	NS	0.82	0.21	0.80	0.66
Mana	1	1.17	2.61	1.43	2.21	3.27	1.53	1.39
	2	1.55	1.08	ND/NS	1.80	1.17	1.22	1.23
	4	1.57	ND	ND/NS	0.32	ND	1.41	1.11
	8	1.37	ND/NS	ND/NS	0.20	ND/NS	0.86	1.09
	12	1.09	ND/NS	ND/NS	1.29	ND	1.11	0.99
	16	0.94	ND/NS	ND/NS	1.11	ND/NS	0.93	0.98

ND: not detected; NS: not predicted by simulation.

atrazine and endosulfan were used as reference compounds. Atrazine was considered likely to leach, and endosulfan was considered unlikely to leach. Transport parameters for the two reference compounds were adopted from Stenemo *et al*.[3]

Comparisons of the AFR index values with the observed COMs at the Poamoho site are shown in Fig. 3. The COMs predicted by the S1D model are also shown in this figure. Figure 3 indicates that the relative leachabilities of the pesticides under study were represented similarly by both the AFR and predicted COMs. However, the exact order of pesticide relative leachabilities given by the COMs and AFR was not obtained (COMs and AFR values did not agree with each other, but the differences were negligible). AFR indices for five of the six tested pesticides were predicted in the narrow range from 3.0 to 3.5 (Fig. 3). Given the uncertainty associated with the AFR index values (about $\pm$0.4 AFR for each pesticide), the exact order of predicted pesticide relative leachabilities may be better characterized by the COMs. Overall, it can be seen that the use of more appropriate model parameters than those used by Dusek *et al*.[18] resulted in predicted index values that were more consistent with field observations.

3.5 Mass recovery

The comparison of calculated and simulated mass recovery, defined as the amount of chemical present in the soil profile per unit area of the plot as a function of time, is shown in Fig. 4. The calculated mass recovery was determined from the measured chemical concentration profile. Reduction in the pesticide mass is primarily caused by degradation or leaching below the sampled zone. Particularly for the shallow soil profile at Kula, it was difficult to conclude from the observed concentration profiles which of these two processes was more significant (Fig. 4a). The S1D model helped to identify degradation as the comparatively greater mechanism for the mass reduction of S-metolachlor at the Kula site where leaching below the sampled zone did not occur (see Section 4.1). Similarly, for sulfometuron-methyl at the Mana site (Fig. 4b), the model indicated that degradation was the primary mechanism of mass reduction of that compound in the soil profile.

3.6 Pesticide leachate and the breakthrough curve

The mass flux of leachate leaving the sampled zone at each of the test sites was simulated using the tier-II model based on optimized transport parameters. Owing to the shallow soil profile sampled

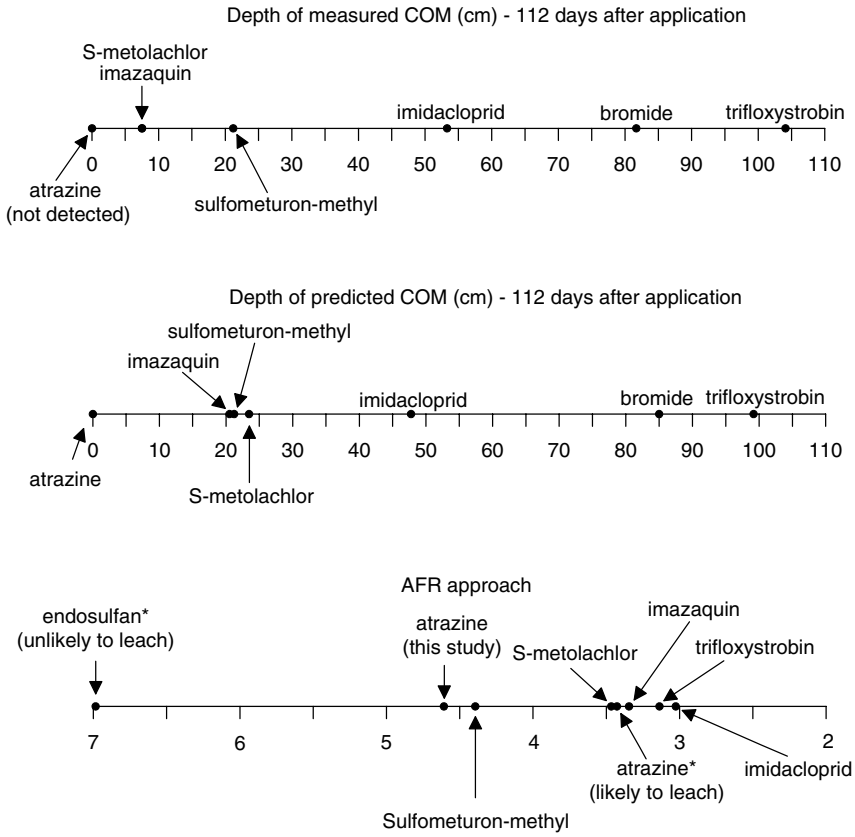

Figure 3. Relative mobility of the pesticides and bromide as indicated by field data, S1D model predictions and AFR index values at the Poamoho site. Values of K_{OC} and $t_{1/2}$ of the two reference compounds (atrazine and endosulfan, marked with asterisks) were taken from Stenemo *et al.*[3] Input parameters for AFR: $\rho = 1200$ kg m^{-3}, $f_{OC} = 1.391\%$, $d = 0.5$ m, $\theta_{FC} = 0.42$, $I = 0.0017$ m day^{-1}, $k = 1$.

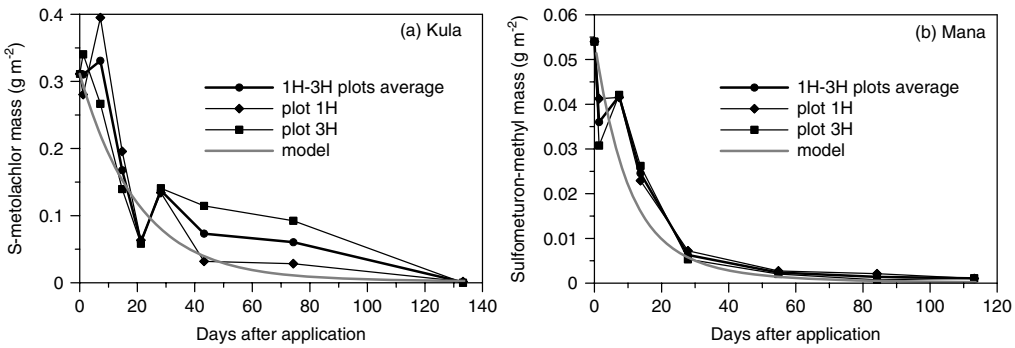

Figure 4. Comparison of simulated and measured mass recovery for (a) S-metolachlor at Kula and (b) sulfometuron-methyl at Mana.

at Kula (i.e. only 64 cm deep), transport simulations predicted pass-through of imazaquin, imidacloprid, sulfometuron-methyl and trifloxystrobin. For all other sites, leaching below the sampled zone (i.e. 210 cm) was predicted only for imidacloprid at Mana and for trifloxystrobin at Poamoho and Waimanalo. Simulations of trifloxystrobin, however, predicted only trace concentrations at Poamoho and Waimanalo (total leachate $<0.002\%$ of the applied mass). The greatest mass loss by leaching was predicted for imazaquin at Kula (59.8% of the applied mass).

Simulated breakthrough curves of the pesticides at a depth of 64 cm at Kula are shown in Fig. 5. The onset of the concentration rise is principally controlled by the K_d values of the respective pesticides. Note that the pesticides were applied at different rates, so the peak concentrations are influenced by K_d and $t_{1/2}$ values as well as by the application rates. As a result, the highest predicted concentration peak was for imidacloprid, applied at termicidal rates at the Kula site.

4 DISCUSSION

4.1 Field data of chemicals

Composite samples were produced from three boreholes for each depth increment during the field leaching experiment. This compositing provided a kind of 'physical averaging' of concentrations from the three sampled holes. However, the variability of the subsample concentrations remained unknown. Comparison of the observed profiles with the predicted results would likely have been more favorable if the range of concentrations given by

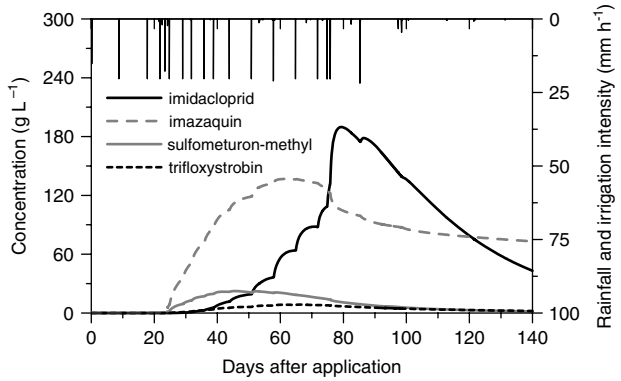

Figure 5. Simulated breakthrough curves of four pesticides at the Kula site (depth of 64 cm).

standard deviations (resulting from analysis of three individual samples rather than the composite sample) at each depth had been determined.

As a result of the implemented sampling plan, bromide and a few of the pesticide compounds leached below the sampled depths early on in the experiment.[18] Deeper sampling from the beginning would have permitted the capture of the complete concentration profiles of the chemicals. However, a majority of the chemicals stayed within the sampled depths at the five sites. So, the mass loss caused by insufficient depth of sampling was minimal as the later samples were extracted from the full depth profile. Nevertheless, the COM analysis in this study suffers from this drawback; the calculated ratios of measured to simulated COMs in the early parts of the experiment will differ slightly from the true ratios.

For some of the pesticides considered in this study, an acceptable match between measured field data and model predictions was difficult to obtain. In a previous study, the field data were subjectively categorized as 'excellent – moderately good – poor'.[18] In this study, assessment was based on RMSE values (Table 1) or comparison of COM values (Table 2). Inconsistencies in some COM comparison (i.e. unexpected changes in COM ratios between samplings) occurred for a few sampling events, and these observations were identified as events of 'poor' data quality. It was not possible to reproduce some of the observed unexpected leaching patterns using standard modeling approaches. It may be hypothesized that the variability in field observations was responsible for the poor predictive performance of the model. Furthermore, it was concluded in the previous study that laboratory analytical difficulties (e.g. pesticide extraction from the soil) and soil heterogeneity contributed to observed variability of resident concentration profiles.[18]

4.2 Estimated parameters

The soil organic carbon sorption coefficients K_{OC} calculated from the optimized K_d values, shown in supporting information Table S3, were compared with K_{OC} values reported in the literature.[37] In the present study, atrazine, sulfometuron-methyl, imidacloprid and trifloxystrobin had smaller K_{OC} values than those found in the FOOTPRINT database.[37] Transport of trifloxystrobin at Poamoho and Waimanalo was exceptional, as this pesticide moved deeper in the soil profile than the bromide tracer. The optimized K_{OC} values of this compound were very low ($K_{OC} < 10$ mL g^{-1}) (supporting information Table S3). For S-metolachlor and imazaquin, the optimized values were within the range of K_{OC} values reported in the literature.

Similarly, the estimated values of dissipation half-lives of the tested pesticides were compared with the field degradation $t_{1/2}$ values reported in the literature,[37] which are listed in supporting information Table S4 (literature values may be longer than the optimized dissipation half-lives). The present model indicated shorter half-life values for atrazine and sulfometuron-methyl than those found in the literature. For S-metolachlor, imazaquin, imidacloprid and trifloxystrobin, the estimated values were within the range of values previously reported in the literature.

The estimated half-life for atrazine at Mana (1.2 days) may appear to be unrealistically short; however, the resident concentration data for a sample withdrawn 28 days after the application revealed no traces of this compound in the whole soil profile, which suggested complete breakdown. The estimated half-life for atrazine at the other four test sites ranged from 2 to 10 days (supporting information Table S4). In an earlier study done in another humid tropical region, atrazine degradation half-life was determined to be as short as 9 days.[38] For specific conditions in Hawaii, storms with total rainfall exceeding 200 mm can occur over a short duration. This can cause surface ponding, leading to rapid leaching of chemicals, including atrazine, which is a known leacher under Hawaii conditions and has been detected in aquifers. However, no such storm events occurred at the test sites during the leaching study.

The optimized reactive parameters shown in supporting information Tables S3 and S4 were also compared with the parameters measured in the laboratory.[18] The optimized K_d values showed a trend generally declining with depth. The greatest difference between measured and optimized K_d values was obtained for trifloxystrobin at Poamoho. As concluded in the previous study,[18] high laboratory-measured K_d values (>2.0 mL g^{-1}) of trifloxystrobin were caused by rapid photodegradation, thus overestimating the 'true' sorption distribution coefficients. Laboratory-determined $t_{1/2}$ values exhibited large differences between half-lives for topsoil and subsoil layers and between different sites.[18] The greatest difference between measured and optimized $t_{1/2}$ values was seen for imazaquin at Poamoho. Inverse modeling for imazaquin generated shorter half-lives compared with laboratory-measured $t_{1/2}$ values. The shorter field $t_{1/2}$ presumably indicated additional degradation at mineral oxide surfaces and possible photodegradation in the first few days after application.[18]

It is important to note that the optimized $t_{1/2}$ values are the field dissipation half-lives, which are not typically used in pesticide registration procedures in the EU. Also, K_d values standardized to reference conditions are employed in the EU pesticide registration procedure. The standardized reference conditions under OECD (Organization for Economic Cooperation and Development) guidelines[39,40] describe the procedure for estimating the reactive transport parameters of pesticides in detail (e.g. soil homogenization methods, the soil to solution ratio, analytical procedures, etc). On the other hand, the literature values of the reactive transport parameters in the FOOTPRINT database are compiled from 'a large number of different sources and not all are of the highest quality' (Lewis K, private communication, University of Hertfordshire). The input transport parameters for FOCUS leaching scenarios,[12] estimated under standardized procedures, are preferably used in pesticide transport simulations. In the present study, however, simulations using literature parameter values and laboratory-measured parameters resulted in poor prediction of COMs and chemical concentration profiles.

4.3 Concentration profile and COM comparisons

RMSE is not a dimensionless measure of fit. For a solute, RMSE has units of concentration, and its absolute value is influenced by weight factors. No weight factors were considered in evaluating the bromide RMSE in this study. Moreover, bromide was applied at higher concentrations than the test pesticides, thus resulting in higher RMSE values compared with those for the test pesticides (see Table 1).

The two criteria (i.e. RMSE and observed-to-predicted COM) used to evaluate the model in this study differ from each other. COM comparisons disregard actual concentration values in the soil; only the relative position of the center of chemical mass in soil profiles is identified. Because of this, RMSE is needed to make comparisons of both actual concentration values and the shapes of concentration profiles in soil. RMSE values are computed from the overall fit of model prediction to experimental data; however, they do not specify the depths of chemical penetration (i.e. overestimation or underestimation). Therefore, COM comparisons can be considered as a convenient complement to existing statistical indices such as RMSE because of the spatial variability and heterogeneity of measured concentration profiles. Previous studies have suggested that COM analysis is an effective tool for the evaluation of solute leaching in soils.[16,24,41]

4.4 Inverse modeling

In Dohnal *et al.*,[42] RMSE values of about 20 cm were obtained by inverse modeling of soil hydraulic parameters. These values were assumed to indicate good agreement between measured and predicted pressure heads. Nearly equal RMSE values were obtained in this study for all five sites after optimization. The optimized soil hydraulic characteristics (α fitting parameter and K_s values) were not correlated, so the inverse solution was considered to be robust. Field measurements of saturated hydraulic conductivity are generally associated with much uncertainty. Thus, it is not surprising that K_s values required adjustment to improve agreement with measured pressure heads. The greatest differences between measured and optimized K_s values were found at the Mana site (supporting information Tables S1 and S2). Measured and optimized K_s values for the other four sites were within one order of magnitude.

Note that the weight factors of unexpected observed concentration profiles (e.g. increased mass found in the profile compared with that in an earlier sampling event) were not decreased. For some pesticides, these unexpected concentration profiles resulted in discrepancies in COM comparisons and high RMSE values (Tables 1 and 2).

The objective function was integrated from two measurements (i.e. actual concentration values and the position of COMs in the soil profile), providing a reasonable compromise in both RMSE and COM measures. Such a composition of the objective function also led to its increased robustness and improved uniqueness of the estimated transport parameters. Although COM analysis could have been hampered by insufficient sampled depth (see Section 4.1), the potential error of the optimized parameters was partly compensated for by the concentration profiles in the objective function (the complete concentration profile was not necessary for inverse modeling). In addition, K_d and $t_{1/2}$ parameters showed low correlation during the optimization. As far as can be ascertained, no attempts have been made to include the depth of measured COM in the objective function in recent modeling studies.

4.5 Adequacy of tier-II modeling

The observed concentration profiles clearly reflect the three-dimensional (3D) nature of the transport driven by the variable irrigation intensities delivered by the sprinkler system, which led to an increase with time in total mass in the soil profile. This is most probably due to the spatially random choosing of the sampling locations (in spite of the averaging of the concentrations by sample compositing). Therefore, the simulated one-dimensional (1D) pesticide transport does not need to be interpreted solely in terms of model success or failure to predict the observed 3D phenomenon. It is obvious that the 3D effects may not be fully predicted by a 1D transport model. However, this should not lead to the conclusion that the 1D model is inadequate for making qualified predictions of vertical pesticide leaching. Some of the 3D effects could probably have been captured using multiple runs of the 1D model in either a deterministic or stochastic (Monte Carlo) framework.[43,44] However, such efforts were beyond the scope of this study.

4.6 Transport processes in soils

Preferential flow and transport in oxisols was not considered in this study, although these soils are known to exhibit preferential flow and transport.[45,46] The reasons for neglecting possible preferential flow and transport in weathered oxisols were twofold: (i) the type of field observations (i.e. pressure head data and concentration profiles) were not suitable for detecting such preferential flow; (ii) the lack of experimental data required to calibrate and run preferential (e.g. dual-continuum) flow models. Continuous sampling of soil pore water[47,48] or flux-averaged concentrations in drain water[49,50] are suitable techniques for detecting preferential transport in the field. In a review of modeling approaches for predicting preferential flow and transport, Gerke[51] concluded that, in spite of significant progress made in experimental techniques and procedures, reliable calibration and parameterization of dual-continuum models remains a challenge.

Well-defined (Gaussian) peaks in concentration profiles were generally not observed for the bromide tracer and pesticides used in this study. This is most likely the result of a complex interaction of sorption and transport processes in the aggregated soils.[24,52] It is also well recognized that adsorption–desorption hysteresis affects the leaching pattern of contaminants.[53] Moreover, chemicals may be retained in intra-aggregate pore spaces of weathered tropical soils and only slowly leach downward.[54] No provision was made to consider these processes in the present conceptual model.

Analysis of the measured COMs of the bromide tracer and the test pesticides revealed possible bromide sorption at a few of the test sites.[18] Table 2 shows the underprediction of simulated COMs of bromide compared with the measured COMs (overall ratio >1.0). The bromide simulations were run with an assumption of no sorption, but the observed COMs were deeper than the predicted COMs. Hence, possible sorption of bromide was not predicted by the numerical modeling.

5 CONCLUSIONS

At all five experimental sites, water flow in the soil profiles was described with reasonable accuracy by the tier-II S1D model after calibration of the soil hydraulic parameters. The predicted pesticide concentration profiles based on laboratory-measured reactive parameters did not provide reasonable agreement with data. Hence, inverse modeling was used to obtain more adequate

reactive transport parameters. RMSE values and COM comparisons suggested that the transport predictions based on optimized K_d and $t_{1/2}$ parameters delivered improved agreement with the actual field data compared with predictions using laboratory-measured reactive parameters. For some chemical profiles, however, it was not possible to reduce the differences between predicted and measured concentrations, even when inverse modeling was utilized to generate the optimized parameters. This can be attributed to a few unexpected observed concentration profiles rather than an inability of the advection-dispersion equation-based model to predict chemical transport in weathered tropical soils. The unexpected pattern of chemical concentration profiles was most likely caused by soil heterogeneity coupled with analytical difficulties. Better results in terms of data–model agreement would be possible with a dataset from an experimental site with more homogeneous soil. A final conclusion addressing the adequacy of an advection-dispersion equation approach to modeling transport processes in tropical soils is thus difficult to formulate. The difficulties encountered in fitting the model to the observed data are largely attributable to the variability of the data obtained during the field leaching experiment.

The chemical profiles observed in the soils did not provide sufficient information to predict the mass flux of pesticide leachate towards the water table. This information, in contrast to expensive field leaching experiments, can only be supplied by tier-II modeling. At two (Kula and Mana) of the five sites, leaching of pesticides below the sampled zone was predicted. The pesticide mass at the other test sites remained within the sampled soil profile. The highest leaching among the pesticides tested was predicted for imazaquin at the Kula site, which may be attributed to the shallow soil profile and low K_d values at that site. It may be expected that, once the chemicals leave the topsoil and shallow subsoil horizons considered in the present study, where sorption and degradation processes are most intensive, the pesticides will leach steadily downwards to groundwater without significant retardation. This hypothesis does not apply to atrazine, a pesticide known to leach in Hawaii conditions. Although atrazine has low K_d (and K_{OC}) values, its rapid degradation caused a breakdown at all sites within the test period of 16 weeks and thus demonstrated only shallow penetrations of the soil profiles.

Numerical modeling helped to identify relevant transport processes in the leaching of pesticides. The reactive transport parameters estimated by tier-II inverse modeling were then used to run the tier-I model. This AFR tier-I modeling delivered index values consistent with observed leaching patterns and S1D-predicted center of mass depths. It was demonstrated that a process-based modeling of water flow and pesticide transport coupled with simple inverse procedures can contribute meaningfully to the evaluation of chemical leaching in Hawaii soils. Furthermore, the tier-II inverse modeling incorporated physical principles into the qualitative AFR approach through the estimated reactive transport parameters.

The Hawaii Department of Agriculture (HDOA) may use the AFR modeling results from this study in current pesticide registration protocols, as the HDOA relies on the results from the tier-I screening model in the decision-making process. Although the estimated reactive transport parameters of the studied pesticides were not determined under standardized reference conditions, they do provide additional information about the pesticides' fate and transport in tropical soils. Four of the six pesticides under study (atrazine, sulfometuron-methyl, imidacloprid and trifloxystrobin) displayed smaller K_{OC} values than those found in the FOOTPRINT database, which is compiled primarily from studies undertaken in temperate regions. The estimated transport parameters may also be used to predict leaching towards groundwater in case the US EPA or the State of Hawaii require this information for registration purposes.

ACKNOWLEDGEMENTS

This study was funded under project number 49506 by the Hawaii Department of Agriculture. Additional support was provided by the research fund of the Ministry of Education of the Czech Republic (MSM 6840770002). The authors sincerely thank Dr Richard E Green, Helena Pavelkova and Dr Martin Sanda for their valuable input and comments. This paper is published as a part of the continuing 'Contributed Papers' series of the Water Resources Research Center, University of Hawaii at Manoa.

SUPPORTING INFORMATION

Supporting information may be found in the online version of this article.

REFERENCES

1 Rao PSC, Hornsby AG and Jessup RE, Indices for ranking the potential for pesticide contamination of groundwater. *Soil Crop Sci Soc Fl* **44**:1–8 (1985).
2 Li ZC, Yost RS and Green RE, Incorporating uncertainty in a chemical leaching assessment. *J Contam Hydrol* **29**:285–299 (1998).
3 Stenemo F, Ray C, Yost R and Matsuda S, A screening tool for vulnerability assessment of pesticide leaching to groundwater for the islands of Hawaii, USA. *Pest Manag Sci* **63**:404–411 (2007).
4 Carsel RF, Smith CN, Mulkey LA, Dean JD and Jowise P, User's manual for the pesticide root zone model (PRZM). Release 1. USEPA-600/3-84-109, USEPA, Washington, DC (1984).
5 Kleveno JJ, Loague K and Green RE, An evaluation of a pesticide mobility index: impact of recharge variation and soil profile heterogeneity. *J Contam Hydrol* **11**:83–99 (1992).
6 Loague KM, Green RE, Liu CCK and Liang TC, Simulation of organic chemical movement in Hawaii soils with PRZM: 1. Preliminary results for EDB. *Pacific Sci* **43**:67–95 (1989).
7 Loague KM, Giambelluca TW, Green RE, Liu CCK, Liang TC and Oki DS, Simulation of organic chemical movement in Hawaii soils with PRZM: 2. Predicting deep penetration of DBCP, EDB, and TCP. *Pacific Sci* **43**:362–383 (1989).
8 Ahuja LR, Rojas KW, Hanson JD, Shaffer JJ and Ma L, *The Root Zone Water Quality Model.* Water Resources Publications LLC, Highlands Ranch, CO (2000).
9 Hutson JL and Wagenet RJ, LEACHM: leaching estimation and chemistry model: a process-based model of water and solute movement, transformations, plant uptake and chemical reactions in the unsaturated zone. Version 3.0. Research Series, Vol. 93-3, Department of Soil, Crop and Atmospheric Sciences, Cornell University, Ithaca, NY (1992).
10 Klein M, PELMO: Pesticide Leaching Model, version 2.01. Fraunhofer Institut für Umweltchemie und Ökotoxikologie, Schmallenberg, Germany (1995).
11 Tiktak A, van den Berg F, Boesten JJTI, Leistra M, van der Linden AMA and van Kraalingen D, Pesticide emission assessment at regional and local scales: user manual of Pearl version 1.1. RIVM Report 711401008, Alterra Report 28, Bilthoven, The Netherlands, 142 pp. (2000).
12 FOCUS groundwater scenarios in the EU review of active substances. Report of the FOCUS Groundwater Scenarios Workgroup, EC Document Reference Sanco/321/2000 rev.2, 202 pp. (2000).
13 Jarvis NJ, The MACRO model (version 3.1). Technical description and sample simulations. Reports and dissert. 19. Department of Soil Science, Swedish University of Agricultural Science, Uppsala, Sweden (1994).

14 Vogel T, Lichner L, Dusek J and Cipakova A, Dual-continuum analysis of a cadmium tracer field experiment. *J Contam Hydrol* **92**:50–65 (2007).
15 Vogel T, Huang K, Zhang R and van Genuchten MTh, The HYDRUS code for simulating one-dimensional water flow, solute transport, and heat movement in variably-saturated media, version 5.0. Research Report No. 140, US Salinity Laboratory, ARS, USDA, Riverside, CA (1996).
16 Alavi G, Dusek J, Vogel T, Green RE and Ray C, Evaluation of dual-permeability models for chemical leaching assessment to assist pesticide regulation in Hawaii. *Vadose Zone J* **6**:735–745 (2007).
17 Köhne JM, Köhne S and Simunek J, A review of model applications for structured soils: (b) Pesticide transport. *J Contam Hydrol* **104**:36–60 (2009).
18 Dusek J, Sanda M, Loo B and Ray C, Field leaching of pesticides at five test sites in Hawaii: study description and results. *Pest Manag Sci* **66**:596–611 (2010).
19 van Genuchten MTh, A closed-form equation for predicting the hydraulic conductivity of unsaturated soils. *Soil Sci Soc Am J* **44**:892–898 (1980).
20 Mualem Y, A new model for predicting the hydraulic conductivity of unsaturated porous media. *Water Resour Res* **12**:513–522 (1976).
21 Vogel T, Cislerova M and Hopmans JW, Porous media with linearly variable hydraulic properties. *Water Resour Res* **27**:2735–2741 (1991).
22 Zacharias S and Heatwole CD, Evaluation of GLEAMS and PRZM for predicting pesticide leaching under field conditions. *T ASAE* **37**:439–451 (1994).
23 Lesikar BJ, Kenimer AL, Hirschi MC, Mitchell JK and Felsot AS, Modeling alachlor movement under spill conditions using LEACHMP. *T ASAE* **40**:953–959 (1997).
24 Gavenda RT, Green RE and Schneider RC, Leaching of pesticides in selected Hawaii oxisols and andisols as influenced by soil profile characteristics. CTAHR Research Series 075, University of Hawaii, Honolulu, HI (1996).
25 Dusek J, Vogel T, Lichner L, Cipakova A and Dohnal M, Simulated cadmium transport in macroporous soil during heavy rainstorm using dual-permeability approach. *Biologia* **61**:S251–S254 (2006).
26 Dusek J, Ray C, Alavi G, Vogel T and Sanda M, Effect of plastic mulch on water flow and herbicide transport in soil cultivated with pineapple crop: a modeling study. *Agr Water Manag* **97**:1637–1645 (2010).
27 Dusek J, Vogel T, Lichner L and Cipakova A, Short-term transport of cadmium during a heavy rain event simulated by a dual-continuum approach. *J Plant Nutr Soil Sci* **173**:536–547 (2010).
28 Ray C, Vogel T and Dusek J, Modeling depth-variant and domain-specific sorption and biodegradation in dual-permeability media. *J Contam Hydrol* **70**:63–87 (2004).
29 Dolezal F, Zumr D, Vacek J, Zavadil J, Battilani A, Plauborg F, *et al.*, Dual permeability soil water dynamics and water uptake by roots in irrigated potato fields. *Biologia* **62**:552–556 (2007).
30 Vogel T, Sanda M, Dusek J, Dohnal M and Votrubova J, Using oxygen-18 to study the role of preferential flow in the hormation of Hillslope runoff. *Vadose Zone J* **9**:252–259 (2010).
31 Vogel T, Dohnal M and Dusek J, Description of the available bench scale modeling approaches with emphasis on the input data requirements and output data structure. Deliverable COMPUTE1.1, Integrated Project AquaTerra (2004).
32 Jury WA, Spencer WF and Farmer WF, Behavior assessment model for trace organics in soil. 1. Model description. *J Environ Qual* **12**:558–564 (1983).
33 Gerke HH, Dusek J, Vogel T and Köhne JM, Two-dimensional dual-permeability analyses of a bromide tracer experiment on a tile-drained field. *Vadose Zone J* **6**:651–667 (2007).
34 Vanderborght J and Vereecken H, Review of dispersivities for transport modeling in soils. *Vadose Zone J* **6**:29–52 (2007).
35 Doherty J, Brebber L and Whyte P, PEST. Model independent parameter estimation. Australian Centre for Tropical Freshwater Research, James Cooke University, Townsville, Australia (1995).
36 Simunek J, Kodesova R, Gribb MM and van Genuchten MTh, Estimating hysteresis in the soil water retention function from cone permeameter experiments. *Water Resour Res* **35**:1329–1345 (1999).
37 *Creating Tools for Pesticide Risk Assessment and Management in European Union FOOTPRINT Program.* [Online]. FOOTPRINT (2007). Available: http://www.eu-footprint.org/ppdb.html [14 September 2010].
38 Bernard H, Chabalier PF, Chopart JL, Legube B and Vauclin M, Assessment of herbicide leaching risk in two tropical soils of Reunion Island (France). *J Environ Qual* **34**:534–543 (2005).
39 OECD guideline for the testing of chemicals 106: Adsorption–desorption using a batch equilibrium method. OECD, adopted 21 January (2000).
40 OECD guideline for the testing of chemicals 307: Aerobic and anaerobic transformation in soil. OECD, adopted 24 April (2002).
41 Asare DK, Sammis TW, Smeal D, Zhang H and Sitze DO, Modeling an irrigation management strategy for minimizing the leaching of atrazine. *Agr Water Manag* **48**:225–238 (2001).
42 Dohnal M, Dusek J and Vogel T, The impact of the retention curve hysteresis on prediction of soil water dynamics. *J Hydrol Hydromech* **54**:258–268 (2006).
43 Dubus IG, Brown CD and Beulke S, Sources of uncertainty in pesticide fate modelling. *Sci Total Environ* **317**:53–72 (2003).
44 Stenemo F, Lindahl AML, Gärdenäs A and Jarvis N, Meta-modeling of the pesticide fate model MACRO for groundwater exposure assessments using artificial neural networks. *J Contam Hydrol* **93**:270–283 (2007).
45 Loague K, Miyahira RN, Green RE, Oki DS, Giambelluca TW and Schneider RC, Chemical leaching near the Waiawa Shaft, Oahu, Hawaii: 2. Modeling results. *Ground Water* **33**:124–138 (1995).
46 Loague K, Bernknopf RL, Green RE and Giambelluca TW, Uncertainty of groundwater vulnerability assessments for agricultural regions in Hawaii: review. *J Environ Qual* **25**:475–490 (1996).
47 BrandiDohrn FM, Dick RP, Hess M and Selker JS, Suction cup sampler bias in leaching characterization of an undisturbed field soil. *Water Resour Res* **32**:1173–1182 (1996).
48 Campbell CG, Ghodrati M and Garrido F, Comparison of time domain reflectometry, fiber optic mini-probes, and solution samplers for real time measurement of solute transport in soil. *Soil Sci* **164**:156–170 (1999).
49 Scorza RP, Smelt JH, Boesten JJTI, Hendriks RFA and van der Zee SEATM, Preferential flow of bromide, bentazon, and imidacloprid in a dutch clay soil. *J Environ Qual* **33**:1473–1486 (2004).
50 Köhne JM and Gerke HH, Spatial and temporal dynamics of preferential bromide movement towards a tile drain. *Vadose Zone J* **4**:79–88 (2005).
51 Gerke HH, Preferential flow descriptions for structured soils. *J Plant Nutr Soil Sci* **169**:382–400 (2006).
52 Rao PSC, Green RE, Balasubramanian V and Kanihero Y, Field study of solute movement in a highly aggregated oxisol with intermittent flooding: II. Picloram. *J Environ Qual* **3**:197–202 (1974).
53 Johnson GR, Gupta K, Putz DK, Hu Q and Brusseau ML, The effect of local-scale physical heterogeneity and nonlinear, rate-limited sorption/desorption on contaminant transport in porous media. *J Contam Hydrol* **64**:35–58 (2003).
54 Rao PSC, Green RE, Balasubramanian V and Kanihero Y, Field study of solute movement in a highly aggregated oxisol with intermittent flooding: I. Nitrate. *J Environ Qual* **2**:359–362 (1973).

Combining dual-continuum approach with diffusion wave model to include a preferential flow component in hillslope scale modeling of shallow subsurface runoff, Advances in Water Resources, 2012.

Advances in Water Resources 44 (2012) 113–125

Contents lists available at SciVerse ScienceDirect

Advances in Water Resources

journal homepage: www.elsevier.com/locate/advwatres

Combining dual-continuum approach with diffusion wave model to include a preferential flow component in hillslope scale modeling of shallow subsurface runoff

Jaromir Dusek [a,*], Tomas Vogel [a], Michal Dohnal [a], Horst H. Gerke [b]

[a] Czech Technical University in Prague, Faculty of Civil Engineering, Prague, Czech Republic
[b] Leibniz-Centre for Agricultural Landscape Research (ZALF), Institute of Soil Landscape Research, Müncheberg, Germany

ARTICLE INFO

Article history:
Received 12 August 2011
Received in revised form 6 March 2012
Accepted 16 May 2012
Available online 23 May 2012

Keywords:
Shallow subsurface runoff
Hillslope discharge
Preferential flow
Dual-permeability model
Richards' equation
Boussinesq equation

ABSTRACT

In the absence of overland flow, shallow subsurface runoff is one of the most important mechanisms determining hydrological responses of headwater catchments to rainstorms. Subsurface runoff can be triggered by preferential flow of infiltrating water frequently occurring in heterogeneous and structured soils as a basically one-dimensional (1D) vertical process. Any attempt to include effects of preferential flow in hydrological hillslope studies is limited by the fact that the thickness of the permeable soil is mostly small compared to the length of the hillslope. The objective of this study is to describe preferential flow effects on hillslope-scale subsurface runoff by combining a 1D vertical dual-continuum approach with a 1D lateral flow equation. The 1D vertical flow of water in a variably saturated soil is described by a coupled set of Richards' equations and the 1D saturated lateral flow of water on less permeable bedrock by the diffusion wave equation. The numerical solution of the combined model was used to study rainfall-runoff events on the Tomsovska hillslope by comparing simulated runoff with observed trench discharge data. The dual-continuum model generated the observed rapid runoff response, which served as an input for the lateral flow model. The diffusion wave model parameters (i.e., length of the contributing hillslope, effective porosity, and effective hydraulic conductivity) indicate that the hillslope length that contributed to subsurface drainage is relatively short (in the range of 25–50 m). Significant transformation of the 1D vertical inflow signal by lateral flow is expected for longer hillslopes, smaller effective conductivities, and larger effective porosities. The physically-based combined modeling approach allows for a consistent description of both preferential flow in a 1D vertical soil profile and lateral subsurface hillslope flow in the simplest way.

1. Introduction

Shallow subsurface runoff (also referred to as interflow, stormflow or throughflow) is recognized as one of the most important mechanisms determining hydrological responses of headwater catchments to rainstorms. It usually develops as shallow saturated lateral flow at the sloping interface between a more permeable surface soil layer and the less permeable underlying soil or bedrock strata. Normally, this type of flow occurs only for a short period of time as an immediate response to an intense rainfall event. The onset of shallow subsurface runoff is commonly accelerated by the presence of preferential pathways in a soil profile. Thus, preferential flow is recognized as a significant factor in runoff formation at the hillslope scale [e.g., 1–3].

Transport processes at the hillslope scale are inherently of three-dimensional (3D) nature. Recently, a few applications of 3D modeling based on Richards' equation for water flow and advection-dispersion equation for solute transport were presented [4–6]. Nevertheless, the water dynamics at the hillslope scale are more frequently described using two-dimensional (2D) models [e.g., 7–9]. However, the 2D approaches are still difficult to apply for large spatial configurations (i.e., hundreds of meters long hillslopes) since computationally demanding numerical solution of the governing equations is required. Therefore, subsurface water dynamics in a hillslope segment was proposed to be decoupled to one-dimensional vertical flow and one-dimensional (1D) lateral flow along the soil/bedrock interface [10–12]. Saturated subsurface flow can be, in principle, described by a one-dimensional diffusion wave (Boussinesq-type) equation. However, the approach of coupling the two one-dimensional models represents a substantial simplification of the reality such that it needs additional experimental evidence. The validity of such simplification for describing fast flow

* Corresponding author. Address: Department of Hydraulics and Hydrology, Faculty of Civil Engineering, Czech Technical University in Prague, Thakurova 7, 166 29 Prague, Czech Republic. Tel.: +420 22435 4355; fax: +420 22435 4793.
E-mail address: dusek@mat.fsv.cvut.cz (J. Dusek).

0309-1708/$ - see front matter © 2012 Elsevier Ltd. All rights reserved.
http://dx.doi.org/10.1016/j.advwatres.2012.05.006

responses at the hillslope scale involving preferential flow effects remains a challenge.

The kinematic wave approximation of saturated subsurface flow was proposed as a simple model for predicting subsurface flow [e.g., 13,14]. The hillslope-storage Boussinesq equation, based on either kinematic or diffusion wave approach, was theoretically developed for various spatial hillslope configurations by Fan and Bras [15], Troch et al. [16,17] and Paniconi et al. [10] focusing on mathematical description of shallow subsurface flow generation. Subsequently, Hilberts et al. [18] introduced a fully coupled model (of 1D vertical Richards' equation and lateral Boussinesq equation) and found a good match with results obtained with a 3D model based on the Richards' equation. However, comparisons of model predictions with experimental data were not presented in these studies, and preferential flow effects were neglected in the modeling approach.

Experimental findings of Vogel et al. [19] based on natural concentrations of the stable oxygen isotope in hillslope discharge demonstrated fast soil water dynamics. In their study, the preferential flow and transport was described using vertical one-dimensional dual-continuum model of Gerke and van Genuchten [20]. At their hillslope discharge analysis, Vogel et al. [19] hypothesized that the contributing hillslope was not long enough to cause any significant modifications in the transformation of the inflow signal (i.e., the lateral component of shallow subsurface flow could be neglected); thus the vertical one-dimensional model could be used alone to predict shallow subsurface runoff and oxygen concentrations. A more detailed analysis of the lateral flow effects contributing to measured shallow subsurface runoff was, however, beyond the scope of their study.

The present study focuses on numerical modeling of shallow subsurface runoff at the hillslope scale. The objective was to develop and test a model that includes a preferential flow component in the description of shallow subsurface runoff along hillslopes with structured soils, and test if the proposed model can represent the most relevant hillslope scale processes. The modeling approach combines two forward-coupled 1D approaches: vertical dual-continuum approach and lateral single-continuum diffusion wave model. The research issues were to test: (i) if the modeling approach works in principle, (ii) if it can be successfully applied to simulate the observed shallow subsurface stormflow hydrographs, and (iii) to confirm that the combined approach is able to transform the rapid preferential-flow-dominated signals into measured runoff responses. More specifically, we analyzed how the signal transformation of vertical flow to lateral runoff depends on hillslope length, effective porosity, and effective hydraulic conductivity.

2. Materials and methods

2.1. Experimental site

The experimental hillslope site Tomsovka is located in the small mountain catchment Uhlirska, Jizera Mountains, Czech Republic. Total area of the catchment is 1.78 km^2, average altitude reaches 820 m above sea level, annual precipitation exceeds 1300 mm/year, and annual mean temperature is 4.7 °C. The studied hillslope is covered with grass (*Calamagrostis villosa*) and spruce (*Picea abies*). The average slope at Tomsovka is about 14%.

Hydrological and micrometeorological conditions are monitored with high temporal resolution at Tomsovka [21]. Subsurface hillslope discharge is measured via an 8 m experimental trench of about 80 cm depth. It consists of two individual sections (A and B), each 4 m wide (Fig. 1). Shallow subsurface hillslope discharge is collected separately in each section at the depth of about 75 cm. The discharge rates are measured continuously by tipping bucket

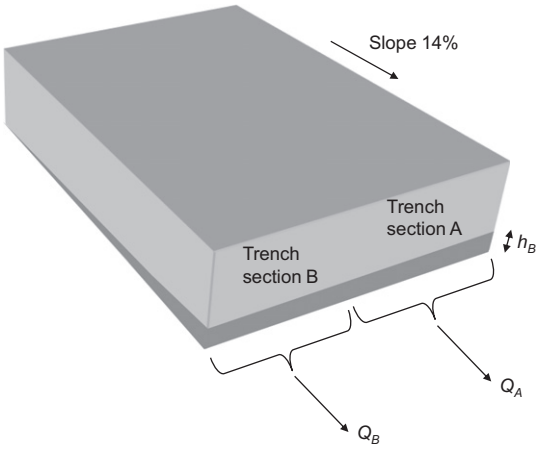

Fig. 1. Schematic of the experimental trench for collecting hillslope discharge at the Tomsovka site. The discharge is collected 75 cm below the soil surface with 4-m long PVC runoff pipes pushed into the soil and measured by tipping buckets separately for the two trench sections (Q_A and Q_B); h_B is the depth of saturated subsurface stream (lateral flow), which occurs episodically in response to major rainstorms.

fluxmeters during the vegetation seasons (from May to October). The hillslope length contributing to measured subsurface discharge was estimated to be about 25 m [22], although the geographic watershed divide is located approximately 130 m above the experimental trench, winding through a gently sloping plateau. The contributing hillslope length estimated by Hrncir et al. [22] resulted from the comparison of trench flow data and discharge observed in the creek gauging station (assuming that the subsurface flow forms a dominant portion of the catchment discharge).

The typical soil profile at Tomsovka is about 70 cm deep; soil is sandy loam classified as Dystric Cambisol. The soil profile consists of three layers with different hydraulic properties. The soil has well-developed internal structure with a broad range of pore sizes. The three soil layers are underlain by a compact transition zone at the depth of about 70 cm, followed by granite bedrock. The soil hydraulic parameters characterizing each layer were derived from laboratory measurements, where undisturbed 100 cm^3 soil samples and 1000 cm^3 soil cores were used to determine soil water retention parameters and saturated hydraulic conductivity, respectively [23]. In addition, saturated hydraulic conductivity of the transition zone was determined using a tension disk infiltrometer.

Significant preferential flow effects, affecting the soil water response to precipitation, were reported for the same site by Sanda and Cislerova [23] and Hrncir et al. [22]. Preferential flow was attributed to highly conductive pathways along decayed tree roots and structural pores as well as by the spatial variability of local soil hydraulic properties. Soil water pressure within the soil profile was monitored using a set of automated tensiometers, installed at five locations at three different depths below the soil surface, between 1 and 20 m distance above the experimental trench. The present study makes use of the data measured at the Tomsovka site over the period from May 2007 to October 2009.

2.2. One-dimensional lateral flow model (LatFlow)

Upon sufficiently intensive rain, infiltrating water percolates vertically downward in the soil profile to the impermeable bedrock (or the top boundary of a low permeable soil layer) where a saturated layer is being gradually formed (Fig. 2). In the saturated layer, water flows laterally in the direction determined by the local gradient of the soil/bedrock interface, which usually does not differ much from the soil surface elevation gradient. The short-term

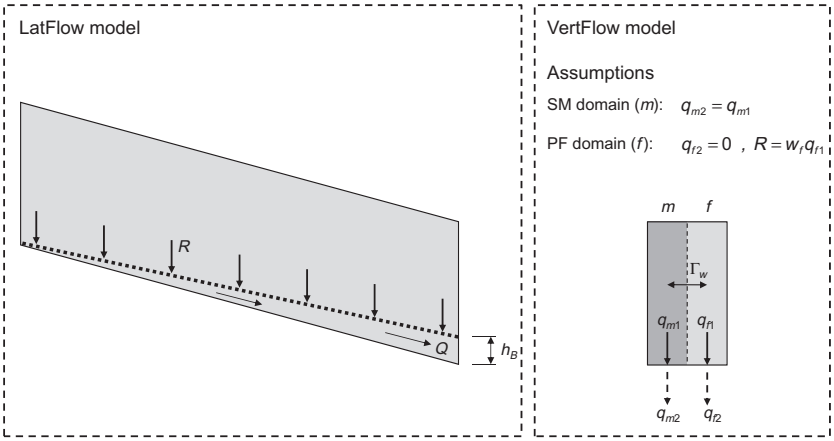

Fig. 2. Schematic of lateral flow in a vertical hillslope segment; R is the recharge intensity feeding the saturated lateral flow, Q is the discharge from the hillslope segment, q_{m1} and q_{f1} are the soil water fluxes generated by the vertical dual-continuum soil water flow model, q_{m2} and q_{f2} fluxes represent seepage to deeper horizons, Γ_w is the inter-domain soil water transfer rate; SM and PF refer to the soil matrix and preferential flow, respectively; w_f is the volume fraction of the PF domain.

saturated subsurface flow (simply referred to as lateral flow) can be approximated by the 1D diffusion wave equation. The diffusion wave rather than kinematic wave approach is suggested to facilitate the prediction of building-up and fading-away stages of saturated subsurface flow episodes [11]. Combining Darcy's law with the assumption of hydrostatic pressure distribution along a vertical section of the saturated stream (i.e., a hillslope analogy to Dupuit's assumption) leads to an equation similar to the one first introduced by Boussinesq [24]:

$$\frac{Q}{W} = -K_B h_B \left(\frac{\partial h_B}{\partial x} + \frac{dz}{dx} \right) \tag{1}$$

where Q is the local hillslope discharge ($m^3\ s^{-1}$), h_B is the depth of lateral flow (m), i.e., the vertical extent of the saturated stream, K_B is the effective saturated hydraulic conductivity ($m\ s^{-1}$), x is the coordinate (m) running along the bedrock slope (positive in the upslope direction), z is the vertical coordinate (positive upwards) dz/dx is the local hillslope gradient (–), and W is the hillslope width (m), here assumed to be invariant along x. This restriction can easily be relaxed; however, the experimental conditions discussed in this study do not involve any complex three-dimensional hillslope configuration (e.g., convergent or divergent hillslope).

The continuity equation for lateral flow can be written as

$$\Theta \frac{\partial h_B}{\partial t} + \frac{1}{W} \frac{\partial Q}{\partial x} = R \tag{2}$$

where Θ is the effective porosity ($m^3\ m^{-3}$), R is the local intensity of vertical recharge ($m\ s^{-1}$), and t is time (s).

The diffusion wave equation for the lateral flow is obtained by substituting the local hillslope discharge into the continuity equation:

$$\Theta \frac{\partial h_B}{\partial t} - \frac{\partial}{\partial x} \left(K_B h_B \left(\frac{\partial h_B}{\partial x} + \frac{dz}{dx} \right) \right) = R \tag{3}$$

This equation with a single dependent variable h_B is solved by the one-dimensional lateral flow model LatFlow. The numerical solution is obtained by the finite element method and implemented in the computer program HYPO [11,25].

2.3. One-dimensional vertical flow model (VertFlow)

The recharge intensity, R, feeding lateral flow, is determined from the soil water flux using a model of vertical water movement in a variably saturated soil profile, more specifically by a numerical solution of the 1D Richards' equation.

The dual-continuum concept is used to solve the vertical water flow through a dual-continuum porous medium, which means that water flow takes place in both the soil matrix (SM) and preferential flow (PF) domains, and Richards' equation describes water flow in each of the two domains. Both equations are coupled using a transfer term, which allows for the dynamic water exchange between the two pore domains. The following pair of governing equations is applied to describe the 1D vertical movement of water (similar to Gerke and van Genuchten [20]):

$$w_f C_f \frac{\partial h_f}{\partial t} = \frac{\partial}{\partial z} \left(w_f K_f \left(\frac{\partial h_f}{\partial z} + 1 \right) \right) - w_f S_f - \Gamma_w \tag{4}$$

$$w_m C_m \frac{\partial h_m}{\partial t} = \frac{\partial}{\partial z} \left(w_m K_m \left(\frac{\partial h_m}{\partial z} + 1 \right) \right) - w_m S_m + \Gamma_w \tag{5}$$

where m denotes the SM domain, f denotes the PF domain, h is the pressure head (m), K is the unsaturated hydraulic conductivity ($m\ s^{-1}$), C is the soil water capacity (m^{-1}), S is the local root water extraction intensity (s^{-1}), Γ_w is the soil water transfer term (s^{-1}) controlling the water exchange between the domains, w_m and w_f are volume fractions of the respective domains ($w_m + w_f = 1$), z is the vertical coordinate (m) directed positive upwards.

The composite volumetric flux of soil water q ($m\ s^{-1}$) is defined as

$$q = w_f q_f + w_m q_m \tag{6}$$

where q_f and q_m are the soil water fluxes in the PF and SM domains, respectively. The domain-specific (local) fluxes are computed using the Buckingham-Darcy law:

$$q_f = -K_f \left(\frac{\partial h_f}{\partial z} + 1 \right) \tag{7}$$

$$q_m = -K_m \left(\frac{\partial h_m}{\partial z} + 1 \right) \tag{8}$$

The water transfer term in Eqs. (4) and (5) is described using the modified first-order approximation of Gerke and van Genuchten [26]:

$$\Gamma_w = \alpha_{ws} K_{ar} (h_f - h_m) \tag{9}$$

where α_{ws} is the water transfer coefficient at saturation ($m^{-1}\ s^{-1}$) and K_{ar} is the relative unsaturated conductivity of the SM-/PF-domain interface [27]. Values of K_{ar} range from 0 to 1 depending

on the SM- and PF-domain conductivities, which are evaluated for upstream soil water pressure [28–30].

The one-dimensional dual-continuum vertical flow model VertFlow is used to predict R. The dual set of governing equations for soil water flow is solved numerically by the computer program S1D using the finite element method. The most recent implementation of the S1D model is described by Vogel et al. [27].

2.4. Forward-coupling procedure

In structured soil, the vertically downward oriented soil water flux can occur in the porous matrix and in the network of cracks, fissures and biopores. The hillslope scale preferential flow is assumed to be triggered by rapid flow through the larger structural porosity. This initially vertically-oriented percolation in soil along hillslope changes into laterally oriented movement after it hits the base of the soil/bedrock interface. Thus, the recharge intensity for lateral subsurface flow is assumed to be dominated by the outflow from the preferential pathways.

The vertical recharge rate for saturated lateral flow can be determined from a simple continuity equation formulated at the soil/bedrock interface, which, at the same time, represents a forward-coupling procedure between the vertical flow (VertFlow) and lateral flow (LatFlow) models:

$$R = R_f + R_m = w_f(q_{f1} - q_{f2}) + w_m(q_{m1} - q_{m2}) \tag{10}$$

where R_f and R_m are the recharge contributions from the PF and SM domains, respectively, q_1 and q_2 are the soil water fluxes above and below the soil/bedrock interface, respectively (m s^{-1}). The q_2 fluxes represent seepage to deeper horizons (see Fig. 2).

In the present application of the model we assume that $q_{m2} = q_{m1}$ and $q_{f2} = 0$, i.e. the deep percolation is associated with the SM-domain flux while only the PF-domain flux contributes to lateral flow. Therefore, the recharge rate is evaluated as

$$R = w_f q_{f1} \tag{11}$$

Note that water flowing through the soil matrix may contribute to q_{f1} as a result of inter-domain exchange processes during the vertical flow in the structured soil.

The lateral saturated flow, simulated by the LatFlow model, develops above the soil/bedrock interface, which is situated at the depth of about 70 cm. The LatFlow model is a single-domain model representing flow in a laterally-continuous system of preferential pathways (this is consistent with our observation that the soil matrix at Tomsovka (see the soil matrix conductivities in Table 1) is incapable of transmitting water laterally fast enough to explain quick responses of hillslope discharge to rainfall). The combined use of vertical dual-continuum model and lateral single-continuum diffusion wave model is henceforward abbreviated as VertFlow + LatFlow model.

Coupling of the VertFlow and LatFlow models was sequential, beginning with the vertical dual-continuum simulations followed by a lateral flow modeling step. Spatial coupling was not explicitly considered, i.e. the recharge rates for the diffusion wave model were assumed invariant along the hillslope length.

2.5. Quasi-steady state lateral flow model (InstLatFlow)

The simplest way to calculate the shallow subsurface runoff from a short and highly permeable hillslope segment (without employing the diffusion wave model) is to apply the assumption of quasi-steady state conditions, in which the effective outflow from the vertical soil column (in our case $R = w_f q_{f1}$) simulated by the VertFlow model is multiplied by the contributing area (i.e., the hillslope micro-catchment area) (similar to Vogel et al. [19]):

$$Q = LWR \tag{12}$$

where Q is the hillslope discharge (m^3 s^{-1}), L is the length of contributing hillslope (m) and W is the width of the subsurface trench section (in our case equal to 4 m). The assumption of quasi-steady state lateral flow is hereafter abbreviated as InstLatFlow model (instantaneous lateral flow). The VertFlow + InstLatFlow model was used as an alternative to the VertFlow + LatFlow model in the following analysis.

2.6. Numerical experiments

The numerical simulations of soil water flow and shallow subsurface runoff were performed for three vegetation seasons (2007, 2008, and 2009), for which data were available. For the VertFlow model, the soil water pressures, measured by tensiometers at the beginning of each vegetation season, were used to characterize the initial condition. The simulations were started assuming a situation of initial equilibrium between the flow domains ($h_f = h_m$). The upper boundary condition involved rainfall and evapotranspiration. Hourly intensities were used to represent the rainfall series. Free drainage condition (equivalent to the unit hydraulic gradient condition) was used for the lower boundary condition for both flow domains (i.e., SM and PF domain) at the depth of 75 cm.

The parameters characterizing hydraulic properties of the different soil layers, required for numerical modeling of vertical flow, were adopted from our previous study, dealing with the stable isotope transport at Tomsovka [19]. The soil hydraulic functions are described by the modified version of the van Genuchten–Mualem parameterization [31]. The parameters of the SM and PF domains are listed in Table 1. The soil hydraulic parameters, derived from laboratory measurements, were then adjusted based on variations of soil water content and soil water pressure observed *in situ* [e.g., 32,33]. The volumetric fraction of the PF domain w_f was set to 7% at the soil surface and 5% at the 75 cm depth, with a linear change between the two boundaries. The values of α_{ws} were also estimated to vary linearly between the soil surface and the lower boundary, i.e. between 1 and 0.01 cm^{-1} d^{-1}, which corresponded to a decreasing trend of saturated hydraulic conductivity of the SM domain.

Daily potential transpiration was calculated using Penman–Monteith equation [34], based on micrometeorological data observed directly at the Tomsovka site. The root water uptake, S, was described according to Feddes et al. [35]. The vertical distribution of the uptake intensity was assumed to be constant for the upper 20 cm soil depth; below it decreased linearly down to

Table 1
The soil hydraulic parameters[a] as used for the one-dimensional dual-continuum model VertFlow.

Domain	Depth (cm)	θ_r (cm^3 cm^{-3})	θ_s (cm^3 cm^{-3})	α (cm^{-1})	n (–)	K_s (cm d^{-1})	h_s (cm)
Matrix	0–8	0.20	0.55	0.050	2.00	567	0.00
	8–20	0.20	0.54	0.050	1.50	67	−0.69
	20–70	0.20	0.49	0.020	1.20	17	−1.48
	70–75	0.20	0.41	0.020	1.20	1.3	−1.88
Preferential	0–75	0.01	0.60	0.050	3.00	5000	0.00

[a] θ_r and θ_s are the residual and saturated water contents, K_s is the saturated hydraulic conductivity, h_s is the air-entry value, and α and n are empirical fitting parameters.

70 cm depth. The plant water stress function was approximated by a standard trapezoidal shape. The optimum uptake rate (implying stress-free conditions) was assumed for the local soil water pressure greater than −600 cm. The applied stress function defined the linear reduction of the optimum rate down to the wilting point, which was set equal to −12 000 cm [32].

As explained above, the soil water flux computed at the lower boundary of the SM domain, q_{m2}, was assumed to percolate to deeper horizons, while the episodic outflow generated at the lower boundary of the PF domain during major rainfall-runoff events, q_{f1}, was supposed to serve as a source for the saturated subsurface flow (see Eq. (11)). For the LatFlow model, zero pressure gradient boundary condition was used at the downslope boundary, while a no-flow boundary condition was applied at the upslope boundary. The slope of the simulated hillslope segment was fixed at 14%.

Two approaches to simulate the lateral flow were applied: (i) vertical flow model and the assumption of quasi-steady state lateral flow (VertFlow + InstLatFlow) and (ii) vertical flow model and diffusion wave model (VertFlow + LatFlow). The hillslope lengths L varied in the range from 12.5 to 100 m to evaluate the effect of the contributing upslope area on simulated subsurface runoff. Since there is a relatively large uncertainty associated with determination of effective parameters for the diffusion wave models [e.g., 36,37], a sensitivity analysis of the two remaining parameters in the LatFlow model (i.e., the effective hydraulic conductivity K_B and effective porosity Θ) was also performed.

2.7. Model efficiency

Shallow subsurface runoff predicted by the model was evaluated using the model efficiency criterion of Nash and Sutcliffe [38]:

$$E = 1 - \frac{\sum_{t=1}^{T}(Q_{ot} - Q_{mt})^2}{\sum_{t=1}^{T}(Q_{ot} - \overline{Q_o})^2} \quad (13)$$

where Q_{ot} is the observed and Q_{mt} the simulated discharge, and $\overline{Q}_o$ is the mean value of the observed discharge. The match between model prediction and observation is increasing as the Nash–Sutcliffe criterion approaches a value of 1.

3. Results

Fig. 3 shows subsurface runoff observed at the two sections of the experimental trench. The selected runoff episodes are marked with numbers for further reference. Superimposed are soil water outflow rates generated by the VertFlow model as lower boundary fluxes ($w_m q_{m1}$ and $w_f q_{f1}$). The temporal resolution of the observed and simulated discharge series is one-hour. The water

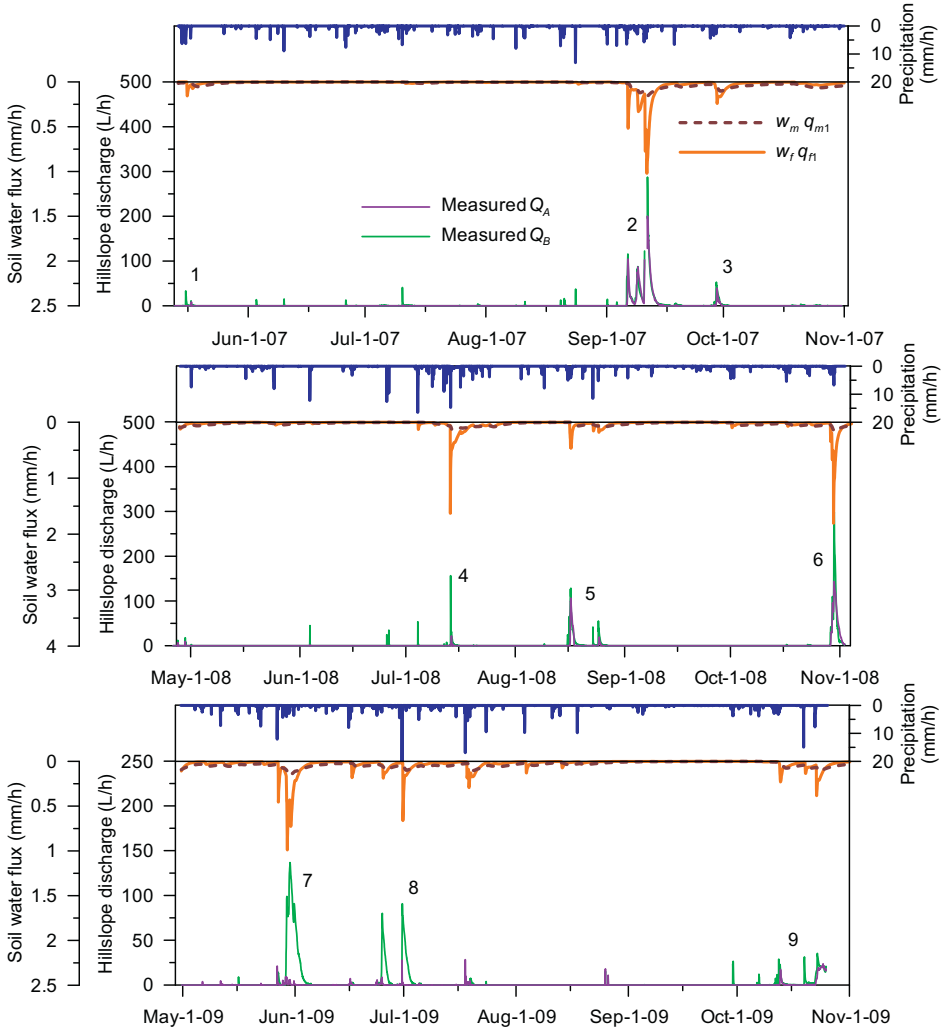

Fig. 3. Observed hillslope discharges (trench section A and B) and the VertFlow model generated outflow rates from the SM and PF domains (denoted as q_{m1} and q_{f1}, respectively). The selected major runoff episodes are labeled with numbers.

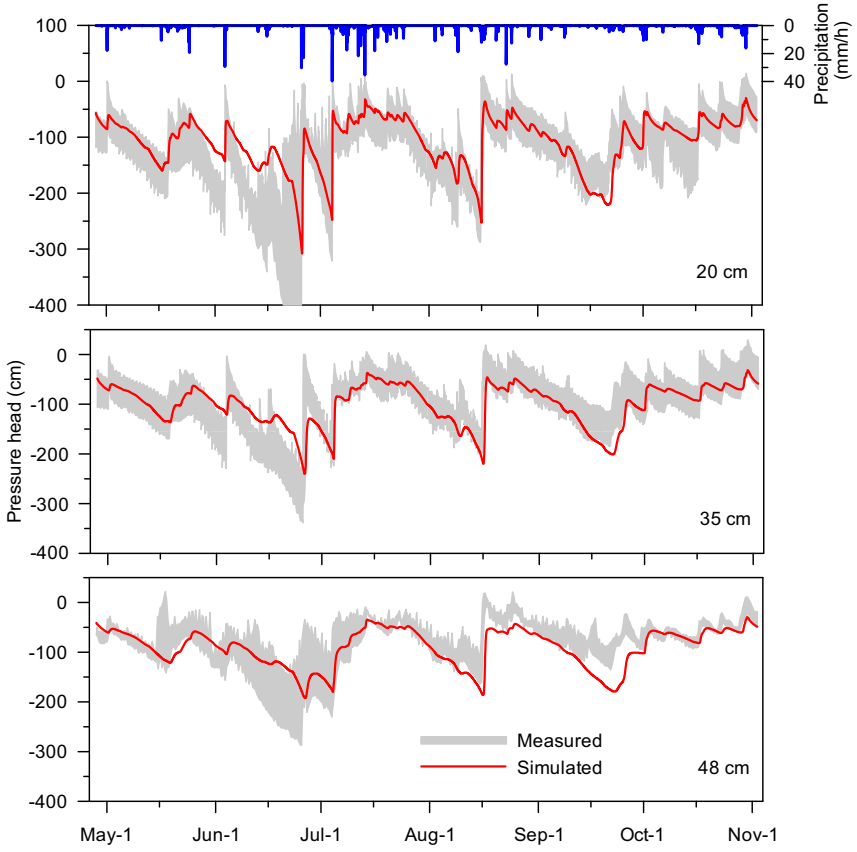

Fig. 4. Simulated (using VertFlow model) and measured pressure heads at three depths in vegetation season 2008. Shaded area represents spatial variability in measured pressure heads obtained from tensiometers at five locations.

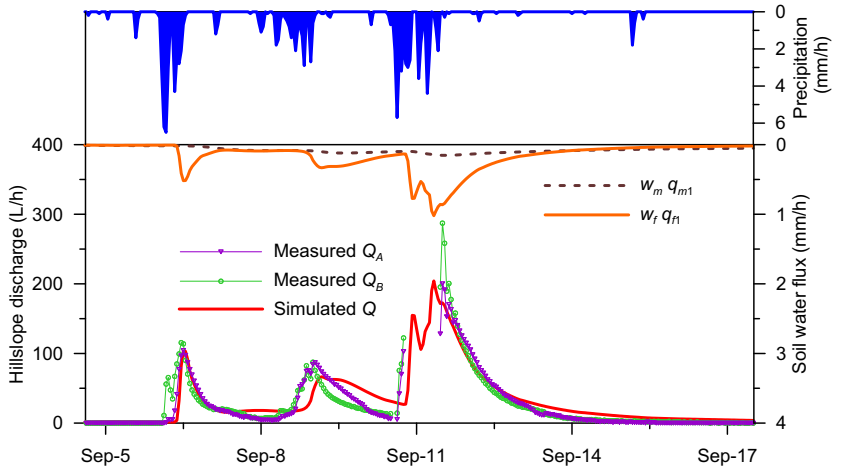

Fig. 5. Observed and simulated hillslope discharges (episode #2, 2007). The predicted subsurface runoff, Q, is calculated using VertFlow + InstLatFlow model based on 50 m hillslope length. The soil water fluxes q_{f1} and q_{m1} were generated by the VertFlow model. Note that two malfunctions of tipping bucket fluxmeters resulted in the incomplete trench data series around September 11.

outflow from the PF domain represents an input signal for subsurface runoff modeling (LatFlow), while the SM-domain outflow is interpreted as deep percolation. This interpretation is supported by the fact that the PF-domain soil water flux is much more coherent with the observed hillslope discharge data compared to the SM-domain flux. This is especially true during major rainfall-runoff events (e.g., September 2007). Nevertheless, a few less significant runoff events, associated with small rainfall intensities, are not well resolved in the VertFlow-generated soil water fluxes.

Comparison of the VertFlow-simulated soil water pressure heads in the SM domain with the experimental data is shown in Fig. 4. The measured and simulated pressure head values are depicted as one-hour averages. Note that while predicted values stayed within the data range during most of the season at 20 and 35 cm depths, the simulated pressure heads were off the shaded area during dry period in June. At 48 cm depth, the data suggested wetter conditions in September.

In Fig. 5, subsurface runoff measured at the two sections of the experimental trench is compared with the model prediction

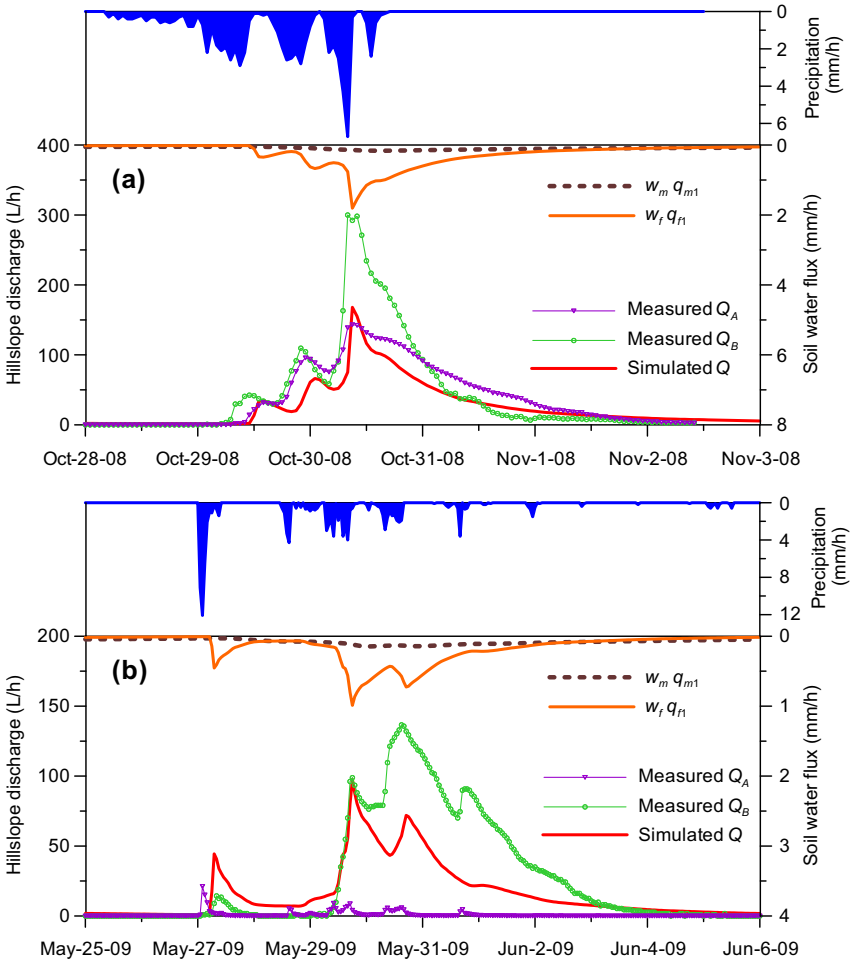

Fig. 6. Observed and simulated hillslope discharges for episode #6 (a) and episode #7 (b). The predicted subsurface runoff, Q, is calculated using VertFlow + LatFlow model ($\Theta = 0.005$ cm^3 cm^{-3} and $K_B = 2500$ cm d^{-1}) based on 25 m hillslope length. The soil water fluxes q_{f1} and q_{m1} were generated by the VertFlow model.

obtained by combining the VertFlow model generated fluxes (q_{f1} and q_{m1}) with the quasi-steady state assumption (InstLatFlow model given by Eq. (12)). The figure shows the most significant runoff event observed during the vegetation season 2007 (episode #2). It can be seen that the subsurface runoff peaks for this episode were relatively well approximated with the simulations based on the 50 m hillslope length. The simulated falling limbs of the discharge series show nearly perfect agreement with the data. Nevertheless, the height of the third simulated hillslope discharge peak (on September 11) was underestimated as compared to the data from the B section of the experimental trench. Furthermore, the simulated hillslope discharge was somewhat delayed compared to observed discharge data, indicating underestimation of the preferential flow by the VertFlow model.

In Fig. 6, subsurface runoff measured at the two sections of the experimental trench is compared with the model prediction obtained by the VertFlow + LatFlow model. The figure shows the two selected runoff episodes during the vegetation season 2008 and 2009 (episodes #6 and #7). Both episodes were approximated with the simulations based on $L = 25$ m. For episode #6, the simulated discharge series showed close agreement with data from trench section A. The timing of the rising limb of the simulated hydrograph of episode #7 compared relatively well with the observed discharge data from trench section B. The weaker response of the trench section A during episode #7 could be related to a malfunction of the fluxmeter.

The rainfall-runoff episode #2, shown in Fig. 5, was used for detailed comparison of the measured subsurface discharges with the model predictions based on the VertFlow + Latflow model with varying input parameters L, Θ, and K_B. The comparison is presented in Fig. 7. The effect of the contributing hillslope length L is shown in Fig. 7a. As expected, the runoff intensity predicted with simulations using different lengths of the contributing hillslope differ nearly proportionally from each other. Increasing the hillslope length, transformation of the inflow signal is more pronounced and the peak is delayed compared to discharge predicted for shorter hillslope lengths. Note that the simulation using $L = 100$ m did not retain the small temporal variations of the recharge signal on September 11.

Fig. 7b illustrates the effect of the effective porosity Θ on simulated hillslope discharge. Smaller value of Θ leads to higher discharge peaks and faster reactions (increase and decrease) in simulated outflow. In contrast, the simulation based on $\Theta = 0.03$ cm^3 cm^{-3} shows more significant transformation of the inflow signal causing complete disappearance of the small temporal variations in the discharge peak on September 11. Similar trend of simulated subsurface runoff was also obtained when varying Θ with other combinations of hillslope length and effective hydraulic conductivity. However, the transformation of the inflow signal is even more significant and the discharge peaks become substantially delayed for smaller values of effective hydraulic conductivity. In general, smaller values of effective porosity lead to narrow

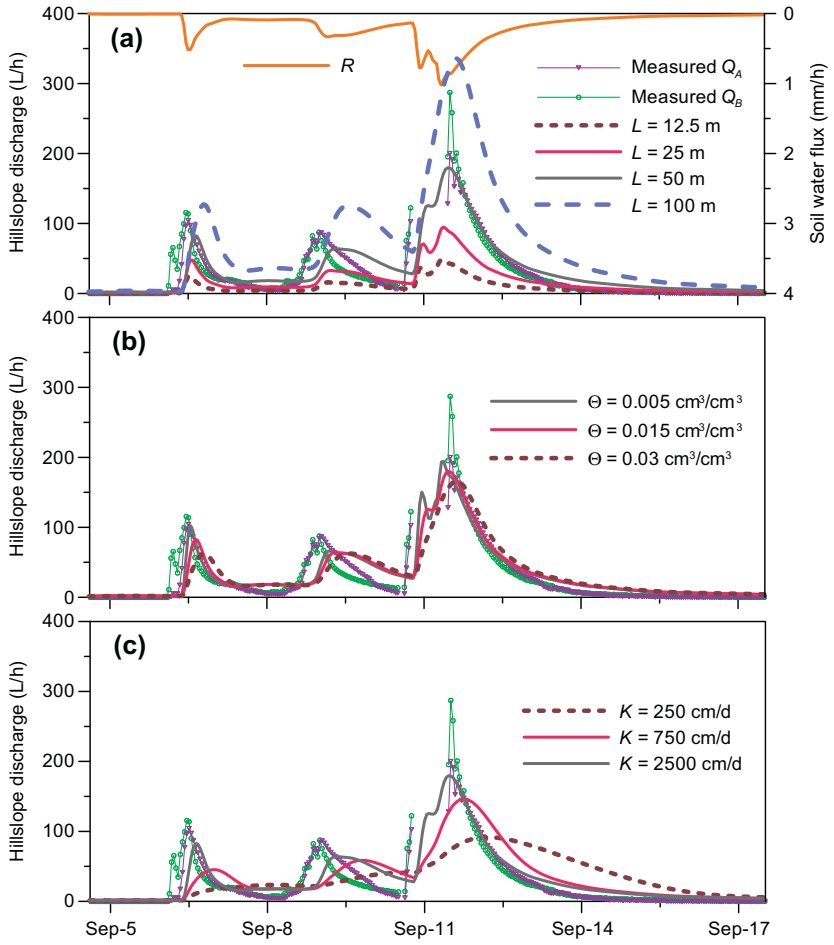

Fig. 7. Subsurface runoff Q predicted by the VertFlow + LatFlow model (episode #2, 2007). The LatFlow model was applied for (a) four different hillslope lengths L ($\Theta = 0.015$ cm^3 cm^{-3} and $K_B = 2500$ cm d^{-1}), (b) three different effective porosities Θ ($K_B = 2500$ cm d^{-1} and $L = 50$ m), and (c) three different effective conductivities K_B ($\Theta = 0.015$ cm^3 cm^{-3} and $L = 50$ m). The recharge rate R generated by the vertical flow model VertFlow is superimposed atop.

discharge hydrograph, higher runoff peak and negligible transformation of the inflow signal.

The effect of varying the effective hydraulic conductivity K_B in the diffusion wave model is shown in Fig. 7c. Maximal deviations among the scenarios with $K_B = 250$ cm d^{-1} and $K_B = 2500$ cm d^{-1} increased to about 45% difference in the main discharge peak height. The simulation using $K_B = 250$ cm d^{-1} is characterized by delayed and smaller height of discharge peaks compared to simulations with higher values of K_B. This response tends to vanish for smaller values of the effective porosity ($\Theta = 0.005$ cm^3 cm^{-3}). In general, higher values of the effective hydraulic conductivity cause higher discharge peak and thus steep rising and falling discharge limbs.

The values of Nash–Sutcliffe criterion for the predictions of hillslope discharge based on the selected combinations of parameters L, Θ, and K_B are presented in Tables 2a–2c. Each vegetation season is represented by a set of three rainfall-runoff episodes per year (numbered according to Fig. 3). The simulations based on the 100 m contributing hillslope length consistently show the lowest efficiency coefficients. For three out of nine episodes (i.e., #1, #3, and #4), the models performed poorly in discharge predictions and the efficiency criteria suggested the contributing hillslope length to be as short as 12.5 m. This is associated with a relatively small measured runoff volume (<0.9 m^3) for these episodes and can perhaps be attributed to dynamically variable contributing area. The model efficiency remained negative for episodes #1 and #4 because of the overestimation of cumulative hillslope discharge. The maximum model efficiency coefficients for the other six significant runoff episodes ranged from 0.406 to 0.890, indicating reasonable agreement between observed and predicted hillslope discharge. These episodes (i.e., #2, #5, #6, #7, #8, and #9) were the major episodes observed within the three simulated vegetation seasons, each characterized by at least 1.4 m^3 of runoff volume with continuous discharge lasting more than 3 days. Excluding the low flow episodes with negative Nash–Sutcliffe values (i.e., episodes #1 and #4), the VertFlow + LatFlow simulation with $L = 25$ m, $\Theta = 0.005$ cm^3 cm^{-3}, and $K_B = 2500$ cm d^{-1} performed better than the simulations using other parameter combinations. However, it should be noted that the combination of the VertFlow + InstLatFlow model (with $L = 25$ m) resulted in comparably good or even better overall prediction of hillslope discharge.

In Table 3, measured cumulative discharges for the three vegetation seasons are compared with the predicted discharges for four different hillslope lengths. The runoff volumes predicted using the VertFlow + InstLatFlow model were the same as those predicted with the VertFlow + LatFlow model (due to the identical recharge signal), irrespective of the selected combination of Θ and K_B parameters. The greatest discrepancies between the observed and predicted cumulative discharges are associated with the shortest and longest contributing hillslope lengths. Taking into account both the model efficiency (Tables 2a–2c) and the water balance (Table 3), the contributing hillslope length can be estimated in the interval of 25–50 m, which confirms the estimates made in the previous studies [e.g., 22].

Table 2a
Values of the Nash–Sutcliffe efficiency coefficients, E, for the discharge predictions obtained with VertFlow + InstLatFlow model and VertFlow + LatFlow model when compared to the measured discharges in vegetation season 2007. The numbering of the rainfall-runoff episodes is introduced in Fig. 3. For the VertFlow + LatFlow model, the efficiency coefficients based on different combinations of effective porosity Θ and effective hydraulic conductivity K_B are shown. The values of E were evaluated separately for sections A and B and then averaged to obtain a single value of E for each combination of model parameters (i.e., $E = (E_A + E_B)/2$). Episodes: #1 (May 15–May 29), #2 (September 6–September 18), and #3 (September 28–October 19).

Episode	Model	K_B (cm d^{-1})	Θ (cm^3 cm^{-3})	Hillslope length, L (m)			
				12.5	25	50	100
#1	VertFlow + InstLatFlow	–	–	−4.60	−18.8	−76.0	−306
	VertFlow + LatFlow	250	0.005	−4.39	−16.1	−57.5	−203
		750		−4.66	−18.4	−69.2	−258
		2500		−5.22	−20.4	−76.1	−293
		250	0.015	−3.60	−12.7	−46.1	−148
		750		−4.47	−16.6	−58.3	−205
		2500		−5.13	−19.9	−70.8	−258
		250	0.03	−3.02	−11.2	−36.1	−98.4
		750		−4.09	−14.4	−50.2	−174
		2500		−5.08	−18.6	−65.7	−229
#2	VertFlow + InstLatFlow	–	–	0.091	0.484	0.811	−0.366
	VertFlow + LatFlow	250	0.005	−0.019	0.460	0.538	−1.50
		750		0.095	0.490	0.746	−1.16
		2500		0.094	0.488	0.802	−0.605
		250	0.015	0.072	0.306	0.151	−1.80
		750		0.104	0.482	0.561	−1.66
		2500		0.096	0.490	0.759	−1.11
		250	0.03	0.009	0.146	−0.132	−1.38
		750		0.103	0.417	0.290	−1.86
		2500		0.101	0.494	0.679	−1.51
#3	VertFlow + InstLatFlow	–	–	0.369	0.285	−1.42	−11.0
	VertFlow + LatFlow	250	0.005	0.313	0.069	−2.13	−11.9
		750		0.359	0.226	−1.66	−11.7
		2500		0.368	0.260	−1.50	−11.2
		250	0.015	0.192	−0.284	−2.48	−9.26
		750		0.317	0.074	−2.13	−12.1
		2500		0.364	0.207	−1.66	−11.7
		250	0.03	0.061	−0.451	−2.12	−6.63
		750		0.260	−0.140	−2.51	−10.9
		2500		0.345	0.144	−1.91	−12.2

4. Discussion

4.1. Discharge data

The experimental data from the subsurface trench showed that only a limited number of discharge episodes during each vegetation season were corresponding to major rainfall-runoff events (Fig. 3). All these events produced saturated subsurface stormflow at the soil/bedrock interface, which led to hillslope discharge observed in the trench. Note that the two sections of the experimental trench responded differently to individual rainfall events. Section B produced significant discharge for a broader range of rainfall events, while section A responded only to a few major events [19]. The difference between the two trench sections could be attributed to spatial variability of the network of preferential pathways, soil heterogeneity, and bedrock topography [e.g., 39–41] among other factors. In this context, the discharge data from the A and B sections in vegetation season 2009 were exceptional. The trench section A showed substantially lower cumulative discharge compared to both previous vegetation seasons and B section in 2009 (Table 3). The weaker response of the trench section A in 2009 could be related to the fluxmeter malfunction.

4.2. Model assumptions

Layered soil profile was assumed in 1D vertical modeling of variably saturated dynamics, whereas the soil hydraulic properties were assumed to be constant along the hillslope in the diffusion wave model. In addition, spatial variability of the rainfall intensity over the hillslope was neglected. These assumptions comply with the original work of Boussinesq, where the recharge rate was considered uniform over the hillslope segment. Boussinesq's theory holds for relatively shallow and highly conductive soils, which corresponds to the conditions at our experimental site. In this study, we used vertical recharge rates generated by the 1D dual-continuum model rather than the rates perpendicular to the bedrock interface, which is in agreement with Chapman [42], who argued that the use of vertical recharge rates for diffusive wave model is more realistic.

In our conceptual model, an ad hoc flow separation of shallow subsurface runoff recharge, associated with the PF-domain soil water flux q_{f1}, and the soil matrix deep percolation, associated with the SM-domain flux q_{m2}, was assumed at the soil/bedrock interface. This simplification of the system arose from the hypothesis that vertical preferential pathways end in the soil above the bedrock (i.e., $q_{f2} = 0$). After reaching the soil/bedrock interface the preferentially-conveyed water turns downslope and flows through the laterally-interconnected network of preferential pathways. The fact that the PF-domain generated soil water fluxes were highly correlated with observed hillslope discharge (Fig. 3) indicates that the separation at the soil/bedrock seems to be realistic. The dominant role of preferential flow in hillslope runoff formation in headwater catchments has already been recognized by many researchers. For instance, Anderson et al. [43] found that the preferential flow component carries most of the shallow subsurface runoff during storms at their experimental hillslope site. However, a hillslope setting with a nearly impervious soil/bedrock interface (as found in e.g., Chicken Creek artificial catchment, see Holländer et al. [44]) would require considering the recharge rates from both the preferential pathways as well as the soil matrix (i.e., $R = w_m q_{m1} + w_f q_{f1}$) to predict lateral runoff adequately.

Table 2b
Values of the Nash–Sutcliffe efficiency coefficients, *E*, for vegetation season 2008. Episodes: #4 (July 13–July 31), #5 (August 15–August 30), and #6 (October 29–November 2).

Episode	Model	K_B (cm d^{-1})	Θ (cm^3 cm^{-3})	Hillslope length, L (m)			
				12.5	25	50	100
#4	VertFlow + InstLatFlow	–	–	−12.2	−54.2	−227	−930
	VertFlow + LatFlow	250	0.005	−10.3	−45.5	−181	−672
		750		−10.8	−47.6	−199	−757
		2500		−11.3	−53.7	−218	−846
		250	0.015	−9.86	−40.6	−149	−503
		750		−10.4	−46.8	−186	−693
		2500		−11.1	−49.3	−202	−778
		250	0.03	−9.45	−36.2	−123	−384
		750		−9.88	−43.2	−165	−585
		2500		−10.3	−49.7	−198	−722
#5	VertFlow + InstLatFlow	–	–	0.216	0.406	0.343	−1.57
	VertFlow + LatFlow	250	0.005	0.172	0.242	−0.103	−1.96
		750		0.208	0.361	0.152	−1.97
		2500		0.208	0.404	0.302	−1.75
		250	0.015	0.082	0.036	−0.362	−1.69
		750		0.176	0.248	−0.105	−2.03
		2500		0.204	0.368	0.168	−1.99
		250	0.03	0.009	−0.071	−0.390	−1.13
		750		0.126	0.118	−0.303	−1.93
		2500		0.192	0.312	0.030	−2.08
#6	VertFlow + InstLatFlow	–	–	0.077	0.655	0.454	−5.38
	VertFlow + LatFlow	250	0.005	−0.017	0.494	0.269	−3.66
		750		0.066	0.632	0.485	−4.48
		2500		0.059	0.658	0.487	−5.01
		250	0.015	−0.107	0.128	−0.398	−1.66
		750		0.029	0.541	0.230	−4.32
		2500		0.057	0.643	0.482	−4.66
		250	0.03	−0.272	−0.239	−0.446	−0.509
		750		−0.008	0.355	−0.277	−3.44
		2500		0.040	0.610	0.420	−4.73

Table 2c
Values of the Nash–Sutcliffe efficiency coefficients, *E*, for vegetation season 2009. Episodes: #1 (May 27–June 10), #2 (Jun 23–July 11), and #3 (October 11–October 25).

Episode	Model	K_B (cm d^{-1})	Θ (cm^3 cm^{-3})	Hillslope length, L (m)			
				12.5	25	50	100
#7[a]	VertFlow + InstLatFlow	–	–	0.209	0.574	0.721	−1.32
	VertFlow + LatFlow	250	0.005	0.206	0.597	0.890	−0.341
		750		0.208	0.582	0.775	−0.862
		2500		0.193	0.576	0.730	−1.23
		250	0.015	0.208	0.578	0.728	−0.604
		750		0.210	0.594	0.877	−0.429
		2500		0.194	0.582	0.763	−0.959
		250	0.03	0.190	0.457	0.373	−0.869
		750		0.212	0.610	0.862	−0.511
		2500		0.194	0.587	0.807	−0.628
#8[a]	VertFlow + InstLatFlow	–	–	0.142	0.408	0.605	−0.336
	VertFlow + LatFlow	250	0.005	0.131	0.356	0.438	−0.561
		750		0.132	0.393	0.583	−0.164
		2500		0.133	0.421	0.611	−0.215
		250	0.015	0.085	0.200	0.043	−0.816
		750		0.114	0.358	0.446	−0.567
		2500		0.123	0.413	0.596	−0.159
		250	0.03	−0.002	0.018	−0.094	−0.679
		750		0.087	0.251	0.175	−0.863
		2500		0.130	0.399	0.543	−0.323
#9	VertFlow + InstLatFlow	–	–	0.279	0.266	−1.91	−14.8
	VertFlow + LatFlow	250	0.005	0.305	0.400	−1.14	−9.69
		750		0.273	0.299	−1.60	−12.6
		2500		0.256	0.251	−1.90	−14.4
		250	0.015	0.319	0.450	−0.545	−4.24
		750		0.291	0.388	−1.20	−10.0
		2500		0.257	0.282	−1.67	-13.0
		250	0.03	0.291	0.419	−0.040	−1.72
		750		0.306	0.428	−0.852	−6.61
		2500		0.262	0.332	−1.43	−11.5

[a] The Nash–Sutcliffe efficiency coefficient was evaluated for section B only.

Table 3
Measured and simulated discharge volumes (expressed in m^3) for the three vegetation seasons and different hillslope lengths.

	Measured in trench section		Simulated with hillslope length, L (m)			
	A	B	12.5	25	50	100
2007	7.86	8.73	3.02	6.04	12.09	24.17
2008	6.87	9.39	5.45	10.89	21.79	43.58
2009	1.82	14.18	4.79	9.58	19.14	38.29

4.3. Input parameters for the diffusion wave model

In case preferential flow occurs in the soil profile, the effective hydraulic conductivity K_B in the diffusion wave equation (Eq. (3)) can be approximated just by the conductivity of the network of preferential pathways. The contribution of soil matrix conductivity is then usually lower or even negligible. In our case, the value of K_B for the diffusion wave model was tested in the range from 250 to 2500 cm d^{-1}. For instance, the value of K_B equal to 750 cm d^{-1} corresponded to the K_s value of the PF domain ($K_B = w_f K_s$) multiplied by the anisotropy factor of three. This value of the anisotropy factor of the lower soil layers was estimated from our previous 2D modeling results [45]. The values of the effective porosity Θ, often referred to as specific yield, were examined in the 0.005–0.03 $cm^3\ cm^{-3}$ range. The higher limit of the effective porosity ($\Theta = 0.03\ cm^3\ cm^{-3}$) was estimated from the parameters of the PF domain (i.e., w_f multiplied by the saturated water content θ_s). Under dynamic conditions (such as in our study), the value of the effective porosity can be only a fraction of the initial value of Θ [e.g., 46]. Note that the LatFlow model predominantly represents the lateral preferential pore network hence the value of Θ is much smaller than the value of the soil porosity (i.e., the SM domain is not considered in the LatFlow model and exchange with the surrounding soil matrix is assumed negligible for saturated conditions). Furthermore, a smaller value of the effective porosity for the LatFlow model can be caused by an imperfect connectivity of preferential pathways along the hillslope.

4.4. Contributing hillslope length

The length of the contributing hillslope can be, in principle, estimated using a field tracer experiment [47]. In the present study, we propose a different approach based on modeling of vertical and lateral flow components. Effective length of the contributing hillslope length most likely also depends on actual soil moisture conditions. Hence, it is not surprising to obtain slightly different contributing hillslope lengths for three distinct seasonal water regimes or even for individual rainfall-runoff events (Tables 2a–2c). Previously estimated contributing hillslope length of 25 m at the Tomsovka site [22] coincides with our modeling results, expressed in the efficiency coefficients (Tables 2a–2c) and discharge balance (Table 3). Although the geographic watershed divide is located approximately 130 m above the experimental trench, the trench seems to effectively drain a much shorter hillslope length. Among the various explanations for this finding, the discontinuity of underlying bedrock was observed by vertical electrical survey [23].

Note that only total contributing area is needed when the VertFlow predictions are combined with the quasi-steady state assumption (InstLatFlow model) to obtain hillslope discharge, i.e. the simulated signal does not undergo any lateral transformation. For the VertFlow + LatFlow model, however, the contributing hillslope length is crucial as the LatFlow model transforms the inflow signal based on the length of hillslope. For our experimental hillslope, the ratio of contributing length-to-width is relatively small thus the VertFlow + InstLatFlow model can be used to predict shallow subsurface runoff. It is worth mentioning that a good agreement between the data and VertFlow + InstLatFlow predictions was achieved not only for hillslope discharge series and discharge balance but also for pressure head comparison using the 25 m hillslope length. It can be speculated that a closer match between the model predictions and observations can be obtained by optimizing the length of contributing hillslope. However, the VertFlow + InstLatFlow model shows higher efficiency coefficients values than the VertFlow + LatFlow model for most runoff episodes (Tables 2a–2c). This further supports the fact that the transformation of the water flow signal by the Boussinesq model is in our case negligible due to relatively short contributing hillslope length.

4.5. Coupling of the models

The complex feedback reactions as in a fully coupled approach of modeling vertical and lateral transport processes at the hillslope scale are not presented in this study, i.e., the effect of shallow saturated depth h_B predicted by the Boussinesq model on 1D vertical water flow was not considered. The emphasis was rather given to the description of relevant processes at the hillslope scale than the full coupling of the models. The runoff response to major rainfall events predicted by the VertFlow + LatFlow model would probably exhibit two opposite effects when the coupling/feedback was more realistically considered. The feedback mechanism will reduce the thickness of the unsaturated zone, leading to the shorter travel times in the unsaturated zone. On the other hand, the response of the VertFlow model will be modified due to the saturated storage effects in the SM domain. Vogel and Dusek [45] presented a comparison of the VertFlow + LatFlow model with a fully coupled two-dimensional model based on dual-continuum approach and found similar behavior of the two conceptually different approaches for the site of interest. Nevertheless, more detailed comparison of these two approaches will be analyzed in a subsequent study.

The depth h_B higher than the soil profile was predicted for the simulation based on the 100 m hillslope length, indicating tendency to the formation of saturation excess overland flow. A few other combinations of Θ and K_B parameters (i.e., smaller Θ and K_B values) for shorter hillslope lengths also led to h_B higher than the soil profile. However, the effective porosity as used in the LatFlow model (Eq. (3)) is much smaller than the retention capacity of the soil profile (including both the soil matrix and preferential pathways). It is important to note that the effect of overland flow triggered by saturation excess is rarely observed at the site of interest and therefore is not considered in this study.

4.6. Sensitivity analysis

The greatest effect among the three tested parameters in the Boussinesq model on subsurface runoff predictions has the contributing hillslope length. This is especially apparent for simulations using $L = 100$ m, where overestimated discharge exhibits a time lag behind the measured values, which produced negative model efficiency coefficients (Tables 2a–2c). The increase of hillslope

length also leads to greater differences in efficiency coefficients among the simulations using different Θ and K_B parameters (Tables 2a–2c), e.g., the simulations scaled for L = 12.5 m show smaller variations in efficiency coefficients than the simulations with longer hillslope length. Significant transformation of the recharge signal from the PF domain was predicted for longer hillslopes, smaller effective conductivities, and larger effective porosities used in the LatFlow simulations (Fig. 7). In addition to the hillslope discharge, the three parameters of the LatFlow model affect the simulated depth of lateral flow h_B. The depth of h_B obviously increases with the increase of the hillslope length L. The simulated depth h_B also tends to build up with decreasing K_B and Θ values, which indicates a possible extension towards surface runoff coupling [48].

5. Conclusions

A one-dimensional model of shallow subsurface flow in a hillslope segment that includes a preferential flow component was described and compared with field data to simulate the mechanism of subsurface runoff formation. The coupling of the LatFlow model, based on a single-continuum diffusion wave approach, with the VertFlow model, based on a vertical dual-continuum Richards' equation approach, allowed for the simulation of the accelerating effect of preferential flow. This effect was shown to be highly important to account properly for water recharge at the hillslope scale. Preferential component of vertical flow was assumed to contribute exclusively to the formation of shallow subsurface runoff. This assumption helped to correctly describe an episodic flow regime in the simulated hillslope segment, i.e., saturated lateral subsurface flow developed after significant rainfalls. The modeling approach used in the present study is process consistent yet simple since it takes into account both preferential flow in a soil profile and lateral preferential flow on the surface of the inclined bedrock. Moreover, the approach seems promising as it describes hillslope discharge and is also suitable for larger spatial configurations of simulated hillslope transects.

The modeling framework of two coupled 1D models showed a good agreement with the experimental data of subsurface runoff dynamics. For the specific case of the Tomsovka hillslope, the analysis confirmed that the diffusion wave model could be replaced by a simple quasi-steady state expression (InstLatFlow model). The significance of lateral transformation would be much greater for longer hillslopes.

Acknowledgments

The study was supported by the Ministry of Environment of the Czech Republic (SP/2e7/229/07). Additional support was provided by the Czech Science Foundation (205/08/1174) the Czech Science Foundation (205/08/1174). The authors wish to thank Dr. Martin Sanda, who supervised the field observations at the Tomsovka site.

Appendix A

List of abbreviations:

SM	soil matrix
PF	preferential flow
VertFlow	vertical flow model based on one-dimensional dual-continuum Richards' equation approach
LatFlow	lateral flow model based on one-dimensional single-continuum diffusion wave approach
InstLatFlow	quasi-steady state lateral flow model (Eq. (12))

References

[1] Wienhofer J, Germer K, Lindenmaier F, Faerber A, Zehe E. Applied tracers for the observation of subsurface stormflow at the hillslope scale. Hydrol Earth Syst Sci 2009;13:1145–61.
[2] van Verseveld WJ, McDonnell JJ, Lajtha K. The role of hillslope hydrology in controlling nutrient loss. J Hydrol 2009;367:177–87. http://dx.doi.org/10.1016/j.jhydrol.2008.11.00.
[3] Fox GA, Wilson GV. The role of subsurface flow in hillslope and stream bank erosion: a review. Soil Sci Soc Am J 2010;74:717–33. http://dx.doi.org/10.2136/sssaj2009.031.
[4] Rigon R, Bertoldi G, Over TM. GEOtop: a distributed hydrological model with coupled water and energy budgets. J Hydrometeorol 2006;7:371–88.
[5] Hopp L, Harman C, Desilets SLE, Graham CB, McDonnell JJ, Troch PA. Hillslope hydrology under glass: confronting fundamental questions of soil–water–biota co-evolution at Biosphere 2. Hydrol Earth Syst Sci 2009;13:2105–18.
[6] Nieber JL, Sidle RC. How do disconnected macropores in sloping soils facilitate preferential flow? Hydrol Process 2010;24:1582–94. http://dx.doi.org/10.1002/hyp.763.
[7] Faeh AO, Scherrer S, Naef F. A combined field and numerical approach to investigate flow processes in natural macroporous soils under extreme precipitation. Hydrol Earth Syst Sci 1997;4:787–800.
[8] Kosugi K, Uchida T, Mizuyama T. Numerical calculation of soil pipe flow and its effect on water dynamics in a slope. Hydrol Process 2004;18:777–89. http://dx.doi.org/10.1002/hyp.136.
[9] Tani M. Analysis of runoff-storage relationships to evaluate the runoff-buffering potential of a sloping permeable domain. J Hydrol 2008;360:132–46. http://dx.doi.org/10.1016/j.jhydrol.2008.07.02.
[10] Paniconi C, Troch PA, van Loon EE, Hilberts AGJ. Hillslope-storage Boussinesq model for subsurface flow and variable source areas along complex hillslopes: 2. Intercomparison with a three-dimensional Richards equation model. Water Resour Res 2003;39:1317. http://dx.doi.org/10.1029/2002WR00173.
[11] Vogel T, Tesař M, Císlerová M. Modeling water regime in a small watershed. In: International conference on small catchment hydrology, Institute of Hydrodynamics of the Czech Academy of Sciences, Prague, Czech Republic; 2003, p. 127–36. ISBN 80-02-01586-X.
[12] Cordano E, Rigon R. A perturbative view on the subsurface water pressure response at hillslope scale. Water Resour Res 2008;44:W05407. http://dx.doi.org/10.1029/2006WR00574.
[13] Beven K. Kinematic subsurface stormflow. Water Resour Res 1981;17:1419–24.
[14] Beven K. Interflow. In: Morel-Seytoux HJ, editor. Unsaturated flow in hydrological modelling – theory and practice. Norwell, Mass.: Kluwer Acad.; 1989. p. 191–219.
[15] Fan Y, Bras R. Analytical solutions to hillslope subsurface storm flow and saturation overland flow. Water Resour Res 1998;34:921–7.
[16] Troch P, van Loon E, Hilberts A. Analytical solutions to a hillslope-storage kinematic wave equation for subsurface flow. Adv Water Resour 2002;25:637–49.
[17] Troch PA, Paniconi C, van Loon EE. Hillslope-storage Boussinesq model for subsurface flow and variable source areas along complex hillslopes: 1. Formulation and characteristic response.. Water Resour Res 2003;39:1316. http://dx.doi.org/10.1029/2002WR00172.
[18] Hilberts AGJ, Troch PA, Paniconi C, Boll J. Low-dimensional modeling of hillslope subsurface flow: relationship between rainfall, recharge, and unsaturated storage dynamics. Water Resour Res 2007;43:W03445. http://dx.doi.org/10.1029/2006WR00496.
[19] Vogel T, Sanda M, Dusek J, Dohnal M, Votrubova J. Using oxygen-18 to study the role of preferential flow in the formation of hillslope runoff. Vadose Zone J 2010;9:252–9. http://dx.doi.org/10.2136/vzj2009.006.
[20] Gerke HH, van Genuchten MT. A dual-porosity model for simulating the preferential movement of water and solutes in structured porous media. Water Resour Res 1993;29:305–19.
[21] Sanda M, Kulasova A, Cislerova M. Hydrological processes in the subsurface investigated by water isotopes and silica. Soil Water Res 2009;4:S83–92.
[22] Hrncir M, Sanda M, Kulasova A, Cislerova M. Runoff formation in a small catchment at hillslope and catchment scales. Hydrol Process 2010;24:2248–56. http://dx.doi.org/10.1002/hyp.761.
[23] Sanda M, Cislerova M. Transforming hydrographs in the hillslope subsurface. J Hydrol Hydromech 2009;57:264–75. http://dx.doi.org/10.2478/v10098-009-0023-z.
[24] Boussinesq J. Essai sur la théorie des eaux courantes. Mem Acad Sci Inst Fr 1877;23:1–680.
[25] Vogel T. Simplified dual continuum approach to modeling subsurface runoff from a hillslope segment. In: General assembly, European Geophysical Union, Vienna, Austria; 2005.
[26] Gerke HH, van Genuchten MT. Evaluation of a first-order water transfer term for variably saturated dual-porosity models. Water Resour Res 1993;29:1225–38.
[27] Vogel T, Brezina J, Dohnal M, Dusek J. Physical and numerical coupling in dual-continuum modeling of preferential flow. Vadose Zone J 2010;9:260–7. http://dx.doi.org/10.2136/vzj2009.009.
[28] Ray C, Vogel T, Dusek J. Modeling depth-variant and domain-specific sorption and biodegradation in dual-permeability media. J Contam Hydrol 2004;70:63–87. http://dx.doi.org/10.1016/j.jconhyd.2003.08.00.

[29] Gerke HH, Dusek J, Vogel T, Köhne JM. Two-dimensional dual-permeability analyses of a bromide tracer experiment on a tile-drained field. Vadose Zone J 2007;6:651–67. http://dx.doi.org/10.2136/vzj2007.003.
[30] Dusek J, Vogel T, Lichner L, Cipakova A. Short-term transport of cadmium during a heavy-rain event simulated by a dual-continuum approach. J Plant Nutr Soil Sci 2010;173:536–47. http://dx.doi.org/10.1002/jpln.20080028.
[31] Vogel T, van Genuchten MT, Cislerova M. Effect of the shape of soil hydraulic properties near saturation on numerical simulation of variably-saturated flow. Adv Water Resour 2000;24:133–44. http://dx.doi.org/10.1016/S0309-1708(00)00037-3.
[32] Dohnal M, Dusek J, Vogel T, Herza J, Tacheci P. Analysis of soil water response to grass transpiration. Soil Water Res 2006;1:85–98.
[33] Dohnal M, Dusek J, Vogel T. The impact of the retention curve hysteresis on prediction of soil water dynamics. J Hydrol Hydromech 2006;54:258–68.
[34] Monteith JL. Evaporation and surface temperature. JCR database 1981;107:1–27.
[35] Feddes RA, Kowalik PJ, Zaradny H. Simulation of field water use and crop yield. Wageningen, The Netherlands: Centre for Agricultural Publishing and Documentation; 1978.
[36] Weiler M, McDonnell JJ. Virtual experiments: a new approach for improving process conceptualization in hillslope hydrology. J Hydrol 2004;285:3–18. http://dx.doi.org/10.1016/S0022-1694(03)00271-3.
[37] Hilberts AGJ, Troch PA, Paniconi C. Storage-dependent drainable porosity for complex hillslopes. Water Resour Res 2005;41:W06001. http://dx.doi.org/10.1029/2004WR00372.
[38] Nash JE, Sutcliffe JV. River flow forecasting through conceptual models part I – a discussion of principles. J Hydrol 1970;10:282–90.
[39] Genereux DP, Hemond HF, Mulholland PJ. Spatial and temporal variability in streamflow generation on the west fork of walker branch watershed. J Hydrol 1993;142:137–66.
[40] Famiglietti JS, Rudnicki JW, Rodell M. Variability in surface moisture content along a hillslope transect: Rattlesnake Hill, Texas. J Hydrol 1998;210:259–81.
[41] Harman C, Sivapalan M. Effects of hydraulic conductivity variability on hillslope-scale shallow subsurface flow response and storage-discharge relations. Water Resour Res 2009;45:W01421. http://dx.doi.org/10.1029/2008WR00722.
[42] Chapman TG. Recharge-induced groundwater flow over a plane sloping bed: solutions for steady and transient flow using physical and numerical models. Water Resour Res 2005;41:W07027. http://dx.doi.org/10.1029/2004WR00360.
[43] Anderson AE, Weiler M, Alila Y, Hudson RO. Subsurface flow velocities in a hillslope with lateral preferential flow. Water Resour Res 2009;45:W11407. http://dx.doi.org/10.1029/2008WR00712.
[44] Holländer HM, Blume T, Bormann H, Buytaert W, Chirico GB, Exbrayat JF, et al. Comparative predictions of discharge from an artificial catchment (Chicken Creek) using sparse data. Hydrol Earth Syst Sci 2009;13:2069–94.
[45] Vogel T, Dusek J. Comparison of two different approaches to modeling subsurface runoff at the hillslope scale. In: General assembly, European Geophysical Union, Vienna, Austria; 2006.
[46] Neuman SP. On methods of determining specific yield. Ground Water 1987;25:679–84.
[47] Jones JAA. Pipeflow contributing areas and runoff response. Hydrol Process 1997;11:35–41.
[48] Weill S, Mouche E, Patin J. A generalized Richards equation for surface/subsurface flow modelling. J Hydrol 2009;366:9–20. http://dx.doi.org/10.1016/j.jhydrol.2008.12.00.

Hillslope hydrograph analysis using synthetic and natural oxygen-18 signatures, Journal of Hydrology, 2012.

Journal of Hydrology 475 (2012) 415–427

Contents lists available at SciVerse ScienceDirect

Journal of Hydrology

journal homepage: www.elsevier.com/locate/jhydrol

Hillslope hydrograph analysis using synthetic and natural oxygen-18 signatures

Jaromir Dusek *, Tomas Vogel, Martin Sanda

Czech Technical University in Prague, Faculty of Civil Engineering, Prague, Czech Republic

ARTICLE INFO

Article history:
Received 18 July 2012
Received in revised form 18 October 2012
Accepted 18 October 2012
Available online 27 October 2012
This manuscript was handled by Peter K. Kitanidis, Editor-in-Chief, with the assistance of Bernhard Wehrli, Associate Editor

Keywords:
Shallow subsurface runoff
Diffusion wave equation
Stable isotope transport in soil
Dual-permeability model
Hillslope hydrograph separation
Preferential flow

SUMMARY

Shallow subsurface runoff is one of the most important mechanisms determining hydrological responses of headwater catchments to rainstorms. In this study, a simplified approach combining one-dimensional dual-continuum vertical flow in a variably saturated soil profile and one-dimensional saturated flow along the soil–bedrock interface was used to study rainfall–runoff events at an experimental hillslope. A dual set of Richards' equations was used to predict vertical flow of water in the soil matrix and preferential pathways. Subsurface flow along the soil–bedrock interface was described by diffusion wave (Boussinesq-type) equation. The observed subsurface runoff and its ^{18}O composition were compared with the model predictions. Contributions of pre-event and event water to hillslope runoff during major rainfall–runoff episodes were evaluated by means of numerical experiments involving synthetic ^{18}O rainfall signatures. Although preferential flow played an important role in the hillslope runoff formation, pre-event water was found to be significant runoff component in most events (it formed 47–74% of total subsurface runoff). The simulation results confirmed the hypothesis of significant mixing between infiltrating rainwater and water stored in the hillslope soil profile. The modeling approach presented in this study was successful in describing both vertical and lateral mixing of water.

1. Introduction

For headwater catchments in temperate climate zone with permeable soils, shallow subsurface flow (also referred to as stormflow, throughflow, or interflow) is recognized as the most important runoff mechanism. Shallow subsurface flow usually develops above the sloping interface of permeable soil and less permeable underlying soil layer or bedrock. It occurs only for a short period of time as an immediate response to intense or long-lasting rainfall event. The onset of shallow subsurface flow is commonly accelerated by the presence of macropores and biopores in a soil profile, potentially forming a network of interconnected preferential pathways. These pathways are known to play a significant role in runoff formation at the hillslope scale, as was experimentally confirmed e.g. by Smettem et al. (1991), Sidle et al. (1995), Heppell et al. (2000), and Buttle and McDonald (2002).

Stable isotopes of water (e.g., ^{18}O and ^{2}H) naturally occurring in rainfall water have the potential to reveal principal transport mechanisms at multiple scales – from soil profile to hillslope and catchment scale (Sveinbjornsdottir and Johnsen, 1992; Mathieu and Bariac, 1996; McGuire and McDonnell, 2010). More specifically, the isotope data are frequently used for runoff separation into pre-event ("old") and event ("new") water by applying a mass balance approach. Thus, the isotopes may help to explain the mechanism of mixing of new and old water at the relevant scales. Natural isotopes are usually treated as conservative tracers when fractionation processes are negligible. Such use benefits from the spatial coherence and relatively high temporal variability of the isotope signal in infiltrating rainwater (Vogel et al., 2010a).

Several experimental case studies showed that event water in hillslope and catchment runoff is a small fraction of the total, even in cases where discharge is expected to be dominated by preferential flow (e.g., McDonnell, 1990; Burns et al., 2001; Kelln et al., 2007). On the contrary, Leaney et al. (1993) estimated contribution of the pre-event soil water to stormflow to be less than 20% as event-driven macropore flow carried substantial part of hillslope runoff. Similarly, event water was hypothesized to form a significant part of the runoff during rainfall–runoff events in studies of Peters and Ratcliffe (1998), Weiler et al. (1999), Monteith et al. (2006), and others. Based on a compilation of studies performed in small- and medium-sized catchments, Buttle (1994) concluded that at least 50% of streamflow is supplied by pre-event water. From these examples it becomes evident that the proportion of pre-event water varies as different hillslope settings result in different transport processes contributing to runoff formation. Nevertheless, consensus made by the hydrologists is that the pre-event water component dominates stormflow in small humid forested catchments (Burns, 2002).

* Corresponding author. Address: Department of Hydraulics and Hydrology, Czech Technical University in Prague, Faculty of Civil Engineering, Thakurova 7, 166 29 Prague, Czech Republic. Tel.: +420 22435 4355; fax: +420 22435 4793.
E-mail address: dusek@mat.fsv.cvut.cz (J. Dusek).

0022-1694/$ - see front matter © 2012 Elsevier B.V. All rights reserved.
http://dx.doi.org/10.1016/j.jhydrol.2012.10.025

To perform the original quantitative hydrograph separation procedure, based on a mass balance approach, hydrometric and isotope field data have to be available in detail temporal resolution and certain basic assumptions have to be met. These restrictions often limit the applicability of runoff separation using isotope data (Van der Hoven et al., 2002). As pointed out by Van der Hoven et al. (2002), the measurement of a single ^{18}O value to characterize the pre-event isotopic composition of soil water in the entire soil profile is hardly adequate. For instance, Kendall and McDonnell (1993) inspected the effect of variable isotope concentration depth profiles on hydrograph separation. The existence of two pore regions in the soil profile (soil matrix and macropores) further invalidates a routine use of the isotopic mass balance approach. Since the assumptions of spatially and temporarily uniform isotope concentrations are rarely fulfilled (^{18}O value of pre-event water is not a constant), a reliable runoff separation is difficult to accomplish. Jones et al. (2006) argued that the role of tracer dispersion is neglected in the hydrograph separation procedures. Van der Hoven et al. (2002) questioned validity of most hydrograph separation studies reported in the literature, which did not consider spatial and temporal variability in individual compartments of subsurface reservoirs. Similarly, Uhlenbrook and Hoeg (2003) demonstrated that the hydrograph separation might deliver only qualitative information on the different runoff contributions while relatively large uncertainties of various sources prevailed when performing the separation. Moreover, it is well known that a significant difference between the isotope concentrations in event and pre-event water is required to separate these contributions (Buttle, 1994). In the past, several improvements and modifications of the original hydrograph separation procedure were suggested (e.g., McDonnell et al., 1990; Harris et al., 1995; Genereux, 1998). For instance, Jones et al. (2006) included surface runoff component in the concept of hydrograph separation at the catchment scale and split subsurface components into contributions from the saturated and unsaturated zones.

The above mentioned drawbacks related to a simplistic use of isotopes in runoff separation studies can be avoided by applying more sophisticated experimental and modeling approaches, ideally including fully distributed process-based multi-dimensional numerical modeling of the relevant hydrological processes. To prevent an excessive computational cost of the numerical solution of two- (2D) or three-dimensional (3D) governing equations of the hillslope scale flow and transport processes, it is possible to decouple the essentially 3D flow into one-dimensional (1D) vertical variably saturated flow and 1D lateral saturated flow along soil–bedrock interface (Fan and Bras, 1998; Troch et al., 2002; Hilberts et al., 2007; and others). This has mostly been achieved by applying Richards' equation to predict 1D vertical flow and 1D Boussinesq equation to describe lateral subsurface flow. It is, however, important to note that complete building-up and fading-away stages of saturated subsurface flow, as predicted by a 2D or 3D solution of Richards' equation, may not be fully captured by the simplified 1D approach (Sloan and Moore, 1984).

Gerke et al. (2007) and Coppola et al. (2009) highlighted the importance of including both water flow data and tracer transport information into a conceptual model to adequately describe flowpaths in soils. In recent literature, the application of isotope transport models was mostly limited to vertical processes under laboratory (Braud et al., 2005) or field conditions (Shurbaji et al., 1995; Singleton et al., 2004; Stumpp et al., 2012). With the exception of our previous study (Vogel et al., 2010a), no attempt has been made to simulate hillslope transport using ^{18}O as environmental tracer in gauged hillslope profiles. Specifically, the lateral component of the isotope transport has not been, to our knowledge, considered in recent modeling studies on the local scale. From the catchment point of view, Iorgulescu et al. (2005, 2007) used a hydrogeochemical stochastic model to predict discharge and tracer concentrations in a stream. Detailed data-model comparisons of isotope transport in unsaturated zone were published in a small number of studies (e.g., Stumpp et al., 2009; Haverd and Cuntz, 2010; Rothfuss et al., 2012). This could be partly attributed to complex requirements for field sampling and laboratory measurements of stable isotope contents. For instance, surface boundary condition for isotope transport modeling is highly uncertain due to short-term variability of isotope content in rainstorm water (McDonnell et al., 1990). The resolution of sampling and number of analyses of isotope contents are often subject to financial limitations.

The present work is a follow-up of the previous studies of Vogel et al. (2010a) and Dusek et al. (2012). Vogel et al. (2010a) applied vertical one-dimensional dual-continuum model to describe soil water dynamics and stable isotope transport in a hillslope soil. In their analysis, the oxygen isotope was used as a natural tracer to study preferential flow effects at the site of interest. In the subsequent study (Dusek et al., 2012), lateral component of rapid shallow subsurface flow at the same site, in addition to preferential vertical movement, was considered, however, lateral transport processes were not addressed.

The primary motivation of the present study originated from the need to improve current understanding of subsurface flow and transport processes occurring in a hillslope segment. To accomplish this goal we combine field observations of hillslope discharge and the associated ^{18}O contents with detailed process-based numerical modeling. The available ^{18}O data from our experimental site indicate significant mixing of pre-event and event water in the soil profile (e.g., Sanda et al., 2009). Sanda and Cislerova (2009), Vogel et al. (2010a), and Dohnal et al. (2012) identified preferential flow as an important factor in runoff formation at the site, in spite of that, the measured ^{18}O contents in hillslope discharge do not show easily identifiable responses to individual rainfall episodes with distinct ^{18}O signatures, but rather a mixture of responses to several antecedent rainfall episodes with varying ^{18}O signatures.

In the present study, we focus on modeling and analysis of processes controlling the isotopic composition of subsurface runoff at the hillslope scale. One-dimensional dual-continuum vertical flow and transport model (based on Richards and advection–dispersion equations) coupled with one-dimensional single-continuum lateral flow and transport model (based on diffusion wave equation for saturated subsurface flow and advection–dispersion equation for isotope transport) were used to simulate the subsurface processes during observed rainfall–runoff episodes. First, we performed long-term simulations, covering three consecutive vegetation seasons, which enabled us to compare observed subsurface hillslope discharge rates and ^{18}O concentrations with the model predictions. Then, model responses to a selected multiple-episode rainfall event were evaluated to study the mixing of pre-event and event water in the hillslope system. To distinguish the partial responses to the individual rainfall episodes, the synthetic ^{18}O signatures were used in the numerical experiments. Finally, separation of pre-event and event water components of hillslope discharge hydrograph was performed.

2. Materials and methods

2.1. Experimental site

The experimental hillslope site Tomsovka is situated in the Uhlirska catchment, Jizera Mountains, Czech Republic. Total area of the catchment is 1.78 km^2, average altitude reaches 820 m above sea level, annual precipitation exceeds 1300 mm, and

average annual temperature is 4.7 °C. The average slope at Tomsovka is about 14%. The studied hillslope is covered with grass (*Calamagrostis villosa*) and spruce (*Picea abies*).

The soil at Tomsovka is sandy loam classified as Dystric Cambisol. The hillslope soil profile consists of three layers with different hydraulic properties (parameterized using a modified version of the van Genuchten–Mualem parameterization (Vogel et al., 2000), (Table 1)). The three soil layers are underlain by a transition zone starting at the depth of about 70 cm, followed by compact granite bedrock. Significant preferential flow effects at Tomsovka, affecting the soil water response to precipitation, were reported by Sanda and Cislerova (2009) and Hrncir et al. (2010). Preferential flow was attributed to highly conductive pathways along decayed tree roots, as well as to soil structure and spatial variability of local soil hydraulic properties. Overland flow is rarely observed due to relatively permeable topsoil layer.

Hydrological and micrometeorological conditions at Tomsovka were monitored with high temporal resolution over the period from May 2007 to October 2009 (Sanda et al., 2009). Soil water pressure within the soil profile was measured using a set of automated tensiometers installed at three different depths below the soil surface. The discharge of shallow subsurface flow was measured by means of experimental trench. Water entering the trench was collected at the depth of about 75 cm below the soil surface into PVC pipes. The pipe discharge was measured by tipping bucket gauges, separately for two trench sections denoted as A and B (each 4 m long). The discharge rates Q_A and Q_B were measured continuously during vegetation seasons (from May to October). The hillslope length contributing to measured subsurface runoff was estimated to be about 25 m (Hrncir et al., 2010), although the geographic catchment divide is located approximately 130 m above the experimental trench, winding through a gently sloping plateau. The contributing hillslope length estimate was based on the comparison of hillslope discharge to the trench and observed catchment outlet discharge (assuming that hillslope subsurface flow represents a dominant part of the catchment response and is uniform across the catchment). For the modeling purposes, the hillslope micro-catchments corresponding to trench sections A and B were assumed to have approximately same geometric and material properties (hillslope length, depth to bedrock, soil stratification, soil hydraulic properties, etc.).

The ^{18}O content at the Tomsovka site was measured in: (i) precipitation collected from the rain gauge, (ii) subsurface hillslope discharge collected from the two sections of the experimental trench, and (iii) soil water extracted from two depths by suction cups.

During the vegetation seasons, rainwater samples of ^{18}O content were collected at daily intervals, provided that the amount of rainfall since the previous sampling had exceeded 5 mm (in 2007) or 1 mm (in 2008 and 2009). As each sample corresponded to cumulative rainfall for the period between two samplings, the measured ^{18}O content represented the average value for this period.

The ^{18}O concentration in hillslope discharge was measured in samples collected at 6-h intervals (3-h intervals in 2009), provided that at least 8.5 L of water had been accumulated since the previous sampling. The ^{18}O content was determined for combined discharge from both trench sections (i.e., separate ^{18}O contents for trench sections A and B were not available). The ^{18}O values measured during intensive outflow episodes represent nearly instantaneous ^{18}O concentrations. In case that discharge rates became lower, mixing of the effluent water occurred and the respective ^{18}O values therefore represent time-averaged concentrations.

To obtain information about resident ^{18}O concentrations, soil water was extracted by suction cups installed at the depths of 30 and 60 cm. Sampling was conducted at monthly intervals over the vegetation seasons. More detailed information on suction cups sampling was given by Vogel et al. (2010a).

The ^{18}O content was measured by a laser spectroscope (LGR Liquid–Water Isotope Analyzer, Los Gatos Research, Inc., CA) (Penna et al., 2010). The $\delta^{18}O$ values (given in parts per thousand) represent relative deviations of measured $^{18}O/^{16}O$ ratios from the isotopic composition of the Vienna Standard Mean Ocean Water ($\delta^{18}O$: ‰ V-SMOW, further referred as ‰ only). Manufacturer declared precision of the ^{18}O measurement is 0.2‰. Based on a long-term use of the LGR laser analyzer the standard deviation is 0.16‰. The weighted average of $\delta^{18}O$ in precipitation at the Tomsovka site is −9.96‰ for the period August 2006–August 2012.

2.2. One-dimensional lateral flow model (LatFlow)

Upon sufficiently abundant rain, water infiltrates through the soil profile vertically down to the impermeable bedrock or, as in our case, the top boundary of a semi-permeable weathered layer where a saturated zone is gradually formed. In this zone, water flows in the direction determined by the local gradient of the soil–bedrock interface, which does not usually differ much from the soil surface elevation gradient. We assume that variably saturated vertical flow is reasonably well described by one-dimensional (1D) Richards' equation while the short-term shallow saturated subsurface flow (simply referred to as lateral flow) can be approximated by the 1D diffusion wave equation, also referred to as Boussinesq equation (Boussinesq, 1877). The diffusion wave equation is considered in the following form:

$$\Theta \frac{\partial h_D}{\partial t} - \frac{\partial}{\partial x}\left(K_D h_D \left(\frac{\partial h_D}{\partial x} + \frac{dz}{dx}\right)\right) = R \quad (1)$$

where Θ is the effective porosity ($m^3\ m^{-3}$), h_D is the depth of lateral flow (m), i.e. the vertical range of the saturated flow zone, K_D is the effective saturated hydraulic conductivity ($m\ s^{-1}$), x is the coordinate (m) running along the bedrock slope (positive in the upslope direction), z is the vertical coordinate (positive upwards), dz/dx is the local hillslope gradient (–), R is the local intensity of vertical recharge ($m\ s^{-1}$), and t is time (s). The local hillslope discharge, Q ($m^3\ s^{-1}$), is expressed as:

Table 1
The soil hydraulic parameters[a] used for the one-dimensional dual-continuum model VertFlow.

Domain	Depth (cm)	θ_r ($cm^3\ cm^{-3}$)	θ_s ($cm^3\ cm^{-3}$)	α (cm^{-1})	n (–)	K_s ($cm\ d^{-1}$)	h_s (cm)
Matrix	0–8	0.20	0.55	0.050	2.00	567	0.00
	8–20	0.20	0.54	0.050	1.50	67	−0.69
	20–70	0.20	0.49	0.020	1.20	17	−1.48
	70–75	0.20	0.41	0.020	1.20	1.3	−1.88
Preferential	0–75	0.01	0.60	0.050	3.00	5000	0.00

[a] θ_r and θ_s are the residual and saturated water contents, respectively, K_s is the saturated hydraulic conductivity, h_s is the air-entry value of Vogel et al. (2000), and α and n are empirical fitting parameters.

$$\frac{Q}{W} = -K_D h_D \left(\frac{\partial h_D}{\partial x} + \frac{dz}{dx}\right) \quad (2)$$

where W is the hillslope width (m), here assumed to be constant along x.

One-dimensional solute transport in a saturated zone above the soil–bedrock interface (here associated with $\delta^{18}O$ transport) can be described by advection–dispersion equation:

$$\frac{\partial \Theta h_D c}{\partial t} + \frac{1}{W}\frac{\partial Q c}{\partial x} - \frac{\partial}{\partial x}\left(\Theta h_D D_D \frac{\partial c}{\partial x}\right) = T \quad (3)$$

where c is the solute concentration (kg m^{-3}), D_D is the effective hydrodynamic dispersion coefficient (m^2 s^{-1}), and T is the vertical solute mass recharge (kg m^{-2} s^{-1}).

The governing equations of lateral flow and transport are solved by the one-dimensional model LatFlow. The numerical solution is obtained by finite element method and implemented in the computer program HYPO (Vogel et al., 2003).

2.3. One-dimensional vertical model (VertFlow)

Vertical movement of water in a variably saturated soil profile is described by one-dimensional dual-continuum model, based on numerical solution of two coupled Richards' equations (similarly to Gerke and van Genuchten (1993a)):

$$w_f C_f \frac{\partial h_f}{\partial t} = \frac{\partial}{\partial z}\left(w_f K_f \left(\frac{\partial h_f}{\partial z} + 1\right)\right) - w_f S_f - \Gamma_w \quad (4)$$

$$w_m C_m \frac{\partial h_m}{\partial t} = \frac{\partial}{\partial z}\left(w_m K_m \left(\frac{\partial h_m}{\partial z} + 1\right)\right) - w_m S_m + \Gamma_w \quad (5)$$

where m and f indicate the soil matrix domain (SM domain) and the preferential flow domain (PF domain), respectively, h is the pressure head (m), K is the unsaturated hydraulic conductivity function (m s^{-1}), C is the soil water capacity (m^{-1}), S is the local root extraction intensity (s^{-1}), Γ_w is the soil water transfer term (s^{-1}) controlling the water exchange between the flow domains, w_m and w_f are volume fractions of the respective domains ($w_m + w_f = 1$), and z is the vertical coordinate (m) positive upwards.

The soil water transfer term is parameterized using a modified first-order approximation of Gerke and van Genuchten (1993b):

$$\Gamma_w = \alpha_{ws} K_{ar} (h_f - h_m) \quad (6)$$

where α_{ws} is the soil water transfer coefficient at saturation (m^{-1} s^{-1}) and K_{ar} is the relative unsaturated conductivity of the SM- and PF-domain interface. Values of K_{ar} range from 0 to 1 depending on the SM- and PF-domain conductivities, which are evaluated for the upstream pressure (Ray et al., 2004; Vogel et al., 2010b).

Similarly to soil water flow, vertical transport of solute is described by a dual set of advection–dispersion equations:

$$\frac{\partial w_f \theta_f c_f}{\partial t} + \frac{\partial w_f q_f c_f}{\partial z} - \frac{\partial}{\partial z}\left(w_f \theta_f D_f \frac{\partial c_f}{\partial z}\right) = -w_f S_f c_f - \Gamma_s \quad (7)$$

$$\frac{\partial w_m \theta_m c_m}{\partial t} + \frac{\partial w_m q_m c_m}{\partial z} - \frac{\partial}{\partial z}\left(w_m \theta_m D_m \frac{\partial c_m}{\partial z}\right) = -w_m S_m c_m + \Gamma_s \quad (8)$$

where θ is the volumetric water content (m^3 m^{-3}), q is the soil water flux (m s^{-1}), D is the hydrodynamic dispersion coefficient (m^2 s^{-1}), and Γ_s is the solute transfer term (kg m^{-3} s^{-1}). The coefficient of hydrodynamic dispersion depends on the respective values of local soil water flux and soil water content as well as dispersivity and molecular-diffusion coefficient (e.g., Jury et al., 1991).

The solute transfer term Γ_s is defined as the mass flux of solute transported from one domain to the other (Gerke and van Genuchten, 1993b):

$$\Gamma_s = \Gamma_w c_i + \alpha_{ss} \theta_{ar} (c_f - c_m) \quad (9)$$

In case that water flows from the PF to SM domain: $c_i = c_f$, for the opposite flow direction: $c_i = c_m$. The first term on the right hand side represents the advective inter-domain exchange of solute driven by the soil water pressure difference. The second term accounts for the diffusive exchange of solute due to the concentration gradient. The rate of diffusive exchange is controlled by the solute transfer coefficient at saturation α_{ss} (s^{-1}) and the value of θ_{ar}, which is the effective degree of saturation at the domain interface. In our model, the coefficient θ_{ar} is assumed to be equal to the relative saturation of the PF domain (Ray et al., 2004).

The governing equations of vertical flow and transport are solved by the one-dimensional dual-continuum model VertFlow. VertFlow is also used to predict the recharge rates R and T needed as input to lateral flow and transport (Eqs. (1) and (3)). The procedure used for evaluation of R and T is described in the next section (see also Fig. 1). The dual sets of governing equations are solved numerically by the computer program S1D using finite element method. The most recent implementation of the S1D code is described in Vogel et al. (2010b).

2.4. Recharge rates for lateral flow and transport

After solving vertical flow and transport equations, the lateral flow recharge rate R can be determined from a simple continuity equation formulated at the soil–bedrock interface, which, at the same time, represents a forward-coupling procedure between the vertical and lateral flow models:

$$R = R_f + R_m = w_f(q_{f1} - q_{f2}) + w_m(q_{m1} - q_{m2}) \quad (10)$$

where R_f and R_m are the contributions from the PF and SM domains, respectively, q_1 and q_2 are the soil water fluxes above and below the soil–bedrock interface, respectively (m s^{-1}). The q_2 fluxes represent seepage to deeper horizons (see Fig. 1).

Similarly to soil water fluxes, the solute mass fluxes at the soil–bedrock interface are assumed to fulfill the continuity equation:

$$T = T_f + T_m = w_f(c_{f1} q_{f1} - c_{f2} q_{f2}) + w_m(c_{m1} q_{m1} - c_{m2} q_{m2}) \quad (11)$$

where T is the composite lateral solute transport recharge, T_f and T_m are the respective contributions from the PF and SM domains, $c_1 q_1$ and $c_2 q_2$ are the solute mass fluxes above and below the soil–bedrock interface, respectively (kg m^{-2} s^{-1}). The $c_2 q_2$ mass fluxes represent leaching of solute to deeper horizons (Fig. 1).

At Tomsovka, partitioning of water and ^{18}O fluxes at the soil–bedrock interface was based on the assumption that the preferential pathways end in the soil above the bedrock (about 70 cm below the soil surface), i.e. $q_{f2} = 0$ and $c_{f2} q_{f2} = 0$. After reaching the soil–bedrock interface the preferentially-conveyed water turns downslope and then flows through the laterally-interconnected network of preferential pathways, while the vertical soil matrix fluxes are assumed to contribute to deep percolation (as specified in Section 3.1). The proposed modeling approach can be, in principle, also applied to different soil–bedrock conditions. For example, nearly impervious soil–bedrock interface would call for including contributions from both pore domains (i.e., the SM and PF domain) in lateral flow recharge. Such conditions were described e.g. in Gerwin et al. (2009).

The combination of forward coupled vertical dual-continuum model and lateral single-continuum diffusion wave model is henceforward abbreviated as the VertFlow + LatFlow model.

2.5. Model performance

The model performance can be evaluated using the model efficiency criterion of Nash and Sutcliffe (1970):

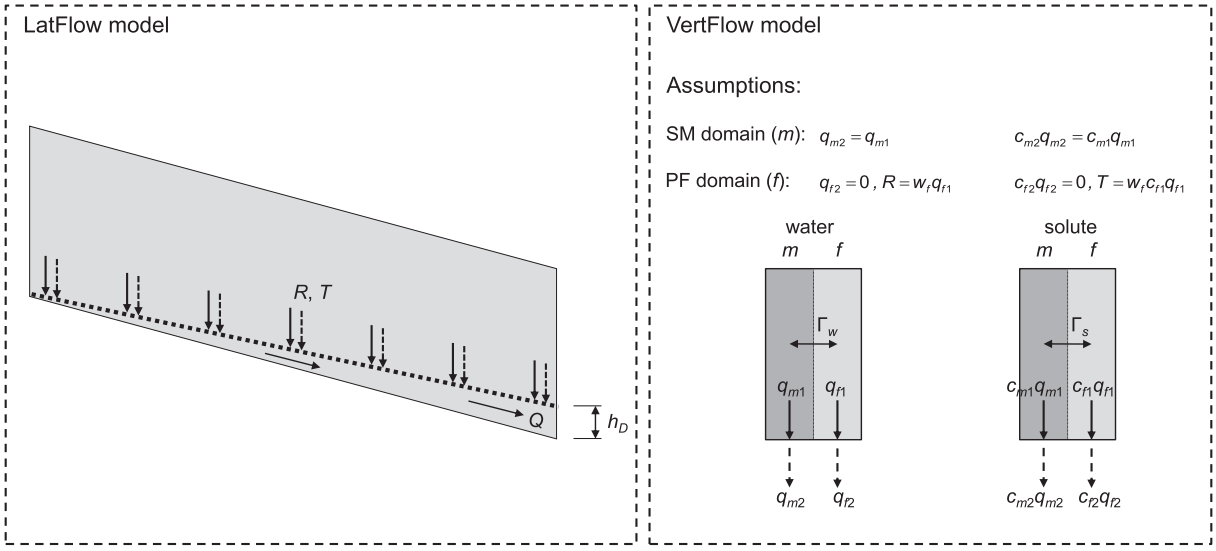

Fig. 1. Schematic of lateral flow in a vertical hillslope segment; R and T are the water and solute mass recharge rates, respectively; Q is the discharge from the hillslope segment; h_D is the depth of lateral flow; q and cq are the soil water and solute mass fluxes generated by the vertical dual-continuum model, respectively; Γ_w and Γ_s are the inter-domain soil water and solute transfer terms, respectively; SM and PF refer to the soil matrix and preferential flow, respectively; w_f is the volume fraction of the PF domain.

$$E = 1 - \frac{\sum_{j=1}^{N}(X_{oj} - X_{mj})^2}{\sum_{j=1}^{N}(X_{oj} - \overline{X_o})^2} \quad (12)$$

in which $E \leqslant 1$, N is the total number of values in a time series, X_o and X_m are the observed and simulated variables, respectively, and $\overline{X_o}$ is the mean value of the observed variable. The match between simulated and observed variables improves with increasing E.

To evaluate the performance of our model, hillslope discharge and ^{18}O mass flux were taken as the observed variables in Eq. (12), respectively. The efficiency coefficients were evaluated separately for each of the three vegetation seasons. The values of E for hillslope discharge were calculated from 1-h time series. The ^{18}O mass fluxes were calculated by multiplying the $\delta^{18}O$ values with the corresponding volumetric discharges of water. The efficiency for ^{18}O mass flux was evaluated using 6-h time resolution (3-h in 2009), consistently with the sampling protocol for ^{18}O concentration in hillslope discharge.

2.6. Mass balance approach for discharge hydrograph separation

To distinguish pre-event and event water in shallow subsurface runoff, mass balance approach has been applied (e.g., Buttle, 1998). The approach is based on a simple set of equations expressing mass balances of water and tracer, respectively:

$$Q = Q_p + Q_e \quad (13)$$

$$cQ = c_p Q_p + c_e Q_e \quad (14)$$

where Q is the total discharge from a hillslope segment, Q_p and Q_e are the contributions from pre-event and event water, respectively, c is the tracer concentration in the hillslope discharge, c_p and c_e are the tracer concentrations in pre-event and event water, respectively. In this concept, the conservative behavior of tracer is assumed, i.e. the tracer concentration changes only by mixing. If c_p and c_e are constant (and are known and sufficiently different from each other), Q_p and Q_e can be calculated by combining Eqs. (13) and (14).

3. Flow and transport simulations

Lateral saturated flow at the Tomsovka hillslope site develops above the soil–bedrock interface, which is situated at the depth of about 70 cm. We assume that the LatFlow model represents flow in a laterally-continuous system of preferential pathways. This assumption is consistent with our observation that the soil matrix at Tomsovka is incapable of transmitting water laterally fast enough to explain quick responses of hillslope discharge to rainfall (cf. the hydraulic conductivities of the soil matrix in Table 1). Saturated lateral flow is episodically recharged through the soil during major rainfall–runoff events and ceases to exist in between these events. The recharge is calculated by the VertFlow model.

In the present study, two types of simulations of subsurface flow and ^{18}O transport in the hillslope profile were performed: (1) long-term simulations based on measured ^{18}O rainfall signatures, covering three consecutive vegetation seasons and (2) simulations of pre-event and event water mixing during a selected multiple-episode rainfall event based on synthetic ^{18}O rainfall signatures.

3.1. Simulations with measured ^{18}O rainfall signatures

The long-term simulations of soil water flow and isotope transport were carried out for vegetation seasons 2007, 2008, and 2009. Soil water pressure data measured by tensiometers at the beginning of each season provided initial conditions for the VertFlow model. The simulations started from initial equilibrium between the flow domains ($h_f = h_m$). The soil–plant–atmosphere interactions were represented by rainfall intensity, input as upper boundary condition, and transpiration, input as root water uptake. Rainfall intensities were arranged in 1-h series. Free drainage condition (equivalent to the unit hydraulic gradient condition) was used for the lower boundary in both domains (i.e., the SM domain and PF domain) at a depth of 75 cm.

Daily potential transpiration was calculated using Penman–Monteith equation (Monteith, 1981), using micrometeorological data observed directly at the Tomsovka site. Root water uptake, S (in Eqs. (4) and (5)), was described according to Feddes et al.

(1978). More detailed information about the implementation of root water uptake in the VertFlow model can be found in Dohnal et al. (2006a) and Vogel et al. (2010a).

The values of soil hydraulic parameters and inter-domain transfer coefficients for the VertFlow model were taken from our previous studies (Vogel et al., 2010a, 2011; Dusek et al., 2012). The soil hydraulic parameters, derived from laboratory measurements, were adjusted based on variations of soil water content and soil water pressure observed *in situ* (Dohnal et al., 2006a,b). The parameters of the SM and PF domains are listed in Table 1. The volumetric fraction of the PF domain w_f was set to 7% at the soil surface and 5% at the lower boundary of the flow domain, with a linear decrease between the two boundaries. The values of α_{ws} and α_{ss} (Eqs. (6) and (9)) were also estimated to decrease linearly between the soil surface and the lower boundary (1 and 0.01 cm^{-1} d^{-1} for α_{ws}, and 0.001 and 0.0001 d^{-1} for α_{ss}), which corresponded to the decreasing trend of saturated hydraulic conductivity of the SM domain.

The soil water flux computed at the lower boundary of the SM domain, q_{m2}, was assumed to percolate to deeper horizons, while the episodic outflow generated at the lower boundary of the PF domain during major rainfall–runoff episodes, q_{f1}, was supposed to serve as the recharge of saturated lateral subsurface flow, i.e. $R = w_f q_{f1}$ (cf. Fig. 1, Eq. (10)). The recharge rate R was assumed to be invariant along the hillslope length. More details about model assumptions were given by Dusek et al. (2012).

Sensitivity analysis of the LatFlow model parameters performed in our previous study (Dusek et al., 2012) suggested following effective parameter values for the diffusion wave model (Eq. (1)): $\Theta = 0.005$ cm^3 cm^{-3}, $K_D = 2500$ cm d^{-1}, and the hillslope length $L = 25$–50 m. The slope of the simulated hillslope segment was fixed at 14%. A zero pressure gradient boundary condition was used at the downslope boundary, while a no-flow boundary condition was applied at the upslope boundary.

For the purpose of ^{18}O transport modeling, the isotope $\delta^{18}O$ values were treated as solute concentrations (denoted as c in the governing advection–dispersion equations). The initial ^{18}O content at the beginning of the simulated period was derived from observed resident concentrations determined in soil water extracted by suction cups. A flux concentration (third-type) boundary condition was used at the soil surface, prescribing measured isotope concentration in precipitation. Zero concentration gradient was used as the lower boundary condition for both VertFlow and LatFlow models, which allowed the isotope to leave the simulated domain freely with the effluent water. The value of vertical dispersivity was set to 5 cm, while dispersivity for lateral model was fixed at 20 cm. The value of lateral dispersivity was found to have negligible effect on simulated ^{18}O concentrations. The molecular diffusion coefficient of ^{18}O, interpreted as self-diffusion coefficient of water (Singleton et al., 2004), was set equal to 2 cm^2 d^{-1}.

In the present application of the VertFlow model we assume following conditions for the advective fluxes of ^{18}O at the soil–bedrock interface (cf. Fig. 1, Eq. (11)): $c_{m2}q_{m2} = c_{m1}q_{m1}$ and $c_{f2}q_{f2} = 0$. Therefore, the mass recharge, T, in the LatFlow model is equal to ^{18}O mass flux at the lower boundary of the PF domain, i.e. $T = w_f c_{f1} q_{f1}$.

In the numerical experiments, we assume that ^{18}O enters the soil profile in concentrations corresponding to the observed $\delta^{18}O$ values in precipitation. Furthermore, based on simultaneous measurements of $\delta^{18}O$ and $\delta^{2}H$ in all samples by means of laser spectroscopy, we carry evidence that no isotope fractionation occurs when soil water is taken up by plant roots for transpiration (in agreement with Allison et al. (1984)) since there is no difference in slope and intercept of mean water line in samples of precipitation, soil pore water, and subsurface stormflow. The soil surface is fully covered with dense vegetation layer of mountain grass, 20 year old spruce plantation, and their organic litter at Tomsovka. As a result, transpiration dominates over direct soil evaporation, which also means that the ^{18}O enrichment of soil water due to soil-surface evaporation is negligible. These assumptions lead to a relatively simple model of the ^{18}O transport – the isotope is subject to advection, hydrodynamic dispersion, and root water uptake only. Advection and dispersion take place in both the SM and PF domains of vertical flow model as well as in the saturated zone of the diffusion wave model. The oxygen isotope may also migrate between the two flow domains of the VertFlow model according to the local soil water pressure and isotope concentration differences.

3.2. Simulations with synthetic ^{18}O rainfall signatures

To study the mixing process determining the pre-event/event water composition of hillslope discharge, additional simulations were performed with synthetic ^{18}O rainfall signatures and initial ^{18}O concentrations in the soil profile. The selected major rainfall–runoff episodes within the three vegetation seasons, labeled in Fig. 2, were used in these simulations. The synthetic ^{18}O rainfall concentrations were chosen to be stepwise constant, so that individual rainfall segments could be distinguished by marking them with a specific ^{18}O signature. In these event-based simulations, the soil water distribution at the beginning of each runoff episode was obtained from the simulations of entire seasons. The ^{18}O concentration of pre-event water in the hillslope soil profile, c_p, was assumed constant prior to all rainfall events and equal to $-12‰$. The rainwater ^{18}O concentration, c_e, was set equal to $-6‰$ during the selected part of the event to make arbitrary yet still reasonable contrast to the pre-event water.

4. Results and discussion

4.1. Results of the simulations with measured ^{18}O rainfall signatures

Fig. 2 depicts subsurface runoff and ^{18}O content measured at two sections of the experimental trench together with the corresponding model predictions based on the one-dimensional dual-continuum model VertFlow, i.e., prior to the additional lateral transformation of the ^{18}O signal simulated by the LatFlow model. The subsequent lateral transformation (not shown in the figure) leads to relatively small ^{18}O signal modification, hardly visible at the time scale of whole vegetation season. This transformation is, however, more apparent in the short-term event-based simulations discussed further below. It can be seen that the soil water flux at the lower boundary of the PF domain, $w_f q_{f1}$, as well as the corresponding ^{18}O content, c_{f1}, are in a relatively good agreement with the trench observations, especially during major rainfall–runoff episodes. As expected, the long-term gradual change of ^{18}O content in the SM domain could not explain the event-driven variations of tracer concentrations measured in the trench. A few measured $\delta^{18}O$ values, associated with low runoff events, were not captured by the VertFlow model. This can be partly explained by the flux-averaging of measured oxygen concentrations during the low runoff events.

In Fig. 3, the simulated spatiotemporal development of the inter-domain soil water transfer Γ_w (Eq. (6)) is shown. The figure illustrates the communication between the PF and SM flow domains during the vegetation season 2009. This figure helps to explain the mechanism governing outflow from the PF domain and thus the transformation of the rainfall signal into the lateral flow recharge R. The figure shows soil water transfer from soil matrix to macropores at the bottom part of the soil profile (above the lowermost soil layer) during and after intensive rainfall events. In the middle part (at the depths of 20–60 cm), the soil water transfer is

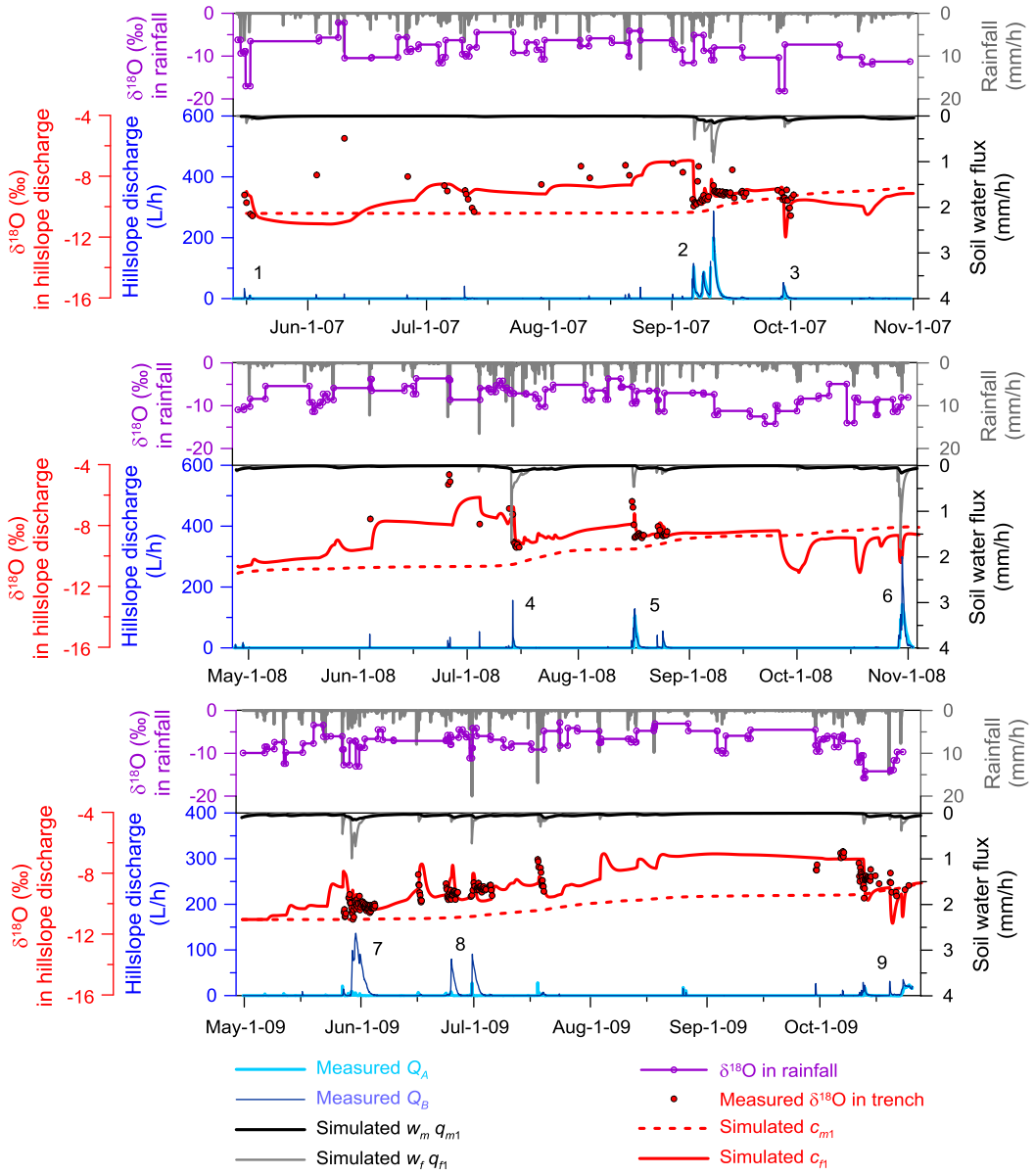

Fig. 2. Observed hillslope discharges (trench sections A and B) and ^{18}O concentrations (A and B combined) compared with the VertFlow model-generated lower boundary soil water fluxes (denoted as q_{m1} for SM domain and q_{f1} for PF domain) and the corresponding ^{18}O concentrations (denoted as c_{m1} and c_{f1}). The selected major rainfall–runoff episodes are labeled with numbers.

directed in the opposite way. Because of high values of water transfer coefficient, α_{ws}, allowing intense communication between both flow domains, significant soil water transfer from SM domain to PF domain was also predicted in the topsoil layer.

It is important to note that there are two different concepts of mixing relevant to hillslope runoff in the present study: (i) mixing between water in the soil matrix and in preferential pathways and (ii) mixing between pre-event and event water. Fig. 3 shows episodic draining of the soil matrix into the PF domain both at the top and at the bottom of the soil profile. Water drained to the network of preferential pathways near the soil–bedrock interface triggers saturated flow along the slope and feeds hillslope discharge. The figure therefore reveals the principal mechanism through which the two mixing concepts are intertwined at Tomsovka. Similar patterns of inter-domain soil water transfer were predicted for 2007 and 2008 seasons.

Three major rainfall–runoff episodes (#2, #8, and #9) were selected for detailed comparison. The episodes were selected on the basis of a noticeable observed hillslope discharge as well as contrasting oxygen composition of precipitation water. These episodes are shown in Fig. 4 where subsurface runoff was simulated by the VertFlow + LatFlow model, i.e., including the lateral transformation. Fig. 5 shows the corresponding model predictions of ^{18}O concentration in hillslope discharge.

The subsurface runoff peaks for the rainfall–runoff episode #2 (September 2007) were more accurately predicted with the simulation based on the contributing hillslope length, L, equal to 50 m (Fig. 4). For the episode #9 (October 2009), the simulation based on $L = 25$ m showed better agreement with the observed hydrograph than the one based on $L = 50$ m. For the episode #8 (June–July 2009), the observation uncertainty, reflected in the differences between the measured discharges of sections A and B (possibly caused by a malfunction of the flow gauge in trench section A), is larger than the model uncertainty caused by uncertain hillslope length (Fig. 4).

Fig. 5 compares the ^{18}O content in hillslope discharge simulated by the VertFlow + LatFlow model with the measured ^{18}O content.

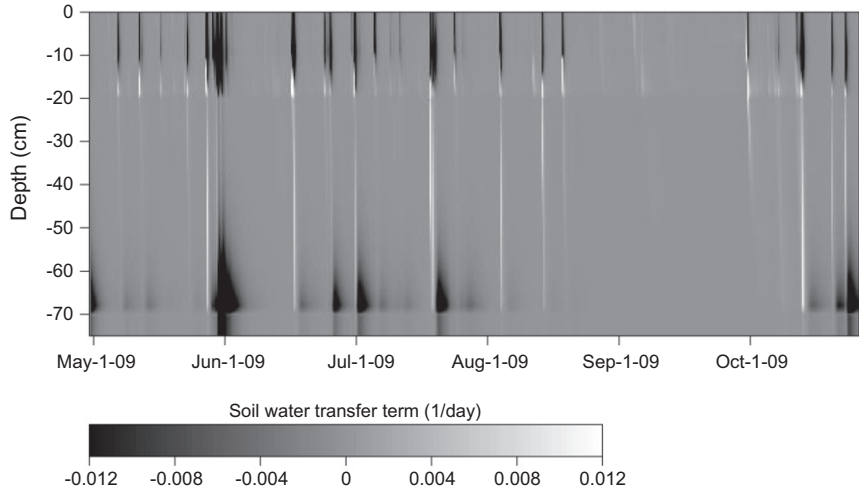

Fig. 3. The simulated depth-time development of the soil water transfer term Γ_w during vegetation season 2009 (VertFlow model). Negative values of transfer term indicate transfer of water from the SM to PF domain; positive values show transfer from macropores to soil matrix.

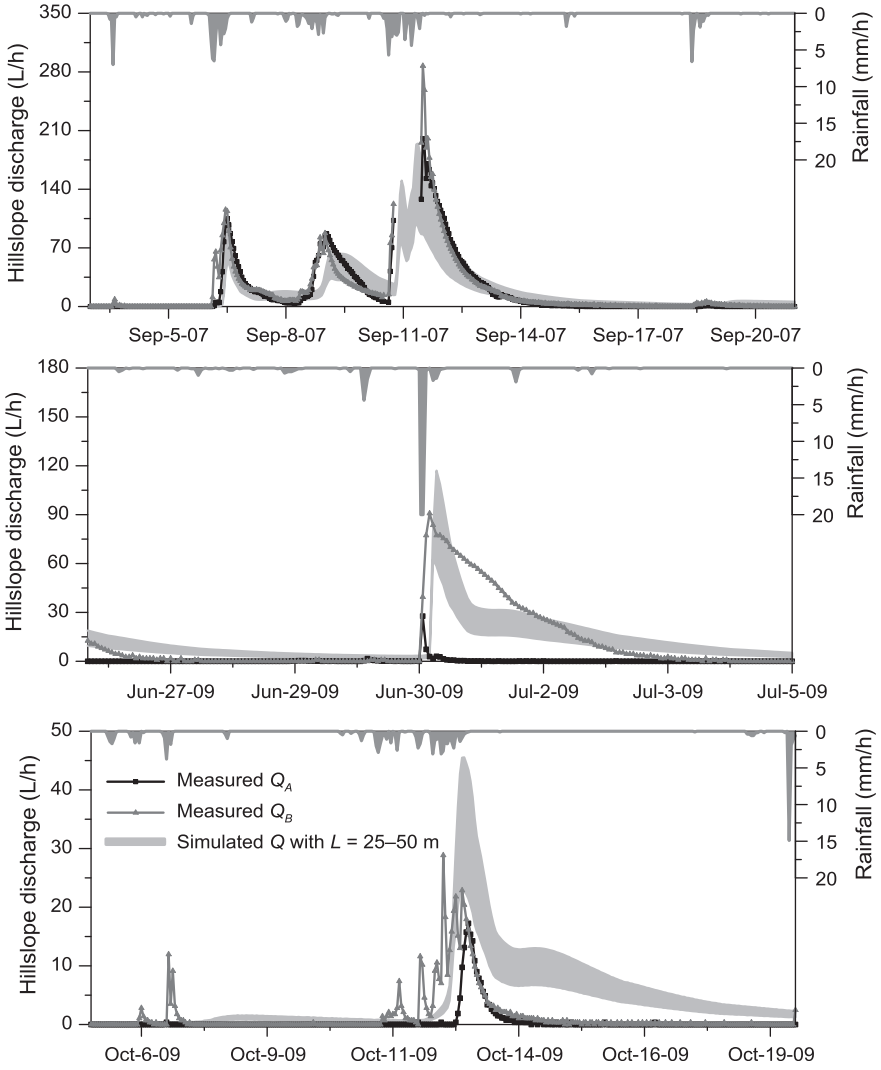

Fig. 4. Observed (trench sections A and B) and simulated (VertFlow + LatFlow) hillslope discharges during three selected rainfall–runoff episodes (#2, #8, and #9). The shaded area of the simulated hydrographs represents the uncertainty in determination of the contributing hillslope length (L = 25–50 m).

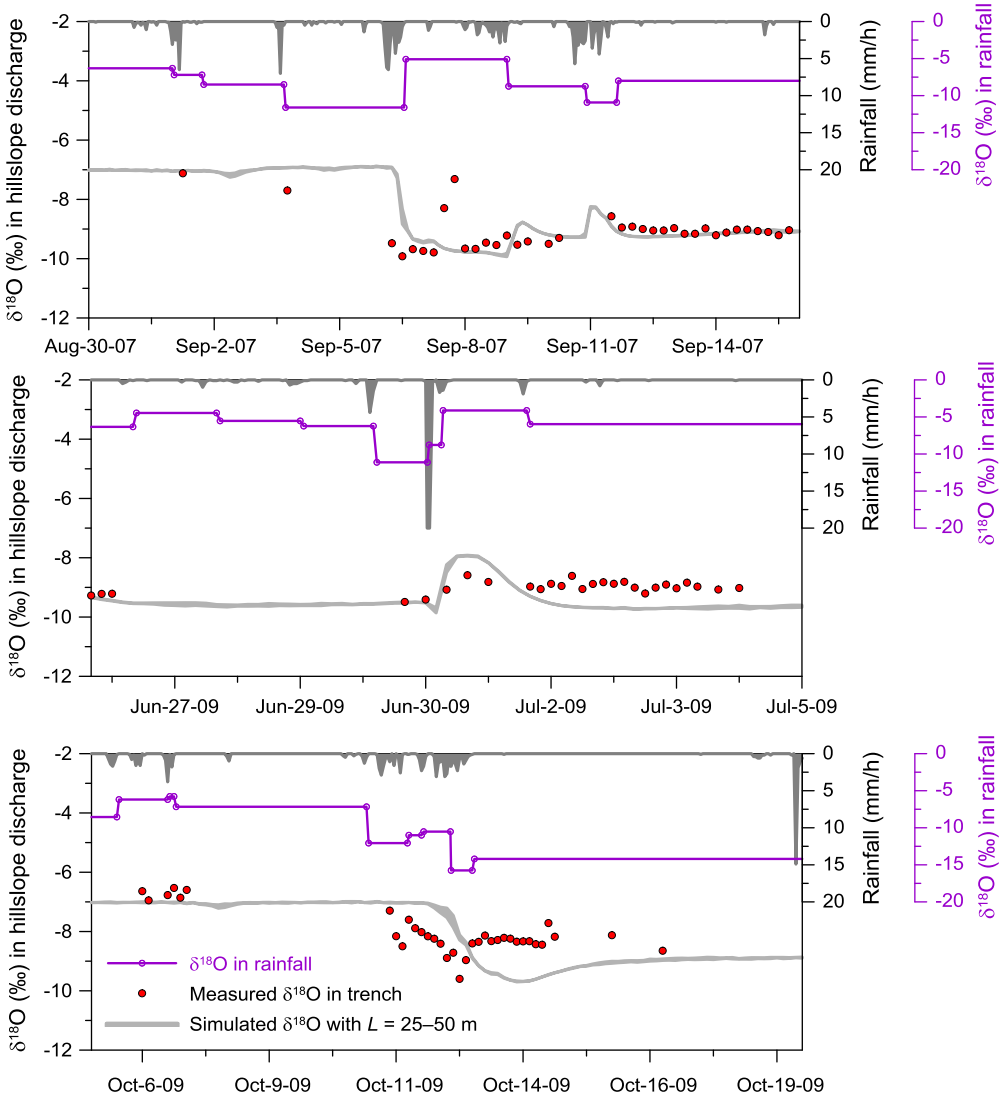

Fig. 5. Observed and simulated (VertFlow + LatFlow) ^{18}O content in hillslope discharge during three selected episodes (#2, #8, and #9). Shaded area of the simulated oxygen content represents the uncertainty in determination of the contributing hillslope length (L = 25–50 m).

The two simulation scenarios based on the 25 m and 50 m hillslope length produced nearly identical $\delta^{18}O$ responses. The simulation results suggest significant mixing of the isotope in a hillslope soil profile. Closer inspection of Fig. 5 shows that the ^{18}O rainfall signatures are not transformed into the hillslope discharge signatures in a simple (intuitively predictable) way. This issue is further addressed in the next section. The predicted ^{18}O contents show a reasonably good agreement with the observed data, although the simulated $\delta^{18}O$ values lag behind the data during the 2009 October episode (bottom figure in Fig. 5).

Nash–Sutcliffe efficiency coefficients for the model predictions assuming two different contributing hillslope lengths are presented in Table 2. Based on the efficiency values, the hillslope length of L = 50 m led to better predictions in vegetation seasons 2007 and 2009, while better model performance for season 2008 was obtained with L = 25 m. The highest efficiency values for hillslope discharge were obtained for the 2007 season. The efficiency values of ^{18}O mass flux showed a similar trend. For ^{18}O transport, the highest efficiency value was obtained for the 2009 season. For 2008, relatively low model efficiency coefficients for ^{18}O mass flux were determined, which could be due to only limited number of data available for comparison (see Fig. 2). In Table 3, measured and simulated discharge volumes and cumulative ^{18}O mass fluxes are summarized for the three vegetation seasons.

Table 2
Nash–Sutcliffe efficiency coefficients E for VertFlow + LatFlow model, reflecting the performance of the model when used to predict hillslope discharge and the corresponding ^{18}O mass flux. Values of E for hillslope discharge are shown separately for trench sections A and B (divided by semicolon). Values of E for isotope mass flux were evaluated from a combined sample from both sections. N/A indicates a possible malfunction of the flow gauge in trench section A.

Hillslope length L (m)	Vegetation season		
	2007	2008	2009
Efficiency for predicting hillslope discharge			
25	0.486; 0.506	0.447; 0.480	N/A; 0.478
50	0.799; 0.719	−0.597; 0.297	N/A; 0.545
Efficiency for predicting ^{18}O mass flux			
25	0.554	0.279	0.569
50	0.584	−2.545	0.741

Based on the simulation results, the following soil water balance components were estimated for the hillslope site: deep percolation, 20%; shallow subsurface runoff, 19%; and evapotranspiration, 61%.

All components were expressed relatively to the total precipitation (2036 mm) over the three vegetation seasons.

The experimental data from the subsurface trench showed only limited number of discharge episodes during each vegetation season, corresponding to major rainfall–runoff episodes (Fig. 2). All these events produced saturated subsurface stormflow at the soil–bedrock interface, which led to hillslope discharge observed in the trench. Note that the two sections of the experimental trench responded differently to individual rainfall events. Trench section B produced significant discharge for a broader range of rainfall events, while section A responded only to a few major events. The difference between the two trench sections could be attributed to a large spatial variability of the network of preferential pathways, soil heterogeneity, and/or bedrock topography (e.g., Genereux et al., 1993; Freer et al., 2002; Harman and Sivapalan, 2009), as well as measurement uncertainties. In this context, the discharge data in vegetation season 2009 were exceptional as trench section A showed substantially lower discharge volume compared to both previous vegetation seasons. Most probably, this could be related to a malfunction of the flow gauge in trench section A in 2009.

The feedback mechanism between lateral saturated flow above the soil–bedrock interface and vertical unsaturated flow was not considered in the present modeling approach. As the saturated layer in the PF domain occurs only for a short time during prominent rainfall–runoff events, the feedback is assumed to be small and mostly captured by the water storage in the soil matrix. On this account, Vogel and Dusek (2006) presented a comparison of the VertFlow + LatFlow model with a fully coupled dual-continuum two-dimensional model and found similar behavior of the two approaches for the site of interest.

4.2. Results of the simulations with synthetic ^{18}O rainfall signatures

For the numerical experiments with synthetic ^{18}O rainfall signatures, the rainfall sequence observed at the beginning of September 2007 (see the top figure of Fig. 5) was taken as input. The sequence was divided into three rainfall sections. The observed isotopic composition of the rainfall was then replaced by a series of simple stepwise-constant ^{18}O signatures as shown in Fig. 6. The figure also shows the superposition of the corresponding ^{18}O output signals (i.e., variations of ^{18}O concentration in hillslope discharge) generated by the VertFlow + LatFlow model. A significant, relatively long-lasting increase of ^{18}O concentration was predicted in response to each of the synthetic ^{18}O rainfall signatures, thus illustrating the difficulties involved in interpreting the causal relationship between ^{18}O concentrations observed in rainwater and those observed in hillslope discharge (cf. Fig. 5).

An added value of using stepwise-constant synthetic ^{18}O rainfall signatures is that such signals exactly fulfill the principal assumption of the mass balance method (as described in Section 2.6), i.e. that the ^{18}O concentrations in pre-event and event water are constant and sufficiently different from each other. This allows for a simple hillslope discharge hydrograph separation into its pre-event and event water components. Let us consider the synthetic ^{18}O rainfall signature (and the corresponding response of ^{18}O concentration in hillslope discharge) from the bottom figure of Fig. 6, and apply the mass balance procedure to separate the hydrograph components. As shown in Fig. 7, the predicted pre-event water in our case dominates total hillslope runoff, especially at the onset of each of the three rainfall sub-events as seen from the steep rising hydrograph limbs of the pre-event water discharge component. The separation further showed that pre-event water comprised about 67% of the total hillslope discharge volume. At the end of this event, about 85% of event water remained in the hillslope soil (i.e., only about 15% of event water was discharged).

The proportion of pre-event water varied from 47% to 74% for selected major rainfall–runoff episodes over the period 2007–2009 (Table 4). Only two rainfall–runoff episodes showed pre-event water contribution less than 50% of the total discharge volume. These two episodes occurred in May 2007 (episode #1) and August 2008 (episode #5) and were characterized by significantly drier soil water conditions prior to rainfall compared to remaining rainfall–runoff episodes. The pre-event water contribution for remaining major episodes was in the 62–74% range of the total discharge volume (Table 4). Thus, the hydrograph separation of hillslope runoff demonstrated that pre-event water made up significant portion of discharge during major rainfall–runoff episodes, suggesting substantial mixing of infiltrating rainwater and water initially stored in the hillslope soil profile. The contribution of pre-event water was strongly affected by antecedent soil water content. As expected, drier soil water conditions prior to rainfall event led to smaller contribution of pre-event water. Sanda et al. (2009) attempted to perform a hydrograph separation for the Uhlirska catchment by analyzing a measured isotopic rainfall/discharge composition during a single rainfall–runoff episode. They found that about 75% and 50% of total runoff originated from pre-event water at the hillslope and catchment scale, respectively, which seems to be in a good agreement with the values estimated in the present study.

As stated above, different hillslope settings lead to different transport processes and thus wide range of pre-event water contribution to discharge. For instance, Anderson et al. (1997) showed slow response to both natural rainfall and artificial irrigation from a steep unchanneled catchment, concluding that nearly all runoff was pre-event water. Kendall et al. (2001) estimated the pre-event water contribution to be about 10% of total discharge. They also pointed out that about 80% of the flow could be attributed to shallow subsurface flow and overland flow. This finding seems unusual since lateral component of shallow subsurface flow is predominantly derived from pre-event water in most catchments (Buttle, 1994). Kienzler and Naef (2008) focused on subsurface flow generation at four different hillslope sites and found a strong dependence of pre-event water fraction on mechanism governing the flow initiation through preferential pathways. Rapid lateral preferential flow originating in a saturated zone above the soil–bedrock interface is a common flow regime in shallow soils of forested hillslopes (e.g., Noguchi et al., 1999; Buttle et al., 2001), where hydraulic conductivity of the soil matrix often decreases with depth.

At our experimental site, drainage from the low conductive SM domain into preferential lateral saturated flow above the soil–bed-

Table 3
Measured and simulated cumulative hillslope discharges and ^{18}O mass fluxes (VertFlow + LatFlow model). Measured discharge volumes are shown separately for trench sections A and B (divided by semicolon). Measured cumulative isotope mass fluxes were evaluated from a combined sample from both sections. N/A indicates a possible malfunction of the flow gauge in trench section A.

Hillslope length L (m)	Vegetation season		
	2007	2008	2009
Measured hillslope discharge volume (m^3)			
	7.86; 8.73	6.87; 9.39	N/A; 14.18
Simulated hillslope discharge volume (m^3)			
25	6.04	10.89	9.58
50	12.09	21.79	19.14
Measured cumulative isotope mass flux (‰ m^3)			
	−74.31	−23.05	−103.23
Simulated cumulative isotope mass flux (‰ m^3)			
25	−49.28	−29.98	−66.39
50	−97.59	−49.33	−130.97

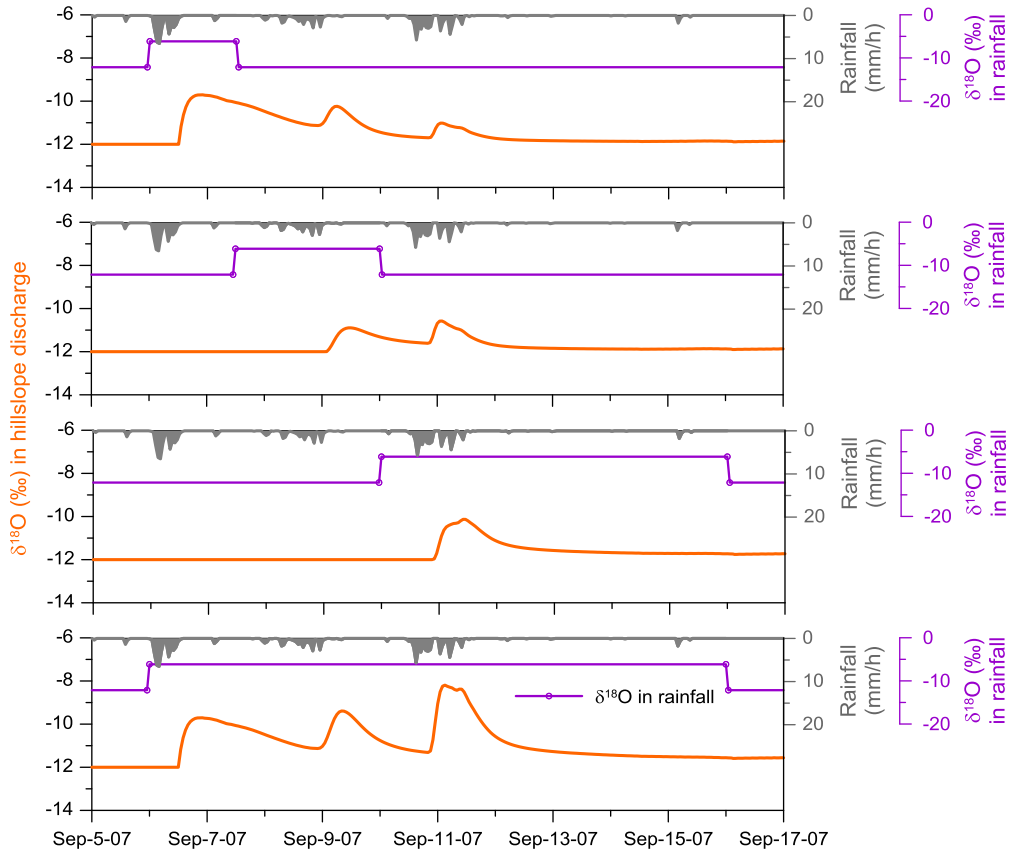

Fig. 6. Simulated (VertFlow + LatFlow) responses of ^{18}O concentration in hillslope discharge to synthetic ^{18}O rainfall signatures (episode #2). The rainfall sequence was divided into three sections, marked with distinct isotope signatures. The individual responses are compared with the composite response (bottom figure). Hillslope length of $L = 50$ m was considered.

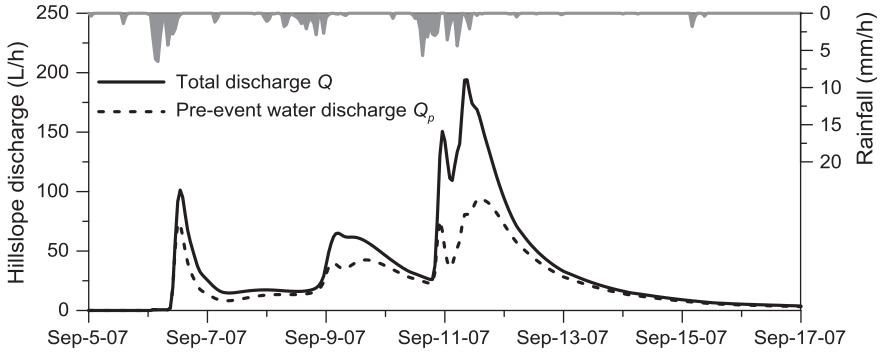

Fig. 7. Separation of total hillslope discharge into pre-event water component for rainfall–runoff episode #2 (VertFlow + LatFlow). Hillslope length of $L = 50$ m was considered.

Table 4
The pre-event water contributions (in %) to total hillslope discharge for major rainfall–runoff episodes[a] estimated using VertFlow + LatFlow model (during vegetation seasons 2007–2009). The numbering of the rainfall–runoff episodes is introduced in Fig. 2.

2007		2008		2009	
#1	49	#4	74	#7	68
#2	67	#5	47	#8	63
#3	74	#6	69	#9	62

[a] Rainfall–runoff episodes: #1 (May 15–29, 2007), #2 (September 6–18, 2007), #3 (September 28–October 19, 2007), #4 (July 13–31, 2008), #5 (August 15–30, 2008), #6 (October 29–November 2, 2008), #7 (May 27–June 10, 2009), #8 (June 23–July 11, 2009), and #9 (October 11–25, 2009).

rock interface had an effect on hillslope discharge and pre-event/event water partitioning. Despite the crucial role of preferential flow on hillslope transport processes, the volume of event water was smaller than the volume of pre-event water contribution for most rainfall–runoff episodes (Table 4). Nevertheless, the contribution of event water seemed significant especially during multiple discharge episodes (see Fig. 7). The analysis of the modeling results also suggested that the contribution of event water in hillslope discharge would be strongly underestimated if flow through preferential pathways was not considered in the conceptual model.

The research debate on mechanisms explaining rapid release of pre-event water into stream channels is still in progress (e.g., Park et al., 2011; Klaus et al., 2012; Fiori, 2012). Numerical experiments

with an isotope tracer carried out to determine pre-event and event water contributions to total hillslope discharge were reported by Weiler and McDonnell (2004), who recognized that if the rainfall is assigned with a distinct constant tracer concentration, the contribution of event water to hillslope discharge can be predicted. This finding was further elaborated on and confirmed in our present study.

5. Summary and conclusions

A one-dimensional model was used to simulate the mechanism of subsurface runoff formation and the associated ^{18}O transport. The episodic saturated flow regime in the hillslope segment was described by a combination of 1D saturated lateral flow model LatFlow, based on the diffusion wave equation, and 1D variably saturated vertical flow model VertFlow, based on the dual-continuum formulation of Richards' equation. Preferential flow was confirmed to be of key importance for an adequate description of flow and transport processes at the hillslope scale.

The simulated hillslope responses showed a reasonable agreement with the experimental data in terms of subsurface runoff and ^{18}O transport dynamics. In particular, the model seems to describe adequately both vertical and lateral mixing of water and ^{18}O in the hillslope segment. It was shown that the contributing hillslope length had significant effect on simulated subsurface discharge and negligible effect on ^{18}O concentration, indicating a dominant role of vertical mixing.

The numerical analysis based on simulations of ^{18}O concentration in subsurface hillslope discharge revealed a complex mechanism of ^{18}O transport in the hillslope soil profile. The simulations involving natural ^{18}O signatures exposed the importance of antecedent rainfall and its varying ^{18}O composition for ^{18}O input/output analysis. The simulations involving multiple synthetic ^{18}O rainfall signatures were helpful in distinguishing hillslope responses to the selected individual rainfall segments. The hillslope hydrograph separation based on synthetic ^{18}O mass balance proved to be a valuable procedure for quantifying subsurface runoff composition in terms of event/pre-event water.

Acknowledgments

The study was supported by the Czech Science Foundation (205/08/1174). Additional support was provided by the research fund of the Ministry of Education of the Czech Republic (MSM 6840770002).

References

Allison, G.B., Barnes, J.B., Hughes, M.W., Leaney, F.W.J., 1984. The effect of climate and vegetation on oxygen-18 and deuterium profiles in soils. In: Isotope Hydrology 1983, IAEA, Vienna, Austria, pp. 105–123.

Anderson, S.P., Dietrich, W.E., Montgomery, D.R., Torres, R., Conrad, M.E., Loague, K., 1997. Subsurface flow paths in a steep, unchanneled catchment. Water Resour. Res. 33 (12), 2637–2653.

Boussinesq, J., 1877. Essai sur la théorie des eaux courantes. Mem. Acad. Sci. Inst. Fr. 23 (1), 1–680.

Braud, I., Bariac, T., Vauclin, M., Boujamlaoui, Z., Gaudet, J.P., Biron, P., Richard, P., 2005. SiSPAT-isotope, a coupled heat, water and stable isotope (HDO and (H_2O)–O-18) transport model for bare soil. Part II. Evaluation and sensitivity tests using two laboratory data sets. J. Hydrol. 309 (1–4), 301–320.

Burns, D.A., McDonnell, J.J., Hooper, R.P., Peters, N.E., Freer, J.E., Kendall, C., Beven, K., 2001. Quantifying contributions to storm runoff through end-member mixing analysis and hydrologic measurements at the Panola Mountain Research Watershed (Georgia, USA). Hydrol. Process. 15 (10), 1903–1924.

Burns, D.A., 2002. Stormflow-hydrograph separation based on isotopes: the thrill is gone – what's next? Hydrol. Process. 16 (7), 1515–1517.

Buttle, J.M., 1994. Isotope hydrograph separations and rapid delivery of pre-event water from drainage basins. Prog. Phys. Geogr. 18 (1), 16–41.

Buttle, J.M., 1998. Fundamentals of small catchments. In: Kendall, C., McDonnell, J.J. (Eds.), Isotope Tracers in Catchment Hydrology. Elsevier, Amsterdam, pp. 1–49.

Buttle, J.M., Lister, S.W., Hill, A.R., 2001. Controls on runoff components on a forested slope and implications for N transport. Hydrol. Process. 15 (6), 1065–1070.

Buttle, J.M., McDonald, D.J., 2002. Coupled vertical and lateral preferential flow on a forested slope. Water Resour. Res. 38 (5), 1060. http://dx.doi.org/10.1029/2001WR000773.

Coppola, A., Comegna, V., Basile, A., Lamaddalena, N., Severino, G., 2009. Darcian preferential water flow and solute transport through bimodal porous systems: experiments and modelling. J. Contam. Hydrol. 104 (1–4), 74–83.

Dohnal, M., Dusek, J., Vogel, T., Herza, J., Tacheci, P., 2006a. Analysis of soil water response to grass transpiration. Soil Water Res. 1 (3), 85–98.

Dohnal, M., Dusek, J., Vogel, T., 2006b. The impact of the retention curve hysteresis on prediction of soil water dynamics. J. Hydrol. Hydromech. 54 (3), 258–268.

Dohnal, M., Vogel, T., Sanda, M., Jelinkova, V., 2012. Uncertainty analysis of a dual-continuum model used to simulate subsurface hillslope runoff involving oxygen-18 as natural tracer. J. Hydrol. Hydromech. 60 (3), 194–205.

Dusek, J., Vogel, T., Dohnal, M., Gerke, H.H., 2012. Combining dual-continuum approach with diffusion wave model to include a preferential flow component in hillslope scale modeling of shallow subsurface runoff. Adv. Water Resour. 44, 113–125. http://dx.doi.org/10.1016/j.advwatres.2012.05.006.

Fan, Y., Bras, R.L., 1998. Analytical solutions to hillslope subsurface storm flow and saturation overland flow. Water Resour. Res. 34 (4), 921–927.

Feddes, R.A., Kowalik, P.J., Zaradny, H., 1978. Simulation of Field Water Use and Crop Yield. Centre for Agricultural Publishing and Documentation, Wageningen, The Netherlands.

Fiori, A., 2012. Old water contribution to streamflow: insight from a linear Boussinesq model. Water Resour. Res. 48, W06601. http://dx.doi.org/10.1029/2011WR011606.

Freer, J., McDonnell, J.J., Beven, K.J., Peters, N.E., Burns, D.A., Hooper, R.P., Aulenbach, B., Kendall, C., 2002. The role of bedrock topography on subsurface storm flow. Water Resour. Res. 38 (12), 1269. http://dx.doi.org/10.1029/2001WR000872.

Genereux, D.P., Hemond, H.F., Mulholland, P.J., 1993. Spatial and temporal variability in streamflow generation on the west fork of walker branch watershed. J. Hydrol. 142 (1–4), 137–166.

Genereux, D., 1998. Quantifying uncertainty in tracer-based hydrograph separations. Water Resour. Res. 34 (4), 915–919.

Gerke, H.H., van Genuchten, M.Th., 1993a. A dual-porosity model for simulating the preferential movement of water and solutes in structured porous media. Water Resour. Res. 29 (2), 305–319.

Gerke, H.H., van Genuchten, M.Th., 1993b. Evaluation of a first-order water transfer term for variably saturated dual-porosity models. Water Resour. Res. 29 (4), 1225–1238.

Gerke, H.H., Dusek, J., Vogel, T., Köhne, J.M., 2007. Two-dimensional dual-permeability analyses of a bromide tracer experiment on a tile-drained field. Vadose Zone J. 6 (3), 651–667.

Gerwin, W., Schaaf, W., Biemelt, D., Fischer, A., Winter, S., Hüttl, R.F., 2009. The artificial catchment "Chicken Creek" (Lusatia, Germany) – a landscape laboratory for interdisciplinary studies of initial ecosystem development. Ecol. Eng. 35 (12), 1786–1796.

Harman, C., Sivapalan, M., 2009. Effects of hydraulic conductivity variability on hillslope-scale shallow subsurface flow response and storage–discharge relations. Water Resour. Res. 45, W01421. http://dx.doi.org/10.1029/2008WR007228.

Harris, D.M., McDonnell, J.J., Rodhe, A., 1995. Hydrograph separation using continuous open system isotope mixing. Water Resour. Res. 31 (1), 157–171.

Haverd, V., Cuntz, M., 2010. Soil-Litter-Iso: a one-dimensional model for coupled transport of heat, water and stable isotopes in soil with a litter layer and root extraction. J. Hydrol. 388 (3–4), 438–455.

Heppell, C.M., Burt, T.P., Williams, R.J., 2000. Variations in the hydrology of an underdrained clay hillslope. J. Hydrol. 227 (1–4), 236–256.

Hilberts, A.G.J., Troch, P.A., Paniconi, C., Boll, J., 2007. Low-dimensional modeling of hillslope subsurface flow: relationship between rainfall, recharge, and unsaturated storage dynamics. Water Resour. Res. 43 (3), W03445. http://dx.doi.org/10.1029/2006WR004964.

Hrncir, M., Sanda, M., Kulasova, A., Cislerova, M., 2010. Runoff formation in a small catchment at hillslope and catchment scales. Hydrol. Process. 24 (16), 2248–2256.

Iorgulescu, I., Beven, K.J., Musy, A., 2005. Data-based modelling of runoff and chemical tracer concentrations in the Haute-Mentue research catchment (Switzerland). Hydrol. Process. 19 (13), 2557–2573.

Iorgulescu, I., Beven, K.J., Musy, A., 2007. Flow, mixing, and displacement in using a data-based hydrochemical model to predict conservative tracer data. Water Resour. Res. 43(3), W03401. http://dx.doi.org/10.1029/2005WR004019.

Jury, W.A., Gardner, W.R., Gardner, W.H., 1991. Soil Physics. John Wiley & Sons, New York.

Jones, J.P., Sudicky, E.A., Brookfield, A.E., Park, Y.-J., 2006. An assessment of the tracer-based approach to quantifying groundwater contributions to streamflow. Water Resour. Res. 42 (2), W02407. http://dx.doi.org/10.1029/2005WR004130.

Kendall, C., McDonnell, J.J., 1993. Effect of intrastorm isotopic heterogeneities of rainfall, soil water, and groundwater on runoff modeling. In: Peters, N.E., Walling, D.E., Hoehn, E., Leibundgut, C., Tase, N. (Eds.), Tracers in Hydrology. Proceedings of the Yokohama Symposium, July 1993, IAHS Publ. No. 215, pp. 41–48.

Kendall, C., McDonnell, J.J., Gu, W., 2001. A look inside 'black box' hydrograph separation models: a study at the Hydrohill catchment. Hydrol. Process. 15 (10), 1877–1902.

Kelln, C., Barbour, L., Qualizza, C., 2007. Preferential flow in a reclamation cover: hydrological and geochemical response. J. Geotech. Geoenviron. 133 (10), 1277–1289.
Kienzler, P.M., Naef, F., 2008. Subsurface storm flow formation at different hillslopes and implications for the 'old water paradox'. Hydrol. Process. 22 (1), 104–116.
Klaus, J., Zehe, E., Elsner, M., Külls, C., McDonnell, J.J., 2012. Macropore flow of old water revisited: where does the mixing occur at the hillslope scale? Hydrol. Earth Syst. Sci. Discuss. 9 (4), 4333–4380. http://dx.doi.org/10.5194/hessd-9-4333-2012.
Leaney, F.W., Smettem, K.R.J., Chittleborough, D.J., 1993. Estimating the contribution of preferential flow to subsurface runoff from a hillslope using deuterium and chloride. J. Hydrol. 147 (1–4), 83–103.
Mathieu, R., Bariac, T., 1996. A numerical model for the simulation of stable isotope profiles in drying soils. J. Geophys. Res.-Atmos. 101(D7), 12685–12696.
McDonnell, J.J., 1990. A rationale for old water discharge through macropores in a steep, humid catchment. Water Resour. Res. 26 (11), 2821–2832.
McDonnell, J.J., Bonell, M., Stewart, M.K., Pearce, A.J., 1990. Deuterium variations in storm rainfall: implications for stream hydrograph separation. Water Resour. Res. 26 (3), 455–458.
McGuire, K.J., McDonnell, J.J., 2010. Hydrological connectivity of hillslopes and streams: characteristic time scales and nonlinearities. Water Resour. Res. 46, W10543. http://dx.doi.org/10.1029/2010WR009341.
Monteith, J.L., 1981. Evaporation and surface temperature. Q. J. Roy. Meteor. Soc. 107 (451), 1–27.
Monteith, S.S., Buttle, J.M., Hazlett, P.W., Beall, F.D., Semkin, R.G., Jeffries, D.S., 2006. Paired-basin comparison of hydrologic response in harvested and undisturbed hardwood forests during snowmelt in central Ontario: II. Streamflow sources and groundwater residence times. Hydrol. Process. 20 (5), 1117–1136.
Nash, J.E., Sutcliffe, J.V., 1970. River flow forecasting through conceptual models part I – a discussion of principles. J. Hydrol. 10 (3), 282–290.
Noguchi, S., Tsuboyama, Y., Sidle, R.C., Hosoda, I., 1999. Morphological characteristics of macropores and the distribution of preferential flow pathways in a forested slope segment. Soil Sci. Soc. Am. J. 63 (5), 1413–1423.
Park, Y.-J., Sudicky, E.A., Brookfield, A.E., Jones, J.P., 2011. Hydrologic response of catchments to precipitation: quantification of mechanical carriers and origins of water. Water Resour. Res. 47 (12), W12515. http://dx.doi.org/10.1029/2011WR010075.
Penna, D., Stenni, B., Sanda, M., Wrede, S., Bogaard, T.A., Gobbi, A., Borga, M., Fischer, B.M.C., Bonazza, M., Charova, Z., 2010. On the reproducibility and repeatability of laser absorption spectroscopy measurements for delta H-2 and delta O-18 isotopic analysis. Hydrol. Earth Syst. Sci. 14 (8), 1551–1566.
Peters, N.E., Ratcliffe, E.B., 1998. Tracing hydrologic pathways using chloride at the Panola Mountain Research Watershed, Georgia, USA. Water Air Soil Pollut. 105 (1–2), 263–275.
Ray, C., Vogel, T., Dusek, J., 2004. Modeling depth-variant and domain-specific sorption and biodegradation in dual-permeability media. J. Contam. Hydrol. 70 (1–2), 63–87.
Rothfuss, Y., Braud, I., Le Moine, N., Biron, P., Durand, J.L., Vauclin, M., Bariac, T., 2012. Factors controlling the isotopic partitioning between soil evaporation and plant transpiration: assessment using a multi-objective calibration of SiSPAT-isotope under controlled conditions. J. Hydrol. 442, 75–88.
Sanda, M., Cislerova, M., 2009. Transforming hydrographs in the hillslope subsurface. J. Hydrol. Hydromech. 57 (4), 264–275.
Sanda, M., Kulasova, A., Cislerova, M., 2009. Hydrological processes in the subsurface investigated by water isotopes and silica. Soil Water Res. 4 (2), S83–S92.
Shurbaji, A.R.M., Phillips, F.M., Campbell, A.R., Knowlton, R.G., 1995. Application of a numerical model for simulating water flow, isotope transport, and heat transfer in the unsaturated zone. J. Hydrol. 171 (1–2), 143–163.
Sidle, R.C., Tsuboyama, Y., Noguchi, S., Hosoda, I., Fujieda, M., Shimizu, T., 1995. Seasonal hydrologic response at various spatial scales in a small forested catchment, Hitachi-Ohta, Japan. J. Hydrol. 168 (1–4), 227–250.
Singleton, M.J., Sonnenthal, E.L., Conrad, M.E., DePaolo, D.J., Gee, G.W., 2004. Multiphase reactive transport modeling of seasonal infiltration events and stable isotope fractionation in unsaturated zone pore water and vapor at the Hanford site. Vadose Zone J. 3 (3), 775–785.
Sloan, P.G., Moore, I.D., 1984. Modeling subsurface stormflow on steeply sloping forested watersheds. Water Resour. Res. 20 (12), 1815–1822.
Smettem, K.R.J., Chittleborough, D.J., Richards, B.G., Leaney, F.W., 1991. The influence of macropores on runoff generation from a hillslope soil with a contrasting textural class. J. Hydrol. 122 (1–4), 235–252.
Stumpp, C., Maloszewski, P., Stichler, W., Fank, J., 2009. Environmental isotope ($d^{18}O$) and hydrological data to assess water flow in unsaturated soils planted with different crops: case study lysimeter station "Wagna" (Austria). J. Hydrol. 369 (1–2), 198–208.
Stumpp, C., Stichler, W., Kandolf, M., Simunek, J., 2012. Effects of land cover and fertilization method on water flow and solute transport in five lysimeters: a long-term study using stable water isotopes. Vadose Zone J. 11 (1). http://dx.doi.org/10.2136/vzj2011.0075.
Sveinbjornsdottir, A.E., Johnsen, S.J., 1992. Stable isotope study of the Thingvallavatn area – groundwater origin, age and evaporation models. Oikos 64 (1–2), 136–150.
Troch, P., van Loon, E., Hilberts, A., 2002. Analytical solutions to a hillslope-storage kinematic wave equation for subsurface flow. Adv. Water Resour. 25 (6), 637–649.
Uhlenbrook, S., Hoeg, S., 2003. Quantifying uncertainties in tracer-based hydrograph separations: a case study for two-, three- and five-component hydrograph separations in a mountainous catchment. Hydrol. Process. 17 (2), 431–453.
Van der Hoven, S.J., Solomon, D.K., Moline, G.R., 2002. Numerical simulation of unsaturated flow along preferential pathways: implications for the use of mass balance calculations for isotope storm hydrograph separation. J. Hydrol. 268 (1–4), 214–233.
Vogel, T., van Genuchten, M.Th., Cislerova, M., 2000. Effect of the shape of soil hydraulic properties near saturation on numerical simulation of variably-saturated flow. Adv. Water Resour. 24 (2), 133–144.
Vogel, T., Tesař, M., Císlerová, M., 2003. Modeling water regime in a small watershed. In: International Conference on Small Catchment Hydrology, Institute of Hydrodynamics of the Czech Academy of Sciences, Prague, Czech Republic, pp. 127–136. ISBN: 80-02-01586-X.
Vogel, T., Dusek, J., 2006. Comparison of two different approaches to modeling subsurface runoff at the hillslope scale. In: General Assembly. European Geophysical Union, Vienna, Austria.
Vogel, T., Sanda, M., Dusek, J., Dohnal, M., Votrubova, J., 2010a. Using oxygen-18 to study the role of preferential flow in the formation of hillslope runoff. Vadose Zone J. 9 (2), 252–259.
Vogel, T., Brezina, J., Dohnal, M., Dusek, J., 2010b. Physical and numerical coupling in dual-continuum modeling of preferential flow. Vadose Zone J. 9 (2), 260–267.
Vogel, T., Dohnal, M., Votrubova, J., 2011. Modeling heat fluxes in macroporous soil under sparse young forest of temperate humid climate. J. Hydrol. 402 (3–4), 367–376.
Weiler, M., Scherrer, S., Naef, F., Burlando, P., 1999. Hydrograph separation of runoff components based on measuring hydraulic state variables, tracer experiments, and weighting methods. In: Leibundgut, C., McDonnell, J., Schultz, G. (Eds.), Integrated Methods in Catchment Hydrology: Tracer, Remote Sensing and New Hydrometric Techniques, vol. 258, pp. 249–255.
Weiler, M., McDonnell, J.J., 2004. Virtual experiments: a new approach for improving process conceptualization in hillslope hydrology. J. Hydrol. 285 (1–4), 3–18.

Transport of iodide in structured soil under spring barley during irrigation experiment analyzed using dual-continuum model, Biologia, 2013.

VERSITA

Biologia **68**/6: 1094—1098, 2013
Section Botany
DOI: 10.2478/s11756-013-0249-4

Transport of iodide in structured soil under spring barley during irrigation experiment analyzed using dual-continuum model**

Jaromír Dušek[1]*, Ľubomír Lichner[2], Tomáš Vogel[1] & Vlasta Štekauerová[2†]

[1] *Czech Technical University in Prague, Faculty of Civil Engineering, Thákurova 7, CZ-16629 Prague, Czech Republic; e-mail: dusek@mat.fsv.cvut.cz*
[2] *Slovak Academy of Sciences, Institute of Hydrology, Račianska 75, SK-83102 Bratislava, Slovakia*
† *Deceased*

Abstract: Transport of radioactive iodide $^{131}I^-$ in a black clay loam soil under spring barley in an early ontogenesis phase was monitored during controlled field irrigation experiment. It was found that iodide bound in the soil matrix could be mobilized by the surface leaching enhanced by mechanical impact of water drops and transported below the root zone of crops via soil cracks. The iodide transport through structured soil profile was simulated by the one-dimensional dual-continuum model, which assumes the existence of two inter-connected flow domains: the soil matrix domain and the preferential flow domain. The model predicted relatively deep percolation of iodide within a short time, in a good agreement with the observed vertical iodide distribution in soil. The dual-continuum approach proved to be an adequate tool for evaluation of field irrigation experiments conducted in structured soils.

Key words: breakthrough curve; dual-permeability model; field tracer experiment; preferential flow; solute transport; water flow

Introduction

Climate change poses the most serious threat to agriculture worldwide. Many areas of southern Slovakia are experiencing increases in the frequency and intensity of heavy rains following long hot, dry periods (Faško et al. 2008), leading to preferential flow, surface runoff, and soil erosion, hence to possible worsening quality of surface water and groundwater.

Agricultural production is dependent upon the addition of fertilizers. Soils have the ability to store nutrients for use in future years; excess nutrients leach out due to surface runoff and preferential flow. Preferential flow in soils develops when water and solutes travel at considerably high velocities through preferential pathways concurrently bypassing the porous matrix. This phenomenon has a direct influence on infiltration, drainage, and specifically on solute transport. Significant effects of preferential flow on solute transport were observed in soils from both ends of grain-size distribution spectrum: fingered flow induced by water repellency in sandy soils (e.g., Lichner et al. 2012) and macropore flow via soil cracks in clay and clay loam soils (e.g., Dohnal et al. 2009).

Mathematical models of water flow and solute transport could be used to characterize flowpaths and residence times in soils. However, reliable model predictions depend on soil hydraulic and transport properties, which are still difficult to estimate for soils with significant preferential flow effects (e.g., Gerke 2006). Unlike dye-staining techniques, restricted to single measurement due to destructive sampling, radioactive tracer techniques have the potential to deliver information from recurrent field experiments as the soil profile is disturbed negligibly (Lichner 1995). Thus, field irrigation experiment combined with radioactive tracer technique may provide valuable data (e.g., spatial and temporal variations of applied tracer), which serve for model calibration and validation (Alaoui et al. 1997).

Shetaya (2011) presented the distribution coefficient K_d of iodide for woodland and arable soil equal to 3.8 and 5.3 L kg^{-1}, respectively, and Mikolajków (2003) found that K_d of nitrate for brown, podsolic, and boggy soil were 5.22, 4.29, and 6.25 L kg^{-1}, respectively. As iodide and nitrate retardation in soils are similar, we used radioactive iodide as a tracer for nitrate movement in clay loam soil. Iodide is immobilized in soils in the form of organically bound iodine through the laccase-catalyzed oxidation (Seki et al. 2013). It was found that iodide was fully transformed into organic forms after 1 day of incubation in highly organic soils and was fully transformed in the studied soils after 60 days (Shetaya 2011).

The aim of this study was to predict iodide transport through clay loam soil during controlled field irrigation experiment following long hot, dry period using

*Corresponding author, **Special Section on Biohydrology, guest-editors Ľubomír Lichner & Kálmán Rajkai

Springer

Table 1. Measured and estimated soil hydraulic properties. SM and PF refer to the soil matrix and preferential flow domain, respectively.

Domain	Depth (cm)	θ_r (cm^3 cm^{-3})	θ_s (cm^3 cm^{-3})	α (cm^{-1})	n (–)	K_s (cm d^{-1})	h_s (cm)	w_f (–)
SM	0–55	0.011	0.489	0.049	1.203	15.7	–0.08	–
	55–85	0.011	0.491	0.028	1.296	15.6	–0.16	–
	85–100	0.011	0.488	0.007	1.287	16.9	–0.68	–
PF	0–100	0.050	0.600	0.145	2.680	700.0	0.00	0.15

dual-continuum approach. The dual-continuum model invokes local nonequilibrium in pressure head and solute concentration between the two pore domains. This is achieved through dividing the liquid phase continuum into a preferential flow domain (further on abbreviated to the PF domain) and a soil matrix flow domain (the SM domain). Model predictions of iodide transport were compared with data from field irrigation experiment.

Material and methods

Field experiment and soil

The study area was located at the Experimental Station of Research Institute of Irrigation at Most pri Bratislave village (48°08′27″ N, 17°14′41″ E). The station is about 133 m above sea level. The average annual air temperature is 9.7 °C, the average annual precipitation is 554 mm. The soil is classified as a Chernozem (WRB 2006) and has a clay loam texture (Soil Survey Division Staff 1993). The soil profile consists of three relatively homogeneous horizons. Physical and chemical properties of the surface horizon were as follows: clay/loam/sand content was 53/46/1%, $CaCO_3$ content 11.2%, C_{org} content 1.9%, pH (H_2O) 8.2, and pH (KCl) 7.8.

The experiment was performed at a 1.4 m × 3.4 m plot after a two weeklong hot and dry period, which resulted in fissures and cracks in the soil profile. Spring barley (*Hordeum vulgare* L.) was growing on the field during the experiment. An original radioactive tracer technique (Lichner 1992) was used to measure the tracer distribution in the soil profile. The measuring probe, used to determine tracer concentrations, consists of a duralumin tube (inner diameter of 8 mm, outer diameter of 12 mm), in which the Geiger-Müller detector (with the length of 21 mm and the diameter of 6.3 mm) and the analog interface unit are connected to a nuclear analyzer with a coaxial cable. Owing to its small size the Geiger-Müller detector can be considered as a point detector. The counting rate recorded by the detector is directly proportional to the activity of the radioactive tracer. Eight probes were installed vertically to the depth of 1.5 m on the plot before the irrigation had started.

Around each of eight probes, a short pulse of $Na^{131}I$ solution with the activity of about 10 MBq was trickled by syringe (Lichner 1995). After the application, radioactive iodide ($^{131}I^-$), bound at the soil matrix, was leached by irrigated water. Water application was conducted manually with a watering can (100 mm in 10 h). The irrigation was then interrupted for 12 h to allow water and tracer redistribution within the soil profile. Following this interruption, another 100 mm of water was applied within 10 h. Vertical distributions of iodide in soil were measured four times during the irrigation experiment, together with the iodide breakthrough curve at the depth of 30 cm.

The soil-water retention curves for the three soil horizons were measured by standard pressure plate apparatus method on undisturbed soil samples and the hydraulic parameters were consequently obtained by fitting van Genuchten's modified prediction model (Vogel et al. 2000) to data points. The measurements of the saturated hydraulic conductivity K_s were carried out by tension infiltrometer at three depths. Five replicate measurements were conducted at each depth. The volumetric portion of the PF domain, w_f, was estimated as 15% of the bulk soil. The retention curve parameters of the PF domain were also estimated based on indirect soil and plot characteristics. The sensitivity of the dual-continuum model to uncertainties associated with preferential flow parameters was studied e.g. by Dohnal et al. (2012). Table 1 summarizes the soil hydraulic parameters for both flow domains. θ_r and θ_s are the residual and saturated water contents, respectively, h_s is the air-entry value of Vogel et al. (2000), and α and n are fitting parameters.

For solute transport, dispersivity value of 5 cm was used. The molecular diffusion coefficient was set equal to 1.3 cm^2 d^{-1}. The values of bulk density within the soil profile were taken from previous study (Nováková 2000). The distribution coefficients were estimated from batch tests performed on soils with similar organic content (Szabová & Čipáková 1988).

Flow and transport model

The dual-continuum approach (Gerke & van Genuchten 1993) assumes that the porous medium consists of two separate domains with specific hydraulic properties. One-dimensional variably saturated water flow in the dual-continuum model was described by a pair of Richards' equations for the PF and the SM domain pore systems. Similarly, a coupled pair of advection-dispersion equations was solved to model solute transport. The exchange of water and solute between the matrix and the fracture domains was assumed to be proportional to the local pressure difference and the concentration gradient between the two pore systems. The dual sets of governing equations for water flow and iodide transport were solved numerically with a finite element scheme using the computer code S1D (Vogel et al. 2010).

Initial and boundary conditions

The iodide tracer was placed at the top 0.1-cm depth of the profile as initial condition. Irrigation water was without iodide. The bottom boundary condition was set to zero concentration gradient, to allow the tracer to pass freely the lower boundary at the depth of 100 cm. Note that iodide concentration in the water entering the soil surface during the experiment was not measured; hence only relative concentrations and masses could be evaluated by the modeling (similarly as in Vogel et al. 2007).

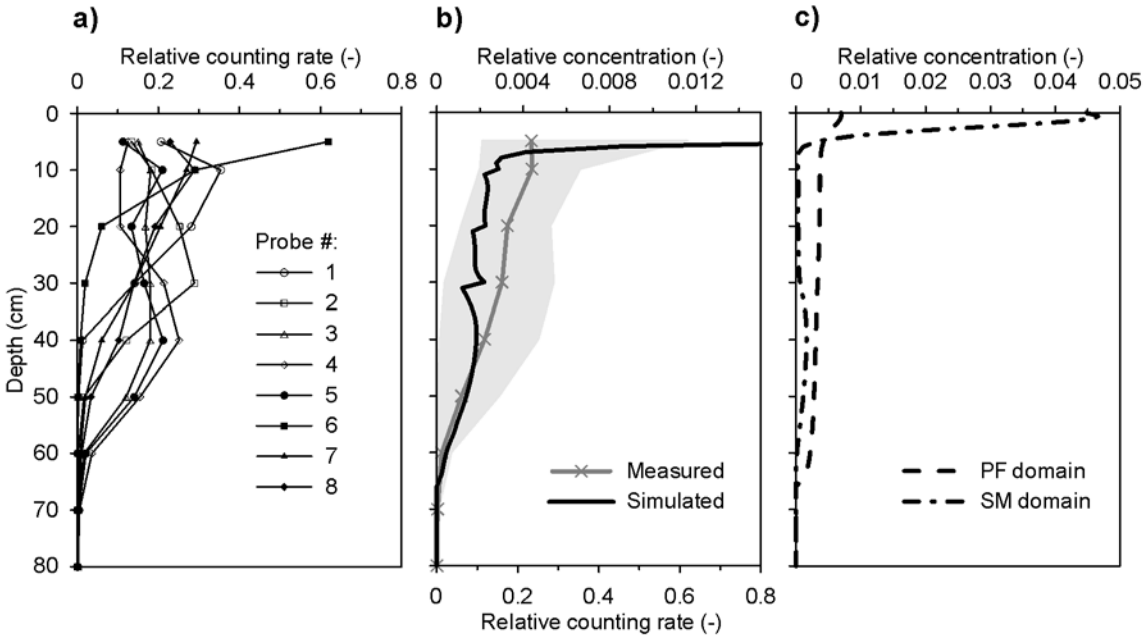

Fig. 1. Vertical iodide distributions in the soil profile: a) – measured iodide profiles along the individual probes for $t = 22$ h (cumulative infiltration rate of 100 mm); b) – simulated composite concentration and mean measured distribution with shaded area representing measurement variability among eight probes; c) – simulated liquid concentrations in the flow domains.

"Atmospheric boundary condition" was postulated at the soil surface. This type of condition allowed for switching between the Neumann and Dirichlet type conditions, i.e. when the top soil was not capable of transmitting water during irrigation, the flux condition was changed to pressure condition. The unit hydraulic gradient condition was used at the lower boundary, allowing water to leave the soil profile at the rate equal to unsaturated hydraulic conductivity. No rainfall had occurred for 14 days before the start of the infiltration experiment, so the initial soil water pressure was set to –700 cm throughout the entire soil profile. No evapotranspiration was taken into account for the simulated period.

Results and discussion

Figure 1 depicts observed and simulated vertical iodide distributions in the soil profile after irrigation of 100 mm water and the following 12 h redistribution period. It can be seen that iodide migrated down to the depth of 70 cm below the surface. Measurement variability among eight probes is clearly visible in Fig. 1a as each probe reflected different transport regime (either in the soil matrix and/or through preferential pathways and other structural soil elements). Simulated composite concentrations showed deep penetration of iodide (Fig. 1b), which is in relatively good agreement with the observed distribution pattern. The concentration increase in the SM domain below 30 cm depth could be attributed to the iodide transfer from the PF to the SM domain (Fig. 1c). Without considering preferential flow effects, iodide distribution was limited in the 0–20 cm part of the topsoil.

As the rooting depth of spring barley can hardly exceed 30 cm at the turn of April/May, it can be concluded that about 2% of iodide, bound in soil matrix and mobilized by the surface leaching enhanced by mechanical impact of water drops, could be transported below the root zone of crops via soil cracks after application of 100 mm water and the following 12 h redistribution period. It should be noted that 3 h precipitation of more than 127 mm was registered in this region e.g. on 10.7.1999. Hourly and daily precipitation data during heavy rain events measured at two meteorological stations in the southwest of Slovakia were presented by Lichner et al. (2006).

Figure 2 shows observed and simulated breakthrough curves at the depth of 30 cm. The simulated concentration increase after 4 h of irrigation is delayed compared to the mean observed breakthrough curve (Fig. 2b); nevertheless the simulated curve remained within the measurement variability. The PF domain showed steep increase of iodide concentrations in response to the first irrigation after 4 h (Fig. 2c). The iodide concentrations in the SM domain were characterized by gradual increase at this depth. The second irrigation induced a slight increase of concentration in the PF domain at about 24 h and negligible response in the SM domain. This could be explained by different vertical distribution of iodide in both flow domains at this time.

Conclusion

Transport of iodide tracer through structured soil during field irrigation experiment was analyzed using dual-continuum model. Observed iodide distributions in the soil profile (i.e., relatively deep percolation within a short time) could not be described with a model based on classical single continuum approach. The applied dual-continuum approach allowed more adequate ap-

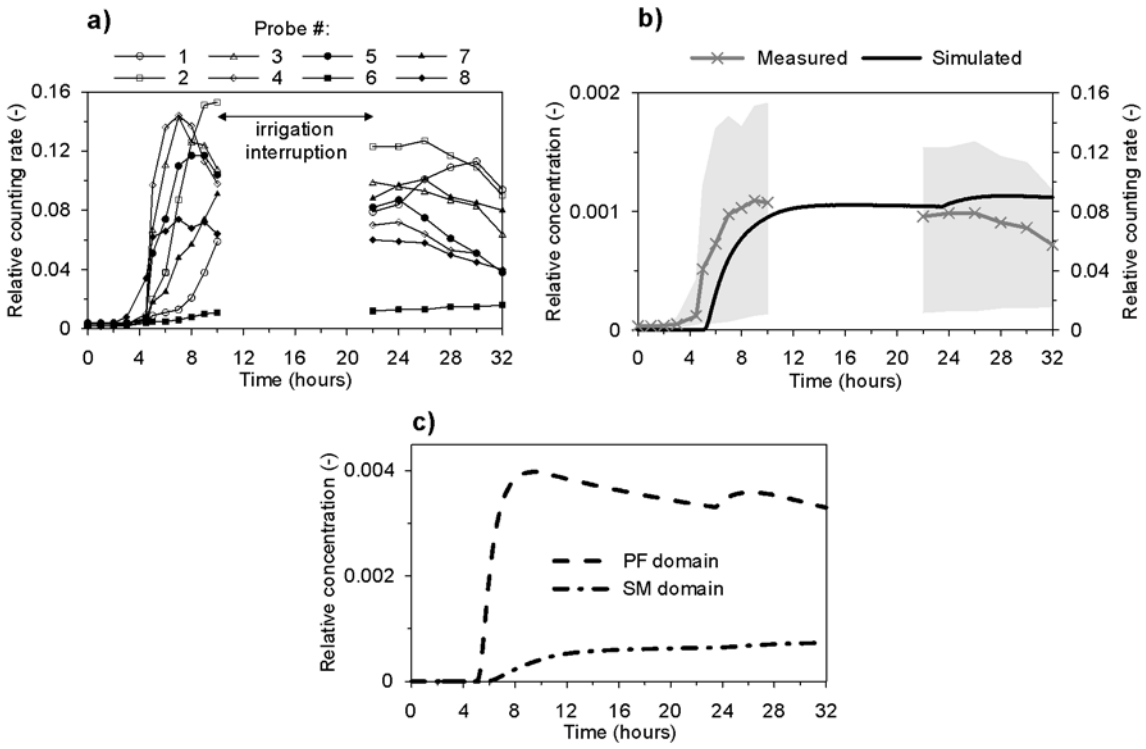

Fig. 2. Iodide breakthrough curves at the depth of 30 cm: a) – iodide concentrations measured by individual probes; b) – mean measured and simulated composite breakthrough curves (the shaded area represents the measurement variability among eight probes); c) – simulated domain-specific iodide concentrations.

proximation of the field data. The dual-continuum model proved to be a useful tool for evaluation of field irrigation experiments conducted in structured soils.

Acknowledgements

The research has been supported by the Ministry of Education of the Czech Republic (MSM 6840770002). Additional support was provided by the Science and Technology Assistance Agency project No. APVT-51-006502 and the Scientific Grant Agency project No. VEGA 2/0073/11.

References

Alaoui A.M., Germann P., Lichner L. & Novak V. 1997. Preferential transport of water and ^{131}iodide in a clay loam assessed with TDR-technique and boundary layer flow theory. Hydrol. Earth Syst. Sci. **1:** 813–822.

Dohnal M., Dušek J., Vogel T., Císlerová M., Lichner Ľ. & Štekauerová V. 2009. Ponded infiltration into soil with biopores – field experiment and modeling. Biologia **64:** 580–584.

Dohnal M., Vogel T., Šanda M. & Jelínková V. 2012. Uncertainty analysis of a dual-continuum model used to simulate subsurface hillslope runoff involving oxygen-18 as natural tracer. J. Hydrol. Hydromech. **60:** 194–205.

Faško P., Lapin M. & Pecho J. 2008. 20-year extraordinary climatic period in Slovakia. Meteorol. Časopis **11**: 99–105.

Gerke H.H. & van Genuchten M.T. 1993. A dual-porosity model for simulating the preferential movement of water and solutes in structured porous media. Water Resour. Res. **29:** 305–319.

Gerke H.H. 2006. Preferential flow descriptions for structured soils. J. Plant Nutr. Soil Sci. **169:** 382–400.

Lichner Ľ. 1992. Laboratory and field measurements of solute transport in soils by means of nuclear tracer technique. Vodohosp. Čas. **40:** 548–561.

Lichner L. 1995. A nuclear tracer technique for investigation of solute transport in the unsaturated zone. In: Proc. Int. Symp. Tracer Technologies for Hydrological Systems, Boulder 1995, IAHS Publ. no. 229, Wallingford, pp. 109–116.

Lichner L., Dlapa P., Sir M., Cipakova A., Houskova B., Fasko P. & Nagy V. 2006. The fate of cadmium in field soils of the Danubian lowland. Soil Till. Res. **85:** 154–165.

Lichner Ľ., Holko L., Zhukova N., Schacht K., Rajkai K., Fodor N. & Sándor R. 2012. Plants and biological soil crust influence the hydrophysical parameters and water flow in an aeolian sandy soil. J. Hydrol. Hydromech. **60:** 309–318.

Mikolajków J. 2003. Laboratory methods of estimating the retardation factor of migrating mineral nitrogen compounds in shallow groundwater. Geol. Quart. **47:** 91–96.

Nováková K. 2000. Soil hydrophysical characteristics influencing rapid transfer of soluble contaminants. In: Heldi A. (ed.): Scientific papers of the Research Institute of Irrigation, Drainage and Landscape Engineering, Bratislava, pp. 243–252. (in Slovak)

Seki M., Oikawa J., Taguchi T., Ohnuki T., Muramatsu Y., Sakamoto K. & Amachi S. 2013. Laccase-catalyzed oxidation of iodide and formation of organically bound iodine in soils. Environ. Sci. Technol. **47:** 390–397.

Shetaya W.H.A.H. 2011. Iodine dynamics in soil. Ph.D. Thesis. University of Nottingham, Nottingham, 171 pp.

Soil Survey Division Staff 1993. Soil survey manual. Soil Conservation Service. U.S. Department of Agriculture Handbook 18, 437 pp.

Szabová T. & Čipáková A. 1988. Determination of adsorption and distribution coefficients of ^{85}Sr, ^{65}Zn, ^{115}Cd, and ^{131}I for several soils. Report No. 1/88. Institute of Radioecology and Applied Nuclear Techniques, Košice. (in Slovak)

Vogel T., van Genuchten M.T. & Císlerová M. 2000. Effect of the shape of soil hydraulic functions near saturation on variably-saturated flow predictions. Adv. Water Resour. **24:** 133–144.

Vogel T., Lichner L., Dusek J. & Cipakova A. 2007. Dual-continuum analysis of a cadmium tracer field experiment. J. Contam. Hydrol. **92:** 50–65.

Vogel T., Brezina J., Dohnal M. & Dusek J. 2010. Physical and numerical coupling in dual-continuum modeling of preferential flow. Vadose Zone J. **9:** 260–267.

WRB 2006. World reference base for soil resources 2006. 2nd ed. World Soil Resources Reports No. 103. FAO, Rome, 128 pp.

Received February 8, 2013
Accepted May 24, 2013

Modeling subsurface hillslope runoff dominated by preferential flow: One- vs. two-dimensional approximation, Vadose Zone Journal, 2014.

Published May 23, 2014

Original Research

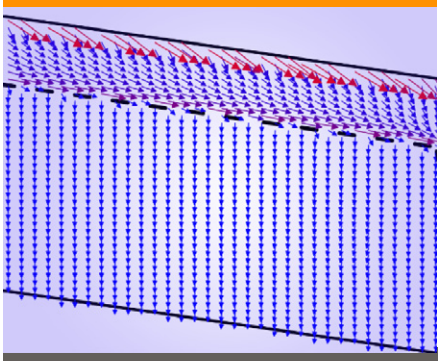

This study deals with episodic shallow lateral subsurface runoff dominated by preferential flow above a semipermeable soil–bedrock interface. Two modeling approaches differing in dimensionality are compared with each other and applied to observed hillslope discharge and soil water pressure data.

Modeling Subsurface Hillslope Runoff Dominated by Preferential Flow: One- vs. Two-Dimensional Approximation

Jaromir Dusek* and Tomas Vogel

Shallow saturated subsurface flow, frequently observed on hillslopes of headwater catchments in humid temperate climates, often dominates hydrologic responses of the catchments to major rainfall events. Typically, these responses are significantly affected by the presence of preferential flow. Reliable prediction of runoff from hillslope soils under such conditions remains a challenge. In this study, two approaches to modeling hillslope responses to rainstorms, which differ in dimensionality and thus also in the complexity of geometric, material, and boundary conditions, were tested and used on the hillslope discharge data observed in an experimental trench. In the one-dimensional (1D) approach, 1D variably saturated vertical soil water flow is combined with 1D lateral saturated flow above the soil–bedrock interface. In this approach, vertical flow is modeled by means of a dual-continuum concept involving two coupled Richards' equations (representing flow in the soil matrix and in the preferential pathways), while lateral flow is described by the diffusion wave equation. In the two-dimensional (2D) approach, the movement of water in a variably saturated hillslope segment is modeled as vertical planar flow (i.e., the vertical and lateral flow components are fully integrated into one flow system). Similar to the 1D approach, the preferential flow effects are implemented in the 2D model by means of the dual-continuum concept. The two model approaches (1D and 2D) resulted in similar hillslope discharge hydrographs, characterized by short-term runoff peaks followed by zero-discharge periods, but the 2D model showed closer agreement between observed and simulated soil water pressure heads near the trench. The sensitivity analysis of soil and bedrock properties confirmed a significant influence of the bedrock saturated hydraulic conductivity on simulated hillslope discharge. The simpler 1D approach, based on the combination of 1D vertical flow and 1D lateral flow, was found to provide a useful approximation of the more complex and flexible 2D system and to be far more efficient in terms of computing time.

Abbreviations: 1D, one-dimensional; 2D, two-dimensional; 3D, three-dimensional; PF, preferential flow; SM, soil matrix.

Czech Technical Univ. in Prague, Faculty of Civil Engineering, Prague, Czech Republic. *Corresponding author (dusek@mat.fsv.cvut.cz).

Vadose Zone J.
doi:10.2136/vzj2013.05.0082
Received 10 May 2013.

Runoff responses of headwater catchments in temperate humid climates to major rainfall events are often dominated by shallow saturated subsurface flow (also referred to as stormflow or throughflow). This type of flow usually develops at the base of a shallow hillslope soil profile above the bedrock (Weiler et al., 2005). The onset and buildup of a saturated layer above the soil–bedrock interface is commonly accelerated by the presence of soil macropores and biopores. The network of preferential pathways also significantly speeds up saturated lateral flow down the slope (Heppell et al., 2000; Buttle and McDonald, 2002). The importance of preferential flow in hillslope runoff formation in headwater catchments is well recognized (e.g., Sidle et al., 2001; Weiler and McDonnell, 2004; Anderson et al., 2010).

With the enormous increase in computational efficiency in recent years, three-dimensional modeling representations of flow and transport processes at the hillslope and catchment

scales have become possible (Rigon et al., 2006; Hopp et al., 2009; Mirus and Loague, 2013). From the large-scale perspective, however, the three-dimensional (3D) impact of local-scale features and processes (e.g., spatial heterogeneity of soil properties and preferential flow) tends to be spatially averaged because the thickness of the permeable soil is usually relatively small compared with the length of the simulated hillslope. Therefore, 1D and 2D approaches often can be successfully applied to predict water discharge from a hillslope soil profile. One-dimensional variably saturated vertical flow has been combined with 1D saturated subsurface flow, for instance, by Fan and Bras (1998), Troch et al. (2002), and Dusek et al. (2012a). Subsurface lateral flow along the soil–bedrock interface has often been described by a 1D Boussinesq-type diffusion wave equation, while models based on a solution of Richards' equation have been used to predict the 1D vertical water flow. The 1D approaches are very efficient in terms of computing speed. This becomes important in cases where the hillslope models are coupled to models used for large, catchment-scale predictions.

Several models of subsurface stormflow of varying complexity, including a 1D diffusion wave model (based on the Boussinesq equation) and the 2D Richards' equation model, were compared by Sloan and Moore (1984). They concluded that these two models predicted the subsurface runoff and water table dynamics equally well. Likewise, Paniconi et al. (2003) performed comparative tests involving a 1D diffusion wave model and 3D Richards' equation model and obtained good agreement between the two models across a wide range of scenarios (various boundary conditions, slope angles, and hillslope shapes). However, the recharge rates needed to solve the Boussinesq equation for saturated lateral flow were not determined by a vertical soil water flow model in these comparisons (a time-invariant recharge rate was used instead). Hilberts et al. (2007) introduced a fully coupled model of 1D vertical Richards' and lateral Boussinesq's equations and performed the benchmark tests for this model and the 3D Richards' equation model. Nevertheless, all these comparisons of 1D predictions with 2D and 3D models considered flow in a homogeneous soil without macropores, i.e., they were not performed for hillslope soils with significant preferential flow effects.

Recently, the description of preferential subsurface stormflow was conceptualized using different approaches including Darcian (with Richards' equation) and non-Darcian (with a kinematic wave equation) type of flow. For example, Faeh et al. (1997) used the 2D dual-permeability model to identify relevant hillslope transport processes, and a 1D module was applied to estimate the exchange of water between the soil matrix and macropores. Beckers and Alila (2004) proposed a model in which vertical macropore flow was initiated by surface ponding and was instantaneously routed to the bedrock surface. Lateral preferential flow was then computed using a Darcy law based approach. The effect of laterally oriented pipes on subsurface stormflow dynamics was examined by Tromp-van Meerveld and Weiler (2008); they concluded that the inclusion of pipe flow had a small influence on simulated subsurface flow. Klaus and Zehe (2010) generated spatially explicit representations of macropore structures for studying preferential flow patterns during irrigation in a tile-drained hillslope. Nevertheless, a systematic and detailed comparison of hillslope discharge data with predictions based on a 2D dual-continuum model (also known as a dual-permeability model) has not, so far, been presented in the literature.

In our previous analyses (Dusek et al., 2012a, 2012b), a 1D model, combining 1D variably saturated soil water flow with 1D saturated lateral flow, was used to simulate the formation of subsurface runoff and the associated mixing of pre-event and event water. In this model, vertical soil water flow was conceptualized as a superposition of flow in the soil matrix and preferential pathways, while the saturated lateral flow component of the model was assumed to represent mainly flow in a laterally connected network of preferential pathways. In these studies, the 1D dual-continuum model described the observed subsurface flow dynamics reasonably well. However, the applied 1D approach was not rigorously verified against a dimensionally more consistent 2D or 3D dual-continuum approach.

In the present study, we compared the 1D model of shallow subsurface flow with a conceptually similar but dimensionally superior 2D model in which both vertical and lateral components of flow are fully integrated into the 2D dual-continuum planar flow model. The primary objective of this study was to verify the simpler 1D approximation of the flow system against its more rigorous 2D analogy. In addition, we drew conclusions about the applicability of these two model approximations to real-world phenomena.

Materials and Methods

Experimental Site

The experimental hillslope site Tomsovka is located in the headwater catchment Uhlirska, Jizera Mountains, North Bohemia, Czech Republic. The total area of the catchment is 1.78 km^2, the average altitude is 820 m asl, the mean annual precipitation is 1380 mm, and the mean annual temperature is 4.7°C. The studied hillslope is covered with grass [*Calamagrostis villosa* (Chaix.) J.F. Gmel.] and spruce [*Picea abies* (L.) H. Karst.]. The average slope at Tomsovka is about 14%.

The present study was based on data measured at the Tomsovka site from May 2007 through October 2009. Hydrologic and micrometeorological conditions were monitored at a 10-min temporal resolution. Subsurface hillslope discharge was measured at an 8-m-long experimental trench. It consisted of two individual sections (labeled as A and B), each 4 m long. Shallow subsurface hillslope discharge was collected separately in each section at a depth of about 75 cm. The discharge rates Q_A and Q_B were measured continuously by tipping buckets during the growing seasons (May–October). Although the geographic watershed divide is located approximately 130 m above the location of

the experimental trench, the trench was found to drain a much shorter hillslope length (25–50 m) (Dusek et al., 2012a). Among the various explanations for this finding, the discontinuity of the underlying bedrock was observed by vertical electrical sounding survey (Sanda and Cislerova, 2009).

For modeling purposes, the hillslope microcatchments corresponding to Trench Sections A and B were assumed to have approximately the same geometric and material properties (hillslope length, depth to bedrock, soil stratification, soil hydraulic properties, etc.). The differences in the measured discharge hydrographs (Q_A vs. Q_B) were attributed to the spatial variability of preferential pathways, especially in terms of their lateral connectivity, bedrock topography, and the measurement uncertainty, related to, e.g., an occasional malfunction of the tipping buckets. The significance of the spatial variability of preferential pathways and bedrock topography in hillslope stormflow generation was already demonstrated, e.g., by Nieber and Sidle (2010) and Freer et al. (2002).

The soil at the Tomsovka site is relatively shallow, about 70 cm deep. The soil is sandy loam classified as a Dystric Cambisol and contains a broad range of pore sizes. The soil profile consists of three layers with different hydraulic properties (Table 1). The soil layers are underlain by a transition zone of weathered granite bedrock, 5 to 10 m thick (Sanda and Cislerova, 2009). This transition zone then changes into a compact porphyritic biotite granite bedrock. The interface between the third soil layer and the transition zone is referred to as the soil–bedrock interface, situated at the depth of 70 cm (Table 1). The soil hydraulic parameters characterizing each soil layer were derived from laboratory measurements, in which undisturbed 100-cm^3 soil samples and 1000-cm^3 soil cores were used to determine the soil water retention parameters and the saturated hydraulic conductivity, respectively (Sanda and Cislerova, 2009). In addition, the saturated hydraulic conductivity of the weathered bedrock surface (70 cm) was determined using a disk infiltrometer.

A set of 28 boreholes (2–3 m deep) at three hillslope transects has been established to survey the stratification of the soil profile and the upper part of the weathered bedrock (Tacheci, 2002). As a complementary method, vertical electrical sounding survey was used (Sanda and Cislerova, 2009). The soil and vertical electrical sounding survey confirmed that the local gradient of the soil–bedrock interface is similar to the local hillslope gradient.

Significant preferential flow effects, affecting the soil water response to precipitation, were reported for the same site by Sanda and Cislerova (2009). Preferential flow was attributed to highly conductive pathways along tree roots as well as the soil structure and the spatial variability of local soil hydraulic properties. Soil water pressure within the soil profile was monitored using a set of automated tensiometers installed in five locations at three different depths below the soil surface (about 20, 35, and 50 cm) between 1- and 20-m distance above the experimental trench. Overland flow is rarely observed at the site due to the highly permeable topsoil layer.

Water Flow Models

One-Dimensional Approach

The 1D approach combines 1D lateral saturated flow along the soil–bedrock interface (described by the diffusion wave equation) and 1D vertical flow (described by a dual set of Richards' equations accounting for flow through the soil matrix and preferential pathways). Here, we summarize the basic features of the 1D vertical and 1D lateral models. More details are available in Dusek et al. (2012a).

One-Dimensional Lateral Flow Model (LatFlow): Upon sufficiently intense rain, infiltrating water percolates vertically down to the impermeable bedrock (or the top boundary of a low-permeability soil layer) where a saturated layer is gradually formed (Fig. 1). In the saturated layer, water flows laterally in a direction determined by the local gradient of the soil–bedrock interface. The intermittent saturated subsurface flow (referred to as lateral flow) can be approximated by the 1D diffusion wave equation.

Table 1. The soil hydraulic parameters (θ_r and θ_s are the residual and saturated water contents, K_s is the saturated hydraulic conductivity, h_s is the air-entry value, and α and n are empirical fitting parameters) as used for the one-dimensional (1D) dual-continuum model VertFlow and two-dimensional (2D) dual-continuum model. The 1D approach was limited to a depth of 75 cm. The 2D approach considered a depth of 300 cm. In the case of the 2D model, the given conductivity values are valid for the vertical direction only (due to anisotropy).

Domain	Approach	Depth	θ_r	θ_s	α	n	K_s	h_s
		cm	— cm^3 cm^{-3} —		cm^{-1}		cm d^{-1}	cm
Soil matrix	1D/2D	0–8	0.20	0.55	0.050	2.00	567	0.00
	1D/2D	8–20	0.20	0.54	0.050	1.50	67	−0.69
	1D/2D	20–70	0.20	0.49	0.020	1.20	17	−1.48
	1D/2D	70–5	0.20	0.41	0.020	1.20	1.3	−1.88
	2D	75–300	0.00	0.21	0.020	1.20	0.4	−2.61
Preferential flow	1D/2D	0–75	0.01	0.60	0.050	3.00	5000	0.00

Using a hillslope analogy to Dupuit's assumption, an equation can be obtained similar to the expression first introduced by Boussinesq (1877):

$$\frac{Q}{W} = -K_D h_D \left(\frac{\partial h_D}{\partial x} + \frac{dz}{dx} \right) \quad [1]$$

where Q is the local hillslope discharge (m^3 s^{-1}), h_D is the depth of lateral flow (m), i.e., the vertical extent of the saturated layer, K_D is the effective saturated hydraulic conductivity (m s^{-1}), x is the coordinate (m) running along the bedrock slope (positive in the upslope direction), z is the vertical coordinate (positive upward), dz/dx is the local gradient of the soil–bedrock interface (dimensionless), and W is the hillslope width (m). In this study, W was assumed to be invariant along

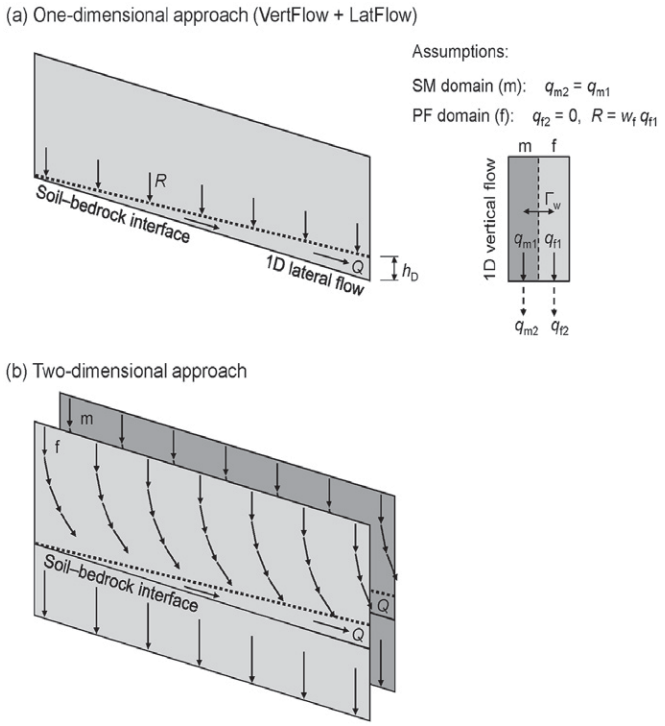

Fig. 1. Schematic of flow in a hillslope segment representing two modeling approaches: (a) a one-dimensional approach, in which R is the recharge intensity feeding the saturated lateral flow (the LatFlow model), h_D is the depth of lateral flow, Q is the hillslope discharge, q_{m1}, q_{m2}, q_{f1}, and q_{f2} are the soil water fluxes generated by the vertical one-dimensional dual-continuum soil water flow model (VertFlow), Γ_w is the interdomain soil water transfer rate, SM and PF refer to the soil matrix and preferential flow domains, respectively, and w_f is the volume fraction of the PF domain; and (b) a two-dimensional approach with two planar flow domains (SM and PF domains).

x. This restriction can easily be relaxed; however, the experimental conditions in this study did not involve any complex 3D hillslope configurations (e.g., convergent or divergent hillslopes).

The continuity equation for lateral flow can be written as

$$\Theta\frac{\partial h_D}{\partial t}+\frac{1}{W}\frac{\partial Q}{\partial x}=R \qquad [2]$$

where Θ is the effective porosity ($m^3\ m^{-3}$), R is the local intensity of vertical recharge ($m\ s^{-1}$), and t is time (s).

The diffusion wave equation for the lateral flow is obtained by substituting the local hillslope discharge into the continuity equation:

$$\Theta\frac{\partial h_D}{\partial t}-\frac{\partial}{\partial x}\left[K_D h_D\left(\frac{\partial h_D}{\partial x}+\frac{dz}{dx}\right)\right]=R \qquad [3]$$

This equation with a single dependent variable h_D is solved by the 1D lateral flow model LatFlow. The numerical solution is obtained by the finite element method and implemented in the computer program HYPO (Vogel et al., 2003).

One-Dimensional Vertical Flow Model (VertFlow): The recharge intensity, R, feeding lateral flow, is determined by the vertical soil water flow model based on the numerical solution of the 1D Richards equation. If a substantial portion of the recharge is caused by preferential flow, the dual-continuum concept is used, which means that the flow of water is assumed to take place in both the soil matrix (SM) and preferential flow (PF) domains, and Richards' equation describes water flow in each of the two domains. Both equations are coupled by means of a transfer term, which allows for the dynamic water exchange between the two pore domains. The following pair of governing equations is applied to describe the 1D vertical movement of water (similar to Gerke and van Genuchten, 1993a):

$$w_f C_f\frac{\partial h_f}{\partial t}=\frac{\partial}{\partial z}\left[w_f K_f\left(\frac{\partial h_f}{\partial z}+1\right)\right]-w_f S_f-\Gamma_w \qquad [4]$$

$$w_m C_m\frac{\partial h_m}{\partial t}=\frac{\partial}{\partial z}\left[w_m K_m\left(\frac{\partial h_m}{\partial z}+1\right)\right]-w_m S_m+\Gamma_w \qquad [5]$$

where subscript m denotes the SM domain and subscript f denotes the PF domain, h is the pressure head (m), K is the unsaturated hydraulic conductivity ($m\ s^{-1}$), C is the soil water capacity (m^{-1}), S is the local root water extraction intensity (s^{-1}), Γ_w is the soil water transfer term (s^{-1}) controlling the water exchange between the domains, w_m and w_f are volume fractions of the respective domains ($w_m + w_f = 1$), and z is the vertical coordinate (m) directed positive upward.

The water transfer term in Eq. [4] and [5] is described by the modified first-order approximation of Gerke and van Genuchten (1993b):

$$\Gamma_w=\alpha_{ws}K_{ar}(h_f-h_m) \qquad [6]$$

where α_{ws} is the water transfer coefficient at saturation ($m^{-1}\ s^{-1}$) and K_{ar} is the relative unsaturated conductivity of the SM–PF domain interface. Values of K_{ar} range from 0 to 1 depending on the SM and PF domain conductivities, which are evaluated for upstream soil water pressure (Gerke et al., 2013).

The dual set of governing equations for soil water flow is solved numerically by the computer program S1D using the finite element method. The most recent implementation of the S1D model was presented by Vogel et al. (2010a).

The 1D dual-continuum vertical flow model VertFlow is used to predict the lateral flow recharge rate R for the LatFlow model. The combined VertFlow + LatFlow model is forward coupled (through the recharge rate R). No backward coupling (the effect of shallow saturated flow on the vertical water flow) is considered. Here, the combined use of the vertical dual-continuum model VertFlow and the lateral single-continuum model LatFlow is referred to as the 1D approach.

Two-Dimensional Approach

In the 2D approach, preferential flow effects are taken into account by formulating the dual set of two-dimensional governing equations, which reflects the dual character of flow in the SM and PF domains. Water flow in the dual-continuum system is described by a pair of Richards' equations (Vogel et al., 2000a):

$$C_f \frac{\partial h_f}{\partial t} = \nabla \cdot (\mathbf{K}_f \nabla h_f) + \nabla \cdot (\mathbf{K}_f \nabla z) - S_f - \frac{\Gamma_w}{w_f} \quad [7]$$

$$C_m \frac{\partial h_m}{\partial t} = \nabla \cdot (\mathbf{K}_m \nabla h_m) + \nabla \cdot (\mathbf{K}_m \nabla z) - S_m + \frac{\Gamma_w}{w_m} \quad [8]$$

where $\mathbf{K}$ is the hydraulic conductivity tensor (m s^{-1}). The soil water transfer term Γ_w is defined identically as in Eq. [6].

The composite boundary flux of soil water q is defined as

$$q = \mathbf{n}\mathbf{q}_f w_f + \mathbf{n}\mathbf{q}_m w_m \quad [9]$$

where $\mathbf{n}$ is the unit normal to the boundary (dimensionless) and $\mathbf{q}_f$ and $\mathbf{q}_m$ are the vectors of the domain-specific soil water fluxes (m s^{-1}). This equation is used to calculate the hillslope discharge Q (shallow subsurface runoff) from the simulated 2D domain.

The dual set of governing equations for soil water flow is solved numerically by the computer program S2D using the fully implicit Galerkin finite elements method (Vogel et al., 2000a).

From the inspection of the governing equations (Eq. [3–5] vs. Eq. [7–8]), it is clear that the 2D approach is more realistic than the 1D approach. This is mainly due to the effective nature of the two coefficients in the 1D lateral flow equation (Θ and K_D in Eq. [3]) compared with more physically based coefficients in the 2D equation, as well as the absence of backward coupling between lateral and vertical flow in the 1D approach. In addition, the 2D approach allows the incorporation of a semipermeable bedrock below the soil profile into the computational flow domain and thus simulation of the flow separation at the soil–bedrock interface without additional assumptions (such as those listed in Fig. 1a for the 1D approach). The main disadvantage of the 2D approach is the fact that it is much more computationally demanding.

Among the questions that we wanted to address in this study are the following ones: Is it possible to simulate the observed hillslope discharge responses with 1D and 2D approaches using a physically coherent set of soil hydraulic properties? Given such properties, does the model with more realistic dimensionality provide significantly better predictions?

Model Inputs

The soil–plant–atmosphere interactions, determining upper boundary conditions for both modeling approaches (1D and 2D), involved natural rainfall and plant transpiration. The rainfall intensities were organized in 1-h series. The daily potential transpiration was calculated using the Penman–Monteith equation (Monteith, 1981) based on micrometeorological data observed directly at the Tomsovka site. The root water uptake, S, was described according to Feddes et al. (1978). More detailed information about the root water uptake parameterization was given by Dohnal et al. (2006b) and Dusek et al. (2012a). The soil water pressure, measured by tensiometers at the beginning of each growing season, was used to characterize the initial condition. The flow simulations were started from the initial equilibrium between the SM domain and PF domain ($h_m = h_f$).

Geometric and Boundary Conditions for the One-Dimensional Approach

The flow domain for the 1D VertFlow model was 75 cm deep, spanning from the soil surface to the depth of 5 cm below the soil–bedrock interface, i.e., containing the upper 5 cm of the semipermeable weathered bedrock layer. In the 1D VertFlow model, a free drainage condition (equivalent to the unit hydraulic gradient condition) was used for the lower boundary condition of both flow domains (i.e., the SM and PF domains). In this study, we assumed that $q_{m2} = q_{m1}$ and $q_{f2} = 0$ (Fig. 1a), i.e., the deep percolation was associated with the SM domain flux while the PF domain flux q_{f1} contributed to lateral flow. Therefore, the recharge rate R of the lateral flow was evaluated as

$$R = w_f q_{f1} \quad [10]$$

The 1D LatFlow subsurface runoff model describes lateral saturated flow that takes place in the PF domain and/or in the laterally continuous pore network above the soil–bedrock interface. The hillslope length (i.e., the length of the 1D lateral computational flow domain) was fixed at 25 m. The slope was set to 14%.

Geometric and Boundary Conditions for the Two-Dimensional Approach

For the 2D flow model, a vertical flow domain of 30 by 3 m was assumed (Fig. 2). The flow domain was extended by 5 m beyond the experimental trench to correctly account for the fluxes in the vicinity of the trench. The hillslope length contributing to discharge was thus 25 m. The slope was fixed at 14%. Identical boundary conditions were used for both flow domains (the PF and SM). The upslope face of the experimental trench was modeled as a seepage face with an effective height of 55 cm (see Fig. 2), permitting water to discharge under saturated conditions only (i.e., for local pressure head values of $h \geq 0$). At the bottom boundary, at the depth of 3 m, a free drainage condition was imposed, allowing water to leave the 2D domain at a rate equal to the unsaturated hydraulic conductivity. At the vertical upslope and downslope sides of the computational domain, no-flow and seepage-face boundary conditions, respectively, were prescribed. The 2D flow domain was discretized into 283,113 triangular elements. The

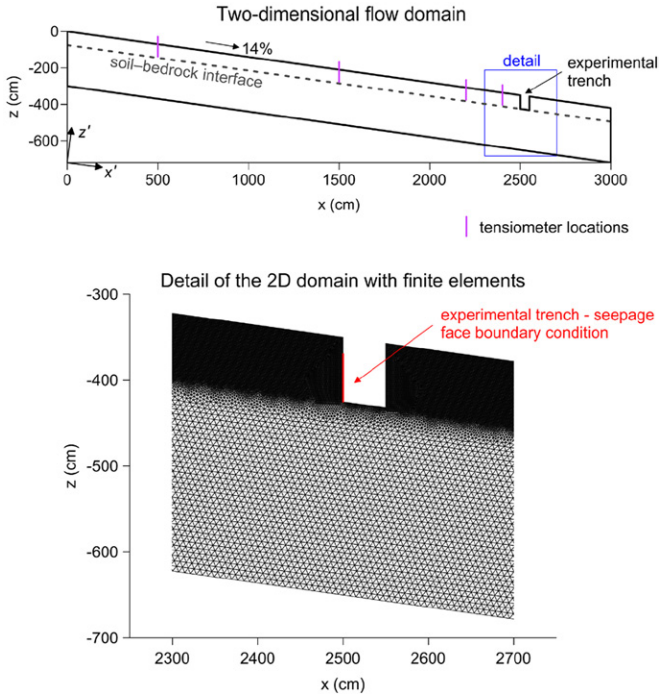

Fig. 2. Two-dimensional (2D) flow domain with the detail of the finite element mesh. The directions of the principal axes x' and z' of the anisotropic hydraulic conductivity tensor **K** are indicated at the origin of the coordinate system.

finite element mesh was refined at the expected high-flow regions, i.e., in the soil profile above the soil–bedrock interface and near the experimental trench.

Soil Hydraulic Properties

The same soil hydraulic properties were used for both the 1D VertFlow model and the 2D model, except for the anisotropy of the hydraulic conductivity tensor. The soil hydraulic characteristics of the soil and bedrock matrices as well as the PF domain were parameterized using a modified van Genuchten model (Vogel and Cislerova, 1988). The modified expressions add extra flexibility in the description of the hydraulic properties near saturation by introducing a nonzero air-entry pressure head value h_s (m). It was shown that the modified approach provides more adequate prediction of the unsaturated hydraulic conductivity function and improves the stability of the numerical solution of Richards' equation for soils with low values of the parameter n (less than about 1.5) (Vogel et al., 2000b).

Soil hydraulic parameters of the respective soil and bedrock layers are given in Table 1. For the 2D approach, the anisotropy ratio for the hydraulic conductivity tensor of the PF domain was set equal to $K_{x'x'}/K_{z'z'} = 10$ above the soil–bedrock interface, indicating the increased conductivity of preferential pathways along the local hillslope gradient. The increased lateral conductivity was assumed to represent the PF continuum formed by pathways along tree roots and biopores as well as the lateral soil structural features. This is consistent with the value of K_D used for the lateral flow component of the 1D model (as explained below). Based on the available information from a regional hydrogeological survey, the saturated hydraulic conductivity of the weathered bedrock was estimated to be 0.4 cm d^{-1}, with the exception of the upper 5-cm layer (at the depth of 70–75 cm), which was assigned a higher hydraulic conductivity value (1.3 cm d^{-1}) determined by disk infiltrometer.

The water transfer coefficient governing the exchange of water between the SM and PF domains as well as the volumetric proportion of the PF domain were set according to Vogel et al. (2010b). The volumetric fraction of the PF domain, w_f, was assumed to vary linearly between 0.07 at the soil surface and 0.05 at the depth of 75 cm. The values of α_{ws} were also estimated to vary linearly between the soil surface and the lower boundary, i.e., between 1 and 0.01 cm^{-1} d^{-1}, which corresponds to a decreasing value of saturated hydraulic conductivity of the SM domain. Higher α_{ws} values lead to less preferential flow conditions, causing faster equilibration of the pressure heads between the SM and PF domains. Such conditions were assumed to prevail in the topsoil horizon. The domains hydraulically communicate, i.e., exchange soil water, mostly under near-saturated conditions. Under dry conditions, they become effectively disconnected due to low interfacial conductivity (at the SM–PF domain interface). More details regarding the parameterization of the soil hydraulic properties of the SM and PF domains at Tomsovka can be found elsewhere (Dohnal et al., 2006a, 2012).

The parameters of the diffusion wave LatFlow model (Θ and K_D) were taken from our previous studies (Dusek et al., 2012a, 2012b), in which the sensitivity of input parameter values was evaluated. The following parameter values were used: the effective porosity $\Theta = 0.005$ cm^3 cm^{-3} and the effective hydraulic conductivity $K_D = 2500$ cm d^{-1}.

The 1D and 2D modeling approaches can be directly compared only if similar soil hydraulic properties are used in both. The properties used to characterize the flow domains in the 1D VertFlow model and in the upper part of the 2D model (to the depth of 75 cm) were identical in respect to the vertical direction (see Table 1). In the 2D model, the anisotropy of hydraulic conductivity $K_{x'x'}/K_{z'z'} = 10$ had to be considered to comply with the effective hydraulic conductivity used in the 1D LatFlow model, $K_D = 2500$ cm d^{-1} (i.e., to account for the increased conductivity of the laterally continuous network of preferential pathways). The anisotropy ratio was estimated using the following approximate formula (sufficiently accurate for small angles between z and z'):

$$\frac{K_{x'x'}}{K_{z'z'}} = \frac{K_D}{w_f K_{sf}} \quad [11]$$

where K_{sf} is the saturated hydraulic conductivity of the PF domain in the vertical direction, $w_f = 0.05$, and $K_{sf} = 5000$ cm d^{-1} (Table

1). The upper limit of the effective porosity Θ for the LatFlow model can be estimated as $\Theta^* = w_f \theta_{sf}$, where θ_{sf} is the saturated soil water content of the PF domain. It is important to note that the LatFlow model exclusively represents flow in the PF domain, so the porosity of the SM domain does not contribute to Θ. Under dynamic conditions (such as in our study), the value of the effective porosity is a fraction of Θ* (e.g., Neuman, 1987). Furthermore, a smaller value of the effective porosity for the LatFlow model can be justified by an imperfect connectivity of preferential pathways along the hillslope.

Numerical Simulations

Numerical simulations of soil water movement in the hillslope segment were performed for three growing seasons (2007, 2008, and 2009). Figure 3 shows the hillslope discharge observed in the two trench sections (A and B) at the Tomsovka experimental site. The two modeling approaches considered (1D and 2D) were subsequently used to simulate subsurface flow during the three growing seasons.

Hillslope discharge data resulting from the two modeling approaches were analyzed separately for each of the selected rainfall–runoff episodes (labeled in Fig. 3). In our previous study (Dusek et al., 2012a), Nash–Sutcliffe coefficients were used to evaluate the agreement between measured and modeled discharge hydrographs predicted by the 1D approach. In the present study, we compared the two modeling approaches in terms of three ratios calculated for: (i) volume of hillslope discharge, (ii) peak value of hillslope discharge, and (iii) centroid time of the discharged volume. The two approaches were also compared using a mutual correlation coefficient. Furthermore, the correlation coefficient and root mean square error (RMSE) were used to compare the model predictions and experimental data.

A simple sensitivity analysis was performed for a selected period (May–June 2009) to evaluate the impact of the PF domain anisotropy, $K_{x'x'}/K_{z'z'}$, and the sensitivity of the 2D model predictions with respect to the magnitude of the saturated hydraulic conductivity of the bedrock matrix—both highly uncertain input parameters. In addition, special attention was paid to the influence of geometric and boundary conditions near the trench.

Depending on the atmospheric boundary condition imposed during the growing season, the computing time of the 2D simulations ranged from 187 to 235 h (Intel Itanium2 1.5 GHz, 4 GB RAM). In contrast, the 1D approach required about 1 min to complete the simulation of one growing season.

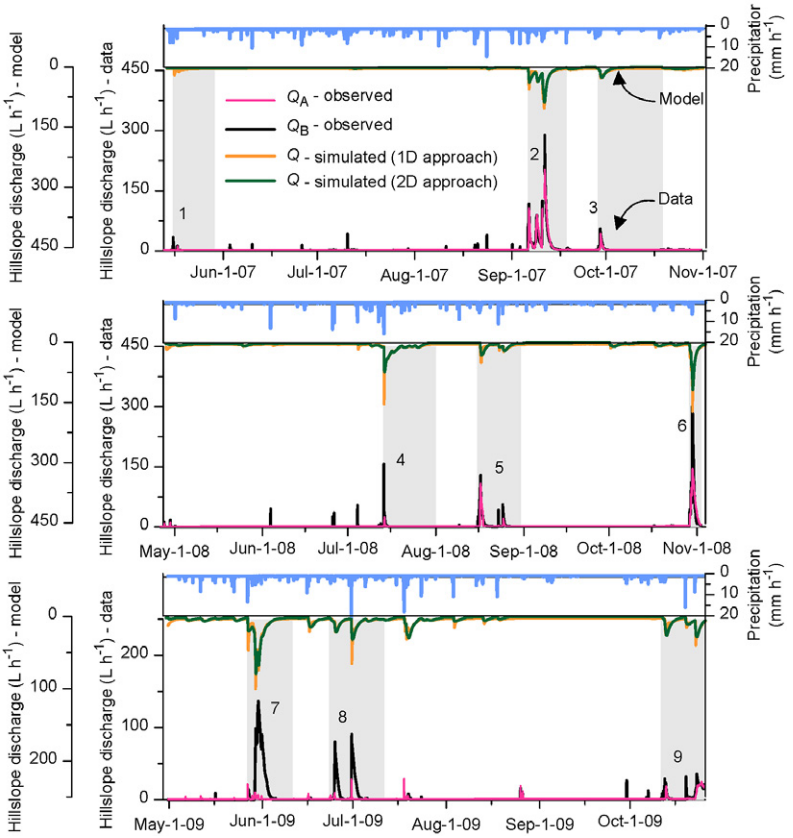

Fig. 3. Observed (Trench Sections A and B) and simulated (using the one- [1D] and two-dimensional [2D] approaches) hillslope discharge during three growing seasons. The selected major rainfall–runoff episodes are labeled with numbers and shown in shaded bars. Lower discharge in Trench Section A in 2009 was probably related to a malfunction of the flow gauge. The scales for observed and simulated hillslope discharges are reversed.

Results and Discussion

Hillslope Discharge

Variations of hillslope discharge during the period of three consecutive growing seasons, simulated by the two modeling approaches (1D and 2D), are shown in Fig. 3. Overall, both modeling approaches captured the shallow stormflow dynamics of the major rainfall–runoff episodes. For some episodes (e.g., Episodes 2 and 8), the simulated hillslope discharge was smaller than the observed discharge. This can be partly explained by the decision to choose the length of the contributing hillslope segment at the lower end of the previously estimated range (25–50 m; Dusek et al., 2012a).

Three rainfall–runoff episodes (6, 7, and 8) were selected for detailed graphical comparison between the simulated hillslope discharge and measured subsurface runoff from the experimental trench (Fig. 4). It can be seen that the simulated hillslope discharge peaks compare relatively well with the measured ones in terms of timing and to a lesser extent also magnitude. The predicted rising limbs of the hillslope discharge hydrographs were delayed by 1 to 5 h compared with the measured hydrographs. The simulated discharge peaks were mostly smaller than those

measured, reaching from 25 to 72% of the measured peaks for Episodes 6, 7, and 8. Both model approaches resulted in similar but not identical responses to rainfall. Steeper rising and falling limbs of the hillslope discharge hydrograph were obtained with the 1D approach, i.e., the 1D approach predicted fast reactions (on the order of hours) to both the beginning and cessation of a rainfall event than did the 2D approach. A few temporal details of the measured discharge hydrographs (29–31 Oct. 2008) were better reproduced with the 1D approach (Fig. 4a).

Hillslope discharges simulated by the two modeling approaches (1D and 2D) were compared for all selected major rainfall–runoff episodes in Table 2. The volume of hillslope discharge predicted by the 2D approach was higher than that predicted by the 1D approach for all selected episodes. The peak discharges were mostly underpredicted by the 2D approach compared with those simulated by the 1D approach (see also Fig. 3). The position of the discharged volume of a given episode (centroid time) showed no pronounced differences between the 1D and 2D predictions. The correlation coefficient suggested a good agreement between the 1D and 2D predictions, except for Episode 5. The 2D approach predicted zero discharge for Episode 1, which was caused by the effect of the initial condition (water initially stored in the soil profile percolated into the bedrock).

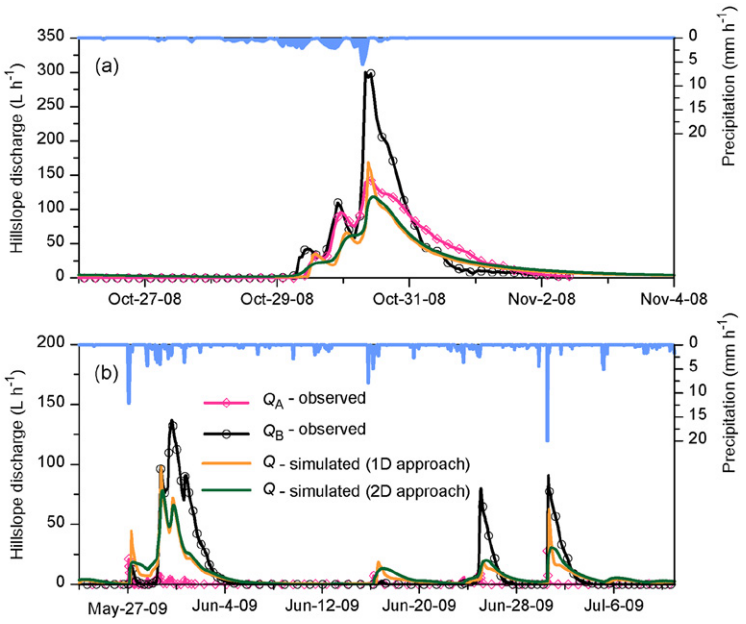

Fig. 4. Observed and simulated hillslope discharge during rainfall episodes in (a) October 2008 (Episode 6) and (b) May to July 2009 (Episodes 7 and 8). The predicted subsurface runoff, Q, was simulated using the one- (1D) and two-dimensional (2D) approaches.

The correlation coefficients and RMSEs comparing the model predictions with the hillslope discharge data are shown in Table 2. For two out of nine episodes (i.e., 1 and 4), both models performed poorly in discharge predictions, with correlation coefficients <0.5. These episodes were characterized by a relatively small measured runoff volume (<0.6 m^3, i.e., <6-mm runoff height) and were previously found to be better approximated using a shorter contributing hillslope length than 25 m (Dusek et al., 2012a). The 2D approach failed to predict Episode 5 (correlation coefficient <0.5). The average correlation coefficients for the seven major runoff episodes (i.e., 2, 3, 5, 6, 7, 8, and 9) using the 1D and 2D approaches were 0.778 and 0.731, respectively, indicating reasonable agreement between the observed and predicted hillslope discharge. The range of the

Table 2. Comparison of simulated hillslope discharge evaluated for selected rainfall–runoff episodes using the one- (1D) and two-dimensional (2D) modeling approaches. Dimensionless ratios are presented for the volume of hillslope discharge, the peak value of hillslope discharge, and the centroid time of discharged volume. The 1D and 2D predictions were evaluated using correlation coefficients and root mean square errors (RMSEs). The runoff difference between Trench Sections A and B was assessed using the RMSE. Correlation coefficient and RMSE values for model-data comparison are shown separately for Trench Sections A and B (divided by a semicolon).

Episode	Ratio (2D/1D) of discharged volume	Ratio (2D/1D) of peak discharge	Ratio (2D/1D) of centroid time	Correlation coefficient (1D–2D)	Correlation coefficient (1D–data)	Correlation coefficient (2D–data)	RMSE (A–B)	RMSE (1D–data)	RMSE (2D–data)
							L h^{-1}		
1 (15–29 May 2007)	0†	0†	0†	–	0.027; 0.030	–	3.171	3.158; 4.140	–
2 (6–18 Sept. 2007)	1.15	0.87	0.98	0.962	0.934; 0.879	0.918; 0.866	13.295	26.435; 31.051	25.357; 29.983
3 (28 Sept.–19 Oct. 2007)	1.12	1.11	0.84	0.980	0.674; 0.645	0.644; 0.657	3.821	4.234; 5.663	5.353; 5.633
4 (13–31 July 2008)	1.12	0.48	1.53	0.919	0.446; 0.344	0.456; 0.355	8.731	17.967; 17.581	18.243; 17.806
5 (15–30 Aug. 2008)	1.29	0.66	0.87	0.767	0.797; 0.594	0.491; 0.345	10.657	12.072; 16.223	15.363; 18.316
6 (29 Oct.–4 Nov. 2008)	1.05	0.70	1.05	0.976	0.928; 0.929	0.963; 0.922	39.565	21.253; 47.975	19.178; 49.935
7 (27 May 27–10 June 2009)	1.08	0.67	1.00	0.977	0.319; 0.871	0.314; 0.886	41.948	22.198; 23.896	22.678; 23.220
8 (23 June–11 July 2009)	1.24	0.49	1.02	0.852	0.035; 0.788	0.058; 0.900	20.647	8.949; 14.581	9.783; 13.276
9 (11 Oct.–7 Nov. 2009)	1.24	0.74	0.85	0.913	0.617; 0.683	0.550; 0.629	5.640	6.937; 6.489	9.063; 7.816

† Zero discharge predicted by the 2D approach.

correlation coefficients for the seven major episodes was 0.345 to 0.963 (Table 2). These episodes were the most significant episodes observed within the three simulated growing seasons, each characterized by at least 0.9 m^3 (9 mm) of runoff volume, with continuous discharge lasting >3 d. Low correlation coefficients for Episodes 7 and 8 (2009 growing season) could have been caused by a tipping bucket malfunction.

The RMSE was also used to evaluate the observation uncertainty (discussed above), reflected in the differences between the observed discharges of Sections A and B (Table 2). It can be seen that the RMSE (A – B) values are of a similar magnitude as the RMSEs that compare the model predictions and hillslope discharge data. For Episodes 7 and 8, the RMSE (A – B) values are larger than the model-data RMSEs.

In Table 3, measured hillslope discharge volumes for the three growing seasons are compared with those simulated with the 1D and 2D approaches. The 2D approach predicted a larger volume of hillslope discharge than did the 1D approach. For the 2009 season, the observation uncertainty, reflected in the differences between the measured discharges of Sections A and B (possibly caused by a malfunction of the flow gauge in Trench Section A) is much larger than the modeling uncertainty, reflected in differences between the 1D and 2D approaches.

Table 3. Volume of hillslope discharge (m^3) measured (in Trench Sections A and B) and simulated by the one- (1D) and two-dimensional (2D) approaches. For the 2D approach, the contribution of the soil matrix to hillslope discharge (m^3) is shown in parenthesis. Low discharge volume in Trench Section A in 2009 was probably related to a malfunction of the flow gauge.

	Hillslope discharge			
	Measured in Trench Section			
Growing season	A	B	1D approach	2D approach
	m^3			
2007	7.86	8.73	6.04	7.74 (0.121)
2008	6.87	9.39	10.89	12.51 (0.188)
2009	1.82	14.18	9.58	11.59 (0.132)

Soil Water Pressure

Figure 5 shows the observed and simulated soil water pressure heads at three depths and horizontal distances above the experimental trench. Obviously, for the 1D approach, the lateral distribution of pressure heads in the hillslope segment could not be considered because only the "effective" vertical flow was simulated (independently of the horizontal position). The 2D approach, on the contrary, took into account the horizontal tensiometer positions above the trench. The 1D-simulated soil water pressure heads suggested drier conditions during the three presented seasons than both the 2D-simulated and observed values. This can be explained by the fact that the 1D approach neglected the effect of the development of a saturated layer above the soil–bedrock interface on vertical flow. This effect was more pronounced near the trench (Fig. 5a).

The agreement between soil water pressure heads alternatively predicted by the 1D and 2D approaches was better under near-saturated conditions (i.e., during and soon after rainfall events). Simulated pressure heads at deeper locations (e.g., at 51 cm below the soil surface, as shown in Fig. 5b) were affected by both different hydraulic conditions at the soil–bedrock interface in the two modeling approaches and the absence of backward coupling between the VertFlow and LatFlow models. The model predictions of soil water pressure were also compared quantitatively using RMSE values. For a 1-m distance above the trench (Fig. 5a), the calculated RMSE values were 87.8 and 31.6 cm for the 1D and 2D approaches, respectively. The RMSE values were 53.0 and 81.7 cm for the 1D and 2D approaches, respectively, at a 3-m distance from the trench (Fig. 5c). A dry period in September 2009 was better approximated using the 1D approach, which led to smaller RMSEs for the entire growing season compared with the 2D simulation. The 2D predictions lay near the observed soil water pressure for the remaining parts of the 2009 season, characterized by more saturated conditions (Fig. 5c). For the 10-m distance

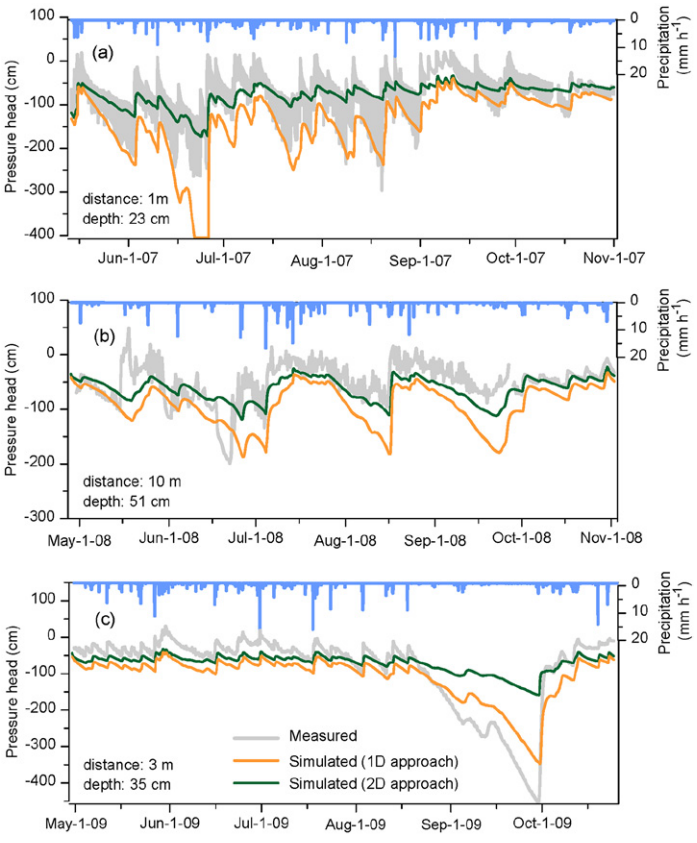

Fig. 5. Time series of soil water pressure heads at three depths: (a) 1 m, (b) 10 m, and (c) 3 m above the trench during growing seasons 2007, 2008, and 2009. Comparison of data with simulated values obtained with the one-dimensional (1D) dual-continuum model (VertFlow) and two-dimensional (2D) dual-continuum model (S2D) for the soil matrix domain. The shaded area in (a) represents the envelope of the available tensiometric data. The gray lines in (b) and (c) represent single sensors.

(Fig. 5b), the RMSE values were 54.6 and 33.1 cm for the 1D and 2D approaches, respectively. Overall, a closer agreement between the observed and simulated pressure heads at the three upslope locations above the trench was obtained with the 2D model.

The predicted soil water pressure heads on the base of the upslope face of the experimental trench indicated that near-saturated conditions were maintained during the three growing seasons (Fig. 6). With the exception of dry periods in 2007 (June) and 2009 (September), the soil water pressure heads in the SM domain remain higher than −40 cm, despite the fact that only three significant rainfall–runoff episodes occurred in each season. The near-saturated conditions in the vicinity of the vertical soil–air interface can be explained by the presence of hydraulic resistance (represented by the seepage-face boundary condition), which allows discharge of water only when local saturation is reached, i.e., the soil water pressure exceeds the atmospheric pressure ($h \geq 0$).

Two-Dimensional Cross-Sections

The two-dimensional fields of pressure head in the SM and PF domains during the rainfall–runoff Episode 2 are shown in Fig. 7, together with the intensity of the interdomain soil water transfer Γ_w. The figure clearly shows the presence of the perched saturated layer in both pore domains above the soil–bedrock interface. It also illustrates the development of a saturated layer below the soil–bedrock interface. Predicted pressure heads near the trench suggest saturated conditions at the upslope face of the trench as well as at the bottom of the trench. This indicates possible trench underflow; however, the water fluxes below the soil–bedrock interface were negligible ($q \approx 0.5$ cm d^{-1}) due to the low hydraulic conductivity of the bedrock (Fig. 8).

The mostly negative soil water transfer rates above the soil–bedrock interface reveal that flow was directed from the SM to PF domains (Fig. 7c). This can be explained by the pressure buildup in the SM domain, caused by the low conductivity of the bedrock and the fact that water from the PF domain was drained by the lateral flow. An intensive water transfer from the SM to PF domains took place also near the soil surface, caused by a higher value of α_{ws} for the topsoil than deeper soil horizons. This also led to a faster interdomain equilibration after the cessation of rainfall events. At the time depicted in Fig. 7, no water transfer was predicted in the middle of the soil profile (about 20–50-cm depth), suggesting equilibrium between the flow domains. However, water transfer in this part of the soil profile was directed from the PF to SM domains during the initial phases of major rainfall events. This was caused by the deeper position of the infiltrating water front in the PF domain than the SM domain.

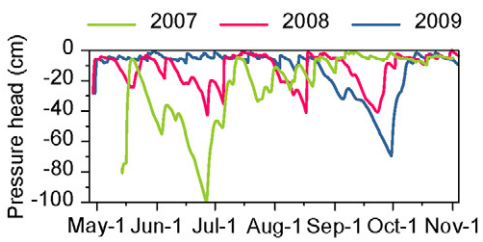

Fig. 6. Simulated soil water pressure heads on the base of the upslope face of the trench during growing seasons 2007, 2008, and 2009. The values were obtained using the two-dimensional dual-continuum model (S2D) for the soil matrix domain, averaged across the 10-cm-high upslope trench face.

The two-dimensional spatial detail of water fluxes in the SM and PF domains during the rainfall–runoff episode in September 2007 is depicted in Fig. 8. It can be seen that the lateral flow component became dominant with increasing depth toward the soil–bedrock interface. In the underlying bedrock, the dominant movement was vertical. The lateral intensities in the PF domain were about 200 times higher than those in the SM domain. The lateral matrix flow would become important in situations when the conductivity and/or connectivity of the lateral preferential pathways is low (which was not our case). Noticeable lateral flow was also predicted in the SM domain near the soil surface; this flow was in fact more intense than that above the soil–bedrock interface (Fig. 8b). This was caused by the sharp decrease in the saturated conductivities between the first and second soil layers (see Table 1).

Sensitivity of Soil Anisotropy and Bedrock Conductivity

The results of the sensitivity analysis performed for the 2D model (involving sensitivities with respect to the degree of soil anisotropy and to the magnitude of the saturated hydraulic conductivity of

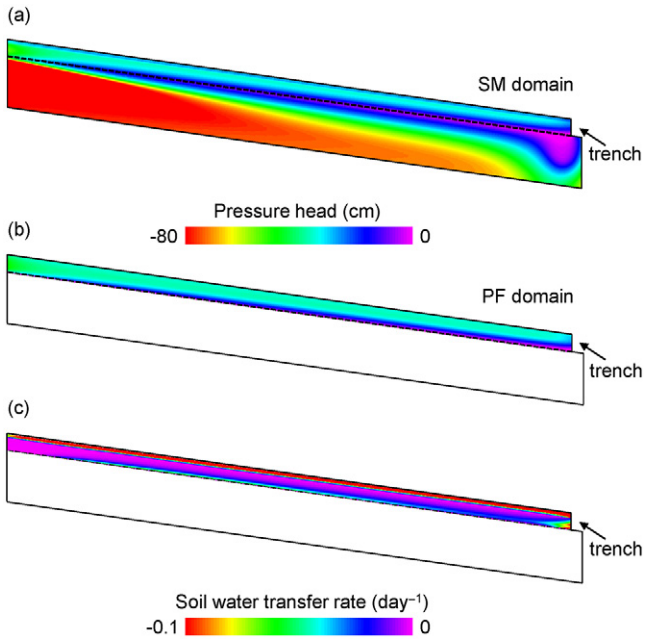

Fig. 7. Vertical cross-sectional distribution of: (a) soil water pressure heads in the soil matrix (SM) domain, (b) soil water pressure heads in the preferential flow (PF) domain, and (c) intensity of soil water transfer Γ_w obtained with the two-dimensional dual-continuum model (rainfall–runoff Episode 2 observed in September 2007). The hillslope segment is 25 m long. The dashed line represents the soil–bedrock interface.

the bedrock) are illustrated in Fig. 9. The figure shows the hillslope discharge hydrographs resulting from the 2D simulations in which the default values of $K_{x'x'}/K_{z'z'} = 10$ and $K_s = 0.4$ cm d^{-1} were subsequently replaced by lower and higher estimates. As seen in Fig. 9a and 9b, the anisotropy factor as well as the K_s value of the bedrock influenced the discharge in terms of both timing and peak values. As expected, a greater value of the anisotropy factor led to a faster and more intense response to rainfall events (Fig. 9a). A larger K_s value of the bedrock resulted in a smaller discharge peak and smaller total discharged volume (Fig. 9b). This simple sensitivity analysis highlights the need to carefully estimate the hydraulic properties of the porous medium in the vicinity of the soil–bedrock interface. The results furthermore suggest that the mobility of water involved in saturated downhill flow is determined by the hydraulic properties of the porous medium above the flow-impeding interface as well as the hydraulic properties of the bedrock.

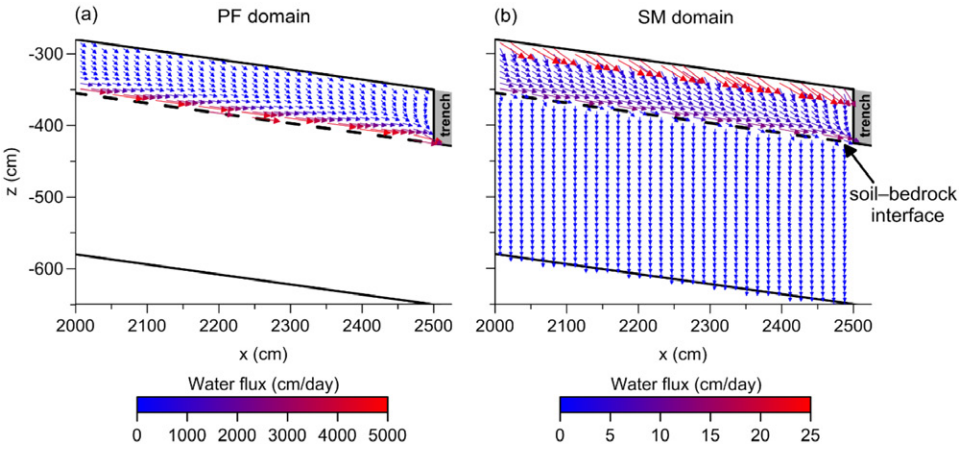

Fig. 8. Vertical distribution of water flux vectors in: (a) the preferential flow (PF) domain and (b) the soil matrix (SM) domain obtained with the two-dimensional dual-continuum model. The hillslope segment 5 m above the trench during a rainfall–runoff episode in September 2007 (Episode 2) is shown. The magnitude of Darcian fluxes is indicated by color coding.

Flow Separation at the Interface

The comparison of the simplified 1D modeling approach with the more rigorous 2D formulation confirms the validity of the flow separation mechanism at the soil–bedrock interface assumed in the 1D model (Fig. 1). The SM domain fluxes contributed to hillslope discharge negligibly (see Table 3 and Fig. 8). The fact that the PF domain soil water fluxes were highly correlated with the observed hillslope discharge (Table 2) indicates that the assumed water-separation mechanism at the soil–bedrock interface is realistic. The assumed separation mechanism is also supported by field observations indicating that the effective preferential pathways at Tomsovka do not extend below the lower boundary of the soil profile (Sanda and Cislerova, 2009). The vertical cross-section of the water transfer rate (Fig. 7c) suggests that the soil matrix is draining episodically into the PF domain above the soil–bedrock interface. Water drained to the network of preferential pathways near the interface triggers saturated flow along the slope, which is the principal mechanism of storm-flow generation at our experimental site.

In general, the flow separation mechanism at the soil–bedrock interface is highly site specific. While our 2D simulations confirmed nearly impervious bedrock at the Tomsovka site (similarly to the sites described, e.g., by Kendall et al. [2001] or Gerwin et al. [2009]), different conditions can be found elsewhere. For instance, Tromp-van Meerveld et al. (2007) questioned an assumption of bedrock impermeability at the Panola Mountain Research Watershed (based on sprinkling experiments). As the deep percolation through bedrock accounted for >90% of the applied water, they concluded that the soil hydraulic properties of the bedrock were of major importance for the formation of shallow subsurface runoff and thus the overall response of the catchment to rainfall. On the same experimental site, the numerical study of Tromp-van Meerveld and Weiler (2008) further confirmed that adequate prediction of long-term water balance in the simulated hillslope segment could only be obtained when the inclusion of bedrock leakage was accounted for.

Main Differences between the One- and Two-Dimensional Approaches

The different dimensionality assumed for the 1D and 2D approaches induces different shapes of the flow paths. The flow

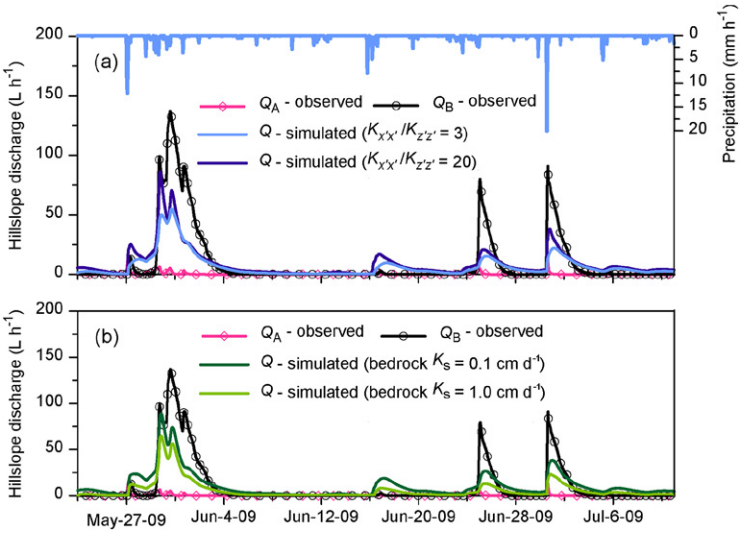

Fig. 9. Sensitivity of the hillslope discharge rates in Trench Sections A and B, Q_A and Q_B, simulated using the two-dimensional approach (Episodes 7 and 8): (a) the effect of the anisotropy of the preferential flow domain hydraulic conductivity ($K_{x'x'}/K_{z'z'}$) and (b) the effect of the saturated hydraulic conductivity K_s of the bedrock.

direction in the 1D approach is vertical and then abruptly turns to follow the local gradient of the soil–bedrock interface, while in the 2D approach the flux vectors are inclined and change continuously to the downslope direction (see Fig. 8). The main differences between the 1D and 2D modeling approaches, in addition to different flow paths, are related to the issues of hydraulic coupling between vertical and lateral flow, the flow separation at the soil–bedrock interface, and the correspondence between the effective parameters of the 1D saturated lateral flow domain (Θ and K_D) and the more physically realistic properties of the 2D variably saturated flow domains (θ_{sf}, θ_{sm}, $\mathbf{K}_{sf}$, and $\mathbf{K}_{sm}$), the first mentioned difference (hydraulic coupling) probably being the most important. There are two opposite effects on hillslope runoff caused by the absence of backward coupling in the 1D approach: (i) overestimation of the depth of the unsaturated zone, resulting in longer vertical travel times, and (ii) underestimation of the saturated storage in the soil matrix, leading to reduction of the hillslope retention capacity. The absence of a backward coupling mechanism prevents the application of the 1D approach in situations where the saturated zone occupies the entire depth of the soil profile (or nearly so) and, of course, this approach cannot be used to simulate exfiltration.

Spatial Heterogeneity

In the present study, we considered a homogeneously layered soil profile. Moreover, spatially heterogeneous hydraulic properties of the bedrock and variable bedrock topography were not taken into account (neither in the 1D nor in the 2D approach). In general, the spatial heterogeneity of soil hydraulic properties can be introduced into the 2D flow model, e.g., by means of stochastically generated 2D fields of scaling factors (Vogel, 2001; Taskinen et al., 2008). The effect of soil spatial heterogeneity on subsurface runoff dynamics could then be studied by multiple forward simulations. For the 1D approach, the recharge rates for the diffusion wave model predicted by the vertical model would differ along the hillslope length as a result of a laterally heterogeneous soil profile.

Summary and Conclusions

Two alternative modeling approaches, the simplified 1D approach combining vertical soil water flow with shallow saturated lateral flow and the fully integrated 2D approach, were used to simulate the formation of subsurface runoff in a hillslope segment. Both approaches involved a preferential flow component based on the dual-continuum formulation. The simulations based on either of the two models yielded a reasonably good agreement between simulated and measured hillslope discharges. The rainfall–runoff episodes characterized by larger discharge volumes were modeled with greater success than the episodes with smaller runoff volumes. This was probably caused by an unaccounted-for spatial variability of preferential pathways in the modeling approach leading to different activation thresholds for preferential flow responses to rainfall events of different magnitudes.

The 1D model predicted short-term runoff peaks with rapidly falling hydrograph limbs, while the 2D model simulated more continuous rising and falling limbs of the discharge hydrographs. The overall volume of hillslope discharge predicted using the 2D model was consistently larger and the peak discharges were smaller than those simulated with the 1D model. The 2D model showed a closer agreement between simulated and observed pressure heads due to a more realistic representation of the hydraulic conditions above the soil–bedrock interface. Both approaches were found useful for studying soil water dynamics in a hillslope segment.

The results of the sensitivity analysis suggested that the mobility of water involved in saturated downhill flow was determined by the hydraulic properties of porous media above as well as below the flow-impeding soil–bedrock interface. This highlighted the importance of careful experimental determination of the hydraulic properties on both sides of the interface. The 2D modeling confirmed the hypothesis that the contribution of the soil matrix flow to hillslope discharge was negligible, i.e., that nearly all hillslope discharge was supplied by the preferential pathways. This also corroborated the principal assumption made for the 1D approach that the lateral flow component was dominated by preferential flow.

The simplified 1D model, based on the combination of 1D vertical two-domain flow and 1D preferential lateral flow, was found to provide a useful approximation of the more complex 2D system. While the 1D approach is, in general, less flexible in terms of the geometric, material, and boundary conditions to which it can be applied, the numerical simulations performed in this study confirmed that it is far more efficient in terms of computing time. Excessive computing power would be necessary to simulate the soil water dynamics when using the 2D two-domain Richards' equation model for hillslopes longer than several tens of meters.

Acknowledgments

The study was supported by the Czech Science Foundation (Project no. 205/08/1174). The Supercomputing Center of CTU in Prague is gratefully acknowledged for the possibility of running the 2D simulations on its computer network.

References

Anderson, A.E., M. Weiler, Y. Alila, and R.O. Hudson. 2010. Piezometric response in zones of a watershed with lateral preferential flow as a first-order control on subsurface flow. Hydrol. Processes 24:2237–2247. doi:10.1002/hyp.7662

Beckers, J., and Y. Alila. 2004. A model of rapid preferential hillslope runoff contributions to peak flow generation in a temperate rain forest watershed. Water Resour. Res. 40:W03501. doi:10.1029/2003WR002582

Boussinesq, J. 1877. Essai sur la théorie des eaux courantes. Mem. Acad. Sci. Inst. Fr. 23:1–680.

Buttle, J.M., and D.J. McDonald. 2002. Coupled vertical and lateral preferential flow on a forested slope. Water Resour. Res. 38(5). doi:10.1029/2001WR000773

Dohnal, M., J. Dusek, and T. Vogel. 2006a. The impact of the retention curve hysteresis on prediction of soil water dynamics. J. Hydrol. Hydromech. 54:258–268.

Dohnal, M., J. Dusek, T. Vogel, J. Herza, and P. Tacheci. 2006b. Analysis of soil water response to grass transpiration. Soil Water Res. 1:85–98.

Dohnal, M., T. Vogel, M. Sanda, and V. Jelinkova. 2012. Uncertainty analysis of a dual-continuum model used to simulate subsurface

hillslope runoff involving oxygen-18 as natural tracer. J. Hydrol. Hydromech. 60:194–205. doi:10.2478/v10098-012-0017-0

Dusek, J., T. Vogel, M. Dohnal, and H.H. Gerke. 2012a. Combining dual-continuum approach with diffusion wave model to include a preferential flow component in hillslope scale modeling of shallow subsurface runoff. Adv. Water Resour. 44:113–125. doi:10.1016/j.advwatres.2012.05.006

Dusek, J., T. Vogel, and M. Sanda. 2012b. Hillslope hydrograph analysis using synthetic and natural oxygen-18 signatures. J. Hydrol. 475:415–427. doi:10.1016/j.jhydrol.2012.10.025

Faeh, A.O., S. Scherrer, and F. Naef. 1997. A combined field and numerical approach to investigate flow processes in natural macroporous soils under extreme precipitation. Hydrol. Earth Syst. Sci. 1:787–800. doi:10.5194/hess-1-787-1997

Fan, Y., and R. Bras. 1998. Analytical solutions to hillslope subsurface storm flow and saturation overland flow. Water Resour. Res. 34:921–927. doi:10.1029/97WR03516

Feddes, R.A., P.J. Kowalik, and H. Zaradny. 1978. Simulation of field water use and crop yield. PUDOC, Wageningen, the Netherlands.

Freer, J., J. McDonnell, K. Beven, N. Peters, D. Burns, R. Hooper, et al. 2002. The role of bedrock topography on subsurface storm flow. Water Resour. Res. 38(12):1269. doi:10.1029/2001WR000872

Gerke, H.H., J. Dusek, and T. Vogel. 2013. Solute mass transfer effects in two-dimensional dual-permeability modeling of bromide leaching from a tile-drained field. Vadose Zone J. 12(2). doi:10.2136/vzj2012.0091

Gerke, H.H., and M.Th. van Genuchten. 1993a. A dual-porosity model for simulating the preferential movement of water and solutes in structured porous media. Water Resour. Res. 29:305–319. doi:10.1029/92WR02339

Gerke, H.H., and M.Th. van Genuchten. 1993b. Evaluation of a first-order water transfer term for variably saturated dual-porosity models. Water Resour. Res. 29:1225–1238. doi:10.1029/92WR02467

Gerwin, W., W. Schaaf, D. Biemelt, A. Fischer, S. Winter, and R.F. Hüttl. 2009. The artificial catchment "Chicken Creek" (Lusatia, Germany): A landscape laboratory for interdisciplinary studies of initial ecosystem development. Ecol. Eng. 35:1786–1796. doi:10.1016/j.ecoleng.2009.09.003

Heppell, C.M., T.P. Burt, and R.J. Williams. 2000. Variations in the hydrology of an underdrained clay hillslope. J. Hydrol. 227:236–256. doi:10.1016/S0022-1694(99)00189-4

Hilberts, A.G.J., P.A. Troch, C. Paniconi, and J. Boll. 2007. Low-dimensional modeling of hillslope subsurface flow: Relationship between rainfall, recharge, and unsaturated storage dynamics. Water Resour. Res. 43:W03445. doi:10.1029/2006WR004964

Hopp, L., C. Harman, S.L.E. Desilets, C.B. Graham, J.J. McDonnell, and P.A. Troch. 2009. Hillslope hydrology under glass: Confronting fundamental questions of soil–water–biota co-evolution at Biosphere 2. Hydrol. Earth Syst. Sci. 13:2105–2118. doi:10.5194/hess-13-2105-2009

Kendall, C., J.J. McDonnell, and W. Gu. 2001. A look inside 'black box' hydrograph separation models: A study at the Hydrohill catchment. Hydrol. Processes 15:1877–1902. doi:10.1002/hyp.245

Klaus, J., and E. Zehe. 2010. Modelling rapid flow response of a tile-drained field site using a 2D physically based model: Assessment of 'equifinal' model setups. Hydrol. Processes 24:1595–1609. doi:10.1002/hyp.7687

Mirus, B.B., and K. Loague. 2013. How runoff begins (and ends): Characterizing hydrologic response at the catchment scale. Water Resour. Res. 49:2987–3006. doi:10.1002/wrcr.20218

Monteith, J.L. 1981. Evaporation and surface temperature. Q. J. R. Meteorol. Soc. 107:1–27. doi:10.1002/qj.49710745102

Neuman, S.P. 1987. On methods of determining specific yield. Ground Water 25:679–684. doi:10.1111/j.1745-6584.1987.tb02208.x

Nieber, J.L., and R.C. Sidle. 2010. How do disconnected macropores in sloping soils facilitate preferential flow? Hydrol. Processes 24:1582–1594. doi:10.1002/hyp.7633

Paniconi, C., P.A. Troch, E.E. van Loon, and A.G.J. Hilberts. 2003. Hillslope-storage Boussinesq model for subsurface flow and variable source areas along complex hillslopes: 2. Intercomparison with a three-dimensional Richards equation model. Water Resour. Res. 39:1317. doi:10.1029/2002WR001730

Rigon, R., G. Bertoldi, and T.M. Over. 2006. GEOtop: A distributed hydrological model with coupled water and energy budgets. J. Hydrometeorol. 7:371–388. doi:10.1175/JHM497.1

Sanda, M., and M. Cislerova. 2009. Transforming hydrographs in the hillslope subsurface. J. Hydrol. Hydromech. 57:264–275. doi:10.2478/v10098-009-0023-z

Sidle, R.C., S. Noguchi, Y. Tsuboyama, and K. Laursen. 2001. A conceptual model of preferential flow systems in forested hillslopes: Evidence of self-organization. Hydrol. Processes 15:1675–1692. doi:10.1002/hyp.233

Sloan, P.G., and I.D. Moore. 1984. Modeling subsurface stormflow on steeply sloping forested watersheds. Water Resour. Res. 20:1815–1822. doi:10.1029/WR020i012p01815

Tacheci, P. 2002. Hydrological regime of the small mountainous catchment and the assessment of the effects of the change of the vegetation cover. (In Czech.) Ph.D. diss. Czech Technical Univ., Prague, Czech Republic.

Taskinen, A., H. Sirvio, and M. Bruen. 2008. Generation of two-dimensionally variable saturated hydraulic conductivity fields: Model theory, verification and computer program. Comput. Geosci. 34:876–890. doi:10.1016/j.cageo.2007.04.010

Troch, P., E. van Loon, and A. Hilberts. 2002. Analytical solutions to a hillslope-storage kinematic wave equation for subsurface flow. Adv. Water Resour. 25:637–649. doi:10.1016/S0309-1708(02)00017-9

Tromp-van Meerveld, H.J., N.E. Peters, and J.J. McDonnell. 2007. Effect of bedrock permeability on subsurface stormflow and the water balance of a trenched hillslope at the Panola Mountain Research Watershed, Georgia, USA. Hydrol. Processes 21:750–769. doi:10.1002/hyp.6265

Tromp-van Meerveld, I., and M. Weiler. 2008. Hillslope dynamics modeled with increasing complexity. J. Hydrol. 361:24–40. doi:10.1016/j.jhydrol.2008.07.019

Vogel, T. 2001. Numerical simulation of flow and transport in a heterogeneous variably saturated hillslope segment. Geophys. Res. Abstr. 3:2837.

Vogel, T., J. Brezina, M. Dohnal, and J. Dusek. 2010a. Physical and numerical coupling in dual-continuum modeling of preferential flow. Vadose Zone J. 9:260–267. doi:10.2136/vzj2009.0091

Vogel, T., and M. Cislerova. 1988. On the reliability of unsaturated hydraulic conductivity calculated from the moisture retention curve. Transp. Porous Media 3:1–15. doi:10.1007/BF00222683

Vogel, T., H.H. Gerke, R. Zhang, and M.Th. van Genuchten. 2000a. Modeling flow and transport in a two-dimensional dual-permeability system with spatially variable hydraulic properties. J. Hydrol. 238:78–89. doi:10.1016/S0022-1694(00)00327-9

Vogel, T., M. Sanda, J. Dusek, M. Dohnal, and J. Votrubova. 2010b. Using oxygen-18 to study the role of preferential flow in the formation of hillslope runoff. Vadose Zone J. 9:252–259. doi:10.2136/vzj2009.0066

Vogel, T., M. Tesař, and M. Císlerová. 2003. Modeling water regime in a small watershed. In: Proceedings of the International Conference on Small Catchment Hydrology, Prague, Czech Republic. 15 Oct. 2003. Inst. of Hydrodynamics of the Czech Acad. of Sci., Prague, Czech Republic. p. 127–136.

Vogel, T., M.Th. van Genuchten, and M. Cislerova. 2000b. Effect of the shape of soil hydraulic properties near saturation on numerical simulation of variably-saturated flow. Adv. Water Resour. 24:133–144. doi:10.1016/S0309-1708(00)00037-3

Weiler, M., and J. McDonnell. 2004. Virtual experiments: A new approach for improving process conceptualization in hillslope hydrology. J. Hydrol. 285:3–18. doi:10.1016/S0022-1694(03)00271-3

Weiler, M., J.J. McDonnell, I. Tromp-van Meerveld, and T. Uchida. 2005. Subsurface stormflow. In: M.G. Anderson, editor, Encyclopedia of hydrological sciences. John Wiley & Sons, New York.

Transport of bromide and pesticides through an undisturbed soil column: A modeling study with global optimization analysis, Journal of Contaminant Hydrology, 2015.

Journal of Contaminant Hydrology 175–176 (2015) 1–16

Contents lists available at ScienceDirect

Journal of Contaminant Hydrology

journal homepage: www.elsevier.com/locate/jconhyd

Transport of bromide and pesticides through an undisturbed soil column: A modeling study with global optimization analysis

Jaromir Dusek [a,*], Michal Dohnal [a], Michal Snehota [a], Martina Sobotkova [a], Chittaranjan Ray [b,c], Tomas Vogel [a]

[a] Czech Technical University in Prague, Faculty of Civil Engineering, Prague, Czech Republic
[b] Civil and Environmental Engineering, Water Resources Research Center, University of Hawaii at Manoa, Honolulu, HI, USA
[c] Nebraska Water Center, University of Nebraska, Lincoln, NE, USA

ARTICLE INFO

Article history:
Received 24 April 2014
Received in revised form 2 February 2015
Accepted 4 February 2015
Available online 12 February 2015

Keywords:
Herbicides
Miscible displacement experiment
Flow interruption
Parameter sensitivity
Latin hypercube sampling
Monte Carlo

ABSTRACT

The fate of pesticides in tropical soils is still not understood as well as it is for soils in temperate regions. In this study, water flow and transport of bromide tracer and five pesticides (atrazine, imazaquin, sulfometuron methyl, S-metolachlor, and imidacloprid) through an undisturbed soil column of tropical Oxisol were analyzed using a one-dimensional numerical model. The numerical model is based on Richards' equation for solving water flow, and the advection–dispersion equation for solving solute transport. Data from a laboratory column leaching experiment were used in the uncertainty analysis using a global optimization methodology to evaluate the model's sensitivity to transport parameters. All pesticides were found to be relatively mobile (sorption distribution coefficients lower than 2 $cm^3\ g^{-1}$). Experimental data indicated significant non-conservative behavior of bromide tracer. All pesticides, with the exception of imidacloprid, were found less persistent (degradation half-lives smaller than 45 days). Three of the five pesticides (atrazine, sulfometuron methyl, and S-metolachlor) were better described by the linear kinetic sorption model, while the breakthrough curves of imazaquin and imidacloprid were more appropriately approximated using nonlinear instantaneous sorption. Sensitivity analysis suggested that the model is most sensitive to sorption distribution coefficient. The prediction limits contained most of the measured points of the experimental breakthrough curves, indicating adequate model concept and model structure for the description of transport processes in the soil column under study. Uncertainty analysis using a physically-based Monte Carlo modeling of pesticide fate and transport provides useful information for the evaluation of chemical leaching in Hawaii soils.

1. Introduction

Reliable model predictions of contaminant fate and transport in soils depend on adequate parameterization of relevant flow and transport processes. Despite significant progress of the analytical and numerical procedures made in past decades, it remains difficult to obtain parameters governing fate and transport of reactive compounds (e.g., pesticides) from field leaching studies due to soil heterogeneity and complex boundary conditions (e.g., Dusek et al., 2011). Thus, laboratory column leaching experiments, also referred to as miscible displacement experiments, are frequently being performed since the experimental conditions (i.e., initial and boundary conditions) may be sufficiently monitored and controlled. The use of independently estimated input parameters for predictions should be the ultimate goal of modeling. However, the conditions of experiments from which the input parameters

* Corresponding author at: Department of Hydraulics and Hydrology, Faculty of Civil Engineering, Czech Technical University in Prague, Thakurova 7, 166 29 Prague, Czech Republic. Tel.: +420 22435 4355; fax: +420 22435 4793.
E-mail address: dusek@mat.fsv.cvut.cz (J. Dusek).

http://dx.doi.org/10.1016/j.jconhyd.2015.02.002
0169-7722/

were estimated differ considerably from the flow and transport conditions on which the model predictions are made. This may therefore lead to modeling results with limited reliability (Vereecken et al., 2011). At present, observed information on solute transport (i.e., spatial or temporal variations of a given chemical in soil and/or soil water) is used to estimate transport parameters by means of inverse modeling.

Several studies suggested that both water flow and chemical transport data are needed for proper model description of transport processes in soils (e.g., Coppola et al., 2009). When transport of solutes is accounted for, different strategies can be followed to obtain soil hydraulic and transport parameters by inverse modeling (Šimůnek et al., 2002). A sequential procedure can be pursued, in which the soil hydraulic parameters are estimated first and then estimation of transport parameters follows (thus two independent optimizations are invoked). Alternatively, water flow data (e.g., soil water pressure, water content, and flux) and transport information (e.g., resident concentration and concentration in the effluent) can be used in a sequential manner. Eventually, combined optimization using water and solute information can be employed to simultaneously estimate both the soil hydraulic and solute transport parameters. Inoue et al. (2000) showed that combined optimization is the most robust approach as it yields smaller estimation errors than a sequential procedure.

Search algorithms based on the Levenberg–Marquardt method (e.g., Clausnitzer and Hopmans, 1995) were recently complemented by prediction uncertainty and parameter sensitivity analysis (Bates and Campbell, 2001; Beven and Binley, 1992) or replaced by so-called global optimization methods (Mertens et al., 2009; Pan and Wu, 1998; Takeshita, 1999). Vrugt et al. (2005) reported on an improved inverse modeling of subsurface flow and transport using a simultaneous optimization and data assimilation method. Beven et al. (2006) presented a method for estimating transport of atrazine at the field scale that accounts for parameter uncertainty by conditioning the parameter distributions and constraining the predictions with the results of laboratory breakthrough experiments. A review of recent developments in inverse modeling procedures relevant for unsaturated flow and transport processes was given by Vrugt et al. (2008). Nevertheless, systematic applications of these optimization methods for reactive transport studies are still scarce.

Experimental breakthrough curves (time series of concentration in the effluent from a soil column) are used to characterize flow and solute processes in soils, e.g., physical and chemical nonequilibrium, biochemical degradation and production, and sorption kinetics. For instance, Fortin et al. (1997) performed an experiment involving flow interruptions on a soil column under saturated conditions and revealed the sorption kinetics of simazine. Bedmar et al. (2004) conducted laboratory leaching experiments on packed soil columns with the herbicides atrazine and metribuzin. In principle, the values of sorption distribution and degradation parameters can be estimated from batch sorption and degradation (incubation) experiments (e.g., Dusek et al., 2010a; Kulluru et al., 2010). However, the use of the coefficients estimated from these independent experiments often leads to discrepancies in prediction of fate and transport under both laboratory and field conditions (see the review from Vereecken et al. (2011)). Hence, the transport parameters can be also estimated directly using data from laboratory (Altfelder et al., 2001; Beigel and Di Pietro, 1999; Gaber et al., 1995) and field leaching studies (Dusek et al., 2011; Kasteel et al., 2010; Roulier and Jarvis, 2003).

Spatial variability of model input parameters as well as uncertainty in their adequate determination propagate through modeling systems in a largely unknown way. Deterministic models coupled with a Monte Carlo framework (e.g., Dubus and Brown, 2002; Lindahl et al., 2005) and stochastic approaches (e.g., Hu and Huang, 2002; Vanderborght et al., 2006) have been used to account for uncertainty analysis in pesticide fate and transport modeling. For pesticides, sorption distribution and degradation parameters have received the greatest attention (Dubus et al., 2003a, 2004; Roulier et al., 2006). Nevertheless, a significant influence of soil properties on pesticide leaching was also noted in several studies (e.g., Vereecken and Dust, 1998; Stenemo and Jarvis, 2007). Dubus et al. (2004) showed that optimized transport parameters depend on the initial values used in their optimization. Dubus et al. (2004) also demonstrated that the sorption distribution and degradation parameters could be both positively and negatively correlated.

Weathered tropical soils are not well understood in respect to transport parameters since the majority of studies have been undertaken in temperate regions (e.g., D'Alessio et al., 2014; Laabs and Amelung, 2005; Racke et al., 1997). Tropical soils often contain aggregates and large portion of fine micropores. Preferential flow effects in aggregated Oxisols have been reported in the literature (Loague et al., 1995, 1996). Besides differences in physical soil properties, soil chemical properties play an important role in controlling pesticide fate. Although the clay content in Oxisols is often high, the cation exchange capacity is low due to weathering of primary minerals. The effect of tropical climates on pesticide fate and transport includes increased volatility and enhanced chemical and microbial degradation rates (Racke et al., 1997). In comparison with temperate regions, field dissipation of pesticides under tropical climate was found to be 5 to 10 times faster (Laabs et al., 2002). Similarly, Laabs et al. (2000) reported short (<14 days) dissipation half-lives of pesticides in a Brazilian Oxisol topsoil. Nevertheless, the presence of pesticides in lysimeter percolate demonstrated that these compounds possess a leaching potential in spite of their fast dissipation in tropical climate (Laabs et al., 2000).

Our previous studies reported on ongoing research aiming to verify the leachability of new pesticides in tropical soils: Dusek et al. (2010a, 2011) summarized the results of a field leaching experiment complemented with modeling of water flow and pesticide transport; Sobotkova et al. (2011) estimated soil hydraulic properties of a laboratory column used for pesticide transport experiments. These studies examined new pesticides under consideration either for new licensing or for license renewal by the Hawaii Department of Agriculture for use in Hawaii. For leaching studies in Hawaii, atrazine is frequently used as the reference pesticide because it has been extensively used in Hawaii and its leaching behavior is well understood in Hawaiian conditions. Based on the fact that atrazine has been found in groundwater in Hawaii, it is a known leacher under Hawaii conditions. Although atrazine has low sorption distribution coefficient, field leaching study conducted on different tropical soils in Hawaii indicated that

atrazine's rapid degradation caused a breakdown within the test period of 16 weeks and thus demonstrated only shallow penetrations of the soil profiles (Dusek et al., 2011). The estimated organic carbon distribution coefficient and field dissipation half-life of atrazine were smaller and shorter than those found in the literature, mostly covering studies undertaken in temperate regions (Dusek et al., 2011).

The objective of the current study was to evaluate the mobility of five pesticides (atrazine, imazaquin, sulfometuron methyl, S-metolachlor, and imidacloprid) through an undisturbed soil column of weathered tropical Oxisol. A laboratory column leaching experiment incorporating flow interruptions combined with one-dimensional numerical modeling of water flow and solute transport was used to achieve this objective. An additional objective was to estimate transport parameters of the pesticides and bromide tracer and to evaluate the effect of parameter uncertainty on model predictions.

2. Materials and methods

2.1. Soil and undisturbed column

The soil column was collected from the Poamoho Agricultural Experiment Station of the University of Hawaii, located on the island of Oahu, Hawaii, USA. The annual average rainfall is about 1000 mm. The climate is tropical with mean annual soil temperatures about 22 °C. The typical soil type is Oxisol (Rhodic Eutrustox, Wahiawa series) (Gavenda et al., 1996). The soil consists of kaolinite, metal oxides, and minimal amount of quartz. The soil is composed of 8% sand (2–0.05 mm), 58% silt (0.05–0.002 mm), and 34% clay particles (<0.002 mm); it is finely textured and contains water-stable silt and sand-sized aggregates. Organic matter content is low, ranging from 1.5% at the soil surface to 0.7% at 0.8 m below the soil surface. The column leaching experiments were conducted on a cylindrical soil column (length 20 cm, diameter 15 cm), taken from the 20–40 cm layer. The column was carefully extracted using a custom-made hydraulic jack-based apparatus (Ray et al., 2007). Computed tomography scanning confirmed that the extraction method prevented crack formation in the soil column (see Sobotkova et al. (2011) for details).

2.2. Column leaching experiment

The undisturbed soil column was used for the leaching experiment with a mixture of four herbicides (atrazine, imazaquin, sulfometuron methyl, S-metolachlor), one insecticide (imidacloprid), and bromide tracer. Atrazine and S-metolachlor are herbicides used in corn, grain, and potato production; imazaquin and sulfometuron methyl are herbicides used for grass and broadleaf weed control; and imidacloprid is an insecticide used for termite and other pest control. Atrazine was used as the reference pesticide because it has been extensively used in Hawaii and its leaching behavior is well understood in Hawaiian conditions. The selection of the pesticides was based on their potential importance in Hawaiian agriculture and urban pest control.

The principle of the column leaching experiment is similar to one presented by Kamra et al. (2001). The column assembly was manufactured from inert materials to prevent pesticide adsorption. Two microtensiometers (Soil Moisture, CA) were installed at 5 cm and 14 cm below the surface of the column to monitor soil water pressures. The column, positioned vertically, was first saturated with a background solution from the bottom. The background solution was prepared from deionized water and 0.0005 M $CaCl_2$. During the experiment, pressure head of −5 cm was maintained on the bottom to induce flow conditions close to saturation. The pressure head was controlled at the outlet by a hanging column similar to that used in the experiment of Seyfried and Rao (1987). Once saturated, a flux (about 15 cm day^{-1}) of background solution was applied during four irrigation periods at the top of the column using a high pressure liquid chromatograph pump (Accuflow Series II, Scientific Systems, PA) (Fig. 1). A thin layer of glass wool covered the top of the soil column. The aim was to distribute the water and tracer/contaminant solution from the six-point drip source over the entire soil surface. After reaching steady state flow, i.e. after applying 22 mm (0.2 pore volume) of background solution, the input was switched to the bromide/pesticide solution. The total volume of the bromide/pesticide solution applied was equivalent to a depth of 708 mm (corresponding to 6 pore volumes). The concentrations in the solution of atrazine, S-metolachlor, imazaquin, sulfometuron methyl, imidacloprid, and bromide were about 10, 10, 5, 5, 5, and 7 mg L^{-1}, respectively. The exact concentrations for each chemical, determined from the control samples, varied slightly during the application. After the application of chemicals was completed, i.e. during the irrigation period 3, the chemicals were leached from the column using the background solution (Fig. 1). Chemical application during irrigation period 3 was shorter than the overall irrigation period to obtain falling part of the breakthrough curve during this irrigation period (see Fig. 1). The average temperature maintained in the laboratory during the experiment was 21.5 ± 1.1 °C. The effluent from the bottom of the sample was taken to a fraction collector at preset intervals (ranging from 23 min to 69 min) and analyzed for the chemical concentrations.

A flow interruption technique (Brusseau et al., 1989; Selim et al., 1999) was imposed during the experiment at rising, steady-state, and falling parts of the breakthrough curve (see Fig. 1). There were three flow interruptions varying in duration from 2.52 day to 20.06 day. The purpose of introducing flow interruptions was to evaluate degradation rates and possibly sorption kinetics for the pesticides. During the flow interruptions, the bottom of the column was sealed off. The top of the column was not fully covered, so evaporation occurred during the interruptions. The evaporation rate was determined from the weight change of the sample during the flow interruptions. The mean value of the evaporation rate slightly varied between the flow interruptions (about 0.05 mm day^{-1} for flow interruption 2 to about 0.09 mm day^{-1} for interruption 1).

Analysis of effluent pesticide concentrations was performed on a liquid chromatograph using a UV detector at the following wavelengths: 269 nm for imidacloprid, 246 nm for imazaquin, and 226 nm for sulfometuron methyl, atrazine, and S-metolachlor. All pesticides were analyzed from one injection. The bromide tracer was analyzed using an ion chromatograph. More detailed information about the analyses was given by Dusek et al. (2010a).

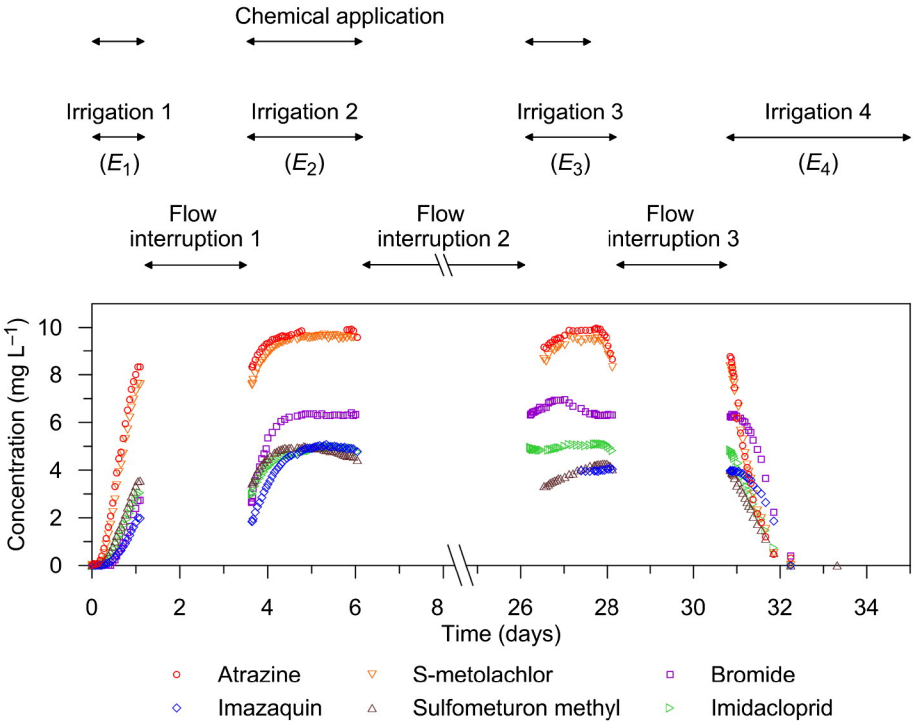

Fig. 1. Breakthrough curves of five pesticides and bromide tracer. The chemical application and irrigation periods as well as flow interruptions are depicted above. (For interpretation of the references to color in this figure legend, the reader is referred to the web version of this article.)

2.3. Flow and transport model

The one-dimensional numerical model S1D (Vogel et al., 2007), the successor to the original HYDRUS code (Vogel et al., 1996), was employed in this study. The model is based on Richards equation for water flow and the advection–dispersion equation for conservative and reactive solute transport. The S1D model has previously been used to consider the transport of heat (Vogel et al., 2011; Votrubova et al., 2012), conservative tracers (Vogel et al., 2010a), pesticides (Dusek et al., 2010b; Ray et al., 2004), and heavy metals (Dusek et al., 2006, 2010c). Water flow is described in the S1D model as:

$$\frac{\partial\theta(h)}{\partial t}=\frac{\partial}{\partial z}\left(K(h)\left(\frac{\partial h}{\partial z}+1\right)\right) \tag{1}$$

where θ is the soil water content ($m^3\ m^{-3}$), h is the soil water pressure head (m), K is the unsaturated hydraulic conductivity ($m\ s^{-1}$), z is the vertical coordinate (assigned positive values for the upward direction in meters), and t denotes time (s). The modified van Genuchten–Mualem formulation (Vogel and Cislerova, 1988; Vogel et al., 2000) is used to describe the soil hydraulic functions in the model.

Transport of solutes is given by the advection–dispersion equation:

$$\frac{\partial\theta c}{\partial t}+\frac{\partial\rho s_1}{\partial t}+\frac{\partial qc}{\partial z}-\frac{\partial}{\partial z}\left(\theta D\frac{\partial c}{\partial z}\right)=-\rho\alpha(\kappa c-s_2)-\lambda\left(\theta c+\rho s_{1,2}\right) \tag{2}$$

where c is the solute concentration ($kg\ m^{-3}$), D is the hydrodynamic dispersion coefficient ($m^2\ s^{-1}$) comprising the molecular diffusion and dispersion, q is the soil water flux ($m\ s^{-1}$) described by Richards equation, s is the adsorbed concentration ($kg\ kg^{-1}$), ρ is the soil bulk density ($kg\ m^{-3}$), and λ is the first-order degradation coefficient (s^{-1}). The subscripts 1 and 2 refer to instantaneous and kinetically controlled sorption sites, respectively; κ refers to the kinetic sorption distribution coefficient at equilibrium ($m^3\ kg^{-1}$) and α is the first-order kinetic sorption reaction rate (s^{-1}). For the instantaneous sorption (immediately in equilibrium with the pore water solution), the sorption distribution coefficient K_d ($kg\ kg^{-1}$: $(kg\ m^{-3})^{-\eta}$) is used to calculate the adsorbed concentration s_1 from the solute concentration c as:

$$s_1=K_d\ c^{\eta} \tag{3}$$

where η is the empirical fitting coefficient (−). If the exponent η is equal to 1, the nonlinear form of the instantaneous sorption isotherm simplifies to a linear isotherm, with dimensions for K_d of $m^3\ kg^{-1}$.

The kinetic sorption is governed by:

$$\frac{\partial\rho s_2}{\partial t}=\rho\alpha(\kappa c-s_2) \tag{4}$$

The reaction rate of the kinetic sorption can be expressed in terms of a sorption reaction half-life $k_{1/2}$ (s) as $\alpha=ln(2)/k_{1/2}$. A small value for the half-life leads to near-instantaneous sorption, whereas a large value leads to the no-sorption case. Using the concept explained in Eqs. (3) and (4), the following sorption mechanisms can be considered: (i) linear instantaneous sorption, (ii) nonlinear instantaneous sorption, and (iii) linear kinetic sorption. The model also enables two-site sorption, in which

both instantaneous and kinetically controlled sorption may coexist.

The governing equations of flow and transport are solved numerically by the computer program S1D using a finite element scheme. The most recent implementation of the S1D code was described by Vogel et al. (2010b).

2.4. Model performance

The Nash–Sutcliffe efficiency E (Nash and Sutcliffe, 1970) was used to evaluate model performance:

$$E = 1 - \frac{\sum_{i=1}^{n}\left(c_{o,i} - c_{s,i}\right)^2}{\sum_{i=1}^{n}\left(c_{o,i} - \overline{c_o}\right)^2} \quad (5)$$

where n is the number of observation times, $c_{o,i}$ is the observed concentration in the effluent at time t_i, $c_{s,i}$ is the corresponding simulated concentration, and $\overline{c}_o$ is the mean of $c_{o,i}$. Values of E may range from $-\infty$ to 1.

2.5. Uncertainty analysis

Uncertainty of model predictions was assessed by informal Bayesian approach (generalized likelihood uncertainty estimation method, e.g. Beven and Binley (1992)). In this context, Vrugt et al. (2009) concluded that informal Bayesian approaches generated very similar uncertainty estimates with those generated by the formal Bayesian approach (based on classical statistical theory and formal mathematics). The methodology based on informal Bayesian approach was used for studying pesticide transport in soils e.g. by Larsbo and Jarvis (2005), Zhang et al. (2006), and Steffens et al. (2013). Our approach utilizes Latin hypercube sampling simulations to determine a quantitative measure of model performance (the likelihood measure) for each combination of model parameters drawn from a selected parametric space. Additionally, likelihood measures were also determined for each of the four parts of the breakthrough curve (E_1, E_2, E_3, and E_4) (Fig. 1). The simulations with high likelihood measure, which simulate the behavior of a real system reasonably well (called behavioral by Beven and Binley (1992)) and less successful simulations (called non-behavioral) were detected. In our case, $E = 0.85$ was used as a threshold value. According to Jin et al. (2010), the use of a higher threshold value results in similar estimates of parameter and model uncertainty as does the formal Bayesian approach.

The resulting model performance distributions were used to assess the model sensitivity to individual transport parameters and to estimate the model prediction uncertainty. To estimate prediction uncertainty, first the model responses were labeled by a likelihood measure and ranked to determine a cumulative probability distribution. The uncertainty quantiles, represented by the prediction limits, were derived from the resulting probability distribution for a selected level of significance, i.e. 5% in this study. This was done separately for each simulation time and each type of observation.

Sensitivity of transport parameters on prediction of concentration in leachate is obtained by comparing prior and posterior parameter distributions (e.g., Larsbo and Jarvis, 2005; Hansson and Lundin, 2006; Dohnal et al., 2012). A significant difference between the two distributions for a parameter indicates a high model sensitivity to that parameter. The posterior distributions are also useful when studying the effect of different contributions of observations (e.g., the four parts of the breakthrough curve). In our case, uniform prior distributions were assumed for all parameters in Latin hypercube sampling. The posterior parameter distributions were constructed as normalized cumulative efficiency distributions determined for each parameter by taking into account the ratio between the number of behavioral model runs associated with a particular parameter value and the number of behavioral runs obtained for the entire parametric space.

3. Model application

3.1. Initial and boundary conditions

The soil water pressure derived from the two tensiometers served as the initial condition for water flow. The soil column was free of chemicals prior to application. The flux (Neumann) boundary condition was prescribed at the top of the sample. The application flux (irrigation intensity) was set according to rate delivered by the pump. The mean value of evaporation rate for each interruption period was set according to observation. On the bottom, a combination of the flux (Neumann) boundary condition with $q = 0$ (during flow interruptions) and the pressure (Dirichlet) boundary condition with $h = -5$ cm (during irrigation periods) was used. A third-type boundary condition with prescribed solute mass flux was employed at the top to match the applied mass of each chemical. The bottom boundary was a zero concentration gradient condition, which allows the chemical to pass through it in discharging water.

3.2. Soil hydraulic parameters

Before the column leaching experiment was performed, a series of infiltration-outflow runs (pressure head boundary condition maintained at the top and seepage face on the bottom) was conducted on the column to obtain the soil hydraulic parameters. Water inflow, outflow, and soil water pressures were monitored during the experiment. Sobotkova et al. (2011) estimated soil hydraulic parameters by means of inverse modeling. The resulting set of soil hydraulic parameters of the main wetting curve of the modified van Genuchten–Mualem parametric model (Vogel and Cislerova, 1988; Vogel et al., 2000) was used in this study: residual water content $\theta_r = 0.339$ cm^3 cm^{-3}, saturated water content $\theta_s = 0.583$ cm^3 cm^{-3}, saturated hydraulic conductivity $K_s = 122$ cm day^{-1}, empirical parameter $n = 1.086$ (−), the parameter of the main wetting curve $\alpha_{WW} = 0.1268$ cm^{-1}, and air-entry value $h_s = -1.52$ cm.

In this study, hysteresis of soil hydraulic function $\theta(h)$ was considered to adequately describe soil water movement during both the irrigation periods and flow interruptions. The simple hysteresis model proposed by Kool and Parker (1987) was used. We assumed that the hysteresis loop is closed at saturation and an empirical parameter n is equal for the two main branches, thus the main branches differ only in empirical parameter α_V. The parameter α_V of the main drying curve was estimated to be two-times smaller than the respective α_V of the main wetting curve, as suggested by Nielsen and Luckner

(1992) and Šimůnek et al. (1999), so the parameter of the main drying curve $\alpha_{VD} = 0.0634$ cm^{-1}. Note that unsaturated hydraulic conductivity function $K(\theta)$ was assumed non-hysteretic.

3.3. Transport parameters

The molecular diffusion coefficient for the pesticides was fixed at a general value of 0.43 cm^2 day^{-1} (Jury et al., 1983). The molecular diffusion coefficient for the bromide tracer (1.2 cm^2 day^{-1}) was taken from literature (Gerke et al., 2007). The value of soil bulk density was 1.2 g cm^{-3} (Dusek et al., 2010a). Dispersivity is usually estimated from the breakthrough curve of a conservative tracer (e.g., Dousset et al., 2007; Katagi, 2013). However, inspection of the observed bromide breakthrough curve (Fig. 1) suggested that the tracer was not completely conservative in the current study (bromide showed the latest appearance in the leachate among all tested chemicals). Therefore, the value of dispersivity was fixed at 2 cm, based on an assumption that the dispersivity is approximately 1/10 of the travel distance (Gelhar et al., 1992).

The first-order degradation coefficient λ was calculated using the half-life value $t_{1/2}$ (s) as $\lambda = ln(2)/t_{1/2}$. The S1D model takes into account the effect of soil water content dynamics on pesticide degradation. This effect was, however, not considered in the current study as the soil column remained close to saturation during the experiment. Furthermore, the effect of temperature on pesticide degradation was neglected since soil temperature did not fluctuate significantly under laboratory conditions.

3.4. Modeling scenarios

The simulations using K_d and $t_{1/2}$ values obtained independently through laboratory batch tests and degradation experiments (Dusek et al., 2010a) showed large discrepancy between observed and predicted breakthrough curves. Hence, the Monte Carlo modeling framework was employed to describe the observed breakthrough curve more adequately. Within this framework, multiple forward simulations, searching through the parametric space, were executed. Transport parameters related to instantaneous sorption and degradation (i.e., K_d, η, and $t_{1/2}$) are usually loaded with high uncertainty (e.g., Dubus et al., 2003a). These parameters were thus allowed to vary within relatively wide ranges of their parameter space. The ranges for K_d and $t_{1/2}$ considered in the analysis are shown in Table 1. Both ranges were set wide enough to contain the value given in the FOOTPRINT database (FOOTPRINT, 2007) and the value estimated in our previous study based on field pesticide leaching (Dusek et al., 2011). The pesticides were allowed to be fully mobile, i.e. lower limit of K_d was set to 0. The empirical exponent η was tested in the 0.8–1.2 range for all pesticides; a similar range was considered by Dubus et al. (2003b). The sorption distribution coefficient and the exponent were also relaxed for bromide tracer considering its sorption to iron-oxide rich tropical Oxisol. In aggregated soils, kinetic sorption model is often applied to describe the experimental breakthrough curves (e.g., Köhne et al., 2009; Ma et al., 1996; Wagenet and Chen, 1998). Hence, it is hypothesized that an improved prediction of pesticide transport in Oxisols may be obtained with sorption kinetics. Therefore, in addition to instantaneous (linear and nonlinear) sorption, parameters governing kinetic sorption (κ and $k_{1/2}$) were allowed to vary for the chemicals. The uniform (prior) distribution was assumed for all varied transport parameters; the parameters were sampled using the Latin hypercube method (Adams et al., 2009; McKay et al., 1979).

The two following modeling scenarios were considered in this study:

Scenario I Based on instantaneous sorption — parameters K_d, η, and $t_{1/2}$ varied in their parametric space;

Scenario II Based on kinetic sorption — parameters κ, $k_{1/2}$, and $t_{1/2}$ varied in their parametric space.

The two-site sorption was not considered in the analysis as the breakthrough data did not allow distinguishing between one- and two-site sorption model. For two-site sorption model, the amount of parameters to be estimated would be too large. Each scenario was based on 50,000 parameter combinations from the parameter ranges presented in Table 1.

4. Results and discussion

4.1. Water flow

Observed and simulated cumulative outflow from the soil sample is shown in Fig. 2a. The outflow of leachate occurred only during the irrigation periods. Very good agreement between observed and predicted outflow curves was obtained (the root mean square error was 11.32 mm). Note that the soil hydraulic parameters were not optimized (adjusted) to obtain closer match between model predictions and data; the soil hydraulic parameters were determined from the infiltration-outflow experiments with boundary conditions different from those used in the column leaching experiment. Comparison

Table 1
Sampling ranges of the transport parameters† considered in Scenarios I and II.

	Atrazine	Imazaquin	Sulfometuron methyl	S-metolachlor	Imidacloprid	Bromide
Scenario I						
K_d (cm$^{3/\eta}$ g$^{-1/\eta}$)	0–5	0–6	0–6	0–6	0–6	0–6
$t_{1/2}$ (day)	2–150	2–150	1–100	1–100	5–300	–
Scenario II						
κ (cm^3 g^{-1})	0–5	0–6	0–6	0–6	0–6	0–6
$k_{1/2}$ (day)	0.04167–50	0.04167–50	0.04167–50	0.04167–50	0.04167–50	0.04167–50
$t_{1/2}$ (day)	2–150	2–150	1–100	1–100	5–300	–

† K_d sorption distribution coefficient; $t_{1/2}$ degradation half-life; κ kinetic sorption distribution coefficient at equilibrium; $k_{1/2}$ kinetic sorption reaction half-life.

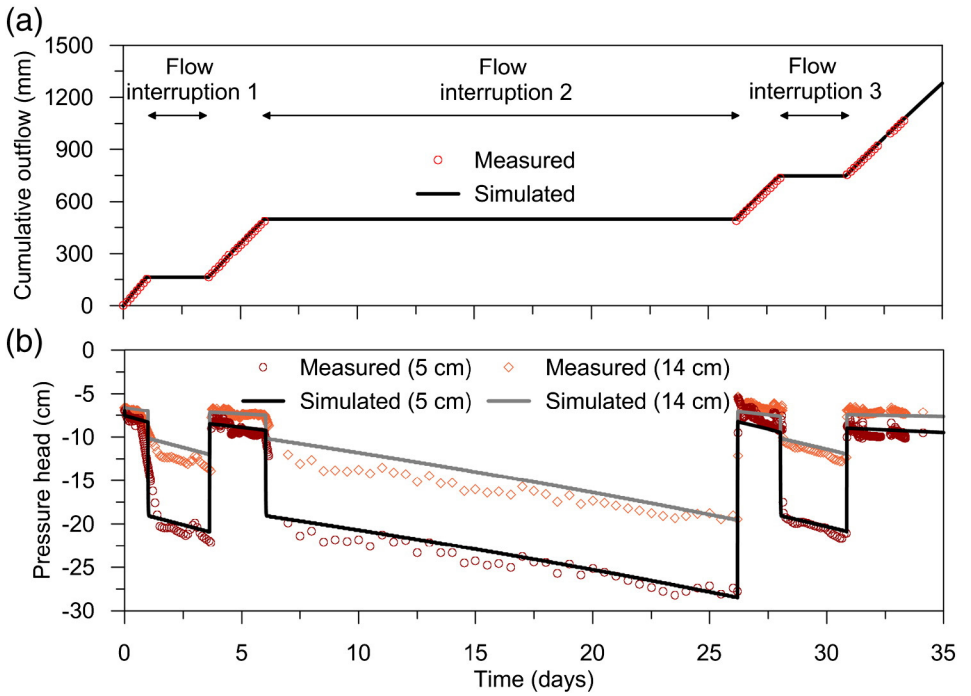

Fig. 2. Measured and simulated cumulative outflow of leachate from the soil sample (a) and soil water pressures at two depths (b).

between observed and simulated soil water pressures at two depths is depicted in Fig. 2b. Variations in irrigation intensity resulted in pressure fluctuations during the irrigation periods. The gradual decline of soil water pressures suggests that evaporation occurred during the three flow interruptions. This was also confirmed by mass loss of the column placed on the balance. Overall, some discrepancies between observed and simulated soil water pressures remained, especially apparent during the flow interruptions (the root mean square error was 1.888 cm and 0.946 cm for depth 5 cm and 14 cm, respectively). The discrepancies can be partly explained by the absence of daily fluctuations of the evaporation flux, which were, for simplicity, not considered in the simulations. Nevertheless, the three flow interruption periods are of less importance in respect to solute leaching.

4.2. Instantaneous sorption (Scenario I)

The relationship between model efficiency and position in parametric space is visualized in Fig. 3. Each dot in a scattergram represents a single model run of atrazine herbicide (one forward simulation). Note that the dot scatter, corresponding to a particular value of a parameter, also reflects the effect of variations in the remaining parameters on model efficiency. Only the simulations with $E > 0$ are shown. The overall as well as the partial E values for each of the four parts of breakthrough curve (irrigation periods 1–4) are further shown as upper envelopes in Fig. 3. There were no simulations with $E_3 > 0$ for the third part of the breakthrough curve. As reflected in negative values of E_3, the data for irrigation period 3 turned out to be highly uncertain. No single simulation was able to explain this part of the breakthrough curve.

The absence of positive values of E_3 could have been caused either by the processes unaccounted for in the applied modeling approach, or measurement deficiencies in the determination of solute concentrations during the third part of the leaching experiment. The longest interruption of water flow during the leaching experiment (flow interruption 2) might have induced competitive sorption between the compounds, hysteretic sorption, and redox-sensitive degradation of chemicals (e.g., Fialips et al., 2010; Köhne et al., 2006; Weber et al., 1991). Oxygen-reduced conditions might have developed in the soil column during the flow interruptions. As a result, the aerobic biodegradation might have been supplemented with anaerobic degradation and possibly with abiotic degradation, which is often seen in Hawaii metal oxide rich soils (D'Alessio et al., 2014). This could have been identified by increased concentrations of soluble metal and manganese oxides in the effluent. Measurement deficiencies are primarily associated with preparation and processing of the effluent samples, photodegradation of the samples in the fraction collector, and the issues related to preparation of chemical solution used for application.

For atrazine, 3432 out of the total number of simulation runs reached $E > 0$ (about 7%). A gradual decline of upper envelopes was predicted for the K_d parameter (Fig. 3a) and poorly defined peaks for sorption exponent η (Fig. 3b). The second part of the breakthrough curve required a substantially smaller K_d value as seen from the rapid drop of partial contribution of E_2 in Fig. 3a. No significant difference between the partial contributions (E_1 through E_4) in respect to the

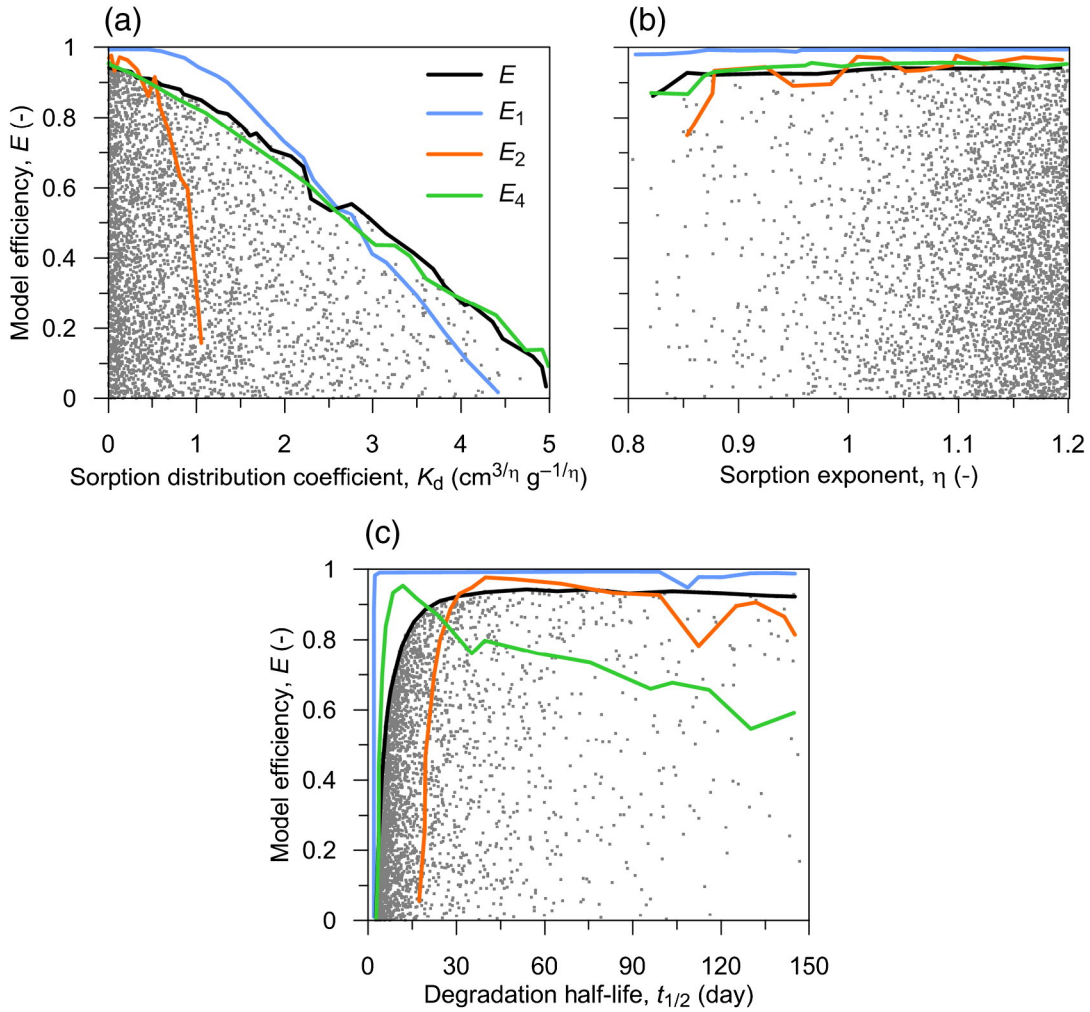

Fig. 3. Scattergrams for atrazine (Scenario I) related to sorption distribution coefficient (a), sorption exponent (b), and degradation half-life (c). The partial contributions (E_1 to E_4) to the overall E value of prediction are shown as upper envelope curves (E_3 envelopes remained negative).

sorption exponent was predicted (Fig. 3b). For degradation half-life, well defined maxima were obtained for the partial E contributions (Fig. 3c). The peak value of $t_{1/2}$ for the E_2 contribution was larger compared to the overall and other contributions. Other chemicals showed similar patterns of overall E as shown in Fig. 3.

In Fig. 4, the upper efficiency envelope curves are shown for the five pesticides and bromide. The model efficiency of the sorption distribution coefficient indicates a declining trend with increasing value of K_d for all chemicals (Fig. 4a). The trend is more pronounced for atrazine and S-metolachlor than for the remaining chemicals. The model efficiencies remain similar for changes in the sorption exponent (Fig. 4b) for all chemicals; only atrazine and S-metolachlor show a drop of E for lower values of η (<0.9). The two different shapes of the upper envelopes of the degradation half-life can be distinguished in Fig. 4c. Imazaquin and sulfometuron methyl are characterized by a peak half-life value ($t_{1/2}$ of about 15–25 days), followed by a gradual decline with increasing $t_{1/2}$. For other three pesticides (atrazine, S-metolachlor, and imidacloprid), the respective peak value of $t_{1/2}$ is then followed by the upper plateau of model efficiency.

The experimental breakthrough curves are compared with the simulations in Fig. 5. The figure shows prediction limits of the breakthrough curves based on 5% and 95% prediction quantiles for all behavioral simulations as well as the simulations based on median values of transport parameters. Note that the number of simulations varied among the chemicals (from 83 simulations for S-metolachlor to 7730 simulations for bromide). The most of measured concentrations during the first and the fourth parts of the breakthrough curves were inside the prediction limits. A few measurement points of the second part of the breakthrough curve fell outside the limits (for example S-metolachlor). The uncertainty in model prediction increased for the third part of the breakthrough curve of the five pesticides resulting in enlarged prediction limits. With the exception of the third part of the breakthrough curve, the prediction limits for atrazine and S-metolachlor were relatively narrow. Greater uncertainty in model predictions, especially of the second and the fourth parts

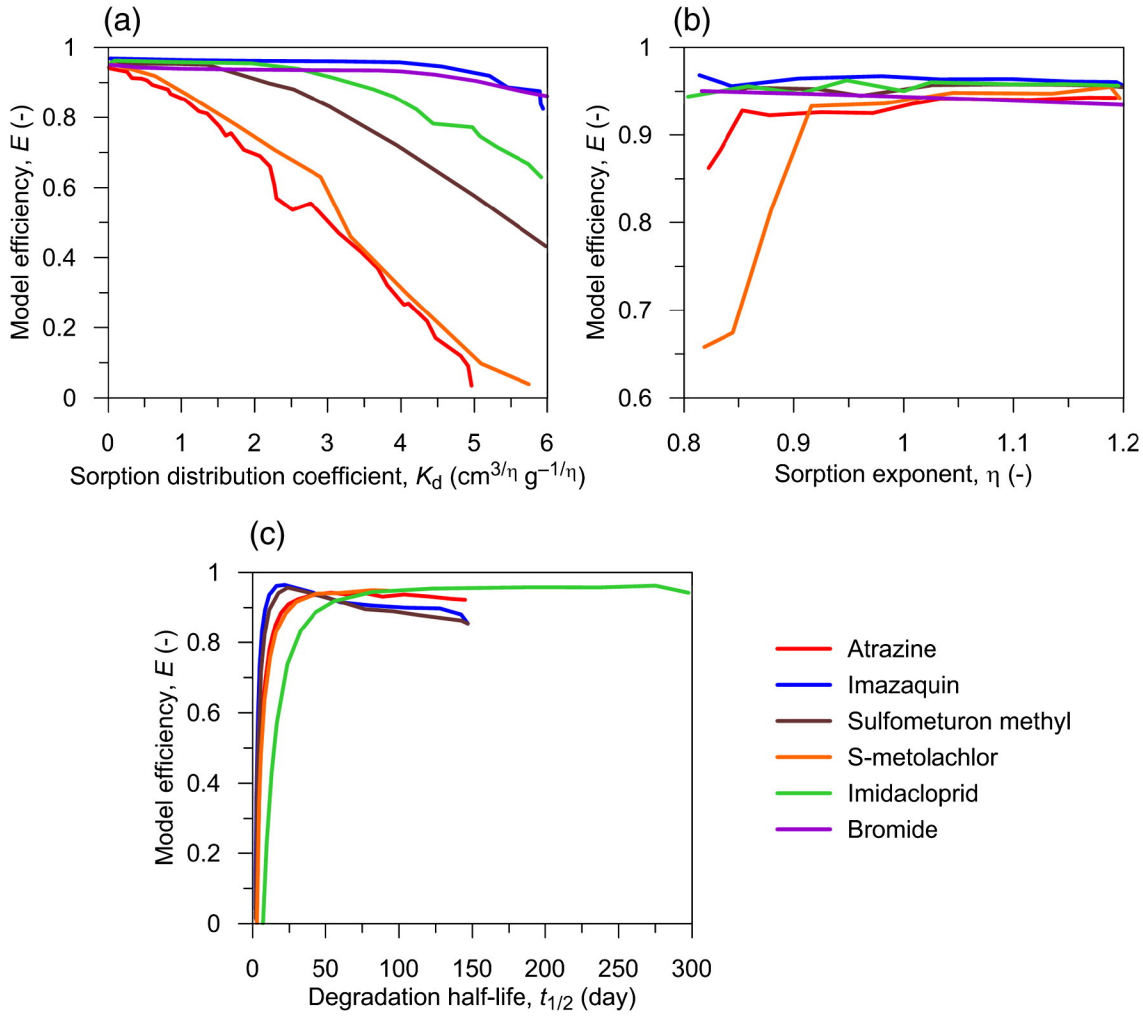

Fig. 4. Upper efficiency envelope curves (Scenario I) related to sorption distribution coefficient (a), sorption exponent (b), and degradation half-life (c).

of the breakthrough curve, can be seen for imazaquin, imidacloprid, sulfometuron methyl, and bromide (Fig. 5).

4.3. Kinetic sorption (Scenario II)

Fig. 6 shows the scattergrams for kinetic sorption of atrazine. The overall upper envelopes and the partial contributions of the breakthrough curve are depicted. Similarly as with instantaneous sorption, the third part of the breakthrough curve had only negative E values. For the atrazine kinetic scenario, 17,464 of all simulation runs were with $E > 0$ (about 35% of total simulations). Flat upper envelopes were seen for the kinetic sorption reaction half-life (Fig. 6b). Well-defined maxima were predicted for degradation half-life, though the difference in peaks between the partial E envelopes is notable (Fig. 6c). For sorption distribution coefficient (Fig. 6a), the E_1 envelope showed no maxima, while the E_2 envelope rapidly declined with increasing κ. This clearly demonstrates that the use of E_1 data alone (i.e., the rising limb of the breakthrough curve) for parameter estimation does not produce a reliable and unique parameter set. Flat E_1 values in full ranges of parameters tested were due to mutual compensation between the transport parameters $\kappa - k_{1/2} - t_{1/2}$.

In Fig. 7, the upper efficiency envelope curves for scenarios based on kinetic sorption are depicted. Overall, atrazine, sulfometuron methyl, and S-metolachlor have the highest E values for the three transport parameters. As seen in the three panels, considerably smaller E values were obtained for the remaining pesticides and bromide tracer. Well-defined maxima of κ (<1 cm^3 g^{-1}) for imazaquin, imidacloprid, and bromide (Fig. 7a) are located around the acceptability limit of $E = 0.85$. A decline of E values in respect to kinetic sorption reaction half-life for imazaquin, imidacloprid, and bromide suggests fast adsorption/desorption, possibly well described by instantaneous sorption model (Fig. 7b). The shapes of the upper envelopes of the degradation half-life were similar for atrazine, sulfometuron methyl, and S-metolachlor (Fig. 7c); imazaquin and imidacloprid were characterized by irregular fluctuations of E value.

The prediction limits, median behavioral simulations, and observations for atrazine, sulfometuron methyl, and S-metolachlor are shown in Fig. 8. The simulations of other pesticides and bromide are not presented since the E values

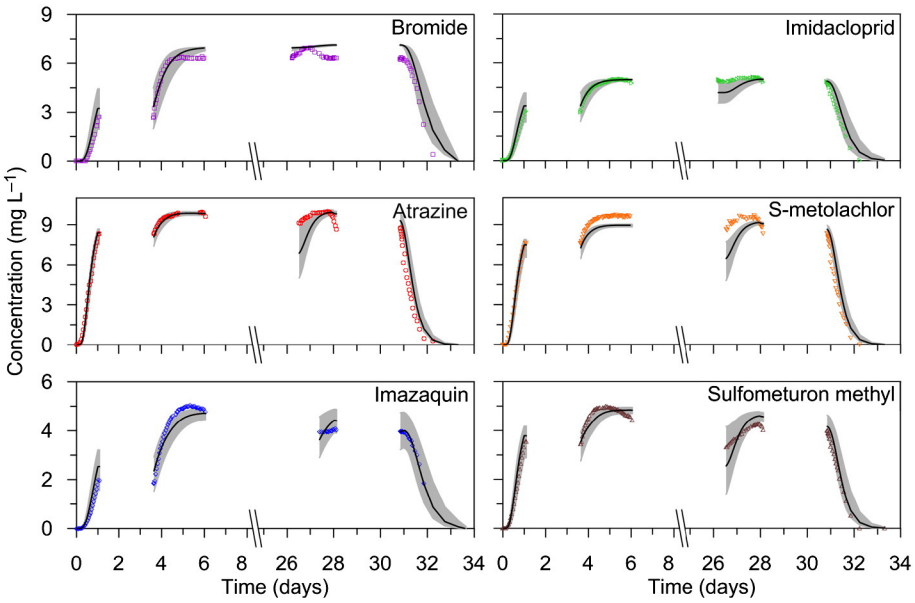

Fig. 5. Observed and predicted breakthrough curves for the five pesticides and bromide (Scenario I). Observed concentrations in the effluent are indicated by the symbols, the shaded areas represent the prediction limits, and black line is the predicted concentration based on median of behavioral simulations.

did not either exceed 0.85 or the total number of behavioral simulations remained too low (<30). Similarly as for Scenario I, the measured concentrations of the breakthrough curves were inside the prediction limits (except part two for S-metolachlor and part three for all three pesticides). The first and the fourth parts of the breakthrough curve showed very narrow prediction limits. Fig. 8 illustrates an apparent mismatch between the simulated and observed concentrations during the third part of the breakthrough curve (as also seen for Scenario I).

4.4. Transport parameter uncertainty

Medians of transport parameters, based on behavioral simulations for each chemical, along with their 95% confidence intervals for both scenarios are presented in Table 2. For scenarios based on kinetic sorption, only atrazine, sulfometuron methyl, and S-metolachlor showed significant amount of simulations with E values >0.85; the transport parameters of the remaining chemicals are not shown. All chemicals were found relatively mobile ($K_d < 2$ cm$^{3/\eta}$ g$^{-1/\eta}$), the sorption exponent was about 1.1 (Scenario I). Bromide tracer was the most sorbing compound. The pesticides underwent relatively fast degradation ($t_{1/2} < 45$ days), with the exception of imidacloprid ($t_{1/2} = 77.7$ days). The estimated $t_{1/2}$ values for pesticides (Scenarios I and II) correspond well to peaks shown in Figs. 4c and 7c. The kinetic sorption reaction half-lives for atrazine, sulfometuron methyl, and S-metolachlor were very similar. Slower degradation and stronger adsorption were obtained for Scenario II than for equilibrium sorption.

The breakthrough curve (Fig. 1) and the estimated K_d value for bromide (Table 2) further indicated that this tracer did not behave conservatively. Interestingly, bromide tracer had higher K_d than atrazine and S-metolachlor (Table 2). The clay mineralogy of weathered tropical soils is typically dominated by kaolinite and the oxides of iron and aluminum. Such mineralogy creates positive charge sites on metal oxide surfaces and the net charge of the soil is then positive. Our results are in agreement with Clay et al. (2004), Wong and Wittwer (2009), and Goldberg and Kabengi (2010), who reported that negatively charged anions such as bromide may undergo sorption in tropical soils. Therefore, we suggest using stable isotopes of water (e.g., ^{18}O and ^{2}H) for transport studies conducted on Oxisols.

The organic carbon normalized distribution coefficient K_{oc} and normalized Freundlich distribution coefficient K_{foc} found in the FOOTPRINT database (FOOTPRINT, 2007) are listed in Table 3 together with the K_{oc} values determined from the batch tests (Dusek et al., 2010a). The value of K_{foc} for each pesticide was calculated by dividing median value of the sorption distribution coefficients K_d estimated in this study by the fraction of the organic carbon content. The normalized distribution coefficients K_{foc} estimated in this study were compared with values found in the FOOTPRINT database as well as those determined from the batch tests, allowing a direct comparison between K_{oc} and K_{foc} values (with an assumption of negligible influence of sorption exponent on normalized distribution coefficients). Values of K_{foc} estimated in this study were smaller than those determined from the batch tests as well as those found in the FOOTPRINT database, with the exception of imazaquin. The differences between K_{foc} estimated in this study and the FOOTPRINT values are substantial (Table 3). The validity of the lower K_d (K_{foc}) values can be supported by the rapid appearance of the studied pesticides in the column leachate as well as the rapid decrease in concentrations of the fourth part of breakthrough curves (Fig. 1). Furthermore, batch tests conducted by Dusek et al. (2010a) suggested linear instantaneous sorption isotherms ($\eta = 1$) for the pesticides tested in the current study, while simulations of the column leaching experiment indicated the sorption exponent to be about 1.1. The Freundlich sorption exponent for all five pesticides from the FOOTPRINT database is

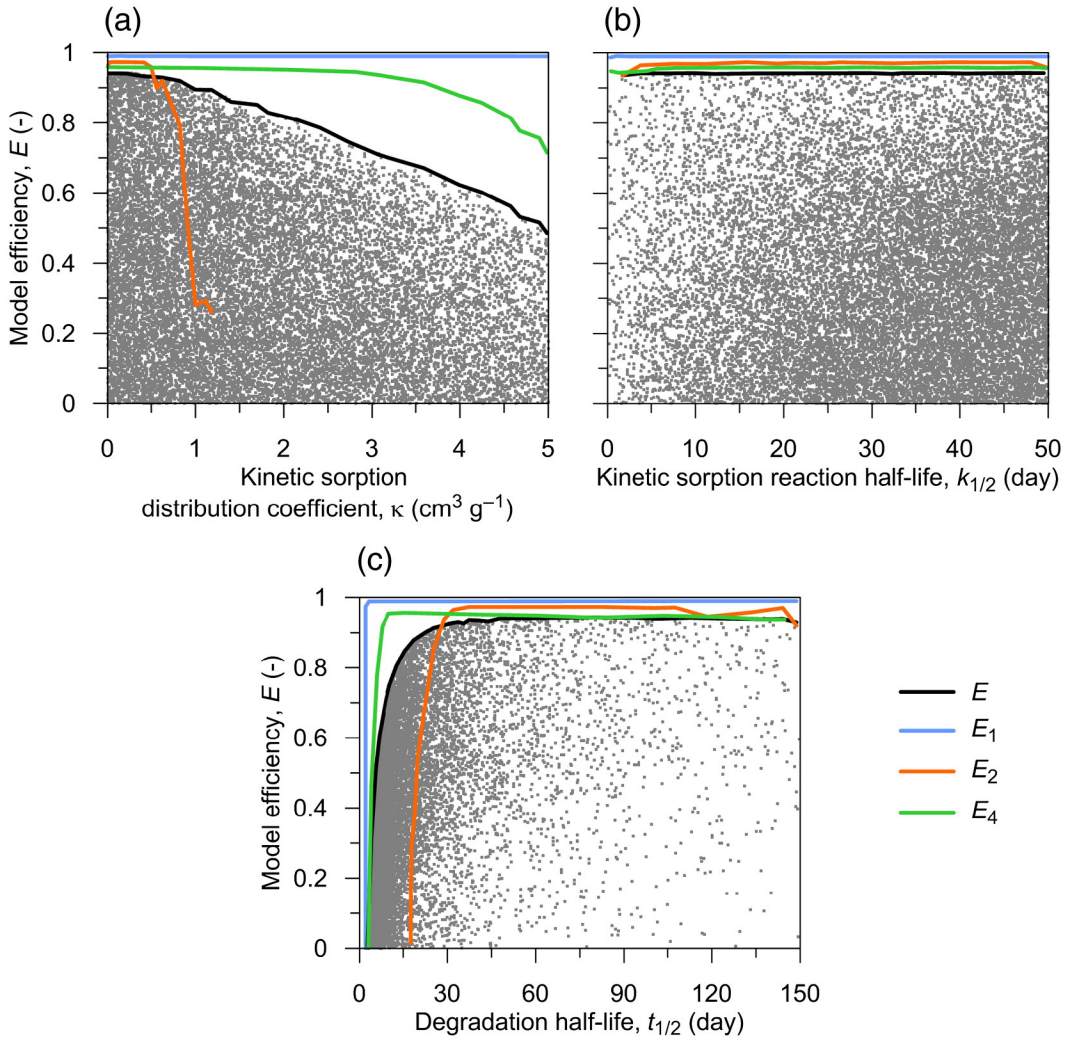

Fig. 6. Scattergrams for atrazine (Scenario II) related to kinetic sorption distribution coefficient (a), kinetic sorption reaction half-life (b), and degradation half-life (c). The partial contributions (E_1 to E_4) to the overall E value of prediction are shown as upper envelope curves (E_3 envelopes remained negative).

smaller than η estimated in this analysis. The difference between sorption characteristics determined from batch tests and those estimated in this study is caused by different assumptions of equilibrium sorption test and column leaching experiment (e.g., homogeneous mixture, contact times of chemicals with the solid phase, the soil/water ratio) (Vereecken et al., 2011). Certainly, the experimental conditions of batch microcosm do not reflect transport conditions imposed during column leaching experiment.

Median values of $t_{1/2}$ estimated in this study (Table 3) were compared with the values found in the FOOTPRINT database. Atrazine, imazaquin, sulfometuron methyl, and imidacloprid showed shorter half-lives in comparison with the FOOTPRINT values. The difference in $t_{1/2}$ values for imazaquin is significant (estimated $t_{1/2} = 16$ days as compared with 94 days found in the literature). Estimated degradation half-life for S-metolachlor was more than two times longer than the FOOTPRINT value. The degradation half-life values estimated in this analysis were consistently smaller than those determined from the incubation experiments of Dusek et al. (2010a). This can be partly explained by different soil layers, which were used for the laboratory incubation experiments and the column leaching study (Table 3).

4.5. Model sensitivity

For atrazine, the posterior distributions of model parameters are compared with prior distributions in Fig. 9. The posterior distributions were constructed for individual parts of the breakthrough curve (E_1, E_2, and E_4). There were no behavioral simulations for the third part of the breakthrough curve (E_3). Note that the number of simulations used to construct the posterior distributions differed between the compounds as only the behavioral simulations were selected. Most posterior distributions differed significantly from the uniform prior distributions, except for $t_{1/2}$ and κ for the first part of breakthrough curve (E_1). Sorption distribution coefficient K_d indicated a high degree of sensitivity of the model to the three breakthrough curve contributions as well as the overall posterior distribution E. For kinetic sorption, the three

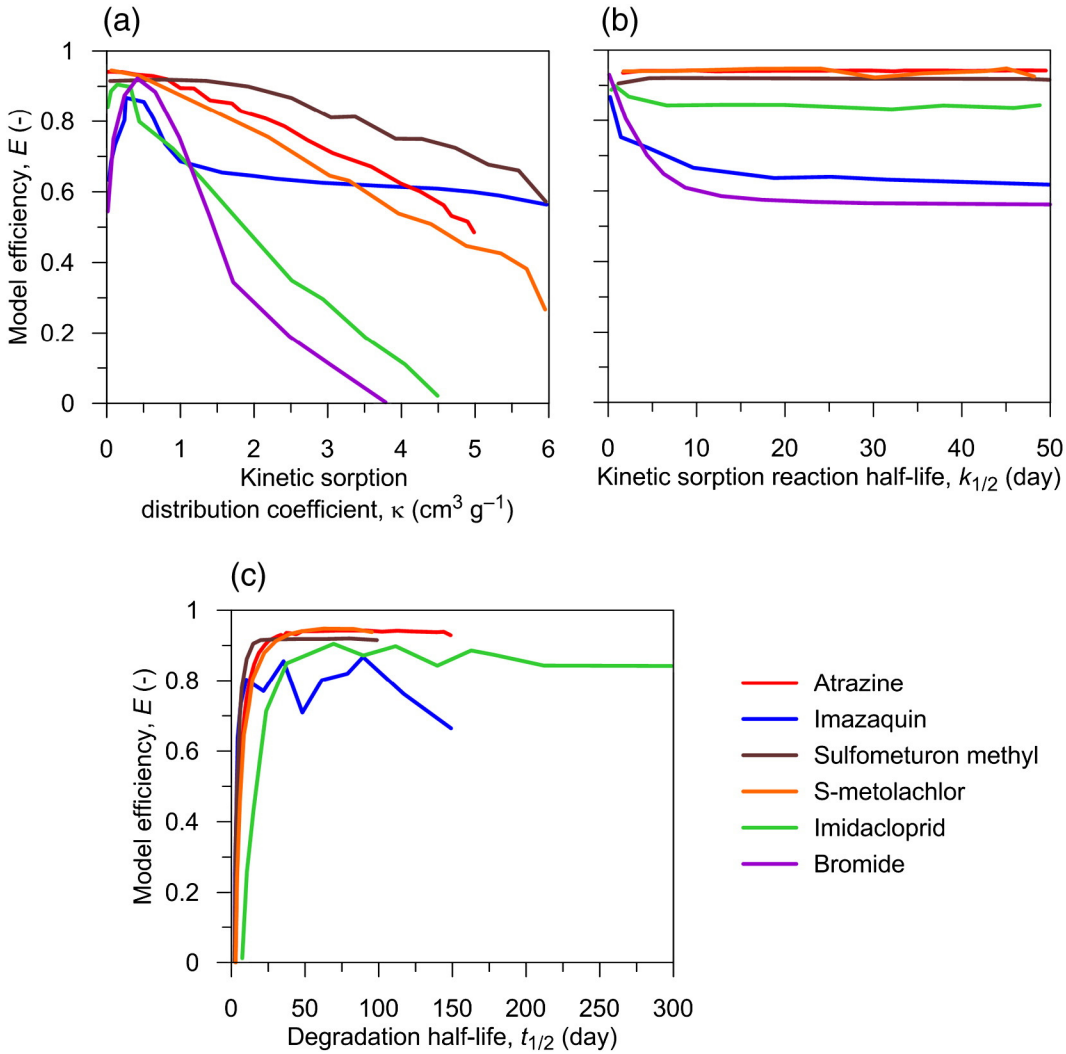

Fig. 7. Upper efficiency envelope curves (Scenario II) related to kinetic sorption distribution coefficient (a), kinetic sorption reaction half-life (b), and degradation half-life (c).

transport parameters had little influence on prediction of the first part of the breakthrough curve (E_1). Kinetic sorption reaction half-life $k_{1/2}$ was found less sensitive in comparison with κ and $t_{1/2}$. The transport parameters of the other four pesticides indicated sensitivity similar to that seen for atrazine (not shown).

4.6. Parameter compensation

The effect of mutual compensation between the transport parameters (K_d, η, and $t_{1/2}$) was studied by running the simulations with parameter ranges narrower than those shown in Table 1. The upper limit of K_d was decreased by a factor of two and the highest $t_{1/2}$ values were reduced three times. Narrow ranges of the transport parameters used for the sampling led to narrower prediction limits of parameters. Moreover, slightly different values of parameters were determined (generally smaller in absolute value). This analysis suggests that a prior knowledge about the physically meaningful and experimentally reasonable values of transport parameters led to a reduction of mutual compensation effects and to an increase of parameter uniqueness.

The effect of compensation between K_d and $t_{1/2}$ and the associated non-uniqueness of the estimated parameters was hypothesized by Dubus et al. (2004) to be caused by using only leaching data (breakthrough curve) in the numerical experiments. Additional data constrains (e.g., residual concentration in the soil column at the end of leaching experiments) were proposed for more robust estimation of parameters. On the contrary, Mertens et al. (2009) used leachate outflow and breakthrough curve data to estimate both the hydraulic and transport parameters through inverse modeling. They concluded that the estimated parameters were unique, approximating the data sufficiently well. In our study, most of the chemicals was leached (>95% of applied) from the soil sample during the experiment due to relatively low K_d (or κ) values. Compared to standard column leaching experiments, a breakthrough curve with several flow interruptions makes it possible to more adequately describe the relevant transport processes. For instance, Fortin et al. (1997) emphasized that the identification

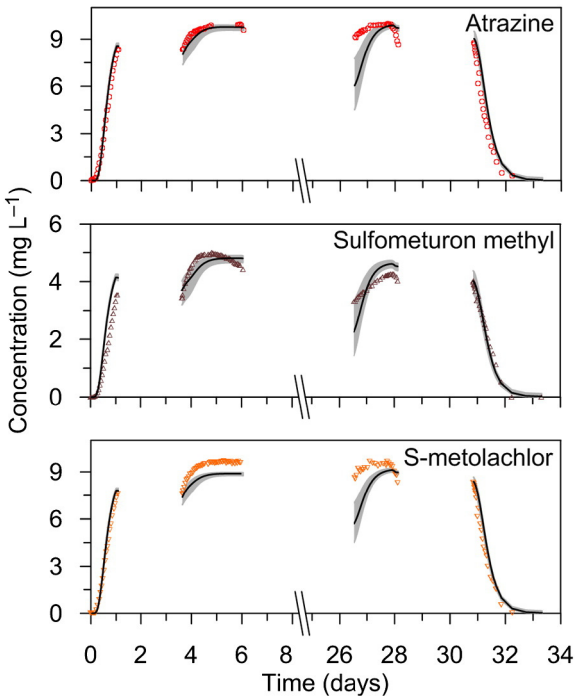

Fig. 8. Observed and predicted breakthrough curves for atrazine, sulfometuron methyl, and S-metolachlor (Scenario II). Observed concentrations in the effluent are indicated by the symbols, the shaded areas represent the prediction limits, and black line is the predicted concentration based on median of behavioral simulations.

of sorption processes from non-interrupted breakthrough curve data may be ambiguous when non-equilibrium is present. In addition, Dubus et al. (2004) did not recommend the optimization of nonlinear exponent η and K_d parameter, due to their mutual correlation/compensation. We allowed these two sorption parameters to vary and further evaluated their mutual relationship.

In this study, the soil hydraulic parameters were taken from previous infiltration-outflow experiments (i.e., the parameters were fixed at previously estimated values). As a result, the uncertainty in the soil hydraulic parameters was not propagated in the uncertainty of the transport parameters (Mertens et al., 2009). The estimation of the soil hydraulic parameters using the Monte Carlo method would lead to many more combinations of possible parametric sets than we used.

4.7. Instantaneous vs. kinetic sorption

The breakthrough curves of atrazine, sulfometuron methyl, and S-metolachlor were well described using the kinetic sorption model. In fact, transport of these three pesticides was reasonably predicted with significantly higher probability using sorption kinetics than utilizing the instantaneous sorption model, as more behavioral simulation runs were obtained for the scenario assuming kinetic sorption (613 atrazine, 696 sulfometuron methyl, and 149 S-metolachlor simulations with $E > 0.85$ for kinetic sorption compared to 205 atrazine, 396 sulfometuron methyl, and 83 S-metolachlor simulations with $E > 0.85$ based on instantaneous sorption). The other chemicals showed either low E values (imazaquin) or short sorption reaction half-life (imidacloprid and bromide), possibly indicating instantaneous sorption. The need to use the sorption kinetics for atrazine, sulfometuron methyl, and S-metolachlor will probably diminish with increasing travel distance (transport modeling at the soil profile scale).

5. Summary and conclusions

Following the estimation of soil hydraulic characteristics of a tropical Oxisol, transport parameters for bromide and five pesticides in this soil were evaluated. The transport parameter space was sampled by the Latin hypercube method. Multiple simulation runs allowed us to estimate the uncertainty of transport parameters and to assess the sensitivity of these parameters.

In the course of laboratory column leaching experiment, the appearance of the studied pesticides in leachate was relatively rapid, with atrazine showing the earliest breakthrough and bromide the latest. Bromide tracer was the most sorbing compound among the tested chemicals. Confirmation of bromide sorption is consistent with the findings from other tropical soils. Imazaquin and sulfometuron methyl showed the fastest degradation. S-metolachlor and imidacloprid were the most persistent chemicals.

The use of sorption kinetics led to improved predictions for three (atrazine, sulfometuron methyl, and S-metolachlor) of the five pesticides. The transport processes of the remaining pesticides (imazaquin and imidacloprid) as well as bromide

Table 2
The statistical characteristics of transport parameters† for scenarios I and II estimated by informal Bayesian approach. Median, 2.5th percentile and 97.5th percentile (in brackets) values are shown.

	Atrazine	Imazaquin	Sulfometuron methyl	S-metolachlor	Imidacloprid	Bromide
Scenario I						
K_d ($cm^{3/\eta}\ g^{-1/\eta}$)	0.138 (0.007–0.771)	1.626 (0.103–4.709)	0.442 (0.006–1.932)	0.220 (0.006–0.877)	0.907 (0.353–3.055)	1.795 (0.112–5.054)
η (−)	1.136 (0.878–1.197)	1.143 (0.927–1.198)	1.146 (0.905–1.198)	1.141 (0.982–1.197	1.145 (0.930–1.198)	1.143 (0.913–1.197)
$t_{1/2}$ (day)	36.1 (18.1–136.4)	16.0 (7.2–90.8)	20.2 (9.7–110.7)	39.8 (20.3–86.5)	77.7 (38.1–263.6)	–
Scenario II						
κ ($cm^3\ g^{-1}$)	0.316 (0.123–1.153)	–	0.559 (0.030–1.950)	0.217 (0.010–0.944)	–	–
$k_{1/2}$ (day)	32.5 (4.4–49.0)	–	33.3 (4.4–49.4)	31.9 (1.7–48.2)	–	–
$t_{1/2}$ (day)	42.3 (18.1–133.6)	–	27.4 (11.2–91.4)	39.8 (20.2–95.6)	–	–

† K_d sorption distribution coefficient; η sorption exponent; $t_{1/2}$ degradation half-life; κ kinetic sorption distribution coefficient at equilibrium; $k_{1/2}$ kinetic sorption reaction half-life.

Table 3
Mean estimated sorption and degradation parameters† for the five pesticides and the literature values.

	Depth (cm)	Atrazine	Imazaquin	Sulfometuron methyl	S-metolachlor	Imidacloprid
This study (Scenario I):						
K_{foc} ($cm^{3/\eta}\ g^{-1/\eta}$)	20–40	13	155	42	21	86
η (−)		1.14	1.14	1.15	1.14	1.15
$t_{1/2}$ (day)	20–40	36.1	16.0	20.2	39.8	77.7
Dusek et al. (2010a):						
K_{oc} ($cm^3\ g^{-1}$)	15–30	95	27	32	95	189
K_{oc} ($cm^3\ g^{-1}$)	30–60	122	27	41	122	161
$t_{1/2}$ (day)	15–30	158	433	58	63	–
FOOTPRINT:						
K_{oc} ($cm^3\ g^{-1}$)		100	–	85	–	–
K_{foc} ($cm^{3/\eta}\ g^{-1/\eta}$)		174	18	–	226	225
η (−)		1.07	1.03	–	1.06	0.80
$t_{1/2}$ (day) – lab at 20 °C		66	94.3	–	14.5	187
$t_{1/2}$ (day) – typical		75	60	24	15	191

† K_{foc} normalized Freundlich distribution coefficient; K_{oc} organic carbon normalized distribution coefficient; η sorption exponent; $t_{1/2}$ degradation half-life.

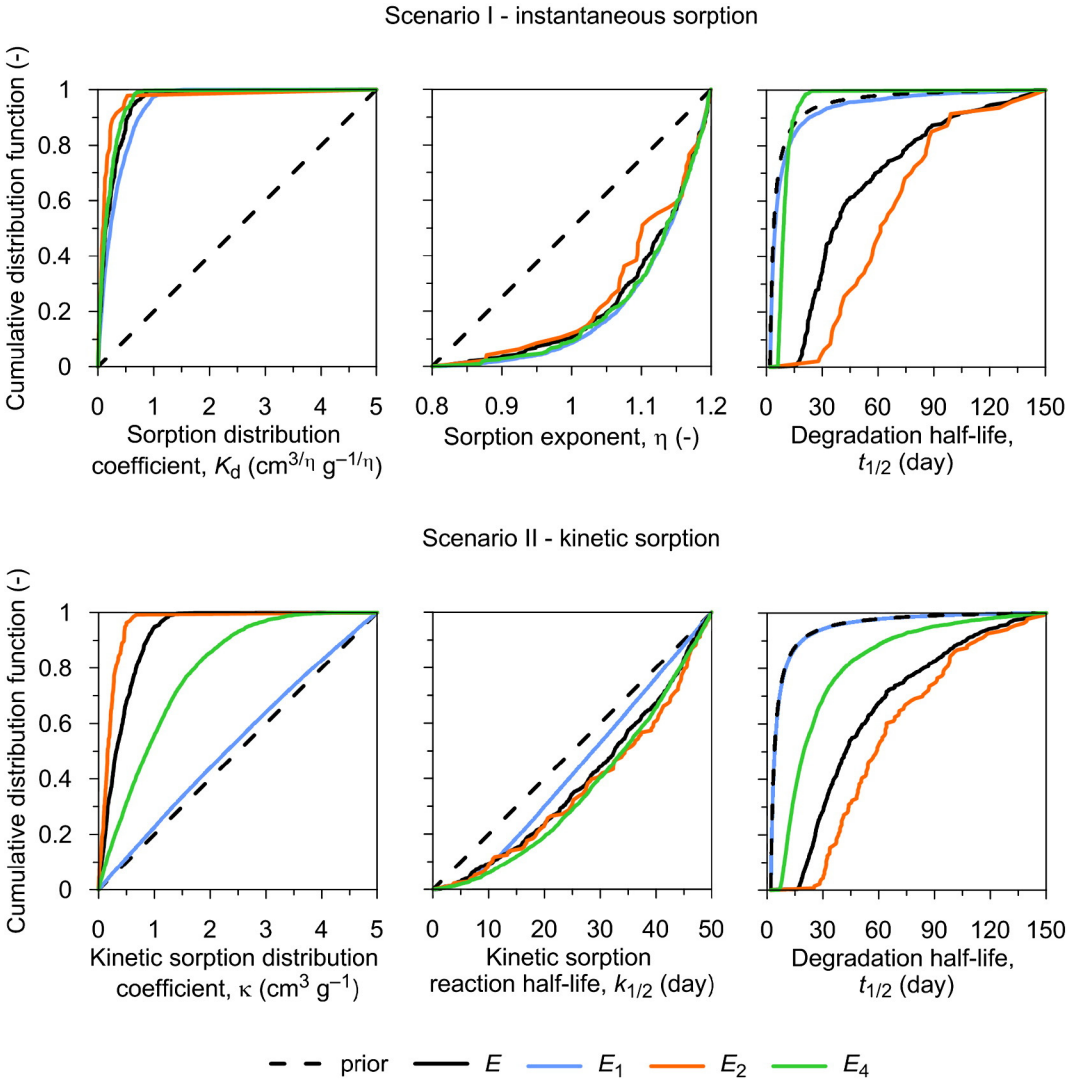

Fig. 9. Cumulative prior and posterior distributions (E) of transport parameters used in the sensitivity analysis (atrazine, Scenarios I and II). The posterior distributions show individual contributions of different parts of breakthrough curve (E_1, E_2, and E_4).

tracer were sufficiently described using the instantaneous sorption model. The values of pesticide sorption distribution coefficients were low compared to values obtained from standard batch sorption tests. All pesticides were found to be relatively mobile (sorption distribution coefficients lower than 2 $cm^3\ g^{-1}$) and less persistent (degradation half-lives smaller than 45 days, with the exception of imidacloprid). Unfavorable sorption was revealed for all chemicals (sorption exponent equal to about 1.1). The estimated degradation half-lives were shorter than those found in the FOOTPRINT database, which is primarily compiled from studies conducted on soils from temperate regions. Numerical experiments confirmed that bromide transport did not follow usual conservative tracer behavior; it was possibly subject to adsorption owing to presence of metal oxides in the soil and soil positive net charge at the prevailing pH. Therefore, stable isotopes of water are recommended as far better alternative to bromide if tracer experiments are performed in Oxisols.

Sensitivity analysis suggested that the model is most sensitive to changes in the sorption distribution coefficient. The prediction limits contained most of the measured points of the experimental breakthrough curves, which indicated that the model concept and model structure seemed adequate for the description of transport processes in the soil column under study. Furthermore, the prediction uncertainty analysis allowed detection of the unaccounted for processes in the modeling approach and/or measurement shortcomings possibly manifested in one part of the breakthrough curve. It was shown that uncertainty analysis using a physically-based Monte Carlo modeling of pesticide transport can contribute meaningfully to the evaluation of chemical leaching in Hawaii soils.

Acknowledgment

Laboratory experiments were conducted at the University of Hawaii under the project “Evaluation of the fate and transport of selected chemicals in Hawaii soils”, Hawaii Department of Agriculture. Numerical evaluation of the experiments was supported by the Czech Science Foundation (project no. 14-03691S) and the Ministry of Education of the Czech Republic (Institutional support for long-term conceptual development).

References

Adams, B.M., Bauman, L.E., Bohnhoff, W.J., Dalbey, K.R., Ebeida, M.S., Eddy, J.P., Eldred, M.S., Hough, P.D., Hu, K.T., Jakeman, J.D., Swiler, L.P., Vigil, D.M., 2009. DAKOTA, a multilevel parallel object-oriented framework for design optimization, parameter estimation, uncertainty quantification, and sensitivity analysis: version 5.3.1 User's manual. Sandia Technical Report SAND2010-2183.

Altfelder, S., Streck, T., Maraqa, M.A., Voice, T.C., 2001. Nonequilibrium sorption of dimethylphthalate — compatibility of batch and column techniques. Soil Sci. Soc. Am. J. 65, 102–111.

Bates, B.C., Campbell, E.P., 2001. A Markov chain Monte Carlo scheme for parameter estimation and inference in conceptual rainfall–runoff modeling. Water Resour. Res. 37, 937–947.

Bedmar, F., Costa, J.L., Suero, E., Gimenez, D., 2004. Transport of atrazine and metribuzin in three soils of the humid pampas of Argentina. Weed Technol. 18, 1–8.

Beigel, C., Di Pietro, L., 1999. Transport of triticonazole in homogeneous soil columns: influence of nonequilibrium sorption. Soil Sci. Soc. Am. J. 63, 1077–1086.

Beven, K., Binley, A., 1992. The future of distributed models: model calibration and uncertainty prediction. Hydrol. Process. 6, 279–298.

Beven, K., Zhang, D., Mermoud, A., 2006. On the value of local measurements for prediction of pesticide transport at the field scale. Vadose Zone J. 5, 222–233.

Brusseau, M.L., Rao, P.S.C., Jessup, R.E., Davidson, J.M., 1989. Flow interruption: a method for investigating sorption nonequilibrium. J. Contam. Hydrol. 4, 223–240.

Clausnitzer, V., Hopmans, J.W., 1995. Non-linear parameter estimation: LM_OPT. General-purpose optimization code based on the Levenberg–Marquardt algorithmLand, Air and Water Resour. Pap. 100032Univ. of California, Davis.

Clay, D.E., Zheng, Z., Liu, Z., Clay, S.A., Trooien, T.P., 2004. Bromide and nitrate movement through undisturbed soil columns. J. Environ. Qual. 33, 338–342.

Coppola, A., Comegna, V., Basile, A., Lamaddalena, N., Severino, G., 2009. Darcian preferential water flow and solute transport through bimodal porous systems: experiments and modelling. J. Contam. Hydrol. 104, 74–83.

D'Alessio, M., Vasudevan, D., Lichwa, J., Mohanty, S.K., Ray, C., 2014. Fate and transport of selected estrogen compounds in Hawaii soils: effect of soil type and macropores. J. Contam. Hydrol. 166, 1–10.

Dohnal, M., Vogel, T., Sanda, M., Jelinkova, V., 2012. Uncertainty analysis of a dual-continuum model used to simulate subsurface hillslope runoff involving oxygen-18 as natural tracer. J. Hydrol. Hydromech. 60, 194–205.

Dousset, S., Thevenot, M., Pot, V., Šimunek, J., Andreux, F., 2007. Evaluating equilibrium and non-equilibrium transport of bromide and isoproturon in disturbed and undisturbed soil columns. J. Contam. Hydrol. 94, 261–276.

Dubus, I.G., Brown, C.D., 2002. Sensitivity and first-step uncertainty analysis for the preferential flow model MACRO. J. Environ. Qual. 31, 227–240.

Dubus, I.G., Brown, C.D., Beulke, S., 2003a. Sources of uncertainty in pesticide fate modeling. Sci. Total Environ. 317, 53–72.

Dubus, I.G., Brown, C.D., Beulke, S., 2003b. Sensitivity analyses for four pesticide leaching models. Pest Manag. Sci. 59, 962–982.

Dubus, I.G., Beulke, S., Brown, C.D., Gottesbüren, B., Dieses, A., 2004. Inverse modelling for estimating sorption and degradation parameters for pesticides. Pest Manag. Sci. 60, 859–874.

Dusek, J., Vogel, T., Lichner, L., Cipakova, A., Dohnal, M., 2006. Simulated cadmium transport in macroporous soil during heavy rainstorm using dual-permeability approach. Biologia 61, S251–S254.

Dusek, J., Sanda, M., Loo, B., Ray, C., 2010a. Field leaching of pesticides at five test sites in Hawaii: study description and results. Pest Manag. Sci. 66, 596–611.

Dusek, J., Ray, C., Alavi, G., Vogel, T., Sanda, M., 2010b. Effect of plastic mulch on water flow and herbicide transport in soil cultivated with pineapple crop: a modeling study. Agric. Water Manage. 97, 1637–1645.

Dusek, J., Vogel, T., Lichner, L., Cipakova, A., 2010c. Short-term transport of cadmium during a heavy-rain event simulated by a dual-continuum approach. J. Plant Nutr. Soil Sci. 173, 536–547.

Dusek, J., Dohnal, M., Vogel, T., Ray, C., 2011. Field leaching of pesticides at five test sites in Hawaii: modeling flow and transport. Pest Manag. Sci. 67, 1571–1582.

Fialips, C.I., Cooper, N.G.A., Jones, D.M., White, M.L., Gray, N.D., 2010. Reductive degradation of p, p′-DDT by Fe(II) in nontronite NAu-2. Clay Clay Miner. 58, 821–836.

FOOTPRINT, 2007. Creating tools for pesticide risk assessment and management in European Union FOOTPRINT Program. [Online]. Available:, http://www.eu-footprint.org/ppdb.html (14 August 2013).

Fortin, J., Flury, M., Jury, W.A., Streck, T., 1997. Rate-limited sorption of simazine in saturated soil columns. J. Contam. Hydrol. 25, 219–234.

Gaber, H.M., Inskeep, W.P., Comfort, S.D., Wraith, J.M., 1995. Nonequilibrium transport of atrazine through large intact soil cores. Soil Sci. Soc. Am. J. 59, 60–67.

Gavenda, R.T., Green, R.E., Schneider, R.C., 1996. Leaching of pesticides in selected Hawaii Oxisols and Andisols as influenced by soil profile characteristics. CTAHR Research Series 075, University of Hawaii, Honolulu, HI.

Gelhar, L.W., Welty, C., Rehfeldt, K.R., 1992. A critical review of data on field-scale dispersion in aquifers. Water Resour. Res. 28, 1955–1974.

Gerke, H.H., Dusek, J., Vogel, T., Köhne, J.M., 2007. Two-dimensional dual-permeability analyses of a bromide tracer experiment on a tile-drained field. Vadose Zone J. 6, 651–667.

Goldberg, S., Kabengi, N.J., 2010. Bromide adsorption by reference minerals and soils. Vadose Zone J. 9, 780–786.

Hansson, K., Lundin, L.-C., 2006. Equifinality and sensitivity in freezing and thawing simulations of laboratory and in situ data. Cold Reg. Sci. Technol. 44, 20–37.

Hu, B.X., Huang, H., 2002. Stochastic analysis of reactive solute transport in heterogeneous, fractured porous media: a dual-permeability approach. Transp. Porous Media 48, 1–39.

Inoue, M., Šimůnek, J., Shiozawa, S., Hopmans, J.W., 2000. Simultaneous estimation of soil hydraulic and solute transport parameters from transient infiltration experiments. Adv. Water Resour. 23, 677–688.

Jin, X., Xu, C.-Y., Zhang, Q., Singh, V.P., 2010. Parameter and modeling uncertainty simulated by GLUE and a formal Bayesian method for a conceptual hydrological model. J. Hydrol. 383, 147–155.

Jury, W.A., Spencer, W.F., Farmer, W.F., 1983. Behavior assessment model for trace organics in soil. 1. Model description. J. Environ. Qual. 12, 558–564.
Kamra, S.K., Lennartz, B., van Genuchten, M.T., Widmoser, P., 2001. Evaluating non-equilibrium solute transport in small soil columns. J. Contam. Hydrol. 48, 189–212.
Kasteel, R., Pütz, T., Vanderborght, J., Vereecken, H., 2010. Fate of two herbicides in zero-tension lysimeters and in field soil. J. Environ. Qual. 39, 1451–1466.
Katagi, T., 2013. Soil column leaching of pesticides. Rev. Environ. Contam. Toxicol. 221, 1–105.
Köhne, J.M., Köhne, S., Šimůnek, J., 2006. Multi-process herbicide transport in structured soil columns: experiments and model analysis. J. Contam. Hydrol. 85, 1–32.
Köhne, J.M., Köhne, S., Šimůnek, J., 2009. A review of model applications for structured soils: b) pesticide transport. J. Contam. Hydrol. 104, 36–60.
Kool, J.B., Parker, J.C., 1987. Development and evaluation of closed-form expressions for hysteretic soil hydraulic properties. Water Resour. Res. 23, 105–114.
Kulluru, P.P., Das, B.S., Panda, P.K., 2010. Evaluation of sorption and leaching potential of malathion and atrazine in agricultural soils of India. Int. J. Environ. Res. 4, 75–90.
Laabs, V., Amelung, W., 2005. Sorption and aging of corn and soybean pesticides in tropical soils of Brazil. J. Agric. Food Chem. 53, 7184–7192.
Laabs, V., Amelung, W., Pinto, A., Altstaedt, A., Zech, W., 2000. Leaching and degradation of corn and soybean pesticides in an Oxisol of the Brazilian Cerrados. Chemosphere 41, 1441–1449.
Laabs, V., Amelung, W., Pinto, A., Zech, W., 2002. Fate of pesticides in tropical soils of Brazil under field conditions. J. Environ. Qual. 31, 256–268.
Larsbo, M., Jarvis, N., 2005. Simulating solute transport in a structured field soil: uncertainty in parameter identification and predictions. J. Environ. Qual. 34, 621–634.
Lindahl, A.M.L., Kreuger, J., Stenström, J., Gärdenäs, A.I., Alavi, G., Roulier, S., Jarvis, N.J., 2005. Stochastic modeling of diffuse pesticide losses from a small agricultural catchment. J. Environ. Qual. 34, 1174–1185.
Loague, K., Miyahira, R.N., Green, R.E., Oki, D.S., Giambelluca, T.W., Schneider, R.C., 1995. Chemical leaching near the Waiawa Shaft, Oahu, Hawaii: 2. Modeling results. Ground Water 33, 124–138.
Loague, K., Bernknopf, R.L., Green, R.E., Giambelluca, T.W., 1996. Uncertainty of groundwater vulnerability assessments for agricultural regions in Hawaii: review. J. Environ. Qual. 25, 475–490.
Ma, Q.L., Ahuja, L.R., Wauchope, R.D., Benjamin, J.G., Burgoa, B., 1996. Comparison of instantaneous equilibrium and equilibrium-kinetic sorption models for simulating simultaneous leaching and runoff of pesticides. Soil Sci. 161, 646–655.
McKay, M.D., Conover, W.J., Beckman, R.J., 1979. A comparison of three methods for selecting values of input variables in the analysis of output from a computer code. Technometrics 21, 239–245.
Mertens, J., Kahl, G., Gottesbüren, B., Vanderborght, J., 2009. Inverse modeling of pesticide leaching in lysimeters: local versus global and sequential single-objective versus multiobjective approaches. Vadose Zone J. 8, 793–804.
Nash, J.E., Sutcliffe, J.V., 1970. River flow forecasting through conceptual models: Part 1—a discussion of principles. J. Hydrol. 10, 282–290.
Nielsen, D.R., Luckner, L.M., 1992. Theoretical aspects to estimate reasonable initial parameters and range limits in identification procedures for soil hydraulic properties. In: van Genuchten, M.T., et al. (Eds.), Proceedings of the International Workshop on Indirect Methods for Estimating the Hydraulic Properties of Unsaturated Soils. University of California, Riverside, pp. 147–160.
Pan, L.H., Wu, L.S., 1998. A hybrid global optimization method for inverse estimation of hydraulic parameters: annealing-simplex method. Water Resour. Res. 34, 2261–2269.
Racke, K.D., Skidmore, M., Hamilton, D.J., Unsworth, J.B., Miyamoto, J., Cohen, S.Z., 1997. Pesticide fate in tropical soils. Pure Appl. Chem. 69, 1349–1371.
Ray, C., Vogel, T., Dusek, J., 2004. Modeling depth-variant and domain-specific sorption and biodegradation in dual-permeability media. J. Contam. Hydrol. 70, 63–87.
Ray, C., Snehota, M., Lichwa, J., Sobotkova, M., 2007. Leaching behavior of selected pesticides: column study of Wahiawa Oxisol from Poamoho. Oahu, Hawaii, WRRC-2007-04, University of Hawaii at Manoa, Final report for HDOA.
Roulier, S., Jarvis, N., 2003. Modeling macropore flow effects on pesticide leaching: inverse parameter estimation using microlysimeters. J. Environ. Qual. 32, 2341–2353.
Roulier, S., Baran, N., Mouvet, C., Stenemo, F., Morvan, X., Albrechtsen, H.J., Clausen, L., Jarvis, N., 2006. Controls on atrazine leaching through a soil-unsaturated fractured limestone sequence at Brevilles, France. J. Contam. Hydrol. 84, 81–105.
Selim, H.M., Ma, L., Zhu, H., 1999. Predicting solute transport in soils: second-order two-site models. Soil Sci. Soc. Am. J. 63, 768–777.
Seyfried, M.S., Rao, P.S., 1987. Solute transport in undisturbed columns of an aggregated tropical soil: preferential flow effects. Soil Sci. Soc. Am. J. 51, 1434–1444.
Šimůnek, J., Kodešová, R., Gribb, M.M., van Genuchten, M.T., 1999. Estimating hysteresis in the soil water retention function from cone permeameter experiments. Water Resour. Res. 35, 1329–1345.
Šimůnek, J., Jacques, D., Hopmans, J.W., Inoue, M., Flury, M., van Genuchten, M.T., 2002. Solute transport during variably saturated flow inverse methods. In: Dane, J.H., Topp, G.C. (Eds.), Methods of Soil Analysis. Part 4. Physical Methods. SSSA Book Ser. 5. SSSA, Madison, WI, pp. 1435–1449.
Sobotkova, M., Snehota, M., Dohnal, M., Ray, C., 2011. Determination of hydraulic properties of a tropical soil of Hawaii using column experiments and inverse modeling. Rev. Bras. Cir. Solo 35, 1229–1239.
Steffens, K., Larsbo, M., Moeys, J., Jarvis, N., Lewan, E., 2013. Predicting pesticide leaching under climate change: importance of model structure and parameter uncertainty. Agric. Ecosyst. Environ. 172, 24–34.
Stenemo, F., Jarvis, N., 2007. Accounting for uncertainty in pedotransfer functions in vulnerability assessments of pesticide leaching to groundwater. Pest Manag. Sci. 63, 867–875.
Takeshita, Y., 1999. Parameter estimation of unsaturated soil hydraulic properties from transient outflow experiments using genetic algorithms. In: van Genuchten, M.T., et al. (Eds.), Characterization and Measurement of the Hydraulic Properties of Unsaturated Porous Media. U.S. Salinity Lab., Riverside, CA, pp. 761–768.
Vanderborght, J., Kasteel, R., Vereecken, H., 2006. Stochastic continuum transport equations for field-scale solute transport: overview of theoretical and experimental results. Vadose Zone J. 5, 184–203.
Vereecken, H., Dust, M., 1998. Modeling water flow and pesticide transport at lysimeter and field scale. ACS Symp. Ser. 699, 189–202.
Vereecken, H., Vanderborght, J., Kasteel, R., Spiteller, M., Schäffer, A., Close, M., 2011. Do lab-derived distribution coefficient values of pesticides match distribution coefficient values determined from column and field-scale experiments? A critical analysis of relevant literature. J. Environ. Qual. 40, 879–898.
Vogel, T., Cislerova, M., 1988. On the reliability of unsaturated hydraulic conductivity calculated from the moisture retention curve. Transp. Porous Media 3, 1–15.
Vogel, T., Huang, K., Zhang, R., van Genuchten, M.T., 1996. The HYDRUS code for simulating one-dimensional water flow, solute transport, and heat movement in variably-saturated media. Version 5.0. Research Report No. 140. US Salinity Laboratory, ARS, USDA, Riverside, CA.
Vogel, T., van Genuchten, M.T., Cislerova, M., 2000. Effect of the shape of soil hydraulic properties near saturation on numerical simulation of variably-saturated flow. Adv. Water Resour. 24, 133–144.
Vogel, T., Lichner, L., Dusek, J., Cipakova, A., 2007. Dual-continuum analysis of a cadmium tracer field experiment. J. Contam. Hydrol. 92, 50–65.
Vogel, T., Sanda, M., Dusek, J., Dohnal, M., Votrubova, J., 2010a. Using oxygen-18 to study the role of preferential flow in the formation of hillslope runoff. Vadose Zone J. 9, 252–259.
Vogel, T., Brezina, J., Dohnal, M., Dusek, J., 2010b. Physical and numerical coupling in dual-continuum modeling of preferential flow. Vadose Zone J. 9, 260–267.
Vogel, T., Dohnal, M., Votrubova, J., 2011. Modeling heat fluxes in macroporous soil under sparse young forest of temperate humid climate. J. Hydrol. 402, 367–376.
Votrubova, J., Dohnal, M., Vogel, T., Tesar, M., 2012. On parameterization of heat conduction in coupled soil water and heat flow modelling. Soil Water Res. 7, 125–137.
Vrugt, J.A., Robinson, B.A., Vesselinov, V.V., 2005. Improved inverse modeling for flow and transport in subsurface media: combined parameter and state estimation. Geophys. Res. Lett. 32, L18408. http://dx.doi.org/10.1029/2005GL023940.
Vrugt, J.A., Stauffer, P.H., Wöhling, T., Robinson, B.A., Vesselinov, V.V., 2008. Inverse modeling of subsurface flow and transport properties: a review with new developments. Vadose Zone J. 7, 843–864.
Vrugt, J.A., ter Braak, C.J.F., Gupta, H.V., Robinson, B.A., 2009. Equifinality of formal (DREAM) and informal (GLUE) Bayesian approaches in hydrologic modeling? Stoch. Env. Res. Risk A. 23, 1011–1026.
Wagenet, R.J., Chen, W., 1998. Coupling sorption rate heterogeneity and physical nonequilibrium in soils. In: Selim, H.M., Ma, L. (Eds.), Physical Nonequilibrium in Soils: Modeling and Application. Ann Arbor Press, Chelsea, MI, pp. 1–33.
Weber, W.J., McGinley, P.M., Katz, L.E., 1991. Sorption phenomena in subsurface systems — concepts, models and effects on contaminant fate and transport. Water Res. 25, 499–528.
Wong, M.T.F., Wittwer, K., 2009. Positive charge discovered across Western Australian wheatbelt soils challenges key soil and nitrogen management assumptions. Aust. J. Soil Res. 47, 127–135.
Zhang, D., Beven, K., Memoud, A., 2006. A comparison of non-linear least square and GLUE for model calibration and uncertainty estimation for pesticide transport in soils. Adv. Water Resour. 29, 1924–1933.

Hillslope-storage and rainfall-amount thresholds as controls of preferential stormflow, Journal of Hydrology, 2016.

Journal of Hydrology 534 (2016) 590–605

Contents lists available at ScienceDirect

Journal of Hydrology

journal homepage: www.elsevier.com/locate/jhydrol

Hillslope-storage and rainfall-amount thresholds as controls of preferential stormflow

Jaromir Dusek *, Tomas Vogel

Czech Technical University in Prague, Faculty of Civil Engineering, Prague, Czech Republic

ARTICLE INFO

Article history:
Received 2 September 2015
Received in revised form 15 January 2016
Accepted 19 January 2016
Available online 27 January 2016
This manuscript was handled by Corrado Corradini, Editor-in-Chief, with the assistance of Renato Morbidelli, Associate Editor

Keywords:
Hillslope hydrology
Rainfall threshold
Rainfall–runoff relationship
Stormflow
Dual-permeability model
Soil–bedrock interface

SUMMARY

Shallow saturated subsurface flow is a dominant runoff mechanism on hillslopes of headwater catchments under humid temperate climate. Its timing and magnitude is significantly affected by the presence of preferential pathways. Reliable prediction of runoff from hillslope soils under such conditions remains a challenge.

In this study, a quantitative relationship between rainfall, stormflow, and leakage to bedrock for hillslopes, where lateral preferential runoff represents a dominant part of the overall response, was sought. Combined effects of temporal rainfall distribution and initial hillslope saturation (antecedent moisture conditions) on stormflow, leakage to bedrock, and overall water balance were evaluated by conducting simulations with synthetic rainfall episodes.

A two-dimensional dual-continuum model was used to analyze hydrological processes at an experimental hillslope site located in a small forested headwater catchment.

Long-term seasonal simulations with natural rainfall indicated that leakage to bedrock occurred mostly as saturated flow during major runoff events. The amount of rainfall needed to initiate stormflow appeared as a dynamic hillslope property, depending on temporal rainfall distribution, initial hillslope storage, and the spatial distribution of soil water within the hillslope. No single valued rainfall threshold responsible for triggering stormflow was found. Rainfall–stormflow as well as rainfall–leakage relationships were found highly nonlinear for low initial hillslope saturations. Temporal rainfall distribution affected the amount of rainfall necessary to initiate stormflow more than it did the amounts of stormflow or leakage to bedrock. In spite of a simple hillslope geometry with constant slope and parallel soil–atmosphere and soil–bedrock interfaces considered in the analysis, the applied model predicted a hysteretic behavior of storage–discharge relationship.

The results showed a mutual interplay of components of hillslope water balance exposing a nonlinear character of the hillslope response. The study provided a quantitatively coherent insight in the hydraulic functioning of hillslopes where preferential flow constitutes a dominant part of stormflow.

1. Introduction

Shallow saturated subsurface flow (also referred to as stormflow or throughflow) is recognized as a dominant runoff mechanism on hillslopes of vegetated headwater catchments under humid temperate climate. The transformation of rainfall into stormflow within a soil profile above the soil–bedrock interface is complex, as several controls affect the runoff process and the related changes of the hillslope storage. The controls can be grouped into static (e.g., hillslope spatial configuration, soil characteristics, and bedrock topography) and dynamic (e.g., storm characteristics, soil water distribution within a hillslope, and vegetation) (Bachmair and Weiler, 2011). These are known to operate simultaneously, thus it remains difficult to identify the effects of individual controls on nonlinear hillslope response to rainfall. Knowledge of temporal and spatial distribution of subsurface runoff has important implications for emerging issues such as carbon dynamics and climate change (e.g., Chaplot and Ribolzi, 2014; Li and Sivapalan, 2014).

The effects of soil depth, slope angle, bedrock topography, bedrock permeability, and the size of storm event were evaluated by Hopp and McDonnell (2009), who considered 72 combinations of these parameters. In their study, some expected results were obtained (e.g., higher stormflow for steeper hillslope) and a few

* Corresponding author at: Department of Hydraulics and Hydrology, Faculty of Civil Engineering, Czech Technical University in Prague, Thakurova 7, 166 29 Prague, Czech Republic. Tel.: +420 22435 4355; fax: +420 22435 4793.
E-mail address: dusek@mat.fsv.cvut.cz (J. Dusek).

http://dx.doi.org/10.1016/j.jhydrol.2016.01.047
0022-1694/

unexpected ones (e.g., peak discharge increased for small and medium slopes and decreased considerably for steeper slope, time to peak discharge was the greatest for medium hillslopes), indicating a complex interplay of these controls. In their case, the connectivity of saturated zone at the soil–bedrock interface was found to explain the governing mechanism of stormflow. The effects of initial condition (antecedent moisture distribution) and temporal rainfall variation on stormflow were not analyzed.

Kampf (2011) examined the persistence of initial condition from the long-term (seasonal) perspective and the effect of initial storage on hillslope discharge. The results showed a straightforward relationship between initial hillslope storage (*IHS*) and stormflow – a nonlinear increase of subsurface stormflow with increasing initial storage. The effect of initial hillslope storage on stormflow and overall hillslope balance seems to be important at the temporal scale of a rainfall–runoff episode (e.g., Cloke et al., 2003; Haga et al., 2005; Tromp-van Meerveld and Weiler, 2008). Also, the contribution of pre-event water to storm hydrograph formation is predetermined by initial hillslope storage (Klaus and McDonnell, 2013). The effects of temporal rainfall distribution were analyzed by using statistical measures of time between rainfalls (McGrath et al., 2007) or by characterizing statistical properties of storms which triggered fracture flow and surface runoff (Struthers et al., 2007). For hillslopes where preferential flow effects are known to represent a significant part of the hillslope response, however, a thorough quantitative evaluation of initial hillslope storage effects on hillslope balance and stormflow has not been considered.

Mathematical modeling of runoff processes can be very helpful in analyses of hillslope responses to rainfall. This is due to the fact that field data are inherently loaded with uncertainty and usually underrepresented in time and space. Another reason is linked to simultaneous effects of various controls on stormflow. Under such circumstances, modeling may be used to isolate individual controls and make further generalizations. The evaluation of field data may lead to biased conclusions and generalizations under specific conditions. Numerical modeling has thus the potential to improve our understanding of runoff mechanisms and processes. A combined approach can be pursued where the modeling and field observations are combined to allow a detailed analysis of mechanisms contributing to runoff (e.g., Bronstert and Plate, 1997; VanderKwaak and Loague, 2001; Hopp et al., 2009).

Preferential flow has been acknowledged as a significant process contributing to stormflow generation in headwater catchments. It has also been given increasing attention in recent modeling applications (e.g., Beckers and Alila, 2004; Weiler and McDonnell, 2007; Klaus and Zehe, 2010). In this context, two-and three-dimensional dual-continuum models of soil water flow have been successfully applied to study hillslope responses to rainfall in a few studies (Faeh et al., 1997; Stadler et al., 2012; Laine-Kaulio et al., 2014). However, the potential of these models to study the combined effects of various controls on the hillslope responses has not been fully exploited.

The hydraulic functioning of the soil–bedrock interface is recognized as one of the most important factors influencing timing and magnitude of stormflow. Based on experimental hillslope data from the Panola Mountain Research Watershed, Tromp-van Meerveld and McDonnell (2006b) and Lehmann et al. (2007) argued that subsurface hydrological connectivity of saturation zones above the soil–bedrock interface is a necessary condition for the initiation of significant stormflow. Tromp-van Meerveld and McDonnell (2006b) proposed fill and spill hypothesis to explain stormflow patterns at the Panola hillslope where variable soil depth formed ridges and depressions at the soil–bedrock interface. At the hillslope scale, fill and spill hypothesis is closely related to a threshold behavior of hillslopes in respect to rainfall input signal. The threshold effect is usually associated with the amount of cumulative rainfall, i.e. how much rainfall is needed to trigger significant stormflow. The threshold relationship between rainfall and stormflow has been accepted as an emergent hillslope property (e.g., Buttle et al., 2004; Weiler et al., 2005; Graham et al., 2010). Beside fill and spill hypothesis, moisture deficit of soil water (Graham and McDonnell, 2010) and strong nonlinearity of hydraulic conductivity function (Steenhuis et al., 2013) were hypothesized to cause the threshold behavior. A modeling study performed by Camporese et al. (2014) suggested that the threshold response was mainly controlled by catchment topography and variable soil depth. According to Tromp-van Meerveld and McDonnell (2006a), the rainfall threshold is a site-specific hillslope property, largely depending on bedrock permeability and topography, soil heterogeneity, the presence of preferential pathways, effective pore storage, etc.

The objective of the present study was to analyze the effects of initial conditions and rainfall characteristics on hillslope runoff at the experimental hillslope site Tomsovka. Different storm rainfall totals as well as temporal variations of rainfall intensity within rainfall–runoff episodes, together with initial hillslope water storages (characterized by spatial distribution of soil water contents within the hillslope segment) were considered in two-dimensional dual-continuum modeling. The causal relationships between initial hillslope storage, rainfall, stormflow, and leakage to bedrock were analyzed. Furthermore, the threshold relationship between rainfall and stormflow as well as hysteresis in the hillslope stormflow–storage relationship were examined.

The present study is organized as follows. First, a brief description of the study area is given in Section 2. Second, two-dimensional model of soil water flow in a hillslope segment, based on dual-continuum approach, is described in Section 2. Third, description of synthetic rainfall episodes derived by scaling from the observed rainfall episodes is presented in Section 2. The simulation results of soil water dynamics in a hillslope during observed and synthetic rainfall–runoff episodes are presented and discussed in Section 3.

2. Materials and methods

2.1. Tomsovka hillslope site

The experimental hillslope site Tomsovka is located in the headwater catchment Uhlirska, Jizera Mountains, North Bohemia, Czech Republic (Fig. 1a). Total area of the catchment is 1.78 km^2, average altitude is 820 m above sea level, mean annual precipitation is 1380 mm, and mean annual temperature is 4.7 °C. The studied hillslope is covered with grass (*Calamagrostis villosa*) and spruce (*Picea abies*).

The soil surface as well as soil–bedrock interface at the Tomsovka hillslope site are approximately planar and parallel. The average slope at Tomsovka is about 14%. The soil at Tomsovka is a sandy loam classified as Cryptopodzol. It is relatively shallow, about 70 cm deep. The soil contains a broad range of pore sizes. The soil profile consists of three layers with different hydraulic properties (Table 1). The topsoil organic layer is of humic character. Below that, a brown sandy loam and light brown soil with a high content of bedrock particles are found (Sanda et al., 2014). The soil layers are underlain by a transition zone of weathered granite bedrock, 5–10 m thick (Sanda and Cislerova, 2009). The transition zone then changes into a compact porphyritic biotite granite bedrock. The interface between the third soil layer and the transition zone is further on referred to as soil–bedrock interface, it is situated at the depth of 70 cm (Table 1). The soil hydraulic parameters characterizing each soil layer were derived from laboratory

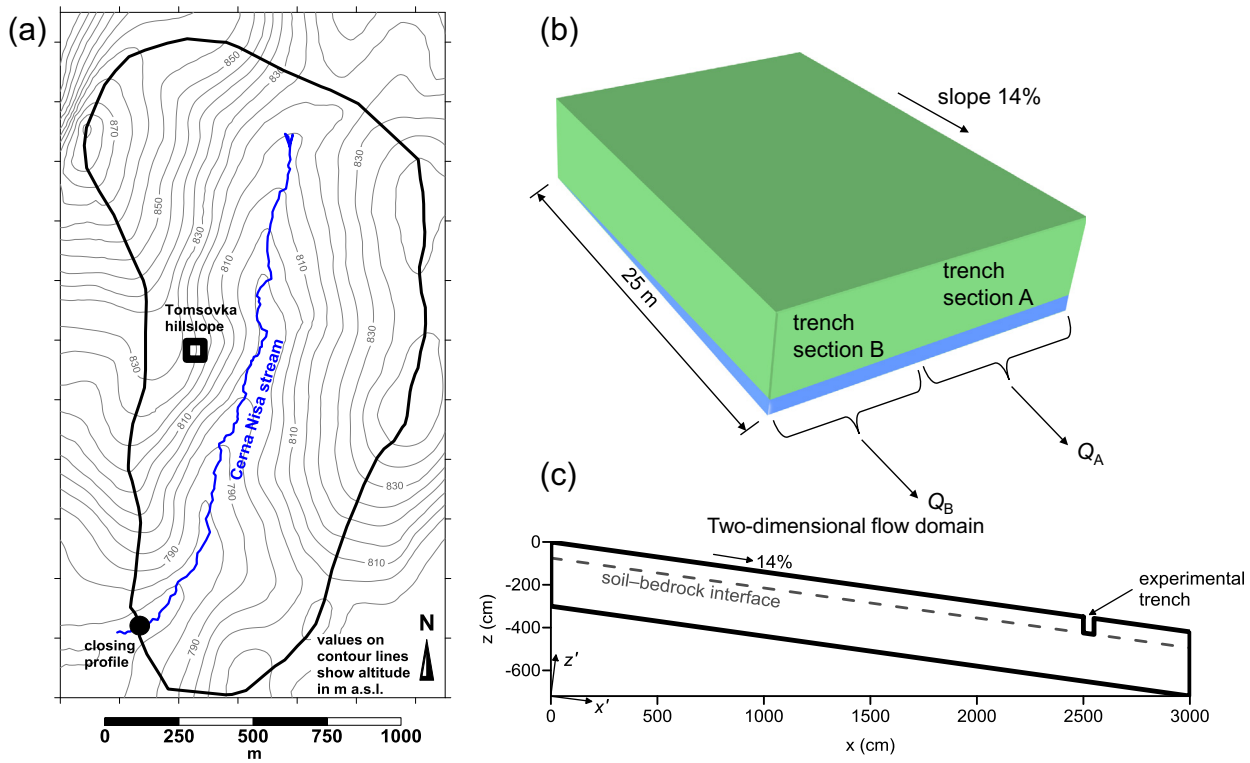

Fig. 1. Uhlirska catchment with the Tomsovka hillslope site (a). Schematic of the experimental trench for collecting hillslope discharge at the Tomsovka site. The discharge is collected 75 cm below the soil surface separately for the two trench sections (Q_A and Q_B) (b). Two-dimensional vertical section of the flow domain. The directions of the principal axes x' and z' of the hydraulic conductivity tensor **K** are indicated at the origin of the coordinate system (c).

Table 1
The soil hydraulic parameters[a] used for the two-dimensional dual-continuum model. The SM and PF abbreviations refer to the soil matrix and preferential flow domain, respectively. Values of saturated hydraulic conductivity are valid for vertical direction.

Domain	Depth (cm)	θ_r ($cm^3\ cm^{-3}$)	θ_s ($cm^3\ cm^{-3}$)	α (cm^{-1})	n (–)	K_s ($cm\ d^{-1}$)	h_s (cm)
SM	0–8	0.20	0.55	0.050	2.00	567	0.00
	8–20	0.20	0.54	0.050	1.50	67	−0.69
	20–70	0.20	0.49	0.020	1.20	17	−1.48
	70–75	0.20	0.41	0.020	1.20	1.3	−1.88
	75–300	0.00	0.21	0.020	1.20	0.4	−2.61
PF	0–75	0.01	0.60	0.050	3.00	5000	0.00

[a] θ_r and θ_s are the residual and saturated water contents, K_s is the saturated hydraulic conductivity, h_s is the air-entry value, and α and n are empirical fitting parameters.

measurements, in which undisturbed 100 cm^3 soil samples and 1000 cm^3 soil cores were used to determine the soil water retention parameters and saturated hydraulic conductivity, respectively (Sanda and Cislerova, 2009). The soil hydraulic parameters derived from the laboratory measurements were adjusted based on variations of soil water content and soil water pressure observed in situ (Dohnal et al., 2006a,b). The resulting hydraulic parameters are listed in Table 1. In addition, the saturated hydraulic conductivity of the weathered bedrock surface (70 cm) was determined by a disk infiltrometer.

Significant preferential flow effects at Tomsovka, affecting the hillslope hydraulic response to rainfall, were reported for the same site by Sanda and Cislerova (2009). Preferential flow was attributed to highly conductive pathways along tree roots as well as to the soil structure and the spatial variability of local soil hydraulic properties. Overland flow is rarely observed at the site due to the highly permeable topsoil layer.

Hydrological and micrometeorological conditions were monitored with 10-min temporal resolution. Subsurface hillslope discharge was measured at an 8 m long experimental trench. The trench consisted of two individual sections (labeled as A and B), each 4 m long (Fig. 1b). Shallow subsurface hillslope discharge was collected separately in each section at the depth of about 75 cm. The discharge rates Q_A and Q_B are measured by tipping buckets during growing seasons (from May to October). Although the geographic watershed divide is located approximately 130 m above the experimental trench, the trench was found to drain a much shorter hillslope length (25–50 m) (Dusek et al., 2012a). This could be explained by a discontinuity of underlying bedrock observed by vertical electrical sounding survey (Sanda and Cislerova, 2009). For the conversion of observed volumetric hillslope discharge to specific stormflow per unit contribution area, the contributing length of 25 m was assumed.

For the modeling purposes, the hillslope micro-catchments corresponding to trench sections A and B were assumed to have approximately the same geometric and material properties (hillslope length, depth to bedrock, soil stratification, soil hydraulic properties, etc.). The differences in the measured discharge hydrographs (Q_A vs. Q_B) were attributed to the spatial variability of preferential pathways, especially in terms of their lateral connectivity.

The significance of spatial variability of preferential pathways and bedrock topography in hillslope stormflow generation was already demonstrated e.g. by Freer et al. (2002), Nieber and Sidle (2010), and Lanni et al. (2013).

2.2. Numerical model

Soil water flow in a hillslope segment is approximated by a dual-continuum approach (Gerke and van Genuchten, 1993a; Vogel et al., 2000a). This approach takes into account the dual character of flow, i.e., flow in the soil matrix and in the preferential pathways. Flow of water in the dual-continuum system is described by a set of two-dimensional Richards' equations:

$$C_f \frac{\partial h_f}{\partial t} = \nabla \cdot (\mathbf{K}_f \nabla h_f) + \nabla \cdot (\mathbf{K}_f \nabla z) - S_f - \frac{\Gamma_w}{w_f} \quad (1)$$

$$C_m \frac{\partial h_m}{\partial t} = \nabla \cdot (\mathbf{K}_m \nabla h_m) + \nabla \cdot (\mathbf{K}_m \nabla z) - S_m + \frac{\Gamma_w}{w_m} \quad (2)$$

where the subscripts f and m stand for the preferential flow (PF) domain and the soil matrix (SM) domain, respectively, C is the soil water capacity (m^{-1}), h is the soil water pressure head (m), $\mathbf{K}$ is the hydraulic conductivity tensor ($m\,s^{-1}$), S is the local root water extraction intensity (s^{-1}), Γ_w is the soil water transfer term (s^{-1}) controlling the water exchange between the domains, w_m and w_f are volume fractions of the respective domains ($w_m + w_f = 1$), and z is the vertical coordinate (m) directed positive upward.

The soil water transfer term in Eqs. (1) and (2) is described by a modified first-order approximation of Gerke and van Genuchten (1993b):

$$\Gamma_w = \alpha_{ws} K_{ar} (h_f - h_m) \quad (3)$$

where α_{ws} is the water transfer coefficient at saturation ($m^{-1}\,s^{-1}$) and K_{ar} is the relative unsaturated conductivity of the SM–PF domain interface. Values of K_{ar} range from 0 to 1 depending on the SM and PF domain conductivities, which are evaluated for the upstream soil water pressure (Gerke et al., 2013).

The composite boundary flux of soil water q is defined as:

$$q = \mathbf{n}\mathbf{q}_f w_f + \mathbf{n}\mathbf{q}_m w_m \quad (4)$$

where $\mathbf{n}$ is the unit normal to the boundary (–), $\mathbf{q}_f$ and $\mathbf{q}_m$ are the vectors of the domain specific soil water fluxes ($m\,s^{-1}$). This equation was used to calculate the hillslope discharge Q (stormflow) from the simulated 2D domain.

The dual set of governing equations (Eqs. (1) and (2)) was solved numerically by the computer program S2D using the fully implicit Galerkin finite elements method (Vogel et al., 2000a).

2.3. Model application

The synthetic rainfall episodes used in this study are based on data measured at the Tomsovka site from May 2007 through October 2009. Details about the application of 2D dual-continuum model at Tomsovka were presented in our previous study (Dusek and Vogel, 2014), where the model predictions of hillslope discharge and soil water status were compared with experimental data.

Soil–plant–atmosphere interactions taken into account in simulations involved natural rainfall, evaporation, and plant transpiration. The rainfall intensities were organized in one-hour series. The daily potential evapotranspiration was calculated using Penman–Monteith equation (Monteith, 1981), based on micrometeorological data observed directly at the Tomsovka site. The root water uptake (represented by the sink term, S, in Eqs. (1) and (2)) was described according to Feddes et al. (1978). Given the humid character of the experimental hillslope site, the actual evapotranspiration calculated by the 2D model was equal to the potential rate. More detailed information about the root water uptake parameterization at Tomsovka was given by Dohnal et al. (2006b) and Dusek et al. (2012a).

The simulations were performed for a 30 m long and 3 m deep 2D vertical cross-section of the hillslope (Fig. 1c). The flow domain spanned 25 m above and 5 m below the experimental trench to correctly account for the fluxes in the vicinity of the trench. The hillslope length contributing to discharge was thus 25 m. A constant slope of 14% was considered. The 2D flow domain was discretized into 283,113 triangular elements. Identical boundary conditions were used for both flow domains (the PF and SM domains). The upslope face of the experimental trench was modeled as a seepage face with the effective height of 55 cm, permitting water to discharge under saturated conditions only (i.e., for local pressure head values of $h \geqslant 0$). For all performed simulation scenarios, the saturated lateral flow was localized in a narrow zone above the soil–bedrock interface, the height of the seepage face therefore did not affect the intensity of stormflow. At the bottom boundary, at the depth of 3 m, free drainage condition was imposed allowing water to leave the 2D domain at the rate equal to unsaturated hydraulic conductivity. At the vertical upslope and downslope sides of the computational domain, no-flow and seepage face boundary conditions were prescribed, respectively.

The soil hydraulic characteristics of the soil and bedrock matrices as well as of the preferential flow domain were parameterized using the modified van Genuchten model (Vogel and Cislerova, 1988; Vogel et al., 2000b). The modified expressions add extra flexibility in the description of the hydraulic properties near saturation by introducing a nonzero air-entry pressure head value h_s. Vogel et al. (2000b) showed that the modified approach provides more adequate prediction of the unsaturated hydraulic conductivity function and improves the stability of the numerical solution of Richards' equation for soils with low values of the parameter n (less than about 1.5).

Soil hydraulic parameters of the respective soil and bedrock layers are given in Table 1. Based on the available information from a regional hydrogeological survey, the saturated hydraulic conductivity of the transition zone of weathered bedrock was estimated to be 0.4 cm d^{-1}. For the depth of 70–75 cm, a higher hydraulic conductivity value was assigned (1.3 cm d^{-1}), which was determined by a disk infiltrometer. The anisotropy ratio in respect to principal directions x' and z' for the hydraulic conductivity tensor of the PF domain was set equal to $K_{x'x'}/K_{z'z'} = 10$ (where x' is directed along the slope and z' is perpendicular to x', see Fig. 1c), indicating the increased conductivity of the laterally continuous network of preferential pathways along the local hillslope gradient. The increased lateral conductivity was assumed to represent the PF domain formed by pathways along tree roots and biopores as well as lateral soil structural features.

The water transfer coefficient, governing exchange of water between the SM and PF domains, as well as the volumetric proportion of the PF domain were set according to Vogel et al. (2010). Soil hydraulic properties of the preferential flow domain (Table 1) were estimated in our previous studies of soil water dynamics at Tomsovka (e.g., Vogel et al., 2003; Dohnal et al., 2006a,b), including field tracer experiments (Cislerova et al., 1998; Sanda et al., 2005) and laboratory column experiments (Snehota et al., 2007). More details regarding the parameterization of soil hydraulic properties of the SM and PF domains at Tomsovka can be found in Dohnal et al. (2006a, 2012). The volumetric fraction of the PF domain, w_f, was assumed to vary linearly between 0.07 at the soil surface and 0.05 at the depth of 75 cm. The decrease of the depth-dependent value of w_f represents variability of the density of the preferential network with depth. The values of α_{ws} were also estimated to vary linearly between the soil surface and the lower

boundary, i.e. between 1 and 0.01 cm^{-1} d^{-1}, which corresponds to a decreasing value of saturated hydraulic conductivity of the SM domain. Higher α_{ws} values lead to less preferential flow conditions, causing faster equilibration of the pressure heads between the SM and PF domains. Such conditions were assumed to prevail in the topsoil horizon. The domains hydraulically communicate, i.e., exchange soil water, mostly under near-saturated conditions. Under dry conditions, they become effectively disconnected due to low interfacial conductivity (at the SM–PF domain interface).

At the soil–bedrock interface, there is a high discontinuity of hydraulic properties of the soil matrix, mainly the saturated hydraulic conductivity. Our previous study showed that a certain amount of the matrix flow is diverted toward the preferential pathways above the semipermeable interface (Dusek and Vogel, 2014). This mechanism causes mixing between old pre-event water stored at the base of the soil profile and new event water during a rainfall event (Dusek et al., 2012b). The exchange is highly nonlinear process and was found to play a key role in control of the soil moisture status and generation of stormflow (e.g., Weiler and Naef, 2003; Pirastru and Niedda, 2010).

To characterize soil water status in the hillslope segment, the hillslope soil water storage (m) and degree of saturation were calculated as follows:

$$HS(t) = \frac{1}{L}\int_{\Omega} \theta(t,x,z) - \theta_r(x,z)d\Omega \quad (5)$$

where L is the contributing hillslope length (25 m), θ is the soil water content (m^3 m^{-3}), θ_r is the residual soil water content (m^3 m^{-3}), and Ω is the specified domain of interest. In our case, Ω corresponded to soil layers above the soil–bedrock interface. The initial value of *HS*, characterizing the antecedent (pre-storm) moisture conditions, is further referred to as *IHS*.

Degree of hillslope saturation (–) is defined as:

$$DS(t) = \frac{HS(t)}{\max HS} \quad (6)$$

where max *HS* (m) is the maximum value of hillslope storage for the soil profile above the trench. The value of max *HS* was equal to 225 mm for the Tomsovka hillslope. The value of *HS* represents the composite volume of water in both flow domains (SM and PF) weighted according to their respective volumetric proportions. The value of *DS* corresponding to initial hillslope storage is further referred to as *IDS*.

In this study, leakage to bedrock refers to deep vertical percolation (groundwater recharge) through the soil–bedrock interface, contributing to catchment baseflow. Note that stormflow at Tomsovka includes only shallow subsurface flow, i.e., without the contribution of overland flow.

2.4. Numerical experiments

The rainfall–stormflow relationship can be preferably obtained from field observation. However, data records have to be extensive to cover the possible range of this relationship. Therefore, numerical experiments may serve as an alternative.

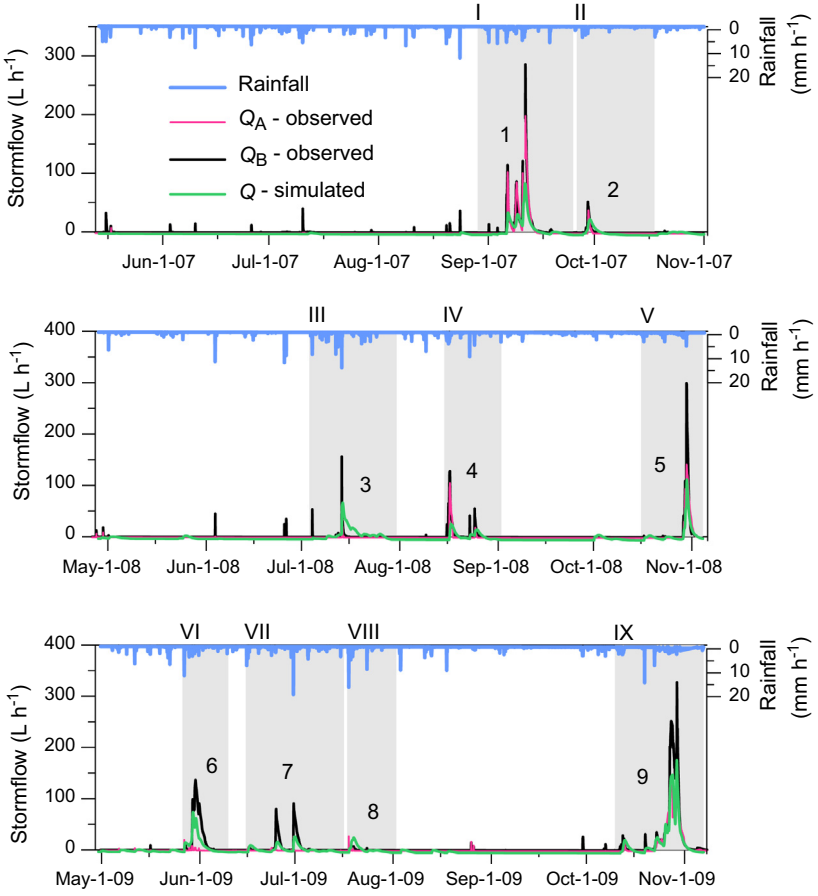

Fig. 2. Observed (trench sections A and B) and simulated hillslope discharge. The selected major rainfall–runoff episodes are marked with Arabic numerals and shown in shaded bars. Roman numerals are used to denote initial conditions for the episodes. (For interpretation of the references to color in this figure legend, the reader is referred to the web version of this article.)

Long-term growing season simulations of subsurface runoff at Tomsovka were compared quantitatively with experimental data (hillslope discharge and soil water pressure) in our previous study (Dusek and Vogel, 2014). The resulting predictions of hillslope discharge are shown in Fig. 2. In the present study, we use the S2D model to analyze the effects of initial soil water status, storm rainfall amount, and the temporal variation of storm rainfall intensity on the formation of saturated subsurface hillslope discharge.

To extend the relatively low number of major rainfall–runoff episodes observed in the experimental trench at Tomsovka, we use synthetic rainfall episodes derived from the nine real events (Fig. 2) by means of scaling. These newly constructed rainfall series were then used in rainfall–runoff simulations to produce functional relationship between rainfall and stormflow for given initial saturations. Initial soil water conditions for each of the nine episodes were obtained from the growing season simulations (Fig. 3). The synthetic rainfall episodes were derived from the observed episodes by scaling the rainfall totals while preserving the relative temporal variations of rainfall intensities during episodes (Fig. 4). The selected observed episodes were characterized by continuous stormflow lasting more than 2 days. The rainfall characteristics of the episodes are presented in Table 2.

The rainfall–runoff simulations were conducted using two different protocols. Under the first protocol (Protocol I), all synthetic rainfall episodes derived from the same observed episode were combined with the same initial soil water condition predicted by the S2D model at the beginning of the observed rainfall episode. Under the second protocol (Protocol II), each synthetic episode was combined with nine different initial conditions corresponding to the nine observed rainfall episodes.

For the first group of simulations (under Protocol I), the values of the scaling factor were varied in 25% steps of the observed rainfall totals (Fig. 4). In some cases, a few additional smaller steps were used (to improve graphical representation of the simulation results in the rainfall–stormflow coordinates). Approximately ten synthetic rainfall episodes were created from each of the nine observed episodes (all together 98 synthetic episodes were generated under Protocol I). The scaling factors ranged from 1% to 600% of the observed rainfall total.

For the second group of simulations (under Protocol II), the scaling factors were adjusted so as to produce 50 mm, 100 mm, 150 mm, and 200 mm cumulative rainfall (Fig. 4). The range of rainfall totals considered under this protocol was chosen to reflect the observed range in 2007–2009 period. The resulting synthetic rainfall episodes were then used in dual-continuum simulations to produce functional relationship between rainfall, initial hillslope storage (*IHS*), stormflow, and leakage to bedrock. In total, 324 simulations (9 *IHS* × 9 rainfall episodes × 4 rainfall amounts) were executed under Protocol II.

Under Protocol I, the evapotranspiration rates for each episode were kept as determined by the Penman–Monteith equation for the respective time period, i.e. they were not scaled with the

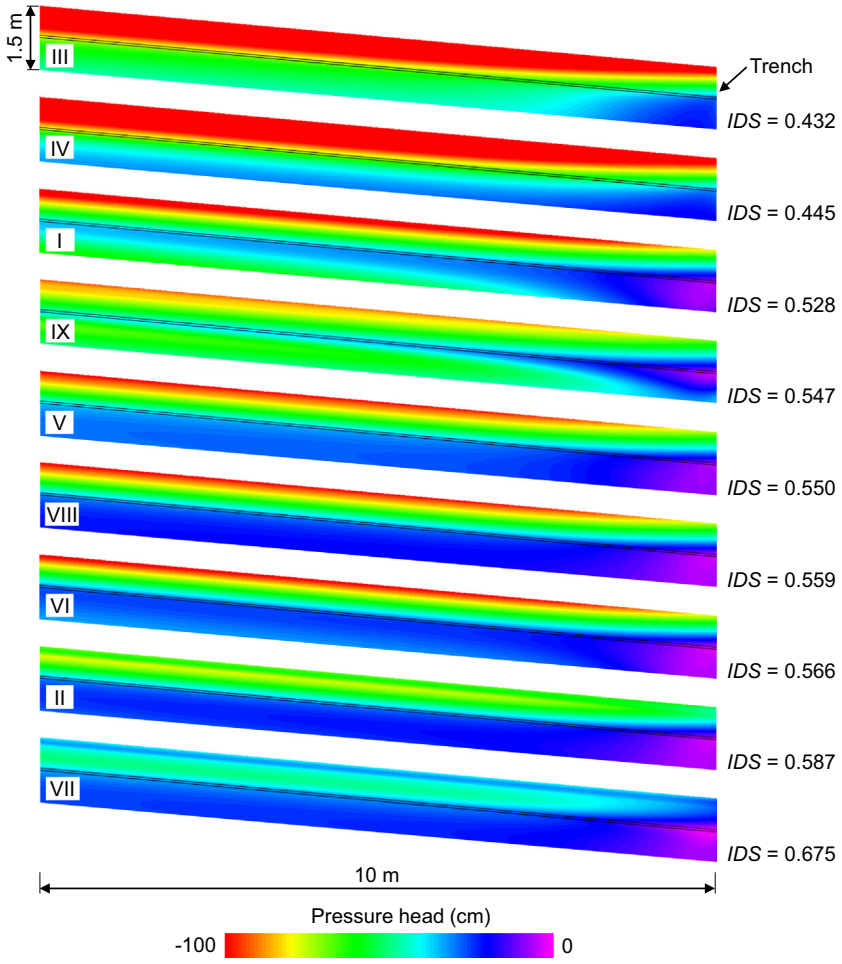

Fig. 3. Initial conditions at the beginning of the selected rainfall episodes (10 m long and 1.5 m deep vertical cross-sections above the trench are shown). Each initial condition (pressure head in the soil matrix domain) is denoted by a Roman numeral and characterized by the value of initial degree of saturation. Two solid lines represent the depths of 70 cm and 75 cm, respectively.

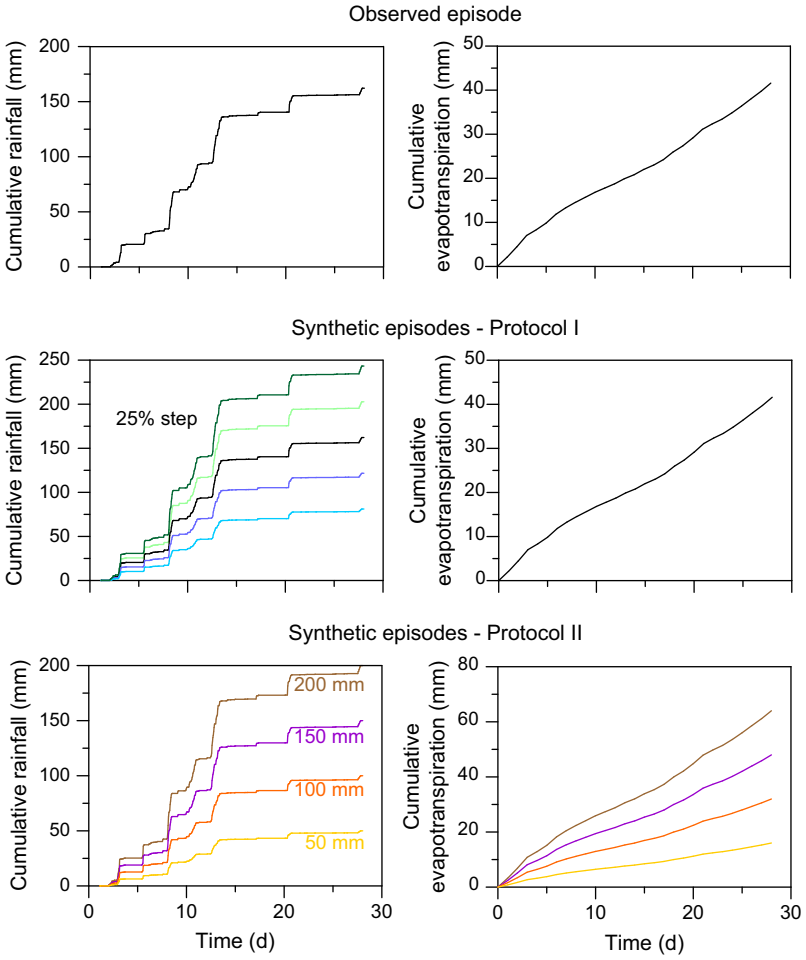

Fig. 4. Rainfall and evapotranspiration rates for synthetic rainfall episodes derived by scaling from the observed rainfall episode #1.

Table 2
Rainfall characteristics for the observed major rainfall–runoff episodes. The episode numbers refer to Fig. 2.

	Rainfall–runoff episodes								
	1	2	3	4	5	6	7	8	9
Average hourly rainfall intensity (mm/h)	1.07	0.69	1.04	1.62	0.91	1.21	0.87	1.31	1.61
Maximum hourly rainfall intensity (mm/h)	7.00	4.40	16.50	11.50	6.70	12.10	14.37	16.90	14.90
Cumulative rainfall (mm)	162	48	196	137	117	113	161	73	221
Episode timespan (days)	27	22	28	18	20	15	32	16	28
Net rainfall duration (h)	152	70	189	85	128	94	186	56	170

rainfall amount. The estimated interception loss was also left unscaled. For the simulations under Protocol II, the combined cumulative evapotranspiration and interception loss was assumed to be 32% of the rainfall, i.e. it was scaled with the rainfall amount. From the long-term water balance at Tomsovka (Dusek et al., 2012b), the combined evapotranspiration and interception loss constituted 61% of rainfall. However, evapotranspiration and interception represented together about 32% of rainfall during major rainfall–runoff episodes. Fig. 4 shows rainfall and evapotranspiration rates for synthetic episodes derived from the observed episode #1.

The treatment of synthetic rainfall episodes under Protocol I represents a simplistic approach in which the only perturbed quantity is the episodic rainfall total, while initial hillslope saturation, evapotranspiration, and interception remain unchanged (for all synthetic episodes derived from one observed episode). This approach was, however, unsuitable for a more complex analysis performed under Protocol II, where initial soil water distribution was varied in addition to rainfall total. The reason is that, under Protocol II, the surplus/lack of rainwater, resulting from under/over-estimated evapotranspiration and interception loss, would obscure the impact of different temporal distributions of rainfall intensities and different initial soil water status on the hillslope water balance.

3. Results and discussion

In the following sections, we discuss both long-term rainfall–runoff simulations (growing seasons 2007, 2008, and 2009) and simulations involving synthetic rainfall episodes. In the discussion,

we focus on the initiation of subsurface stormflow as well as on the changes of overall hillslope water balance at Tomsovka.

3.1. Long-term simulations of subsurface stormflow and leakage to bedrock

Observed (trench sections A and B) and simulated variations of subsurface stormflow during the period of three consecutive growing seasons are presented in Fig. 2. Overall, the two-dimensional model approach captured the shallow stormflow dynamics of the major rainfall–runoff episodes. The simulated stormflow remained smaller than the observed discharge. This can be partly explained by the decision to choose the length of the contributing hillslope segment at the lower end of the previously estimated range (25–50 m; Dusek et al., 2012a). Lower discharge in trench section A in 2009 was probably related to a malfunction of the flow gauge.

In Fig. 5, spatiotemporal development of soil water pressure head along the soil–bedrock interface is depicted together with the observed and simulated stormflow. Two major rainfall–runoff episodes observed in 2009 are shown (episodes #6 and #7). The complex rainfall pattern with several distinct sub-episodes induced shallow saturated stormflow from the hillslope. The length of the near-saturated part of the interface corresponds to the peak values of the hillslope discharge. Several distinct periods of increased saturation of the soil–bedrock interface, related to stormflow periods, can be recognized. The length of the near-saturated part of the interface was different during the individual sub-episodes. The maximum length was less than 5 m above the trench (May 30). In the vicinity of the trench, close to saturation conditions prevailed during the entire period depicted in Fig. 5. Positive pressure heads were predicted in the soil matrix domain, but remained small ($h \leqslant 2$ cm). This was caused by the transfer of water toward the PF domain above the interface and the fact that water from the preferential pathways was drained by lateral flow along the interface (contributing to stormflow). Near-saturated conditions in the SM domain in the vicinity of the trench were sufficient to predict significant stormflow.

The simulated leakage to bedrock during the three growing seasons is depicted in Fig. 6a. It is associated with fluxes directed from the soil matrix to bedrock. Near-saturated conditions prevailed at the soil–bedrock interface near the trench (see Fig. 5). As a result, this part of the interface contributed to the leakage more that the upslope part. During the summer periods, a negative trend in leakage to bedrock was predicted (Fig. 6a), indicating an upward

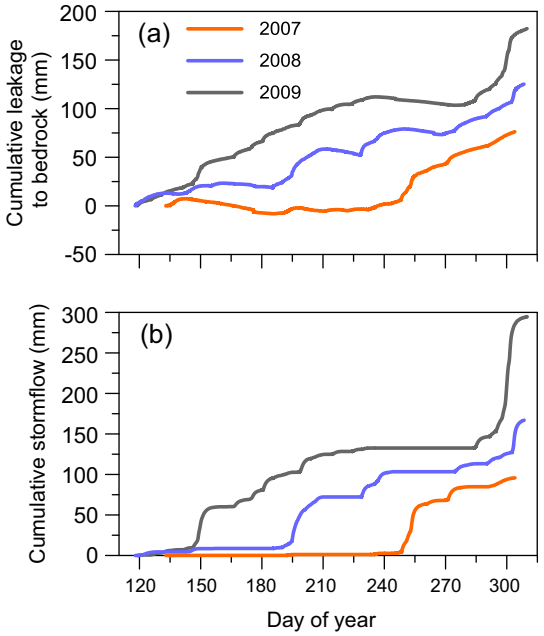

Fig. 6. Simulated leakage to bedrock (a) and stormflow (b).

movement of soil water across the interface as demanded by increased evapotranspiration. On average, the upward cumulative rate amounted to 18 mm per growing season. An upward leakage was also predicted in a numerical study of Broda et al. (2011); however, the partitioning of leakage along a hillslope was found to be controlled by the hillslope geometry. The combined hillslope balance of growing seasons 2007, 2008, and 2009 involved: rainfall 2232 mm, evapotranspiration 1264 mm (57% of rainfall), stormflow 568 mm (26%), and leakage to bedrock 384 mm (17%). Winter periods with reduced evapotranspiration and increased precipitation input would lead to higher proportion of both stormflow and leakage to bedrock. Heppner et al. (2007) estimated annual percolation under a grass lysimeter as 32% of rainfall.

In our model, leakage to bedrock is a product of both unsaturated and saturated flow across the interface. The saturated leakage took place during stormflow episodes, when the saturated zone developed above the soil–bedrock interface. During stormflow episodes, leakage represented about 86% of total leakage (on the basis of the three seasons). Unsaturated flow, associated with

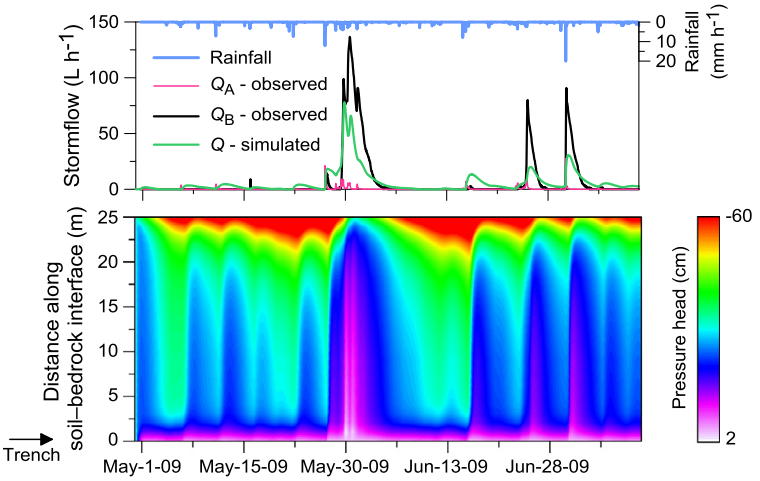

Fig. 5. Spatiotemporal development of pressure head (in the soil matrix domain) at the soil–bedrock interface (episodes #6 and #7). The stormflow rates are superimposed atop.

the periods where no stormflow was predicted, accounted for the remaining 14% of total leakage to bedrock. At Panola experimental hillslope, Appels et al. (2015) found that unsaturated leakage was the prevailing groundwater recharge mechanism accounting for 60% of annual recharge.

In Fig. 6b, cumulative stormflow during the three growing seasons is shown. The stormflow associated with the matrix flow was negligible compared to stormflow formed in the preferential continuum. The preferential stormflow made up 98% of total stormflow. For instance, Beckers and Alila (2004) concluded that simulated streamflow was almost entirely derived from preferential flow while the matrix flow contribution remained negligible during high flow rainfall–runoff events.

3.2. Synthetic rainfall–runoff simulations under Protocol I

Fig. 7 shows the effect of varying episodic rainfall amount on hillslope stormflow for synthetic rainfall episodes derived from the individual observed episodes. Each symbol in this figure represents one simulation. It can be seen that for smaller initial hillslope storages ($IDS < 0.5$), the stormflow response became highly nonlinear (episodes #3 and #4). For large rainfall inputs (about 400 mm), the simulations converged to a narrow range of stormflow (240–270 mm), regardless of *IDS*. Due to positive pressure heads developed within the hillslope for the simulations with extreme rainfall amounts, predicted hillslope storages approached value of max *HS* (225 mm), indicating tendency to the formation of saturation excess overland flow if the amounts were further increased. Stormflow was confirmed to depend strongly on *IDS* for smaller rainfall amounts (<100 mm). For rainfall amounts larger than 100 mm, initial saturation was less important. The pattern shown in Fig. 7 is similar to that presented by Hrncir et al. (2010).

The synthetic episodes derived from the episode #7 with $IDS = 0.675$ ($IHS = 151.7$ mm) represented an extreme case, in which the stormflow was triggered even by negligible rainfall (<10 mm) due to high initial saturation at the soil–bedrock interface in the trench vicinity. High initial saturation also induced similar stormflow in the 10–30 mm rainfall range. Only this set of synthetic episodes produced convex character of the rainfall–stormflow relationship (Fig. 7). This was caused by the greatest evapotranspiration (82 mm) during the episode. As the cumulative evapotranspiration rate was not scaled under Protocol I, the ET/rainfall ratio of the episode #7 was the greatest among all episodes, leading to lower stormflow in the 30–220 mm rainfall range than seen for the other episodes.

The difference in absolute values of initial saturation in this study with those shown by Hrncir et al. (2010) was due to different assumptions in respect to soil layering. In the present study, we followed the soil stratification as suggested by Vogel et al. (2010), where the soil hydraulic parameters were further refined for the purpose of numerical modeling of stormflow responses at the hillslope scale. Furthermore, the soil profile saturation assumed by Hrncir et al. (2010) was based on the observation located 1 m above trench section B, in contrast to integral hillslope saturation used in this study.

Hrncir et al. (2010) hypothesized that a threshold value of rainfall amount was needed to initiate significant stormflow; they estimated rainfall threshold 60–70 mm. In a follow up study, Steenhuis et al. (2013) estimated the threshold in the range of 35–75 mm, depending on *IDS*. The hypothesis of the threshold-like behavior was not confirmed by our simulations. The simulation results showed an exponential relationship between rainfall and stormflow for different initial saturations (Fig. 7). However, it was difficult to find a single value of threshold necessary to trigger significant stormflow. Depending on *IDS*, the rainfall amount between 10 mm and 90 mm produced similar stormflow. This could be explained by the limited number of observed stormflow episodes in the 10–90 mm rainfall range included in the studies of Hrncir et al. (2010) and Steenhuis et al. (2013). The rainfall threshold estimation is elaborated in more detail in the following section.

3.3. Synthetic rainfall–runoff simulations under Protocol II

3.3.1. Rainfall–stormflow relationship for different initial saturations

The adoption of Protocol II makes it possible to distinguish between the effects of initial hillslope saturation and temporal rainfall distribution. The functional relationship between rainfall and stormflow obtained for the simulated synthetic rainfall–runoff episodes for different initial saturations is shown in Fig. 8. A non-unique nonlinear dependence of stormflow on rainfall was obtained (i.e., a convex shape of the rainfall–stormflow relationship). The simulations with $IDS > 0.5$, however, showed a nearly linear relationship. The stormflow variability due to temporal rainfall distribution is reflected in the spread of stormflow amounts at the individual cumulative rainfall levels (50 mm, 100 mm, 150 mm, and 200 mm).

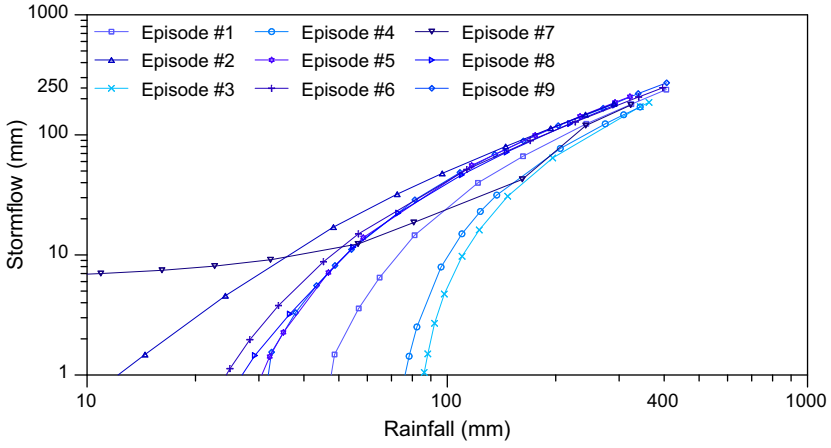

Fig. 7. The relationship between rainfall and stormflow for synthetic rainfall episodes derived from the selected observed episodes. Symbols represent responses to synthetic episodes derived from the same observed episode.

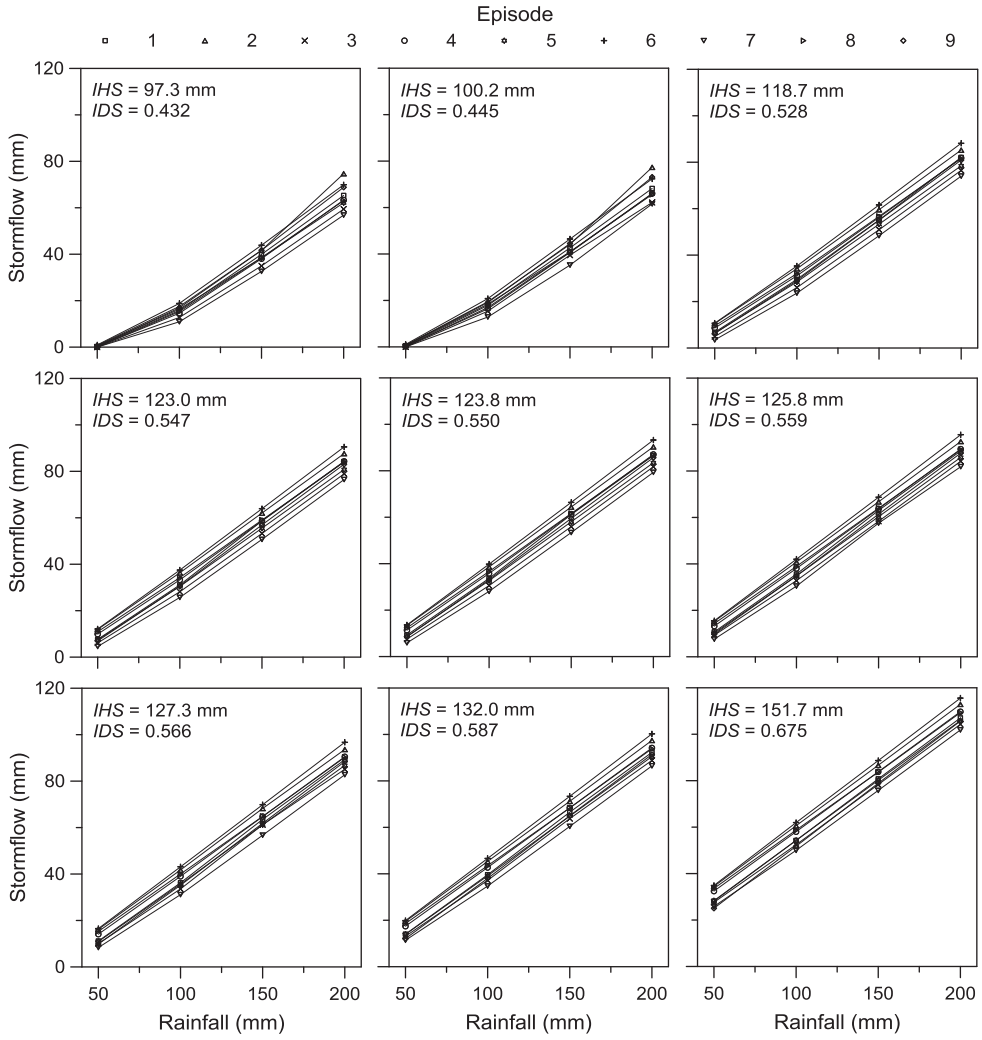

Fig. 8. Rainfall–stormflow relationship for the nine initial hillslope saturations, nine rainfall episodes, and four rainfall amounts. Each symbol represents a single simulation of synthetic rainfall–runoff episode. The lines connect synthetic episodes derived from the same observed episode.

The same relationship (involving rainfall, initial saturation, and stormflow) in a different projection is shown in Fig. 9. The figure illustrates the stormflow variability due to temporal rainfall distribution within episodes. The increase of stormflow amount for different initial hillslope saturations (represented by Roman numerals in Fig. 9) was not proportional, indicating

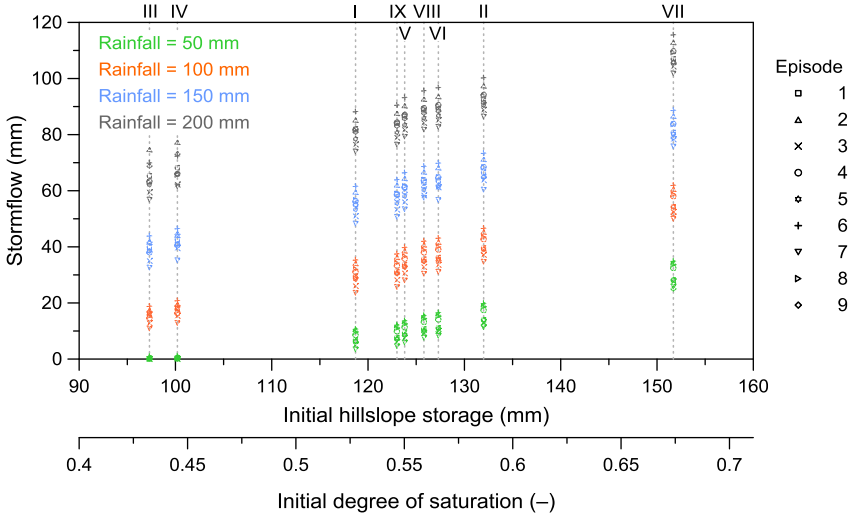

Fig. 9. The relationship between initial saturation and stormflow for four rainfall amounts. Each symbol represents one rainfall–runoff simulation reflecting the hillslope response to a particular synthetic rainfall episode. Episode numbers refer to the observed rainfall episodes, from which the synthetic episodes were derived. Initial saturations are labeled with Roman numerals following the chronological order of the observed episodes.

a nonlinear relationship between hillslope storage and stormflow.

The effect of different temporal rainfall distribution is reflected in different simulated stormflow amounts produced by synthetic rainfall episodes with the same rainfall amount but derived from different observed rainfall episodes. In overall, the smallest stormflow was produced during synthetic episodes derived from the observed episodes #3 and #7. Note that these synthetic episodes had a relatively low average intensity and long rainfall duration. The highest stormflow was generated by synthetic episodes derived from the episodes #2 and #6 (these two episodes had very similar rainfall characteristics). Surprisingly, synthetic episodes derived from the episode #8 with the shortest rainfall duration and the greatest average and maximum intensity did not cause the highest stormflow (it scored third). This confirmed that the rainfall characteristics alone did not explain stormflow generation sufficiently well.

3.3.2. Leakage to bedrock

Leakage to bedrock as a function of initial hillslope saturation and rainfall amount is shown in Fig. 10. As expected, the leakage increased with increasing rainfall amount and *IDS* values. A nonlinear pattern was obtained for lower values of initial saturation (*IDS* < 0.528, initial conditions III and IV), with a lower rate of increase of leakage with increasing rainfall (i.e., a concave shape of the rainfall–leakage relationship). Leakage to bedrock mostly originated from the saturated zone above the soil–bedrock interface (the contribution of unsaturated flow was negligible). For lower values of initial saturation (*IDS* < 0.528), the variability of the results due to the temporal rainfall distribution increased considerably with increasing rainfall amount (as reflected in a large spread of leakage values among the episodes). Synthetic episodes derived from the observed episode #2 showed remarkably small increase of leakage for rainfall increase from 150 mm to 200 mm (*IDS* = 0.432 and 0.445, initial conditions III and IV). This was counterbalanced by increasing stormflow; the increase of stormflow with increasing rainfall was found progressively nonlinear for low initial saturations (see Fig. 8). The simulations with higher initial saturations showed a linear rainfall–leakage relationship and relatively low variability between different rainfall episodes (Fig. 10).

The relationship between initial saturation and leakage to edrock for four different rainfall amounts is shown in Fig. 11. An overlap of the leakage values based on 200 mm rainfall with those caused by smaller rainfalls was predicted for lower values of initial saturation (*IDS* ⩽ 0.445, initial conditions III and IV). For the

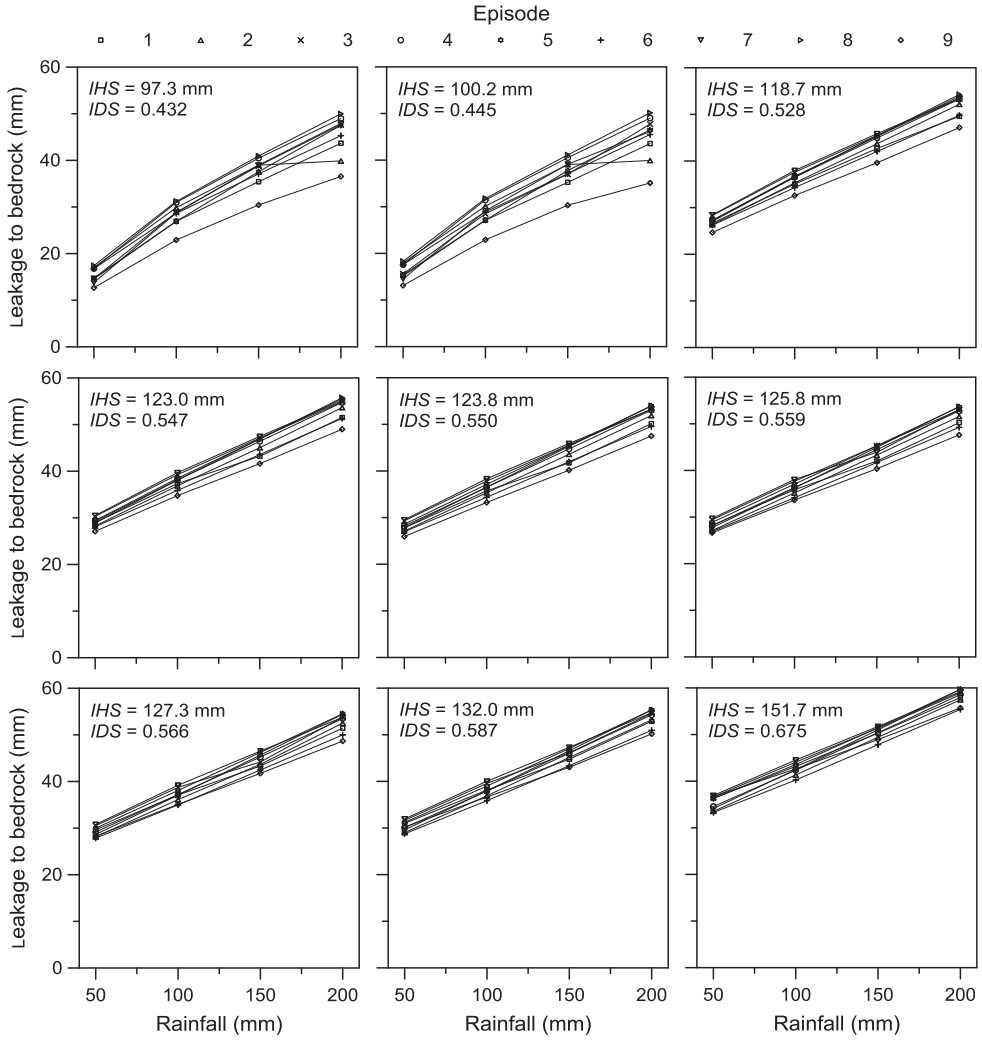

Fig. 10. Rainfall–leakage relationship for the nine initial hillslope saturations, nine rainfall episodes, and four rainfall amounts. Each symbol represents a single simulation of synthetic rainfall–runoff episode. The lines connect synthetic episodes derived from the same observed episode.

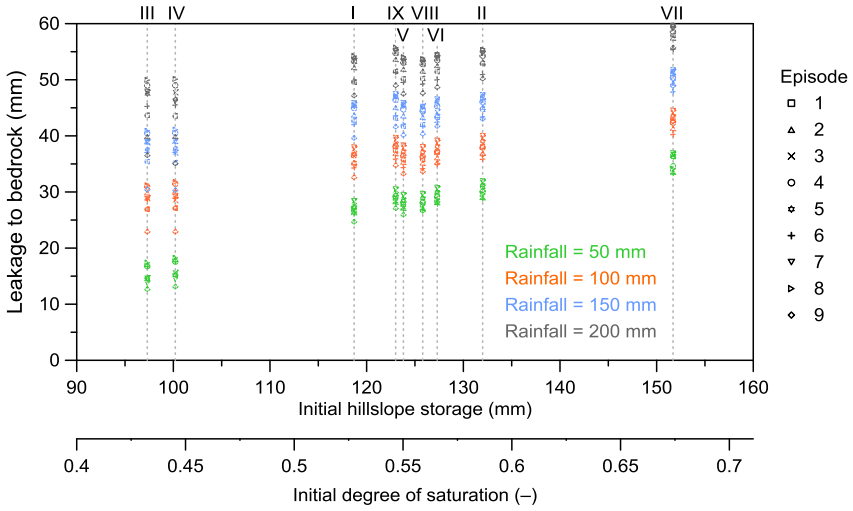

Fig. 11. The relationship between initial saturation and leakage to bedrock for four rainfall amounts. Each symbol represents one rainfall–runoff simulation reflecting the hillslope response to a particular synthetic rainfall episode. Episode numbers refer to the observed rainfall episodes, from which the synthetic episodes were derived. Initial saturations are labeled with Roman numerals following the chronological order of the observed episodes.

intermediate initial saturations (*IDS* between 0.528 and 0.587, initial conditions I, IX, V, VIII, VI, and II), the leakage showed both increasing and decreasing trends. This resulted from the interplay between components of the hillslope water balance induced by different initial distributions of soil water above the soil–bedrock interface. For instance, the synthetic episodes based on initial condition IX (*IDS* = 0.547) showed greater leakage than the episodes based on initial condition V (*IDS* = 0.550). This was caused by a larger vertical pressure gradient between the soil and the weathered bedrock for initial condition IX (see Fig. 3).

The temporal rainfall distribution affected leakage to bedrock as well. As shown in Fig. 11, the lowest leakage to bedrock was predicted for synthetic episodes derived from the observed episode #9, the episode with the smallest average rainfall intensity. The highest stormflow delivered by the synthetic episodes derived from the episodes #2 and #6 was not accompanied by the lowest leakage to bedrock (these episodes scored sixth and eighth in leakage, respectively). Depending on initial hillslope saturation, two different leakage regimes were identified. Within the first regime, the largest leakage was associated with synthetic episodes derived from the observed episode #8 for small *IDS* values (⩽0.445); the synthetic episodes were characterized by the highest average and maximum rainfall intensities and the shortest rainfall durations. Within the second regime, the largest leakage was produced by synthetic episodes derived from the observed episode #7 for *IDS* values larger than 0.445; the largest leakage for these episodes was accompanied by the smallest stormflow. There was a significant interplay among initial saturation, spatial distribution of soil water, and temporal rainfall distribution affecting overall ranking of leakage to bedrock among the episodes (reflected in the position in rainfall–leakage relationship shown in Fig. 10). Unexpectedly, leakage amounts switched the ranking positions for different rainfall amounts more readily than in case of rainfall–stormflow relationship (compare Figs. 8 and 10).

3.3.3. Hillslope water balance

In Table 3, the components of hillslope water balance are summarized for all synthetic rainfall–runoff simulations executed under Protocol II. The variability of stormflow and leakage to bedrock was expressed for all considered *IDS* by giving their ranges

Table 3
The ranges of simulated hillslope water balance components (%) for different values of the initial degree of saturation and selected rainfall amounts. The sum of cumulative evapotranspiration and interception loss for all synthetic rainfall–runoff simulations was assumed to be 32% of the rainfall amount. The ranges were obtained from the nine synthetic episodes. Initial saturations are labeled with Roman numerals.

	Initial degree of saturation, *IDS* (–)								
	0.432 III	0.445 IV	0.528 I	0.547 IX	0.550 V	0.559 VIII	0.566 VI	0.587 II	0.675 VII
50 mm rainfall									
Stormflow	0–1.9	0–2.2	6.9–21.3	9.1–24.3	11.8–27.2	15.2–31.1	16.6–33.0	22.7–39.7	50.1–69.8
Leakage to bedrock	25.3–34.8	26.2–36.6	49.3–56.9	54.2–61.0	51.9–59.0	53.3–59.4	55.7–61.6	57.5–63.9	66.5–73.9
Change of hillslope water storage[a]	31.3–42.7	29.2–41.8	−10.2 to 11.8	−17.3 to 4.7	−18.2 to 4.3	−22.5 to −0.5	−26.6 to −4.3	−35.6 to −12.2	−75.7 to −48.6
100 mm rainfall									
Stormflow	10.9–18.8	12.9–20.8	23.6–35.3	25.7–37.5	28.1–39.8	30.4–42.0	31.1–43.1	34.7–46.6	50.0–61.9
Leakage to bedrock	22.9–31.2	22.9–31.8	32.6–38.0	34.8–39.7	33.2–38.3	33.6–38.1	35.0–39.2	35.9–40.0	40.2–44.5
Change of hillslope water storage[a]	18.0–34.2	15.4–32.2	−5.3 to 11.8	−9.2 to 7.5	−10.1 to 6.7	−12.1 to 4.0	−14.3 to 1.9	−18.6 to −2.6	−38.4 to −22.2
150 mm rainfall									
Stormflow	21.7–29.3	23.5–31.0	32.2–41.1	33.8–42.6	35.6–44.3	38.4–45.8	37.8–46.6	40.3–48.9	50.5–59.1
Leakage to bedrock	20.3–27.3	20.2–27.4	26.4–30.6	27.8–31.6	26.8–30.6	26.9–30.2	27.8–31.0	28.7–31.5	29.2–34.5
Change of hillslope water storage[a]	11.4–26.0	9.6–24.3	−3.7 to 9.4	−6.2 to 6.4	−6.9 to 5.6	−8.0 to 2.7	−9.6 to 2.4	−12.4 to −1.0	−25.6 to −11.7
200 mm rainfall									
Stormflow	28.4–37.3	30.8–38.7	37.0–44.1	38.2–45.3	39.7–46.6	40.9–47.8	41.4–48.4	43.2–50.1	50.9–57.8
Leakage to bedrock	18.3–25.0	17.5–25.1	23.6–27.1	24.5–27.9	23.7–27.0	23.8–26.8	24.3–27.3	25.1–27.7	27.7–29.8
Change of hillslope water storage[a]	5.7–21.3	4.2–19.7	−3.2 to 7.4	−5.2 to 5.3	−5.6 to 4.6	−6.6 to 3.3	−7.7 to 2.3	−9.8 to −0.3	−19.6 to −10.6

[a] Positive value denotes an increase of hillslope storage during the episode, while negative value indicates depletion of hillslope storage.

reflecting the impact of different temporal rainfall distributions. The ranges were calculated as the difference between min and max values of predicted stormflow and leakage. The values of stormflow and leakage are expressed relatively to the rainfall amounts (in %) and thus represent the respective episodic runoff coefficients. The changes in hillslope water storage were calculated after removal of the evapotranspiration and interception loss.

Three different regimes of soil water balance in the simulated hillslope segment were identified (Table 3). (1) The first regime was characterized by a net increase of hillslope storage for smaller initial saturations ($IDS \leqslant 0.445$). (2) For the second regime, *HS* acted as a source for evapotranspiration, leakage to bedrock, and stormflow for larger initial saturations, showing depletion of *HS* over the episode. For instance, the simulation with $IDS = 0.675$ showed a *HS* depletion by 49–76% (2nd regime), while an increase of *HS* by 31–43% was obtained for the scenario based on $IDS = 0.432$ (1st regime). (3) For intermediate initial saturations ($IDS = 0.528$–0.566, initial conditions I, IX, V, VIII, and VI), less significant changes of the hillslope water storage were predicted (3rd regime). The change of overall hillslope water balance was also accompanied by differences in the two runoff components (stormflow and leakage to bedrock). Note that even a significant increase of rainfall amount was incapable of causing a significant change in the overall soil water balance regime, at least for the rainfall amounts considered. It was the initial hillslope saturation, which governed the regime. The largest difference in hillslope water balance among different *IDS* scenarios was obtained for 50 mm rainfall, i.e. the most significant impact of *IDS* on the hillslope water balance was for the lowest rainfall amount.

3.3.4. Thresholds

The rainfall volumes initiating stormflow (*RIS*) are shown in Fig. 12a. It can be seen that the *RIS* volumes gradually changed with initial hillslope saturations. As expected, a decrease of *RIS* for increasing initial saturation was predicted. It was not possible to find a single value or a range of *RIS* triggering significant stormflow. The *RIS* volumes ranged from 0 to 96 mm for all considered simulations. The value of *RIS* converged to 0 mm for *IDS* equal to 0.566 (initial condition VI) and 0.675 (initial condition VII), these are indicated by the arrows in Fig. 12a. There are different reasons for each of the two cases. Because of high initial hillslope saturation, stormflow lasting several days was predicted for the simulation with initial condition VII even after a modest rainfall (reflected by $RIS = 0$ mm). This is consistent with the stormflow response of episode #7 shown in Fig. 7. For the case with $IDS = 0.566$, *RIS* equal 0 mm was caused by a particular soil water distribution in the hillslope segment. Specifically, the soil saturation above the soil–bedrock interface caused stormflow independently of the received rainfall amount. The simulation with $IDS = 0.566$ was characterized by higher initial saturation along the soil–bedrock interface than the scenario based on $IDS = 0.587$ (for which $RIS > 0$ was obtained). Hence, the initial distribution of soil water within the hillslope was a key factor in stormflow generation. These results point to study of Kampf (2011), who also obtained different stormflow for the same value of initial saturation due to different spatial distribution of soil water in a hillslope.

The value of *RIS* increased with increasing cumulative rainfall input for the majority of scenarios (more apparent for initial conditions I, IX, V, and VIII in Fig. 12a). The increased rainfall amounts induced increased hillslope storage before stormflow was initiated, as documented in Fig. 12b. This was because of the high infiltration fluxes resulting from the high rainfall intensities occurring within a short time (before stormflow commenced); less rainfall amount to initiate stormflow was required under different temporal rainfall distributions, which is demonstrated by the synthetic episodes based on smaller rainfall amounts (Fig. 12a). Obviously, the time needed to initiate stormflow was shorter for the simulations with higher cumulative rainfall amount and/or higher initial saturation.

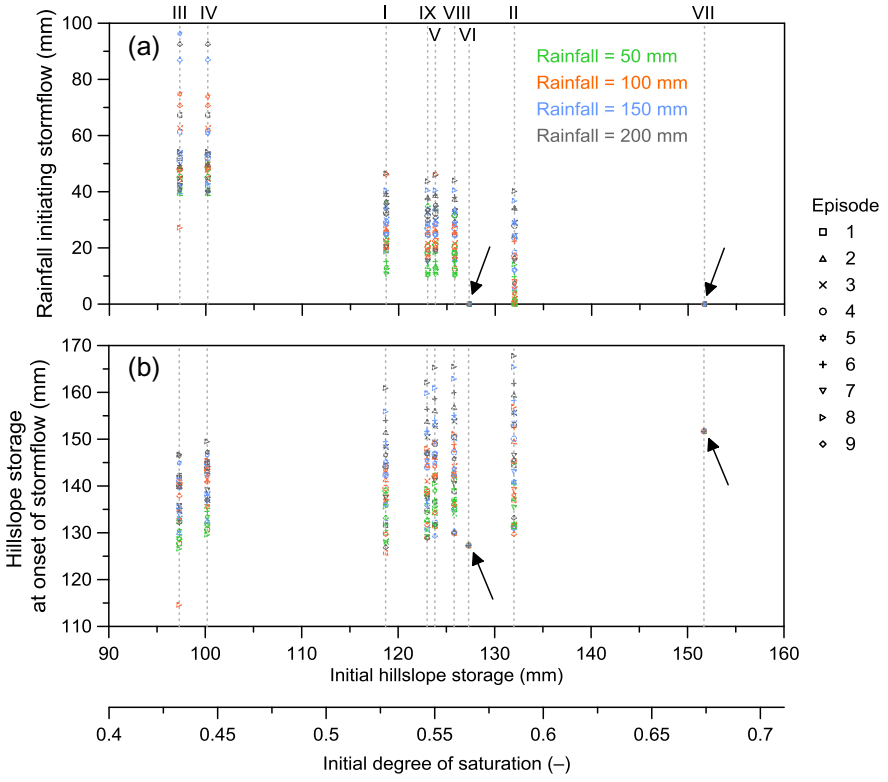

Fig. 12. The rainfall volume initiating stormflow (*RIS*) for different synthetic rainfall episodes (distinguished by episode number and rainfall total) as a function of initial saturation (a). Hillslope storage at the onset of stormflow (*HSOS*) as a function of initial saturation (b). The arrows indicate convergence of *RIS* and *HSOS* values related to different rainfall episodes. The initial saturations are labeled with Roman numerals.

The *RIS* volume is a function of both rainfall amount and initial hillslope storage. Similarly to the *RIS* volume, the hillslope storage at the onset of stormflow (*HSOS*) can be also used to characterize the conditions at the beginning of stormflow. The *HSOS* values for different *IHS* values and rainfall amounts are depicted in Fig. 12b. The predicted values of *HSOS* ranged from 115 to 168 mm for all considered rainfall–runoff episodes. The variability of the surface boundary condition (temporal distribution of rainfall and evapotranspiration fluxes) was reflected in relatively large spread of the *HSOS* values. The onset of stormflow was controlled by the combination of initial hillslope storage and temporal rainfall distribution. The *HSOS* values for the simulations with *IDS* = 0.566 (initial condition VI) and 0.675 (initial condition VII) converged to a single value for different rainfall scenarios similarly to their respective *IHS* values. Interestingly, the values of *HSOS* for the simulations with *IDS* = 0.566 belonged to the smallest *HSOS* values. Similarly to *RIS*, this was caused by a particular initial distribution of soil water, namely saturation along the soil–bedrock interface. A significant effect of temporal rainfall distribution was seen on both *RIS* and *HSOS* thresholds (Fig. 12). The hillslope storage at the cessation of stormflow converged to a narrow range of values (*HS* from 124.6 to 129.4 mm, *DS* = 0.554–0.575) for all considered simulations.

Although the experimental records from many gauged hillslopes (e.g., Peters et al., 1995; Tani, 1997; Noguchi et al., 2001; Uchida et al., 2005) indicated a threshold rainfall–stormflow behavior, there might have been insufficient data to fully prove such behavior. Other data sets show an exponential relation instead (Tromp-van Meerveld and McDonnell, 2006a). A threshold-like response was often associated with flow in soil pipes. The idea of moisture deficit as the cause of threshold behavior was supported by an apparent threshold change under different antecedent moisture conditions (Graham and McDonnell, 2010). This can lead to continuous change of rainfall threshold for different antecedent soil water contents. In this study, we used a wide range of scenarios combining different initial saturations, rainfall amounts, and temporal rainfall distribution to assess the possible causes of the threshold behavior at our experimental catchment.

3.3.5. Hysteretic behavior of stormflow–storage relationship

The evolution of stormflow–storage relationship in response to four synthetic rainfall episodes is depicted in Fig. 13. This figure was constructed for four synthetic rainfall episodes derived from the observed episode #6. The hysteretic loop of stormflow–storage relationship was consistently oriented in clockwise direction, indicating higher *HS* for the rising limbs of stormflow hydrograph than *HS* associated with falling limbs. The onset of stormflow was thus characterized by higher *HS* than the conditions at the cessation of stormflow. The hysteretic behavior was obtained without any additional provisions for hysteresis of soil hydraulic characteristics, variable soil depth, and variable soil–bedrock topography. The hysteretic pattern can be explained by the difference in timing between the responses in hillslope storage and stormflow. In our case, hillslope storage responded faster than stormflow. Such response is expected for flow of water in the subsurface, when saturated zone must be developed before stormflow commences. Nonlinear dynamics of the hillslope runoff processes, manifested in hysteresis of stormflow–storage relationship, is dictated by a nonlinear character of governing equations.

Hrncir et al. (2010) showed a similar hysteretic relationship between stormflow and hillslope saturation at the Uhlirska catchment (based on soil water content data from three depths located 1 m above the trench). Penna et al. (2011) identified two opposite trends in discharge–saturation relationship, allowing both clockwise and anticlockwise directions. In their study, saturation of topsoil layer was averaged from four discrete locations along the hillslope. The direction was found to be governed by the initial condition, i.e. clockwise and anticlockwise direction was associated with wet and dry conditions, respectively. In our analysis, the direction of the hysteretic loop was not affected by the hillslope saturation. Nevertheless, when the hillslope storage was determined from local soil water storages instead of using the

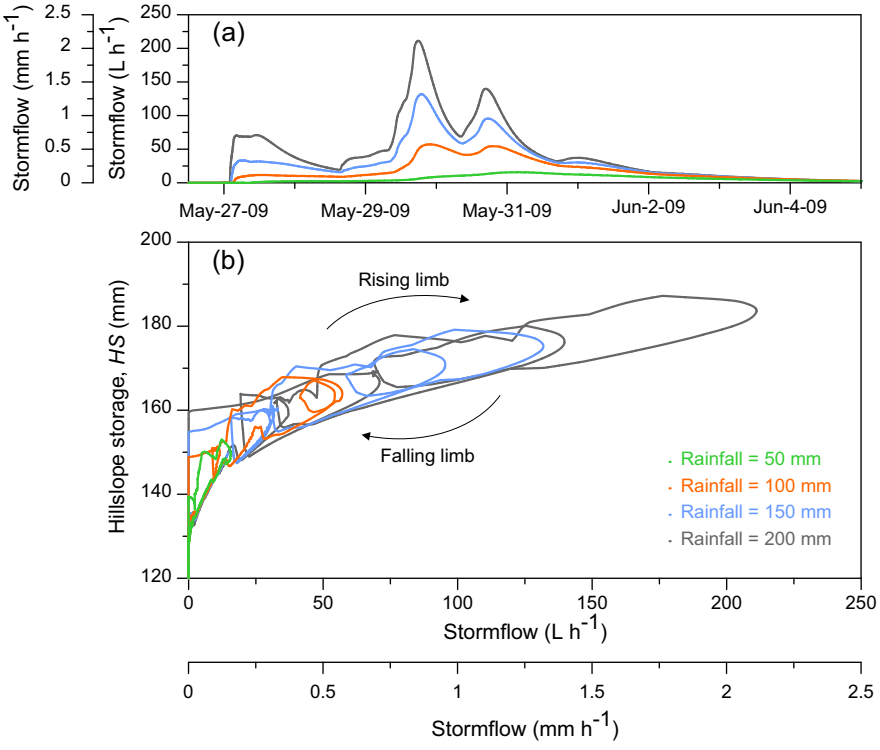

Fig. 13. Simulated stormflow hydrograph (a) and hysteretic relationship between stormflow and hillslope storage (b) for four synthetic rainfall episodes derived from the observed episode #6 (*IDS* = 0.559).

integral hillslope storage, the orientation of the hysteretic loop did reverse (not shown), similarly to Penna et al. (2011).

4. Summary and conclusions

Hillslope discharge responses to rainfall events were analyzed using numerical experiments. The analysis was conducted for a hillslope characterized by significant preferential flow conditions above the soil–bedrock interface. Combined effects of initial hillslope saturation, temporal distribution of rainfall intensities, and storm rainfall totals on hillslope water balance were evaluated by two-dimensional dual-continuum modeling.

It was demonstrated that a larger part of the leakage to bedrock (>85%) was associated with stormflow episodes. During summer, when increased transpiration demands existed, an upward water movement across the soil–bedrock interface was predicted.

Quantitative relationships between the individual components of the hillslope water balance were evaluated. The effect of initial hillslope saturation on simulated stormflow diminished with increasing rainfall amount (>100 mm). The rainfall–stormflow relationship was increasingly linear with increasing initial hillslope saturation and rainfall amount. Similarly, the relationship between the rainfall amount and the amount of leakage to bedrock showed more linear behavior for high initial hillslope saturations.

The simulation results indicated that there was no single valued rainfall threshold responsible for the activation of preferential flow and initiation of stormflow. We revisited previous studies on a threshold-like behavior performed for the Tomsovka hillslope site and further refined the rainfall–stormflow relationship for smaller rainfalls and higher initial saturations (utilizing synthetic rainfall episodes). The rainfall amount needed to initiate stormflow ranged from 0 to 96 mm among the simulated rainfall–runoff events, greatly depending on initial hillslope saturation, initial spatial distribution of soil water, and temporal rainfall distribution.

The performed numerical experiments indicated that the spatial distribution of soil water stored in the hillslope segment prior to the rainfall event affected stormflow dynamics and overall hillslope discharge response. A hysteretic behavior of hillslope stormflow–storage relationship was predicted (hillslope storage responded faster than stormflow), in which the direction of the hysteretic loop was not affected by the initial hillslope saturation. The simulation results also indicated that near-saturated conditions along the soil–bedrock interface were sufficient to trigger significant stormflow even after a modest rainfall. The temporal distribution of rainfall during individual rainfall–runoff episodes had a noteworthy impact on both stormflow and leakage to bedrock. For low initial hillslope saturations, high rainfall intensity induced large leakage to bedrock, not stormflow.

The two-dimensional numerical model was useful in evaluating different hillslope water balance components. It also proved to be numerically stable as hundreds of simulations were run successfully, involving many different combinations of initial saturations, rainfall amounts, and temporal rainfall distributions.

A more thorough analysis of storage–stormflow relationship based on hillslope observations at contrasting initial saturations can answer questions that remain open. Likewise, the threshold behavior between rainfall and stormflow should be further examined. The developed modeling approach will be used to study the transport of natural stable isotopes and dissolved organic compounds in the hillslope segment.

Acknowledgments

This study was supported by the Czech Science Foundation, project No. 14-15201J. We thank the Supercomputing Center of the CTU in Prague for the possibility of running the 2D simulations on its computer network.

References

Appels, W.M., Graham, C.B., Freer, J.E., McDonnell, J.J., 2015. Factors affecting the spatial pattern of bedrock groundwater recharge at the hillslope scale. Hydrol. Process. 29, 4594–4610. http://dx.doi.org/10.1002/hyp.10481.

Bachmair, S., Weiler, M., 2011. New dimensions of hillslope hydrology. In: Levia, D. F. et al. (Eds.), Forest Hydrology and Biogeochemistry: Synthesis of Past Research and Future Directions. Ecological Studies, vol. 216. http://dx.doi.org/10.1007/978-94-007-1363-5_23.

Beckers, J., Alila, Y., 2004. A model of rapid preferential hillslope runoff contributions to peak flow generation in a temperate rain forest watershed. Water Resour. Res. 40, W03501. http://dx.doi.org/10.1029/2003WR002582.

Broda, S., Paniconi, C., Larocque, M., 2011. Numerical investigation of leakage in sloping aquifers. J. Hydrol. 409, 49–61. http://dx.doi.org/10.1016/j.jhydrol.2011.07.035.

Bronstert, A., Plate, E.J., 1997. Modelling of runoff generation and soil moisture dynamics for hillslopes and micro-catchments. J. Hydrol. 198, 177–195. http://dx.doi.org/10.1016/S0022-1694(96)03306-9.

Buttle, J.M., Dillon, P.J., Eerkes, G.R., 2004. Hydrologic coupling of slopes, riparian zones and streams: an example from the Canadian Shield. J. Hydrol. 287, 161–177. http://dx.doi.org/10.1016/j.jhydrol.2003.09.022.

Camporese, M., Penna, D., Borga, M., Paniconi, C., 2014. A field and modeling study of nonlinear storage–discharge dynamics for an Alpine headwater catchment. Water Resour. Res. 50, 806–822. http://dx.doi.org/10.1002/2013WR013604.

Chaplot, V., Ribolzi, O., 2014. Hydrograph separation to improve understanding of dissolved organic carbon dynamics in headwater catchments. Hydrol. Process. 28, 5354–5366. http://dx.doi.org/10.1002/hyp.10010.

Cislerova, M., Sanda, M., Blazkova, S., Mazac, O., Grünwald, A., Zeithammerova, J., Tacheci, P., 1998. Ecological Aspects of the Water Resources Protection: Transport Processes in a Watershed Affected by Abrupt Changes of Runoff Conditions (Jizera Mountains). Res. Rep. VaV/510/3/96-DÚ 01. Ministry of Environment, Czech Republic, Prague (in Czech).

Cloke, H.L., Renaud, J.-P., Claxton, A.J., McDonnell, J.J., Anderson, M.G., Blake, J.R., Bates, P.D., 2003. The effect of model configuration on modelled hillslope–riparian interactions. J. Hydrol. 279, 167–181. http://dx.doi.org/10.1016/S0022-1694(03)00177-X.

Dohnal, M., Dusek, J., Vogel, T., 2006a. The impact of the retention curve hysteresis on prediction of soil water dynamics. J. Hydrol. Hydromech. 54, 258–268.

Dohnal, M., Dusek, J., Vogel, T., Herza, J., Tacheci, P., 2006b. Analysis of soil water response to grass transpiration. Soil Water Res. 1, 85–98.

Dohnal, M., Vogel, T., Sanda, M., Jelinkova, V., 2012. Uncertainty analysis of a dual-continuum model used to simulate subsurface hillslope runoff involving oxygen-18 as natural tracer. J. Hydrol. Hydromech. 60, 194–205. http://dx.doi.org/10.2478/v10098-012-0017-0.

Dusek, J., Vogel, T., 2014. Modeling subsurface hillslope runoff dominated by preferential flow: one- vs. two-dimensional approximation. Vadose Zone J. 13. http://dx.doi.org/10.2136/vzj2013.05.0082.

Dusek, J., Vogel, T., Dohnal, M., Gerke, H.H., 2012a. Combining dual-continuum approach with diffusion wave model to include a preferential flow component in hillslope scale modeling of shallow subsurface runoff. Adv. Water Resour. 44, 113–125. http://dx.doi.org/10.1016/j.advwatres.2012.05.006.

Dusek, J., Vogel, T., Sanda, M., 2012b. Hillslope hydrograph analysis using synthetic and natural oxygen-18 signatures. J. Hydrol. 475, 415–427. http://dx.doi.org/10.1016/j.jhydrol.2012.10.025.

Faeh, A.O., Scherrer, S., Naef, F., 1997. A combined field and numerical approach to investigate flow processes in natural macroporous soils under extreme precipitation. Hydrol. Earth Syst. Sci. 1, 787–800. http://dx.doi.org/10.5194/hess-1-787-1997.

Feddes, R.A., Kowalik, P.J., Zaradny, H., 1978. Simulation of Field Water Use and Crop Yield. PUDOC, Wageningen, The Netherlands.

Freer, J., McDonnell, J.J., Beven, K.J., Peters, N.E., Burns, D.A., Hooper, R.P., Aulenbach, B., Kendall, C., 2002. The role of bedrock topography on subsurface storm flow. Water Resour. Res. 38, 1269. http://dx.doi.org/10.1029/2001WR000872.

Gerke, H.H., van Genuchten, M.Th., 1993a. A dual-porosity model for simulating the preferential movement of water and solutes in structured porous media. Water Resour. Res. 29, 305–319. http://dx.doi.org/10.1029/92WR02339.

Gerke, H.H., van Genuchten, M.Th., 1993b. Evaluation of a first-order water transfer term for variably saturated dual-porosity models. Water Resour. Res. 29, 1225–1238. http://dx.doi.org/10.1029/92WR02467.

Gerke, H.H., Dusek, J., Vogel, T., 2013. Solute mass transfer effects in two-dimensional dual-permeability modeling of bromide leaching from a tile-drained field. Vadose Zone J. 12. http://dx.doi.org/10.2136/vzj2012.0091.

Graham, C.B., McDonnell, J.J., 2010. Hillslope threshold response to rainfall: (2) development and use of a macroscale model. J. Hydrol. 393, 77–93. http://dx.doi.org/10.1016/j.jhydrol.2010.03.008.

Graham, C.B., Woods, R.A., McDonnell, J.J., 2010. Hillslope threshold response to rainfall: (1) a field based forensic approach. J. Hydrol. 393, 65–76. http://dx.doi.org/10.1016/j.jhydrol.2009.12.015.

Haga, H., Matsumoto, Y., Matsutani, J., Fujita, M., Nishida, K., Sakamoto, Y., 2005. Flow paths, rainfall properties, and antecedent soil moisture controlling lags to peak discharge in a granitic unchanneled catchment. Water Resour. Res. 41, W12410. http://dx.doi.org/10.1029/2005WR004236.

Heppner, C.S., Nimmo, J.R., Folmar, G.J., Gburek, W.J., Risser, D.W., 2007. Multiple-methods investigation of recharge at a humid-region fractured rock site, Pennsylvania, USA. Hydrogeol. J. 15, 915–927. http://dx.doi.org/10.1007/s10040-006-0149-6.

Hopp, L., Harman, C., Desilets, S.L.E., Graham, C.B., McDonnell, J.J., Troch, P.A., 2009. Hillslope hydrology under glass: confronting fundamental questions of soil-water-biota co-evolution at Biosphere 2. Hydrol. Earth Syst. Sci. 13, 2105–2118. http://dx.doi.org/10.5194/hess-13-2105-2009.

Hopp, L., McDonnell, J.J., 2009. Connectivity at the hillslope scale: identifying interactions between storm size, bedrock permeability, slope angle and soil depth. J. Hydrol. 376, 378–391. http://dx.doi.org/10.1016/j.jhydrol.2009.07.047.

Hrncir, M., Sanda, M., Kulasova, A., Cislerova, M., 2010. Runoff formation in a small catchment at hillslope and catchment scales. Hydrol. Process. 24, 2248–2256. http://dx.doi.org/10.1002/hyp.7614.

Kampf, S.K., 2011. Variability and persistence of hillslope initial conditions: a continuous perspective on subsurface flow response to rain events. J. Hydrol. 404, 176–185. http://dx.doi.org/10.1016/j.jhydrol.2011.04.028.

Klaus, J., McDonnell, J.J., 2013. Hydrograph separation using stable isotopes: review and evaluation. J. Hydrol. 505, 47–64. http://dx.doi.org/10.1016/j.jhydrol.2013.09.006.

Klaus, J., Zehe, E., 2010. Modelling rapid flow response of a tile-drained field site using a 2D physically based model: assessment of 'equifinal' model setups. Hydrol. Process. 24, 1595–1609. http://dx.doi.org/10.1002/hyp.7687.

Laine-Kaulio, H., Backnäs, S., Karvonen, T., Koivusalo, H., McDonnell, J.J., 2014. Lateral subsurface stormflow and solute transport in a forested hillslope: a combined measurement and modeling approach. Water Resour. Res. 50, 8159–8178. http://dx.doi.org/10.1002/2014WR015381.

Lanni, C., McDonnell, J., Hopp, L., Rigon, R., 2013. Simulated effect of soil depth and bedrock topography on near-surface hydrologic response and slope stability. Earth Surf. Process. Landforms 38, 146–159. http://dx.doi.org/10.1002/esp.3267.

Lehmann, P., Hinz, C., McGrath, G., Tromp-van Meerveld, H.J., McDonnell, J.J., 2007. Rainfall threshold for hillslope outflow: an emergent property of flow pathway connectivity. Hydrol. Earth Syst. Sci. 11, 1047–1063. http://dx.doi.org/10.5194/hess-11-1047-2007.

Li, H.Y., Sivapalan, M., 2014. Functional approach to exploring climatic and landscape controls on runoff generation: 2 timing of runoff storm response. Water Resour. Res. 50, 9323–9342. http://dx.doi.org/10.1002/2014WR016308.

McGrath, G.S., Hinz, C., Sivapalan, M., 2007. Temporal dynamics of hydrological threshold events. Hydrol. Earth Syst. Sci. 11, 923–938. http://dx.doi.org/10.5194/hess-11-923-2007.

Monteith, J.L., 1981. Evaporation and surface temperature. Quart. J. R. Meteorol. Soc. 107, 1–27. http://dx.doi.org/10.1002/qj.49710745102.

Nieber, J.L., Sidle, R.C., 2010. How do disconnected macropores in sloping soils facilitate preferential flow? Hydrol. Process. 24, 1582–1594. http://dx.doi.org/10.1002/hyp.7633.

Noguchi, S., Tsuboyama, Y., Sidle, R.C., Hosoda, I., 2001. Subsurface runoff characteristics from a forest hillslope soil profile including macropores, Hitachi Ohta, Japan. Hydrol. Process. 15, 2131–2149. http://dx.doi.org/10.1002/hyp.278.

Penna, D., Tromp-van Meerveld, H.J., Gobbi, A., Borga, M., Dalla Fontana, D., 2011. The influence of soil moisture on threshold runoff generation processes in an alpine headwater catchment. Hydrol. Earth Syst. Sci. 15, 689–702. http://dx.doi.org/10.5194/hess-15-689-2011.

Peters, D.L., Buttle, J.M., Taylor, C.H., LaZerte, B.D., 1995. Runoff production in a forested, shallow soil, Canadian Shield basin. Water Resour. Res. 31, 1291–1304. http://dx.doi.org/10.1029/94WR03286.

Pirastru, M., Niedda, M., 2010. Field monitoring and dual permeability modelling of water flow through unsaturated calcareous rocks. J. Hydrol. 392, 40–53. http://dx.doi.org/10.1016/j.jhydrol.2010.07.045.

Sanda, M., Cislerova, M., 2009. Transforming hydrographs in the hillslope subsurface. J. Hydrol. Hydromech. 57, 264–275. http://dx.doi.org/10.2478/v10098-009-0023-z.

Sanda, M., Cislerova, M., Picek, T., 2005. Ponded infiltration test in field using fluorescent dye. In: Geophysical Research Abstracts 7. Hydrological Sciences HS2. Abstr. no. EGU05-A-06394. Copernicus, Katlenburg-Lindau. <http://www.cosis.net/abstracts/EGU05/06394/EGU05-J-06394.pdf>.

Sanda, M., Vitvar, T., Kulasova, A., Jankovec, J., Cislerova, M., 2014. Run-off formation in a humid, temperate headwater catchment using a combined hydrological, hydrochemical and isotopic approach (Jizera Mountains, Czech Republic). Hydrol. Process. 28, 3217–3229. http://dx.doi.org/10.1002/hyp.9847.

Snehota, M., Sobotkova, M., Ray, C., Cislerova, M., 2007. Characterization of potential preferential pathways in soil columns by X-ray tomography and infiltration experiments. In: Eos Trans. AGU, 88(52), Fall Meet. Suppl., Abstract H53F-1500.

Stadler, L., Hinkelmann, R., Helmig, R., 2012. Modeling macroporous soils with a two-phase dual-permeability model. Transp. Porous Media 95, 585–601. http://dx.doi.org/10.1007/s11242-012-0064-3.

Steenhuis, T.S., Hrncir, M., Poteau, D., Luna, E.J.R., Tilahun, S.A., Caballero, L.A., Guzman, C.D., Stoof, C.R., Sanda, M., Yiteferu, B., Cislerova, M., 2013. A saturated excess runoff pedotransfer function for vegetated watersheds. Vadose Zone J. 12. http://dx.doi.org/10.2136/vzj2013.03.0060.

Struthers, I., Sivapalan, M., Hinz, C., 2007. Conceptual examination of climate–soil controls upon rainfall partitioning in an open-fractured soil II: response to a population of storms. Adv. Water Resour. 30, 518–527. http://dx.doi.org/10.1016/j.advwatres.2006.04.005.

Tani, M., 1997. Runoff generation processes estimated from hydrological observations on a steep forested hillslope with a thin soil layer. J. Hydrol. 200, 84–109. http://dx.doi.org/10.1016/S0022-1694(97)00018-8.

Tromp-van Meerveld, H.J., McDonnell, J.J., 2006a. Threshold relations in subsurface stormflow: 1. A 147-storm analysis of the Panola hillslope. Water Resour. Res. 42, W02410. http://dx.doi.org/10.1029/2004WR003778.

Tromp-van Meerveld, H.J., McDonnell, J.J., 2006b. Threshold relations in subsurface stormflow: 2. The fill and spill hypothesis. Water Resour. Res. 42, W02411. http://dx.doi.org/10.1029/2004WR003800.

Tromp-van Meerveld, I., Weiler, M., 2008. Hillslope dynamics modeled with increasing complexity. J. Hydrol. 361, 24–40. http://dx.doi.org/10.1016/j.jhydrol.2008.07.019.

Uchida, T., Tromp-van Meerveld, I., McDonnell, J.J., 2005. The role of lateral pipe flow in hillslope runoff response: an intercomparison of non-linear hillslope response. J. Hydrol. 311, 117–133. http://dx.doi.org/10.1016/j.jhydrol.2005.01.012.

VanderKwaak, J.E., Loague, K., 2001. Hydrologic-response simulations for the R-5 catchment with a comprehensive physics-based model. Water Resour. Res. 37, 999–1013. http://dx.doi.org/10.1029/2000WR900272.

Vogel, T., Cislerova, M., 1988. On the reliability of unsaturated hydraulic conductivity calculated from the moisture retention curve. Transp. Porous Media 3, 1–15. http://dx.doi.org/10.1007/BF00222683.

Vogel, T., Cislerova, M., Sanda, M., 2003. Modeling formation of runoff in soil with preferential pathways. Acta Hydrol. Slovaca 4, 307–312.

Vogel, T., Gerke, H.H., Zhang, R., van Genuchten, M.Th., 2000a. Modeling flow and transport in a two-dimensional dual-permeability system with spatially variable hydraulic properties. J. Hydrol. 238, 78–89. http://dx.doi.org/10.1016/S0022-1694(00)00327-9.

Vogel, T., van Genuchten, M.Th., Cislerova, M., 2000b. Effect of the shape of soil hydraulic properties near saturation on numerical simulation of variably-saturated flow. Adv. Water Resour. 24, 133–144. http://dx.doi.org/10.1016/S0309-1708(00)00037-3.

Vogel, T., Sanda, M., Dusek, J., Dohnal, M., Votrubova, J., 2010. Using oxygen-18 to study the role of preferential flow in the formation of hillslope runoff. Vadose Zone J. 9, 252–259. http://dx.doi.org/10.2136/vzj2009.0066.

Weiler, M., Naef, F., 2003. Simulating surface and subsurface initiation of macropore flow. J. Hydrol. 273, 139–154. http://dx.doi.org/10.1016/S0022-1694(02)00361-X.

Weiler, M., McDonnell, J.J., 2007. Conceptualizing lateral preferential flow and flow networks and simulating the effects on gauged and ungauged hillslopes. Water Resour. Res. 43, W03403. http://dx.doi.org/10.1029/2006WR004867.

Weiler, M., McDonnell, J.J., Tromp-van Meerveld, I., Uchida, T., 2005. Subsurface stormflow. In: Anderson, M.G. (Ed.), Encyclopedia of Hydrological Sciences. John Wiley & Sons, New York. http://dx.doi.org/10.1002/0470848944.hsa119.

Dynamics of dissolved organic carbon in hillslope discharge: Modeling and challenges, Journal of Hydrology, 2017.

Journal of Hydrology 546 (2017) 309–325

Contents lists available at ScienceDirect

Journal of Hydrology

journal homepage: www.elsevier.com/locate/jhydrol

Research papers

Dynamics of dissolved organic carbon in hillslope discharge: Modeling and challenges

Jaromir Dusek [a,*], Tomas Vogel [a], Michal Dohnal [a], Johannes A.C. Barth [b], Martin Sanda [a], Anne Marx [b], Jakub Jankovec [a]

[a] Czech Technical University in Prague, Faculty of Civil Engineering, Prague, Czech Republic
[b] Friedrich-Alexander University Erlangen-Nuremberg, Department of Geography and Earth Sciences, Erlangen, Germany

ARTICLE INFO

Article history:
Received 8 November 2016
Received in revised form 21 December 2016
Accepted 29 December 2016
Available online 31 December 2016
This manuscript was handled by Corrado Corradini, Editor-in-Chief, with the assistance of Bartolomé Andreo-Navarro, Associate Editor

Keywords:
Water oxygen isotope
Dissolved organic carbon
Preferential transport
Dual-permeability model
DOC sorption
DOC decomposition
Monte Carlo analysis

ABSTRACT

Reliable quantitative prediction of water movement and fluxes of dissolved substances – specifically organic carbon – at both the hillslope and the catchment scales remains a challenge due to complex boundary conditions and soil spatial heterogeneity. In addition, microbially mediated transformations of dissolved organic carbon (DOC) are recognized to determine the balance of DOC in soils. So far, only few studies utilized stable water isotope information in modeling and even fewer linked dissolved carbon fluxes to mixing and/or transport models. In this study, stormflow dynamics of $^{18}O/^{16}O$ ratios in the water molecules (expressed as $\delta^{18}O$) and DOC were analyzed using a physically-based modeling approach. A one-dimensional dual-continuum vertical flow and transport model was used to simulate the subsurface transport processes in a forest hillslope soil over a period of 2.5 years. The model was applied to describe the transformation of input signals of $\delta^{18}O$ and DOC into output signals observed in the hillslope stormflow. To quantify uncertainty associated with the model parameterization, Monte Carlo analysis in conjunction with Latin hypercube sampling was applied. $\delta^{18}O$ variations in hillslope discharge and in soil pore water were predicted reasonably well. Despite the complex nature of microbial transformations that caused uncertainty in model parameters and subsequent prediction of DOC transport, the simulated temporal patterns of DOC concentration in stormflow showed similar behavior to that reflected in the observed DOC fluxes. Due to preferential flow, the contribution of the hillslope DOC export was higher than the amounts that are usually found in the available literature.

1. Introduction

One of the key challenges in environmental sciences is to quantify interactions of water and carbon turnover as growing evidence indicates that their cycles strongly interact (Battin et al., 2009). Within the aqueous carbon cycle, the main carbon forms include dissolved organic carbon (DOC), particulate organic carbon (POC), and dissolved inorganic carbon (DIC). Recently, numerous studies reported increasing concentrations of DOC in surface waters (e.g., Worrall et al., 2004; Weyhenmeyer, 2008; Zhang et al., 2010), which generated concern for the treatment of drinking water (Delpla et al., 2009; Oulehle and Hruška, 2009). The mass fluxes of the main carbon forms and their relative concentration changes in surface- and subsurface aqueous compartments of streams, reservoirs, and lakes are important environmental markers for release and uptake of carbon and for environmental sources of carbon as well as for carbon interactions with the biosphere. For instance, variable mass fluxes of DOC are known to be related to storm events, droughts, changes in temperature, and/or atmospheric deposition (Tipping et al., 1999; Clark et al., 2005; Monteith et al., 2007). A need for improved understanding of DOC movement in the soil compartment was emphasized by Hagedorn et al. (2000), who highlighted the role of changing hydrologic pathways for DOC transport even during a single rainfall–runoff event.

Dissolved organic carbon in soil solutions originates from plant litter, soil organic matter, microbial biomass, and root exudates (Kalbitz et al., 2000). DOC is very important for a large number of processes, including global carbon cycling, pedogenesis, and pollutant transport in soils (Herbert and Bertsch, 1995; Kalbitz et al., 2000; Jansen et al., 2014). Both biotic and abiotic processes contribute to observed DOC concentrations in soils. The DOC concentration in soils is determined by processes associated with

* Corresponding author at: Department of Hydraulics and Hydrology, Faculty of Civil Engineering, Czech Technical University in Prague, Thakurova 7, 166 29 Prague, Czech Republic.
E-mail address: jaromir.dusek@fsv.cvut.cz (J. Dusek).

http://dx.doi.org/10.1016/j.jhydrol.2016.12.054
0022-1694/

sources such as leaching from soil organic matter (humus) and litter or desorption from the solid phase and sinks such as adsorption or decomposition. The biotic transformation processes, mediated by decomposer communities in soils (microorganisms and fungi), depend on environmental factors such as temperature and soil moisture. Moreover, abiotic processes are also controlled by physical and chemical characteristics of soils.

Mathematical modeling of DOC transport processes in soils and streams is an increasingly important topic as it can be very helpful in predictive analyses of soil organic matter dynamics. The main goal of modeling is to improve our understanding of DOC transport and transformation mechanisms. Modeling thus also offers a unique opportunity to study the effects causing shifts in long-term patterns as well as to provide a framework for testing of hypotheses such as preferential transport during increased runoff or temperature controls on DOC turnover. It also has the potential to separate individual controls and to study combined effects on DOC mobility and turnover. Since the biogeochemistry of carbon phases is complex and often difficult to observe at the field scale, modeling also plays an essential role in advancing our knowledge of relevant processes such as DOC sorption and desorption, production and decomposition. Several approaches for DOC modeling at the hillslope and catchment scales were proposed. These include regression models (Worrall and Burt, 2005; Köhler et al., 2009; Winterdahl et al., 2011), lumped models (Boyer et al., 2000; Xu et al., 2012; Charlier et al., 2012), and physically-based models (Neff and Asner, 2001; Yurova et al., 2008; Mei et al., 2014). In these approaches, the headwater catchment is frequently conceptualized as an assembly of several water reservoirs and carbon pools (e.g., hillslopes, riparian zones, and groundwater) where DOC mixing with respective flow rates occurs and causes DOC temporal variations in stream discharge (e.g., Hornberger et al., 1994; Dick et al., 2015). Likewise, simplified approaches were used that integrate both the key hydrological and biogeochemical processes (e.g., Weiler and McDonnell, 2006; Seibert et al., 2009; Hartmann et al., 2016).

Biogeochemical processes were recognized as the most important control on DOC transport in some modeling approaches, in which the complexity of transformations and soil water chemistry (e.g., changes in S and N deposition) for long-term predictions were considered (e.g., Erlandsson et al., 2008; Futter et al., 2011; Oulehle et al., 2012). However, flow dynamics during rainfall–runoff events in such model approaches are often neglected as most models apply coarse time steps of daily to yearly intervals. In contrast, Michalzik et al. (2003) developed a simplified model to account for water flow in soil, with possible exchange of DOC between the macropores and micropores. They explicitly considered transformation of organic litter into humic fractions and CO_2. Fan et al. (2010) studied transport of different fractions of DOC through top organic layers using a two-site model, however, they excluded the underlying mineral soil. This approach allowed to distinguish between instantaneous and kinetic adsorption/desorption of DOC to solid phase. In addition, CO_2 efflux from the organic layer to atmosphere was predicted, originating from the heterotrophic respiration of microorganisms.

Reliable parametrization of carbon-related transformations in soils is a key issue in modeling of DOC fate and transport. This aspect is reflected in most recent studies based on model analysis (e.g., Futter et al., 2007; Yurova et al., 2008; Köhler et al., 2009). Enormous soil spatial heterogeneity, encountered in natural catchments, may also propagate to spatial heterogeneity of DOC transformations. In addition, initial and boundary conditions of field experiments cannot be as well defined and monitored as in laboratory experiments. On the other hand, the experiments carried out under laboratory conditions (e.g., batch tests evaluating adsorption/desorption characteristics of DOC, leaching on soil column) are characterized by an artificial water flow regime, which differs significantly from field conditions. The discrepancy between laboratory and field conditions leads to different estimates of contact (residence) times between the solid and solution phases, influencing the sorption potential and overall decomposition (Jardine et al., 2006). Moreover, the temperature effects seen in controlled laboratory incubations can become masked under more realistic *in situ* conditions (Campbell and Paustian, 2015). As a result, transport parameters obtained at the laboratory scale are often hardly suited for model predictions at the field scale. These aspects make modeling efforts challenging and thus predictions remain loaded with substantial uncertainty. Kalbitz et al. (2000) even argued that quantitative prediction of DOC fluxes is impossible under field conditions.

A prerequisite for modeling of water isotope and DOC is the spatiotemporal information on water fluxes in soils. This is not a trivial task in heterogeneous porous media and/or in soils where preferential flow effects are known to affect the hydrological response to rainfall (Dusek and Vogel, 2016). Leaching of DOC at pedon- and hillslope scales for soils with active preferential pathways is not well understood so far. On hillslopes with shallow soil profile, saturated subsurface flow (stormflow) may be triggered laterally along the slope upon intensive or long-lasting rainfall (e.g., Weiler et al., 2005; Ameli et al., 2016). This type of flow may carry significant DOC fluxes. For instance, McGlynn and McDonnell (2003) quantified the hillslope contribution to total catchment DOC export with 21–41% during a single rainfall–runoff event. Similarly, the upland DOC contribution was found to form about 30% of the stream DOC flux (Lambert et al., 2014).

The objective of this study was to develop a conceptual model of DOC transport in a shallow forest hillslope soil. A physically-based water flow and solute transport model (taking into account preferential flow effects) was used to predict DOC fluxes in the soil profile and DOC concentrations in hillslope discharge. The impact of model parameter uncertainty was studied by means of Monte Carlo analysis. The ^{18}O isotope was used as a conservative natural tracer to contrast the behavior of DOC that undergoes complex transformations in the soil environment. As observed $\delta^{18}O$ and DOC signatures in hillslope stormflow suggested highly dynamic temporal variations, rapid transport of these elements through preferential pathways was a key factor in our conceptual model. To account for temperature dependent DOC transformations, heat transport was also considered by solving conduction-advection equation.

2. Materials and methods

2.1. Experimental hillslope site

The experimental hillslope site Tomsovka is located in the headwater catchment Uhlirska, Jizera Mountains, North Bohemia, Czech Republic (Fig. 1). The total area of the catchment is 1.78 km^2, its average altitude is 820 m above sea level, mean annual precipitation is 1380 mm, and the mean annual temperature is 4.7 °C. The hillslope is covered with grass (*Calamagrostis villosa*) and spruce (*Picea abies*). The stream discharge is strongly affected by rainfall, causing rapid and frequent event-related discharge variations (Votrubova et al., 2017). The mean specific discharge, reported for the hydrological year 2013, is 41 L s^{-1} km^{-2} (Sanda et al., 2017).

The soil surface as well as soil–bedrock interface at the Tomsovka hillslope site are approximately parallel. The average slope is about 14%. The soil at Tomsovka is a sandy loam classified as Cryptopodzols and Podzols with a depth of 70 cm. The soil contains a broad range of pore sizes as reflected in gradually changing retention curve. The soil profile consists of three layers with

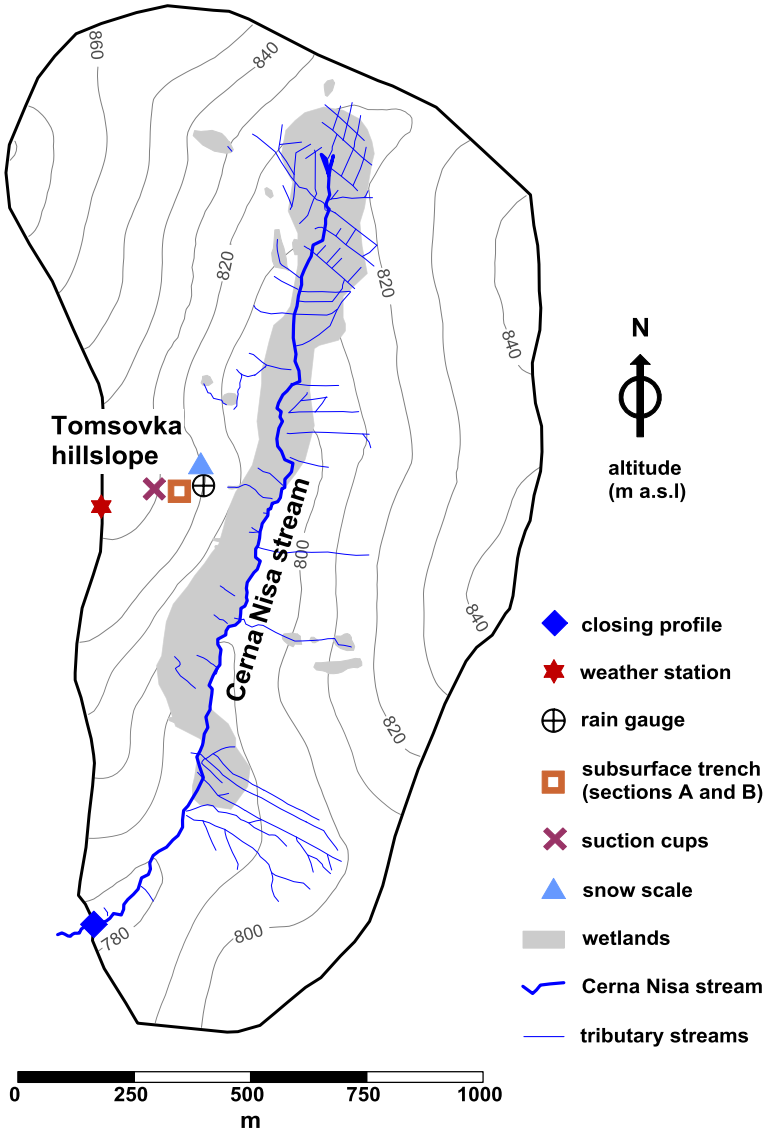

Fig. 1. Schematic of Uhlirska catchment with the Tomsovka hillslope site.

different hydraulic properties (Table 1). The topsoil organic layer is of humic character, containing recent litter. Below this layer, a brown sandy loam with a mixture of organic material overlies a light brown soil with a high content of bedrock particles (Sanda et al., 2014). The value of pH (H_2O) is 3.81 and 4.51 for soil from 0–10 cm and 20–40 cm depth, respectively. The average values of total organic carbon content are 10.4% and 2.4% for soils from 0–10 cm and 20–40 cm depth. The concentration of Fe and Al in the topsoil (0–10 cm depth), extracted by $BaCl_2$, is 78 mg kg^{-1} and 592 mg kg^{-1}, respectively. The soil layers are underlain by a transition zone of weathered granite bedrock that is 5–10 m thick (Sanda and Cislerova, 2009). The interface between the third soil layer and the transition zone is further on referred to as the soil–bedrock interface. It is mostly situated at the depth of 70 cm. The soil hydraulic parameters of each soil layer are listed in Table 1.

Significant preferential flow effects at Tomsovka, affecting the hydrologic hillslope response to rainfall, were reported for the same site by Sanda and Cislerova (2009). Preferential flow was

Table 1
The soil hydraulic parameters for the one-dimensional dual-continuum model. The SM and PF abbreviations refer to the soil matrix and preferential flow domain, respectively. θ_r and θ_s are the residual and saturated water contents, K_s is the saturated hydraulic conductivity, h_s is the air-entry value, and α and n are empirical fitting parameters (Vogel et al., 2000). The value of K_s shown for the PF domain is valid for soil water flow and ^{18}O transport simulations.

Domain	Depth (cm)	θ_r ($cm^3\ cm^{-3}$)	θ_s ($cm^3\ cm^{-3}$)	α (cm^{-1})	n (–)	K_s ($cm\ d^{-1}$)	h_s (cm)
SM	0–8	0.20	0.55	0.050	2.00	567	0.00
	8–20	0.20	0.54	0.050	1.50	67	−0.69
	20–70	0.20	0.49	0.020	1.20	17	−1.48
	70–75	0.20	0.41	0.020	1.20	1.3	−1.88
PF	0–75	0.01	0.60	0.050	3.00	5000	0.00

attributed to highly conductive pathways along tree roots as well as to the soil structure and the spatial variability of local soil hydraulic properties. Overland flow was rarely observed at the hillslope site due to the highly permeable topsoil.

2.1.1. Hillslope discharge

Meteorological conditions at the Tomsovka hillslope site were continuously monitored by a weather station. Meteorological data, including relative humidity, wind speed, air temperature, and net solar radiation, were recorded with 10-min temporal resolution. Subsurface hillslope discharge was measured at an 8 m long experimental trench. The trench consists of two individual adjacent sections (labeled as A and B), each 4 m long. Shallow subsurface hillslope discharge was collected separately in each section at a depth of about 75 cm (Fig. 2). The discharge rates Q_A and Q_B were measured by tipping buckets. Although the geographic watershed divide is located approximately 130 m above the experimental trench, the trench was found to drain a much shorter hillslope length (25–50 m) (Dusek et al., 2012a). For the conversion of the observed volumetric hillslope discharge to specific stormflow per unit contribution area, the contributing length of 25 m was assumed (Fig. 2).

For the modeling, the hillslope micro-catchments corresponding to trench sections A and B were assumed to have approximately the same vegetation characteristics, and geometric and material properties. Differences in the measured discharge hydrographs (Q_A vs. Q_B) were attributed to the spatial variability of preferential pathways, especially their lateral connectivity.

2.1.2. Sampling for oxygen isotope and DOC

The $^{18}O/^{16}O$ ratio in water is commonly expressed as ‰ with the $\delta^{18}O$ nomenclature (e.g., van Geldern and Barth, 2012). It represents the relative deviations of the measured $^{18}O/^{16}O$ ratios from the isotopic composition of the Vienna Standard Mean Ocean Water.

At Tomsovka, $\delta^{18}O$ values were measured in: (i) precipitation collected from the rain gauge, (ii) subsurface hillslope discharge collected from the experimental trench, and (iii) soil water extracted from two depths by suction cups.

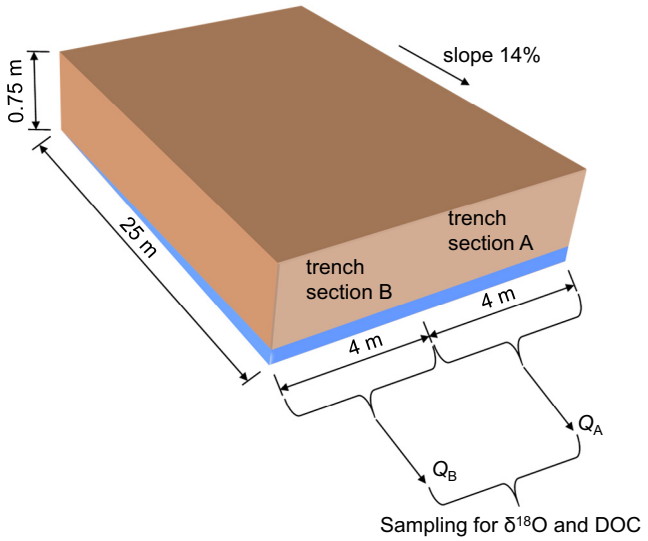

Fig. 2. Schematic of the experimental trench for collecting hillslope discharge at the Tomsovka site. The discharge is collected separately for the two trench sections (Q_A and Q_B). Stormflow samples for $\delta^{18}O$ and DOC analyses were combined from both sections of the trench.

During the growing seasons (from May to October), rainwater samples were collected at daily intervals, provided that the amount of rainfall since the previous sampling had exceeded 1 mm. Once the amount of rain exceeded 10 mm, the next bottle was used for sampling on top of the daily interval rule. Because each sample represents cumulative rainfall for the period between the two sampling events, the measured $\delta^{18}O$ value was averaged over the time interval of collection. During winter, weekly precipitation totals were measured by a storage gauge (rain–snow standpipe). The snow water equivalent was measured by a snow scale and snow density was measured by a snow sampling tube. Melting of snowpack was computed from the change of weight of the snowpack measured by snow scale. The storage gauge water was sampled weekly to determine the $\delta^{18}O$ values.

Due to logistic reasons, the sampling of subsurface hillslope discharge for $\delta^{18}O$/DOC analyses was limited to growing seasons. The discharge was sampled at 6-h intervals, provided that at least 3 L of the subsurface water had been collected since the previous sampling. Samples were taken from a 2-L bucket (allowing overflow of any excess water), into which the discharge from both sections of the trench was piped. During intensive stormflow events, the measured $\delta^{18}O$ and DOC values represent nearly instant concentrations. However, when the discharge rate becomes lower, mixing of the effluent water takes place and the $\delta^{18}O$ and DOC values represent time-averaged concentrations.

Soil water was extracted by suction cups installed at the depths of 30 cm and 60 cm below the soil surface. At the beginning of the soil water extraction, the air was pumped out from the probe with a hand vacuum pump until a pressure head of about −500 cm of water column was reached. A soil water sample was then collected in 2–4 day intervals, depending on the soil moisture conditions. The extraction time was adjusted so as to obtain at least a 20 mL water sample. The pressure head increase in the probe during the extraction was about 100 cm. Sampling was repeated at approximately monthly intervals over the period of interest. The water sampled from the suction cups was used to determine $\delta^{18}O$ within the soil profile. Unfortunately, the suction cups installed at Tomsovka were not suitable for sampling of DOC due to sorption on porous ceramics. This leaves out for now the interpretation of DOC directly sampled from the soil compartment. However, the most important calibration was still possible with the DOC collected in the hillslope runoff that was sampled and analyzed correctly.

The $\delta^{18}O$ measurements were carried out by a laser spectroscope (LGR Liquid-Water Isotope Analyzer version 2, Los Gatos Research Inc., Mountain View, CA). More information on $\delta^{18}O$ measurement can be found in Penna et al. (2010). The manufacturer declared precision of the measurement is 0.2‰. Based on a long-term use of the LGR laser analyzer the standard deviation is 0.16‰. For DOC measurements, DOC samples were filtered through syringe disk filters with 0.45 μm pore size (Minisart High-Flow PES, Sartorius AG, Germany) into 40 mL amber glass vials in the field. The vials fulfill the specifications of the US Environmental Protection Agency (so-called EPA vials) and were poisoned with 2 μL saturated $HgCl_2$ solution to avoid biological activity after sampling. Syringe and membrane were pre-washed with the sample before filling the glass vials. After collection, DOC samples were kept in the dark at 4 °C until analysis. In the laboratory, DOC concentrations were measured with an Aurora 1030 W instrument (OI Analytical, College Station, Texas) via an internal non-dispersive infrared sensor (NDIR) and a set of calibration standards with known concentrations prepared from analytical (A.C.S.) grade potassium hydrogen phthalate (KHP). Areas of the sample peaks are directly proportional to the amount of CO_2 generated by the reaction of the sample with sodium persulfate. Precision based

on repeated analyses of control standard (C_3 sugar) during all runs was better than 0.6 mg C L^{-1} (2σ).

2.2. Flow and transport model

A one-dimensional numerical model, based on dual-permeability approach of Gerke and van Genuchten (1993a), was applied. The model is based on the assumption that soil water flow and transport of dissolved substances take place in a system of two parallel, mutually communicating flow domains: the soil matrix domain (further abbreviated as SM domain) and the preferential flow domain (PF domain). The PF domain represents macropores, biopores, soil cracks and other highly conductive structural elements in soils.

The governing equations for soil water flow and transport of heat and solutes are solved numerically using finite element method. The numerical solver is implemented in the dual-continuum model S1D developed at CTU in Prague. More details about the S1D code can be found in Vogel et al. (2010a, 2011).

2.2.1. Soil water flow model

Variably saturated flow of water is described by a dual set of one-dimensional Richards' equations. These equations are coupled through a first-order soil water transfer term, which enables dynamic exchange of water between the preferential flow and the soil matrix domain. The governing equations are formulated as:

$$\frac{\partial \theta_m}{\partial t} - \frac{\partial}{\partial z}\left(K_m\left(\frac{\partial h_m}{\partial z} + 1\right)\right) = -S_m + \frac{\Gamma_w}{w_m} \tag{1}$$

$$\frac{\partial \theta_f}{\partial t} - \frac{\partial}{\partial z}\left(K_f\left(\frac{\partial h_f}{\partial z} + 1\right)\right) = -S_f - \frac{\Gamma_w}{w_f} \tag{2}$$

where the subscripts m and f indicate the soil matrix and the preferential flow domain, respectively, θ is the volumetric soil water content ($m^3\ m^{-3}$), h is the soil water pressure head (m), K is the soil hydraulic conductivity ($m\ s^{-1}$), S is the intensity of root water uptake (s^{-1}), Γ_w represents the soil water transfer term (s^{-1}) controlling the water exchange between the flow domains, w_m and w_f are volume fractions of the respective domains ($w_m + w_f = 1$), z is the vertical coordinate (m) positive upward. Values of θ_m, θ_f, K_m, and K_f depend on the respective pressure heads h_m and h_f through the domain-specific soil water retention and soil hydraulic conductivity functions.

The soil water transfer term in Eqs. (1) and (2) is described by a modified first-order approximation of Gerke and van Genuchten (1993b):

$$\Gamma_w = \alpha_{ws} K_{ar}(h_f - h_m) \tag{3}$$

where α_{ws} is the water transfer coefficient at saturation ($m^{-1}\ s^{-1}$) and K_{ar} is the relative unsaturated conductivity of the SM–PF domain interface. Values of K_{ar} range from 0 to 1 depending on the conductivities of the SM and PF domains that were evaluated for the upstream soil water pressure (Gerke et al., 2013).

The soil water fluxes q_m and q_f ($m\ s^{-1}$) are defined as:

$$q_m = -K_m(h_m)\left(\frac{\partial h_m}{\partial z} + 1\right) \tag{4}$$

$$q_f = -K_f(h_f)\left(\frac{\partial h_f}{\partial z} + 1\right) \tag{5}$$

The composite flux of soil water q is defined as:

$$q = q_m w_m + q_f w_f \tag{6}$$

2.2.2. Soil heat, oxygen isotope and dissolved organic carbon transport model

The transport of heat is necessary to allow temperature dependent transformations of DOC. In a soil profile, it is described by the following set of governing equations:

$$\frac{\partial C_m T_m}{\partial t} + \frac{\partial q_m c_w T_m}{\partial z} - \frac{\partial}{\partial z}\left(\kappa_m \frac{\partial T_m}{\partial z}\right) = -S_m c_w T_m + \frac{\Gamma_H}{w_m} \tag{7}$$

$$\frac{\partial C_f T_f}{\partial t} + \frac{\partial q_f c_w T_f}{\partial z} - \frac{\partial}{\partial z}\left(\kappa_f \frac{\partial T_f}{\partial z}\right) = -S_f c_w T_f - \frac{\Gamma_H}{w_f} \tag{8}$$

where T is the soil temperature (K), C is the volumetric heat capacity of soil ($J\ m^{-3}\ K^{-1}$), c_w is the volumetric heat capacity of water ($J\ m^{-3}\ K^{-1}$), κ is the apparent thermal conductivity ($W\ m^{-1}\ K^{-1}$), and Γ_H is the soil heat transfer term ($W\ m^{-3}$).

The soil heat transfer term Γ_H is defined as the flux of heat directed from one domain to the other. In analogy to soil water transfer and solute transfer terms used in dual-continuum models (e.g., Gerke and van Genuchten, 1993a, 1993b), the following simple first-order formula is assumed:

$$\Gamma_H = \Gamma_w c_w T_i + \alpha_H(T_f - T_m) \tag{9}$$

where α_H is the soil heat transfer coefficient ($W\ m^{-1}\ K^{-1}$). When water flows from the PF domain to the soil matrix: $T_i = T_f$, for the opposite direction: $T_i = T_m$. The first term on the right hand side of Eq. (9) represents the advective interdomain exchange of soil heat, driven by the soil water pressure difference. The second term accounts for the conduction of heat due to the temperature difference.

Transport of ^{18}O in a dual-continuum porous system is considered as conservative and described using a dual set of standard advection-dispersion equations. Transport predictions of dissolved organic carbon rely on the same governing equations but modified to account for microbial transformations. In this study, the zero- and first-order microbial processes, linear equilibrium sorption, and the effects of soil water content and soil temperature on effective transformation coefficients were considered. The governing equations are written as:

$$\frac{\partial R_m \theta_m c_m}{\partial t} + \frac{\partial q_m c_m}{\partial z} - \frac{\partial}{\partial z}\left(\theta_m D_m \frac{\partial c_m}{\partial z}\right) = -\lambda_w \theta_m c_m - \lambda_s \rho K_D c_m + \gamma \theta_m - S_m c_m + \frac{\Gamma_s}{w_m} \tag{10}$$

$$\frac{\partial R_f \theta_f c_f}{\partial t} + \frac{\partial q_f c_f}{\partial z} - \frac{\partial}{\partial z}\left(\theta_f D_f \frac{\partial c_f}{\partial z}\right) = -\lambda_w \theta_f c_f - \lambda_s \rho K_D c_f + \gamma \theta_f - S_f c_f - \frac{\Gamma_s}{w_f} \tag{11}$$

where c is the $\delta^{18}O$ or DOC concentration in soil water (‰ or $kg\ m^{-3}$, respectively), R is the dimensionless retardation factor, D is the hydrodynamic dispersion coefficient ($m^2\ s^{-1}$), λ_w and λ_s are the first-order degradation coefficients for the liquid (water) and solid phases (s^{-1}), γ is the zero-order production coefficient for the liquid phase ($kg\ m^{-3}\ s^{-1}$), ρ is the soil bulk density ($kg\ m^{-3}$), K_D is the sorption distribution coefficient ($m^3\ kg^{-1}$), and Γ_s is the mass transfer term (‰ s^{-1} or $kg\ m^{-3}\ s^{-1}$, respectively) mediating the exchange of ^{18}O or DOC between the domains.

The mass transfer term Γ_s is defined as the mass flux transported from one domain to the other (Gerke and van Genuchten, 1993b):

$$\Gamma_s = \Gamma_w c_i + \alpha_{ss}\theta_{ar}(c_f - c_m) \tag{12}$$

where α_{ss} is the solute transfer coefficient at saturation (s^{-1}) and θ_{ar} is the effective degree of saturation at the SM–PF domain interface. When water flows from the PF to SM domain, $c_i = c_f$ and for the

opposite flow direction we establish $c_i = c_m$. The first term on the right hand side represents the advective interdomain exchange, driven by the soil water pressure difference. The second term accounts for the diffusive exchange due to the concentration gradient. The rate of diffusive exchange is controlled by the values of α_{ss} and θ_{ar}. In our model, the coefficient θ_{ar} is assumed to be equal to the relative saturation of the PF domain (Ray et al., 2004).

2.2.3. Transformations of DOC in soil

First, dissolved organic carbon is subject to sorption to solid phase. In this study, we assumed linear equilibrium sorption. The retardation factor R is formulated as:

$$R = 1 + \frac{\rho}{\theta} K_D \tag{13}$$

The sorption distribution coefficient K_D was used to calculate the adsorbed concentration of DOC, s (kg kg^{-1}), as:

$$s = cK_D \tag{14}$$

Second, it is well recognized that microbial transformations affect DOC balance in soils (e.g., Yurova et al., 2008; Mei et al., 2012; Sierra et al., 2015). Therefore, the zero-order production and the first-order decomposition (degradation) processes were considered to account for microbially mediated transformations of DOC. The rate of microbial transformations has been found to strongly depend on soil water content (moisture) and also on soil temperature (Rodrigo et al., 1997). Thus, the functions $f(\theta)$ and $f(T)$ were used to account for the effects of soil water content and soil temperature on microbial transformations of DOC, respectively.

The respiration rate of soil microorganisms has been found to decrease in dry soils (low soil water pressure heads) as well as in saturated soils (high pressure heads) (e.g., Miller and Johnson, 1964; Glinski and Stepniewski, 1985; Davidson et al., 2000). Based on the available literature, Rodrigo et al. (1997) concluded that optimal production and decomposition rates range from $h = -500$ cm to -100 cm. The main processes restricting the activity of microorganisms in dry soils are the reduction in water transport and nutrient diffusion, leading to limited physiological performance of microorganisms. The reduction of the respiration rate near saturation (under anaerobic conditions) has been explained by the low diffusion rate through the soil. Šimůnek and Suarez (1993) assumed that the soil water content reduction function $f(\theta)$ is defined for the three different intervals of soil water content:

$$\begin{aligned} f(\theta) &= \frac{\theta - \theta_1}{\theta_2 - \theta_1} \quad \theta \in (\theta_1, \theta_2) \\ f(\theta) &= 1 \quad \theta \in (\theta_2, \theta_3) \\ f(\theta) &= \frac{\theta_4 - \theta}{\theta_4 - \theta_3} \quad \theta \in (\theta_3, \theta_4) \end{aligned} \tag{15}$$

where values of θ_1, θ_2, θ_3, and θ_4 define the soil water content reduction function $f(\theta)$. The range of soil water content (θ_2, θ_3) represents optimal soil water conditions for microbial activity (i.e., $f(\theta) = 1$) and θ_1 is the soil water content when the transformations cease. The reduction function was assumed to be zero when close to saturation for $\theta > \theta_4$ (indicating anaerobic conditions) as well as in very dry conditions for $\theta < \theta_1$.

The rate of biological processes generally increases exponentially as the temperature increases above the freezing point (Rodrigo et al., 1997). A modified Van't Hoff equation was used to account for the effect of soil temperature on DOC transformations:

$$f(T) = Q_{10}^{(T - T_{ref})/10} \tag{16}$$

where $f(T)$ is the temperature function, Q_{10} is the coefficient representing the increase in metabolic rates per 10 °C increase of temperature (–), T_{ref} is a reference temperature at which the basal rates of microbial production γ and degradation λ were estimated.

The functions of soil temperature and soil water were assumed to affect both the zero-order production and the first-order decomposition coefficients as follows:

$$\gamma(\theta, T) = \gamma_{ref} f(\theta) f(T) \tag{17}$$

$$\lambda(\theta, T) = \lambda_{ref} f(\theta) f(T) \tag{18}$$

where γ_{ref} and λ_{ref} is the reference production and decomposition rate, respectively. Note that the resulting effective transformation rates are spatially and temporally dependent.

2.3. Uncertainty analysis

For DOC transport, uncertainty of model predictions was assessed by informal Bayesian approach (generalized likelihood uncertainty estimation method proposed by Beven and Binley (1992)). Latin hypercube sampling simulations (Adams et al., 2009; McKay et al., 1979) with uniform prior distributions for all parameters were utilized. Each combination of model parameters was assessed by the likelihood measure (i.e., quantitative measure of model performance). The simulations with high likelihood measure, which simulate the behavior of a real system reasonably well, were identified as behavioral simulations; less successful simulations were called non-behavioral (Beven and Binley, 1992). A multiple-objective function was formulated since multiple datasets (e.g., effluent DOC concentration, instantaneous DOC mass flux, and cumulative DOC mass flux) were considered.

The resulting model performance distributions were used to assess the model sensitivity to individual transport parameters and to estimate the model prediction uncertainty. To estimate prediction uncertainty, first the model responses were labeled by a likelihood measure and ranked to determine a cumulative probability distribution (Dusek et al., 2015). The uncertainty quantiles, represented by the prediction limits, were derived from the resulting probability distribution for a selected level of significance, i.e. 5% in this study. This was done separately for each simulation time and each type of observation. The uncertainty quantiles was shown to depend on the choice of objective function and on the threshold value (Larsbo and Jarvis, 2005).

The Nash-Sutcliffe model efficiency E (Nash and Sutcliffe, 1970) was used as a quantitative measure of model performance. The match between simulated and observed variables improves with increasing values of E. The value of criterion for hillslope discharge was calculated from 1-h time series. The $\delta^{18}O$ and DOC mass fluxes were calculated by multiplying the $\delta^{18}O$ values and DOC concentrations with the corresponding volumetric discharges of water. The efficiency for $\delta^{18}O$ and DOC mass flux was evaluated using a 6-h time resolution, consistent with the sampling protocol for $\delta^{18}O$ and DOC concentrations in hillslope discharge.

3. Model application

3.1. Water flow simulation

The numerical simulation of soil water flow and transport of heat, $\delta^{18}O$, and DOC was performed for the period from May 2012 to November 2014. For soil water flow, the initial condition corresponded to the soil water pressure profile measured by tensiometers at the beginning of the growing season 2012. After snowmelt (beginning of the growing season 2012), high soil water pressures were observed by tensiometers, corresponding to high soil water saturation. Under such conditions, the soil matrix

domain and preferential flow domain pressures tend to equilibrate. Therefore, the simulation started from initial equilibrium between the flow domains ($h_f = h_m$). The free drainage condition (equivalent to the unit hydraulic gradient condition) was used as the lower boundary condition at the depth of 75 cm below the soil surface for both domains (i.e., the SM domain and the PF domain). The episodic outflow generated at the lower boundary of the PF domain was assumed to feed the saturated subsurface flow during major rainfall–runoff events. To obtain the subsurface discharge to the trench, the vertical PF-domain fluxes were multiplied by the upslope contributing area. The soil water flux computed at the lower boundary of the SM domain was assumed to percolate vertically to deeper bedrock horizons. More details on applications of such one-dimensional vertical flow models are provided by Vogel et al. (2010b) and Dusek et al. (2012a).

Soil–plant–atmosphere interactions taken into account in simulations involved natural rainfall and evapotranspiration. The upper atmospheric boundary condition combined natural rainfall and snowmelt. The rainfall intensities were organized in one-hour series during growing seasons. Intensity of snowmelt was derived from snowpack measurement. Daily time steps were used for rainfall and snowmelt during winter seasons. The daily potential evapotranspiration was calculated using Penman–Monteith equation (Monteith, 1981), based on micrometeorological data observed directly at the Tomsovka hillslope. The root water uptake (represented by the sink term, S, in Eqs. (1) and (2)) was described according to Feddes et al. (1978). The highest density of the root system is located in the upper 20 cm soil depth. In addition, negligible evapotranspiration was assumed during the winter seasons. Given the humid character of the experimental hillslope, the actual evapotranspiration calculated by the model was equal to the potential rate. More detailed information about the root water uptake parameterization at Tomsovka was given by Dohnal et al. (2006a) and Dusek et al. (2012a).

3.2. Parameters of dual-continuum system

The soil hydraulic characteristics of the soil/bedrock matrix as well as of the preferential flow domain were parameterized using the modified van Genuchten model (Vogel and Cislerova, 1988; Vogel et al., 2000). The soil hydraulic parameters that were used for the one-dimensional dual-continuum model are listed in Table 1. The water transfer coefficient, governing the exchange of water between the SM and PF domains, as well as the volumetric proportion of the PF domain were set according to Vogel et al. (2010b). The volumetric fraction of the PF domain, w_f, was assumed to vary linearly between 0.07 at the soil surface and 0.05 at the depth of 75 cm. The decrease of the depth-dependent value of w_f represents variability of the density of the preferential network with depth. The values of α_{ws} and α_{ss} were also estimated to decrease linearly between the soil surface and the lower boundary, i.e. 1 and 0.01 $cm^{-1}\,d^{-1}$ for α_{ws} and 0.001 and 0.0001 d^{-1} for α_{ss}, which corresponds to a decreasing value of saturated hydraulic conductivity of the SM domain. Higher α_{ws} values lead to less preferential flow conditions, causing faster equilibration of the pressure heads between the SM and PF domains. Such conditions were assumed to prevail in the topsoil horizon. The domains hydraulically communicate and exchange soil water mostly under near-saturated conditions. Under dry conditions, they become effectively disconnected due to low interfacial conductivity (at the SM–PF domain interface). More details regarding the parameterization of soil hydraulic properties of the SM and PF domains at Tomsovka can be found in Dohnal et al. (2012).

3.3. Transport of heat

Transport of heat at the Tomsovka hillslope site was analyzed in detail by Vogel et al. (2011). Briefly, the initial condition was derived from measured soil temperature profile. The upper boundary condition of the Dirichlet type with prescribed resident temperature was used. Resident temperature was assigned at the lower boundary of 75 cm, which was determined by the simulation considering a 3-m soil/bedrock profile. The inclusion of the bedrock mass in the simulation was found to be essential for the long-term temperature distribution in the upper soil profile. The soil thermal conductivity function of each domain of the dual-continuum system was evaluated using the approach of Côté and Konrad (2005). The volumetric heat capacities of soil constituents (inorganic solid matter and organic matter) were set equal to their standard values reported in the literature (e.g., Hillel, 1998).

3.4. Transport of ^{18}O

For the purpose of modeling, the isotope $\delta^{18}O$ values were treated as conventional solute concentrations, denoted as c in the governing advection–dispersion equations and referred to as ^{18}O concentration. The initial $\delta^{18}O$ distribution at the beginning of the simulation period was derived from observed resident concentrations in soil water extracted by suction cups. The bottom boundary condition was defined as a zero concentration gradient to allow the tracer to leave the profile freely with the effluent water (i.e., stormflow). Previous studies of Vogel et al. (2010b) and Dusek et al. (2012b) indicated that the short-term variations of $\delta^{18}O$ observed in trench were explained by the fluctuations of the PF-domain $\delta^{18}O$ signal. The third-type (Cauchy) boundary condition was used for the soil surface, prescribing the measured isotope concentration in the rainfall (or snowmelt or both). A dispersivity value was fixed at 5 cm. This estimate lies within the commonly used range of 1/10 to 1/20 of the transport spatial scale (Gelhar et al., 1992). The molecular diffusion coefficient, interpreted as the self-diffusion coefficient of water (Singleton et al., 2004), was set equal to 2 $cm^2\,d^{-1}$. The isotope ^{18}O was subject to root water uptake via the sink terms in Eqs. (10) and (11). Recently, the uncertainty analysis of ^{18}O transport modeling at the hillslope of interest was performed by Dohnal et al. (2012).

The above assumptions led to simplified model of ^{18}O transport, in which the isotope was subject to advection, hydrodynamic dispersion, and root water uptake only. We assumed that no fractionation of oxygen isotopes occurred when soil water is taken up by plant roots for transpiration (Allison et al., 1984). During vegetation seasons, the soil surface is fully covered with dense vegetation layer and infiltration is rapid. Thus, we could safely assume that transpiration dominates over direct soil evaporation. This meant that the ^{18}O enrichment of soil water due to soil-surface evaporation could be neglected. Furthermore, the isotope fractionation due to snow sublimation was also assumed to be insignificant (Friedman et al., 1991). With this, the $\delta^{18}O$ signal can be interpreted as a conservative tracer and the advection and dispersion took place in both the SM domain and the PF domain. The $\delta^{18}O$ signal could also migrate between the two domains according to the local soil water pressure and concentration differences.

3.5. Transport of dissolved organic carbon

Preliminary long-term simulation over a two-year period was used as a warm up period to obtain initial condition of DOC. The warm up period started with exponential decrease of DOC concentration with depth, as derived from the literature (Thurman, 2012). The concentration profile obtained at the end of this starting period

was used as an initial condition for all DOC transport simulations performed.

All transformations of DOC (sorption, production, and decomposition) were assumed to take place exclusively in the soil matrix, i.e. the parameters R_f, γ, λ_w, and λ_s in Eq. (11) were set equal zero for the PF domain. This seems reasonable because the transformations in the preferential pathways can be assumed negligible. In the soil matrix domain, DOC production and decomposition varied with soil water content and temperature according to Eqs. (17) and (18). The reference decomposition rates in the liquid and solid phase, λ_w^{ref} and λ_s^{ref}, and sorption distribution coefficient K_D were assumed constant with depth. Production of DOC in the soil matrix, γ, was assumed to be present in organic carbon-rich soil horizons only (0–20 cm). Moreover, no external DOC sources were assumed with zero mass flux of DOC on soil surface. In analogy to isotope modeling, a zero concentration gradient was used also at the lower boundary for DOC transport simulation. A molecular diffusion coefficient of 1 $cm^2\ d^{-1}$ was adopted from Yurova et al. (2008).

The parameters of Q_{10} and T_{ref} were fixed at 1.7 and 20 °C, respectively, as previously applied in several studies (e.g., Mei et al., 2012; Yurova et al., 2008). The water contents θ_2 and θ_3 defining the optimum production and decomposition rates in Eq. (15) were chosen to correspond to pressure heads of −500 cm and −100 cm, respectively. Parameters θ_1 and θ_4 were set equal to the water contents corresponding to pressure heads −1000 cm and zero, respectively. In addition, no DOC uptake by the root system was assumed ($S = 0$ in Eqs. (10) and (11)).

The above assumptions led to a conceptual model of the DOC transport, in which the dissolved organic carbon was subject to advection and hydrodynamic dispersion. The advection and dispersion took place at different rates in both the SM domain and the PF domain of the dual-continuum soil system. Sorption of DOC to the solid phase, production in the water phase, and decomposition in both water and solid phases were assumed to take place in the soil matrix only. The DOC could be transferred between the two domains according to differences in local soil water pressures and concentrations.

3.6. Uncertainty analysis of DOC transport parameters

The impact of uncertain DOC transport parameters on predicted DOC fluxes was studied by means of Monte Carlo analysis. Multiple forward simulations were executed to examine the properties of the respective objective function. Transport parameters related to instantaneous sorption, zero-order production, and first-order decomposition (i.e., K_D, γ_{ref}, λ_w^{ref}, and λ_s^{ref}) were allowed to vary within relatively wide ranges of their parameter space. The ranges considered in the analysis were set wide enough to contain the values found in literature (Table 2). In addition to DOC transport parameters, saturated hydraulic conductivity of the PF domain (K_{sf}) was included in the analysis to examine the effects of water flow regime (stormflow fluxes) on DOC predictions. The uncertainty analysis was based on 100,000 parameter combinations drawn from the selected parameter ranges. In this study, a threshold value of model efficiency defining acceptable (behavioral) simulations was chosen to be 0.40.

4. Results and discussion

4.1. Stormflow dynamics

Observed and simulated variations of subsurface stormflow during the period of three growing seasons and two winter seasons are presented in Fig. 3. The predicted water flux from the preferential pathways at the base of the soil profile is compared with stormflow measurements at trench sections A and B. Overall, the one-dimensional modeling approach predicted the shallow stormflow dynamics reasonably well. The simulated stormflow was similar to observed hillslope discharge in respect to both timing and magnitude. The model efficiency E comparing observed and predicted stormflow was 0.239 and 0.696 for trench section A and B, respectively. The same comparison yielded root mean square error (RMSE) values of 34.1 L h^{-1} and 38.3 L h^{-1}, respectively. The prediction of internal storage of soil water within the hillslope segment was compared with the observed storage in our previous studies (Dohnal et al., 2006b; Dusek et al., 2012a).

4.2. Transport of oxygen isotope

The predictions of soil water movement dynamics were supplemented with ^{18}O transport simulations (Figs. 4 and 5). Here, $\delta^{18}O$ observed in stormflow were compared with the model predictions in Fig. 4. It shows that the general patterns of ^{18}O variations were predicted reasonably well. Minor discrepancies can partly be explained by the flux-averaging of measured $\delta^{18}O$ concentrations during the low runoff events. The model efficiency for $\delta^{18}O$ isotope in stormflow was 0.695 and value of RMSE was 0.871 ‰. The model efficiency for isotope mass flux was 0.799. In contrast to dynamic fluctuations of $\delta^{18}O$ in stormflow, the $\delta^{18}O$ values in soil pore water reflect seasonal (long-term) variations of ^{18}O concentrations in the soil matrix (Fig. 5). The ^{18}O concentrations in the soil matrix were in good agreement with the observed concentrations at the two depths of 30 cm and 60 cm. The seasonal variations of $\delta^{18}O$ were mostly caused by distinctively different isotope ratios of summer and winter precipitation. A progressive depletion of ^{18}O concentration during the winter seasons were mostly driven by isotopically lighter rainfall and meltwater. On the other hand, rainwater that was enriched in $\delta^{18}O$ produced higher ^{18}O concentrations during the warmer seasons.

Table 2
A priori sampling ranges and a posteriori confidence intervals of DOC transport parameters. Parameter sampling ranges were set based on the listed literature. Estimated parameter medians together with their confidence intervals resulting from the uncertainty analysis (defined by 5th and 95th percentiles) are shown in the last column.

Parameter	Symbol	Units	Sampling range		Estimated median and confidence interval
			Interval	Source	
Sorption distribution coefficient	K_D	$cm^3\ g^{-1}$	2–40	Moore et al. (1992)	28.50 (12.94–38.90)
Reference production coefficient (0–20 cm depth)	γ_{ref}	mg $cm^{-3}\ d^{-1}$	0.0001–0.01	Yurova et al. (2008)	0.0043 (0.0026–0.0067)
Reference decomposition coefficient in liquid phase	λ_w^{ref}	d^{-1}	6.93e−4–1.73e−2	Yurova et al. (2008), Mei et al. (2012, 2014)	0.0093 (0.0016–0.0166)
Reference decomposition coefficient in solid phase	λ_s^{ref}	d^{-1}	3.47e−4–8.66e−3		0.0012 (0.00049–0.0020)
Saturated hydraulic conductivity of the PF domain	K_{sf}	cm d^{-1}	1000–10000	Dohnal et al. (2012)	5954 (3292–9372)

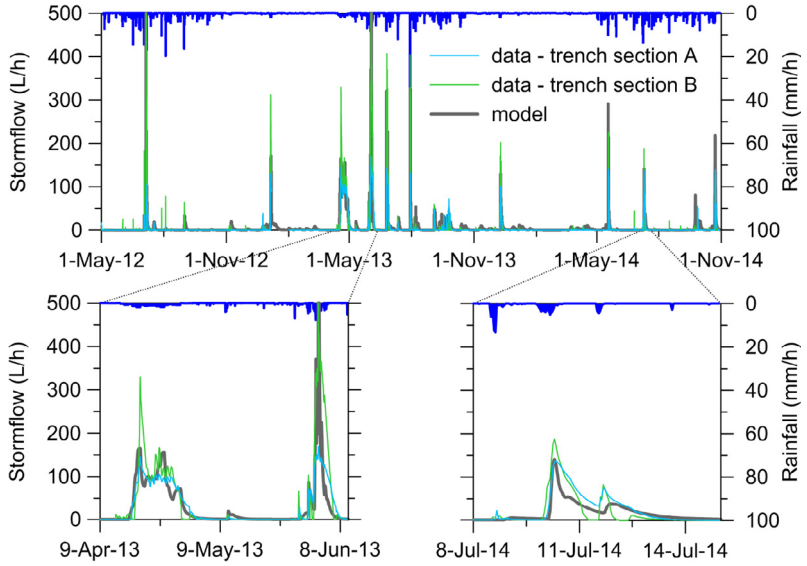

Fig. 3. Observed (trench sections A and B) and simulated hillslope discharge.

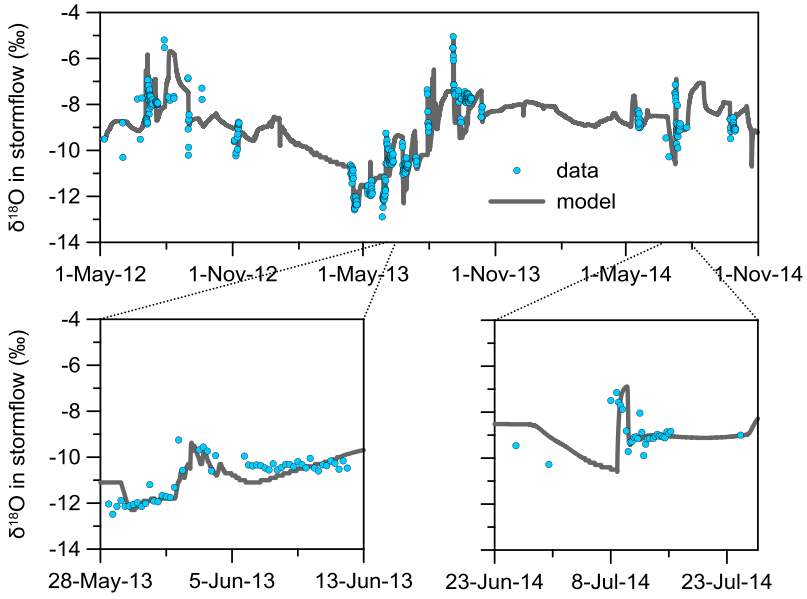

Fig. 4. Observed $\delta^{18}O$ (trench sections A and B combined) compared with the model-generated concentrations.

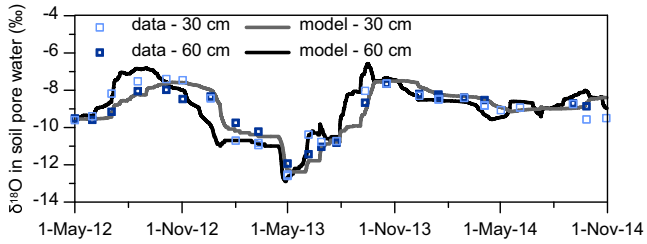

Fig. 5. Observed and simulated ^{18}O concentrations at two depths below the soil surface. The isotope content was measured in soil water extracted by suction cups.

The simulated spatiotemporal development of $\delta^{18}O$ in the soil profile is shown in Fig. 6a and b. The figures illustrate different transport regimes in the SM and PF domains during the considered period. In the soil matrix, a gradual movement of surface water was predicted. Water isotope values in the preferential pathways showed rapid responses to changing surface boundary conditions. Winter seasons were characterized by lower $\delta^{18}O$ values when compared to growing seasons.

4.3. Transport of dissolved organic carbon

The behavioral simulations characterized by model efficiency with the acceptable threshold ($E \geqslant 0.40$) amounted to 2000 out of the total number of 100,000 simulation runs. The relationship between model efficiency and position in parametric space is visualized in Fig. 7. Each dot in this scattergram represents a single model run (one forward simulation) conditioned with DOC concentration data in stormflow only. Note that the dot scatter, corresponding to a particular value of a parameter, reflects the effect of variations in the remaining parameters on the entire model efficiency. The shape of the model responses to changes in the

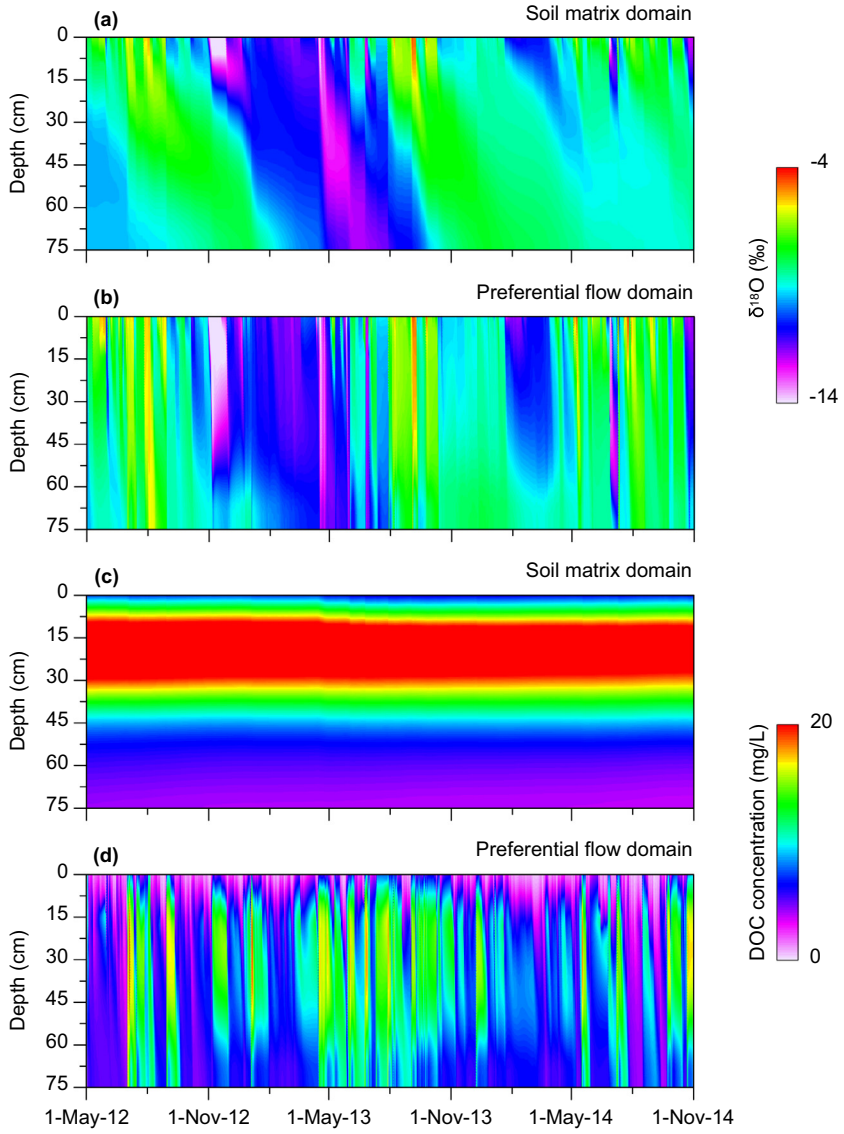

Fig. 6. Predicted spatiotemporal development of $\delta^{18}O$ and DOC concentrations in the SM and PF domains during the simulated period. Predicted $\delta^{18}O$ in the soil matrix (a) and the preferential pathways (b). Predicted DOC concentration (liquid phase) in the soil matrix (c) and the preferential pathways (d). The prediction of DOC concentrations is based on the best behavioral simulation.

parameters is shown for the entire E range (from −90 to 0.46) in Fig. 7. Two of the five parameters (decomposition coefficient in liquid phase and saturated hydraulic conductivity) showed no clear trend of model efficiency within the selected sampling ranges, suggesting a poor ability to identify these parameters.

The upper envelopes of model efficiency scattergrams are depicted in Fig. 8 for each contribution to the objective function (effluent DOC concentration, instantaneous DOC mass flux, and cumulative DOC mass flux). It shows that the efficiencies for mass flux contributions were higher than those for DOC concentrations. Fig. 8 also shows that each data set produced different conditioning of the hydraulic and DOC transport parameters. This is especially apparent for the production coefficient γ (Fig. 8a). Well-defined trends and maxima were predicted for DOC production, sorption distribution coefficient, decomposition in solid phase, and saturated hydraulic conductivity of the PF domain. Limited apparent sensitivity was observed for decomposition rates in the liquid phase (Fig. 8c). In the Monte Carlo analysis performed by Yurova et al. (2008), values of Willmott index and RMSE for DOC concentration predictions at the catchment scale ranged from 0.60 to 0.90 and from 7.2 to 16.1 mg L^{-1}, respectively. For comparison, in the present study, the best behavioral simulations in terms of DOC concentrations corresponded to Willmott index of agreement higher than 0.77 and RMSE values smaller than 2.2 mg L^{-1}.

Fig. 9 shows the comparison of DOC concentrations observed in stormflow with the predicted DOC concentration at the lower boundary of the PF domain. The figure shows prediction limits of the DOC concentrations based on 5% and 95% prediction quantiles for behavioral simulations as well as the results of the best behavioral simulation. Dynamic variance of DOC leaching was observed during stormflows. The DOC concentrations ranged between 5 and 25 mg L^{-1} during individual rainfall–runoff events. Here, measured DOC concentrations mostly remained within the prediction limits. However, DOC concentration variations during several rainfall–runoff events were not fully captured by the model.

Fig. 6c and d shows the predicted spatiotemporal development of DOC concentration in the SM and PF domains during the simulated period (based on the best behavioral simulation). Temporal variations of DOC concentrations in the PF domain are highly

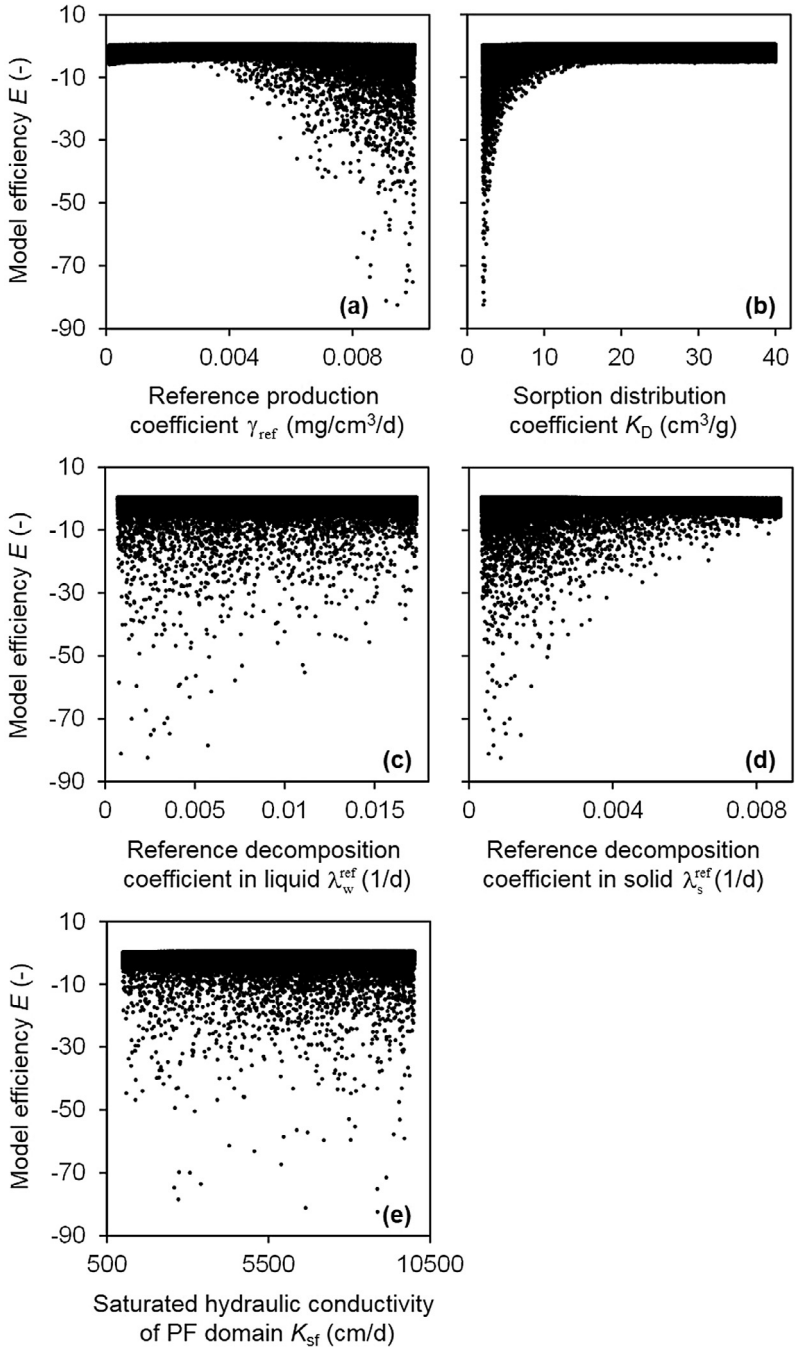

Fig. 7. Efficiency scattergrams conditioned by DOC concentration in stormflow for the individual DOC transport parameters: reference production coefficient in 0–20 cm depth (a), sorption distribution coefficient (b), reference decomposition coefficient in liquid phase (c), reference decomposition coefficient in solid phase (d), and saturated hydraulic conductivity of the PF domain (e).

dynamic and respond to major rainfall events. The DOC in the SM domain shows stable distribution in time due to strong DOC adsorption. Nevertheless, a cluster of significant rainfall events during the growing season of 2013 caused downward movements of DOC in the soil matrix. This movement of a DOC plume was counterbalanced by the DOC production in the topsoil.

4.4. Transport regimes

Highly episodic transport in the preferential pathways, documented by rapid leaching during major rainfall–runoff events, was predicted for both ^{18}O and DOC. However, the transport regime in the soil matrix was different among these two substances (cf. Fig. 6a and c). For ^{18}O transport, the water entered the soil profile with precipitation. For DOC transport, the source of DOC was assumed in the organic rich layers and limited to the soil matrix only. To initiate downward leaching of DOC in the preferential pathways, a mass transfer of DOC from the soil matrix to the PF domain was required. DOC in the soil matrix did not show breakthrough in deeper layers due to strong sorption in the subsoil (Fig. 6c). In contrast, ^{18}O moved freely as fully conservative tracer. Predicted patterns in the soil matrix showed a reasonable correlation with the $\delta^{18}O$ distribution observed in soil pore water at two depths (Fig. 5).

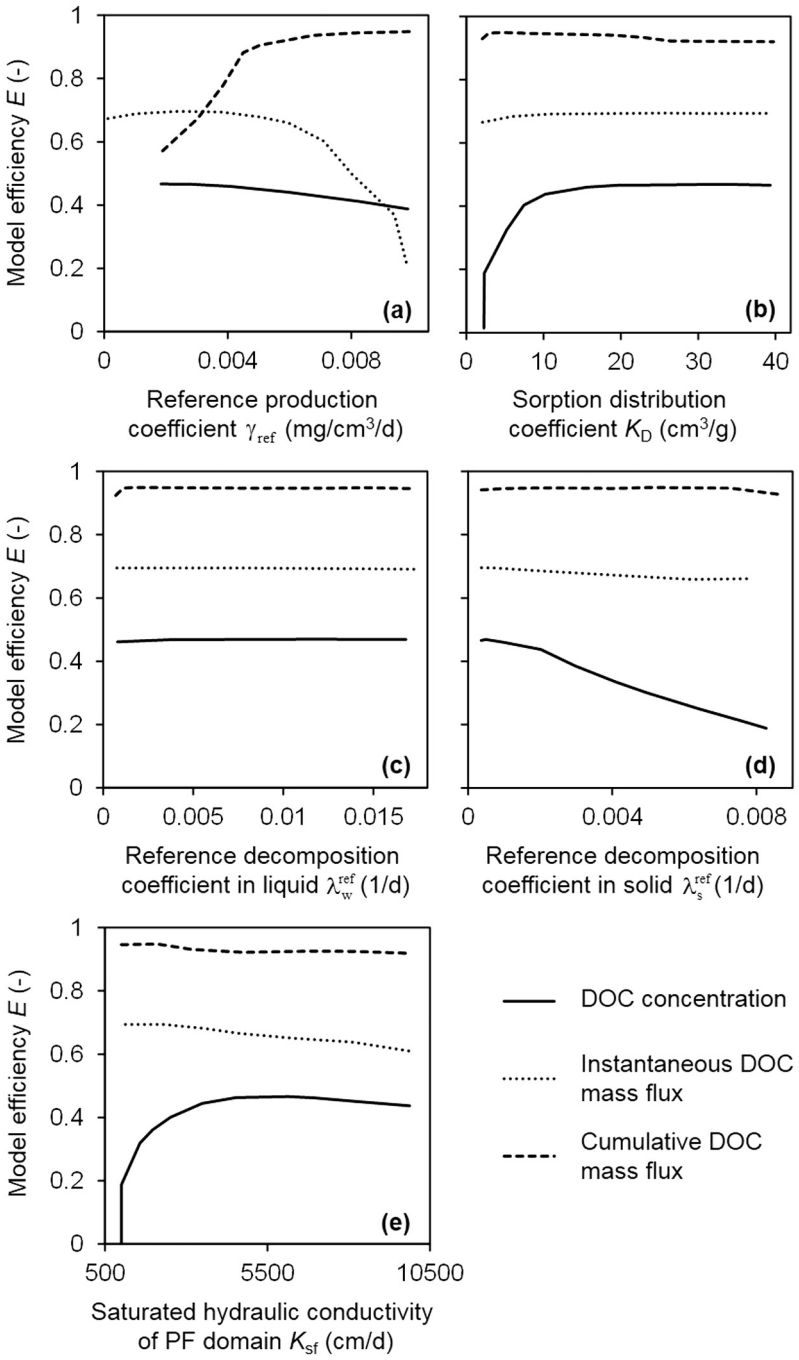

Fig. 8. The partial contributions of three different types of data in the objective function. The upper envelope curves of the efficiency scattergrams are shown for reference production coefficient in 0–20 cm depth (a), sorption distribution coefficient (b), reference decomposition coefficient in liquid phase (c), reference decomposition coefficient in solid phase (d), and saturated hydraulic conductivity of the PF domain (e).

During early stages of significant runoff events, faster water fluxes in the PF domain caused transfer of solutes from the PF to the SM domain. Later, the flow was directed from the SM to the PF domain because preferential pathways drained fast and contributed to stormflow. For DOC transport, the mass transfer toward the PF domain was the most intense in the top 20 cm depths of the profile, where the concentration gradient between the domains was highest and water flow directed from the SM to the PF domain occurred most readily. Above the soil–bedrock interface (at 70 cm depth), the water exchange between the two flow domains was directed likewise, however, the associated DOC mass transfer was much smaller.

Temporal variations of DOC concentrations in soils are known to occur on both seasonal and (storm) event scales. Substantial variations of DOC concentrations were predicted during a single rainfall–runoff event (Fig. 9). The predicted DOC concentrations in stormflow also showed seasonal variations. The peak DOC concentrations during winter seasons were characterized by lower values compared to growing seasons. The base of DOC concentrations at the bottom of the soil profile showed fairly constant values during the simulated period (around 5 mg L^{-1}). In our conceptual model, DOC contents in throughfall were neglected, even though throughfall may contain DOC concentrations leached from aboveground canopy (Moore, 1998). Such concentrations of DOC in

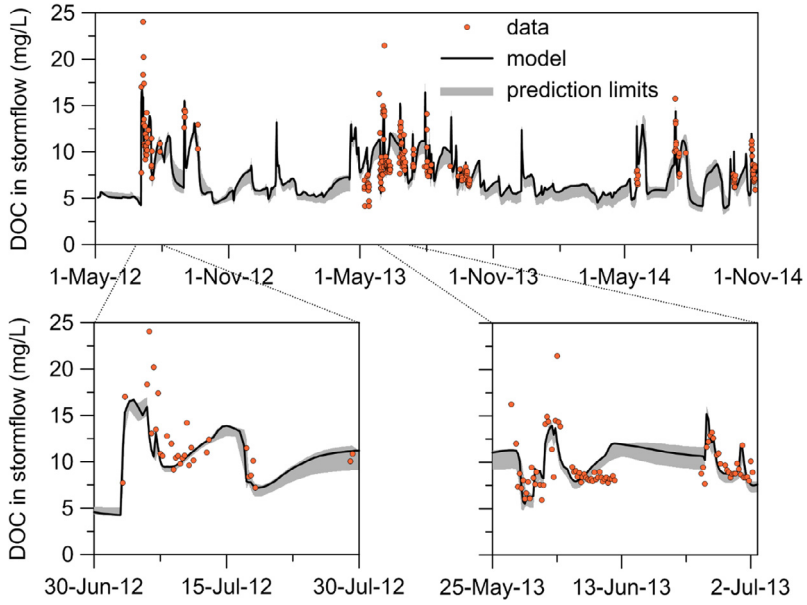

Fig. 9. Observed DOC concentrations (trench sections A and B combined) compared with simulated DOC concentrations in hillslope discharge. Observed concentrations in the effluent are represented by symbols, the shaded area represents prediction limits, and the solid line represents the predicted concentration based on the best behavioral simulation.

throughfall can be high at the early stages of the rainfall events (Kalbitz et al., 2000). This may be one of the reasons why DOC concentrations remain mostly underpredicted during storm events (Fig. 9). Nevertheless, such DOC sources are generally small in boreal coniferous forests (Fröberg et al., 2007).

4.5. Transport parameters

Medians of estimated transport parameters, based on behavioral simulations (2000 model realizations), along with their confidence intervals are presented in Table 2. DOC was found relatively immobile in the soil matrix ($K_D > 25$ cm^3 g^{-1}). It underwent relatively fast decomposition in the liquid phase with half-life value of 75 d, while its decomposition in solid phase was slow with half-life value of 575 d. The median of K_{sf} was similar to the value used for the transport simulations of water oxygen isotopes. The largest uncertainty among the transport parameters, represented by the ratio between the confidence interval and the initial sampling range, had the coefficient of decomposition in the liquid phase λ_w^{ref}. This indicates that λ_w^{ref} was not well conditioned with the concentration data.

Recent modeling studies suggested that DOC adsorption/desorption is more accurately described by kinetic reactions than by a simplification based on equilibrium (Yurova et al., 2008; Mei et al., 2012, 2014). In addition to estimate of the sorption distribution coefficient, kinetic approaches would require a supplementary parameter such as the sorption reaction half-life, which mediates intensity of DOC exchange between soil solution and solid phase. However, the use of the sorption reaction half-life values led to either no-sorption (Mei et al., 2012) or equilibrium sorption (Yurova et al., 2008). The batch experiments conducted by Dahlgren and Marrett (1991) showed relatively fast adsorption and desorption of DOC to Spodosol, i.e. both processes were completed within several hours. Batch sorption experiments on dozens of soil samples performed by Moore et al. (1992) suggested that DOC sorption to soil phases can be adequately described using linear isotherms based on equilibrium sorption. Evaluation of transport experiments on soil columns by Jardine et al. (1992) suggested that local equilibria between DOC and solid phases were not achieved due to high water flow. Such hydraulic conditions were mimicked in the network of the preferential pathways in this study, where DOC was mobile and not subject to adsorption.

A progressive decrease of DOC with depth in the soil matrix was predicted, which is similar to previous studies reviewed by Herbert and Bertsch (1995) and Kalbitz et al. (2000). This was due to strong sorption of DOC onto the solid phase in the lower soil horizons rather than decomposition of DOC. The sorption process of DOC can also be affected by the pH and presence of sulfate in soil solutions (e.g., Kennedy et al., 1996; Kaiser and Zech, 1998). Moreover, sulfate and phosphate anions in soil solution were recognized to compete with DOC for adsorption sites in forest soils (Vance and David, 1992; Gu et al., 1994). On the other hand, adsorption of DOC on iron and aluminum oxides/hydroxides was shown to increase with decreasing pH (Davis, 1982; Rahman et al., 2013). This finding was in agreement with relatively high K_D values estimated in our analysis. At present, limited information on biodegradability of DOC is available, especially for field conditions (Kalbitz et al., 2000). For the sake of simplicity, we, therefore, did not introduce depth-variant decomposition rates, but rather prescribed constant values within the soil profile found in literature. Furthermore, adsorbed DOC was expected to be less accessible by microbes for decomposition (e.g., Miltner and Zech, 1998). This was also confirmed by smaller values of λ_s^{ref} compared with λ_w^{ref} (Table 2).

4.6. Conceptual model

The conceptual model yielded a complex mechanism of DOC leaching at the hillslope scale. The principal characteristics of the proposed model of DOC leaching are: (i) fully mobile DOC in the preferential pathways, (ii) DOC transformations (production, decomposition, and sorption) occurring predominantly in the soil matrix, and (iii) DOC transfer from the soil matrix to the preferential pathways initiating leaching during stormflow events. The water flow regime was identified as a key factor in transport and DOC leaching pattern at the hillslope scale. In this study, we present one of the first complex yet holistic model approaches, in which DOC transport parameters and their corresponding

uncertainties were evaluated. Only one DOC transport parameter was allowed to be spatially resolved (the reference zero-order production coefficient γ_{ref}). Simulated DOC concentrations had lower sensitivity to the DOC transformation parameters related to soil temperature and soil water content (θ_1 to θ_4, Q_{10}, and T_{ref}) than to parameters related to instantaneous sorption, zero-order production, first-order decomposition, and saturated hydraulic conductivity of the preferential pathways (K_D, γ_{ref}, λ_w^{ref}, λ_s^{ref}, and K_{sf}).

4.7. Reduction functions

A product of reduction functions $f(T)$ and $f(\theta)$, evaluated according to Eqs. (15) and (16), is shown in Fig. 10. The resulting function governs the microbially mediated transformations of DOC (production and decomposition) in response to changes of soil temperature and soil water content. The function of $f(T)f(\theta)$ has a distinct sinusoidal character due to seasonal variation of temperature. A decline in the absolute value of $f(T)f(\theta)$ and less dynamic fluctuations of the function with depth were obtained. Several dry periods, predicted in the topsoil during growing seasons, caused $f(T)f(\theta)$ a drop to zero. This effectively ceased production and decomposition processes during these short periods. The soil temperature higher than T_{ref} (20 °C) on the soil surface produced values of $f(T)f(\theta) > 1$. However, the $f(T)f(\theta)$ function mostly reduced the reference rates of production and decomposition ($f(T)f(\theta) < 1$). For about 40% of the simulated period, the optimum range of soil water content ($f(\theta) = 1$) was predicted for the two depths shown in Fig. 10. Other approaches to consider soil water content and soil temperature interactions on DOC transformations, beside those assumed in Eqs. (17) and (18), exist. For instance, a minimum or linear combination of $f(T)$ and $f(\theta)$ functions were proposed (Rodrigo et al., 1997).

4.8. DOC flushing

Flushing was proposed as a delivery mechanism of DOC to streams during snowmelt events (Boyer et al., 1997). As pointed out by Burns (2005), the use of flushing terms in recent literature is often ambiguous and may lead to confusion. DOC flushing is the transport mechanism during which increased DOC concentrations in organic topsoil is flushed by rising saturated zone or infiltrating rainfall. Unless this reservoir is quickly re-filled or very large, this may result in diminished or limited supplies of DOC for later periods of storm events or subsequent rain storms (Boyer et al., 1997; Brooks et al., 1999; McGlynn and McDonnell, 2003). The flushing mechanism is typically evidenced by increased concentrations on the rising limb and lower concentrations on the falling limb of stream hydrographs. Transport of DOC is known to display transport-limited flushing mechanisms. This can be explained by an inability of storms to flush the abundance of DOC concentration in the soil profile (Burns, 2005). We found no evidence of flushing mechanisms at the hillslope scale since DOC peaks predicted in this study occurred at or after the hydrograph peaks. Our finding rather indicated that mass transfer and mixing between the soil matrix and preferential pathways controlled the DOC dynamics.

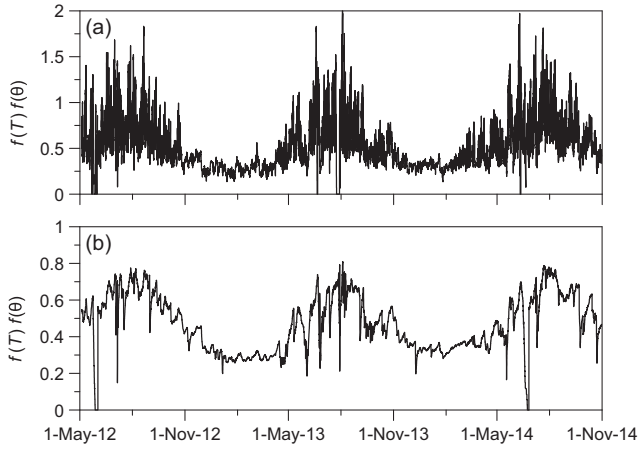

Fig. 10. Temporal variations of the combined reduction function $f(T)f(\theta)$ at the soil surface (a) and at the depth of 20 cm (b) for the best behavioral simulation.

4.9. Hillslope export of $\delta^{18}O$ and DOC

Hillslope soils usually deliver smaller DOC amounts to streams compared to organic rich peatland areas of headwater catchments (e.g., McGlynn and McDonnell, 2003; Lambert et al., 2014). In this study, export of DOC associated with preferential stormflow and deep bedrock percolation was 134.8 g C m^{-2} y^{-1} and 1.3 g C m^{-2} y^{-1}, respectively (based on the best behavioral simulation of two growing and two winter seasons). Separation of DOC fluxes at the soil–bedrock interface followed the concept proposed in our previous studies, where stormflow was exclusively fed by preferential flow while the flow in the soil matrix represented deep vertical percolation (Vogel et al., 2010b; Dusek et al., 2012b; Dusek and Vogel, 2014). Predicted DOC export in this study was larger than reported subsurface fluxes (2–69 g C m^{-2} y^{-1}) by Neff and Asner (2001). This higher DOC export is attributed to the inclusion of preferential flow in our conceptual model. Note that vertical percolation of DOC, associated with the matrix flow, contributes to increase DOC concentration of deep groundwater.

In Table 3, measured and simulated cumulative $\delta^{18}O$ and DOC mass fluxes are summarized for the three growing seasons. Data-to-model comparison was done for events with available observations of both $\delta^{18}O$ and DOC concentrations only. Note that the inter-annual differences of $\delta^{18}O$ and DOC hillslope export were due to different number of major rainfall–runoff events occurring each growing season. They also originated from a different number of samples, i.e. some runoff events were not sampled simultaneously for $\delta^{18}O$ and DOC, see Figs. 4 and 9. The model underpredicted $\delta^{18}O$ and DOC fluxes during the growing seasons, except for DOC mass fluxes in 2014 when the best behavioral simulation overpredicted the observed DOC export. Compared to observations during all three growing seasons, the predicted mass fluxes were lower by 15% and 18% for $\delta^{18}O$ and DOC, respectively. For $\delta^{18}O$, underpredicted stormflow peaks (see Fig. 3) might have caused the discrepancy. In addition to stormflow, the omission of DOC in throughfall is hypothesized to affect the export of DOC. However, this influence was assumed to have a minor effect in our study.

4.10. Future challenges

The distribution of dissolved organic matter in soil solutions is determined by a mixture of various pools with different physicochemical and biochemical properties. The pools are composed of different organic substances such as humic, fluvic, and hydrophilic acids, carbohydrates, amino and carboxylic acids, and hydrocarbons (Herbert and Bertsch, 1995). Each substance may have different transport parameters that influence the overall DOC decomposition rates (Qualls and Haines, 1992) as well as their sorption characteristics (Jardine et al., 1989). Transformations of DOC (production, decomposition, and sorption processes) are still under debate and ongoing research, showing widely varying findings in different soil systems under different boundary conditions (Kalbitz et al., 2000). This inherently leads to an uncertainty in parametrization of the transformation processes and thus in model

Table 3
Observed and simulated cumulative $\delta^{18}O$ and DOC mass fluxes in stormflow. Simulated DOC mass fluxes are based on the best behavioral simulation, ranges in parentheses represent prediction limits of behavioral simulations determined for 5th and 95th percentiles.

Growing season	Cumulative $\delta^{18}O$ mass flux (‰ m^3)		Cumulative DOC mass flux (g C)	
	Observed	Simulated	Observed	Simulated
2012	−68.9	−57.4	139.9	81.3 (69.3–82.5)
2013	−329.4	−273.0	364.4	288.9 (274.0–296.2)
2014	−80.8	−74.7	105.7	131.7 (108.9–134.1)

predictions due to under parameterization of key processes in transport modeling of DOC in soils.

Several possible effects on DOC transport in soils have not been accounted for in the proposed conceptual model. These include the effects of atmospheric deposition, ionic strength of soil solution, anions (e.g., sulfate), pH of soil solution, and variation of DOC concentrations in throughfall on transport behavior of DOC. For instance, Gu et al. (1994) indicated that DOC can become irreversibly sorbed to iron oxides and Kaiser and Zech (1997) showed that DOC adsorption decreased under anaerobic conditions. Systematic incorporation of these effects into numerical models represents a challenging tasks for the future. New field and laboratory experiments with defined boundary conditions are required to examine and parametrize each factor affecting overall DOC fate and transport. The complexity of the soil system with multiple direct and indirect interactions between different processes and factors to be considered in modeling seems considerable and still needs future efforts of geochemists, biologists, soil physicists and modelers (e.g., Vereecken et al., 2016; Jarvis et al., 2016).

5. Summary and conclusions

In this study, a one-dimensional dual-continuum model was used to predict stormflow and the associated transport of natural stable isotope ^{18}O and dissolved organic carbon in the forest macroporous soil developed under humid temperate climate. A quantitative comparison of observed and simulated $\delta^{18}O$ and DOC concentrations in stormflow was performed.

The flow regime (i.e. preferential versus matrix flow) was identified as a key factor in controlling DOC leaching patterns. Specifically, flow and transport through preferential pathways were found to be the most important drivers. This type of flow was activated during major rainfall–runoff events, which caused significant hillslope DOC export (>100 g C m^{-2} y^{-1}). In addition, DOC concentrations in stormflow showed considerable variations during a single storm event. Given the conceptual DOC transport model, in which the DOC transformations take place exclusively in the soil matrix and DOC was fully mobile in the preferential pathways, the mass transfer between the two pore domains was found to be of major importance. Simultaneous analysis of ^{18}O and DOC transport patterns made it possible to assess the impact of different flow regimes in preferential flow and soil matrix domains on DOC transport, as well as to distinguish between the effects of parameters controlling transport by advection–dispersion and those controlling DOC transformations in the soil profile.

Monte Carlo analysis applied in this study indicated that the uncertainties associated with the parameterization of DOC transport in soils remain high. The prediction limits contained most of DOC concentrations observed in hillslope stormflow. However, some observations fell outside the prediction limits, which suggested possibly unaccounted-for processes or factors in the modeling approach.

Despite uncertainties associated with the parametrization of DOC transformation processes, the model provided reasonable predictions of DOC dynamics in stormflow. The variability of simulated DOC effluent signal was significantly larger than the uncertainty represented by the prediction limits. It was shown that the model can be used to establish mass fluxes at the hillslope scale and may serve as a basis for upscaling this information to the catchment scale.

Most of the recent studies considered DOC fluxes at larger scales than in this analysis. As a result, numerous processes influencing DOC dynamics in soils were inevitably simplified or neglected. In our study, the mechanisms behind mobilization and storage of DOC at the source (soil profile and hillslope scales) were thoroughly examined. Such analysis should contribute to better understanding of relevant transport processes and DOC transformations under field conditions.

Acknowledgments

This study was supported by a bilateral Czech-German project funded by the Czech Science Foundation under project No. 14-15201J and the German Research Foundation (DFG) under project No. BA 2207/10-1. We thank Dr. Filip Oulehle from the Czech Geological Survey, who helped with chemical characterization of the soil profile at Tomsovka.

References

Adams, B.M., Bauman, L.E., Bohnhoff, W.J., Dalbey, K.R., Ebeida, M.S., Eddy, J.P., Eldred, M.S., Hough, P.D., Hu, K.T., Jakeman, J.D., Swiler, L.P., Vigil, D.M., 2009. DAKOTA, a multilevel parallel object-oriented framework for design optimization, parameter estimation, uncertainty quantification, and sensitivity analysis: version 5.3.1 User's manual. Sandia Technical Report SAND2010-2183.

Ameli, A.A., McDonnell, J.J., Bishop, K., 2016. The exponential decline in saturated hydraulic conductivity with depth: a novel method for exploring its effect on water flow paths and transit time distribution. Hydrol. Process. 30, 2438–2450.

Allison, G.B., Barnes, J.B., Hughes, M.W., Leaney, F.W.J., 1984. The effect of climate and vegetation on oxygen-18 and deuterium profiles in soils. In: Isotope hydrology. IAEA, Austria, Vienna, pp. 105–123.

Battin, T.J., Luyssaert, S., Kaplan, L.A., Aufdenkampe, A.K., Richter, A., Tranvik, L.J., 2009. The boundless carbon cycle. Nat. Geosci. 2, 598–600.

Beven, K., Binley, A., 1992. The future of distributed models: model calibration and uncertainty prediction. Hydrol. Process. 6, 279–298.

Boyer, E.W., Hornberger, G.M., Bencala, K.E., McKnight, D.M., 1997. Response characteristics of DOC flushing in an alpine catchment. Hydrol. Process. 11, 1635–1647.

Boyer, E.W., Hornberger, G.M., Bencala, K.E., McKnight, D.M., 2000. Effects of asynchronous snowmelt on flushing of dissolved organic carbon: a mixing model approach. Hydrol. Process. 14, 3291–3308.

Burns, D., 2005. What do hydrologists mean when they use the term flushing? Hydrol. Process. 19, 1325–1327.

Brooks, P.D., McKnight, D.M., Bencala, K.E., 1999. The relationship between soil heterotrophic activity, soil dissolved organic carbon (DOC) leachate, and catchment-scale DOC export in headwater catchments. Water Resour. Res. 35, 1895–1902.

Campbell, E.E., Paustian, K., 2015. Current developments in soil organic matter modeling and the expansion of model applications: a review. Environ. Res. Lett. 10, 123004.

Charlier, J.B., Bertrand, C., Mudry, J., 2012. Conceptual hydrogeological model of flow and transport of dissolved organic carbon in a small Jura karst system. J. Hydrol. 460, 52–64.

Clark, J.M., Chapman, P.J., Adamson, J.K., Lane, S.N., 2005. Influence of drought-induced acidification on the mobility of dissolved organic carbon in peat soils. Glob. Change Biol. 11, 791–809.

Côté, J., Konrad, J.M., 2005. A generalized thermal conductivity model for soils and construction materials. Can. Geotech. J. 42, 443–458.

Dahlgren, R.A., Marrett, D.J., 1991. Organic carbon sorption in arctic and subalpine spodosol B horizons. Soil Sci. Soc. Am. J. 55, 1382–1390.
Davis, J.A., 1982. Adsorption of natural dissolved organic matter at the oxide/water interface. Geochim. Cosmochimi. Ac. 46, 2381–2393.
Davidson, E.A., Verchot, L.V., Cattânio, J.H., Ackerman, I.L., Carvalho, J.E.M., 2000. Effects of soil water content on soil respiration in forests and cattle pastures of eastern Amazonia. Biogeochemistry 48, 53–69.
Delpla, I., Jung, A.V., Baures, E., Clement, M., Thomas, O., 2009. Impacts of climate change on surface water quality in relation to drinking water production. Environ. Int. 35, 1225–1233.
Dick, J.J., Tetzlaff, D., Birkel, C., Soulsby, C., 2015. Modelling landscape controls on dissolved organic carbon sources and fluxes to streams. Biogeochemistry 122, 361–374.
Dohnal, M., Dusek, J., Vogel, T., Herza, J., Tacheci, P., 2006a. Analysis of soil water response to grass transpiration. Soil Water Res. 1, 85–98.
Dohnal, M., Dusek, J., Vogel, T., 2006b. The impact of the retention curve hysteresis on prediction of soil water dynamics. J. Hydrol. Hydromech. 54, 258–268.
Dohnal, M., Vogel, T., Sanda, M., Jelinkova, V., 2012. Uncertainty analysis of a dual-continuum model used to simulate subsurface hillslope runoff involving oxygen-18 as natural tracer. J. Hydrol. Hydromech. 60, 194–205.
Dusek, J., Vogel, T., Dohnal, M., Gerke, H.H., 2012a. Combining dual-continuum approach with diffusion wave model to include a preferential flow component in hillslope scale modeling of shallow subsurface runoff. Adv. Water Resour. 44, 113–125.
Dusek, J., Vogel, T., Sanda, M., 2012b. Hillslope hydrograph analysis using synthetic and natural oxygen-18 signatures. J. Hydrol. 475, 415–427.
Dusek, J., Vogel, T., 2014. Modeling subsurface hillslope runoff dominated by preferential flow: one- vs. two-dimensional approximation. Vadose Zone J. 13. http://dx.doi.org/10.2136/vzj2013.05.0082.
Dusek, J., Dohnal, M., Snehota, M., Sobotkova, M., Ray, C., Vogel, T., 2015. Transport of bromide and pesticides through an undisturbed soil column: a modeling study with global optimization analysis. J. Contam. Hydrol. 175–176, 1–16.
Dusek, J., Vogel, T., 2016. Hillslope-storage and rainfall-amount thresholds as controls of preferential stormflow. J. Hydrol. 534, 590–605.
Erlandsson, M., Buffam, I., Fölster, J., Laudon, H., Temnerud, J., Weyhenmeyer, G.A., Bishop, K., 2008. Thirty-five years of synchrony in the organic matter concentrations of Swedish rivers explained by variation in flow and sulphate. Glob. Change Biol. 14, 1191–1198.
Fan, Z., Neff, J.C., Wickland, K.P., 2010. Modeling the production, decomposition, and transport of dissolved organic carbon in boreal soils. Soil Sci. 175, 223–232.
Feddes, R.A., Kowalik, P.J., Zaradny, H., 1978. Simulation of field water use and crop yield. PUDOC, Wageningen, The Netherlands.
Friedman, I., Benson, C.S., Gleason, J., 1991. Isotopic changes during snow metamorphism. In: Taylor Jr., H.P., et al. (Eds.), Stable Isotope Geochemistry: A Tribute to Samuel Epstein. Spec. Publ. 3. Geochemical Society, San Antonio, TX, pp. 211–221.
Fröberg, M., Berggren Kleja, D., Hagedorn, F., 2007. The contribution of fresh litter to dissolved organic carbon leached from a coniferous forest floor. Eur. J. Soil Sci. 58, 108–114.
Futter, M.N., Butterfield, D., Cosby, B.J., Dillon, P.J., Wade, A.J., Whitehead, P.G., 2007. Modeling the mechanisms that control in-stream dissolved organic carbon dynamics in upland and forested catchments. Water Resour. Res. 43. http://dx.doi.org/10.1029/2006WR004960.
Futter, M.N., Löfgren, S., Köhler, S.J., Lundin, L., Moldan, F., Bringmark, L., 2011. Simulating dissolved organic carbon dynamics at the Swedish integrated monitoring sites with the integrated catchments model for carbon, INCA-C. Ambio 40, 906–919.
Gelhar, L.W., Welty, C., Rehfeldt, K.R., 1992. A critical review of data on field-scale dispersion in aquifers. Water Resour. Res. 28, 1955–1974.
Gerke, H.H., van Genuchten, M.Th., 1993a. A dual-porosity model for simulating the preferential movement of water and solutes in structured porous media. Water Resour. Res. 29, 305–319.
Gerke, H.H., van Genuchten, M.Th., 1993b. Evaluation of a first-order water transfer term for variably saturated dual-porosity models. Water Resour. Res. 29, 1225–1238.
Gerke, H.H., Dusek, J., Vogel, T., 2013. Solute mass transfer effects in two-dimensional dual-permeability modeling of bromide leaching from a tile-drained field. Vadose Zone J. 12. http://dx.doi.org/10.2136/vzj2012.0091.
Glinski, J., Stepniewski, W., 1985. Soil Aeration and Its Role for Plants. CRC Press, Boca Raton, FL.
Gu, B., Schmitt, J., Chen, Z., Liang, L., McCarthy, J.F., 1994. Adsorption and desorption of natural organic matter on iron oxide: mechanisms and models. Environ. Sci. Technol. 28, 38–46.
Hagedorn, F., Schleppi, P., Waldner, P., Flühler, H., 2000. Export of dissolved organic carbon and nitrogen from Gleysol dominated catchments–the significance of water flow paths. Biogeochemistry 50, 137–161.
Hartmann, A., Kobler, J., Kralik, M., Dirnböck, T., Humer, F., Weiler, M., 2016. Model-aided quantification of dissolved carbon and nitrogen release after windthrow disturbance in an Austrian karst system. Biogeosciences 13, 159–174.
Herbert, B.E., Bertsch, P.M., 1995. Characterization of dissolved and colloidal organic matter in soil solution: a review. In: Kelly, J.M., McFee, W.W. (Eds.), Carbon Forms and Functions in Forest Soils. SSSA, Madison, WI, pp. 63–88.
Hillel, D., 1998. Environmental Soil Physics. Academic Press. 771pp.
Hornberger, G.M., Bencala, K.E., McKnight, D.M., 1994. Hydrological controls on dissolved organic carbon during snowmelt in the Snake River near Montezuma, Colorado. Biogeochemistry 25, 147–165.
Jansen, B., Kalbitz, K., McDowell, W.H., 2014. Dissolved organic matter: linking soils and aquatic systems. Vadose Zone J. 13. http://dx.doi.org/10.2136/vzj2014.05.0051.
Jardine, P.M., Weber, N.L., McCarthy, J.F., 1989. Mechanism of dissolved organic carbon adsorption on soil. Soil Sci. Soc. Am. J. 53, 1378–1385.
Jardine, P.M., Dunnivant, F.M., McCarthy, J.F., Selim, H.M., 1992. Comparison of models for describing the transport of dissolved organic carbon in aquifer columns. Soil Sci. Soc. Am. J. 56, 393–401.
Jardine, P.M., Mayes, M.A., Mulholland, P.J., Hanson, P.J., Tarver, R.J., Luxmoore, R.J., McCarthy, J.F., Wilson, G.V., 2006. Vadose zone flow and transport of dissolved organic carbon at multiple scales in humid regimes. Vadose Zone J. 5, 140–152.
Jarvis, N., Koestel, J., Larsbo, M., 2016. Understanding preferential flow in the vadose zone: recent advances and future prospects. Vadose Zone J. 15. http://dx.doi.org/10.2136/vzj2016.09.0075.
Kaiser, K., Zech, W., 1997. About the sorption of dissolved organic matter to forest soils. Z. Pflanz. Bodenkunde 160, 295–301.
Kaiser, K., Zech, W., 1998. Soil dissolved organic matter sorption as influenced by organic and sesquioxide coatings and sorbed sulfate. Soil Sci. Soc. Am. J. 62, 129–136.
Kalbitz, K., Solinger, S., Park, J.-H., Michalzik, B., Matzner, E., 2000. Controls on the dynamics of dissolved organic matter in soils: a review. Soil Sci. 165, 277–304.
Kennedy, J., Billett, M.F., Duthie, D., Fraser, A.R., Harrison, A.F., 1996. Organic matter retention in an upland humic podzol; the effects of pH and solute type. Eur. J. Soil Sci. 47, 615–625.
Köhler, S.J., Buffam, I., Seibert, J., Bishop, K.H., Laudon, H., 2009. Dynamics of stream water TOC concentrations in a boreal headwater catchment: controlling factors and implications for climate scenarios. J. Hydrol. 373, 44–56.
Lambert, T., Pierson-Wickmann, A.C., Gruau, G., Jaffrézic, A., Petitjean, P., Thibault, J. N., Jeanneau, L., 2014. DOC sources and DOC transport pathways in a small headwater catchment as revealed by carbon isotope fluctuation during storm events. Biogeosciences 11, 3043–3056.
Larsbo, M., Jarvis, N., 2005. Simulating solute transport in a structured field soil: uncertainty in parameter identification and predictions. J. Environ. Qual. 34, 621–634.
McGlynn, B.L., McDonnell, J.J., 2003. Role of discrete landscape units in controlling catchment dissolved organic carbon dynamics. Water Resour. Res. 39. http://dx.doi.org/10.1029/2002WR001525.
McKay, M.D., Conover, W.J., Beckman, R.J., 1979. A comparison of three methods for selecting values of input variables in the analysis of output from a computer code. Technometrics 21, 239–245.
Mei, Y., Hornberger, G.M., Kaplan, L.A., Newbold, J.D., Aufdenkampe, A.K., 2012. Estimation of dissolved organic carbon contribution from hillslope soils to a headwater stream. Water Resour. Res. 48, W09514. http://dx.doi.org/10.1029/2011WR010815.
Mei, Y., Hornberger, G.M., Kaplan, L.A., Newbold, J.D., Aufdenkampe, A.K., 2014. The delivery of dissolved organic carbon from a forested hillslope to a headwater stream in southeastern Pennsylvania. USA. Water Resour. Res. 50. http://dx.doi.org/10.1002/2014WR015635.
Michalzik, B., Tipping, E., Mulder, J., Lancho, J.F.G., Matzner, E., Bryant, C.L., Clarke, N., Lofts, S., Esteban, M.A.V., 2003. Modelling the production and transport of dissolved organic carbon in forest soils. Biogeochemistry 66, 241–264.
Miller, R.D., Johnson, D.D., 1964. The effect of soil moisture tension on carbon dioxide evolution, nitrification, and nitrogen mineralization. Soil Sci. Soc. Am. Proc. 28, 644–647.
Miltner, A., Zech, W., 1998. Carbohydrate decomposition in beech litter as influenced by aluminium, iron and manganese oxides. Soil Biol. Biochem. 30, 1–7.
Monteith, J.L., 1981. Evaporation and surface temperature. Quart. J. R. Meteorol. Soc. 107, 1–27.
Monteith, D.T., Stoddard, J.L., Evans, C.D., de Wit, H.A., Forsius, M., Høgåsen, T., Wilander, A., Skjelkvåle, B.L., Jeffries, D.S., Vuorenmaa, J., Keller, B., 2007. Dissolved organic carbon trends resulting from changes in atmospheric deposition chemistry. Nature 450, 537–540.
Moore, T.R., De Souza, W., Koprivnjak, J.F., 1992. Controls on the sorption of dissolved organic carbon by soils. Soil Sci. 154, 120–129.
Moore, T.R., 1998. Dissolved organic carbon: sources, sinks, and fluxes and role in the soil carbon cycle. In: Lal, R., Kimble, J.M., Follett, R.E., Stewart, B.A. (Eds.), Soil Processes and the Carbon Cycl. Advances in Soil Science. CRC Press, Boca Raton, FL, pp. 281–292.
Nash, J.E., Sutcliffe, J.V., 1970. River flow forecasting through conceptual models Part I – a discussion of principles. J. Hydrol. 10, 282–290.
Neff, J.C., Asner, G.P., 2001. Dissolved organic carbon in terrestrial ecosystems: synthesis and a model. Ecosystems 4, 29–48.
Oulehle, F., Hruška, J., 2009. Rising trends of dissolved organic matter in drinking-water reservoirs as a result of recovery from acidification in the Ore Mts, Czech Republic. Environ. Pollut. 157, 3433–3439.
Oulehle, F., Cosby, B.J., Wright, R.F., Hruška, J., Kopáček, J., Krám, P., Evans, C.D., Moldan, F., 2012. Modelling soil nitrogen: the MAGIC model with nitrogen retention linked to carbon turnover using decomposer dynamics. Environ. Pollut. 165, 158–166.
Penna, D., Stenni, B., Šanda, M., Wrede, S., Bogaard, T.A., Gobbi, A., Borga, M., Bonazza, M., Chárová, Z., 2010. On the reproducibility and repeatability of laser absorption spectroscopy measurements for δ^2H and $\delta^{18}O$ isotopic analysis. Hydrol. Earth Syst. Sci. 14, 1551–1566.
Qualls, R.G., Haines, B.L., 1992. Biodegradability of dissolved organic matter in forest throughfall, soil solution and stream waters. Soil Sci. Soc. Am. J. 56, 578–586.

Rahman, M.S., Whalen, M., Gagnon, G.A., 2013. Adsorption of dissolved organic matter (DOM) onto the synthetic iron pipe corrosion scales (goethite and magnetite): effect of pH. Chem. Eng. J. 234, 149–157.
Ray, C., Vogel, T., Dusek, J., 2004. Modeling depth-variant and domain-specific sorption and biodegradation in dual-permeability media. J. Contam. Hydrol. 70, 63–87.
Rodrigo, A., Recous, S., Neel, C., Mary, B., 1997. Modelling temperature and moisture effects on C-N transformations in soils: comparison of nine models. Ecol. Model. 102, 325–339.
Sanda, M., Cislerova, M., 2009. Transforming hydrographs in the hillslope subsurface. J. Hydrol. Hydromech. 57, 264–275.
Sanda, M., Vitvar, T., Kulasova, A., Jankovec, J., Cislerova, M., 2014. Run-off formation in a humid, temperate headwater catchment using a combined hydrological, hydrochemical and isotopic approach (Jizera Mountains, Czech Republic). Hydrol. Process. 28, 3217–3229.
Sanda, M., Sedlmaierova, P., Vitvar, T., Seidler, C., Kändler, M., Jankovec, J., Kulasova, A., Paska, F., 2017. Pre-event water contributions and streamwater residence times in different land use settings of the transboundary mesoscale Lužická Nisa catchment. J. Hydrol. Hydromech. 65. http://dx.doi.org/10.1515/johh-2017-0003.
Seibert, J., Grabs, T., Köhler, S., Laudon, H., Winterdahl, M., Bishop, K., 2009. Linking soil- and stream-water chemistry based on a riparian flow-concentration integration model. Hydrol. Earth Syst. Sci. 13, 2287–2297.
Sierra, C.A., Trumbore, S.E., Davidson, E.A., Vicca, S., Janssens, I., 2015. Sensitivity of decomposition rates of soil organic matter with respect to simultaneous changes in temperature and moisture. J. Adv. Model. Earth Syst. 7, 335–356.
Singleton, M.J., Sonnenthal, E.L., Conrad, M.E., DePaolo, D.J., Gee, G.W., 2004. Multiphase reactive transport modeling of seasonal infiltration events and stable isotope fractionation in unsaturated zone pore water and vapor at the Hanford site. Vadose Zone J. 3, 775–785.
Šimůnek, J., Suarez, D.L., 1993. Modeling of carbon dioxide transport and production in soil: 1. Model development. Water Resour. Res. 29, 487–497.
Thurman, E.M., 2012. Organic Geochemistry of Natural Waters. Dordrecht Martinus Nijhoff/Dr. W. Junk Publishers.
Tipping, E., Woof, C., Rigg, E., Harrison, A.F., Inneson, P., Taylor, K., Benham, D., Poskitt, J., Rowland, A.P., Bol, R., Harkness, D.D., 1999. Climatic influences on the leaching of dissolved organic matter from upland UK moorland soils, investigated by a field manipulation experiment. Environ. Int. 25, 83–95.
Vance, G.F., David, M.B., 1992. Dissolved organic carbon and sulfate sorption by spodosol mineral horizons. Soil Sci. 154, 136–144.
van Geldern, R., Barth, J.A., 2012. Optimization of instrument setup and post-run corrections for oxygen and hydrogen stable isotope measurements of water by isotope ratio infrared spectroscopy (IRIS). Limnol. Oceanogr: Methods 10, 1024–1036.
Vereecken, H., Schnepf, A., Hopmans, J.W., Javaux, M., Or, D., Roose, T., Vanderborght, J., et al., 2016. Modeling soil processes: review, key challenges, and new perspectives. Vadose Zone J. 15. http://dx.doi.org/10.2136/vzj2015.09.0131.
Vogel, T., Cislerova, M., 1988. On the reliability of unsaturated hydraulic conductivity calculated from the moisture retention curve. Transp. Porous Media 3, 1–15.
Vogel, T., van Genuchten, M.Th., Cislerova, M., 2000. Effect of the shape of soil hydraulic properties near saturation on numerical simulation of variably saturated flow. Adv. Water Resour. 24, 133–144.
Vogel, T., Brezina, J., Dohnal, M., Dusek, J., 2010a. Physical and numerical coupling in dual-continuum modeling of preferential flow. Vadose Zone J. 9, 260–267.
Vogel, T., Sanda, M., Dusek, J., Dohnal, M., Votrubova, J., 2010b. Using oxygen-18 to study the role of preferential flow in the formation of hillslope runoff. Vadose Zone J. 9, 252–259.
Vogel, T., Dohnal, M., Votrubova, J., 2011. Modeling heat fluxes in macroporous soil under sparse young forest of temperate humid climate. J. Hydrol. 402, 367–376.
Votrubova, J., Dohnal, M., Vogel, T., Sanda, M., Tesar, M., 2017. Episodic runoff generation at Central European headwater catchments studied using water isotope concentration signals. J. Hydrol. Hydromech. 65. http://dx.doi.org/10.1515/johh-2017-0002.
Weiler, M., McDonnell, J.J., Tromp-van Meerveld, I., Uchida, T., 2005. Subsurface stormflow. In: Anderson, M.G. (Ed.), Encyclopedia of Hydrological Sciences. John Wiley & Sons, New York.
Weiler, M., McDonnell, J.J., 2006. Testing nutrient flushing hypotheses at the hillslope scale: a virtual experiment approach. J. Hydrol. 319, 339–356.
Weyhenmeyer, G.A., 2008. Water chemical changes along a latitudinal gradient in relation to climate and atmospheric deposition. Climatic Change 88, 199–208.
Winterdahl, M., Temnerud, J., Futter, M.N., Löfgren, S., Moldan, F., Bishop, K., 2011. Riparian zone influence on stream water dissolved organic carbon concentrations at the Swedish Integrated Monitoring sites. Ambio 40, 920–930.
Worrall, F., Harriman, R., Evans, C.D., Watts, C.D., Adamson, J., Neal, C., Tipping, E., et al., 2004. Trends in dissolved organic carbon in UK Rivers and lakes. Biogeochemistry 70, 369–402.
Worrall, F., Burt, T., 2005. Predicting the future DOC flux from upland peat catchments. J. Hydrol. 300, 126–139.
Xu, N., Saiers, J.E., Wilson, H.F., Raymond, P.A., 2012. Simulating streamflow and dissolved organic matter export from a forested watershed. Water Resour. Res. 48, W05519. http://dx.doi.org/10.1029/2011WR011423.
Yurova, A., Sirin, A., Buffam, I., Bishop, K., Laudon, H., 2008. Modeling the dissolved organic carbon output from a boreal mire using the convection-dispersion equation: importance of representing sorption. Water Resour. Res. 44, W07411. http://dx.doi.org/10.1029/2007WR006523.
Zhang, J., Hudson, J., Neal, R., Sereda, J., Clair, T., Turner, M., Jeffries, D., Dillon, P., Molot, L., Somers, K., Hesslein, R., 2010. Long-term patterns of dissolved organic carbon in lakes across eastern Canada: evidence of a pronounced climate effect. Limnol. Oceanogr. 55, 30–42.